Immune function and responses to COVID-19 vaccines in immunocompromised people

Sam M. Murray
Green Templeton College
University of Oxford

Thesis submitted for the degree of Doctor of Philosophy in Clinical Medicine
Hilary Term, 2025

Supervisors: Professor Eleanor Barnes, Dr Nicholas Provine, Professor Paul Klenerman and Professor Susanna Dunachie

Abstract
Immune function and responses to COVID-19 vaccines in immunocompromised people

Sam M. Murray
Green Templeton College
A thesis submitted for the degree of Doctor of Philosophy
Hilary Term, 2025

mRNA and ChAdOx1-vectored COVID-19 vaccines were highly effective at protecting against severe SARS-CoV-2 infection, but factors relating to the vaccine regimen and the recipient of the vaccine have been identified that impact vaccine immunogenicity. In particular, immunocompromising conditions increased the risk of severe COVID-19 even after vaccination. The aim of this thesis is to investigate the impact of the vaccine regimen and various immunocompromising conditions (diseases and/or immunosuppressive therapies) on SARS-CoV-2-specific antibody and T cell responses induced by COVID-19 vaccines.

First, I present data from two large observational cohort studies of COVID-19 vaccine immunogenicity and SARS-CoV-2 infection outcomes in individuals from 14 different immunocompromising conditions and healthy donors. These studies identify clinical subgroups at particular risk of immune non-responsiveness to vaccine, demonstrate the impact of SARS-CoV-2 mutations on vaccine-induced immune responses in immunocompromised individuals, and reveal the association between vaccine immunogenicity and subsequent COVID-19 severity in the immunocompromised cohort.

Next, I demonstrate the dominant impact of the vaccine dosing interval on the quality of antigen-specific T cells induced by mRNA and ChAdOx-1-vectored COVID-19 vaccines in healthy individuals. Through the combination of an activation induced marker assay and single-cell RNA- and T cell receptor sequencing, I provide insight into the broad functional and clonal heterogeneity of vaccine-induced T cells.

To understand how immunocompromising conditions shape the immune landscape prior to vaccination, I perform a comparative analysis of the transcriptome, inflammatory proteome and immune cell phenotype using pre-vaccination blood samples from immunocompromised individuals known to have poor immune responses to vaccines. By integrating this data with vaccine immunogenicity measures, I identify pre-vaccine immune signatures that are predictive of vaccine immune responsiveness in immunocompromised individuals.

Finally, I apply combined single-cell sequencing approaches to characterise COVID-19 vaccine-induced antigen-specific B and T cells and broader peripheral blood immune cells in immunocompromised individuals. This analysis characterises disease-specific vaccine-induced B and T cell populations and identifies new pathways of immune dysfunction in immune-vulnerable patient groups.

Overall, this thesis provides a comprehensive characterisation of the impact of immunocompromising diseases and therapeutics on COVID-19 vaccine responses and identifies new avenues to optimise vaccination strategies in at-risk populations.

Acknowledgements

As I near the end of my DPhil, I feel extremely lucky to be able to look back upon it and say with honesty that I enjoyed (almost!) every moment of it. On reflection, I think that is a testament to the people that I shared the journey with that provided support, guidance, and most of all a sense of happiness that made every experience and challenge worthwhile.

Firstly, I would like to thank my brilliant supervision team, whose passion for science is contagious and was a never-ending source for inspiration. Ellie Barnes, Nick Provine, Paul Klenerman and Susie Dunachie - I have greatly enjoyed working with each of you. Particularly, I would like to thank Ellie and Nick, I am truly appreciative for the generosity of your support and the effort you have put into making my DPhil as successful and enjoyable as possible. Our long discussions on all things science and non-science (but mostly science!) have brought new ideas and fun throughout. Your mentorship has helped me to develop so much over the past four years, and I very much look forward to seeing what more we can achieve together.

There are numerous people to thank from the cohort studies that formed the basis of all my work. In particular, I would like to thank all those at the Birmingham Cancer Research UK Clinical Trials Unit, for managing the OCTAVE trials, Tom Marjot for his leadership of the EASL COVID-Hep 2.0 study, and to Susie and Paul for allowing me access to samples and data from the PITCH study. Beyond that, I would like to thank the hundreds of donors who went out of their way to make these studies a reality.

Next, I would like to thank my friends – old and new - that reminded me what fun there is outside of the lab; and friends within the Barnes/Klenerman groups: Becky Strain, Katia Sayaf, Georgi Meacham, Tom Marjot, Stavros Dimitriadis, Anthony Brown, Jordan Rolt that showed me what fun there is within the lab, and helped me through some long days.

To my mum, Ann, and brother, Ben, your support throughout my life is a constant, and without it I wouldn't be the person I am today. Thank you to both of you for always being there to push me on. And thank you to my adopted family, Alison and Emily, for putting up with me on your doorstep after all this time - hopefully it has been worth the effort!

Finally, to Lucy, who has been the best companion a person could ask for. Your patience, kindness and friendship has made every day a better one. I'm endlessly grateful to have you in my life, and your support throughout this DPhil just reinforces that gratitude. I can't wait to get through more challenges like this one, with you. Thank you.

Thesis contributors

All work included in this thesis was authored and produced by me. As my work includes data generated as part of large human cohort studies, this was done in collaboration with colleagues, specific contributions are provided below and noted throughout:

Chapter 3

Georgina Meacham, Dr Sophie Irwin

Assisted with IFNγ ELISpots

Anthony Brown

Pooled SARS-CoV-2 spike peptide pools for IFNγ ELISpots, assisted with importing PBMC and serum samples from European sites into UK.

Dr Ashley Otter (UK Health Security Agency)

Provided additional Roche antibody data for PITCH healthy controls for EASL COVID-Hep 2.0 study

Dr Marc Lütgehetmann, Dr Golda Schaub and Dr Paul Duengelhoef, Dr Melanie Wittner, Dr Julian Schulze zur Wiesch

Provided PBMC, Roche antibody, demographic and SARS-CoV-2 infection data for liver transplant recipients in EASL COVID-Hep 2.0 study.

Maria-Carlota Londoño, Elisa Pose, Virginia Hernandez-Gea, Francesco Paolo Russo, Massimo Iavarone, Pietro Lampertico

Provided PBMC, demographic and SARS-CoV-2 infection data for liver disease patients in EASL COVID-Hep 2.0 study.

Dr Thomas Marjot

Oversaw EASL COVID-Hep 2.0 study, assisted with importing PBMC and serum samples from European sites into UK, provided critical feedback for EASL COVID-Hep 2.0 data analysis.

Dr Sandra Adele, Eloise Philipps,Tom Malone (Dunachie lab)

Performed IFNγ ELISpot experiments on PITCH participants.

Dr Tom Tipton, Saoirse Healy (Professor Miles Carroll lab)

Provided SARS-CoV-2 variant ACE-2 inhibition and IgG binding assay and microneutralization data for EASL COVID-Hep 2.0 and OCTAVE studies.

OCTAVE Clinical Trials Team

Provided PBMC from OCTAVE DUO study.

OCTAVE DUO Clinical Trials Team

Provided PBMC from OCTAVE DUO study.

Dr Amanda Kirkham, Amit Patel, Charlotte Gaskell (OCTAVE and OCTAVE DUO Statistician team)

Provided processed and filtered demographic, clinical, SARS-CoV-2 infection and adaptive

immune outcome data from OCTAVE and OCTAVE DUO trials

Chapter 4

Dr Nicholas Provine

Developed and performed activation induced marker experiment and prepared libraries for single cell RNA-sequencing

Dr Helen Ferry

Performed fluorescence-activated cell sorting

Dr Ali Amini, Dr Lucy Garner (Klenerman lab)

Collected and processed peripheral blood mononuclear cells (PBMC) in PITCH study.

Dr Barbara Kronsteiner (Dunachie lab)

Provided samples from PITCH study

Dr Sagida Bibi, Prof Teresa Lambe, Prof Andrew Pollard

Provided PBMC samples from COV001 study

Chapter 5

Georgina Meacham

Assisted with RNA extraction from whole blood Tempus tubes. Assisted with preparing samples for Olink proteomics.

Dr Rory Peters

Assisted with design and optimisation of the Aurora immunophenotyping flow cytometry panel.

Vishal Rao

Assisted with RNA extraction from whole blood Tempus tubes.

Jordan Rolt

Assisted with some batches of the Aurora experiments by helping to prepare PBMC and acquire on flow cytometer.

Anthony Brown

Pooled SARS-CoV-2 spike peptide pools for Aurora ICS experiment

OCTAVE DUO Clinical Trials Team

Provided PBMC, Tempus tubes and serum samples from OCTAVE DUO study.

Dr Amanda Kirkham, Amit Patel (OCTAVE DUO Statistician team)

Provided processed and filtered demographic, clinical and adaptive immune outcome data from OCTAVE DUO trial

Dr Edward Carr and Professor Rupert Beale

Provided live neutralization assay data for OCTAVE DUO study

Chapter 6

Georgina Meacham

Assisted with thawing PBMC

Dr Helen Ferry

Performed fluorescence-activated cell sorting

Kyla Dooley and Amelia Heslington (Uhlig lab)

Assisted with single-cell RNA sequencing library preparations

Dr Barbara Kronsteiner (Dunachie lab)

Provided samples from PITCH study

OCTAVE DUO Clinical Trials Team

Provided PBMC from OCTAVE DUO study.

Dr Amanda Kirkham, Amit Patel (OCTAVE DUO Statistician team)

Provided processed and filtered demographic, clinical and adaptive immune outcome data from OCTAVE DUO trial

List of publications

Publications arising from introduction

Murray, S.M., Ansari, A.M., Frater, J. *et al.* The impact of pre-existing cross-reactive immunity on SARS-CoV-2 infection and vaccine responses. *Nat Rev Immunol* **23**, 304–316 (2023).

Publications arising from Chapter 3

Murray, S.M., Barbanti, M., Campbell, C., *et al.* Impaired humoral and cellular response to primary COVID-19 vaccination in patients less than 2 years after allogeneic bone marrow transplant. *Br J Haematol*. **198**, 668–679 (2022).

Murray, S.M, Pose, E., Wittner, M., *et al.* Immune responses and clinical outcomes after COVID-19 vaccination in patients with liver disease and in liver transplant recipients. *Journal of Hepatology,* **80**(1): 109-123 (2023).

Perez-Campuzano, V., Rautou, P-E, Marjot, T, … , **Murray S.M.** Impact of SARS-CoV-2 vaccination in patients with vascular liver diseases: Observations from a VALDIG multicenter study. *JHEP Reports* **6:12,** (2024).

Goodyear,C.S.*, Patel A.*, Barnes E.*, Willicombe M.*, Siebert S.*, de Silva T.I.*, … , **Murray, S.M.**, *et al.* Immunogenicity of third dose COVID-19 vaccine strategies in patients who are immunocompromised with suboptimal immunity following two doses (OCTAVE-DUO): an open-label, multicentre, randomised, controlled, phase 3 trial. *The Lancet Rheumatology* **6:6**, e339 - e351(2024).

Barnes, E.*, Goodyear, C.S., Willicombe, M. *, Gaskell, C.*, Siebert, S.*, de Silva, T., **Murray, S.M.,** *et al.* SARS-CoV-2-specific immune responses and clinical outcomes after COVID-19 vaccination in patients with immune-suppressive disease. *Nat Med* **29**, 1760–1774 (2023).

Publications arising from Chapter 4

Murray S.M, Amini A., Ferry H., *et al.* The dominant impact of dosing interval on the quality of T cells induced by SARS-CoV-2 mRNA and adenoviral vaccines. In revision, *Science Immunology.* (2025)

Publications arising from design of peptide pools in chapter 3

Moore S.C, Kronsteiner B., Longet S., Adele S., … , **Murray S.M,** Evolution of long-term vaccine-induced and hybrid immunity in healthcare workers after different COVID-19 vaccine regimens. *Med* **4***,* 191-215 (2023)

Table of Contents

List of Figures

List of Tables

List of Abbreviations

6-MP - 6-mercaptopurine
AAV - ANCA-associated vasculitis
aCD20 - anti-CD20
ADT - antibody-derived tag
AdV - adenovirus
AIM - Activation induced marker
aTNF - anti-tumour necrosis factor
B NHL - B cell non-Hodgkins lymphoma
BCR - B cell receptor
CD - Crohn's disease
ChAd - chimpanzee adenovirus
CITE-seq - cellular indexing of transcriptomes and epitopes
CM - central memory
CNI - calcineurin inhibitors
COVID-19 - coronavirus disease 2019
DMARD - disease modifying anti-rheumatic drug
EM- effector memory
EMRA - Effector memory re-expression CD45RA
FACS - Fluorescence-Activated Cell Sorting
HC - healthy control
HM - haematological malignancy
HSCT - haematopoietic stem cell transplant
IBD - inflammatory bowel disease
ICS - Intracellular cytokine staining
IFN - interferon
Ig - immunoglobulin
IMPDH - inosine-5′-monophosphate dehydrogenase
ISG - Interferon stimulated gene
LD - liver disease
LT - liver transplant
MHC - Major histocompatibility complex
MMF - mycophenolate mofetil
mTOR - mechanistic target of rapamycin
MTX - methotrexate
NFAT - nuclear factor of activated T cells
PAMP/DAMP - pattern/damage associated molecular pattern
PBMC - peripheral blood mononuclear cells
PCA - principal component analysis
PCR - polymerase chain reaction
PID - primary immunodeficiency

QC - quality control
RA - rheumatoid arthritis
RBD - receptor binding domain
RC - rheumatic condition
RT - renal transplant
SARS-CoV-2 - Severe acute respiratory syndrome coronavirus 2
scRNA-seq - single-cell RNA sequencing
Secondary immunodeficiencies - SIs
SFU - spot forming unit
SOT - solid organ transplant
TCR - T cell receptor
Tfh - T follicular helper
Th - T helper
TNF - tumour necrosis factor
TNF - tumour necrosis factor
UC - ulcerative colitis
UMAP - uniform manifold approximation and projection
V - vaccine
VoC- variant of concern

1 Introduction

1.1 COVID-19 pandemic and its impact on immune vulnerable people

The corona virus disease (COVID)-19 pandemic, caused by the severe acute respiratory syndrome coronavirus 2 (SARS-CoV-2) was a global health emergency which necessitated the rapid design and deployment of immunogenic and protective anti-viral vaccines. The pandemic caused millions of deaths (*1*), socio-economic disruption (*2*) and long-term health issues (*3*). COVID-19 was particularly impactful to individuals who had immune compromising conditions or chronic diseases that made them particularly susceptible to severe disease (*4-6*). In 2020, 29.3% of individuals in the United Kingdom (UK) had one or more long-term health conditions, including 82.9% of individuals over the age of 80 years (*7*) and 3.9% of the population of England were defined as severely immunosuppressed in 2023 (*4*). The rapid development of SARS-CoV-2 targeting vaccines in the COVID-19 pandemic was essential to protect individuals against severe disease and facilitate global socio-economic recovery (*8*). Given the association between vaccine immunogenicity and effectiveness at protecting against severe disease, understanding the factors associated with COVID-19 vaccine immunogenicity, particularly in immune-vulnerable individuals, was critical to determine protection against COVID-19.

1.2 SARS-CoV-2 and COVID-19 clinical course

SARS-CoV-2 is a member of a large family of positive-sense RNA human coronaviruses (HCoVs) which include the alphacoronaviruses (α-CoVs) 299E and NL63 and the betacoronaviruses (β-CoVs) HKU1, OC43, MERS-CoV, SARS-CoV and SARS-CoV-2 (*9*). These HCoVs contain genes that code for structural proteins: spike (S), envelope (E), membrane (M), nucleocapsid (N), and accessory and non-structural proteins (NSPs) (*10*). SARS-CoV-2 infection varies from asymptomatic infection to infection causing acute respiratory failure, septic shock, multiple organ failure and death (*11*). In healthy people, an estimated 20% of SARS-CoV-2 infections were asymptomatic (*12*), 60-70% of symptomatic

infections presented with mild illness with fever, cough and shortness of breath (*13*), 23% presented with severe disease and 6% resulted in death (*14*).

1.2 Vaccination for infectious disease

Vaccines have proven to be effective mechanisms of protection against infectious disease for over 200 years (*15*). Prophylactic administration of an inert form of pathogen-associated antigen causes the generation of an adaptive immune response to the antigen of interest (*16*). The adaptive immune response, in the form of B and T cells and antibodies, persists after the initial vaccination and provides protection against subsequent infection with the target pathogen (*16*). Many different forms of vaccines now exist that are variably effective at inducing adaptive immune responses. Vaccine immunogenicity is affected by factors relating to the vaccine platform, including the delivery vector, the target antigen, adjuvants and the vaccination regimen (*16*). Vaccine immunogenicity is also affected by factors relating to the vaccine recipient, including genetic, environmental and clinical factors – in particular, immune compromising conditions (*16-18*).

1.3 COVID-19 vaccines

Various vaccine platforms were used to develop many different types of COVID-19 vaccines (*19*). In the UK, relatively new vaccine platforms such as adenoviral-vectored and mRNA vaccines were quickly deployed and demonstrated high real-world efficacy against severe disease in immunocompetent populations (*19*). Their efficacy in this setting highlighted their utility as highly immunogenic antigen-delivery platforms. mRNA and adenoviral-vectored vaccines are therefore increasingly being applied to a number of disease contexts, including for emerging viruses (*20-22*), bacteria (*23, 24*) and cancer (*25*).

1.4 COVID-19 vaccines: platforms

1.4.1 Adenoviral vector vaccines

Adenoviruses (AdV) were first used as gene delivery vehicles in the 1980s (*26*). AdV are non-enveloped double-stranded DNA viruses natively found in vertebrates, with over 150 primate

and 56 human AdV serotypes (*27, 28*). AdVs have several features which makes them ideal viral vectors for transgene delivery and vaccination (*29*). They are easily genetically modified, allowing for transgene insertion and removal of replication-essential genes (E1 and/or E3). They exhibit broad tissue tropism via the coxsackievirus and adenovirus receptor, enabling transgene expression in multiple cell types. Additionally, they transiently express transgenes without integrating viral DNA into the host genome and are well tolerated with good safety profiles in humans (*30*).

A limitation of AdVs as vaccine vectors in humans is their reduced efficacy due to pre-existing neutralizing antibodies and CD8+ T cell responses against the vector itself (*31*). Given the widespread circulation of AdVs in human populations, this pre-existing immunity significantly limits their practicality as vaccine platforms (*31*). To address this, less commonly circulating AdV strains (such as Ad26) or non-human AdVs (such as chimpanzee adenovirus (ChAd)) have been developed as vaccine vectors. Replication deficient ChAd vectors with the capacity to express genetic products in human cells were first described in 2001 (*32*) and several immunogenic vectors have since been developed and tested in clinical trials (*33, 34*).

The ChAdOx1 vector is a modified strain of the Y25 ChAd with the E1 coding region (required for viral replication) removed, and genetically modified E3 and E4 regions (*35*). Prior to use as a vaccine against SARS-CoV-2, the immunogenicity of ChAdOx1 was demonstrated in small-animal models and clinical trials against antigens from several viruses including influenza (*36, 37*), Middle East respiratory syndrome (MERS) coronavirus (*38, 39*) and others (*22*). These studies demonstrated the induction of robust polyfunctional $CD4^+$ and $CD8^+$ T cell responses after a single dose, with relatively low induction of neutralizing antibodies.

1.4.2 mRNA vaccines

Since the first demonstration of in vitro transcription and protein production from exogenous mRNA in 1990 (*40*), significant advances in mRNA vaccine technology have led to its successful usage as a COVID-19 vaccine. mRNA has many advantages as a gene delivery

mechanism (*41*). It is highly flexible in its range of potential genetic cargo and is translated and degraded through endogenous cellular processes. It is non-infectious, cannot be integrated into the genome and does not induce anti-vector adaptive immunity, as is observed in some viral-vectored vaccines (*41*).

However, several key innovations were required to enable mRNA as a viable vaccine platform. First, mRNA is targeted by exonucleases for degradation and therefore is inherently unstable. To address this, modifications to the 5' cap, 5' and 3' UTR and poly(A) tail of the coding mRNA enhanced its stability and translatability by improving ribosome targeting and reducing RNA degradation (*42*). Second, mRNA delivery is inefficient due to high rates of extracellular degradation and limited mechanisms of cellular entry (*42*). To address this, lipid nanoparticles (LNPs), composed of cationic lipids and polymers, were developed to encapsulate and protect mRNA, enhance uptake, and provide an adjuvant effect (*43, 44*). Third, exogenous mRNA activates innate immune responses through nucleic acid sensors like TLRs 3, 7, and 8, as well as cytoplasmic receptors (RIG-1, MDA-5, and OAS), triggering interferon (IFN) signalling that degrades RNA and inhibits protein expression (*45-47*). Through this mechanism, mRNA gene delivery and subsequent immunogenicity is highly sensitive to IFN signalling (*48, 49*). To reduce sensing of the exogenous mRNA, nucleoside modifications such as pseudouridine or N1-methylpseudouridine were introduced which reduced TNF and IFNa production by dendritic cells (*50-52*). These nucleoside modifications increased vaccine-induced immunogenicity (antibody titres) in mice in a manner negatively correlated with inflammatory signalling (*49*).

These innovations were incorporated into the widely deployed SARS-CoV-2 mRNA vaccines BNT162b2 (Pfizer-BioNTech) and mRNA-1273 (Moderna), enabling their success as vaccine vectors against COVID-19.

1.5 COVID-19 vaccines: SARS-CoV-2 antigen selection

There is a high degree of homology between hCoVs in both structural and non-structural

proteins between members (*53, 54*). Based on work done to rationally design vaccines targeting MERS- and SARS- coronaviruses, ChAdOx1 and mRNA COVID-19 vaccines were developed against SARS-CoV-2 using pre-fusion stabilised SARS-CoV-2 spike protein as the vaccine immunogen (*55-58*).

1.6 COVID-19 vaccines: pre-clinical studies and clinical trials in healthy individuals

1.6.1 ChAdOx1 nCoV-19

The initial studies of ChAdOX1 nCoV-19 in mice and rhesus macaques demonstrated generation of anti-SARS-CoV-2 spike and neutralising antibodies that significantly increased in titre after a second dose (*59*). IFNγ T cell responses were also induced, but were not further boosted by a second dose (*59*). These findings were recapitulated in healthy adult humans (aged 18-55 years) in phase I/II clinical trials, which indicated that binding and neutralising antibody titres were similar to those induced by COVID-19 infection (*58, 60*).

1.6.2 mRNA

In the UK, the available mRNA vaccines for initial priming vaccine doses were BNT162b2 and, to a lesser extent, mRNA-1273. Both vaccines were shown to be immunogenic in pre-clinical and clinical trials (*57, 61, 62*). Direct comparison of BNT162b2 and mRNA-1273 demonstrated similar induction of spike-specific binding and neutralising antibody titres and similar levels of activated or cytokine producing spike-specific $CD4^+$ and $CD8^+$ T cells (*63*).

1.7 COVID-19 vaccines: vaccine regimen

1.7.1 ChAdOx1 versus mRNA platforms

While similar immunogenicity was observed between mRNA platforms, the immunogenicity induced by mRNA and ChAdOx1 was significantly different. Comparison of BNT162b2 and ChAdOx1 homologous prime-boost in a randomised controlled trial (RCT) of healthy young adults demonstrated that BNT162b2 induced 10-fold higher titres of anti-spike IgG 28 days post boosting dose (1392ELU/mL ChAdOx1 vs 14080ELU/mL BNT162b2, (*64*)). In RCTs ChAdOx1 nCoV-19 induced stronger T cell responses after the priming dose than BNT162b2,

but two of three trials reported higher responses with BNT162b2 following a booster (i.e., second) vaccination (*65-67*). Observational studies also showed higher magnitude T cell responses after one or two doses of adenovirus vector vaccines (ChAdOx1 or Ad26) compared with mRNA-LNP (BNT162b2 or mRNA-1273) vaccination (*68-70*). These studies indicated that there were differences in the quantity of SARS-CoV-2 spike-specific T cells induced by different vaccine platforms but lacked insights into the quality or multi-faceted functionality of the induced T cells.

Interestingly, heterologous prime-boosting with a single dose of ChAdOx1 nCoV-19 followed by a single dose of BNT162b2 induced significantly higher antibody titres than homologous ChAdOx1 vaccination and higher IFNγ T cell responses compared to homologous doses of either vaccine (*64*). This indicates that ChAdOx1 and mRNA vaccination may act synergistically in combination to induce higher immunogenicity.

1.7.2 Prime-boost dosing interval

Initial studies of mRNA and ChAdOx1 COVID-19 demonstrated that a booster (second) dose increased vaccine immunogenicity, particularly antibody titres (*57, 58*). Large studies of BNT162b2 and ChAdOx1 immunogenicity additionally observed that increasing the length of time between first and second vaccine doses (the vaccine dosing interval) was associated with differences in vaccine-induced antibody and T cell responses (*71-74*). Anti-SARS-CoV-2 spike antibody titres 28 days after vaccination with a second dose of either vaccine was increased by extending the dosing interval from 3-4 weeks to over 10 weeks (*71-74*). Extended dosing intervals were also associated with increased or equivalent vaccine efficacy against symptomatic COVID-19 infection after either vaccine (*73, 75*). In contrast to antibody responses, RCTs and observational cohort studies showed that an extended dosing interval marginally decreased the frequency of vaccine-induced IFNγ$^+$ T cells (*66, 71, 76*), highlighting a disconnect between humoral and cellular vaccine-induced immune responses. Nevertheless, the frequency of IFNγ$^+$ T cells is only a single measure of cellular immunity, and

further work is required to broaden these results to the full diversity of T cell functionality.

1.8 COVID-19 vaccines: vaccine induced responses in the context of coronavirus cross-reactivity and SARS-CoV-2 variants

1.8.1 Seasonal coronaviruses

Unexpectedly, SARS-CoV-2 specific immune responses were identified in samples taken prior to the emergence of SARS-CoV-2 in 2019 (*77, 78*). Due to the high homology of SARS-CoV-2 with other HCoV's, cross-reactivity between pre-existing memory immune responses to circulating seasonal coronaviruses with conserved SARS-CoV-2 epitopes was the proposed source of these unexpected SARS-CoV-2 responses. Much work has been done to investigate the role of this pre-existing immunity in SARS-CoV-2 and COVID-19 vaccination outcomes. I reviewed this in detail in (*79*) (**Appendix 1**).

Evidence for the effect of pre-existing immunity on SARS-CoV-2 immunogenicity that is beneficial (boosts/augments subsequent SARS-CoV-2 responses), neutral (has no effect on response) or detrimental (reduces SARS-CoV-2 responses) have been described. Most of the reported evidence supports a beneficial role for pre-existing T cells in subsequent SARS-CoV-2 immune responses and a broadly neutral or detrimental role for pre-existing B cell mediated responses (*79*). Observed beneficial roles for pre-existing T cells include the identification of a pool of pre-existing memory responses that 'abort' SARS-CoV-2 infection (clear the virus before the occurrence of symptomatic disease) or can be quickly recalled to contribute to the *de novo* response and protect against severe disease (*80, 81*). However, the exact contribution of pre-existing T cell clones to vaccine immunogenicity remains an open question. For B cell mediated responses, pre-existing antibodies had no association with protection against disease or subsequent antibody responses (*82, 83*), and weak observational evidence found that pre-existing antibodies were associated with an increased probability of developing severe COVID-19 (*84*). Thus, there is a nuanced and potentially conflicting role for pre-existing adaptive immune responses on subsequent SARS-CoV-2 responses – with their contribution

to vaccine-induced responses still not precisely clear.

1.8.2 SARS-CoV-2 variants

Since the initial emergence of SARS-CoV-2, multiple viral variants emerged through mutation or recombination events that had a significant impact on viral fitness and pathogenicity (*85, 86*) **(Fig. 1.1)**. The increasing prevalence of immunity – by COVID-19 vaccination and SARS-CoV-2 infection - to SARS-CoV-2 provided increased evolutionary pressure for SARS-CoV-2 to develop mutations which evaded the protective immune response (*85*). Based on criteria of disease severity and prevalence, SARS-CoV-2 variants were categorised (in descending order of risk) as variants of concern (VoC), variants of interest (VoI) or variants under monitoring (VUM). Between September 2020 and March 2025, there were 70 unique SARS-CoV-2 variants labelled under one of these categories, with no VoCs and only two VoI's (Omicron BA.2.86 and KP.3) circulating in Europe in March 2025 (*87*).

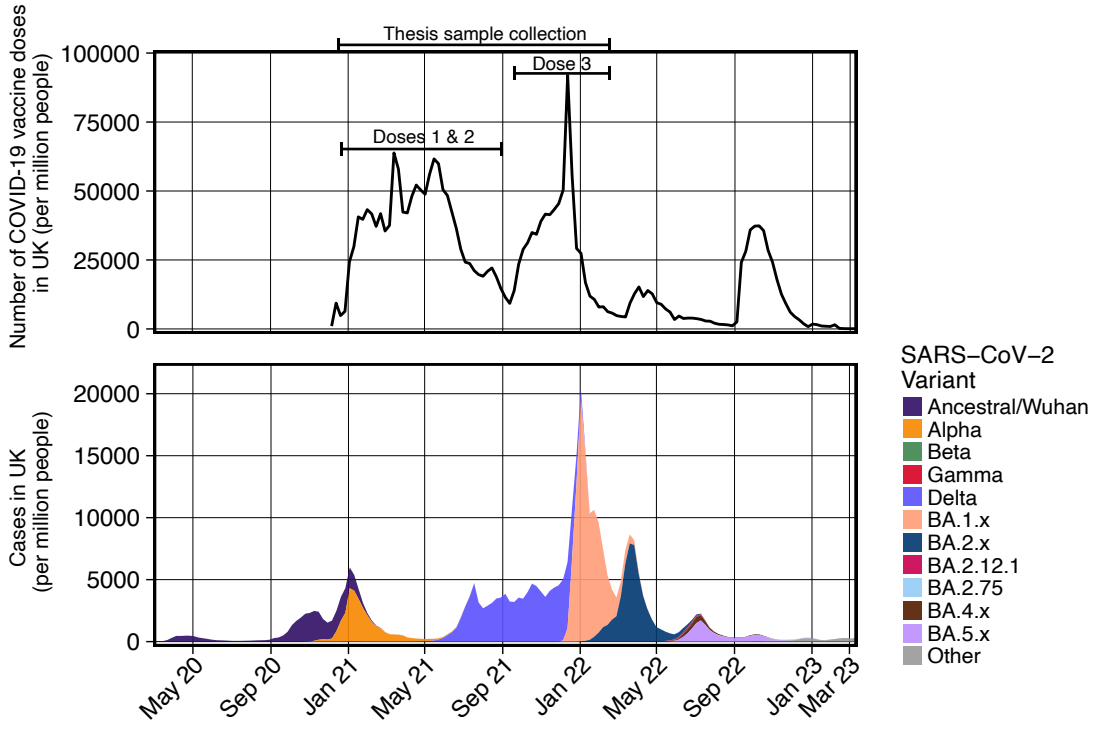

Fig. 1.1 COVID-19 vaccination and SARS-CoV-2 variant infection rate over time in the United Kingdom up until March 2023

The COVID-19 vaccination rate (top panel) and SARS-CoV-2 infection rate by variant per million people in the United Kingdom (UK). Vaccine data taken from NHS England COVID-19 vaccinations archive. Infection data downloaded from World Health Organisation and variant data from GISAID (Section 3.5.4).

Most of the work in my thesis was performed on human samples collected up until April 2022, when Omicron sub-variants BA.1 to XBB.1 were the most recent dominant SARS-CoV-2 variants. At this time, the impact of SARS-CoV-2 mutations on vaccine immunogenicity was largely unknown – especially in immunocompromised individuals. Since, much work has been done to show the immune evasion of emerging variants (*88, 89*).

The emergence of the delta variant in Autumn 2021 and subsequent emergence of Omicron BA.1 prompted the global deployment of a 'booster' third vaccine dose. Omicron BA.1 presented a major step change in the COVID-19 pandemic, with 30 substitutions plus the deletion of 6 and insertion of 3 residues in the spike protein of BA.1 compared to ancestral SARS-CoV-2 (*90*). These mutations significantly reduced the neutralisation capacity of antibodies generated to ancestral vaccines in healthy individuals (*88, 91, 92*), contributing to a surge in SARS-CoV-2 infections in the UK and globally. Interestingly, Omicron BA.1 was associated with reduced COVID-19 severity compared to prior variants (*93*). In healthy individuals, cross-neutralisation of variants was associated with high titres of ancestral-binding antibodies (*88*). With the emergence of SARS-CoV-2 variants with mutations that further evaded immune responses to ancestral vaccines, subsequent mRNA vaccines that encoded spike proteins from SARS-CoV-2 variants were deployed to improve protection against new SARS-CoV-2 variants (*94*). However, the focus of this thesis will be on ancestral SARS-CoV-2 spike encoding vaccines.

1.9 COVID-19 vaccines: host factors relating to vaccine immunogenicity

While both ChAdOx1 and mRNA vectored COVID-19 vaccines induce potent adaptive immune responses in healthy individuals, there is considerable variation between recipients in vaccine immunogenicity. Within immunocompetent populations, several host factors (demographic/environmental) are associated with vaccine-induced responses, including previous COVID-19 infection (*71*), sex (*95*) and age.

1.9.1 Age

Studies examining the impact of age on immune responses to the ChAdOx1 COVID-19 vaccine showed that vaccine-induced antibody titres were consistent across different age groups (*60, 96*). There was no significant decrease in SARS-CoV-2 spike antibody binding titres or IFNγ T cell responses in older adults (56 years and older) or younger participants (aged 6-17 years) compared to adults aged 18-55 years (*60, 96*). However, this study only included elderly individuals who were in good health, with no uncontrolled comorbidities or high frailty scores, and so is not representative of the general elderly population (*60, 97*).

In mRNA vaccination, there is contrasting evidence supporting the impact of age on vaccine immunogenicity. A small sub-study of the mRNA-1273 phase I clinical trial identified no difference in binding or neutralising antibody titres between adults aged 18-55 years and those over 56 years old (*98*). No difference in induced antibody or T cell responses was also observed in individuals that were over 80 years old compared to 51-79 year old individuals after two doses of BNT162b2 vaccination (*99*). However, other, larger, studies observed that anti-spike antibody titres induced 21-28 days after one or two doses of BNT162b2 or mRNA-1273 decreased with increasing age (*71, 100-102*). Studies of the effect of human aging on vaccine immunogenicity are often limited by the confounding effects of comorbidity and frailty, both of which increase in prevalence with age (*103*) and may impact vaccine immunogenicity (*104*). Heterogenous prevalence of comorbidities/frailty in these studies therefore likely explains the contrasting conclusions on vaccine immunogenicity.

1.10 Secondary immunodeficiencies

As highlighted above, the adaptive immune response to vaccines is central to their effectiveness at protecting against infection, including SARS-CoV-2. The adaptive immune response is carefully regulated to reduce responsiveness to self-antigen while maximising responsiveness to invasive external antigen (*105*). In rare circumstances, failure to properly downregulate the adaptive immune response to self-antigen may manifest clinically as autoimmune diseases (*106*). In other circumstances, such as in transplantation, adaptive

immune responses to allogeneic (donor) tissue are generated appropriately but are counteractive to the clinical intervention and therefore are detrimental to health (*107*). Autoimmune conditions that are studied in this thesis include rheumatoid arthritis (RA) (*108*), anti-neutrophil cytoplasmic antibody (ANCA)-associated vasculitis (AAV) (*109*) and autoimmune hepatitis (AIH) (*110*). Transplantation includes haematopoietic stem cell (HSCT) (*111*) and solid organ transplant (SOT) including liver (*112*) (LT) and kidney (renal) transplant (RT) (*113*).

For both autoimmunity and organ transplantation, medication designed to interfere with the generation of the adaptive immune response is prescribed with the aim of suppressing immune-induced pathology (*114*). Chronic inflammatory conditions, such as inflammatory bowel diseases (IBD) also require immunosuppression to reduce immune-mediated inflammation and organ damage (*115*). Such immunosuppressive agents have been transformative to clinical outcomes. However, they lack antigen-specificity and lead to systemic dysregulation of one or more central functions of the adaptive immune system. Thus, they may inadvertently also impair immune responses to exogenous antigens such as infectious agents or vaccines.

In addition to the use of immunosuppressive medications, immune dysregulation may be caused through disease-mediated mechanisms. Examples of disease-mediated immune dysfunction include chronic diseases such as liver cirrhosis (*116*), and haematological malignancies (HM) (*117*), and chronic viral infection such as infection with human immunodeficiency virus (HIV) (*118*), cytomegalovirus (CMV) (*119, 120*) and Epstein-Barr virus (EBV) (*121, 122*). In the case of chronic diseases, immune dysregulation may additionally be exacerbated by the clinical intervention (e.g. immunosuppressive therapeutic or haematological stem cell transplant) employed to treat the disease.

Together, conditions of immunodeficiency caused by non-heritable factors are referred to as secondary immunodeficiencies (SIs). Individuals living with SIs are at increased risk of

infection and cancer and as such have higher rates of morbidity and mortality compared to immunocompetent populations (*123, 124*). Vaccines offer potential solutions to the risks associated with both infection and cancer, so understanding vaccine immunogenicity in such populations is of considerable importance.

1.11 Secondary immunodeficiencies: immunosuppressive medications

Several classes of immunosuppressive medications exist that inhibit adaptive immune responses (**Table 1.1, Fig. 1.2**). Broadly, they impair immune responses through one of four mechanisms: 1) reduction of proliferation of adaptive immune cells, 2) depletion of immune cell populations, 3) impair adaptive immune cell activation and 4) blockade of inflammatory signalling pathways. Different immunosuppressive drug classes act through one or more of these mechanisms to impair immune responses. This overview will focus on adaptive immune related mechanisms of action/pathology for immunosuppressive therapeutics included in the thesis.

1.11.1 Immunophilin inhibitors (calcineurin and mTOR inhibitors)

Immunophilins are cytosolic proteins that positively regulate T cell action by interacting with nuclear factor of activated T cells (NFAT) or mechanistic target of rapamycin (mTOR). The immunophilin which interacts with NFAT is cyclophilin A, which is inhibited by calcineurin inhibitors such as tacrolimus and cyclosporin A (*125, 126*). The mTORC1 complex is inhibited by mTOR inhibitors such as everolimus and sirolimus (*127*).

Through blockade of NFAT translocation, calcineurin inhibitors inhibit the expression of cytokines including IL-2 and early activation genes (including *c-Myc*) after TCR stimulation – blocking required signals for T cell activation and proliferation (*125*). mTOR inhibitors block intracellular signalling after CD28 and IL-2 receptor (CD25) engagement which is also key for T cell activation (*128*) (*129*). Importantly, TCR signalling in the absence of mTOR mediated IL2/CD28 signalling leads to lack of T cell activation or T cell anergy (*127*). mTOR inhibitors additionally can block B cell proliferation, survival and differentiation into antibody-producing

plasma cells (*130*). Together, immunophilins act to suppress the activation and proliferation of predominantly T cells, causing disruption to $CD4^+$ T follicular helper (T_{FH}) (*131*), cytotoxic and effector $CD4^+$ T cells ($T_H1/T_H2/T_H17$) (*132*), regulatory $CD4^+$ T cells (T_{reg}) (*133, 134*) and $CD8^+$ T cells (*135*).

Immunophilins are commonly used as immunosuppressive agents in liver and kidney transplantation and in autoimmune conditions such as rheumatoid arthritis (*136*). mTOR inhibitors are also increasingly being used in cancer (*137*).

Table 1.1 Relevant immunosuppressive therapy types, their mechanism of action and associated disease groups.

Drug class	Mechanism of action	Common use:
Antibody therapy	Various: including B cell depletion (anti-CD20), and TNF inhibition (anti-TNF) (*138*)	RA, IBD, HSCT, AIH, HM, AAV
Calcineurin inhibitors	Impairs transcription of T cell activation cytokines (IL-2 etc) to inhibit T cell function (*139*).	RA, AAV, SOT, HSCT, AAV
mTOR inhibitors	Inhibition of T cell proliferation	SOT, HM
Antiproliferative/ Antimetabolite	Inhibit B and T cell proliferation by blocking purine base synthesis(*140*)	RA, AAV, SOT, AIH
Methotrexate	T cell apoptosis	RA, AAV, IBD
Glucocorticoids	Various, including down-regulation of pro-inflammatory cytokines(*141*)	RA, AAV, IBD, HSCT, SOT, HM

ATGs = antithymocyte globulins; RA = rheumatoid arthritis ; SOT = solid organ transplant; HSCT = haematological stem cell transplant; AIH = autoimmune hepatitis; IBD = inflammatory bowel disease; RT = renal transplant; HM = haematological malignancy; AAV = ANCA-associated vasculitis

1.11.2 Antiproliferative/Antimetabolite

Anti-proliferative/anti-metabolites inhibit T and B cell proliferation by blocking or reducing cell cycling and include azathioprine, mercaptopurine (6-MP) (collectively referred to as thiopurines), methotrexate, and mycophenolate mofetil.

T cells require the *de novo* synthesis of purine and pyrimidine nucleotides for mitosis in response to activation signals (*142*). The anti-metabolite class of immunosuppressants block T cell cycling by disrupting the generation of these nucleotides (*35).* Thiopurines are purine nucleotide analogues that block aminotransferase enzymes, including inosine-5′-monophosphate dehydrogenase (IMPDH) (*143*). Mycophenolate mofetil specifically binds to and inhibits IMPDH – also blocking purine synthesis (*143, 144*).

At high doses, methotrexate blocks lymphocyte proliferation through inhibition of dihydrofolate reductase (*145*). At lower doses, methotrexate causes the cellular accumulation and release of adenosine, which potently inhibits inflammatory pathways (*145*). It also leads to reactive oxygen species accumulation in T cells, resulting in increased T cell sensitivity to apoptosis through increased JUN N-terminal kinase activation (*146*).

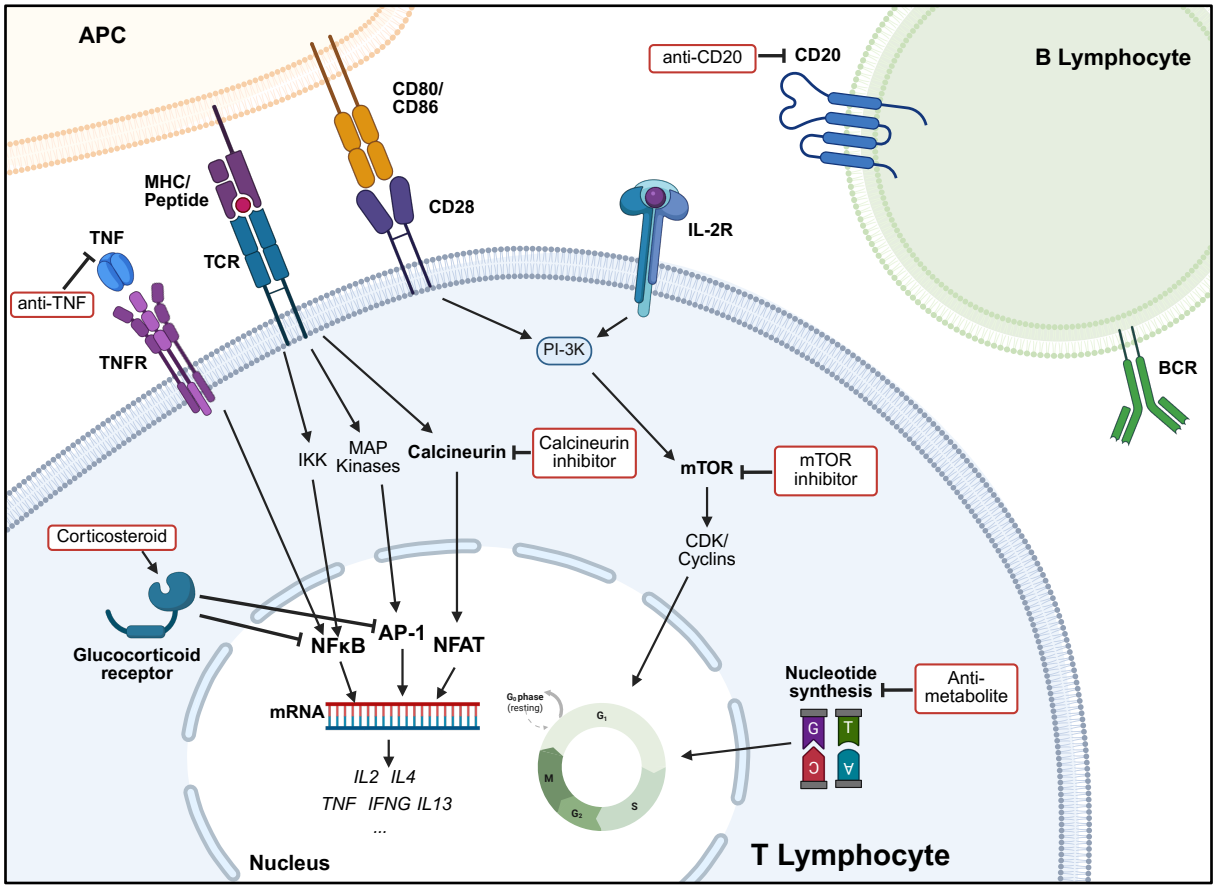

Fig. 1.2 Targets of immunosuppressive therapeutics
The mechanisms of immunosuppressive agents used in patient groups in this thesis. Made using BioRender, IKK = IκB kinase, MAP = Mitogen-activated protein, CDK = Cyclin-dependent kinase, PI-3K = Phosphatidylinositol 3-kinase, AP-1 = Activator Protein-1, NFAT = nuclear factor of activated T cells, APC = antigen presenting cell

Thiopurines are commonly used as immunosuppressive agents in autoimmune hepatitis (AIH) (*147*), kidney transplantation (*148*), RA (*149*), and inflammatory bowel disease (IBD) (*150*). Mycophenolate mofetil is used in SOT, RA and AIH and commonly in combination with calcineurin inhibitors in SOT, due to its dose sparing effect (*151*). Methotrexate is commonly used in the treatment of IBD and RA (*145*).

1.11.3 Glucocorticoids

Glucocorticoid therapeutics, such as prednisolone and dexamethasone, induce systemic anti-inflammatory and immunosuppressive effects. The glucocorticoid receptor is an almost ubiquitously expressed transcription factor which exerts control over multiple inflammatory and homeostatic processes. The primary anti-inflammatory role of corticosteroids is mediated through its repression of NFκB and AP-1 transcription factors which are both central regulators of cytokine production and cellular proliferation, differentiation and apoptosis in T cells (*141, 152*). Corticosteroids also suppress IL-2 production and inhibit T cell activation and differentiation by blocking JAK-STAT signalling in T cells and by inhibiting production of co-stimulatory cytokines (IL-6, IL-2, TNF) by dendritic cells (*153, 154*).

Owing to their various immunosuppressive and anti-inflammatory roles, glucocorticoids are commonly used in many immune-mediated conditions, including RA, SOT, IBD, HSCT and haematological malignancies (*152, 155*).

1.11.4 Biologics (antibody therapies)

Biologics are a diverse class of immunomodulatory therapeutics, primarily consisting of antibodies or recombinant proteins. These therapies leverage the high binding specificity of recombinant proteins or antibodies to ensure precise interaction with a target molecule. Depending on the target, biologic agents can induce various downstream effects and numerous biologics are currently used as immunosuppressive therapies, reviewed in (*114*). Biologics that are relevant to this thesis are infliximab/adalimumab - which inhibit TNF binding to TNFR1/TNFR2 receptors (*156*) - and rituximab which binds to CD20 and depletes B cells

through cellular- and complement-dependent cytotoxicity (*157, 158*). Because of the pleiotropic effects of TNF, its blockade interrupts many aspects of inflammatory cytokine production and impairs T cell activation (*159, 160*). In contrast, aCD20 therapy specifically disrupts B cells (*161*).

Infliximab and adalimumab are commonly used in IBD and RA (*159, 160*). Rituximab is used in severe rheumatological conditions including ANCA-associated vasculitis (AAV) and RA (*161*), and haematological malignancies including B cell lymphomas (including Hodgkins and non-Hodgkins lymphomas) (*162*).

1.12 Secondary immunodeficiencies: chronic disease

1.12.1 Cirrhosis

In addition to immunosuppressive agents, chronic disease can cause immune dysfunction. An example of this is cirrhosis-associated immune dysfunction (CAID), which is a term that covers the systemic inflammation and immune cell deficiency associated with liver cirrhosis (*163*). Cirrhosis is a progressive disease of the liver that comprises two stages, an often-asymptomatic early stage referred to as 'compensated disease' and a 'decompensated' phase associated with failure of hepatic function (*163*). Although ostensibly a disease of the liver, cirrhosis is considered a systemic disease because it impacts most systems of the body (*116*). Systemic inflammation in CAID is evidenced by increased plasma concentration of acute-phase proteins, cytokines (including IL-6, TNF, IFNγ and IL-17 (*164*)) and endothelial activation markers (including intracellular adhesion molecule 1 (ICAM1), vascular cell adhesion protein 1 (VCAM1) and vascular endothelial growth factor (VEGF)(*165*). Increased intestinal permeability in cirrhosis causes increased bacterial translocation and sensing of pattern/danger associated molecular patterns (PAMP/DAMP) (*166*), which leads to increased pro-inflammatory cytokine production from monocytes and T cells (*167, 168*). Serum concentration of these inflammatory factors increases with cirrhosis severity (*164*) and is associated with broad activation of circulating lymphocytes, vasodilation and further systemic

inflammation (*116, 169*). Immune cell function and phenotype are altered in cirrhosis. Depletion of neutrophils (*170*), $CD4^+$ T cells (*171*) and memory B cells (*172*), and functional impairment of inflammatory monocytes (*173, 174*) have been observed in cirrhosis, and are related to the increased systemic inflammation and DAMP/PAMP sensing from cirrhosis-associated bacterial translocation.

1.12.2 Haemodialysis

Haemodialysis, a therapeutic approach to artificially filter blood in end-stage kidney disease, is associated with broad immune suppression. Chronic inflammation in end-stage kidney disease patients on haemodialysis is caused by uraemia and the associated accumulation of pro-inflammatory cytokines including TNF, IL-1β and IL-6 (*175*). Additional inflammation is caused by routine exposure to the bio-incompatible membranes of the dialysis catheters, causing endothelial nitric oxide production and oxidative stress (*176*). Some patients with haemodialysis additionally receive immunosuppression for other comorbidities or to prevent rejection of previous unsuccessful kidney transplantation – leading to further immune dysfunction (*177*).

1.13 Secondary immunodeficiencies: impact on vaccine immunogenicity

1.13.1 Non-COVID-19 vaccines

Adaptive immune responses are reduced to several vaccines in individuals with SIs compared to healthy people. Rates of serological response to HBV, influenza or pneumococcal vaccines are decreased in patients with cirrhosis (*178, 179*), RA patients on methotrexate (MTX)(*180*), IBD patients on TNF inhibitors (*181*), SOT recipients (*182*) and HSCT recipients (*183*) compared to healthy individuals. RA patients treated with anti-CD20 therapy also had severely reduced serological responses to influenza vaccine than those on MTX or compared to healthy individuals (*184*). Relatively few studies investigated T cell responses to vaccination in immunocompromised patients in comparison to healthy donors, but those that did have also described reduced vaccine-induced cellular responses in immunocompromised patients (*185,*

186).

1.13.2 COVID-19 vaccines

Multiple studies demonstrated reduced immunogenicity of the primary course (doses one and two) of COVID-19 vaccines in SI groups compared to healthy individuals (*187-199*). Many of the early studies focused on single vaccine types and primarily reported only anti-SARS-CoV-2 antibody responses as a measure of vaccine immunogenicity. Many studies focused on a single disease type, thereby limiting observations to a single mechanism of immunosuppression and not providing comparative analysis of the impact of different immunosuppressive conditions on vaccine responsiveness. There was a critical need therefore for large comparative studies of antibody and T cell immunogenicity across immunosuppressive conditions.

With the emergence of SARS-CoV-2 variants, booster vaccine doses were recommended to increase vaccine immunogenicity. These were particularly prioritised for individuals with SIs – however the capacity of additional vaccine doses to increase SARS-CoV-2 immune responses in individuals with SIs was largely unknown. More recently, several large prospective cohorts of immunocompromised individuals have provided insight into the vaccine-induced antibody response and effectiveness at preventing severe COVID-19 in these groups (*200, 201*). As of Autumn 2024, immunocompromised individuals in the UK were offered up to their 10th booster dose of COVID-19 vaccine, including doses of variant-adapted COVID-19 vaccines (*200-202*). Work is ongoing to understand the immunogenicity of this number of vaccine doses.

1.14 Systems vaccinology approaches

There are many immune pathways involved in the generation of a successful immune response to vaccines (*16*). As discussed above, SIs and other host factors may impair vaccine immunogenicity through disruption of any number of these pathways. With the aim to study the concerted biology of the vaccine-related response, “systems vaccinology” approaches have been developed (*16*). Such approaches use high-dimensional technologies to measure

large numbers of parameters/analytes simultaneously to provide a holistic view by which to assess vaccine immunogenicity. These technologies include methods to assess gene expression (transcriptomics), protein concentration (proteomics), and high-dimensional flow cytometry approaches. These techniques can be used to assess whole tissue samples (bulk) or single-cell immune cell phenotypes. In combination, they provide complementary data sources to identify complex immunological networks, which in the context of vaccination, can be used to understand pathways associated with immunogenicity.

1.4.1 Transcriptomic sequencing, bulk and single-cell RNA-sequencing

High-throughput next-generation sequencing approaches have revolutionised transcriptomic analysis by facilitating the sequencing of tens of millions to billions of DNA sequences in days (*203*). As such, the transcriptome of bulk immune cells in blood can now be assessed to capture a snapshot of the broad composition of the circulating immune system. Bulk transcriptomic assessment of whole blood has been used successfully in vaccine studies to detect broad differences in expression profiles before and after vaccination and identify transcriptomic signatures predictive of vaccine responsiveness (*204-208*). In 2009, the first published work of mRNA sequencing of a single cell demonstrated that cell-to-cell transcriptional heterogeneity could be explored using single cell RNA-sequencing (scRNA-seq) (*209*). Development of droplet-based scRNA-seq approaches (*210*) greatly expanded the number of cells that could be individually sequenced and facilitated the use of this approach in vaccine studies. Since, scRNA-seq has been used in healthy people to identify several features associated with vaccine responsiveness, including: early within-cell type transcriptional signatures (*208*); interactions between biological sex and past viral exposures (*211*) and underlying host variation (*212*). Integration of RNA sequencing with adjunct single-cell sequencing measures such as surface protein sequencing (CITE) and adaptive immune receptor sequencing (V(D)J sequencing) provides a platform to study adaptive immune responses to vaccination at very high resolution.

1.4.2 Proteomics

While transcriptomic approaches can quantify expression of genes, not all genes are translated into proteins, and post-translational modifications can alter protein functionality (*213*). Assessment of the proteome of tissues and cells therefore gives vital insight into their functionality, beyond transcriptional approaches. In addition, protein concentrations in blood can be used as proxy measures of tissue dysregulation and as such have been used successfully as diagnostic/prognostic indicators of disease (*214, 215*), to identify disease targets (*216*), and to integrate genomic and proteomic traits (*217, 218*). Several approaches to measure proteomes have developed and vary in the number of protein analytes measured simultaneously and include unsupervised and supervised approaches. Mass spectrometry has been used to assess the whole human proteome (*213*) and can measure many thousands of proteins and protein variants in a single analysis run without pre-selecting proteins of interest (unsupervised) (*219*). Affinity-based platforms, such as those developed by SomaLogic and Olink, use DNA oligomer-tagged antibodies or aptamers that are specific to pre-selected (supervised approaches) target proteins (*220, 221*). Through quantification of the bound antibodies/aptamers using next-generation sequencing or microarrays respectively, pre-designed panels of tens to thousands of proteins can be measured simultaneously (*217*). Finally, multiplexed bead assays, such as Luminex and Meso-scale Discovery (MSD) use fluorescence-based approaches to quantify concentration of 10s to 100s of proteins simultaneously (*219*). The methodologies vary by specificity and sensitivity (*219*), but have been used to give insight into vaccine-induced inflammation (*208, 222*) and the impact of pre-vaccine inflammation on vaccine immune responsiveness (*223*).

1.4.3 Spectral-flow cytometry

Flow cytometry is a core technique that has been central to the improvement in understanding of cellular immune responses (*224*). Flow cytometry was invented in the late 1960s at which point it could be used to detect one fluorescently labelled antibody and the size of the cell

(*225*). Since, polychromatic ("conventional") flow cytometry has been improved to the extent that up-to 20 distinct fluorescently labelled proteins can be measured on single cells simultaneously (*226*). Development of spectral flow cytometry techniques, which quantifies the entire emission spectra of flow cytometry fluorophores rather than specific fluorescence 'bandwidths' as in conventional cytometry (*226*), has revolutionised this approach such that over 50 protein targets can be measured on single cells simultaneously (*227*). Spectral flow cytometry therefore provides the opportunity to quantify surface and intracellular expression of known proteins in millions of cells rapidly. In vaccinology, it has been used to provide broad insight into the phenotype and function of vaccine responsive immune cells across many studies (*228, 229*).

1.15 Knowledge gaps

Both mRNA and ChAdOx1-vectored COVID-19 vaccines induce robust antibody and T cell responses in healthy humans. However, factors relating to the vaccine regimen and to the vaccine recipient have been shown to impact vaccine-induced immunogenicity. This thesis aims to provide further insight into the impact of some of these factors on vaccine immunogenicity. Specifically, it will focus on the following:

1.15.1 Factors relating to vaccine regimen

ChAdOx1 nCoV-19 induces higher magnitudes of SARS-CoV-2 spike-specific IFNγ producing T cells than mRNA-vectored vaccines. However, beyond cytokine production, little is understood about the impact of the vaccine vector on the phenotype or functionality of spike-specific T cells.

In addition, the antibody and T cell response to a second dose of COVID-19 vaccine, particularly mRNA-vectored COVID-19 vaccines, is altered depending on the time-interval between first and second vaccine doses. Beyond its impact on IFNγ T cell production, little is known about the impact of vaccine dosing-interval on the phenotype or function of spike-specific T cells induced by mRNA or ChAdOx1 COVID-19 vaccines.

1.15.2 Factors relating to vaccine recipient

SIs impair normal immune function through broad and varied mechanisms. These mechanisms differentially act on different immune compartments and have been shown to variably impact vaccine-induced immune responses. However, little work has been done to directly compare the impact of different SIs on responses induced to a given vaccine antigen.

Early in the COVID-19 pandemic, little was known about the immunogenicity of new vaccine platforms (mRNA and ChAdOx1) in individuals with SIs. The impact of different immunosuppressive therapeutics on the phenotype and function of vaccine-induced antigen-specific B and T cells remains largely unknown. Additionally, the vaccine-related immunophenotype of individuals with SIs has not been mapped in sufficient detail to identify specific pathways that linked immunosuppressive conditions with vaccine immunogenicity.

Considerable work has been performed to identify pre-vaccine biological predictors of vaccine immunogenicity in healthy people. However much of this work has focussed on predicting vaccine-induced antibody responsiveness, it has not been performed in mRNA vaccination, and its applicability to immunocompromised populations is unknown.

1.16 Aims of thesis

In this thesis, I aim to profile the impact of host and vaccine regimen related factors on COVID-19 vaccine immunogenicity. First, I will establish the immunogenicity of mRNA and ChAdOx1-vectored COVID-19 vaccines in individuals with various SIs compared to healthy individuals in large cohort studies. Second, I will demonstrate the impact of vaccine platform and vaccine dosing interval on SARS-CoV-2 spike-specific T cell functionality and clonality using a single-cell sequencing approach. Third, I will identify differences in the immunophenotype of individuals with various SIs using systems approaches and link these differences to COVID-19 vaccine immunogenicity. Finally, I will use single cell sequencing approaches to demonstrate the impact of SIs on the single cell transcriptome of COVID-19 vaccine-induced antigen-specific B and T cells and other circulating immune cells.

2 Methods

2.1 Data generation: Preparation of peripheral blood mononuclear cells (PBMCs)

PBMCs were isolated from whole blood by density gradient centrifugation (Lymphoprep, Axis-Shield) and cryopreserved in 90% foetal calf serum (FCS) and 10% dimethyl sulfoxide (DMSO). PBMCs were thawed for use washed in R10 (RPMI 1640 (Sigma-Aldrich), 10% FCS, 1% Penicillin-Streptomycin (ThermoFisher).

2.2 Data generation: IFNγ ELISpot

Thawed PBMC were rested for 3-4 hours at 37°C in R10 + 1mg/mL DNase (Roche). Multiscreen-I 96 ELISpot plates (Millipore) were incubated with 10 µg/mL ELISpot basic kit capture antibody (clone 1-D1K) from the Human IFNγ ELISpot Basic kit (Mabtech 3420-2A) diluted in sterile Dulbecco's phosphate-buffered saline (DPBS; Fisher Scientific) for 3 hours at room temperature (RT). Plates were then washed 3x with DPBS and blocked with 100µL R10 for 1-2 hours at RT. 50µL of stimulation media were diluted to final concentrations in R10 and added to wells in duplicate or triplicate as follows: 2µg/mL DMSO (unstimulated control); 2µg/mL pools of overlapping peptides covering SARS-CoV-2 ancestral or variant proteins, 2µg/mL cytomegalovirus, Epstein–Barr virus and influenza peptides (CEF, Proimmune) or concanavalin A (ConA; Sigma-Aldrich) (positive controls). PBMC were washed in R10 and 200,000 cells per well added to the plate and incubated at 37°C for 16-18 hours overnight. The plate was washed 6x with phosphate buffered saline (PBS, Sigma-Aldrich) + 0.05% (v/v) Tween-20 (Sigma-Aldrich) and incubated with ELISpot Basic kit streptavidin-ALP, diluted in PBS at 1 µg/mL for 1.5 hours. Spots were detected by adding 50µL/well of filtered RT BCIP/NBT stock and incubating for 5-7 minutes and counted on CTL immunocapture (Cellular Technology Limited) using Smartcount® settings.

2.3 Data generation: Serological assays

2.3.1 SARS-CoV-2 spike binding assays: Elecsys® Anti-SARS-CoV-2 S

The Elecsys® Anti-SARS-CoV-2 total Ig (Roche) was used to assess total serum Ig binding

to the receptor binding domain (RBD) of SARS-CoV-2 spike and SARS-CoV-2 nucleocapsid proteins. These assays were performed by Dr Ashley Otter or Dr Marc Lütgehetmann and Golda Schaub. Assays were performed as per manufacturer instructions. The lower limit of detection (LoD) for the assay is 0.4AU/mL and upper LoD is 2500AU/mL. Samples were serially diluted to quantify concentrations above this, up to $2.5x10^5$ or $2.5x10^4$ (EASL COVID-Hep 2.0 study). The manufacturer defined negative cutoff for response is 0.8AU/mL.

2.3.2 SARS-CoV-2 variant IgG binding and angiotensin-converting enzyme 2 (ACE2) inhibition assays

IgG binding titres or functional antibody responses (ACE2 inhibition) were assessed to wild-type SARS-CoV-2 and nine of the most prevalent SARS-CoV-2 variants of concern as of February 2023: 1.529/BA.1/BA.1.15, BA.2.75, BA.2.75.2, BA.4.6, BA.5, BF.7, BQ.1, BQ.1.1, and XBB.1, using a multiplexed MSD® immunoassay (K15668U and K15679U). Assays were performed as per manufacturer instructions with 1:10,000 and 1:30,000 dilutions of serum/plasma for binding assays and 1:10 and 1:100 dilutions for ACE2 inhibition assays.

2.3.3 Live neutralisation of SARS-CoV-2 ancestral, delta and omicron BA.1

High-through live virus microneutralisation assays were performed at The Francis Crick Institute under the leadership of Dr Edward Carr and Professor Rupert Beale, following a previously published protocol *(230)*. The fold-dilution of serum required to inhibit 50% of viral replication was defined as the IC_{50}. Some samples fell below or above the limit of quantification (LoQ) of the assay and were assigned a representative IC_{50} value: no signal detected and below LoQ = 5, signal detected but below LoQ = 10, above LoQ = 4000.

2.4 Data generation: Flow cytometry

2.4.1 Activation induced marker assay for sorting of spike-specific B and T cells and CD45+ PBMC

Thawed PBMC were stimulated for 24 hours at 37°C with pools of overlapping peptides (15mers with 11 amino acid overlap) which covered the entire SARS-CoV-2 spike protein

(Cambridge Biosciences), at a final concentration of 1µg/mL. 1x vial of PBMCs per participant was thawed and split across stimulation wells at 1 x 10^6 PBMC per well. 1x10^6 cells per donor was incubated for 24 hours with 1µg/mL DMSO as an unstimulated control. 1x10^6 cells per experiment were incubated for 24 hours with 1:500 diluted leukocyte activation cocktail as a positive control for sorting (BioLegend). Plates were washed with FACS buffer (PBS + 0.05% bovine serum albumin + 1 mM EDTA, Sigma-Aldrich) and incubated with fluorophore or DNA-oligomer tagged monoclonal antibodies for flow cytometric staining/sorting and cellular-indexing of transcriptomes and epitopes (CITE) sequencing (**Table 2.1**). Staining was performed in a final volume of 50µL for 30mins at 4°C in the dark. Cells were then prepared for FACS as per **Section 2.4.3**.

2.4.2 CellTrace Violet (CTV) assay to detect pre-existing SARS-CoV-2 specific clones

5.25 × 10^6 cells per donor were collected and labelled with CTV (ThermoFisher), as described (*231*). Briefly, cells were thawed and washed 2x with sterile PBS. After washing, cells were resuspended in 1mL of PBS and incubated with 1:2000 CTV for 10 minutes at RT. After incubation, 4mL of ice-cold FCS was added to cells to quench staining. Cells were washed in 5mL of RH10 (RPMI-1640 + 10% human AB serum + 1% Penicillin/Streptomycin), incubated for 5mins at RT, then resuspended in fresh RH10 at 2.5 × 10^6 cells per mL. 100µL of cells were incubated with 100µL of RH10 and the following stimulation mixes: 2µg/mL DMSO (unstimulated control), 2µg/mL overlapping peptide pools (15mers with 11 amino acid overlap) covering the SARS-CoV-2 spike protein (Cambridge Biosciences), 2µg/mL PHA (positive control). Cells were incubated for 7 days at 37 °C, and 5% CO_2 for 7 days. On day 4, the plate was centrifuged (1800 rpm for 3 min) and 100µL of media was removed and replaced with fresh, pre-warmed RH10. After incubation, cells were washed 3x in FACS buffer and stained using a cocktail of FITC-CD19 (HIB19), FITC-CD14 (M5E2), AF700-CD8α (SK1), BV650-CD4 (OKT4), BV785-CD3 (OKT3) antibodies in a final volume of 50µL for 30mins at 4°C in the dark. Cells were then prepared for FACS as per **Section 2.4.3**.

2.4.3 Fluorescence-activated cell sorting (FACS)

After staining, cells were washed three times with FACS buffer, resuspended in 100µl of FACS buffer, and transferred to a 1.5mL RNase-free Microfuge tube. SYTOX Green was pre-diluted 1:60 in PBS + 0.04% BSA, then diluted 1:100 in each sample. Sorting was on a BD FACSAria III (BD Biosciences) using an 85-micron nozzle. Sorted cells were collected into sorting buffer (RPMI-1640 + 1% NEAA + 1% Na Pyruvate + 2.5% HEPES + 10% FBS, Sigma-Aldrich) and stored at 4°C until use for single-cell RNA sequencing. All FACS was performed at the translational gastroenterology and liver unit (TGLU) Flow Cytometry Facility by Dr. Helen Ferry.

2.4.4 Preparation of PBMC for immunophenotyping and intracellular cytokine staining using spectral flow cytometry

1x vial of PBMC was thawed per individual, $2x10^6$ cells were retained for the immunophenotyping panel and $1x10^6$ retained for each ICS stimulation condition. For immunophenotyping, PBMC were stained at RT in the dark with fluorophore-conjugated antibodies **(Table 2.2)**, washed 2x in FACS buffer and stored at 4°C prior to acquisition on the Cytek Aurora.

For ICS, 96-well flat-bottom plates were prepared by pre-coating one well per donor with 100µL of 1µg/mL anti-CD3 monoclonal antibody (CD3-2; MabTech) and incubating for 1-2 hours at 37°C. After incubation, wells were washed 3x with PBS and the following stimulation conditions were prepared in 50µL R10 and added to the plate: 1µg/mL DMSO (unstimulated control), 2µg/mL 18mer peptides with 11amino acid overlap covering entire ancestral SARS-CoV-2 spike, R10 only (added to anti-CD3 coated wells). 50uL of co-stimulation mix (**Table 2.3**) and 100µL of $1x10^7$ PBMC per well was added to all wells and incubated for 2 hours at 37°C. 50µL of 1:1000 Brefeldin A and 1:1000 Monensin (BioLegend) in R10 were added to each well, pipette mixed, and samples were incubated for a further 16-18 hours at 37°C. After incubation, the samples were washed 2x in FACS buffer and stained for surface markers

(**Table 2.3**) for 30 minutes at 4°C in the dark. Cells were then fixed and permeabilised for 30 minutes at 4°C using Cytofix/Cytoperm (BD Biosciences), washed 2x with Perm/Wash buffer (BD Biosciences) and stained for intracellular markers (**Table 2.3**) for 30 minutes at 4°C in the dark. After staining, samples were washed 2x in Perm/Wash buffer, resuspended in FACS buffer and stored at 4°C in the dark until acquisition on the Cytek Aurora. Jordan Rolt assisted with sample preparation and acquisition.

2.4.5 Preparation of reference controls for spectral flow cytometric acquisition on Cytek Aurora

All single stain or unstained media-only reference controls were generated following the sample preparation protocols in **Section 2.4.4**. Reference controls for live/dead staining were generated using heat-killed (65°C for 10 minutes followed by 5 minutes on ice) PBMC. CompBeads (BD Biosciences) or PBMC were used for single stain controls as per (**Table 2.2**).

Single stain reference controls were matched with each experiment for batch, fluorophore and specificity. For B cell baits, monoclonal antibodies with the same fluorophore conjugate (BV421 or PE) targeting a marker on the target cell type (B cells). Reference controls were stored and reused across multiple runs of the same flow cytometry panel, up until 3 months after their generation, or a new batch of staining antibody was used in the experiment, whichever occurred first.

2.5 Data generation: Olink proteomics

Plasma samples were analysed using the proximity-extension assay: Olink® Explore 384 Inflammation I library (*232*) (Olink Proteomics). This followed the standard protocol and was performed at the Wellcome Centre for Human Genetics, Oxford Genomics Centre (University of Oxford) Olink certified proteomics core facility. Samples were randomised across two plates alongside internal and external controls.

2.6 Data generation: whole blood RNA-sequencing

Whole blood from donors was collected in Tempus™ tubes (ThermoFisher). Samples were

thawed at RT in batches and RNA was extracted using Tempus™ Spin RNA Isolation Kit (ThermoFisher) as per manufacturer guidelines. All work surfaces were pre-treated with RNAse AWAY (Thermo Fisher) and DNAZap (ThermoFisher). Processed RNA was quantified and QC performed first using NanoDrop 2000 (ThermoFisher) and again prior to library preparation using 4200 TapeStation (Agilent) electrophoresis at Oxford Genomic Centre or Novogene. RNA extraction was performed by me, Georgina Meacham or Vishal Rao**.** RNA libraries were prepared and sequenced across two batches at Oxford Genomics Centre or Novogene and using ribosomal and haemoglobin gene depletion followed by poly-A enrichment library preparation protocols. Paired-end 150bp sequencing of prepared libraries was performed using NovaSeq6000 (Illumina, Oxford Genomics Centre) or NovaSeq X Plus (Illumina, Novogene) sequencers.

2.7 Data generation: Single-cell cellular indexing of transcriptomes and epitopes (CITE) and V(D)J sequencing sample and library preparation

FACS sorted samples were either directly used for 10x Genomics single-cell RNA sequencing or underwent additional surface staining with DNA-barcoded Total-Seq-C Human Universal Cocktail (BioLegend) as per manufacturer guidelines. Cells from each participant were labelled with Total-Seq hashing antibodies either after or during flow cytometric staining. Cells were prepared in emulsions and loaded onto a Chromium Next GEM Single Cell 5' Kit v2 chip or Chromium Next GEM Single Cell 5’ high throughput (HT) chips and processed using Chromium X (10x Genomics) as per manufacturer guidelines. For v2 chips, an average of 23,000 cells per channel were loaded. For HT chips, an average of 40,000 cells per channel were loaded.

Gene expression, cell surface protein (ADT) and V(D)J sequencing libraries were prepared as per manufacture guidelines. The following library construction kits from 10x Genomics were used: Library Construction Kit (1000190), Chromium 5’ Feature Barcode Kit (1000541), Chromium Single Cell TCR and BCR Amplification Kits (1000252, 1000253) and Dual Index

Kits TT and TN Set A (1000215, 1000250). The prepared libraries were sequenced using NovaSeq PE150 (Illumina, Novogene, UK) or NovaSeq6000 (Illumina, Wellcome Sanger Institute, Cambridge, UK) sequencers. In chapter 4, all libraries were prepared by Dr Nicholas Provine. In chapter 6, libraries were prepared by me, with assistance from Kyla Dooley and Amelia Heslington.

2.8 Data analysis: IFNγ ELISpot

The mean spots of the negative control wells were subtracted from the test wells and then multiplied by 5 to give antigen specific responses expressed as spot-forming units (SFU)/10^6 PBMCs.

2.9 Data analysis: Flow cytometry, data normalisation and analysis

Data from conventional flow cytometry were analysed in FlowJo 11 (FlowJo, LLC). Data from Aurora Cytek was unmixed using SpectroFlo 3.2.1 (Cytek) with auto-fluorescence subtraction. Manual gating of unmixed spectral flow cytometry data was performed using FlowJo 11.

2.10 Data analysis: Olink Proteomics

2.10.1 QC and pre-processing

Quality control (QC) and intensity normalisation was performed by the certified team at the Oxford Genomics Centre. 162 of 176 (92%) analysed samples passed QC for all markers, with only few analytes per sample not meeting QC criteria for 14 of 176 (8%). The inter and intra- assay %CV was 11% and 8% respectively, which was within accepted range. Protein expression value data was outputted as Normalized Protein eXpression (NPX) on the Log_2 scale. As the NPX value is normalised for each analyte based on the on-plate controls, NPX values for different analytes are not directly comparable.

2.10.2 Analysis and visualisation

Olink proteomics data was analysed in R (v4.3.1). Data normality was assessed by visual expression of data distributions or Shapiro-Wilk tests. PCA was performed on the NPX values. Generalised linear models were generated to explore the association of NPX values with

variables of interest. The caret (v6.0-94) package was used to separate data into test and training datasets and to generate glmnet, random forest and nnet models. Differential expression of proteins was assessed using EdgeR or ANCOVA tests.

2.11 Data analysis: whole blood RNA-sequencing

2.11.1 QC and pre-processing

RNA-sequencing reads were quality controlled and trimmed using the fastp package (v0.23.4)(*233*) with default settings. Reads were then quantified using Salmon (v1.8.0)(*234*) mapped to a GRCh38.86 reference genome with the –-seqBias option enabled. Samples from different experimental batches were integrated using the ComBat_seq function from the sva package (v3.5.0). This uses a negative binomial model to regress out unwanted variation while maintaining the integer nature of the count data (*235*). Adjusted counts were then normalised using median of ratios method (DESeq2, v1.40.2) or $\log_2$ counts per million (CPM) with a prior of 1 for downstream analysis.

2.11.2 Differential gene expression, geneset expression quantification and geneset enrichment analysis

Differential gene expression was performed on ComBat_Seq adjusted counts using the negative binomial model method included in the DESeq2 package (*236*). Genes were filtered to have a minimum of 10 counts in total across the cohort.

Geneset variation analysis (GSVA, v1.48.3) was used to quantify expression of genesets on a per sample basis (*237*). Genesets used for this method include blood transcriptomic modules (*238*) or genesets from Human MSigDB Hallmark or the Gene Ontology Biological Process databases.

Geneset enrichment analysis was performed on lists of genes resultant from differential gene expression analysis. Genes were pre-ranked by the false discovery rate (FDR) multiplied by the sign of the average $\log_2$ fold change (FC), or by the average $\log_2$ FC and enrichment was assessed using fgsea (v1.26.0) (*239*) or clusterProfiler (v4.8.1) packages (*240*).

2.11.3 Data Visualisation

Data were visualised using PCA and in heatmaps generated using the ComplexHeatmaps package (*241*).

2.12 Data analysis: Single-cell RNA-sequencing

2.12.1 Read mapping, quality control, hashtag demultiplexing and clustering

FASTQ files were generated from BCL files using Illumina bcl2fastq. FASTQ files for all modalities were mapped to the GRCh38-2020-A reference genome and a custom ADT marker list using the Cell Ranger 7.0.0 multi pipeline for count, ADT and VDJ data. The filtered_contig_annotations.csv file was filtered to retain only high-confidence, full-length, productive contigs corresponding to TCRα or TCRβ chains.

Data analysis was primarily performed using the Seurat package (v4.3.0) (*242*) in R (v4.3.0). Quality control was performed as follows: low quality cells were removed (based on low UMI and gene count and high percent mitochondrial reads), doublets were flagged and removed using scDblFinder (*243*). Immunoglobulin and TCR gene segments were removed from the gene expression object, except for the following genes: *IGHM, IGHG1, IGHG2, IGHG3, IGHG4, IGHD, IGHE, IGHA1, TRAV1-2, TRAV24, TRDV1, TRDV2, TRDV3*. Hashtags for each unique individual within a single experiment were demultiplexed using MULTIseqDemux (*244*) and then data from each experiment were merged into a single Seurat object. Gene counts were log-normalised (NormalizeData function), variable features were found (n=3000, FindVariableFeatures function) and features were scaled using default Seurat parameters (ScaleData function). The top variable features were used for nearest-neighbour and Louvain clustering (resolution 0.7) and to generate principal components, the top 30 of which were used to generate uniform manifold approximation and projections (UMAP).

2.12.2 Differential abundance analysis

Differential abundance analysis was performed using the edgeR package (v3.42.2) (*245*), with the function glmQLFtest with flags robust=TRUE and abundance.trend=FALSE and

dispersions estimated using estimateDisp with the flag trend="none".

2.12.3 Differential gene expression and geneset enrichment, overrepresentation and variation analysis

For comparisons between individuals in different groups, differentially expressed genes were defined using Limma or Model-based Analysis of Single-cell Transcriptomics (MAST) with Bonferroni corrected p values for genes with an average FC of >0.05 and minimum percent expression within each compared cluster of 25% (FindMarkers function). For within-individual comparisons (e.g. those across timepoints), differential expression of genes was assessed using the Seurat FindMarkers function with the test.use="LR" flag, with individual as a latent variable.

Genesets used for GSEA and overrepresentation analyses were obtained from Human MSigDB Hallmark or the Gene Ontology Biological Process database and filtered to include genesets related to cytokines, T helper and cytotoxic subsets, and antigen presentation pathways. A $CD8^+$ T cell cytotoxicity associated geneset was obtained from (*246*). Stimulated MAIT cell genesets were obtained from (*247*) by taking the top 100 differentially expressed genes from sorted MAIT cells that were most differentiated from unstimulated cells after stimulation with a TCR (MR1/5-OP-RU), cytokine (IL-12 + IL-18), or TCR and cytokine stimulus. GSEA and overrepresentation analysis were performed using the fgsea (v1.26.0) (*239*) or clusterProfiler (v4.8.1) packages (*240*)**.** Genesets were quantified on a per cell basis using the Seurat AddModuleScore function with default parameters, or with GSVA on aggregated, pseudo-bulked counts of the relevant cell type.

2.12.4 TCR analysis

Paired αβ TCR chains were compiled for each cell using the scRepertoire package (v2.0.4), which loads filtered_contig_annotation files (output from 10x CellRanger multi) and combines them with the Seurat object for downstream analysis. Briefly, createHTOContigList was used with groups based on the called hashtag IDs and combineTCR with default settings. Clones

were called based on paired CDR3 amino acid chain calling within each individual at each timepoint. Visualisation of overlapping TCR clones was performed using the circlize package (v0.4.15) (*248*). Visualisation of selected TCR amino acid sequences motifs was performed using the ggseqlogo package (v0.1). For analysis over time, clones were called as those with identical paired αβ TCR chains, and 'recalled clones' were defined as those present at more than one timepoint.

2.13 Tables

Table 2.1 Activation induced marker panel

Fluorophore	Marker	Clone	Dilution (1 in x)
PE	S1-tet	--	50
PE-Dazzle594	CD69	FN50	100
PE-Cy7	CD45	HI30	100
APC	4-1BB (CD137)	4B4-1	100
APC	OX-40 (CD134)	Ber-ACT35	100
AF700	CD8a	SK1	100
APC-Cy7	CD19	HIB19	100
BV421	S1-tet	--	50
BV650	CD4	OKT4	100
BV785	CD3	OKT3	100

Table 2.2 Cytek Aurora Immunophenotyping panel

Fluorphore	Marker	Vendor	Use per 200ul/Sample	Incubation time (mins)	Reference Type
LD/ Fixable - UV	Live/Dead	Thermofisher Sci.	4µL of 1/40 dilution	15*	Dead Cells
BV421	CCR7	Biolegend	5ul	50	Beads
BUV563	CCR5	BD Biosciences	2.5ul	40	Beads
BV750	CXCR5 (CD185)	BD Biosciences	1.2ul	40	Cells
BV711	CCR6 (CD196)	Biolegend	1.2ul	40	Beads
PE-Cy7	CXCR3 (CD183)	Thermofisher Sci.	2.5ul	40	Beads
PerCP-eFlour710	TCRgd (B1.1)	Thermofisher Sci.	1.2ul	35	Beads
APC-R700	CD127	BD Biosciences	6ul	25**	Beads
FITC	CD57	Biolegend	1.2ul	25**	Beads
Spark Blue 550	CD14	Biolegend	2.5ul	25**	Beads
PerCP-Cy5.5	CD11b	Biolegend	5ul	25**	Beads
AF647	CD1c	Biolegend	5ul	25**	Beads
Spark NIR685	CD19	Biolegend	1.2ul	25**	Beads
APC-Fire810	CD38	Biolegend	1ul	25**	Beads
SuperBright436	CD123	Thermofisher Sci.	2.5ul	25**	Beads
eFlour450	CD161	Thermofisher Sci.	5ul	25**	Beads
Pacific Orange	CD20	Thermofisher Sci.	5ul	25**	Cells
PerCP	CD45	Thermofisher Sci.	2.5ul	25**	Cells
PE	CD25	Thermofisher Sci.	2.5ul	25**	Beads
PE-eFluor 610	CD24	Thermofisher Sci.	5ul	25**	Beads
PECy5	CD95	Thermofisher	1.2ul	25**	Beads

		Sci.			
APC	CD27	Thermofisher Sci.	2.5ul	25**	Beads
APC-eFluor780	HLA-DR	Thermofisher Sci.	2.5ul	25**	Cells
BUV395	CD45RA	BD Biosciences	1.2ul	25**	Beads
BUV496	CD16	BD Biosciences	0.6ul	25**	Beads
BUV615	CD4	BD Biosciences	1ul	25**	Beads
BUV661	CD11c	BD Biosciences	2.5ul	25**	Beads
BUV737	CD56	BD Biosciences	1.2ul	25**	Beads
BUV805	CD8	BD Biosciences	1.2ul	25**	Cells
BV480	IgD	BD Biosciences	0.6ul	25**	Cells
BV605	IgG	BD Biosciences	5ul	25**	Beads
BB515	CD141	BD Biosciences	2.5ul	25**	Beads
BV510	CD3	Biolegend	5ul	25**	Cells
BV570	IgM	Biolegend	2.5ul	25**	Beads
BV650	CD28	Biolegend	2.5ul	25**	Beads
BV785	PD-1	Biolegend	5ul	25**	Beads

** After incubation cells were spun, resuspended in 90µL Aurora wash buffer, 10µL Brilliant Violet Stain Buffer Plus (BD Biosciences) and 5µL True-Stain Monocyte blocker (Biolegend), then other dyes were added.*

*** Added as mastermix*

Table 2.3 Aurora intracellular cytokine staining panel

Co-stimulatory mix			
Fluorophore	Marker	Clone	Dilution (1 in X)
--	anti-CD28		1000
--	anti-CD49d		1000
BV786	CD107a	H4A3	100
Surface			
Fluorophore	Marker	Clone	Dilution (1 in X)
Blue	Live/dead	--	250
BUV661	CD3	OKT3	200
BUV737	CD25	2A3	800
BUV805	CD4	SK3	100
BV421	S1 tetramer	--	100
AF405	CD8	3B5	100
VioBlue	KLRG1	REA261	100
BV480	CD38	HIT2	100
Superbright 702	CD45RA	HI100	100
PE	S1 tetramer	--	100
AF532	CD20	2H7	50
PerCP eF710	CD27	O323	100
PE-Cy7	CD57	HNK-1	200
Spark NiR 685	CD19	CD19.11	200
AF700	IgD	IA6-2	100
Intracellular			
Fluorophore	Marker	Clone	Dilution (1 in X)
BUV395	TNF	MAb11	100
BUV563	CD71	M-A712	100
BV605	IL2	MQ1-17H12	100
BV650	IFNγ	4S.B3	50
BV711	IL-17A	BL168	50
BV750	CD69	FN50	100
FITC	IL-4	MP4-25D2	100
APC	IL-10	JES3-9D7	100
APC eF780	Ki67	SolA15	100
PE-dazzle 594	PD1	EH12.2H7	100
PerCP-Cy5.5	CCR7	G043H7	50

3 Results: Immunogenicity and efficacy of ChAdOx1 and mRNA COVID-19 vaccines in immunocompromised and healthy individuals

3.1 Introduction

SARS-CoV-2 vaccines were highly effective in the management of the Coronavirus Disease 2019 (COVID-19) pandemic and induced protection against severe disease in healthy people after two doses (*249, 250*). Epidemiological evidence demonstrated that COVID-19 vaccines prevent wild-type SARS-CoV-2 infection and protect against severe disease from other SARS-CoV-2 variants, including Omicron BA.1 (*251*). However, epidemiological and disease cohort studies showed that individuals with various comorbidities, chronic diseases or immune-compromising conditions were at increased risk of severe COVID-19 before (*5, 252*) and after (*6, 253, 254*) COVID-19 prime-boost vaccination. Therefore, understanding the immunogenicity of COVID-19 vaccines in immunocompromised cohorts, and determining which groups were at highest risk of vaccine non-responsiveness is important.

Many studies demonstrated suboptimal COVID-19 vaccine immune responses in cohorts of patients with SIs (**Section 1.13)**. In general, these studies focused on specific disease cohorts, and few robustly evaluated cellular immune responses. As SARS-CoV-2 variants of concern (VoC) emerged and displayed considerable immune evasion in healthy individuals (*88, 255*), understanding the cross-reactivity of vaccine-induced immune responses to SARS-CoV-2 VoC in immunocompromised individuals was essential to understand their ongoing vulnerability to COVID-19. With the emergence of the delta VoC in Autumn 2021, 'booster' vaccine doses were deployed, which increased titres of neutralising antibodies to delta and subsequently to omicron BA.1 in healthy individuals (*88, 256*). However, at this time the effectiveness of the booster vaccine dose in immunocompromised people was largely unknown.

In addition, the cross-reactivity of vaccine-induced T cell responses to SARS-CoV-2 variants was initially unclear but appeared to be more conserved compared to antibodies in healthy individuals (*257*). If vaccine-induced T cells in immunocompromised individuals had equivalent

cross-reactivity to SARS-CoV-2 VoCs as vaccine-induced T cells in healthy individuals was largely unknown. Furthermore, it was not known if the quality or magnitudes of vaccine-induced antibodies and T cells generated by individuals with SIs were sufficient to protect against severe COVID-19.

3.2 Summary of chapter rationale

The primary vaccination schedule of mRNA and ChAdOx1 COVID-19 vaccines was demonstrated to be highly efficacious against the ancestral strain of COVID-19 in healthy individuals. This efficacy was related to the high antibody and T cell immunogenicity of the COVID-19 vaccines. Individuals with certain secondary immunodeficiencies were more vulnerable to severe COVID-19, even after vaccination. The cross-reactivity of antibodies and T cells induced by ancestral COVID-19 vaccines to SARS-CoV-2 variants of concern was unknown in immunocompromised individuals. Understanding the immunogenicity of COVID-19 vaccines to ancestral and variant SARS-CoV-2 strains was essential for determining groups at risk of severe COVID-19 and those that should be prioritised for alternative therapy. Additionally, assessing how the vaccine-induced T cell and antibody response related to subsequent protection against severe COVID-19 was key to identifying measures associated with vaccine-mediated protection in immunocompromised groups.

3.3 Hypotheses and aims

The central hypotheses of this chapter are as follows:

1) Secondary immunodeficiencies impair the antibody and T cell immunogenicity of COVID-19 vaccines compared to healthy individuals.
2) ChAdOx1 nCoV-19 and COVID-19 mRNA vaccines induce different magnitudes of anti-SARS-CoV-2 spike antibodies and T cells.
3) Increasing the number of vaccine doses will increase vaccine immunogenicity in individuals with secondary immunodeficiencies.
4) Antibody and T cell responses induced to ancestral COVID-19 vaccines in individuals

with secondary immunodeficiencies are less effective against SARS-CoV-2 variants.

5) Vaccine induced antibody and T cell responses are related to protection against severe COVID-19 in immunocompromised individuals.

To address these hypotheses, in this chapter I aim to:

1) Assess antigen-specific antibody and IFNγ T cell responses to COVID-19 vaccines in individuals with secondary immunodeficiencies and healthy control individuals.
2) Assess the effect of factors relating to vaccine regimen on SARS-CoV-2 antibody and T cell responses:
    a. Vaccine types
    b. Number of vaccine doses
3) Assess the effect of host or viral factors on SARS-CoV-2 antibody and T cell responses including:
    a. Immunosuppressive diseases/therapeutic agents compared to healthy controls or other immunosuppressive conditions.
    b. Age, Comorbidities
4) Compare the effect of factors relating to the virus on vaccine induced antibody and T cell responses:
    a. SARS-CoV-2 variant spike mutations – specifically Omicron variants.
5) Assess the relationship of vaccine-induced antibodies and T cells with subsequent COVID-19 severity.

3.4 Chapter overview

To address these aims, I contributed to several large observational cohort studies to investigate vaccine-induced antibody and T cell responses across several secondary immunodeficiencies. The results of two of these studies are included in this chapter.

Firstly, I performed T cell experiments and analysis of antibody data to understand antibody and T cell responses within a sub cohort of the UK-wide OCTAVE study. I additionally curated

and analysed data from the entire cohort to assess the immunological factors associated with protection against severe COVID-19. I took a leading role on the interpretation of data in the OCTAVE trial and co-wrote the associated manuscript (**Appendix 2)**:

- Barnes, E.*, Goodyear, C.S.*, Willicombe, M. *, Gaskell, C.*, Siebert, S.*, de Silva, T., **Murray, S.M.,** *et al.* SARS-CoV-2-specific immune responses and clinical outcomes after COVID-19 vaccination in patients with immune-suppressive disease. *Nat Med* **29**, 1760–1774 (2023).

Secondly, I performed T cell experiments, data curation and analysis of antibody and T cell data from the EASL COVID-Hep 2.0 multi-centre observational cohort study. This study investigated the immunogenicity of up to three doses of ChAdOx1 or mRNA COVID-19 vaccines in a pan-liver disease cohort. I led the synthesis and writing of the associated manuscript (**Appendix 3)**:

- **Murray, S.M**, Pose, E., Wittner, M., *et al.* Immune responses and clinical outcomes after COVID-19 vaccination in patients with liver disease and in liver transplant recipients. *Journal of Hepatology,* **80**(1): 109-123 (2023).

3.5 Chapter specific methods

3.5.1 Ethical and regulatory approvals

The OCTAVE study was coordinated by the Cancer Research UK Clinical Trials Unit (CRCTU) at the University of Birmingham, which was the sponsor. It was approved by the London and Chelsea Research Ethics Committee (REC ref.: 21/HRA/0489) and funded by UKRI. All centres involved in the EASL (European association for the study of the liver) COVID-Hep 2.0 vaccine registry recruited participants through local ethics approvals and was funded by EASL. All studies were conducted in compliance with relevant ethical regulations for work with human participants according to the principles of the Declaration of Helsinki (2008) and written informed consent was obtained for all included participants (*258, 259*).

3.5.2 Clinical phenotyping and definitions

Clinical data for all participants were uploaded electronically from participating sites using REDCap (Research Electronic Data Capture) databases hosted by the University of Oxford or University of Birmingham. Clinical data comprised information on demographics, vaccination type, comorbidities, and disease-specific phenotyping including Child-Pugh (CP) class and aetiology of cirrhosis, and type and dose of immunosuppression for patients with AIH and LT recipients. Model for end-stage liver disease (MELD) score included serum sodium, creatinine, bilirubin and international normalised ratio (*260, 261*).

3.5.3 Capture of breakthrough SARS-CoV-2 infection and severity data

Information regarding breakthrough SARS-CoV-2 infection after vaccination was collected by screening electronic hospital records and/or contacting individual patients. Positive cases were defined as those confirmed via self-reported PCR assay or lateral flow antigen test. Captured data included the date of infection and COVID-19 severity. In the EASL COVID-Hep 2.0 study, data was collected up until December 2022. In the OCTAVE study, data was collected at two follow-up timepoints, 6months post-V2 and 12months post-V1. Severe COVID-19 was defined according to the World Health Organisation classification or based on hospitalisation status (*262*).

3.5.4 Rates of breakthrough infection over time with emergence of SARS-CoV-2 variants of concern

In the OCTAVE study, infection with a given SARS-CoV-2 variant of concern was assessed by chronological binning into time ‘epochs’, where infections reported within a given timeframe were assumed to be associated with the SARS-CoV-2 variant most prevalent (>80% of circulating strain) in the UK at that time. Defined as: alpha, 14 January 2021 (study start) to 24 May 2021; delta, 24 May 2021 to 20 December 2021 and finally omicron BA.1 from 20 December 2021 onwards.

In the EASL COVID-Hep 2.0 study, country-specific proportions of SARS-CoV-2 variants were calculated based on data shared via GISAID (*263*) EpiCoV database, downloaded 23 March 2023. The date on which Omicron became the dominant variant (defined as representing >90% of circulating variants) was 1st January 2022 in the UK, 16th January 2022 in Italy and Spain, and 23rd January 2022 in Germany.

3.6 Results

3.6.1 OCTAVE: cohort and study design

The OCTAVE study was a multi-centre observational cohort study to investigate the immunogenicity and breakthrough SARS-CoV-2 infections after one or two doses of BNT162b2 or ChAdOX1 nCoV-19 in individuals with a range of SIs. In total, 2,686 individuals were recruited from 13 different SIs **(Fig. 3.1A).** 674 patients were enrolled into the 'deep immunophenotyping' cohort, whereby serum and PBMC samples were taken immediately before first (pre-V1) and second vaccine doses (pre-V2) and 28 days following second vaccine dose (V2+28d); and 2,012 individuals were enrolled into the 'serology' cohort where only serum samples were collected at V2+28d **(Fig. 3.1B)**. All enrolled individuals were also contacted up to 12months post-V1 to collect data on breakthrough SARS-CoV-2 infections received after vaccination (n=1,617) **(Fig. 3.1B)**. In addition, 236 matched healthy control individuals (UK Health Security Agency (UKHSA) CONSENSUS and PITCH cohorts) were available for comparative analysis for immunogenicity data **(Fig. 3.1B)**.

Demographic data was available in 2,645 patients and 236 healthy controls, outlined in **Table 3.1**. Overall, 1,430 of 2,881 (50%) participants were male, but distribution varied by disease cohort. Most participants, 2,629 of 2,881 (91%), were younger than 75 years of age; 2,038 of 2,881 (70%) reported White ethnicity; 479 of 2,881 (17%) reported Asian ethnicity; and 150 of 2,881 (5%) reported Black ethnicity. Pre-vaccination SARS-CoV-2 infection (SARS-CoV-2 polymerase chain reaction (PCR) positive or anti-nucleocapsid or anti-spike antibody detected

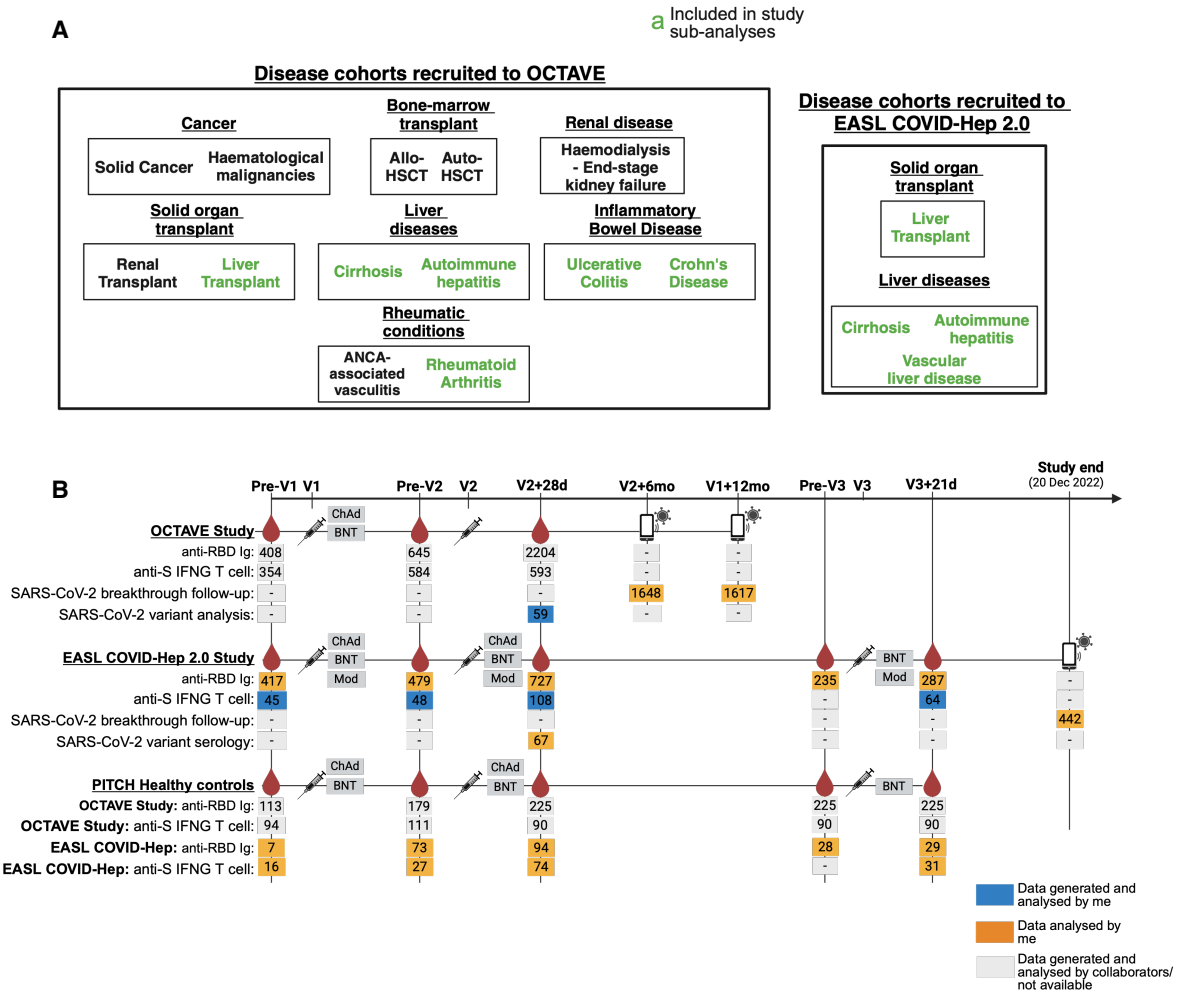

Fig. 3.1 Overview of studies included in Chapter 3
A) Overview of patient cohorts included in the observational cohort studies included in Chapter 4.

B) Study overview for each observation cohort study included in Chapter 4. The number indicated is the number of individuals included for the given analysis/study. The vaccine given at each dose is indicated for each study/timepoint. The symbol indicates the sample taken at each timepoint, either a peripheral blood draw (red droplet) or follow-up contact to gather information on SARS-CoV-2 infection. Colours at each timepoint represents my contribution to the data presented in this analysis. Where data that was generated and analysed by collaborators, only relevant data is presented to illustrate the immunogenicity cohort overviews. BNT = BNT162b2, ChAd = ChAdOx1 nCoV-19, Mod = mRNA-1273

at pre-V1) was reported in 398 of 2,881 (14%) individuals, with higher rates in some disease cohorts (for example, haemodialysis in 104/211 (49%)). Of 2,881 participants (44%), 1,249 had overweight or obesity, and 567 (20%) had type 1 or type 2 diabetes. Of 2,881 participants, 1,876 (65%) received ChAdOx1 nCoV-19, and 975 (34%) received BNT162b2. Three participants received mRNA-1273 and vaccine type was not reported for 27 individuals. Individuals in the OCTAVE cohort received a large and variable range of different immunosuppressive therapeutics.

3.6.2 Total binding Ig to SARS-CoV-2 receptor binding domain varies by immunosuppressive group and is reduced compared to healthy controls

Peak anti-SARS-CoV-2 receptor binding domain (RBD) serum Ig titres were assessed in 2,204 patients and 225 matched healthy controls at the V2+28d timepoint. Compared to the healthy control group, V2+28d anti-RBD Ig titres were decreased in the ANCA-associated vasculitis, inflammatory arthritis, kidney transplant, liver transplant, Crohn's disease and allo-HSCT cohorts (**Fig. 3.2A**).

V2+28d anti-RBD Ig titres were stratified into 'no response' (<0.8AU/mL, manufacturer defined) and 'low response' (<380AU/mL, the upper value of the lowest decile of anti-RBD Ig responses in the healthy control cohort) to assess the rates of individuals who were seronegative or had responses below the range expected in healthy individuals, respectively **(Fig. 3.2B)**. There were significantly higher rates of seropositivity in the healthy control group (222 of 225; 99%) compared with the overall OCTAVE cohort (1,949 of 2,204; 88%; Fisher's exact test, $P<0.001$). Rates of seropositivity were significantly decreased in several disease groups within the OCTAVE cohort, including: ANCA-associated vasculitis (8 of 29, 28%), haemodialysis on immunosuppression (24 of 30, 80%), kidney transplant (317 of 458, 69%), liver transplant (61 of 81, 75%), auto-HSCT (28 of 33, 85%), allo-HSCT (83 of 96, 86%) and CAR-T (4 of 8, 50%) disease groups (Fisher's exact test, Bonferroni-adjusted P value < 0.05) **(Fig. 3.2B)**. All other groups had a similar rate of seropositivity to healthy controls and cirrhosis, Crohn's disease and ulcerative colitis had 100% seropositivity rates.

In addition to decreased rates of seropositivity, there was a greater number of individuals with low (or no) serological response at V2+28d in the OCTAVE cohort (844 of 2,204; 39%) compared with healthy controls (37 of 225; 16%; Fisher's exact test, p < 0.001) **(Fig. 3.2B)**. Rates of low or no serological responsiveness were significantly increased in ANCA-associated vasculitis (26 of 29; 90%), inflammatory arthritis (233 of 690; 34%), haemodialysis on immunosuppression (13 of 30; 43%), kidney transplant (279 of 458; 61%), liver transplant

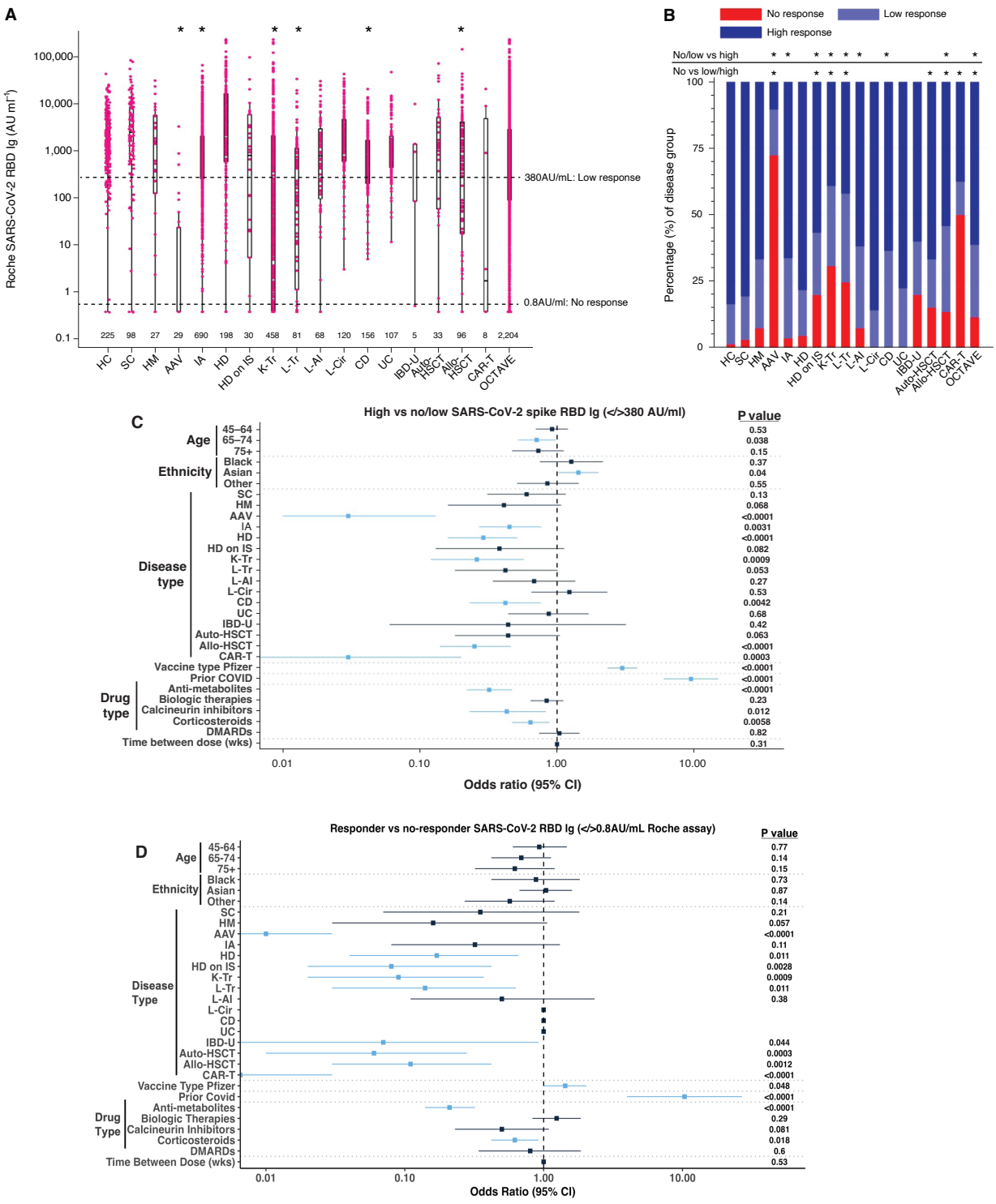

Fig. 3.2 Total binding Ig responses to SARS-CoV-2 receptor binding domain after two doses of COVID-19 vaccines in immunocompromised and matched healthy individuals

A) Magnitude of serological response in disease groups and healthy controls at V2+28d timepoint (n=2,204). Mann-Whitney U tests comparing disease group to healthy controls are presented.

B) Proportion of non (<0.8 AU ml^{-1}), low (<380 AU ml^{-1}) and high (>380 AU ml^{-1}) anti-SARS-CoV-2 spike RBD total Ig responses (n=2,204). Fisher's exact test comparisons in disease groups compared to healthy controls are presented.

C&D) Forest plot of multivariable logistic regression model fitted on V2+28d anti-SARS-CoV-2 RBD-binding total Ig antibody in 2,204 patients in the OCTAVE cohort and 225 matched healthy controls. Odds ratio of high response status compared with no or low response status (C) or seropositive compared with seronegative (D) is depicted, with whiskers as 95% confidence interval.

SC = Solid cancer, HM = Haematological malignancy, AAV = ANCA-associated vasculitis, IA = Inflammatory arthritis, HD = Haemodialysis, HD on IS = haemodialysis on immunosuppression, K-Tr = Kidney transplant, L-Tr = Liver transplant, L-AI = Autoimmune hepatitis, L-Cir = cirrhosis, CD = Crohn's disease, UC = Ulcerative colitis, IBD-U = Inflammatory bowel disease unclassified. HSCT = haematopoietic stem cell transplant

Primary analysis performed by OCTAVE statistics team

(47 of 81; 58%), autoimmune liver disease (26 of 68; 38%), Crohn's disease (57 of 156; 37%) and allo-HSCT (44 of 96; 46%) groups compared to the healthy control group (Fisher's exact test, Bonferroni-adjusted P value < 0.05) **(Fig. 3.2B)**.

Multivariate analysis, including clinical and vaccine regimen data was used to investigate factors associated with V2+28d serological responsiveness. Patients aged 65–74 years had significantly lower odds of having a robust serological response compared to patients in the 15–44-year age group (**Fig. 3.2C**). Patients of Asian versus White ethnicity had significantly higher odds of having a robust serological response (**Fig. 3.2C**). Disease groups more likely to have low or no serological response (compared to the healthy control group) included ANCA-associated vasculitis, inflammatory arthritis, haemodialysis, kidney transplant, Crohn's disease, allo-HSCT and CAR-T (**Fig. 3.2C**). Patients receiving anti-metabolites, calcineurin inhibitors and corticosteroids were each more likely to have a low or absent serological response compared to healthy controls (**Fig. 3.2C**). Prior SARS-CoV-2 infection and vaccination with BNT162b2 vaccine also significantly increased the odds of having a high serological response (**Fig. 3.2C**).

These findings were generally recapitulated when analysing the OR of likelihood of anti-RBD Ig seropositivity (**Fig. 3.2D**), but liver transplant and haemodialysis on immunosuppression disease groups were additionally associated with a decreased rate of seropositivity compared to the healthy control group.

3.6.3 IFNγ T cell responses to COVID-19 vaccines are impaired in select immunocompromised groups

T cell responses to peptide pools covering SARS-CoV-2 spike and nucleocapsid were evaluated at pre-V1, pre-V2 and V2+28d timepoints using the Oxford Immunotec T-SPOT Discovery IFNγ ELISpot assay in 656 patients and 210 matched healthy controls. Compared with healthy controls, the magnitude of IFNγ T cell responses at V2+28d were significantly reduced only in liver transplant and allo-HSCT disease groups **(Fig. 3.3A)**. Rates of IFNγ T

Fig. 3.3 IFNγ T cell responses to SARS-CoV-2 spike after COVID-19 vaccination in immunocompromised and matched healthy individuals

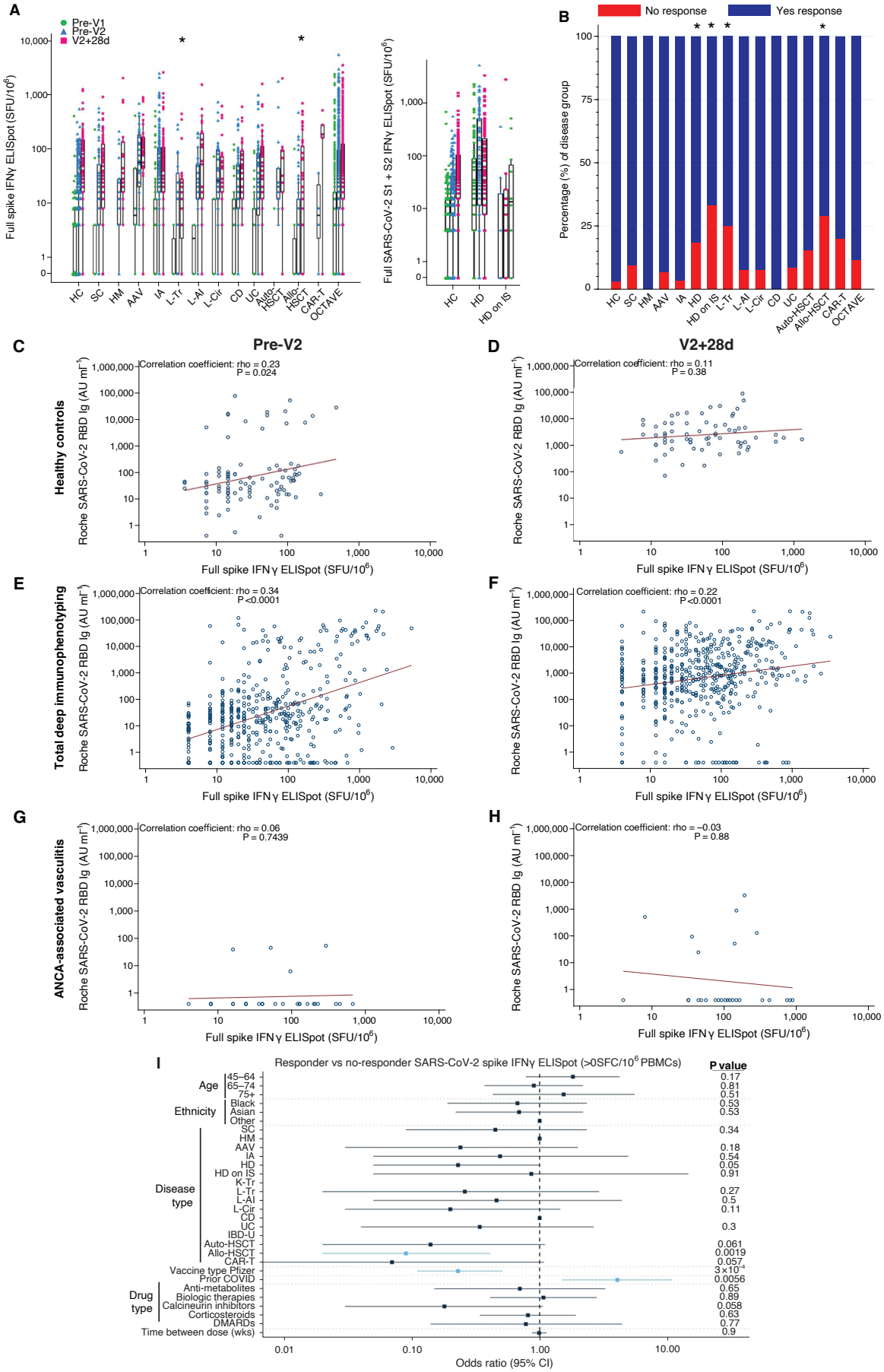

Fig. 3.3 IFNγ T cell responses to SARS-CoV-2 spike after COVID-19 vaccination in immunocompromised and matched healthy individuals

A&B) IFNγ T cell response to SARS-CoV-2 spike measured by Oxford Immunotec presented as the magnitude at pre-V1, pre-V2 and V2+28d timepoints (A) and as the proportion of individuals with or without an anti-SARS-CoV-2 spike T cell response at V2+28d (B) in 645 individuals in OCTAVE and 189 healthy controls. Mann-Whitney U-test of disease group compared to healthy controls (HC) at V2+28d.

C-H) Selected examples of the correlation of anti-SARS-CoV-2 receptor binding domain (RBD) binding total Ig with IFNγ T cell response to ancestral SARS-CoV-2 spike at pre-V2 (C,E,G) and V2+28d (D,F,H) timepoints in healthy individuals (C&D), all 645 individuals in OCTAVE with paired T and antibody data (deep immunophenotyping cohort) (E,F) and ANCA-associated vasculitis patients (G&H). Spearman's rank-sum ρ with Bonferroni adjusted p value presented.

I) Forest plot of multivariable logistic regression model fitted on V2+28d IFNγ T cell responses in 645 individuals in the OCTAVE cohort and 189 matched healthy controls. Odds ratio (OR) of anti-SARS-CoV-2 spike IFNγ T cell response >0 SFU per 10^6 PBMCs and 95% CI depicted. $P<0.05$ is marked with blue lines.

SC = Solid cancer, HM = Haematological malignancy, AAV = ANCA-associated vasculitis, IA = Inflammatory arthritis, HD = Haemodialysis, HD on IS = haemodialysis on immunosuppression, K-Tr = Kidney transplant, L-Tr = Liver transplant, L-AI = Autoimmune hepatitis, L-Cir = cirrhosis, CD = Crohn's disease, UC = Ulcerative colitis, IBD-U = Inflammatory bowel disease unclassified. HSCT = haematopoietic stem cell transplant, SFU = spot forming units

Primary analysis performed by OCTAVE statistics team

cell responsiveness (any responsiveness, i.e. > 0 SFC/10^6) were significantly (Bonferroni adjusted $p < 0.05$) reduced in haemodialysis (23 of 124, 19%), haemodialysis on immunosuppression (4 of 12; 33%), liver transplant (6 of 24; 25%) and allo-HSCT (11 of 38; 29%) groups compared with healthy control individuals (2 of 66; 3%), but not across the entire cohort (67 of 580; 12%; Bonferroni adjusted p = 0.51) **(Fig. 3.3B)**. 100% of individuals in haematological malignancy and Crohn's disease groups had IFNγ T cell responses at V2+28d.

We next assessed the association of vaccine-induced T cell and antibody responses in the cohorts. In healthy controls, there was weak significant positive correlation between the magnitudes of anti-RBD Ig and IFNγ T cell responses at the pre-V2 timepoint, but not at the V2+28 timepoint (**Fig. 3.3C&D)**. In the entire OCTAVE cohort we observed significant positive correlation at both timepoints, but the strength of the correlation was reduced at V2+28 (**Fig. 3.3E&F)**. Notably, there were some clinical subgroups within the OCTAVE cohort that did not follow the overall trend, including the ANCA-associated vasculitis group where T cells but not antibodies were induced by the vaccine **(Fig. 3.3G&H)**. This is consistent with the use of B cell depleting monotherapies in this disease group.

In multivariate analysis, the only disease group significantly enriched for T cell non-responsiveness compared with healthy controls was allo-HSCT, however haemodialysis, auto-HSCT and CAR-T groups all demonstrated near significant odds of T cell non-responsiveness (**Fig. 3.3l)**. In contrast to the serological results, vaccination with BNT162b2 was associated with significantly decreased odds of generating a cellular response (**Fig. 3.3l)**. Previous SARS-CoV-2 infection significantly increased the odds of generating a cellular response (**Fig. 3.3l)**.

3.6.4 COVID-19 vaccine-induced T cells, but not antibodies, are responsive to SARS-CoV-2 variants of concern in immunocompromised groups.

On the basis of the reduced antibody and T cell immunogenicity we observed in response to the vaccine immunogen (**Figs. 3.2&3.3),** we hypothesised that the cross-reactivity of vaccine-induced antibodies and T cells to SARS-CoV-2 variants of concern may also be reduced in immunodeficient populations. To address this hypothesis, we selected a group of 59 individuals from liver transplant, autoimmune liver disease, cirrhosis and inflammatory arthritis cohorts. ChAdOx1 nCoV-19 vaccinees with detectable ancestral (wild-type, WT) RBD binding Ig that spanned the full range of V2+28d anti-RBD Ig titres (range 257–29,332 AU/mL by Roche assay) were selected.

I first assessed the cross-reactivity of vaccine-induced Ig by analysing SARS-CoV-2 VoC antibody binding and surrogate neutralisation data produced by Dr. Tom Tipton. Compared to ancestral, spike binding IgG titres were significantly decreased against all variants except

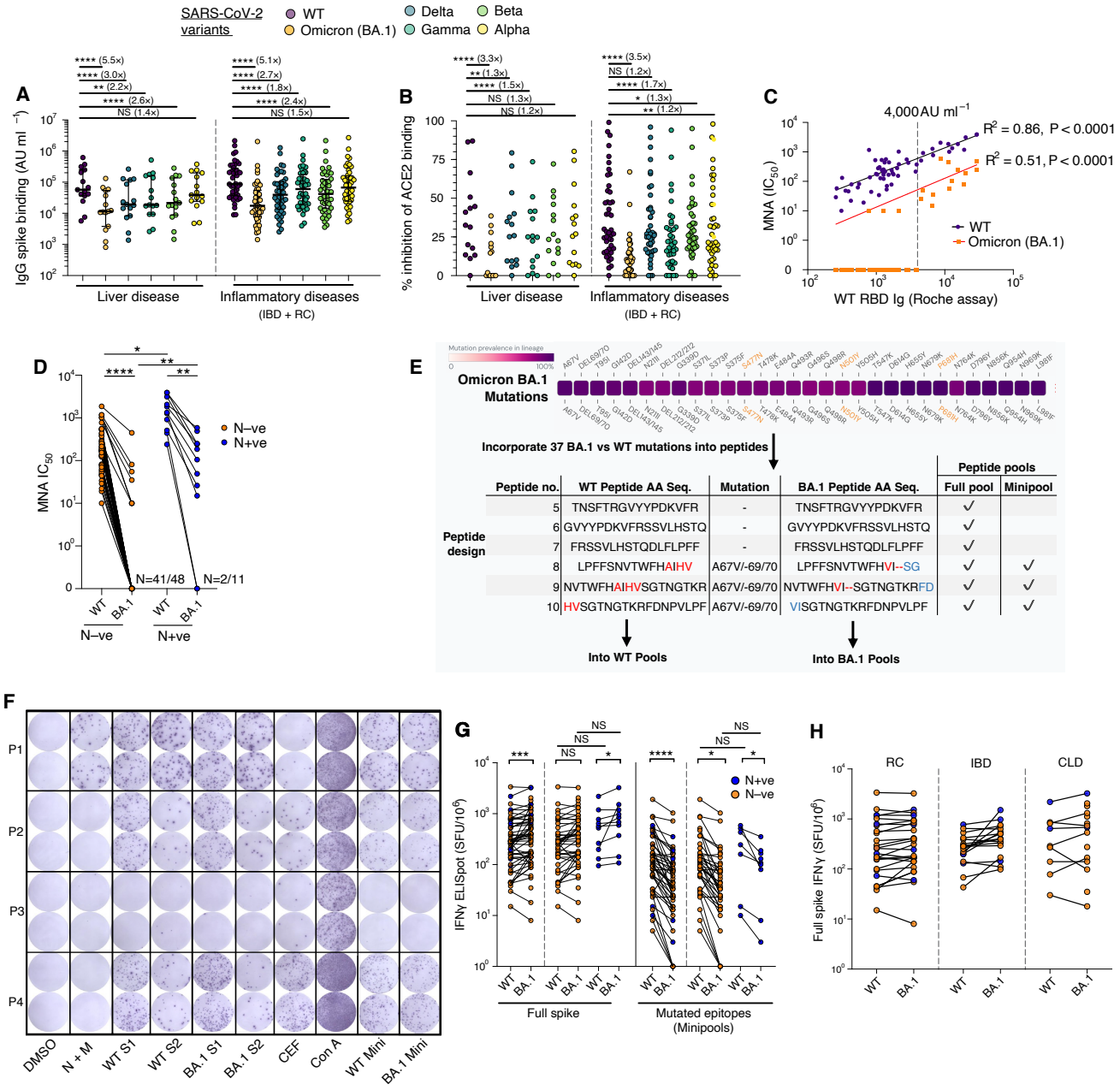

Fig. 3.4 Antibody and T cell responses to SARS-CoV-2 variants of concern in 59 immunocompromised individuals 28d after two doses of ChAdOx1 nCoV-19 vaccine

A&B) Serum IgG binding to SARS-CoV-2 variants of concern (VOC) spike protein (A) or Inhibition of SARS-CoV-2 VOC spike binding to hACE2 by participant serum (B) at V2+28d.

C&D) Microneutralisation of live ancestral (WT) or omicron BA.1 SARS-CoV-2 at the V2+28d timepoint: correlation of microneutralisation IC_{50} with ancestral anti-SARS-CoV-2 RBD-binding total Ig (C) and microneutralisation IC_{50} separated by previous SARS-CoV-2 infection status (D).

E) Graphic to depict design process for Omicron BA.1 peptide pools.

F) Exemplar IFNγ ELISpot layout to assess T cell responses to WT and omicron BA.1 spike proteins. Relevant to G&H

G&H) IFNγ T cell response to ancestral and Omicron BA.1 spike or pools of peptides covering regions mutated in BA.1 and their ancestral equivalents (minipools) at V2+28d. By previous SARS-CoV-2 infection (G) or disease group (H).

* indicates statistically significant by Bonferroni-adjusted alpha. ***adjusted P<0.001, ****adjusted P<0.0001. IBD, inflammatory bowel disease. RC, rheumatic conditions. CLD, chronic liver disease. N, nucleoprotein. M, membrane protein. MNA, microneutralisation assay.

Alpha, with the largest fold change-decrease between WT and Omicron BA.1(5.5-fold in liver disease, 5.1-fold in IBD and rheumatic conditions, RC) **(Fig. 3.4A)**. This was consistent in liver disease and inflammatory diseases, and similar to that seen in healthy individuals in other studies **(Fig. 3.4A)** (*255*). Surrogate neutralisation of variants was also decreased compared to WT and although detectable ACE2-inhibition was observed against WT spike in most individuals (57 of 59 ; 97%), only 29 of 59 (49%) exhibited any inhibition of Omicron BA.1 spike binding to ACE2 **(Fig. 3.4B)**. Live neutralisation assays similarly demonstrated a significant reduction in the functionality of vaccine-induced Ig **(Fig. 3.4C&D)**. All individuals neutralised ancestral SARS-CoV-2 (mean half-maximal inhibitory concentration, mean IC_{50} = 589), but there was a 13-fold decrease in the neutralisation Omicron BA.1 (mean IC_{50} = 44) and only 23 of 59 (27%) of patients could neutralise Omicron BA.1 **(Fig. 3.4C&D)**. There was a significant positive correlation between anti-RBD Ig titres and ancestral and Omicron BA.1 neutralisation, notably, those with a V2+28d Roche anti-RBD Ig titre of <4,000 AU ml^{-1} were largely unable to neutralise Omicron **(Fig. 3.4C)**. Patients with previous SARS-CoV-2 infection had significantly higher microneutralisation IC_{50} than naive patients **(Fig. 3.4D)**, with a higher proportion able to neutralise Omicron (9 of 11 versus 7 of 48, $P < 0.0001$, Fisher's exact test).

I next assessed T cell cross-reactivity between WT and Omicron BA.1 by designing peptide pools for use in IFNγ ELISpots **(Fig. 3.4E)**. The consensus sequence (derived from Global Initiative on Sharing All Influenza Data; GISAID) from Omicron BA.1 was used to adapt existing overlapping 18-mer peptide pools covering the entire WT SARS-CoV-2 spike protein (separated into S1 and S2 pools (*264*)). Peptides effected by insertion/deletion mutations were lengthened/shortened accordingly, without shifting subsequent amino acid sequences of peptides (e.g. peptides 8-10, **Fig. 3.4E)** and substitutions were replaced. Variant and non-mutated peptides covering the entire BA.1 spike (full spike pool), and variant peptides only ("minipools') were then pooled for comparison against equivalent WT pools **(Fig. 3.4F)**.

The IFNγ T cell response to Omicron BA.1 full spike was maintained compared to WT and did not differ depending on prior SARS-CoV-2 infection status (**Fig. 3.4G).** In contrast, IFNγ ELISpot magnitudes to only the peptides mutated in BA.1 (minipools) were reduced compared with the equivalent WT peptide minipools **(Fig. 3.4G)**. All individuals that did not respond to the mutated BA.1 pool (4 of 59; 7%) had low responses to the WT minipool and were SARS-CoV-2 infection naive **(Fig. 3.4G)**. These findings were consistent across different immunocompromised disease groups **(Fig. 3.4H)**. There was strong positive correlation between anti-RBD total Ig (Roche assay) and each of the serological measures of variant spike binding but low overall correlation between WT S1 and S2 T cell responses with serological measures of vaccine immunogenicity, particularly against SARS-CoV-2 variants (**Fig. 3.5)**.

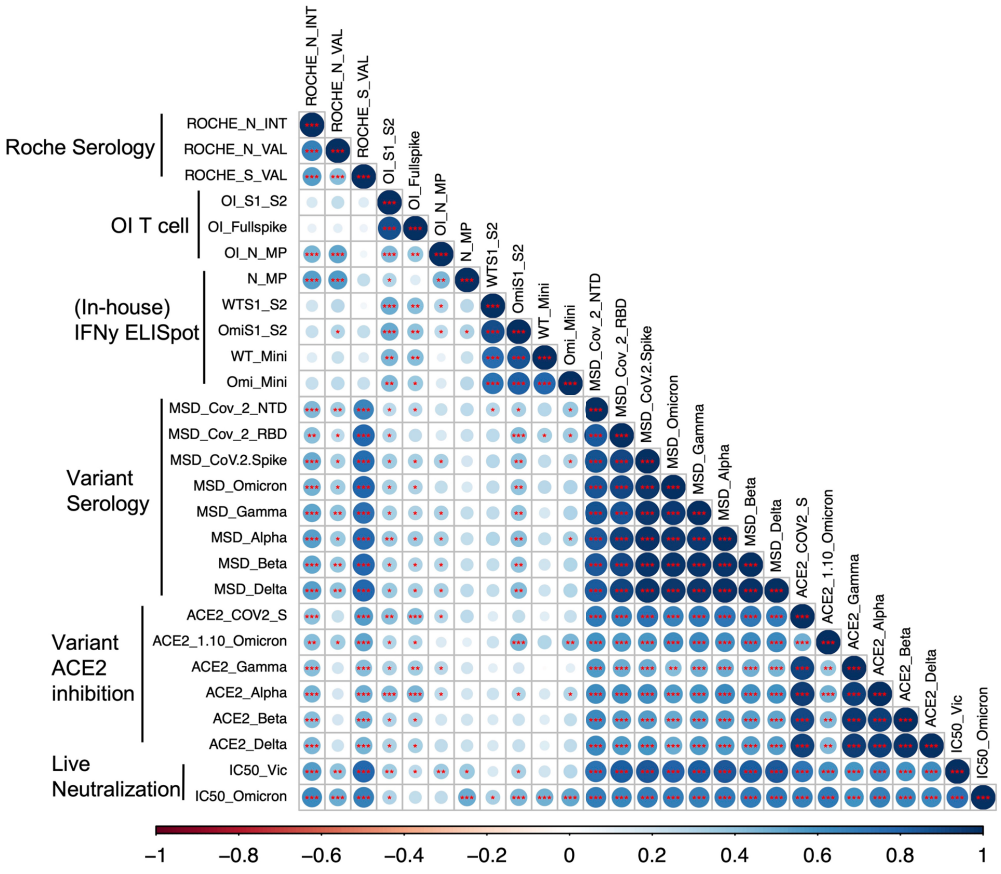

Fig. 3.5 Correlation of V2+28d second vaccine immune assay responses.

Correlation plot of all assays used to evaluate serological and cellular responses at V2+28d in the 59 sub-cohort participants. Spearman rank sum test used. Spearman ρ depicted by area of circle and colour legend. * P value < 0.05; ** P value < 0.01, ***; P value < 0.001.

3.6.5 EASL COVID-Hep 2.0 cohort and study design

The OCTAVE Study assessed the impact of a broad range of different SIs on COVID-19 vaccine immunogenicity and highlighted several disease states that were enriched for vaccine non-responsiveness. However, I next aimed to study the interaction between vaccine regimen and immunosuppressive conditions in more detail in patients with liver disease. To do this, we conducted the "EASL COVID-Hep 2.0" study of vaccine-immunogenicity in individuals with liver-associated diseases (**Fig. 3.1A)**.

The study was performed with an identical protocol to the OCTAVE study across multiple centres in multiple European countries. PBMC and serum samples were taken at identical timepoints with respect to the first two doses of COVID-19 vaccine, with additional samples taken immediately pre (pre-V3) and 21 days after a third dose of vaccine (V3+21d) **(Fig. 3.1B)**. Data from 127 individuals recruited into the PITCH study were included as healthy controls. In total, 722 patients with liver disease were recruited between March and September 2021 and included for immunogenicity analysis.

The liver disease patient cohort comprised 355 (49%) individuals with cirrhosis, 257 (36%) LT recipients, 74 (10%) individuals with AIH, and 36 (5%) with VLD. In the entire cohort, the primary two-dose vaccination course included ChAdOx1 (n = 246), BNT162b2 (n = 460), and mRNA-1273 (n = 118). An additional 13 individuals received heterologous vaccination with ChAdOx1 for first vaccination followed by an mRNA platform (BNT162b2 or mRNA-1273) for the second vaccination. Data were available for 307 participants after a third vaccination which included 187 (61%) receiving BNT162b2, 110 (36%) receiving mRNA-1273, and 10 (3%) where the vaccine type was unknown.

Across the entire liver disease cohort, the median age was 60 years (IQR 52–68), 425 (59%) were male, and 76 (11%) had previous evidence of SARS-CoV-2 infection **(Table 3.2)**. In the HC cohort, the median age was 36 years (IQR 25–45), 40 (31%) were male, and 40 (31%) had evidence of previous SARS-CoV-2 infection. Nineteen patients became newly positive for nucleocapsid antibody at the V3+21d timepoint. For the analysis, 21 (29%) patients with

AIH and concurrent cirrhosis were included in the AIH group and not the cirrhosis group as they were recipients of immunosuppressive therapy.

Several disease group-specific parameters are highlighted in **(Table 3.2).** 254 of 257 (99%) of LT recipients, 66 of 74 (89%) AIH, 7 of 355 (2%) cirrhosis and 2 of 36 (6%) VLD received at least one immunosuppressive therapeutic. Included in the cirrhosis cohort were 113 (32%) individuals with decompensated cirrhosis (**defined in Section 1.12.1**), and the commonest cirrhosis aetiology was alcoholic liver disease (152 of 355; 43%).

3.6.6 anti-RBD Ig titres vary across liver disease phenotypes, number of vaccine doses, and type of vaccine

Longitudinal assessment of antibody responses using the Roche anti-RBD assay across all liver disease phenotypes and HCs is presented in **(Fig. 3.6A)**. Prior SARS-CoV-2 infection was associated with a significant increase in anti-RBD titres across all disease groups **(Fig. S3.1A)** and therefore previously infected individuals were removed from the primary analysis (n = 76 with liver disease and n = 40 HCs excluded). Across the total liver disease cohort, there was a graded incremental increase in median antibody titres after each consecutive vaccine dose ($p < 0.0001$). This observation remained significant after excluding 19 patients who had become newly positive for nucleocapsid antibody between enrolment and V3+21d (**Fig. S3.1B**). A decrease in antibody titre between the V2+28d and pre-V3 timepoint was observed in both liver disease and HC groups and was subsequently boosted by the administration of a third vaccine dose (**Table 3.4**). mRNA platforms were associated with significantly higher V2+28d anti-RBD titres compared to ChAdOx1 in both liver disease ($p = 0.0005$) and HC cohorts ($p < 0.001$). Thirteen patients who received heterologous first and second vaccines had significant elevations in V2+28d antibody titres compared to homologous ChAdOx1 ($p = 0.0002$) and homologous mRNA regimens ($p = 0.004$) (**Fig. 3.6B**). In disease groups where data were available for both BNT162b2 or mRNA-1273 vaccinated individuals,

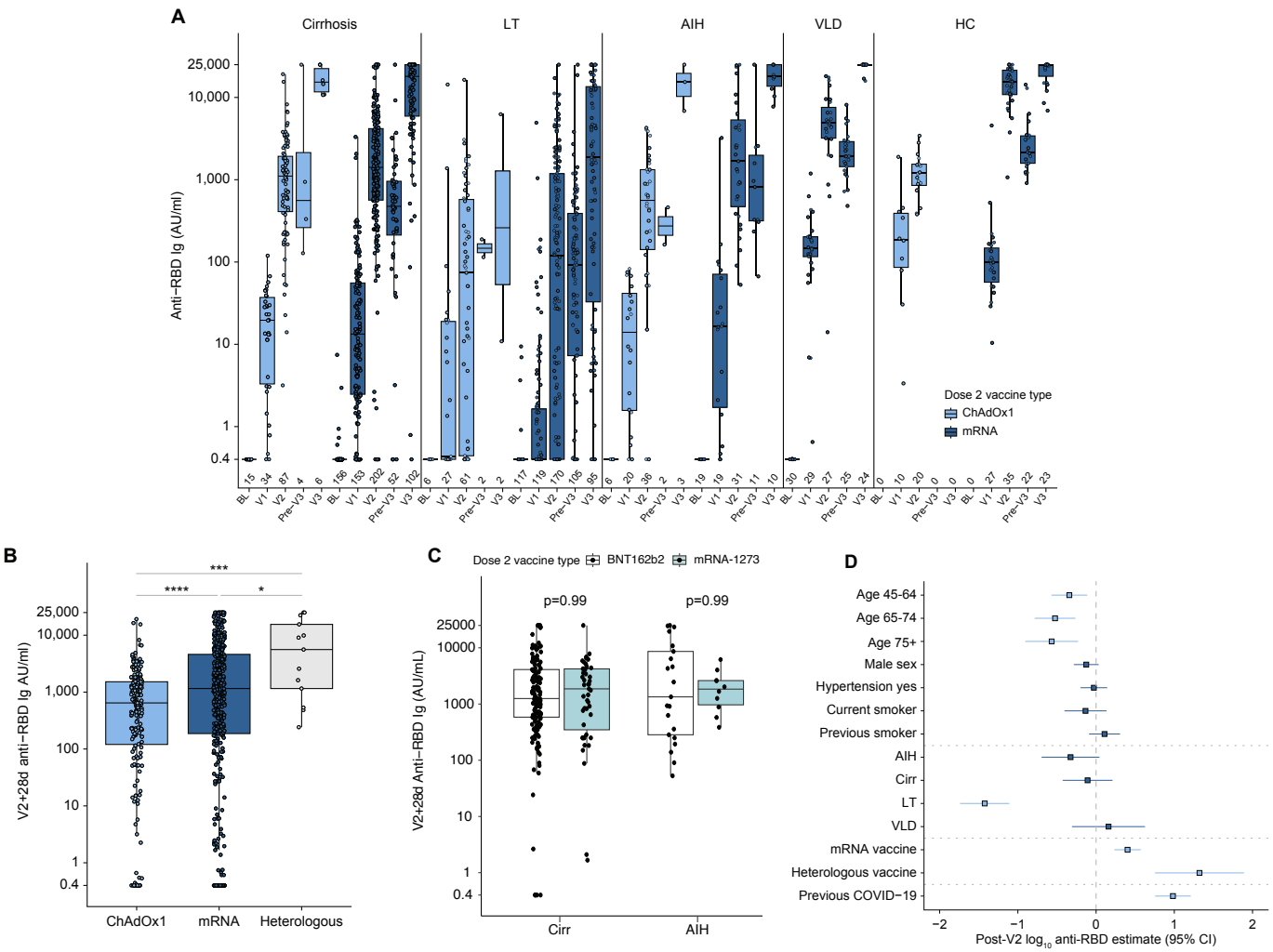

Fig. 3.6 COVID-19 vaccine-induced anti-SARS-CoV-2 RBD total Ig in EASL COVID Hep 2.0 Study

A) Assessment of anti-RBD total binding Ig at baseline (BL), post first vaccine (V1), 28 days after second vaccine (V2), immediately prior to third vaccine (pre-V3) and 21 days after third vaccine (V3). All participants had an mRNA vaccine as their third dose, individuals vaccinated with a heterologous prime-boost vaccine regimen and previous SARS-CoV-2 infection were excluded. N number shown.

B) Comparison of vaccination platforms at the post-V2 timepoint. Mann-Whitney U test with Bonferroni adjustment.

C) Comparison BNT162b or mRNA-1273 at V2+28d timepoint in cirrhosis or AIH groups. Mann-Whitney U test with Bonferroni adjustment.

D) Forest plot depicting results from multivariable linear regression model of post-V2 $\log_{10}$ transformed anti-SARS-CoV-2 RBD Ig in all participants. Point represents odds ratio, whiskers 95% CI. Dark blue indicates significantly predictive variables ($p < 0.05$).

$*p < 0.05$, $***p < 0.001$. AIH, autoimmune hepatitis; Cirr, cirrhosis; HCs, healthy controls; LT, liver transplant; RBD, receptor binding domain; VLD, vascular liver disease.

there were no significant differences in anti-RBD at the V2+28d timepoint; therefore, both mRNA vaccines were grouped for further analysis (**Fig. 3.6C**).

Within the entire study cohort (patients and HCs) multivariable analyses showed that the factors significantly associated with lower antibody response after V2 were advancing age

and inclusion in the LT recipient group, and factors associated with greater response were mRNA vaccination, heterologous prime-boost vaccination and previous COVID-19 infection (**Fig. 3.6D**).

At the V2+28d and V3+21d timepoints LT recipients mounted lower antibody titres compared to all other disease groups and HCs regardless of vaccine type **(Table 3.5)**. mRNA-vaccinated patients with cirrhosis had reduced V2+28d antibody titres compared to mRNA-vaccinated HCs, but ChAdOx1-vaccinated patients with cirrhosis had comparable V2+28d titres to ChAdOx1-vaccinated HCs.

There were variable non-response rates across disease groups depending on vaccine type and timepoint **(Table 3.6)**. No HCs were seronegative after either two or three vaccine doses. LT recipients had the highest rates of serological non-response with 18 of 52 (35%) and 52 of 179 (29%) having absent responses after two doses of ChAdOx1 and mRNA vaccines, respectively. Non-response rates were reduced at the V3+21d timepoint in all disease groups, with only 9 of 97 (9%) LT recipients and 2 of 108 (2%) patients with cirrhosis not having a serological response to vaccine at the V3+21d timepoint.

3.6.7 Immunosuppressive therapeutic regimen significantly impacts vaccine-induced Ig titres in liver transplant recipients

To assess the impact of immunosuppressive agents on vaccine immunogenicity, I compared anti-RBD Ig titres between individuals within the LT recipient group on different immunosuppressive combinations **(Fig. 3.7A)**. The commonest immunosuppressive therapy combinations for LT recipients were calcineurin inhibitor (CNI) alone (81 of 257; 32%), CNI plus mycophenolate mofetil (MMF) (79 of 257; 31%), CNI plus non-MMF other (81 of 257; 31%) or mTor inhibitor only (13 of 257; 5%). For AIH, 38 of 74 (51%) individuals were treated with a purine synthesis inhibitor (azathioprine or 6-mercaptopurine; 6-MP), 33 of 74 (43%) received corticosteroids and 15 received MMF and/or CNI (**Table 3.2**, **Fig. 3.7A)**.

There was a downward trend in V2+28d anti-RBD titres associated with increasing intensity

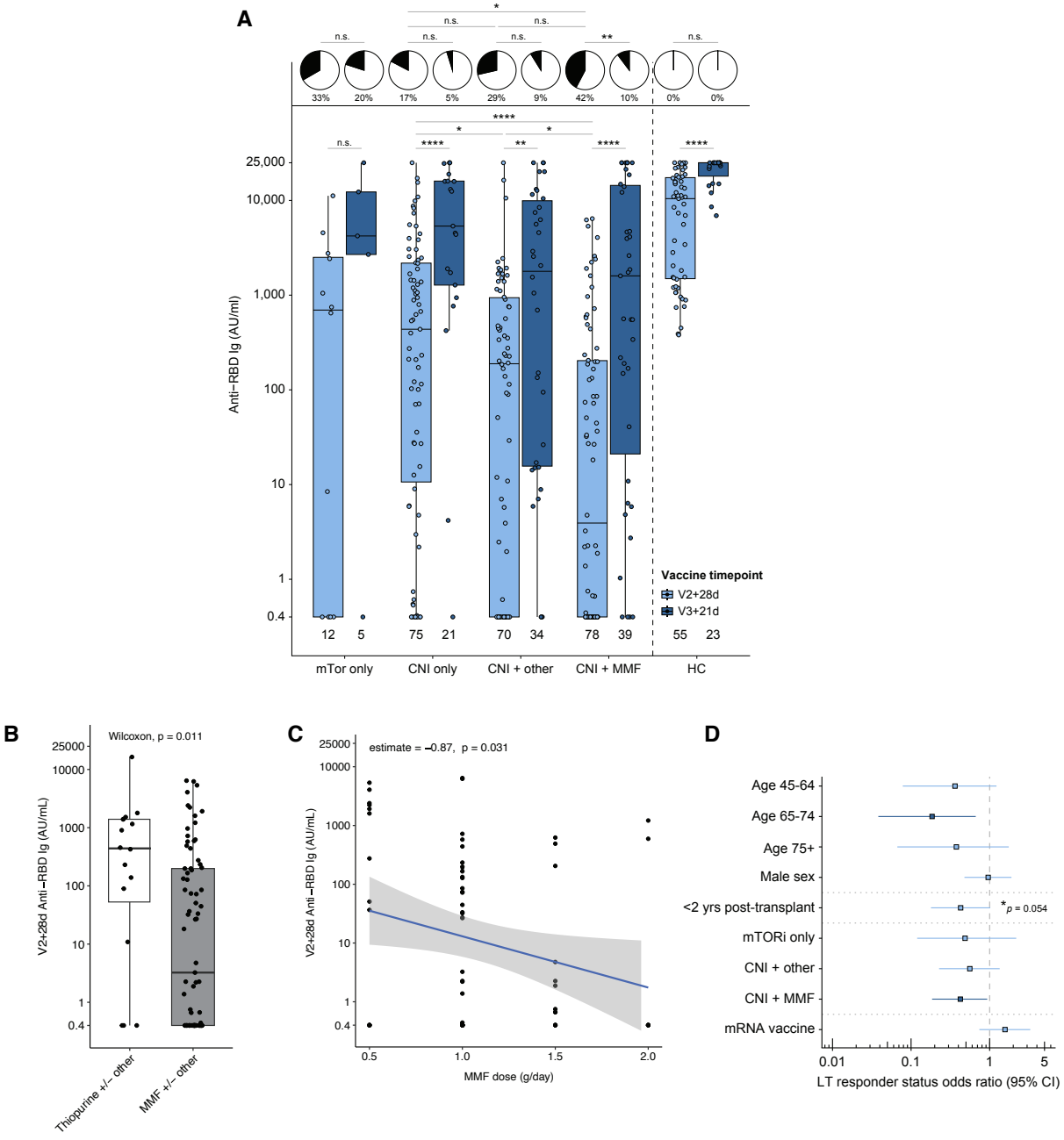

Fig. 3.7 Serological responses to COVID-19 vaccines in liver transplant recipients.

A) Magnitude of anti-SARS-CoV-2 RBD Ig in SARS-CoV-2 infection-naïve liver transplant recipients and healthy controls (HC). Proportions of seropositive (white) and seronegative (black) (<0.8 AU/ml) patients in each subgroup presented in pie charts. Statistical comparison with Mann-Whitney U or Fisher's exact tests.

B) Comparison of thiopurine (Azathioprine or 6-mercaptopurine) or Mycophenolate mofetil (MMF) as an immunosuppressive therapeutic in LT recipient. Participants may have received other immunosuppressive therapeutics in addition.

C) MMF dose breakdown (gram/day) in SARS-CoV-2 infection naïve LT recipients at V2+28d timepoint. Linear model of $\log_{10}$ transformed Anti-RBD Ig compared with daily MMF dose.

D) Forest plot of multivariable logistic regression showing odds of seropositivity at the V2+28d timepoint within the liver transplant cohort. Point represents odds ratio, whiskers 95% CI. Dark blue indicates significantly associated variables ($p < 0.05$).

MMF = Mycophenolate mofetil, CNI = calcineurin inhibitor, LT = liver transplant

of immunosuppression, with significant reductions observed in patients on a calcineurin inhibitor (CNI) plus mycophenolate mofetil (MMF) vs. a CNI alone, and in patients on a CNI plus another immunosuppressant other than MMF, compared to CNI alone (**Fig. 3.7A)**. LT recipients on MMF additionally had significantly reduced responses compared to those on thiopurines (p = 0.011, **Fig. 3.7B**) – relevant as thiopurines are commonly used instead of MMF in practice in European sites but not in the UK (*265, 266*). In LT recipient on CNI + MMF, increasing daily dose of MMF was significantly associated with decreased anti-RBD titres at the V2+28d timepoint (p = 0.031) (**Fig. 3.7C**). A third vaccine dose significantly increased antibody responses across all groups, except with mTOR inhibitor monotherapy where cohort numbers were small (**Fig. 3.7A**). LT recipients had high rates of antibody non-response, with non-response rates at the V2+28d timepoint of 4 of 12 (33%) in the mTOR inhibitor only group, 13 of 75 (17%) in the CNI only group, 20 of 70 (29%) in the CNI plus other immunosuppression group and 33 of 78 (42%) in the CNI plus MMF group (**Fig. 3.7A**). The rate of serological non-responsiveness was significantly higher in the CNI plus MMF group compared to the CNI alone group (**Fig. 3.7A**). A third vaccine dose led to improvement in rates of non-response across all subgroups of immunosuppression (mTOR inhibitor only 1 of 5; 20%, CNI only 1 of 21; 5%, CNI plus other immunosuppression 3 of 34; 9%, CNI plus MMF 4 of 39; 10%) (**Fig. 3.7A**). Among LT recipients, both multivariable analyses showed that the factors significantly associated with reduced odds of seropositivity at V2+28d were age (65-74 age group) and CNI plus MMF (**Fig. 3.7D**). LT recipients with previous SARS-CoV-2 infection were removed from the logistic regression, as all of these patients had a detectable response at V2+28d.

3.6.8 Immunosuppression in patients with autoimmune hepatitis had a reduced impact on anti-RBD Ig titres compared to LT recipients

Patients with AIH had higher V2+28d antibody responses than LT recipients with both ChAdOx1 and mRNA platforms despite both groups being immunocompromised and being of similar age (61 years [49–69] vs. 60 years [52–68], **Tables 3.2 & 3.4**). Additionally, after a

third vaccine dose, anti-RBD Ig titres in the AIH group were boosted to titres similar to those observed at V3+21d in HC (**Table 3.4)**. Unlike LT recipients, there were no significant differences in serological response between class and intensity of immunosuppression at V2+28d (**Fig. 3.8A**), despite the fact some patients with AIH (6/8 with MMF dose data) were on high dose (2 g/day) MMF. There were also no differences in response when the AIH cohort was split by the presence or absence of cirrhosis (**Fig. 3.8B**). Multivariable analyses showed that the factors significantly associated with higher antibody responses at V2+28d were mRNA vaccination and previous COVID-19 (**Fig. 3.8C**).

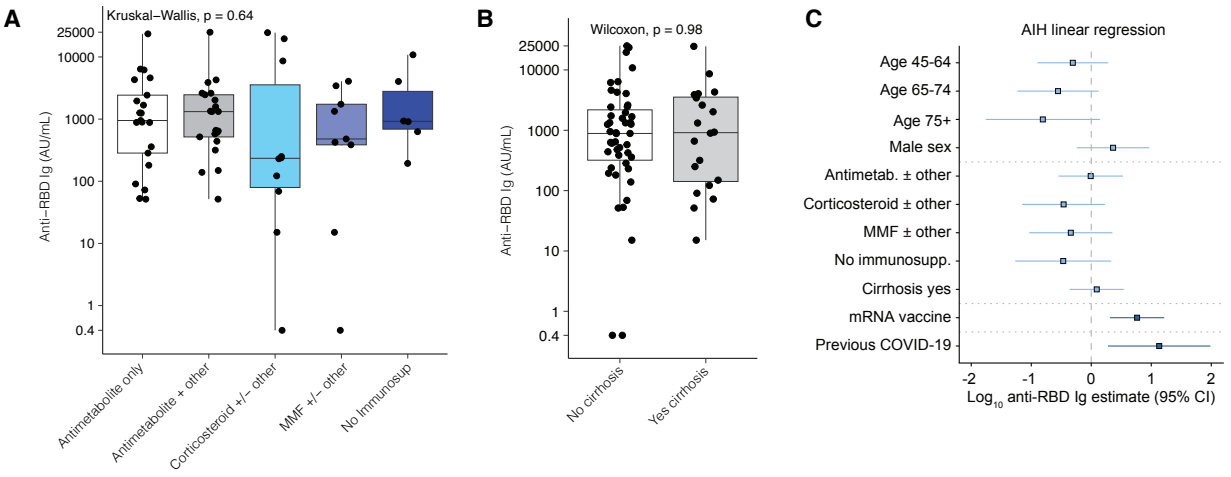

Fig. 3.8 Serological responses to COVID-19 vaccines in patients with autoimmune hepatitis.

A&B) SARS-CoV-2 infection naïve patients with autoimmune hepatitis at V2+28d timepoint, comparing A) immunosuppressive therapies and B) presence of cirrhosis. Boxes represent median and IQR, whiskers represent +/- 1.5x IQR. Kruskal Wallis (A) or Two-sided Mann-Whitney U test (B).

C) Results of multivariable linear regression of $\log_{10}$ anti-SARS-CoV-2 RBD Ig at V2+28d timepoint in autoimmune hepatitis cohort. Dark blue indicates significantly associated variables ($p < 0.05$) Antimetabolites include 6-mercaptopurine and azathioprine. MMF = Mycophenolate mofetil.

3.6.9 Unique interactions of COVID-19 vaccine type and disease severity on anti-RBD Ig titres in patients with cirrhosis

Assessment of anti-RBD Ig in cirrhosis patients revealed a dynamic interaction between number of doses, severity of cirrhosis, and vaccine type **(Fig. 3.9A)**. At pre-V2 there were no differences in antibody titres between compensated (CP-A) and decompensated (CP–B/C) cirrhosis when vaccinated with ChAdOx1 **(Section 1.12.1)**. However, CP-A had higher antibodies than CP-B/C at pre-V2 when vaccinated with mRNA. At post-V1, both CP-A and

CP-B/C had lower antibody titres than HC with both vaccine types. At V2+28d, there were no significant differences between CP-A and CP-B/C or between patients and HCs when vaccinated with ChAdOx1. Whereas at V2+28d for mRNA, HCs had higher titres than patients with cirrhosis irrespective of CP class. At V3+21d, there were no significant differences between any groups **(Fig. 3.9A)**. Broadly, this suggested an association between liver disease

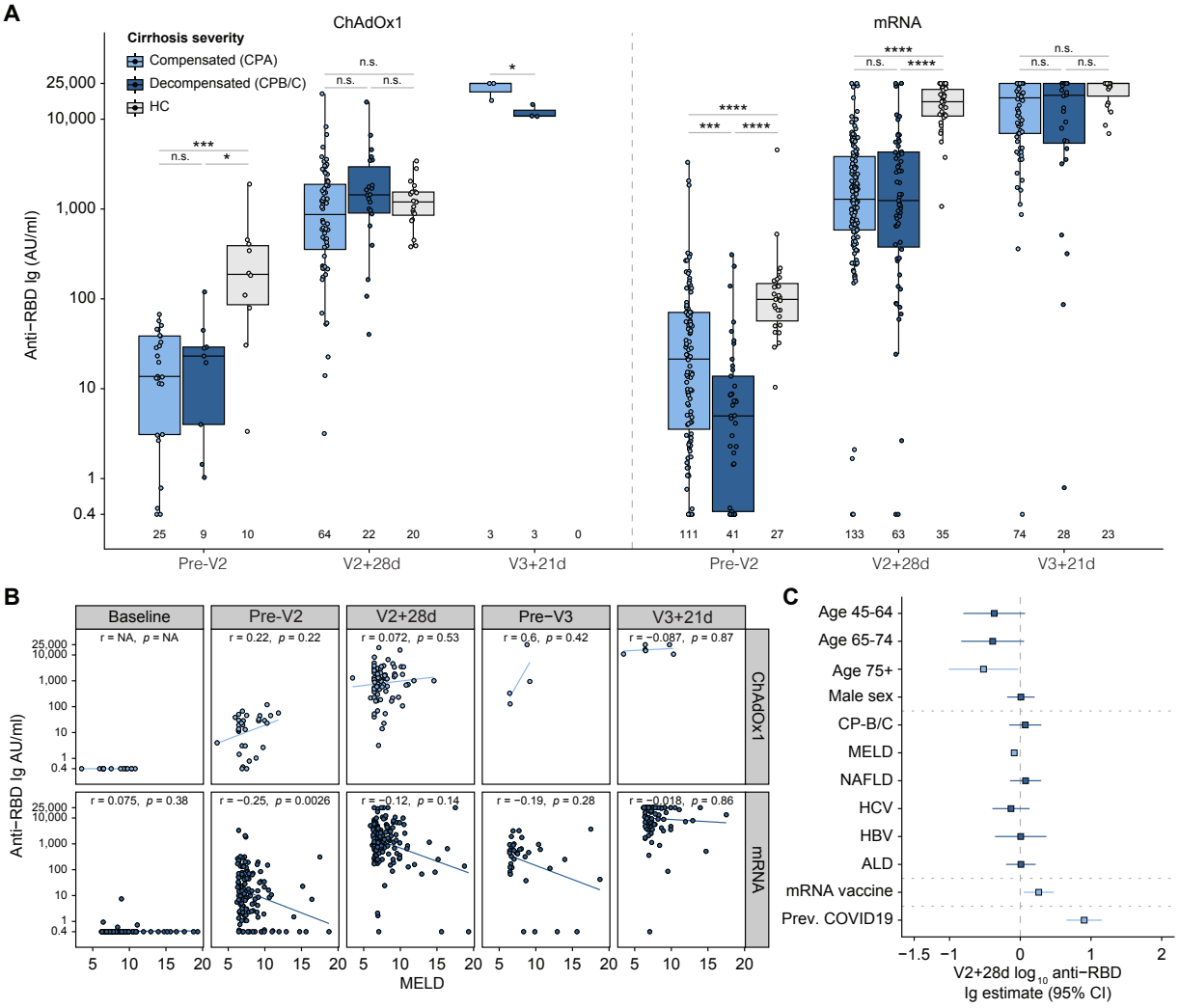

Fig. 3.9 Serological responses to COVID-19 vaccines in patients with cirrhosis.

A) Magnitude of vaccine responses in SARS-CoV-2 infection-naïve patients with cirrhosis and healthy controls. Vaccine type is for first two vaccine doses. Kruskal-Wallis with *post hoc* Dunn's test adjusted with Holm-Bonferroni method.

B) Spearman correlation of MELD score with anti-SARS-CoV-2 RBD Ig in same cirrhosis patients as A. Line represents linear regression, output from Spearman regression shown

C) Forest plot depicting results of multivariable linear regression of $\log_{10}$ anti-SARS-CoV-2 RBD Ig at V2+28d timepoint in cirrhosis cohort. Point represents odds ratio, whiskers 95% CI. Dark blue indicates significantly associated variables (p <0.05).

n.s., non-significant, $**p < 0.01$, $***p < 0.001$, $****p < 0.0001$. ALD, alcohol-related liver disease; CP, Child-Pugh class; HC, healthy control; NALFD, non-alcoholic fatty liver disease.

severity and reduced antibody responses when vaccinated with mRNA but not the ChAdOx1 platform, particularly early in the vaccination course.

To explore the interaction between disease severity and vaccine type further, I plotted the correlation between Model for End-stage Liver disease (MELD) score and anti-RBD titres **(Fig. 3.9B)**. The MELD score is a semi-linear scoring system for end-stage liver disease severity (*260, 261*). At pre-V2, this again showed that increasing disease severity was associated with decreased anti-RBD Ig titres when vaccinated with mRNA platform but not with ChAdOx1. This trend persisted after V2 and V3, although it was non-significant. Among patients with cirrhosis, multivariable analyses showed that age over 75 years and increasing MELD score were associated with a lower antibody response, whereas mRNA platform and previous COVID-19 were associated with higher titres (**Fig. 3.9C**).

3.6.10 A third dose of COVID-19 vaccine improves the cross-reactivity of antibodies to SARS-CoV-2 variants in individuals with liver disease but not healthy individuals

Similar to **Section 3.6.4**, I assessed the cross-reactivity of vaccine-induced antibodies in a subset of liver disease patients and healthy individuals at V2+28d and V3+21d timepoints, by analysing data on SARS-CoV-2 variant binding and ACE2 inhibition generated by Dr. Tom Tipton. Panels of the commonest circulating VoC at the time of analysis were included.

Within the combined cohort (liver disease and HCs) at both timepoints, serological titres to all Omicron subvariants (except for BF.7 and BQ.1) were significantly lower compared to WT SARS-CoV-2 **(Fig. 3.10A**). The subvariants with the greatest decrease in IgG binding compared to WT were BA2.75.2 (median fold decrease: x8.93 V2+28d and x6.12 V3+21d) and BA.4.6 (x4.46 V2+28d and x3.2 V3+21d) which were both first identified in autumn 2022 **(Fig. 3.10A)**. Notably, the magnitude of reduction in IgG binding to Omicron subvariants relative to WT was lower following V3 compared to V2+28d **(Fig. 3.10A**). The same trends were observed when IgG binding was split by liver disease aetiology **(Fig. 3.10B & Fig. S3.2A**). However, HCs had less of a decrease in IgG binding to Omicron subvariants relative

to WT than seen in patients with liver disease **(Fig. 3.10B)**. Serum from most participants inhibited ACE2 binding to WT RBD at V2+28d and V3+21d **(Fig. 3.10C)**, whereas there was a significant decrease in inhibition across all Omicron subvariants relative to WT. Again, the decrease in ACE2 binding at V3+21d was less pronounced compared to V2+28d **(Fig. 3.10C)**. There was also less of a decrease at the V2+28d and V3+21d timepoints in HCs compared to patients with liver disease **(Figs. 3.10D and S3.2B)**.

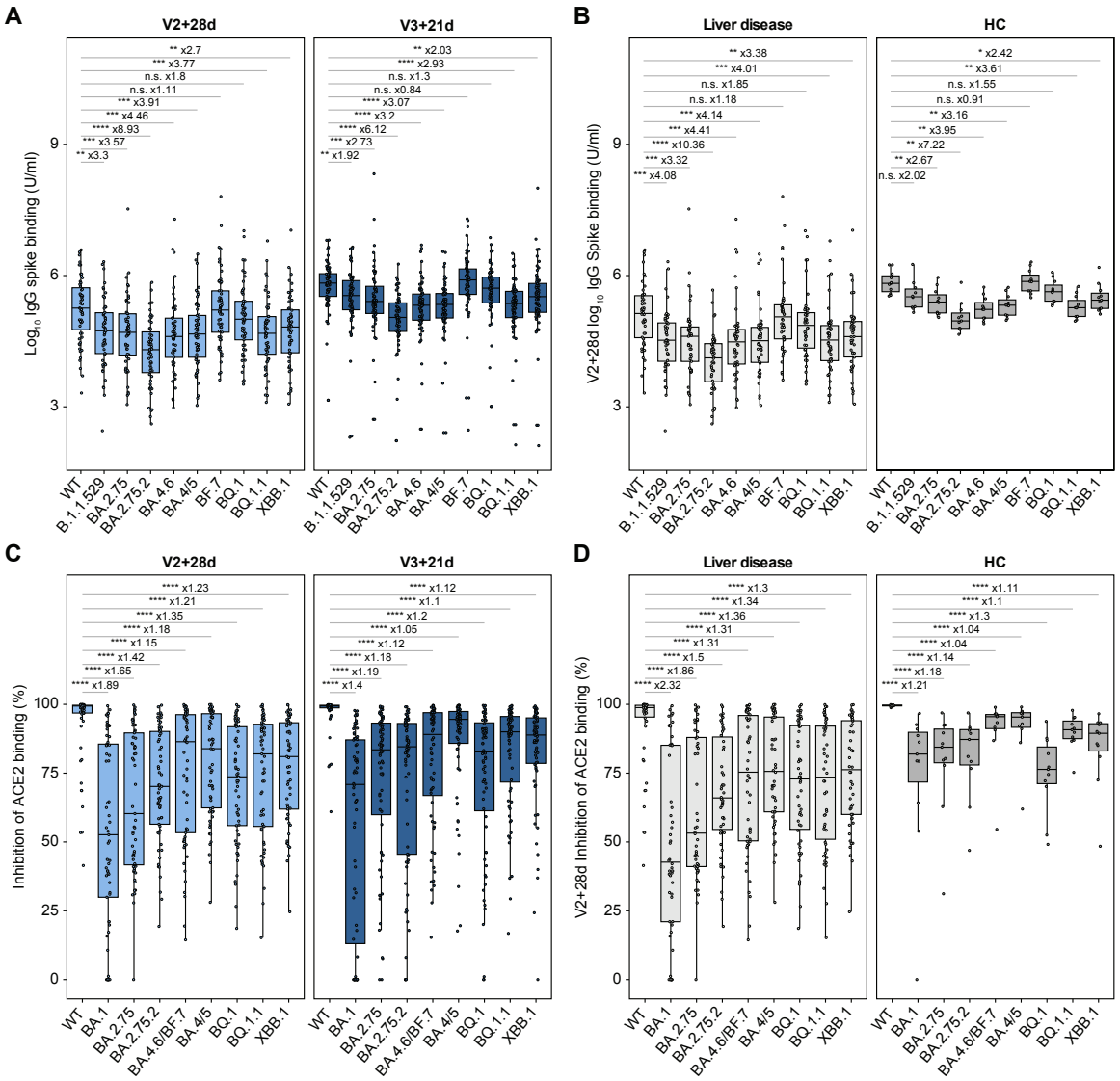

Fig. 3.10 COVID-19 vaccine-induced serological responses to Omicron subvariants.

A&B) IgG to subvariant spike protein and **(C,D)** inhibition of ACE2 binding to subvariant RBD in 68 individuals. **(A,C)** Includes all individuals split by timepoint and **(B,D)** are post-V2 responses separated by liver disease (inc. liver transplant) and HCs. Mann-Whitney *U* test with Holm-Bonferroni adjustment. Fold-change of median depicted.

$*p < 0.05$, $**p < 0.01$, $***p < 0.001$, $****p < 0.0001$. ACE2, angiotensin-converting enzyme 2; HCs, healthy controls; RBD, receptor binding domain; WT, wild-type.

The ratio of IgG binding to WT spike compared to VoC spike was significantly increased by a third vaccine in the liver disease group, but no change was observed between two and three vaccine responses in HCs (**Fig. 3.11A**). There were significant positive correlations at V2+28d and V3+21d timepoints when comparing the Roche anti-RBD titre with VoC binding IgG, ACE2

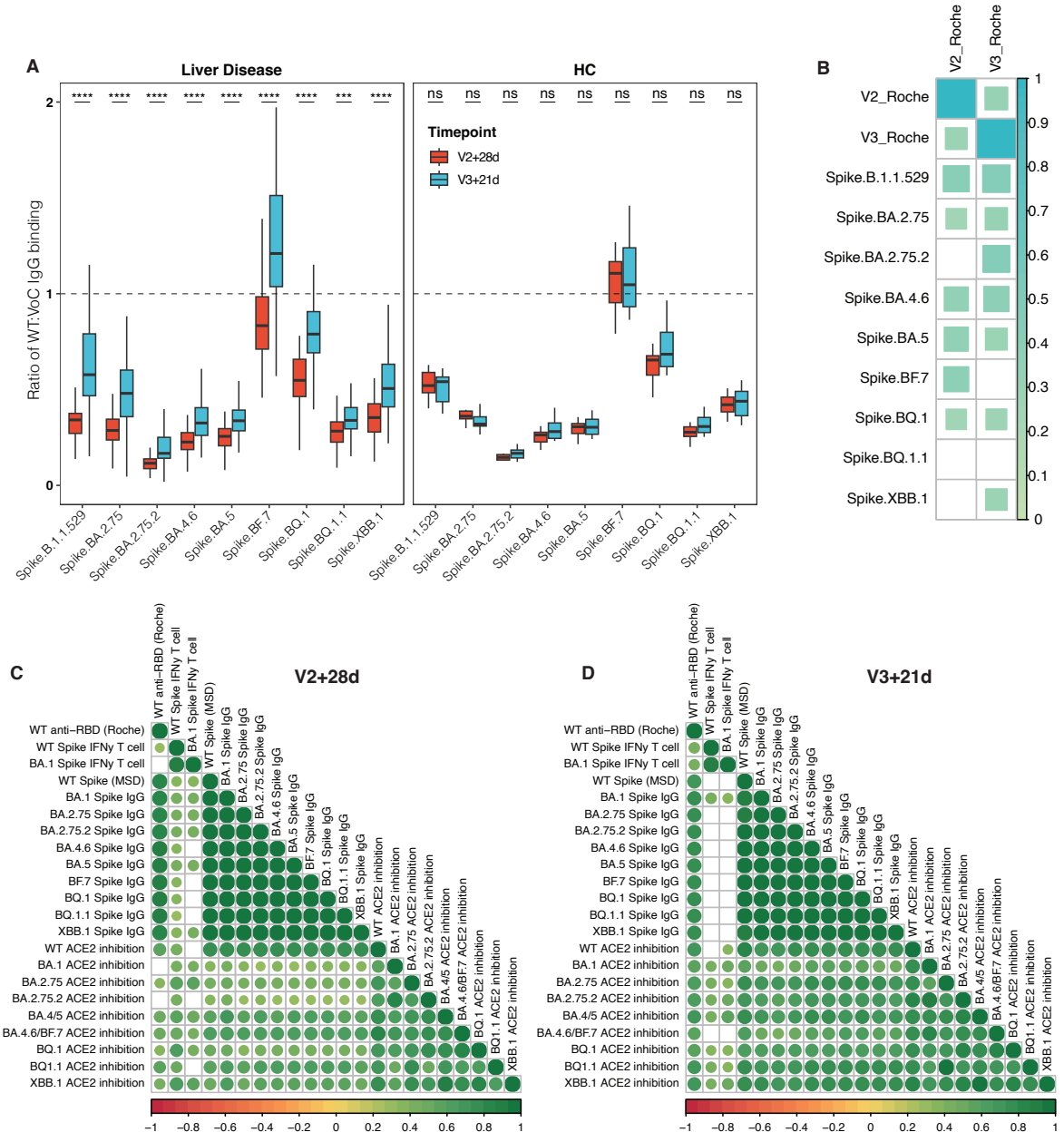

Fig. 3.11 Cross-reactivity of vaccine-induced antibodies to SARS-CoV-2 variants of concern (VoC) and correlation with wild-type anti-receptor binding domain antibodies

A) Ratio of IgG binding to WT and each respective SARS-CoV-2 variant of concern (VoC) at V2+28d and V3+21d timepoints in liver disease and healthy controls (HC). Two-sided Mann-Whitney U test adjusted with Holm-Bonferroni.

B) Correlation of anti-RBD Ig titres (measured by Roche assay) with the ratio of IgG binding to WT and each respective SARS-CoV-2 VoC at V2+28d and V3+21d timepoints.

C&D) Correlation of all assessed VoC antibody and T cell measure at V2+28d (C) and V3+21d timepoints (D)

WT = wild-type. * = P<0.05, ** = P<0.01, *** = P<0.001, **** = P < 0.0001. Only significant correlations (P<0.05) are shown. Spearman's correlation. Size and shade of spots/squares represent r value.

inhibition, and with the ratio between WT to VoC binding IgG (**Figs. 3.11B-D**).

3.6.11 T cell responses to WT and Omicron BA.1 SARS-CoV-2 across liver disease phenotypes

Having identified differences between disease groups in anti-RBD Ig titres, I next investigated IFNγ T cell magnitudes to SARS-CoV-2 spike peptide pools in a random subset of individuals from each group across multiple timepoints **(Fig. 3.12A)**. Most patients across the cohort had positive T cell responses (>26 SFU/10^6 PBMCs) after at least one dose of vaccination **(Fig. 3.12A)**. Within the liver disease cohort all patients generated a positive T cell response after V2 except for 3 of 10 (30%) in LT, 4 of 24 (17%) cirrhosis, and 1/12 (8%) AIH groups **(Fig. 3.12A)**. Despite significant heterogeneity, all groups except for LT recipients had a significant increase in the magnitude of IFNγ responses after two or three vaccine doses **(Fig. 3.12A)**. Considerable IFNγ T cell responses were observed at baseline in all disease groups and HC **(Fig. 3.12A)**. Within the total liver disease cohort, patients with previous COVID-19 had significantly higher IFNγ responses at pre-V2, V2+28d and V3+21d **(Fig. 3.12B)**. There were positive correlations between V2+28d T cell responses to WT spike, anti-RBD binding antibodies to WT, and functional antibody responses to all variants (ACE2 binding inhibition) **(Figs. 3.12C and 3.11C)**.

To determine the cross-reactivity of vaccine-induced cellular responses I additionally assessed IFNγ T cell responses to peptides covering the Omicron (BA.1) spike protein using peptides pools (**as in Fig. 3.12D)**. Compared to the WT antigen, T cell responses to BA.1 spike were well preserved regardless of disease group at V2+28d and V3+28d timepoints. However, when only assessing responses to peptides that differed between WT and BA.1 spike (minipools) there were significant reductions in BA.1 peptide-specific reactivity compared to WT in all groups (**Fig. 3.12E**), indicating that T cell responses specifically to mutated epitopes were reduced but overall responses were maintained.

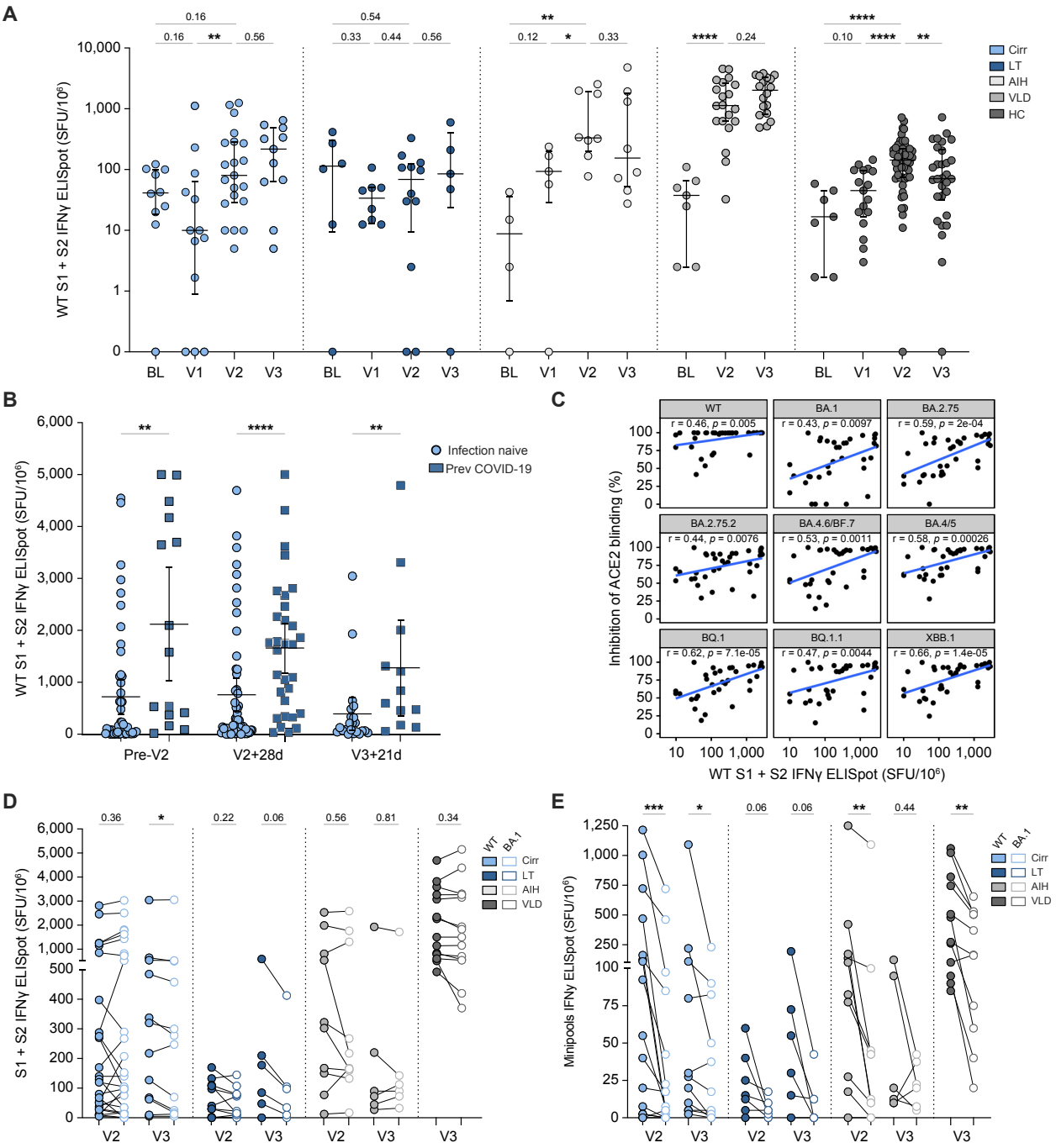

Fig. 3.12 IFNγ T cell responses to COVID-19 vaccination.

A) Magnitude of IFNγ T cell response to WT SARS-CoV-2 spike peptides across time in a subgroup of SARS-CoV-2-naïve individuals with cirrhosis (Cirr, n = 24), autoimmune hepatitis (AIH, n = 12), or vascular liver disease (VLD, n = 22), liver transplant recipients (LTRs, n = 12) and healthy controls (HCs, n = 28). Baseline data are from same individuals as later timepoints. Mann-Whitney *U* test. Healthy control ELISpots data was provided by Dr. Barbara Kronsteiner from the PITCH study

B) IFNγ T cell responses in SARS-CoV-2-naïve (n = 68) and previously infected individuals (n = 31) across all disease groups.

C) Spearman correlation between magnitude of IFNγ T cell responses to WT spike and percent inhibition of ACE2 binding to Omicron subvariant RBD by serum at post-V2 timepoint.

D,E) Magnitude of IFNγ T cell responses to WT (filled circles) and Omicron BA.1 (open circles) peptides after two or three vaccines covering (D) whole spike and (E) minipools. Wilcoxon matched-paired signed rank test.

n.s., non-significant, $*p < 0.05$,$**p < 0.01$,$***p < 0.001$,$****p < 0.0001$. AIH, autoimmune hepatitis; BL, baseline; RBD, receptor binding domain; SFU, spot-forming units; WT, wild-type.

3.6.12 Association of vaccine-induced anti-SARS-CoV-2 immune responses with breakthrough COVID-19 severity in OCTAVE and EASL COVID-Hep 2.0 studies

In both the OCTAVE and EASL COVID-Hep 2.0 studies there was large heterogeneity in vaccine-induced antibody and T cell responses across SI groups. In healthy individuals, both antibody and T cell vaccine-responses have been associated with protection against severe COVID-19 (*267-270*). Therefore, I next aimed to assess the relationship of vaccine-induced immune responses with COVID-19 outcomes in individuals with SIs, using immunological and follow-up SARS-CoV-2 infection and symptom severity data collected in OCTAVE and EASL COVID-Hep 2.0 studies (**Section 3.5.3**).

3.6.12.1 OCTAVE study

In the OCTAVE cohort, a total of 474 SARS-CoV-2 infections were reported including one Alpha infection, 110 Delta and 335 Omicron (BA.1 or BA.2) infection. 113 of 474 (24%) infections occurred within 6 months of V2, and 361 of 474 (76%) occurred between 6 months post-V2 and 12-months post-V1 **(Table 3.7)**. Most infections occurred in patients with kidney transplant, inflammatory arthritis and Crohn's disease, with infection rates of 123/456 (27%), 79/689 (11%) and 67/156 (43%), respectively **(Fig. 3.13A, Table 3.7)**. Within group infection rates varied from 6.2% (auto-HSCT) to 43% (Crohn's disease and CAR-T) **(Fig. 3.13A)**.

Most infections of known severity were mild (397/440, 90.2%), including asymptomatic infection (49 of 440; 11%) and symptomatic infection that did not require hospitalization (348 of 440, 79%) **(Fig. 3.13B & Table 3.8**). Severe disease requiring hospitalization or COVID-19-related death was reported in 43 of 440 (9.8%) infections; 15 of 440 (3.4%) patients required oxygen; three patients were admitted to the intensive treatment unit (ITU) (0.7%); and 10 of 440 patients died (2.3%) **(Fig. 3.13B & Table 3.8**). Infections occurring within 6 months after V2 (11 of 107; 10%) were not more severe (hospitalised or died) than those at more than 6 months after V2 (32 of 333; 9.6%) (**Table 3.8**). However, of 434 patients with known severity and precise date of infection, more severe infections occurred in those infected

in Delta versus the Omicron time epochs (eight died and 23 severe/107 Delta versus two died and 17 severe/327 Omicron; $P<0.0001$).

Disease severity varied per group and certain disease groups were enriched for more severe outcomes, including AAV, HD and HD on IS, K-Tr, auto-HSCT and CAR-T groups **(Fig. 3.13B)**. COVID-19 related deaths were found only within these groups **(Table 3.8)**. Notably, all of these groups had reduced anti-RBD Ig titres at V2+28d (**Fig. 3.2C&D)** and HD, HD on IS and auto-HSCT groups were enriched for T cell non-responsiveness at V2+28d compared to healthy individuals **(Fig. 3.3B)**.

The finding that disease groups that were enriched for severe disease outcomes were also associated with reduced immune responses to COVID-19 vaccines was striking. To further investigate this, I next assessed post-vaccine SARS-CoV-2 infection rates and COVID-19 outcomes stratified by V2+28d anti-SARS-CoV-2 immune responses. There was a higher rate of infection (infections per 1,000 d after V2) in patients with absent serological or T cell responses compared to those with high responses (**Fig. 3.13C&D).** Five patients died of COVID-19 without serological titres taken and were excluded from subsequent analysis. Of 434 patients with known severity and precise date of infection, more severe infections occurred in those infected in the Delta versus the Omicron time epochs (eight died and 23 severe/107 Delta versus two died and 17 severe/327 Omicron; $P<0.0001$).

Infection severity was increased in patients with no (20 of 61; 32.3% severe) or low (13 of 89; 14.6%) post-V2 serological response compared to those with high serological response (10 of 290; 3.4%) (no versus low and high, $P<0.0001$) **(Fig. 3.13E&F & Table 3.8)**, but V2+28d T cell responder status was not significantly associated with increased COVID-19 severity (4 of 18; 22.2% non-response vs 7 of 80; 8.8% response ($P=0.11$)) **(Fig. 3.13G&H & Table 3.9)**. Of the COVID-19-related deaths, eight of 10 individuals had no detectable or low V2+28d

Fig. 3.13 SARS-CoV-2 infection outcomes after two COVID-19 vaccines in the OCTAVE study

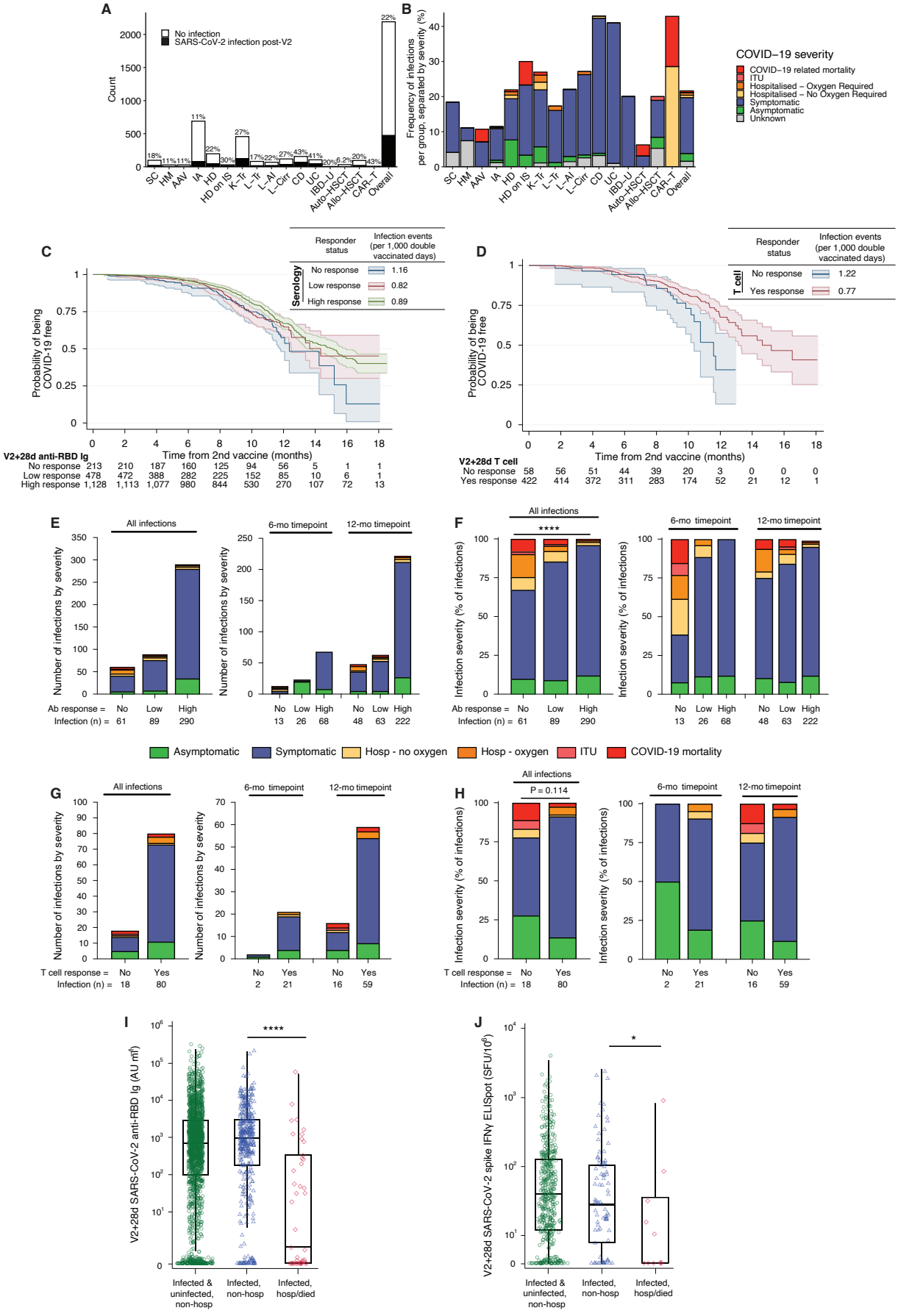

Fig. 3.13 SARS-CoV-2 infection outcomes after two COVID-19 vaccines in the OCTAVE study

A) Number of reported infections in post-V2 SARS-CoV-2 infection follow-up. Percent of total per group is reported.

B) Proportion of individuals within given group that were infected at any time post-V2 with given disease severity (n = 474).

C&D) COVID-19 incidence-free progression over time after second vaccine and infection rate per 1,000 double-vaccinated days, stratified by V2+28d receptor binding domain (RBD) binding Ig response status (n=1,617) (C) or V2+28d SARS-CoV-2 spike IFNγ T cell response status (*n*=359) (D). Lines represent COVID-19-free progression, and shading 95% CI.

E-H) Total number (E&G) and proportion (F&H) of SARS-CoV-2 infections stratified by COVID-19 disease severity and SARS-CoV-2 RBD-binding total Ig (*n*=440)(E&F) or SARS-CoV-2 spike IFNγ T cell (*n*=98) (G&H) response status. 6-month post-V2, 12-month post-V1 and combined timepoints are shown. P values derived from Fisher's exact tests.

I&J) V2+28d RBD-binding total Ig (*n*=2,191) (I) and SARS-CoV-2 spike IFNγ T cell response (*n*=573) (J) stratified by COVID-19 infection/severity. Includes all non-hospitalised individuals with or without SARS-CoV-2 infection (infected and uninfected, non-hospitalised), SARS-CoV-2 infected individuals who were not hospitalised with COVID-19 (infected, non-hospitalised) and individuals who were hospitalised or died with COVID-19 (infected, hospitalised). P values derived from two-sided Mann–Whitney rank-sum test.

**P*<0.05, *****P*<0.0001.

serological response, and two of four (50%) individuals had no detectable T cell response (**Tables 3.7 & 3.8)**. The magnitude of V2+28d anti-SARS-CoV-2 RBD Ig and spike-specific T cells were each significantly reduced (Ig: P<0.0001, T cell: P=0.033) in patients with severe COVID-19 compared to mild disease **(Fig. 3.13I&J)**.

3.6.12.2 EASL COVID Hep 2.0 study

Of the 422 individuals with post second vaccine SARS-CoV-2 infection follow up in the EASL COVID-Hep 2.0 study **(Fig. 3.14A)**, 122 developed infection after at least two vaccine doses; 40 of 122 (33%) occurred between V2 and V3, 47 of 122 (39%) between V3 and V4 and 35 of 122 (29%) after V4 **(Fig. 3.14B)**. Due to variability in the prevalence of COVID-19 variants in different countries, I plotted the cumulative incidence of SARS-CoV-2 post-vaccine infections alongside the frequency of SARS-CoV-2 variants in the given country **(Fig. 3.14A)**. This identified that the majority (101 of 122, 83%) of breakthrough infections occurred after the emergence of Omicron as the dominant SARS-CoV-2 variant in each recruiting country. It also demonstrated a stepwise increase in breakthrough infection rate coinciding with the occurrence of a new dominant SARS-CoV-2 variant in each country. Most notably, the emergence of the BA.5 variant in Italy in July 2022 coincided with SARS-CoV-2 infections in

an additional 9.8% of Italy-based recruits **(Fig. 3.14A)**. Post-vaccine infection occurred in 51 of 181 (28%) LT recipients, 46 of 179 (26%) patients with cirrhosis, 18 of 47 (38%) with AIH and 8 of 35 (23%) with VLD, in individuals with available data **(Fig. 3.14B)**.

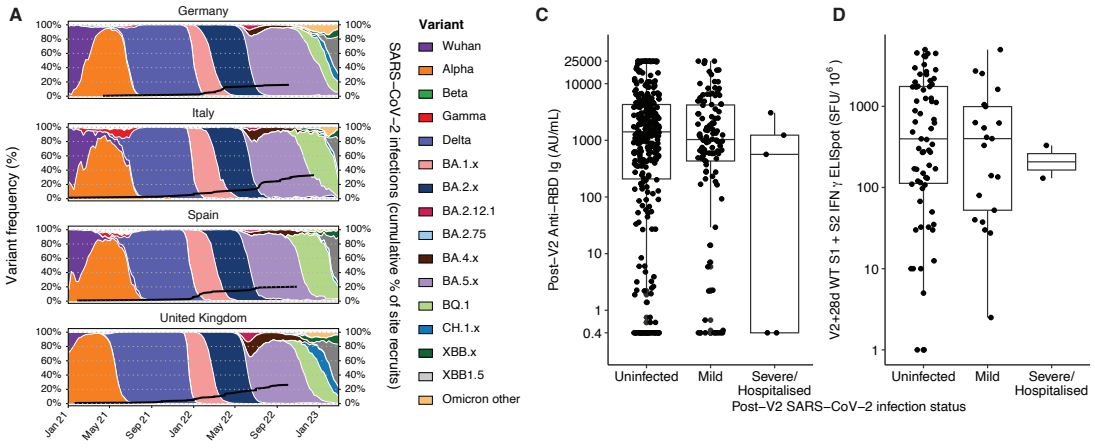

B

	Infection summary		COVID-19 severity	
	Uninfected (n = 320)	**Infected (n = 122)**	**Mild-moderate COVID-19 (n = 117)**	**Severe/ hospitalised (n = 5)**
Age*	60 (51, 68)	59 (49, 66)	60 (49, 66)	58 (54, 68)
Unknown	0	1	1	0
Sex (F)	137 (43%)	54 (44%)	53 (45%)	1 (20%)
Obesity				
No	206 (64%)	72 (59%)	70 (60%)	2 (40%)
Yes	70 (22%)	37 (30%)	35 (30%)	2 (40%)
Unknown	44 (14%)	13 (11%)	12 (10%)	1 (20%)
Disease type				
AIH	29 (9.1%)	18 (15%)	18 (15%)	0 (0%)
Cirr	133 (42%)	46 (38%)	45 (38%)	1 (20%)
LT	130 (41%)	51 (42%)	47 (40%)	4 (80%)
VLD	28 (8.8%)	7 (5.7%)	7 (6.0%)	0 (0%)
LT specific				
<2yr post-Tx	26/130 (20%)	5/51 (9.8%)	4/47 (8.5%)	1/4 (25%)
Immunosup. MMF	47 (36%)	17 (14%)	15 (32%)	2 (40%)
Child-Pugh score				
Non-cirrhotic	146 (50%)	66 (57%)	69 (59%)	4 (80%)
A	83 (29%)	38 (33%)	37 (32%)	1 (20%)
B	43 (15%)	9 (8%)	9 (7.7%)	0 (0%)
C	19 (6.5%)	2 (2%)	2 (1.7%)	0 (0%)
Infection timepoint				
Post-V2	-	40 (33%)	38 (32%)	2 (40%)
Post-V3	-	47 (39%)	47 (40%)	0 (0%)
Post-V4	-	35 (29%)	32 (27%)	3 (60%)
Time-post vaccination (days)*	-	143 (76, 218)	143 (72, 231)	142 (122,165)
Post-V2 anti-RBD serological status				
High	196 (70%)	91 (76%)	88 (77%)	3 (60%)
Low	50 (18%)	15 (12%)	15 (13%)	0 (0%)
No	36 (13%)	14 (12%)	12 (10%)	2 (40%)
Post-V2 anti-RBD Ig*	1,410 (208, 4,288)	1,020 (410, 3,718)	1,032 (432, 4,212)	565 (0, 1,234)
Unknown	16	2	2	0

Fig. 3.14 SARS-CoV-2 infection outcomes after two COVID-19 vaccines in the EASL COVID-Hep 2.0 study

A) Reported SARS-CoV-2 infection after second dose vaccine split across recruitment site countries. Frequency of SARS-CoV-2 and Omicron subvariants per country per week with cumulative proportion of infected individuals out of total individuals recruited at each site (black line).

B) Demographics and immunogenicity of cases with breakdown of severity (bottom panel).

C&D) Binding Ig to SARS-CoV-2 receptor binding domain (RBD) (n=359) (C) or WT S1+S2 IFNγ T cell responses (n=90) (D) at V2+28d timepoint in immunocompromised individuals, stratified by COVID-19 severity post-second vaccine.

Age* = Median and IQR. AIH, autoimmune hepatitis; Cirr, cirrhosis; LT, liver transplant; MMF, mycophenolate mofetil; VLD, vascular liver disease.

117 of 122 (96%) were mild-moderate (including asymptomatic and symptomatic) and 5 of 122 (4%) were severe (hospitalised cases). Of those with severe breakthrough COVID-19, 4 of 5 (80%) were LT recipients, two of whom were immunosuppressed with MMF and had absent anti-RBD responses at V2+28d (**Fig. 3.14B)**. Although the small sample size prevented robust statistical comparisons, the median post-V2 anti-RBD titre was numerically lower in those with severe COVID-19 compared to mild-moderate disease (565 AU/ml IQR [0-1,234] severe; 1,032 AU/ml mild-moderate [432-4,212]) (**Fig. 3.14C**) and did not differ between those that reported infections and those that did not. Two of five individuals with severe symptomatic breakthrough infection had PBMCs available at the post-V2 timepoint and had similar T cell responses to WT spike (163 SFU/10^6 PBMCs and 65 SFU/10^6 PBMCs) as other LT recipients (median 65 SFU/106 PBMCs) (**Fig. 3.14D).**

3.7 Discussion

In this chapter, I present immunogenicity and SARS-CoV-2 infection data from two large prospective observational studies and demonstrate the variability in immune responses and protection against severe COVID-19 induced by COVID-19 vaccines across different Sis groups. Analysis of anti-RBD Ig data from these studies identified that the majority of immunocompromised individuals developed antibody and/or T cell responses to COVID-19 vaccines – but that certain groups had a higher likelihood of vaccine immune non-responsiveness compared to healthy controls. Overall, two doses of an mRNA COVID-19 vaccine generated higher antibody titres compared to two doses of ChAdOx1 nCoV-19, but ChAdOx1 nCoV-19 induced significantly stronger V2+28d T cell responses in the OCTAVE study. T cell responses after two or three vaccine doses remained highly conserved between the original vaccine strain (WT SARS-CoV-2) and the Omicron BA.1 variant. In contrast, functional antibody analysis showed a substantial reduction in the binding and neutralising capacity of antibodies to SARS-CoV-2 VoC compared to WT after two vaccine doses in immunocompromised and healthy individuals. Among individuals with liver disease, a third

vaccine dose enhanced antibody cross-reactivity to VoC. Finally, analysis of SARS-CoV-2 infection data following two vaccine doses revealed that immunocompromised individuals with low antibody or T cell levels 28 days after vaccination faced a higher risk of severe COVID-19.

3.7.1 Vaccine-induced responses to SARS-CoV-2 across immunosuppressive diseases and SARS-CoV-2 variants

Many studies have now demonstrated the sub-optimal COVID-19 vaccine immune responses in cohorts of patients with SIs (*187-199, 271-275*). The OCTAVE and EASL COVID-Hep 2.0 made unique contributions to this knowledge by assessing responses to large numbers of individuals across multiple different immune-suppressive diseases in a robust manner, with uniform sampling timepoints and laboratory assays. This approach allowed us to assess the relative impact of chronic disease and immunosuppressive therapies on vaccine responsiveness and identify groups at particular risk of vaccine immune non-responsiveness.

Assessment of specific immunosuppressive therapeutics in liver transplant recipients identified that MMF use, in addition to CNI, was particularly associated with reduced anti-RBD Ig titres in this group. This was consistent with data from kidney transplant recipients (*276*) and supports evidence from other patient groups that short-term discontinuation or dose reductions of immunosuppressive therapy (including MMF) may improve antibody responses to vaccination (*277, 278*). Evaluation of draining lymph node fine-needle aspiration samples in healthy donors and kidney transplant recipients on CNI + MMF therapy demonstrated reduced lymph node T_{FH} and germinal centre memory B cells in these patients (*279*). The impact of these immunosuppressive agents on T cell signalling and expansion (*126, 280*) or direct impairment of B cell function (*281*) likely both contribute to the reduced antibody secretion observed here. Interestingly, comparison of AIH and LT recipients on high-dose MMF demonstrated that MMF alone did not significantly reduce anti-RBD Ig responses in AIH patients, suggesting that the combination of immunosuppressive agents and transplantation

was necessary for reduced antibody responses to COVID-19 vaccines in LT recipients.

Reassuringly for patient groups, a third dose of COVID-19 vaccination significantly boosted anti-RBD Ig responses and antibody cross-reactivity to SARS-CoV-2 VoC in all groups in the EASL COVID-Hep 2.0 study, including LT recipients. More recently other studies have demonstrated that the majority of LT recipients have detectable anti-SARS-CoV-2 Ig responses after four or five COVID-19 vaccine doses (*282*), indicating that booster doses of mRNA vaccines can overcome the impaired immunogenicity observed after two doses. In OCTAVE, there was a strong positive correlation between WT anti-RBD Ig titres and binding/neutralising SARS-CoV-2 VoC. Interestingly, individuals below 4000AU/mL failed to neutralise Omicron BA.1. In the EASL COVID-Hep 2.0 study, IgG VoC cross-reactivity was boosted in individuals with liver disease at V3+21d compared to V2+28d, but was not boosted in healthy controls. Together these data support the idea that a minimum threshold of binding antibody titres is required to have an antibody repertoire with sufficient breadth to cross-protect against SARS-CoV-2 variants (*283*). Above this threshold titre, the likelihood of having neutralising antibody titres to VoC is no longer increased and so antibody cross-reactivity is not increased.

In contrast to the antibody data, T cell cross-reactivity using whole spike antigens against Omicron was maintained, consistent with healthy individuals (*284*), but responses to pools of peptides specifically mutated in BA.1 demonstrated a slight reduction in IFNγ T cell magnitude. This incongruency is possibly due to technical limitations of the IFNγ ELISpot, whereby increased numbers of peptides in a single well (in the full spike vs the minipools) may reduce the specificity of the response by increasing bystander activation (*285*). Nevertheless, high levels of T cell cross-reactivity to SARS-CoV-2 variants continues to be observed with more recently emerged SARS-CoV-2 variants and after SARS-CoV-2 variant vaccination (*286, 287*).

3.7.2 SARS-CoV-2 vaccine platforms

In the OCTAVE study, two doses of BNT162b2 vaccine were associated with higher antibody titres but lower IFNγ T cell magnitudes when compared to ChAdOx1 nCoV-19 vaccination. This observation has also been described in healthy populations (*19, 69, 288-291*) and in other publications of vaccine immunogenicity in immunocompromised groups (*196, 292*). Why ChAd vaccines generate higher T cell but lower antibody responses than mRNA vaccines is unknown, but may relate to differences in the biodistribution and duration of antigen expression by each platform (*293, 294*).

It is possible the mechanisms of immunogenicity of each platform are variably impacted by immunosuppressive diseases/therapeutics. Early in the vaccination course, we identified that increased severity of cirrhosis (indicated by CP class and MELD score) was associated with lower antibody responses to mRNA but not ChAdOx1. Cirrhosis-associated immune dysfunction is associated with systemic inflammation and immune dysregulation (**Section 1.12.1**). It is possible that this inflammatory environment is particularly detrimental to mRNA vaccine immunogenicity because it is highly sensitive to interferon signalling (*48, 49*). A similar observation was made in auto-HSCT recipients, where neutralising antibody responses induced by ChAdOx1 nCoV-19 were better preserved between auto-HSCT and HC compared to those induced by mRNA vaccines (*295*). Further study of the pathways that impact mRNA but not ChAdOx1 immunogenicity may give insight into the differential mechanisms of immunogenicity by each platform.

Consistent with studies in healthy individuals (*64*), heterologous prime-boost of ChAdOx1 followed by mRNA COVID-19 vaccine boosted Ig titres in individuals with liver diseases to higher than those seen with homologous ChAdOx1, and comparable to homologous mRNA vaccination. This indicates that the combination of vaccine platforms may act synergistically to overcome dysregulated immune pathways in immunocompromised individuals.

3.7.3 Post-vaccine SARS-CoV-2 infection severity

Defining immunological parameters associated with vaccine-mediated protection against

infection is challenging as it necessitates the recruitment of large numbers of individuals, deployment of large-scale immunological assays and routine follow-up to assess infection outcomes. Several high-throughput methods for measurement of anti-SARS-CoV-2 binding (*296*) and neutralising antibodies (*297*) were developed in 2020, including the Roche Elecsys platform used to measure anti-RBD Ig in the studies in this chapter. However, measurement of vaccine-induced T cells at the scale required to assess correlates of protection is more difficult due to the requirement of peripheral blood processing facilities and relatively more complex laboratory procedures. As such, many studies in healthy individuals or in a limited number of immunocompromised individuals have reported solely on the association of binding or neutralisation with protection against SARS-CoV-2 infection (*267, 298-300*).

Some studies in healthy individuals have used IFNγ release assays on venous or capillary blood samples to assess SARS-CoV-2 induced T cell responses at scale and found association with SARS-CoV-2 infection (*268*). Studies of host genetics identified HLA polymorphisms that were associated with asymptomatic COVID-19 infection (HLA-B*15:01) and vaccine immunogenicity and protection against breakthrough COVID-19 infection (HLA-DQB1*06) – supporting direct and indirect roles for T cells in COVID-19 protection (*12, 301*). In the OCTAVE study the Oxford Immunotec IFNγ ELISpot assay was used on a large cohort of 674 individuals. This assay broadly correlated with the in-house ELISpot assay used to conduct T cell responses in the EASL COVID-Hep 2.0 study, but with reduced sensitivity (*302*), and facilitated assessment of the relationship between vaccine-induced T cell responses and SARS-CoV-2 infection outcomes in immunocompromised individuals for the first time.

Accurately assessing SARS-CoV-2 infection incidence is challenging, as SARS-CoV-2 infection is often asymptomatic (*303*) – and is therefore not systematically captured by self-reporting. Routine lab-confirmed PCR tests for SARS-CoV-2 infection is the gold standard for assessing protection against infection, but this approach is highly resource-intensive to employ at scale (*73, 304, 305*). In the OCTAVE and EASL COVID-Hep 2.0 studies we

captured symptomatic SARS-CoV-2 infection through patient interviews and systematic review of electronic patient records. In both studies, SARS-CoV-2 infection rates varied among disease subtypes and were higher in patients with no detectable antibody or T cells. However, infection rates cannot be confidently ascribed to disease phenotype, as social shielding behaviour and subsequently, SARS-CoV-2 exposure, are likely to have differed between groups. Due to limitations in the methods used to capture SARS-CoV-2 infection and confounding differences in SARS-CoV-2 exposure, infection rates should be interpreted cautiously in these studies.

Nevertheless, COVID-19 severity in the reported infections was systematically captured and therefore could be correlated with vaccine immunogenicity measures. Most individuals in OCTAVE and EASL studies had asymptomatic or mild infection, but a substantial number (33 of 440 in OCTAVE, 5 of 122 in EASL) had severe disease and 15 patients in OCTAVE died of COVID-19. Failure to seroconvert and the magnitude of the serological and cellular response to prior COVID-19 vaccination were each associated with severe disease. However, one quarter of patients with severe disease seroconverted and had antibody levels similar to healthy controls, highlighting that other factors contribute to disease susceptibility—for example, disease phenotype and/or comorbidities. Notably, study participants likely had additional COVID-19 vaccines (third and fourth doses) during the SARS-CoV-2 infection follow-up period and immunogenicity data following these vaccines was not available. Despite the incomplete capture of immunogenicity data on intervening vaccine doses, the fact that V2+28d vaccine immunogenicity was associated with future COVID-19 severity suggests that the immunogenicity measurement after the second dose has lasting relevance to COVID-19 outcomes.

3.7.4 Limitations

There are some limitations to both the OCTAVE and EASL studies. Due to the rapid delivery of the vaccination programme in vulnerable groups, baseline data were incomplete. For both

studies, healthy control data were generated from samples recruited separately in the PITCH cohort of health care workers that were generally younger with fewer comorbidities than the diseased population. To improve comparability, studies used standardised timepoints and procedures, and healthy controls in the OCTAVE study were matched to study participants for age and sex. In EASL, multivariable models which account for age and sex were employed to address such potential confounding factors.

As observational studies, there was no randomisation of vaccines within groups and in the EASL study certain vaccine platforms in particular groups were lacking, including mRNA-1273-vaccinated HCs, third dose of ChAdOx1 in HCs, and ChAdOx1-or BNT162b2-vaccinated patients with VLD. Furthermore, we only assessed vaccine immunogenicity after one, two or three COVID-19 vaccines, whereas most vulnerable individuals have now had multiple vaccine doses.

Assessment of T cell immunogenicity only by IFNγ ELISpot is limited as it gives only a single measure of T cell function and does not give insight into the phenotype or clonality of T cells. In the context of immunosuppressive disease, these factors are likely highly influential in the outcome of vaccine-induced T cell responses. However, as this chapter aimed to assess T cell responses between a large number of individuals, the relative scalability of the IFNγ ELISpot assay (*306*) made it the most suitable available approach.

Finally, in the SARS-CoV-2 infection follow-up data, it remains impossible to account for important confounding variables such as local SARS-CoV-2 prevalence, viral load exposure, further vaccine doses, and individual patient behaviours including shielding measures. Furthermore, we were unable to systematically collect accurate data on the use of antiviral medications and recombinant antibodies due to incomplete documentation in electronic hospital records and geographic variability in access to these agents.

3.8 Conclusions

In conclusion, although the majority of immunocompromised individuals generated antigen-

specific antibody or T cell responses to two or three doses of COVID-19 vaccines, some immunocompromised groups were enriched for individuals with no or low vaccine-induced immune response. mRNA vaccines were associated with the generation of higher anti-SARS-CoV-2 antibody titres but lower magnitudes of IFNγ producing T cells compared to ChAdOx1 nCoV-19 in immunocompromised individuals. COVID-19 vaccine induced T cells, but not antibodies, maintained responsiveness to SARS-CoV-2 variants of concern. An ability to seroconvert and increased magnitudes of serological and cellular responses at 28 days following a second COVID-19 vaccine dose were associated with less severe COVID-19 after vaccination.

3.9 Tables

Table 3.1 Demographics of the OCTAVE study

	HC (236)		SC (112)		HM (33)		AAV (35)		IA (707)		HD (211)		HD on IS (36)		K-Tr (743)		L-Tr (83)		L-AI (73)		L-Cir (126)		CD (170)		UC (115)		IBD-U (5)		Auto-HSCT (43)		Allo-HSCT (145)		CAR-T (8)		Total (2,881)	
Sex																																		
Male	104	(44%)	9	(8%)	21	(64%)	19	(54%)	236	(33%)	119	(56%)	20	(56%)	474	(64%)	52	(63%)	24	(33%)	68	(54%)	97	(57%)	70	(61%)	3	(60%)	26	(60%)	83	(57%)	5	(63%)	1430	(50%)
Female	132	(56%)	103	(92%)	12	(36%)	16	(46%)	470	(66%)	92	(44%)	16	(44%)	269	(36%)	31	(37%)	49	(67%)	58	(46%)	73	(43%)	45	(39%)	2	(40%)	17	(40%)	62	(43%)	3	(38%)	1450	(50%)
Unknown	0	(0%)	0	(0%)	0	(0%)	0	(0%)	1	(0%)	0	(0%)	0	(0%)	0	(0%)	0	(0%)	0	(0%)	0	(0%)	0	(0%)	0	(0%)	0	(0%)	0	(0%)	0	(0%)	0	(0%)	1	(0%)
Age (years)																																		
15–44	22	(9%)	24	(21%)	2	(6%)	10	(29%)	130	(18%)	18	(9%)	5	(14%)	153	(21%)	17	(20%)	10	(14%)	8	(6%)	113	(66%)	69	(60%)	5	(100%)	4	(9%)	42	(29%)	4	(50%)	636	(22%)
45–64	63	(27%)	55	(49%)	19	(58%)	17	(49%)	393	(56%)	61	(29%)	19	(53%)	361	(49%)	39	(47%)	39	(53%)	65	(52%)	54	(32%)	38	(33%)	0	(0%)	22	(51%)	72	(50%)	4	(50%)	1321	(46%)
65–74	101	(43%)	24	(21%)	9	(27%)	4	(11%)	152	(21%)	58	(27%)	9	(25%)	172	(23%)	23	(28%)	19	(26%)	45	(36%)	3	(2%)	6	(5%)	0	(0%)	16	(37%)	30	(21%)	0	(0%)	671	(23%)
75+	50	(21%)	9	(8%)	3	(9%)	4	(11%)	32	(5%)	73	(35%)	3	(8%)	57	(8%)	4	(5%)	5	(7%)	8	(6%)	0	(0%)	2	(2%)	0	(0%)	1	(2%)	1	(1%)	0	(0%)	252	(9%)
Unknown	0	(0%)	0	(0%)	0	(0%)	0	(0%)	0	(0%)	1	(0%)	0	(0%)	0	(0%)	0	(0%)	0	(0%)	0	(0%)	0	(0%)	0	(0%)	0	(0%)	0	(0%)	0	(0%)	0	(0%)	1	(0%)
Ethnicity																																		
White	193	(82%)	84	(75%)	26	(79%)	28	(80%)	625	(88%)	50	(24%)	14	(39%)	319	(43%)	76	(92%)	61	(84%)	116	(92%)	159	(94%)	104	(90%)	5	(100%)	40	(93%)	131	(90%)	7	(88%)	2038	(71%)
Black	11	(5%)	7	(6%)	2	(6%)	0	(0%)	4	(1%)	54	(26%)	6	(17%)	59	(8%)	2	(2%)	0	(0%)	1	(1%)	1	(1%)	1	(1%)	0	(0%)	1	(2%)	1	(1%)	0	(0%)	150	(5%)
Asian	16	(7%)	1	(1%)	2	(6%)	1	(3%)	10	(1%)	96	(45%)	14	(39%)	308	(41%)	1	(1%)	10	(14%)	4	(3%)	7	(4%)	5	(4%)	0	(0%)	1	(2%)	2	(1%)	1	(13%)	479	(17%)
Mixed/ Other	12	(5%)	17	(15%)	1	(3%)	2	(6%)	20	(3%)	9	(4%)	1	(3%)	36	(5%)	3	(4%)	2	(3%)	3	(2%)	3	(2%)	3	(3%)	0	(0%)	0	(0%)	4	(3%)	0	(0%)	116	(4%)
Not known	4	(2%)	3	(3%)	2	(6%)	4	(11%)	48	(7%)	2	(1%)	1	(3%)	21	(3%)	1	(1%)	0	(0%)	2	(2%)	0	(0%)	2	(2%)	0	(0%)	1	(2%)	7	(5%)	0	(0%)	98	(3%)
BMI																																		
Under weight	1	(0%)	1	(1%)	0	(0%)	0	(0%)	10	(1%)	8	(4%)	1	(3%)	3	(0%)	0	(0%)	3	(4%)	0	(0%)	6	(4%)	4	(3%)	0	(0%)	0	(0%)	6	(4%)	1	(13%)	44	(2%)
Healthy weight	14	(6%)	31	(28%)	11	(33%)	7	(20%)	163	(23%)	35	(17%)	4	(11%)	62	(8%)	30	(36%)	24	(33%)	25	(20%)	92	(54%)	54	(47%)	5	(100%)	15	(35%)	57	(39%)	2	(25%)	631	(22%)
Overweight	7	(3%)	20	(18%)	10	(30%)	8	(23%)	261	(37%)	32	(15%)	4	(11%)	81	(11%)	26	(31%)	28	(38%)	34	(27%)	39	(23%)	39	(34%)	0	(0%)	14	(33%)	42	(29%)	4	(50%)	649	(23%)
Obese	1	(0%)	28	(25%)	10	(30%)	15	(43%)	257	(36%)	42	(20%)	4	(11%)	71	(10%)	26	(31%)	14	(19%)	60	(48%)	28	(16%)	14	(12%)	0	(0%)	10	(23%)	20	(14%)	0	(0%)	600	(21%)
Unknown	5	(2%)	32	(29%)	2	(6%)	5	(14%)	16	(2%)	94	(45%)	23	(64%)	526	(71%)	1	(1%)	4	(5%)	7	(6%)	5	(3%)	4	(3%)	0	(0%)	4	(9%)	20	(14%)	1	(13%)	749	(26%)
Data unavailable	208	(88%)	0	(0%)	0	(0%)	0	(0%)	0	(0%)	0	(0%)	0	(0%)	0	(0%)	0	(0%)	0	(0%)	0	(0%)	0	(0%)	0	(0%)	0	(0%)	0	(0%)	0	(0%)	0	(0%)	208	(7%)
Prior COVID																																		
No confirmed infection	198	(84%)	95	(85%)	30	(91%)	33	(94%)	637	(90%)	106	(50%)	23	(64%)	692	(93%)	76	(92%)	69	(95%)	111	(88%)	154	(91%)	101	(88%)	5	(100%)	36	(84%)	112	(77%)	5	(63%)	2483	(86%)
Yes	38	(16%)	17	(15%)	3	(9%)	2	(6%)	70	(10%)	105	(50%)	13	(36%)	51	(7%)	7	(8%)	4	(5%)	15	(12%)	16	(9%)	14	(12%)	0	(0%)	7	(16%)	33	(23%)	3	(38%)	398	(14%)
Vaccine type																																		
ChAdOx nCoV-19	156	(66%)	44	(39%)	19	(58%)	33	(94%)	591	(84%)	127	(60%)	29	(81%)	326	(44%)	62	(75%)	52	(71%)	93	(74%)	140	(82%)	99	(86%)	3	(60%)	37	(86%)	61	(42%)	4	(50%)	1876	(65%)
BNT162b2	80	(34%)	61	(54%)	13	(39%)	2	(6%)	116	(16%)	84	(40%)	7	(19%)	410	(55%)	21	(25%)	21	(29%)	33	(26%)	30	(18%)	16	(14%)	2	(40%)	5	(12%)	70	(48%)	4	(50%)	975	(34%)
mRNA1273	0	(0%)	1	(1%)	0	(0%)	0	(0%)	0	(0%)	0	(0%)	0	(0%)	0	(0%)	0	(0%)	0	(0%)	0	(0%)	0	(0%)	0	(0%)	0	(0%)	0	(0%)	2	(1%)	0	(0%)	3	(0%)
Unknown	0	(0%)	6	(5%)	1	(3%)	0	(0%)	0	(0%)	0	(0%)	0	(0%)	7	(1%)	0	(0%)	0	(0%)	0	(0%)	0	(0%)	0	(0%)	0	(0%)	1	(2%)	12	(8%)	0	(0%)	27	(1%)
Smoking status																																		
Never smoked	20	(8%)	26	(23%)	14	(42%)	15	(43%)	369	(52%)	41	(19%)	7	(19%)	163	(22%)	45	(54%)	34	(47%)	40	(32%)	96	(56%)	69	(60%)	4	(80%)	7	(16%)	47	(32%)	6	(75%)	1003	(35%)
Previous smoker	1	(0%)	18	(16%)	2	(6%)	8	(23%)	255	(36%)	17	(8%)	2	(6%)	37	(5%)	28	(34%)	25	(34%)	55	(44%)	49	(29%)	30	(26%)	0	(0%)	4	(9%)	27	(19%)	1	(13%)	559	(19%)
Current smoker	0	(0%)	7	(6%)	0	(0%)	4	(11%)	72	(10%)	12	(6%)	0	(0%)	10	(1%)	2	(2%)	10	(14%)	23	(18%)	23	(14%)	13	(11%)	1	(20%)	0	(0%)	4	(3%)	0	(0%)	181	(6%)
Diabetes																																		
No	24	(10%)	101	(90%)	31	(94%)	27	(77%)	641	(91%)	107	(51%)	22	(61%)	473	(64%)	66	(80%)	59	(81%)	71	(56%)	165	(97%)	113	(98%)	5	(100%)	37	(86%)	138	(95%)	8	(100%)	2088	(72%)
Yes	0	(0%)	6	(5%)	2	(6%)	7	(20%)	62	(9%)	104	(49%)	14	(39%)	269	(36%)	17	(20%)	14	(19%)	55	(44%)	5	(3%)	2	(2%)	0	(0%)	4	(9%)	6	(4%)	0	(0%)	567	(20%)
Not known	4	(2%)	5	(4%)	0	(0%)	1	(3%)	4	(1%)	0	(0%)	0	(0%)	1	(0%)	0	(0%)	0	(0%)	0	(0%)	0	(0%)	0	(0%)	0	(0%)	2	(5%)	1	(1%)	0	(0%)	18	(1%)
Data unavailable	208	(88%)	0	(0%)	0	(0%)	0	(0%)	0	(0%)	0	(0%)	0	(0%)	0	(0%)	0	(0%)	0	(0%)	0	(0%)	0	(0%)	0	(0%)	0	(0%)	0	(0%)	0	(0%)	0	(0%)	208	(7%)

Table 3.2 Demographics of EASL COVID-Hep 2.0 Study

	LT (n = 257)	AIH (n = 74)	Cirr (n = 355)	VLD (n = 36)	HC (n = 127)	Total (N = 849)
Age (years, IQR)	60 (50-67)	61 (49-69)	62 (55-69)	46 (40-49)	36 (25-45)	58 (46-66)
Unknown	2 (0.8%)	0 (0%)	2 (0.6%)	0 (0%)	1 (0.8%)	5 (0.5%)
Sex						
Female	98 (38%)	61 (82%)	123 (35%)	15 (42%)	86 (68%)	383 (45%)
Male	159 (62%)	13 (18%)	232 (65%)	21 (58%)	40 (31%)	465 (55%)
Unknown	0 (0%)	0 (0%)	0 (0%)	0 (0%)	1 (0.8%)	1 (0.1%)
Ethnicity						
Asian	1 (0.4%)	5 (6.8%)	7 (2.0%)	0 (0%)	16 (13%)	29 (3.4%)
Black	2 (0.8%)	0 (0%)	8 (2.3%)	1 (2.8%)	1 (0.8%)	12 (1.4%)
Other	3 (1.2%)	2 (2.7%)	7 (2.0%)	4 (11%)	4 (3.1%)	20 (2.4%)
White	132 (51%)	65 (88%)	293 (83%)	31 (86%)	84 (66%)	605 (71%)
Unknown	119 (46%)	2 (2.7%)	40 (11%)	0 (0%)	22 (17%)	183 (22%)
Obesity						
No	156 (61%)	51 (69%)	220 (62%)	31 (86%)	82 (65%)	540 (64%)
Yes	49 (19%)	14 (19%)	116 (33%)	4 (11%)	5 (3.9%)	188 (22%)
Unknown	52 (20%)	9 (12%)	19 (5.4%)	1 (2.8%)	40 (31%)	121 (14%)
Smoking status						
Never smoked	227 (88%)	44 (59%)	188 (53%)	25 (69%)	117 (92%)	601 (71%)
Previously smoked	28 (11%)	22 (30%)	107 (30%)	2 (5.6%)	10 (7.9%)	169 (20%)
Currently smoke	2 (0.8%)	8 (11%)	60 (17%)	9 (25%)	0 (0%)	79 (9.3%)
Diabetes						
Yes	25 (9.7%)	10 (14%)	102 (29%)	2 (5.6%)	0 (0%)	139 (17%)
Hypertension						
Yes	87 (34%)	12 (16%)	136 (38%)	0 (0%)	3 (2.9%)	238 (29%)
Prior SARS-CoV-2 infection						
No confirmed infection	241 (94%)	68 (92%)	307 (86%)	30 (83%)	87 (69%)	733 (86%)
Previously infected	16 (6.2%)	6 (8.2%)	48 (14%)	6 (17%)	40 (31%)	116 (14%)
Vaccine type - dose 1						
ChAdOx1 nCoV-19	73 (28%)	38 (51%)	112 (32%)	0 (0%)	39 (31%)	262 (31%)
BNT162b2	175 (68%)	23 (31%)	176 (50%)	0 (0%)	87 (69%)	461 (54%)
mRNA-1273	7 (2.7%)	13 (18%)	64 (18%)	36 (100%)	1 (0.8%)	121 (14%)
Unknown	2 (0.8%)	0 (0%)	3 (0.8%)	0 (0%)	0 (0%)	5 (0.6%)
Vaccine type - dose 2						
ChAdOx1 nCoV-19	66 (26%)	37 (50%)	104 (29%)	0 (0%)	39 (31%)	246 (29%)
BNT162b2	180 (70%)	22 (30%)	180 (51%)	0 (0%)	87 (69%)	469 (55%)
mRNA-1273	9 (3.5%)	14 (19%)	64 (18%)	33 (92%)	1 (0.8%)	121 (14%)
Unknown	2 (0.8%)	1 (1.4%)	7 (2.0%)	3 (8.3%)	0 (0%)	13 (1.5%)
Vaccine type - dose 3*						
BNT162b2	88 (85%)	4 (24%)	70 (52%)	0 (0%)	25 (89%)	187 (61%)
mRNA-1273	9 (8.7%)	13 (76%)	61 (46%)	24 (100%)	3 (11%)	110 (36%)
Unknown	7 (6.7%)	0 (0%)	3 (2.2%)	0 (0%)	0 (0%)	10 (3.3%)
<2 years post LT						
Yes	37 (14%)	—	—	—	—	—
Indication for LT						
Acute liver failure	21 (8%)	—	—	—	—	—
Decompensated cirrhosis	99 (39%)	—	—	—	—	—
HCC	33 (13%)	—	—	—	—	—
Other	40 (16%)	—	—	—	—	—
Unknown	64 (25%)	—	—	—	—	—
IS						
Azathioprine	16 (6.2%)	21 (29%)	2 (0.6%)	—	—	—
Sirolimus	6 (2.3%)	0 (0%)	—	—	—	—
Everolimus	44 (17%)	0 (0%)	—	—	—	—
6-MP	5 (1.9%)	27 (37%)	1 (0.3%)	—	—	—
MMF	79 (31%)	9 (12%)	1 (0.3%)	1 (3%)	—	—
MTX	—	—	2 (0.6%)	—	—	—
Corticosteroids	50 (19%)	33 (43%)	1 (0.3%)	1 (3%)	—	—
Ciclosporin	41 (16%)	0 (0%)	—	—	—	—
Tacrolimus	195 (76%)	6 (8.2%)	—	—	—	—
No. IS therapies						
0	3 (1.2%)	8 (11%)	—	—	—	—
1	95 (37%)	36 (49%)	—	—	—	—
2	132 (51%)	23 (32%)	—	—	—	—
3	27 (11%)	6 (8.2%)	—	—	—	—
IS combinations						
CNI only	81 (32%)	—	—	—	—	—
mTori only	13 (5.1%)	—	—	—	—	—

(continued on next page)

6-MP, 6-mercaptopurine; AIH, autoimmune hepatitis; ALD, alcohol-related liver disease; BCS, Budd-Chiari syndrome; Cirr, cirrhosis; CNI, calcineurin inhibitor; HCs, healthy controls; HCC, hepatocellular carcinoma; IS, immunosuppression; LT, liver transplant; MMF, mycophenolate mofetil; mTORi, mTOR inhibitor; MTX, methotrexate; NAFLD, non- alcoholic fatty liver disease; NCPVT, non-cirrhotic non-tumoral portal vein thrombosis; PBC, primary biliary cholangitis; PSC, primary sclerosing cholangitis; PSVD, porto- sinusoidal vascular disorder; VLD, vascular liver disease. *Numbers only given for individuals with third dose anti-RBD Ig titre data available.

Table 3.3 Demographics of EASL COVID-Hep 2.0 Study (continued)

	LT (n = 257)	AIH (n = 74)	Cirr (n = 355)	VLD (n = 36)	HC (n = 127)	Total (N = 849)
CNI + MMF (+/- other)	79 (31%)	—	—	—	—	—
CNI + other (+/- other)	81 (32%)	—	—	—	—	—
Cirrhosis severity						
MELD score (median, IQR)	—	—	7.25 (6.67, 8.43)	—	—	—
Unknown	—	—	60 (17%)	—	—	—
Child-Pugh class						
A	—	19 (26%)	232 (65%)	—	—	—
B	—	2 (2.7%)	82 (23%)	—	—	—
C	—	1 (1.4%)	31 (8.7%)	—	—	—
No cirrhosis	—	52 (70%)	0 (0%)	—	—	—
Unknown	—	—	10 (2.8%)	—	—	—
Cirrhosis aetiology						
NAFLD	—	1 (5%)	98 (28%)	—	—	—
ALD	—	1 (5%)	152 (43%)	—	—	—
HCV	—	2 (9%)	80 (22%)	—	—	—
HBV	—	1 (5%)	24 (6.7%)	—	—	—
PBC	—	2 (9%)	12 (2.8%)	—	—	—
PSC	—	2 (9%)	12 (3.1%)	—	—	—
Unknown	—	15 (68%)	33 (9.3%)	—	—	—
VLD aetiology						
NCPVT	—	—	—	16 (44%)	—	—
BCS	—	—	—	9 (25%)	—	—
PSVD	—	—	—	11 (31%)	—	—

6-MP, 6-mercaptopurine; AIH, autoimmune hepatitis; ALD, alcohol-related liver disease; BCS, Budd-Chiari syndrome; Cirr, cirrhosis; CNI, calcineurin inhibitor; HCs, healthy controls; HCC, hepatocellular carcinoma; IS, immunosuppression; LT, liver transplant; MMF, mycophenolate mofetil; mTORi, mTOR inhibitor; MTX, methotrexate; NAFLD, non- alcoholic fatty liver disease; NCPVT, non-cirrhotic non-tumoral portal vein thrombosis; PBC, primary biliary cholangitis; PSC, primary sclerosing cholangitis; PSVD, porto- sinusoidal vascular disorder; VLD, vascular liver disease. *Numbers only given for individuals with third dose anti-RBD Ig titre data available.

Table 3.4 Comparison of vaccine response over multiple vaccine doses

In SARS-CoV-2 infection naïve individuals, Roche anti-RBD antibody response to one, two and three doses of COVID-19 vaccine, separated by vaccine type and disease group.1 comparison of Baseline and Pre-V2, 2 comparison of Pre-V2 and Post-V2, 3 comparison of Post-V2 and Pre-V3, 4 comparison of Pre-V3 and Post-V3, 4 comparison of Post-V2 and Post-V3. Kruskal Wallis with Dunn's post-hoc test, adjusted for multiple comparisons using Bonferroni correction. Cir = Cirrhosis, AIH = Autoimmune hepatitis, LT = Liver transplant, Az = AstraZeneca vaccine

		Baseline		Post-V1			Post-V2			Pre-V3			Post-V3			
Vaccine Type	Disease group	N	Median (IQR)	N	Median (IQR)	P val[1]	N	Median (IQR)	Pval[2]	N	Median (IQR)	P val[3]	N	Median (IQR)	P val[4]	P val[5]
ChAdOx1	Cirr	15	0.4 (0.4-0.4)	34	19.6 (3.3-37.1)	1	85	1106 (395-1838)	$7.2x10^{-11}$	4	637 (281-6956)	1	6	15368 (11784-22791)	1	0.3
	AIH	6	0.4 (0.4-0.4)	20	15.1 (1.6-41.9)	1	34	498 (129-1323)	$4.3x10^{-4}$	2	312 (237-387)	1	3	15401 (11133-20201)	1	1
	LT	6	0.4 (0.4-0.4)	27	0.4 (0.4-19.0)	1	52	63 (0.4-608)	0.1	2	151 (133-170)	1	2	3133 (1572-4694)	1	1
	HC	-	-	10	187.5 (87.0-392)	N/A	20	1198 (855-1546)	0.02	-	-	N/A	-	-	N/A	N/A
mRNA	Cirr	156	0.4 (0.4-0.4)	153	13.3 (2.5-55.6)	$9.2x10^{-11}$	204	1413.5 (578-4140)	$6.6x10^{-23}$	52	476 (214-958)	0.35	102	18015 (5927-25000)	$1.5x10^{-8}$	$2.2x10^{-6}$
	AIH	19	0.4 (0.4-0.4)	19	16.6 (1.8-71.6)	0.87	33	1341 (577-4605)	0.002	11	815 (316-2035)	1	10	18280.5 (13784-25000)	0.73	1
	LT	117	0.4 (0.4-0.4)	119	0.4 (0.4-1.6)	0.09	179	114 (0.4-1113)	$2.9x10^{-13}$	105	92 (7-390)	1	95	1861 (34-13534)	0.003	$9.4x10^{-5}$
	VLD	30	0.4 (0.4-0.4)	29	147 (116-203)	0.10	27	4880 (3203-7663)	$4.7x10^{-4}$	25	1943 (1441-2907)	1	24	25000 (25000-25000)	0.002	0.1
	HC	-	-	27	98.7 (57.2-148)	N/A	35	15634 (10829-21445)	$3.2x10^{-11}$	22	2171 (1584-3416)	0.007	23	25000 (18359-25000)	$2.1x10^{-5}$	1

Table 3.5 Comparison of vaccine responses between liver disease groups

In infection naïve individuals, comparison of Roche anti-RBD antibody response across disease groups at post-V2 and post-V3. Comparisons at post-v3 in AstraZeneca vaccinated individuals not made due to low n numbers. Kruskal Wallis with Dunn's post-hoc test, adjusted for multiple comparisons using Benjamini Hochberg. Cir = Cirrhosis, AIH = Autoimmune hepatitis, LT = Liver transplant, Az = AstraZeneca vaccine. * indicates statistical significance (P<0.05)

	Comparison groups		Timepoints	
	Group 1	Group 2	Post-V2 (p val)	Post-V3 (p val)
AstraZeneca	Cirr	AIH	0.06	-
	Cirr	LT	2.00E-08*	-
	Cirr	HC	0.57	-
	AIH	LT	0.01*	-
	AIH	HC	0.06	-
	LT	HC	0.000017*	-
mRNA	Cirr	AIH	0.69	0.50999
	Cirr	LT	2.00E-15*	1.98E-08*
	Cirr	VLD	0.0039*	0.00031*
	Cirr	HC	1.30E-10*	0.06007
	AIH	LT	3.40E-06*	0.00219*
	AIH	VLD	0.05	0.12800
	AIH	HC	5.96E-06*	0.57498
	LT	VLD	5.90E-12*	9.10E-13*
	LT	HC	1.28E-27*	1.6641E-07*
	VLD	HC	0.03*	0.23352

Table 3.6 Rates of antibody responsiveness across liver disease groups and healthy controls

In infection naïve individuals, comparison of Roche anti-RBD antibody response rate across disease groups at post-V2 and post-V3. Seropositive defined as >0.8AU/mL by anti-RBD Ig assay. Cir = Cirrhosis, AIH = Autoimmune hepatitis, LT = Liver transplant, VLD = Vascular liver disease; HC = healthy control

Disease group	Vaccine platform	Timepoint	Seronegative (%)	Seropositive (%)
Cir	ChAdOx1	Post-V1	4 (12%)	30 (88%)
		Post-V2	-	85 (100%)
		Post-V3	-	6 (100%)
	mRNA	Post-V1	20 (13%)	133 (87%)
		Post-V2	4 (2%)	200 (98%)
		Post-V3	2 (2%)	100 (98%)
LT	ChAdOx1	Post-V1	14 (52%)	13 (48%)
		Post-V2	18 (35%)	34 (65%)
		Post-V3	-	2 (100%)
	mRNA	Post-V1	80 (67%)	39 (33%)
		Post-V2	52 (29%)	127 (71%)
		Post-V3	9 (9%)	86 (91%)
AIH	ChAdOx1	Post-V1	4 (20%)	16 (80%)
		Post-V2	2 (6%)	32 (94%)
		Post-V3	-	3 (100%)
	mRNA	Post-V1	4 (21%)	15 (79%)
		Post-V2	-	33 (100%)
		Post-V3	-	10 (100%)
VLD	mRNA	Post-V1	1 (3%)	28 (97%)
		Post-V2	-	27 (100%)
		Post-V3	-	24 (100%)
HC	ChAdOx1	Post-V1	-	10 (100%)
		Post-V2	-	20 (100%)
		Post-V3	-	-
	mRNA	Post-V1	-	27 (100%)
		Post-V2	-	35 (100%)
		Post-V3	-	23 (100%)

Table 3.7 Rates of SARS-CoV-2 infection after COVID-19 vaccination in OCTAVE cohort, separated by antibody and T cell responsiveness

Summary of SARS-CoV-2 infections reported in combined follow-up periods after COVID-19 vaccination for all immunocompromised patients in OCTAVE, split by disease subgroup and based on Roche anti-RBD Ig assay result ≥0.8 AU ml^{-1}, low response <380 AU ml^{-1} and high response >380 AU mL^{-1} and IFNγ T cell responsiveness at the post-V2 timepoint. # (%) of total OCTAVE infections.

				SARS-CoV-2 infection (Whole OCTAVE cohort)																
	Follow-up period	Responder status	Infection status	SC	HM	AAV	IA	HD	HD on IS	K-Tr	L-Tr	L-AI	L-Cirr	CD	UC	IBD-U	Auto-HSCT	Allo-HSCT	CAR-T	OCTAVE
Serology breakdown	<6months post-V2	No response	Not Infected	0 (0%)	1 (50%)	1 (5%)	7 (28%)	7 (88%)	5 (83%)	128 (91%)	1 (5%)	1 (20%)	-	-	-	0 (0%)	0 (0%)	6 (46%)	0 (0%)	157 (62%)
			Infected	1 (33%)	0 (0%)	1 (5%)	1 (4%)	0 (0%)	0 (0%)	9 (6%)	0 (0%)	0 (0%)	-	-	-	0 (0%)	0 (0%)	2 (15%)	2 (50%)	16 (6%)
			Uk/NA	2 (67%)	1 (50%)	19 (90%)	17 (68%)	1 (13%)	1 (17%)	3 (2%)	19 (95%)	4 (80%)	-	-	-	1 (100%)	5 (100%)	5 (38%)	2 (50%)	80 (32%)
			Total#	3 (1%)	2 (1%)	21 (8%)	25 (10%)	8 (3%)	6 (2%)	140 (55%)	20 (8%)	5 (2%)	0 (0%)	0 (0%)	0 (0%)	1 (0%)	5 (2%)	13 (5%)	4 (2%)	253
		Low response	Not infected	3 (19%)	5 (71%)	0 (0%)	72 (35%)	31 (91%)	6 (86%)	131 (95%)	1 (4%)	1 (5%)	1 (6%)	11 (19%)	4 (17%)	0 (0%)	2 (33%)	15 (48%)	0 (0%)	283 (47%)
			Infected	1 (6%)	0 (0%)	0 (0%)	10 (5%)	1 (3%)	0 (0%)	5 (4%)	0 (0%)	2 (10%)	0 (0%)	2 (4%)	0 (0%)	0 (0%)	0 (0%)	5 (16%)	0 (0%)	26 (4%)
			Uk/NA	12 (75%)	2 (29%)	4 (100%)	125 (60%)	2 (6%)	1 (14%)	2 (1%)	26 (96%)	18 (86%)	16 (94%)	44 (77%)	20 (83%)	1 (100%)	4 (67%)	11 (35%)	1 (100%)	289 (48%)
			Total#	16 (3%)	7 (1%)	4 (1%)	207 (35%)	34 (6%)	7 (1%)	138 (23%)	27 (5%)	21 (4%)	17 (3%)	57 (10%)	24 (4%)	1 (0%)	6 (1%)	31 (5%)	1 (0%)	598
		High response	Not Infected	60 (76%)	11 (61%)	3 (100%)	409 (89%)	147 (95%)	16 (94%)	172 (97%)	17 (50%)	32 (76%)	66 (65%)	55 (56%)	54 (67%)	2 (67%)	19 (90%)	30 (59%)	2 (100%)	1095 (82%)
			Infected	7 (9%)	1 (6%)	0 (0%)	25 (5%)	3 (2%)	0 (0%)	4 (2%)	3 (9%)	1 (2%)	5 (5%)	13 (13%)	5 (6%)	0 (0%)	1 (5%)	3 (6%)	0 (0%)	71 (5%)
			Uk/NA	12 (15%)	6 (33%)	0 (0%)	23 (5%)	4 (3%)	1 (6%)	2 (1%)	14 (41%)	9 (21%)	30 (30%)	31 (31%)	22 (27%)	1 (33%)	1 (5%)	18 (35%)	0 (0%)	174 (13%)
			Total#	79 (6%)	18 (1%)	3 (0%)	457 (34%)	154 (11%)	17 (1%)	178 (13%)	34 (3%)	42 (3%)	101 (8%)	99 (7%)	81 (6%)	3 (0%)	21 (2%)	51 (4%)	2 (0%)	1,340
		Overall	Not Infected	63 (64%)	17 (63%)	4 (14%)	488 (71%)	185 (94%)	27 (90%)	431 (95%)	19 (23%)	34 (50%)	67 (57%)	66 (42%)	58 (55%)	2 (40%)	21 (66%)	51 (54%)	2 (29%)	1535 (70%)
			Infected	9 (9%)	1 (4%)	1 (4%)	36 (5%)	4 (2%)	0 (0%)	18 (4%)	3 (4%)	3 (4%)	5 (4%)	15 (10%)	5 (5%)	0 (0%)	1 (3%)	10 (11%)	2 (29%)	113 (5%)
			Uk/NA	26 (27%)	9 (33%)	23 (82%)	165 (24%)	7 (4%)	3 (10%)	7 (2%)	59 (73%)	31 (46%)	46 (39%)	75 (48%)	42 (40%)	3 (60%)	10 (31%)	34 (36%)	3 (43%)	543 (25%)
			Total#	98 (4%)	27 (1%)	28 (1%)	689 (31%)	196 (9%)	30 (1%)	456 (21%)	81 (4%)	68 (3%)	118 (5%)	156 (7%)	105 (5%)	5 (0%)	32 (1%)	95 (4%)	7 (0%)	2,191
	6months post-V2 - 12months post-V1	No response	Not Infected	1 (33%)	0 (0%)	1 (5%)	4 (16%)	4 (50%)	4 (67%)	93 (66%)	0 (0%)	0 (0%)	-	-	-	0 (0%)	0 (0%)	6 (46%)	1 (25%)	114 (45%)
			Infected	0 (0%)	1 (50%)	2 (10%)	2 (8%)	3 (38%)	2 (33%)	37 (26%)	1 (5%)	1 (20%)	-	-	-	0 (0%)	0 (0%)	1 (8%)	0 (0%)	50 (20%)
			Uk/NA	2 (67%)	1 (50%)	18 (86%)	19 (76%)	1 (13%)	0 (0%)	10 (7%)	19 (95%)	4 (80%)	-	-	-	1 (100%)	5 (100%)	6 (46%)	3 (75%)	89 (35%)
			Total#	3 (1%)	2 (1%)	21 (8%)	25 (10%)	8 (3%)	6 (2%)	140 (55%)	20 (8%)	5 (2%)	0 (0%)	0 (0%)	0 (0%)	1 (0%)	5 (2%)	13 (5%)	4 (2%)	253
		Low response	Not infected	2 (13%)	4 (57%)	0 (0%)	69 (33%)	21 (62%)	5 (71%)	101 (73%)	0 (0%)	1 (5%)	1 (6%)	7 (12%)	2 (8%)	0 (0%)	2 (33%)	15 (48%)	0 (0%)	230 (38%)
			Infected	1 (6%)	1 (14%)	0 (0%)	6 (3%)	6 (18%)	1 (14%)	31 (22%)	1 (4%)	2 (10%)	0 (0%)	14 (25%)	3 (13%)	0 (0%)	0 (0%)	2 (6%)	1 (100%)	69 (12%)
			Uk/NA	13 (81%)	2 (29%)	4 (100%)	132 (64%)	7 (21%)	1 (14%)	6 (4%)	26 (96%)	18 (86%)	16 (94%)	36 (63%)	19 (79%)	1 (100%)	4 (67%)	14 (45%)	0 (0%)	299 (50%)
			Total#	16 (3%)	7 (1%)	4 (1%)	207 (35%)	34 (6%)	7 (1%)	138 (23%)	27 (5%)	21 (4%)	17 (3%)	57 (10%)	24 (4%)	1 (0%)	6 (1%)	31 (5%)	1 (0%)	598
		High response	Not Infected	46 (58%)	11 (61%)	3 (100%)	392 (86%)	110 (71%)	9 (53%)	136 (76%)	12 (35%)	24 (57%)	53 (52%)	39 (39%)	28 (35%)	2 (67%)	20 (95%)	25 (49%)	2 (100%)	912 (68%)
			Infected	8 (10%)	0 (0%)	0 (0%)	35 (8%)	30 (19%)	6 (35%)	37 (21%)	9 (26%)	9 (21%)	27 (27%)	38 (38%)	35 (43%)	1 (33%)	1 (5%)	6 (12%)	0 (0%)	242 (18%)
			Uk/NA	25 (32%)	7 (39%)	0 (0%)	30 (7%)	14 (9%)	2 (12%)	5 (3%)	13 (38%)	9 (21%)	21 (21%)	22 (22%)	18 (22%)	0 (0%)	0 (0%)	20 (39%)	0 (0%)	186 (14%)
			Total#	79 (6%)	18 (1%)	3 (0%)	457 (34%)	154 (11%)	17 (1%)	178 (13%)	34 (3%)	42 (3%)	101 (8%)	99 (7%)	81 (6%)	3 (0%)	21 (2%)	51 (4%)	2 (0%)	1340
		Overall	Not Infected	49 (50%)	15 (56%)	4 (14%)	465 (67%)	135 (69%)	18 (60%)	330 (72%)	12 (15%)	25 (37%)	54 (46%)	46 (29%)	30 (29%)	2 (40%)	22 (69%)	46 (48%)	3 (43%)	1256 (57%)
			Infected	9 (9%)	2 (7%)	2 (7%)	43 (6%)	39 (20%)	9 (30%)	105 (23%)	11 (14%)	12 (18%)	27 (23%)	52 (33%)	38 (36%)	1 (20%)	1 (3%)	9 (9%)	1 (14%)	361 (16%)
			Uk/NA	40 (41%)	10 (37%)	22 (79%)	181 (26%)	22 (11%)	3 (10%)	21 (5%)	58 (72%)	31 (46%)	37 (31%)	58 (37%)	37 (35%)	2 (40%)	9 (28%)	40 (42%)	3 (43%)	574 (26%)
			Total#	98 (4%)	27 (1%)	28 (1%)	689 (31%)	196 (9%)	30 (1%)	456 (21%)	81 (4%)	68 (3%)	118 (5%)	156 (7%)	105 (5%)	5 (0%)	32 (1%)	95 (4%)	7 (0%)	2191
T cell Breakdown	<6months post-V2	No response	Not Infected	4 (67%)	-	0 (0%)	2 (50%)	21 (95%)	4 (100%)	-	1 (17%)	1 (50%)	2 (100%)	-	1 (25%)	-	2 (100%)	6 (55%)	0 (0%)	44 (67%)
			Infected	0 (0%)	-	0 (0%)	0 (0%)	0 (0%)	0 (0%)	-	0 (0%)	0 (0%)	0 (0%)	-	0 (0%)	-	0 (0%)	2 (18%)	0 (0%)	2 (3%)
			Uk/NA	2 (33%)	-	2 (100%)	2 (50%)	1 (5%)	0 (0%)	-	5 (83%)	1 (50%)	0 (0%)	-	3 (75%)	-	0 (0%)	3 (27%)	1 (100%)	20 (30%)
			Total#	6 (9%)	0 (0%)	2 (3%)	4 (6%)	22 (33%)	4 (6%)	-	6 (9%)	2 (3%)	2 (3%)	0 (0%)	4 (6%)	-	2 (3%)	11 (17%)	1 (2%)	66
		Yes response	Not infected	37 (65%)	13 (76%)	4 (15%)	47 (43%)	94 (94%)	8 (100%)	-	6 (33%)	13 (54%)	10 (42%)	22 (54%)	26 (63%)	-	8 (73%)	19 (70%)	2 (67%)	309 (61%)
			Infected	4 (7%)	1 (6%)	1 (4%)	8 (7%)	2 (2%)	0 (0%)	-	1 (6%)	0 (0%)	3 (13%)	1 (2%)	2 (5%)	-	0 (0%)	1 (4%)	0 (0%)	24 (5%)
			Uk/NA	16 (28%)	3 (18%)	21 (81%)	55 (50%)	4 (4%)	0 (0%)	-	11 (61%)	11 (46%)	11 (46%)	18 (44%)	13 (32%)	-	3 (27%)	7 (26%)	1 (33%)	174 (34%)
			Total#	57 (11%)	17 (3%)	26 (5%)	110 (22%)	100 (20%)	8 (2%)	-	18 (4%)	24 (5%)	24 (5%)	41 (8%)	41 (8%)	-	11 (2%)	27 (5%)	3 (1%)	507
		Overall	Not Infected	41 (65%)	13 (76%)	4 (14%)	49 (43%)	115 (94%)	12 (100%)	-	7 (29%)	14 (54%)	12 (46%)	22 (54%)	27 (60%)	-	10 (77%)	25 (66%)	2 (50%)	353 (62%)
			Infected	4 (6%)	1 (6%)	1 (4%)	8 (7%)	2 (2%)	0 (0%)	-	1 (4%)	0 (0%)	3 (12%)	1 (2%)	2 (4%)	-	0 (0%)	3 (8%)	0 (0%)	26 (5%)
			Uk/NA	18 (29%)	3 (18%)	23 (82%)	57 (50%)	5 (4%)	0 (0%)	-	16 (67%)	12 (46%)	11 (42%)	18 (44%)	16 (36%)	-	3 (23%)	10 (26%)	2 (50%)	194 (34%)
			Total#	63 (11%)	17 (3%)	28 (5%)	114 (20%)	122 (21%)	12 (2%)	-	24 (4%)	26 (5%)	26 (5%)	41 (7%)	45 (8%)	-	13 (2%)	38 (7%)	4 (1%)	573
	6months post-V2 - 12months post-V1	No response	Not Infected	3 (50%)	-	0 (0%)	0 (0%)	12 (55%)	2 (50%)	-	0 (0%)	1 (50%)	2 (100%)	-	0 (0%)	-	2 (100%)	7 (64%)	0 (0%)	29 (44%)
			Infected	0 (0%)	-	0 (0%)	2 (50%)	8 (36%)	2 (50%)	-	1 (17%)	0 (0%)	0 (0%)	-	1 (25%)	-	0 (0%)	1 (9%)	1 (100%)	16 (24%)
			Uk/NA	3 (50%)	-	2 (100%)	2 (50%)	2 (9%)	0 (0%)	-	5 (83%)	1 (50%)	0 (0%)	-	3 (75%)	-	0 (0%)	3 (27%)	0 (0%)	21 (32%)
			Total#	6 (9%)	0 (0%)	2 (3%)	4 (6%)	22 (33%)	4 (6%)	-	6 (9%)	2 (3%)	2 (3%)	0 (0%)	4 (6%)	-	2 (3%)	11 (17%)	1 (2%)	66
		Yes response	Not infected	30 (53%)	12 (71%)	4 (15%)	45 (41%)	76 (76%)	5 (63%)	-	5 (28%)	7 (29%)	8 (33%)	13 (32%)	14 (34%)	-	8 (73%)	17 (63%)	2 (67%)	246 (49%)
			Infected	4 (7%)	1 (6%)	2 (8%)	10 (9%)	11 (11%)	3 (38%)	-	2 (11%)	5 (21%)	4 (17%)	10 (24%)	14 (34%)	-	1 (9%)	1 (4%)	0 (0%)	68 (13%)
			Uk/NA	23 (40%)	4 (24%)	20 (77%)	55 (50%)	13 (13%)	0 (0%)	-	11 (61%)	12 (50%)	12 (50%)	18 (44%)	13 (32%)	-	2 (18%)	9 (33%)	1 (33%)	193 (38%)
			Total#	57 (11%)	17 (3%)	26 (5%)	110 (22%)	100 (20%)	8 (2%)	-	18 (4%)	24 (5%)	24 (5%)	41 (8%)	41 (8%)	-	11 (2%)	27 (5%)	3 (1%)	507
		Overall	Not Infected	33 (52%)	12 (71%)	4 (14%)	45 (39%)	88 (72%)	7 (58%)	-	5 (21%)	8 (31%)	10 (38%)	13 (32%)	14 (31%)	-	10 (77%)	24 (63%)	2 (50%)	275 (48%)
			Infected	4 (6%)	1 (6%)	2 (7%)	12 (11%)	19 (16%)	5 (42%)	-	3 (13%)	5 (19%)	4 (15%)	10 (24%)	15 (33%)	-	1 (8%)	2 (5%)	1 (25%)	84 (15%)
			Uk/NA	26 (41%)	4 (24%)	22 (79%)	57 (50%)	15 (12%)	0 (0%)	-	16 (67%)	13 (50%)	12 (46%)	18 (44%)	16 (36%)	-	2 (15%)	12 (32%)	1 (25%)	214 (37%)
			Total#	63 (11%)	17 (3%)	28 (5%)	114 (20%)	122 (21%)	12 (2%)	-	24 (4%)	26 (5%)	26 (5%)	41 (7%)	45 (8%)	-	13 (2%)	38 (7%)	4 (1%)	573

Table 3.8 COVID-19 severity reported after COVID-19 vaccination in OCTAVE study, serological breakdown.

Summary of COVID-19 severity reported in combined follow-up periods after COVID-19 vaccination for all immunocompromised patients in OCTAVE, split by disease subgroup and based on Roche anti-RBD Ig assay result ≥0.8 AU ml^{-1}, low response <380 AU ml^{-1} and high response >380 AU mL^{-1} at the post-V2 timepoint. # (%) of total OCTAVE infections.

		Anti-RBD Ig breakdown - <6months post-v2 - 12months post-V1 (n (%))															
		SC	HM	AAV	IA	HD	HD on IS	K-Tr	L-Tr	L-AI	L-Cirr	CD	UC	IBD-U	Auto-HSCT	Allo-HSCT	CAR-T	OCTAVE
No Response	Asymptomatic	0 (0%)	0 (0%)	0 (0%)	0 (0%)	0 (0%)	1 (50%)	5 (11%)	0 (0%)	0 (0%)	-	-	-	-	-	0 (0%)	0 (0%)	6 (9%)
	Symptomatic	1 (100%)	1 (100%)	2 (67%)	1 (33%)	2 (67%)	0 (0%)	25 (54%)	1 (100%)	1 (100%)	-	-	-	-	-	1 (33%)	0 (0%)	35 (53%)
	Hospitalised - No Oxygen Required	0 (0%)	0 (0%)	0 (0%)	0 (0%)	0 (0%)	0 (0%)	3 (7%)	0 (0%)	0 (0%)	-	-	-	-	-	0 (0%)	2 (100%)	5 (8%)
	Hospitalised - Oxygen Required	0 (0%)	0 (0%)	0 (0%)	1 (33%)	0 (0%)	0 (0%)	8 (17%)	0 (0%)	0 (0%)	-	-	-	-	-	0 (0%)	0 (0%)	9 (14%)
	ITU	0 (0%)	0 (0%)	0 (0%)	1 (33%)	0 (0%)	0 (0%)	0 (0%)	0 (0%)	0 (0%)	-	-	-	-	-	0 (0%)	0 (0%)	1 (2%)
	COVID-19 related mortality	0 (0%)	0 (0%)	1 (33%)	0 (0%)	1 (33%)	1 (50%)	2 (4%)	0 (0%)	0 (0%)	-	-	-	-	-	0 (0%)	0 (0%)	5 (8%)
	Unknown/NA	0 (0%)	0 (0%)	0 (0%)	0 (0%)	0 (0%)	0 (0%)	3 (7%)	0 (0%)	0 (0%)	-	-	-	-	-	2 (67%)	0 (0%)	5 (8%)
	Total[#]	1 (2%)	1 (2%)	3 (5%)	3 (5%)	3 (5%)	2 (3%)	46 (70%)	1 (2%)	1 (2%)	0 (0%)	0 (0%)	0 (0%)	0 (0%)	0 (0%)	3 (5%)	2 (3%)	66
Low response	Asymptomatic	0 (0%)	0 (0%)	-	0 (0%)	2 (29%)	0 (0%)	5 (14%)	0 (0%)	0 (0%)	-	0 (0%)	0 (0%)	-	-	1 (14%)	0 (0%)	8 (8%)
	Symptomatic	1 (50%)	0 (0%)	-	13 (81%)	4 (57%)	0 (0%)	24 (67%)	1 (100%)	3 (75%)	-	15 (94%)	3 (100%)	-	-	4 (57%)	0 (0%)	68 (72%)
	Hospitalised - No Oxygen Required	0 (0%)	0 (0%)	-	1 (6%)	0 (0%)	0 (0%)	5 (14%)	0 (0%)	0 (0%)	-	0 (0%)	0 (0%)	-	-	0 (0%)	0 (0%)	6 (6%)
	Hospitalised - Oxygen Required	0 (0%)	0 (0%)	-	1 (6%)	1 (14%)	0 (0%)	1 (3%)	0 (0%)	0 (0%)	-	0 (0%)	0 (0%)	-	-	0 (0%)	0 (0%)	3 (3%)
	ITU	0 (0%)	0 (0%)	-	0 (0%)	0 (0%)	0 (0%)	0 (0%)	0 (0%)	0 (0%)	-	0 (0%)	0 (0%)	-	-	1 (14%)	0 (0%)	1 (1%)
	COVID-19 related mortality	0 (0%)	0 (0%)	-	0 (0%)	0 (0%)	1 (100%)	1 (3%)	0 (0%)	0 (0%)	-	0 (0%)	0 (0%)	-	-	0 (0%)	1 (100%)	3 (3%)
	Unknown/NA	1 (50%)	1 (100%)	-	1 (6%)	0 (0%)	0 (0%)	0 (0%)	0 (0%)	1 (25%)	-	1 (6%)	0 (0%)	-	-	1 (14%)	0 (0%)	6 (6%)
	Total[#]	2 (2%)	1 (1%)	0 (0%)	16 (17%)	7 (7%)	1 (1%)	36 (38%)	1 (1%)	4 (4%)	0 (0%)	16 (17%)	3 (3%)	0 (0%)	0 (0%)	7 (7%)	1 (1%)	95
High response	Asymptomatic	0 (0%)	0 (0%)	-	5 (8%)	13 (39%)	0 (0%)	11 (27%)	1 (8%)	1 (10%)	1 (3%)	1 (2%)	0 (0%)	0 (0%)	0 (0%)	2 (22%)	-	35 (11%)
	Symptomatic	12 (80%)	0 (0%)	-	48 (80%)	17 (52%)	6 (100%)	25 (61%)	10 (83%)	9 (90%)	27 (84%)	45 (88%)	39 (98%)	1 (100%)	1 (50%)	5 (56%)	-	245 (78%)
	Hospitalised - No Oxygen Required	0 (0%)	0 (0%)	-	0 (0%)	2 (6%)	0 (0%)	2 (5%)	0 (0%)	0 (0%)	0 (0%)	1 (2%)	0 (0%)	0 (0%)	0 (0%)	0 (0%)	-	5 (2%)
	Hospitalised - Oxygen Required	0 (0%)	0 (0%)	-	0 (0%)	1 (3%)	0 (0%)	0 (0%)	1 (8%)	0 (0%)	1 (3%)	0 (0%)	0 (0%)	0 (0%)	0 (0%)	0 (0%)	-	3 (1%)
	ITU	0 (0%)	0 (0%)	-	0 (0%)	0 (0%)	0 (0%)	0 (0%)	0 (0%)	0 (0%)	0 (0%)	0 (0%)	0 (0%)	0 (0%)	0 (0%)	0 (0%)	-	0 (0%)
	COVID-19 related mortality	0 (0%)	0 (0%)	-	0 (0%)	0 (0%)	0 (0%)	1 (2%)	0 (0%)	0 (0%)	0 (0%)	0 (0%)	0 (0%)	0 (0%)	1 (50%)	0 (0%)	-	2 (1%)
	Unknown/NA	3 (20%)	1 (100%)	-	7 (12%)	0 (0%)	0 (0%)	2 (5%)	0 (0%)	0 (0%)	3 (9%)	4 (8%)	1 (3%)	0 (0%)	0 (0%)	2 (22%)	-	23 (7%)
	Total[#]	15 (5%)	1 (0%)	0 (0%)	60 (19%)	33 (11%)	6 (2%)	41 (13%)	12 (4%)	10 (3%)	32 (10%)	51 (16%)	40 (13%)	1 (0%)	2 (1%)	9 (3%)	0 (0%)	313
Total	Asymptomatic	0 (0%)	0 (0%)	0 (0%)	5 (6%)	15 (35%)	1 (11%)	21 (17%)	1 (7%)	1 (7%)	1 (3%)	1 (1%)	0 (0%)	0 (0%)	0 (0%)	3 (16%)	0 (0%)	49 (10%)
	Symptomatic	14 (78%)	1 (33%)	2 (67%)	62 (78%)	23 (53%)	6 (67%)	74 (60%)	12 (86%)	13 (87%)	27 (84%)	60 (90%)	42 (98%)	1 (100%)	1 (50%)	10 (53%)	0 (0%)	348 (73%)
	Hospitalised - No Oxygen Required	0 (0%)	0 (0%)	0 (0%)	1 (1%)	2 (5%)	0 (0%)	10 (8%)	0 (0%)	0 (0%)	0 (0%)	1 (1%)	0 (0%)	0 (0%)	0 (0%)	0 (0%)	2 (67%)	16 (3%)
	Hospitalised - Oxygen Required	0 (0%)	0 (0%)	0 (0%)	2 (3%)	2 (5%)	0 (0%)	9 (7%)	1 (7%)	0 (0%)	1 (3%)	0 (0%)	0 (0%)	0 (0%)	0 (0%)	0 (0%)	0 (0%)	15 (3%)
	ITU	0 (0%)	0 (0%)	0 (0%)	1 (1%)	0 (0%)	0 (0%)	0 (0%)	0 (0%)	0 (0%)	0 (0%)	0 (0%)	0 (0%)	0 (0%)	0 (0%)	1 (5%)	0 (0%)	2 (0%)
	COVID-19 related mortality	0 (0%)	0 (0%)	1 (33%)	0 (0%)	1 (2%)	2 (22%)	4 (3%)	0 (0%)	0 (0%)	0 (0%)	0 (0%)	0 (0%)	0 (0%)	1 (50%)	0 (0%)	1 (33%)	10 (2%)
	Unknown/NA	4 (22%)	2 (67%)	0 (0%)	8 (10%)	0 (0%)	0 (0%)	5 (4%)	0 (0%)	1 (7%)	3 (9%)	5 (7%)	1 (2%)	0 (0%)	0 (0%)	5 (26%)	0 (0%)	34 (7%)
	Total[#]	18 (4%)	3 (1%)	3 (1%)	79 (17%)	43 (9%)	9 (2%)	123 (26%)	14 (3%)	15 (3%)	32 (7%)	67 (14%)	43 (9%)	1 (0%)	2 (0%)	19 (4%)	3 (1%)	474

Table 3.9 COVID-19 severity reported after COVID-19 vaccination in OCTAVE study, T cell breakdown

Summary of COVID-19 severity reported in combined follow-up periods after COVID-19 vaccination for all immunocompromised patients in OCTAVE, split by disease subgroup and based on IFNγ ELISpot response to SARS-CoV-2 spike at the post-V2 timepoint. No response = 0SFU/106; yes response > 0SFU/106. * Kidney transplant and undefined inflammatory bowel disease groups were not included in group 1.

		T cell breakdown - <6months post-v2 - 12months post-V1 (n (%))																
		SC	HM	AAV	IA	HD	HD on IS	K-Tr *	L-Tr	L-AI	L-Cirr	CD	UC	IBD-U*	Auto-HSCT	Allo-HSCT	CAR-T	OCTAVE
No response	Asymptomatic	-	-	-	0 (0%)	3 (38%)	1 (50%)	-	0 (0%)	-	-	-	0 (0%)	-	-	1 (33%)	0 (0%)	5 (28%)
	Symptomatic	-	-	-	2 (100%)	3 (38%)	1 (50%)	-	1 (100%)	-	-	-	1 (100%)	-	-	1 (33%)	0 (0%)	9 (50%)
	Hospitalised - No Oxygen Required	-	-	-	0 (0%)	1 (13%)	0 (0%)	-	0 (0%)	-	-	-	0 (0%)	-	-	0 (0%)	0 (0%)	1 (6%)
	Hospitalised - Oxygen Required	-	-	-	0 (0%)	0 (0%)	0 (0%)	-	0 (0%)	-	-	-	0 (0%)	-	-	0 (0%)	0 (0%)	0 (0%)
	ITU	-	-	-	0 (0%)	0 (0%)	0 (0%)	-	0 (0%)	-	-	-	0 (0%)	-	-	1 (33%)	0 (0%)	1 (6%)
	COVID-19 related mortality	-	-	-	0 (0%)	1 (13%)	0 (0%)	-	0 (0%)	-	-	-	0 (0%)	-	-	0 (0%)	1 (100%)	2 (11%)
	Unknown/NA	-	-	-	0 (0%)	0 (0%)	0 (0%)	-	0 (0%)	-	-	-	0 (0%)	-	-	0 (0%)	0 (0%)	0 (0%)
	Total#	0 (0%)	0 (0%)	0 (0%)	2 (11%)	8 (44%)	2 (11%)	-	1 (6%)	0 (0%)	0 (0%)	0 (0%)	1 (6%)	-	0 (0%)	3 (17%)	1 (6%)	18
Yes response	Asymptomatic	0 (0%)	0 (0%)	0 (0%)	4 (22%)	4 (31%)	0 (0%)	-	0 (0%)	1 (20%)	1 (14%)	0 (0%)	0 (0%)	-	0 (0%)	1 (50%)	-	11 (12%)
	Symptomatic	6 (75%)	0 (0%)	2 (67%)	7 (39%)	8 (62%)	3 (100%)	-	2 (67%)	4 (80%)	2 (29%)	11 (100%)	16 (100%)	-	0 (0%)	1 (50%)	-	62 (67%)
	Hospitalised - No Oxygen Required	0 (0%)	0 (0%)	0 (0%)	1 (6%)	0 (0%)	0 (0%)	-	0 (0%)	0 (0%)	0 (0%)	0 (0%)	0 (0%)	-	0 (0%)	0 (0%)	-	1 (1%)
	Hospitalised - Oxygen Required	0 (0%)	0 (0%)	0 (0%)	1 (6%)	1 (8%)	0 (0%)	-	1 (33%)	0 (0%)	1 (14%)	0 (0%)	0 (0%)	-	0 (0%)	0 (0%)	-	4 (4%)
	ITU	0 (0%)	0 (0%)	0 (0%)	0 (0%)	0 (0%)	0 (0%)	-	0 (0%)	0 (0%)	0 (0%)	0 (0%)	0 (0%)	-	0 (0%)	0 (0%)	-	0 (0%)
	COVID-19 related mortality	0 (0%)	0 (0%)	1 (33%)	0 (0%)	0 (0%)	0 (0%)	-	0 (0%)	0 (0%)	0 (0%)	0 (0%)	0 (0%)	-	1 (100%)	0 (0%)	-	2 (2%)
	Unknown/NA	2 (25%)	2 (100%)	0 (0%)	5 (28%)	0 (0%)	0 (0%)	-	0 (0%)	0 (0%)	3 (43%)	0 (0%)	0 (0%)	-	0 (0%)	0 (0%)	-	12 (13%)
	Total#	8 (9%)	2 (2%)	3 (3%)	18 (20%)	13 (14%)	3 (3%)	-	3 (3%)	5 (5%)	7 (8%)	11 (12%)	16 (17%)	-	1 (1%)	2 (2%)	0 (0%)	92
Total	Asymptomatic	0 (0%)	0 (0%)	0 (0%)	4 (20%)	7 (33%)	1 (20%)	-	0 (0%)	1 (20%)	1 (14%)	0 (0%)	0 (0%)	-	0 (0%)	2 (40%)	0 (0%)	16 (15%)
	Symptomatic	6 (75%)	0 (0%)	2 (67%)	9 (45%)	11 (52%)	4 (80%)	-	3 (75%)	4 (80%)	2 (29%)	11 (100%)	17 (100%)	-	0 (0%)	2 (40%)	0 (0%)	71 (65%)
	Hospitalised - No Oxygen Required	0 (0%)	0 (0%)	0 (0%)	1 (5%)	1 (5%)	0 (0%)	-	0 (0%)	0 (0%)	0 (0%)	0 (0%)	0 (0%)	-	0 (0%)	0 (0%)	0 (0%)	2 (2%)
	Hospitalised - Oxygen Required	0 (0%)	0 (0%)	0 (0%)	1 (5%)	1 (5%)	0 (0%)	-	1 (25%)	0 (0%)	1 (14%)	0 (0%)	0 (0%)	-	0 (0%)	0 (0%)	0 (0%)	4 (4%)
	ITU	0 (0%)	0 (0%)	0 (0%)	0 (0%)	0 (0%)	0 (0%)	-	0 (0%)	0 (0%)	0 (0%)	0 (0%)	0 (0%)	-	0 (0%)	1 (20%)	0 (0%)	1 (1%)
	COVID-19 related mortality	0 (0%)	0 (0%)	1 (33%)	0 (0%)	1 (5%)	0 (0%)	-	0 (0%)	0 (0%)	0 (0%)	0 (0%)	0 (0%)	-	1 (100%)	0 (0%)	1 (100%)	4 (4%)
	Unknown/NA	2 (25%)	1 (50%)	0 (0%)	3 (15%)	0 (0%)	0 (0%)	-	0 (0%)	0 (0%)	0 (0%)	0 (0%)	0 (0%)	-	0 (0%)	0 (0%)	0 (0%)	6 (5%)
	Total#	8 (7%)	2 (2%)	3 (3%)	20 (18%)	21 (19%)	5 (5%)	-	4 (4%)	5 (5%)	7 (6%)	11 (10%)	17 (15%)	-	1 (1%)	5 (5%)	1 (1%)	110

3.10 Supplementary Figures

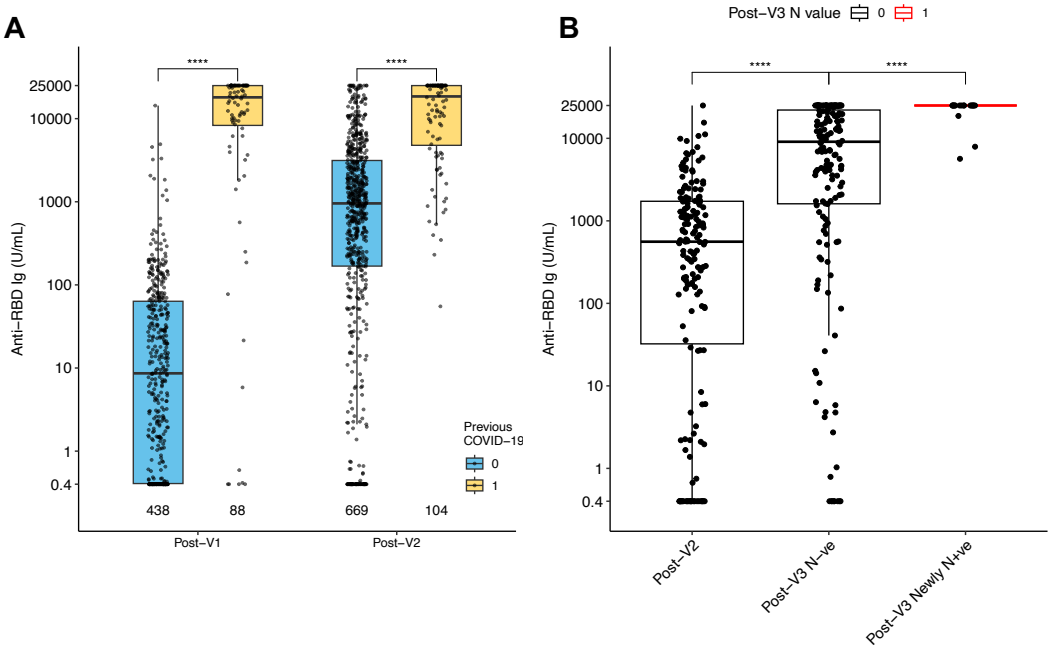

Fig. S3.1 Impact of previous SARS-CoV-2 infection on anti-RBD Ig in individuals with liver disease

A) Magnitude of anti SARS-CoV-2 RBD Ig in infection naïve and previously SARS-CoV-2 infected individuals at post-V1 and post-V2 timepoints.

B) Magnitude of anti SARS-CoV-2 RBD Ig in Naïve individuals at post-V2 and post-V3 timepoints and in individuals who became nucleocapsid positive between second and third vaccines (Post-V3 Newly N+ve).

Boxes represent median and IQR, whiskers represent +/- 1.5x IQR. Mann Whitney U test used, adjusted P value presented.

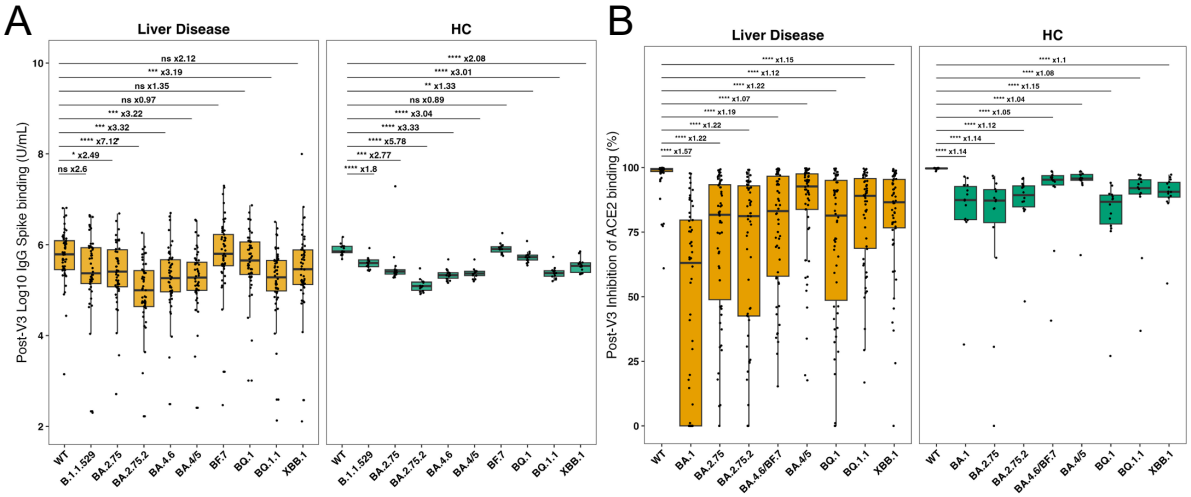

Fig. S3.2 V3+21 days binding IgG and ACE2 inhibition against SARS-CoV-2 VoC in individuals liver disease and healthy controls

V3+21d IgG (A) and ACE2 inhibition (B) to SARS-CoV-2 VoC, separated by liver disease versus healthy controls.

Two-sided Mann-Whitney U test adjusted with Holm-Bonferroni. Fold-change of median depicted. Boxes represent median and IQR, whiskers represent +/- 1.5x IQR. HC = healthy controls; ACE2 = angiotensin-converting enzyme 2, WT = wild-type. * = P<0.05, ** = P<0.01, *** = P<0.001, **** = P < 0.0001.

4 Results: Impact of vaccine platform and dosing interval on SARS-CoV-2 spike-specific T cell function, phenotype and clonality

4.1 Introduction

In Chapter 3 I used IFNγ ELISpot assays to identify differences in functional T cell responses to SARS-CoV-2 spike peptide pools between immunocompromised and healthy individuals. While IFNγ ELISpot assays are a useful and commonly used measure of functional antigen-specific T cells, it delineates only a single functional output – IFNγ release. T cell responses to vaccines represent the activation of multiple heterogeneous cell subsets (i.e., $CD8^+$, $CD4^+$, T_H1, T_H2, T_H17, T_{FH} and T_{reg}) with diverse effector functions (e.g., cytokine production, cytotoxicity, cell-cell contact-dependent functions) (*307*)**.** Therefore, more detailed study is required to capture the multiple facets of an effective T cell response to vaccination, including the functionality, phenotype and clonality of responding T cells.

Flow cytometry-based assays, including intracellular cytokine staining (ICS), proliferation assays, MHC tetramer, and activation-induced marker (AIM) assays, enable simultaneous assessment of multiple functional and phenotypic markers (*285, 308-314*). AIM assays have recently emerged as an effective method to quantify antigen-specific $CD4^+$ and $CD8^+$ T cells independently of cytokine production. By measuring surface markers associated with TCR and costimulatory signalling (e.g., OX-40, CD40L, CD107a, ICOS, PD-1, 4-1BB, CD69, CD25), AIM assays capture high frequencies (compared to ICS (*63*)) of diverse T cell phenotypes (*315-318*). Additionally, AIM^+ T cells remain viable for downstream analyses, enabling further functional and phenotypic characterization. When combined with transcriptomics, AIM assays facilitate deep profiling of polyclonal antigen-responsive T cells across biological contexts, including vaccination. Recent studies have leveraged this approach to reveal persistent transcriptional changes in SARS-CoV-2-specific T cells post-mRNA vaccination (*319*) and a hyper-effector phenotype in mRNA-vaccinated XLA patients (*320*), underscoring AIM's utility in dissecting T cell functional diversity.

Several factors related to the vaccine regimen have been identified that impact the magnitude of COVID-19 T cell responses, measured by IFNγ ELISpot, AIM assay or ICS. These factors include the vaccine type (*64, 65*), the number of vaccine doses (*71, 73*), the interval between vaccine doses (*71, 73*), pre-vaccine anti-SARS-CoV-2 T cell responses (*79*) and the length of time between the vaccine dose and sampling timepoint (*73, 321*). Crucially however, these studies do not give insight into the quality or potential breadth of responses induced by COVID-19 vaccines. Study of the factors associated with vaccine-induced T cell quality is essential for future optimisation of vaccine regimen and to enhance our knowledge of pathways of vaccine immunogenicity.

4.2 Summary of chapter rationale

Multiple experimental approaches have been used to assess antigen-specific T cell responses to COVID-19 vaccines, highlighting various elements of the vaccine regimen that influence the magnitude of SARS-CoV-2-specific T cells. However, these methods provide limited resolution of the functionality of antigen-specific T cells and may not fully capture the complexity of vaccine-induced responses. Additionally, they do not assess T cell clonality, which is likely important for understanding the longevity of vaccine-induced immunity. Advancing our understanding of T cell functionality will help define optimal immunogenicity, identify key determinants of effective T cell responses, and guide improvements in vaccine regimen design.

4.3 Hypothesis and Aims

The central hypotheses of this chapter are as follows:

1) SARS-CoV-2 spike-specific T cells differ in functionality and clonality depending on the type of SARS-CoV-2 stimulus (e.g. vaccine or infection)
2) Factors relating to the vaccine regimen alter the quality of SARS-CoV-2 T cells that are induced by vaccines
3) Pre-existing T cells that are cross-reactive to SARS-CoV-2 will impact the phenotype

of vaccine-induced T cells

This chapter aims to address these main aims:

1) Broadly characterise the function, phenotype and clonality of SARS-CoV-2 responsive T cells induced by COVID-19 stimuli, captured by the AIM assay
2) Investigate the relationship between T cell phenotype and T cell clonality
3) Assess the contribution of various factors relating to the vaccine regimen on the phenotype, function and clonality of antigen-responsive T cells, including:
    a. vaccine type
    b. number of vaccine doses
    c. the interval between vaccine doses
    d. pre-vaccine anti-SARS-CoV-2 T cell responses
    e. duration from vaccine dose
4) Assess the phenotype and function of T cells induced by COVID-19 vaccines and compare them with T cells induced by COVID infection

4.4 Chapter overview

To address these aims, I analysed a single-cell CITE- and TCR-sequencing dataset generated by Dr. Nicholas Provine. This dataset included SARS-CoV-2 spike peptide-responsive T cells sorted by flow cytometry from PBMC samples taken before and after one or two doses of either BNT162b2 or ChAdOx1 nCoV-19 vaccination in healthy individuals. To compare vaccine prime-boosting intervals, individuals with either a short (3-4week) or long (8-12week) dosing interval were included. To compare the observed vaccine-induced responses with immune responses following SARS-CoV-2 infection (ancestral strain), SARS-CoV-2 spike responsive T cells were additionally captured at two timepoints following mild COVID-19.

The work performed in this chapter is under review for publication, the manuscript is appended (**Appendix 4**):

Murray S.M, Amini A., Ferry H., *et al.* The dominant impact of dosing interval on the quality of

T cells induced by SARS-CoV-2 mRNA and adenoviral vaccines. In revision, *Science Immunology.* (2025)

4.5 Chapter specific methods

4.5.1 AIM$^+$ T cell pre-processing

Following Louvain clustering and manual annotation of cell clusters, several developmentally distinct cell populations were found to co-cluster based on gene expression and were manually separated as follows: MAIT_2 were separated from the co-clustered VD2 and CD8_Tem populations based on co-expression of SLC4A10 and TRAV1-2; VD1_Eff were separated from the co-clustered CD8_IFNG population based on lack of expression of abTCR chains.

4.5.2 Baseline spike-responsive T cell data pre-processing

Single-cell RNA-sequencing data on CTV^{lo} baseline reactive T cells underwent QC as per above. Integration of data from different experiments was performed using SCTransform with 3000 variable features. As above, the VD2 population was separated from CD8_IFNG and CD8_GZMA populations based on lack of expression of abTCR chains.

4.5.3 CellPhoneDB

To find putative cell-cell interactions, CellPhoneDB (v5, (*322*)) was applied to the entire pre-processed and filtered dataset, or subsets of cells including only BNT162b2 or ChAdOx1 nCoV-19 vaccinated individuals. Differentially expressed genes for each cluster were identified using Limma and used for interaction analysis.

4.5.4 CoNGA analysis of TCRs

To identify the relationship between TCR physiochemical properties and gene expression, and identify clones enriched in our dataset compared with simulated 'background' TCR repertoires, we performed analysis using the CoNGA package (v0.1.2) (*323*) in Python (v3.9). A PCA-based approach was used to reduce cells with identical abTCR sequences to a single representative cell and TCRdist was used to calculate TCR distance metrics between clones. Neighbourhoods of gene and TCRdist similarity were defined using PCs of gene expression

and TCR distance data. Significant CoNGA scores represent clonotypes that are present in neighbourhoods with significant overlap in gene expression and TCR space.

To identify TCR meta-clonotypes that were antigen-enriched, TCR clumping analysis was performed. A background VDJ repertoire was simulated and individual TCR neighbourhoods in the observed data were tested for overrepresentation compared to the null model (background) of VDJ recombination. Meta-clonotypes with >10 participating clonotypes were selected for further analysis, and clustalOmega within the msa (v1.32.0) package was used to derive consensus sequences for α and β CDR3 regions separately.

4.5.5 Mixed linear models to identify impact of vaccine type and interval

For analysis of the interactions between vaccine, interval and timepoint, sex and age, mixed-effects linear models with estimated precision weights were assessed using the dream method of variancePartition (v1.3.0) (*324*), based on analysis performed in (*212*). Briefly, gene counts within a given individual * timepoint * cluster combination were aggregated using the edgeR function Seurat2PB and filtered and normalized. voomWithDreamWeights was used to normalize data and estimate precision weights for dream analysis. Dream analysis was performed using the formula ~ 0 + group.time + Age + Sex + (1|ID) to estimate regression coefficients for each gene and empirical bayes shrinkage was applied using the eBayes function of variancePartition.

4.6 Results

4.6.1 Study population and experimental design

Individuals vaccinated with ChAdOx1 nCoV-19 ("ChAd") or BNT162b2 ("BNT") with a short or long dosing interval were sampled immediately before their first vaccine ("T0"), and before ("T1-short" and "T1-long", respectively) and 28-days after ("T2") their second vaccine dose (**Fig. 4.1A**). Paired samples from T0, T1 and T2 were assessed from six individuals in each of the ChAd-long, ChAd-short, BNT-long and BNT-short groups. Samples from the short ChAd group were from participants in COV001, while samples from all other groups were from the

PITCH study.

Also included were a group of six unvaccinated individuals with mild COVID-19, sampled approximately 28 days (range 17-28 days, T1-Short) and 56 days (range 53-61 days, T1-Long) after SARS-CoV-2 PCR positivity (“COVID”). Groups were broadly balanced for age

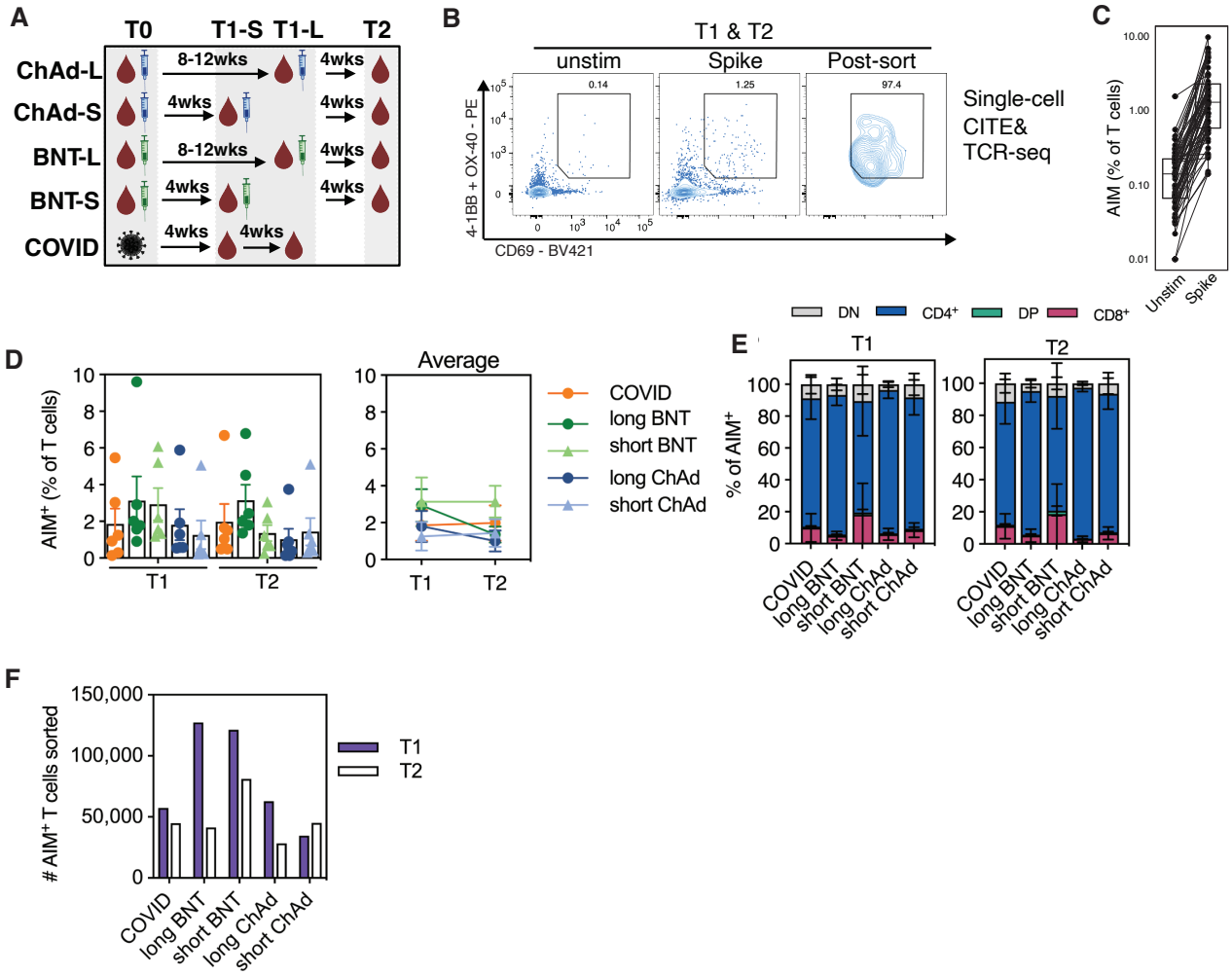

Fig. 4.1 Experimental overview and AIM+ T cell flow cytometry

A) Study overview.

B) Flow cytometric staining of unstimulated and pre- and post- sort SARS-CoV-2 spike peptide stimulated peripheral blood.

C) Proportion of activation induced marker (AIM)+ CD3+ T cells following 24 hour stimulation.

D) Frequency of CD69+, 4-1BB+/OX-40+ (activation induced marker, AIM) CD3+ T cells after stimulation with SARS-CoV-2 spike peptide.

E) Frequency of CD4+, CD8+, CD4+CD8+ (Double positive, DP) and CD4–CD8– (Double negative, DN) AIM+ CD3+ T cells.

F) Total number of AIM+ T cells sorted for single-cell RNA sequencing.

and sex (**Table 4.1**).

To capture SARS-CoV-2 spike peptide-reactive T cell responses we used an AIM assay in all participants at T1 and T2 timepoints (**Fig. 4.1B**). AIM markers included CD69 and 4-1BB/OX-40 – with 4-1BB/OX-40 on the same fluorophore (**Fig. 4.1B**). On average, 2% of $CD3^+$ T cells were AIM^+ (**Fig. 4.1C**), with little difference between study groups or timepoints (**Fig. 4.1D**). Median percentages of $CD4^+$, $CD8^+$ and CD4/CD8 double negative (DN) AIM^+ T cells identified by flow cytometry were 86%, 7% and 6%, respectively (**Fig. 4.1E**). All AIM^+ $CD3^+$ T cells were isolated by flow cytometric cell sorting for multi-modal (RNA, TCR and eight selected cell-surface phenotyping and AIM protein markers) single-cell sequencing, with the largest numbers of AIM^+ $CD3^+$ T cells obtained from BNT vaccinees (**Fig. 4.1F**).

4.6.2 AIM^+ T cells elicited by COVID-19 infection and vaccination display diverse phenotypes

To assess the phenotypes of AIM^+ T cells captured after COVID-19 vaccination or infection I first analysed the dataset as a whole, combining timepoints from all groups. After sequencing and QC (**Section 2.12.1**), the final dataset of AIM^+ T cells contained 128,017 cells (**Fig. 4.2A**). PCA and UMAP were used to reduce the dimensionality of the transcriptomic data for visualisation and Louvain clustering was used to group cells based on their transcriptional similarity (**Fig. 4.2A)**. Clusters of $CD4^+$ and $CD4^-$ T cells were observed **(Fig 4.2B)**.

Following clustering and manual annotation of cell clusters, several developmentally distinct cell populations were found to co-cluster within the non-CD4 populations **(Fig 4.2C)**. Cluster 9 included cells which expressed genes unique to mucosal-associated invariant T cells (*SLC4A10*, *TRAV1-2*), Vδ2 γδT cells (*TRDV2*) and non-MAIT $CD8^+$ T cells **(Fig 4.2C)**. Cluster 11 included a mixed population of effector Vδ1 γδT cells (expressing *TDRV1*) and αβ $CD8^+$ T cells. Owing to the known developmental differences of these cell types (*325, 326*), these

Fig. 4.2 COVID-19 vaccines induce heterogenous SARS-CoV-2 spike responsive T cell populations

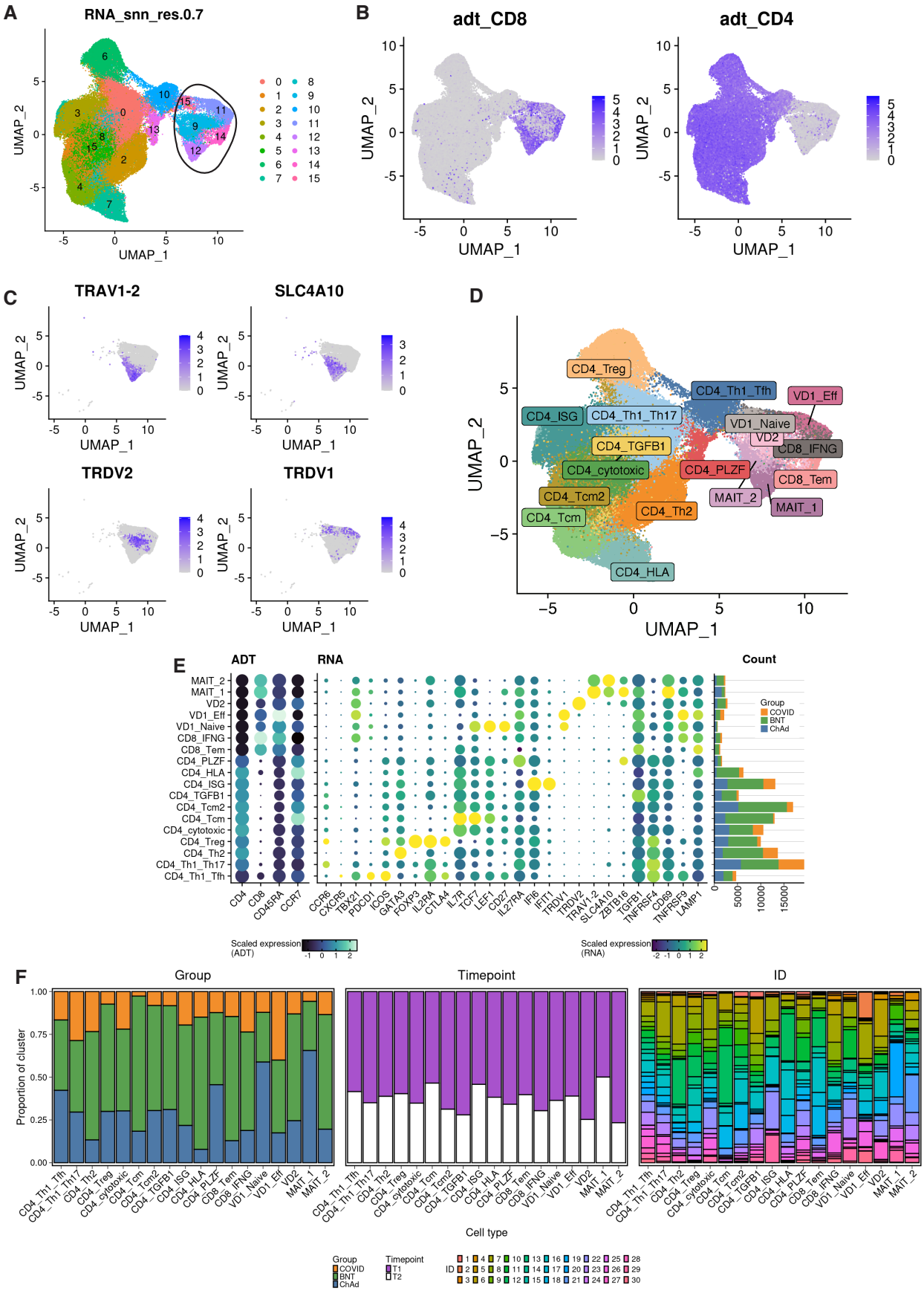

Fig. 4.2 COVID-19 vaccines induce heterogenous SARS-CoV-2 spike responsive T cell populations

A) Uniform manifold approximation and projection (UMAP) embedding of combined T1 and T2 AIM+ T cell transcriptomic data, clustered using Louvain clustering at 0.7 resolution (pre-clean up).

B) Scaled normalized expression of CD8 and CD4 surface protein (ADT)

C) Scaled normalized expression of mucosal associated invariant T cell (MAIT) (*SLC4A10* and *TRAV1-2*) and γδT cell (*TRDV2* and *TRDV1*) associated genes.

D) UMAP representation of gene expression data from sorted AIM+ CD3+ T cells, with manual annotation after separation of clusters 11 and 9.

E) Selected surface protein and RNA features used for manual annotation.

F) Proportion of study group (left), timepoint (middle), and donor (right) of AIM$^+$ T cell clusters defined by single-cell RNA sequencing

populations were manually sub-clustered based on expression thresholds of their subset-defining genes (**Section 4.5.1**).

18 final clusters were identified: 11 were identified as CD4$^+$ T cells, two as CD8$^+$ T cells, two as mucosal-associated invariant T (MAIT) cells, and three as γδT cell populations **(Fig 4.2D)**. All vaccine types, both timepoints and the majority (80%) of donors contributed to all clusters **(Fig. 4.2E&F)**.

CD4$^+$ T cell clusters comprised multiple populations with clear parallels to known polarized subsets, including a hybrid T_H1/T_{FH} cluster (CD4_Th1_Tfh), a hybrid T_H1/T_H17 cluster (CD4_Th1_Th17), a T_H2 cluster (CD4_Th2), and a T_{reg} cluster (CD4_Treg) **(Fig. 4.2E&F)**. Several clusters exhibited phenotypes not associated with T_H polarization, including a cytotoxic population (CD4_cytotoxic) and memory states (CD4_Tcm and CD4_Tcm2). Finally, four clusters of CD4$^+$ T cells were defined by distinctive expression of specific markers (*TGFB1,* interferon stimulated genes [ISGs], HLA molecules, and *ZBTB16* [encodes PLZF], respectively) and could not be easily assigned to known CD4$^+$ populations (CD4_TGFB1, CD4_ISG, CD4_HLA, and CD4_PLZF). The two clusters of CD8$^+$ T cells corresponded to activated IFNγ-producing effector CD8$^+$ T cells (CD8_IFNG) and more quiescent effector memory T_{EM} cells (CD8_Tem) **(Fig. 4.2E&F)**.

Detection of some of these clusters was surprising. MAIT and γδT cells were not expected to respond to SARS-CoV-2 spike peptides, as their cognate antigens are not peptides (*325, 326*).

It was also unexpected to find transcriptionally resting/undifferentiated cells such as the CD4_HLA, CD4_Tcm and CD8_Tem populations. As such, I next investigated the phenotype of these cells further.

4.6.3 Resting AIM$^+$ T cells have defined transcriptional characteristics

In the conventional AIM assay, background subtraction of the small fraction of T cells that are AIM$^+$ at rest gives a very good signal-to-noise ratio (*315-317*). However, these cells cannot be excluded from sorting gates when isolating cells by flow cytometric cell sorting. Therefore, a small fraction of the recovered cells may be background activated.

To identify cell types enriched for background activated phenotypes, I identified baseline AIM$^+$ cells by surface expression of CD69, CD134 (OX-40), and CD137 (4-1BB) in a published CITE-seq dataset of unstimulated T cells prepared in a similar manner to our dataset (*327*) **(Fig 4.3A)**. Based on the cluster annotations from the original publication, MAIT cells were the population most over-represented in the baseline AIM$^+$ population (**Fig. 4.3B**). When T1 and T2 AIM$^+$ cluster labels were mapped onto the baseline AIM$^+$ population, nearly all cells mapped to CD4_Tcm, CD8_Tem, VD2, and MAIT_1 cells (**Fig. 4.3C**). Critically, many of the polarized CD4$^+$ T cell clusters we identified (e.g., T_H1) did not have a corresponding baseline AIM$^+$ population and therefore are distinct activated populations.

4.6.4 AIM$^+$ MAIT cells have signatures of cytokine-driven activation

As evidenced by our analysis of baseline AIM$^+$ T cells, the detection of MAIT and γδT cells is at least partially attributable to their expression of AIM markers at rest. Baseline AIM$^+$ MAIT cells only mapped to our MAIT_1 cluster, suggesting the MAIT_2 phenotype was activation induced (**Fig. 4.3C**). MAIT cells and γδT cells can become “bystander activated”, by cytokine stimulation independent of their TCR specificity (*247*), perhaps explaining their detection in the AIM assay. To determine if bystander activation of MAITs could be observed here, I first confirmed that the TCR characteristics of the MAIT_1 and MAIT_2 clusters mirrored those

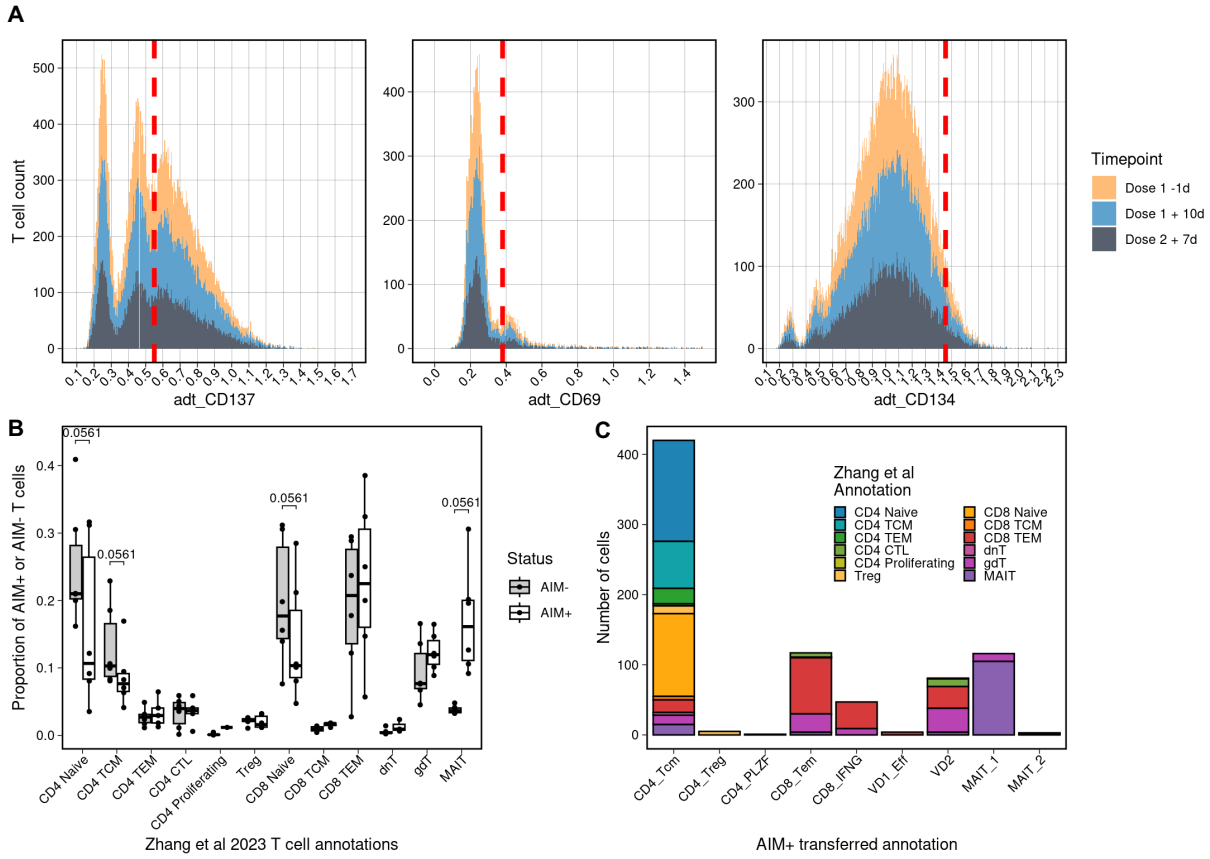

Fig. 4.3 Re-analysis of publicly available unstimulated AIM+ cells identifies background populations

Cellular indexing of transcriptomes and epitopes (CITE) sequencing analysis of RNA and surface protein expression on unstimulated T cells from dataset derived from Zhang *et al* 2023

A) Normalized expression of activation induced marker surface expression on unstimulated T cells. For CD137 (4-1BB) and CD69, red lines represent manually defined expression cut-off. For CD134 (OX-40), a clear positivity cut-off could not be defined, so a 95% expression level cut-off was used.

B) Proportion of Zhang et al defined T cell subpopulations in AIM$^+$ (CD69$^+$, 4-1BB$^+$/OX-40$^+$, defined using thresholds in A) and AIM$^-$ T cells in the unstimulated T cells.

C) Projection of annotations defined on spike-responsive AIM$^+$ T cells in the present study onto unstimulated AIM$^+$ T cells in Zhang *et al* 2023 dataset.

seen previously in sorted MAIT cells (*247*) (**Fig. 4.4A-D**). Clonal overlap was observed between the two clusters and across timepoints, suggesting the two clusters reflected plastic phenotypes (**Fig. 4.4E**). Notably, the MAIT_2 cluster had a signature of cytokine-mediated or dual TCR and cytokine (IL-12 and IL-18) stimulation, while the MAIT_1 cluster had a signature of TCR-driven activation (**Fig. 4.4F&G**). Thus, the MAIT_2 cluster appears to represent an effector population responding in a secondary manner to cytokines produced by antigen-

specific T cells.

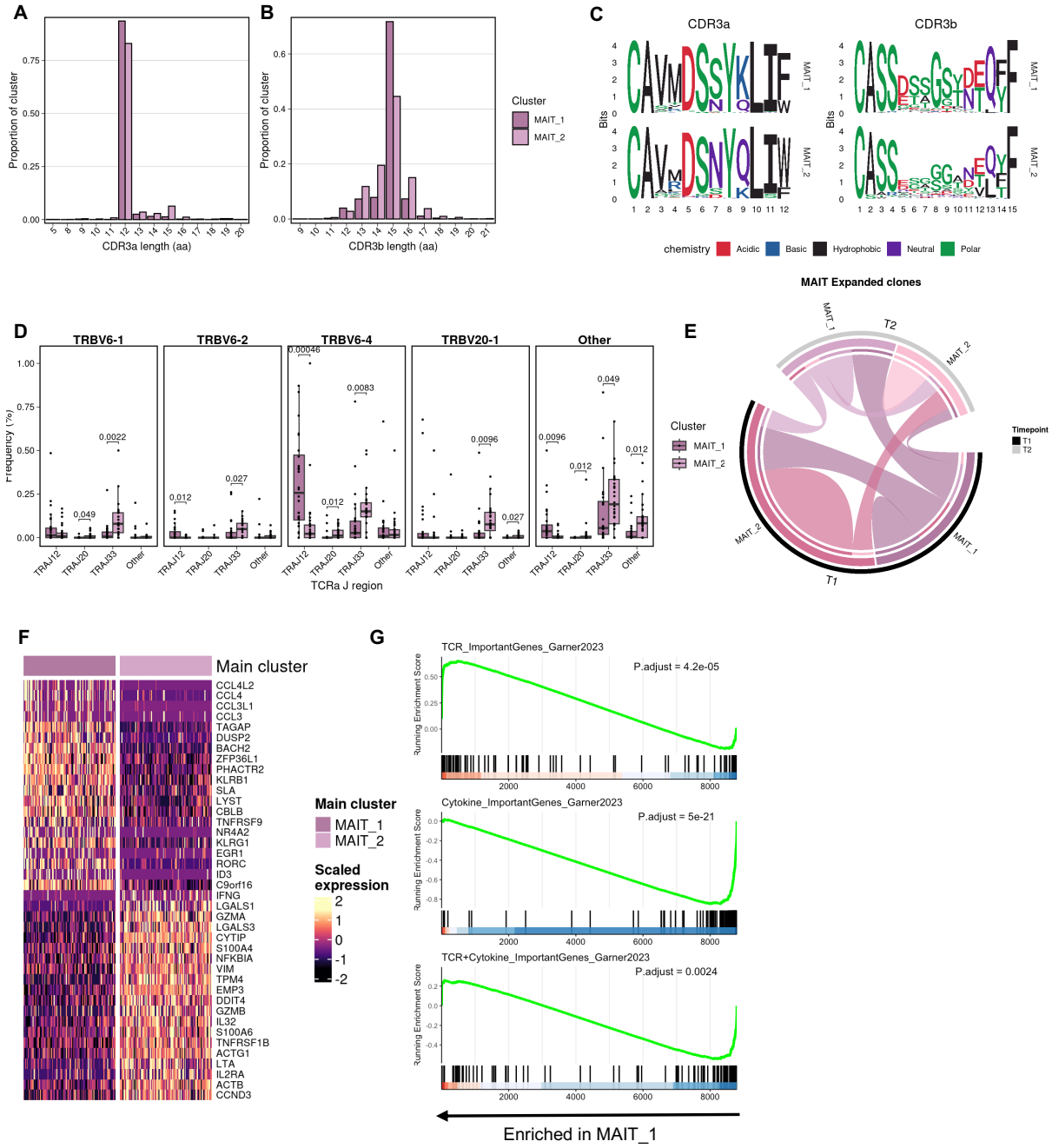

Fig. 4.4 Identification of cytokine and TCR stimulated AIM+ mucosal-associated invariant T cell populations

A&B) CDR3 length of α (A) and β (B) TCR chains in MAIT_1 and MAIT_2 AIM+ T cell populations.

C) CDR3 amino acid motifs of most common length α and β TCR chains from MAIT_1 and MAIT_2 AIM+ T cell populations.

D) Frequency of TRAJ and TRBV gene usage combinations.

E) Overlap of paired αβ CDR3 amino acid sequence clones between MAIT populations and across timepoints.

F) Scaled RNA expression of the top 20 significant differentially expressed genes between MAIT subtypes.

G) Geneset enrichment of genesets derived from sorted MAIT cells stimulated with TCR, cytokine (IL-12 and IL-18) or TCR and cytokine (IL-12 and IL-18) in (Garner et al. 2023**).** Genes were ranked based on average log fold change between MAIT clusters.

4.6.5 SARS-CoV-2 responsive T cells have diverse functional characteristics

Having identified sources of background in the recovered populations, I next assessed the functional characteristics of the AIM$^+$ populations. In line with the annotated transcriptomic phenotype, canonical effector molecules of given T cell polarization states were produced as expected: *IFNG* was produced by the T_H1/T_{FH}, T_H1/T_H17, CD8$^+$ T cell and unconventional T cell populations; *IL2* and *IL21* were produced by the T_H1/T_{FH} cluster, *IL17F* and *IL22* were produced by the T_H1/T_H17 cluster, and *IL4* and *IL13* was produced by the T_H2 cluster **(Fig. 4.5A&B)** (*328*). Cytotoxic molecules and the inflammatory chemokines *CCL3* and *CCL4* were expressed by the CD8$^+$ T cell and unconventional T cell clusters, as expected (*329*). *TNF* was broadly expressed and in some cases was the only detectable effector cytokine. Interestingly, the CD4$^+$ cytotoxic cluster expressed cytotoxic granules *GZMA*, *GZMB* and *PRF1* at levels comparable to the differentiated Th1 and Th17 populations but did not express any *IFNG* or *IL2*. CD4_HLA, CD4_TGFB1, CD4_Tcm and CD8_Tem clusters had the lowest overall expression of cytokines, concordant with their resting phenotype **(Fig. 4.5A & 4.2E)**. The T_{reg} cluster notably did not produce *IL10 (330, 331)* **(Fig. 4.5A)**. Interestingly, the populations with the highest expression of *IFNG* and *TNF* were the MAIT_2 and Vδ2 populations **(Fig 4.5A)**.

Different combinations of AIMs can be used to identify peptide-reactive cells (*315-318*). In addition to CD69, OX-40 and 4-1BB which were included in the staining panel, CITE-seq staining for other commonly used AIM markers was performed: CD107a, CD40L, ICOS and PD-1 (**Fig. 4.5C**). RNA transcript expression for CD69, OX-40 and 4-1BB was consistent with the expected protein-level expression for each AIM (**Fig. 4.2E & 4.5C**). However, comparison of the surface protein expression of the other AIMs revealed interesting patterns. CD40L was expressed in CD4$^+$ T cell clusters as compared to CD8$^+$ T cell clusters, with the marked exception of T_{reg} cells that had low expression (**Fig. 4.5C**). ICOS was also more strongly expressed on CD4$^+$ T cell clusters as compared to CD8$^+$ T cell clusters, with strongest expression on the T_H1/T_{FH} and T_{reg} clusters (**Fig. 4.5C**). Finally, PD-1 expression was biased

towards clusters associated with type 1 immunity (T_H1/T_{FH}), with low expression on most CD4+ T cell clusters. Thus, depending on the combination of AIMs used, markedly distinct T cell populations, particularly CD4+ T cell populations, are recovered.

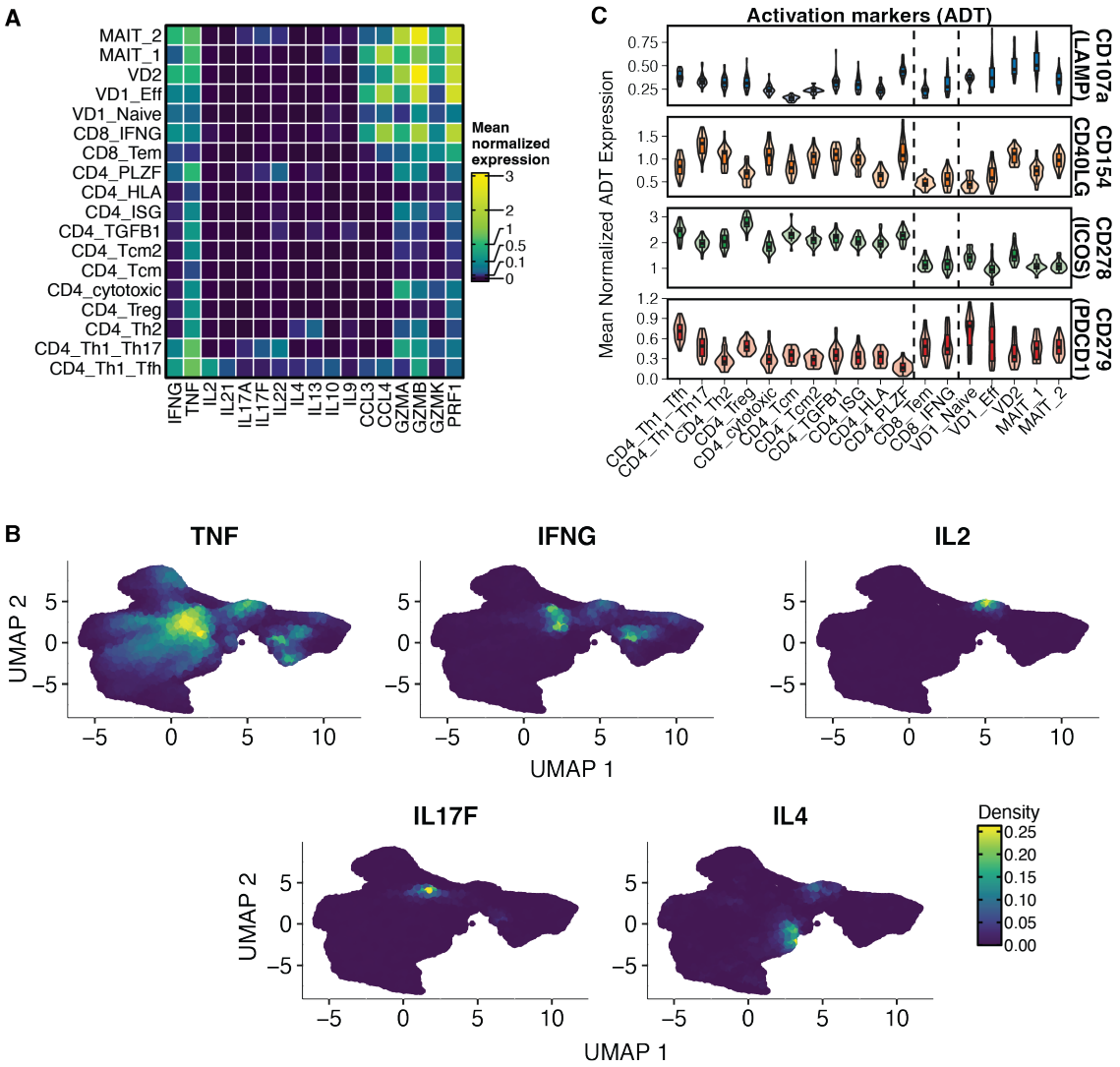

Fig. 4.5 SARS-CoV-2 spike responsive T cell clusters are functionally heterogenous

A) Mean normalized RNA expression of selected functional genes across clusters.

B) Mean normalized ADT expression of surface activation induced proteins.

C) Projection of the RNA expression density of selected functional cytokines onto gene expression UMAP.

4.6.6 AIM+ T cell populations have varied effector and inhibitory interactions.

To better understand the function of AIM+ T cells, we examined putative cell-cell interactions between clusters using CellphoneDB, with the caveat that only T cell – T cell interactions could be examined in this dataset. CellphoneDB uses a curated database of experimentally derived and predicted cell-cell interactions, which are mapped to clusters by examining the relative

expression patterns of ligands and their receptors (*322, 332*).

Overall, CD4+ T cells sent and received proportionally fewer signals than CD8+ T cells and unconventional T cells (**Fig. 4.6A-C**). Classification of these using pre-prepared biological classifications interactions highlights diverse biology (**Fig. 4.6B**). The majority of interactions were classified within human leukocyte antigen (HLA), TNF, Intercellular Adhesion Molecule

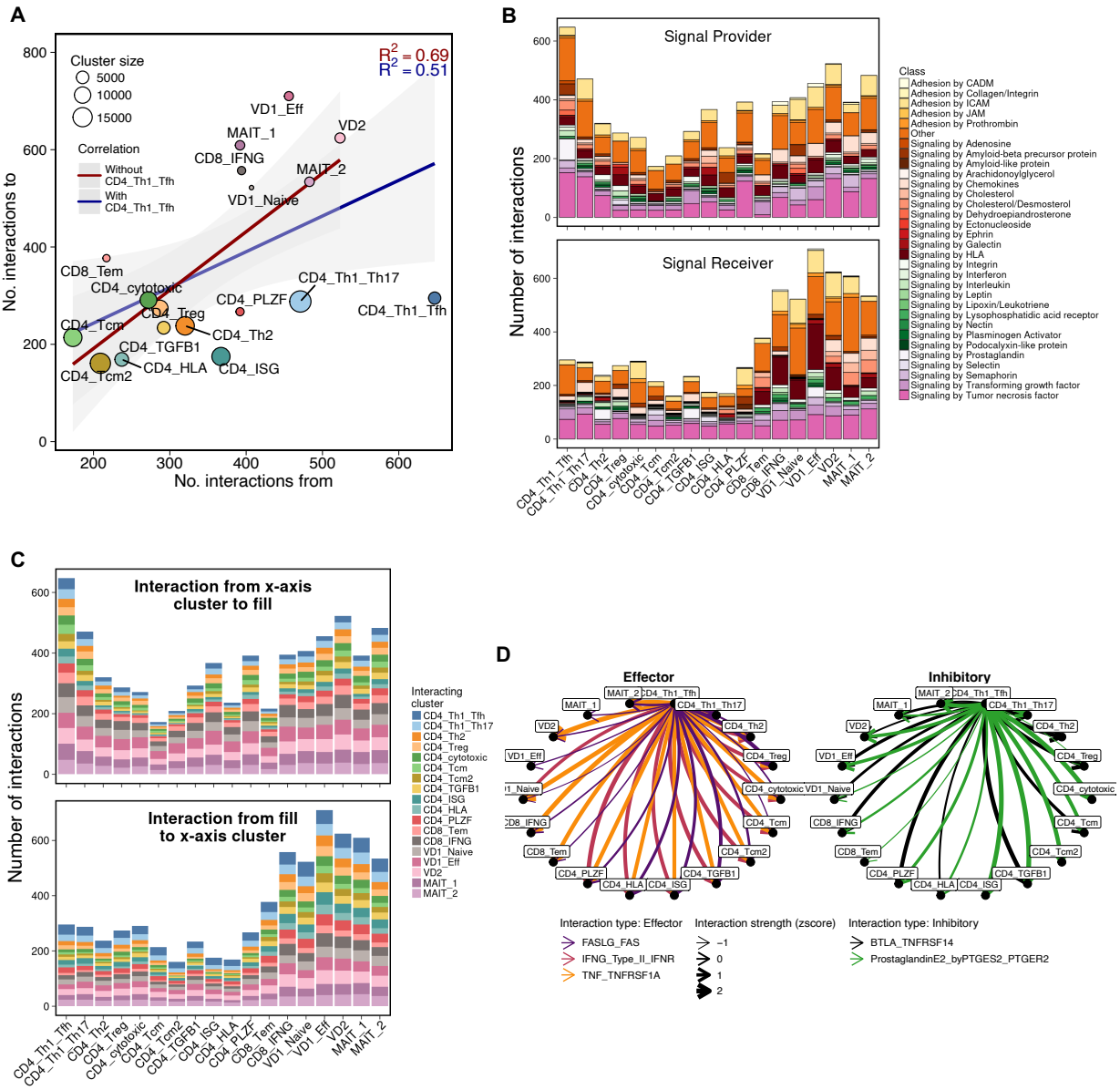

Fig. 4.6 Unique effector and inhibitory interactions between SARS-CoV-2 spike responsive T cell clusters

A) Pearson correlation of total number of interactions to and from a given cell type, with or without CD4_Th1_Tfh cluster. Point size is scaled by number of cells per cluster.

B&C) Significant CellphoneDB derived interactions from (top) or to (bottom) each spike-responsive T cell cluster, separated by B) broad biological interaction class or C) cell type interaction partner.

D) Selected effector and inhibitory interactions that originate from the CD4_Th1_Tfh cluster. Arrow points in direction of interaction and is scaled by interaction strength.

(ICAM) and "other" groups, which includes broad cytokine signalling pathways (*322, 332*). The T_H1/T_{FH} cluster sent the greatest number of signals to other clusters, suggesting a "hub" role for these cells (**Fig. 4.6A&C**). Examination of specific interactions revealed both immune stimulatory (e.g., IFNγ, TNF and FASL interaction with their receptors) and immunomodulatory (e.g., BTLA and Prostaglandin E2 interaction with their receptors) interactions between the T_H1/T_{FH} cluster and all other clusters (**Fig. 4.6D**).

4.6.7 Antigen-specific and expanded clones are shared across T cell subsets

Analysis of the transcriptional and surface protein expression of AIM^+ T cell subsets identified diverse T cell populations. Some analysis suggests that T cell clonality and TCR specificity are related to T cell function, with relevance to T cell memory formation (*333-335*). Therefore, I next explored the relationship of T cell clonality and function amongst the SARS-CoV-2 responsive T cells. Clusters did not show specific enrichment of TCRα or TCRβ chains, with the exception of the CD4_PLZF cluster (**Fig. 4.7A&B**), which was enriched for *TRAV10*, *TRBV4-1, TRAJ18* and *TRBV12-5* genes. Expanded clones were found across all clusters and at both timepoints, but were proportionally more abundant in T_H2 cells, cytotoxic $CD4^+$ T cells, ISG^{hi} $CD4^+$ T cells and $IFN\gamma^+$ $CD8^+$ T cells (**Fig. 4.7C**). A large proportion of captured cells in each cluster were unexpanded. In expanded clones, there was considerable clonal sharing between $CD4^+$ T cell clusters, with notable exception of the T_{reg} population (**Fig. 4.8A&B**). A major contribution to this clonal sharing was population interconversion between timepoints (**Fig. 4.8C**).

4.6.8 For a given effector state, T cell functionality is related to clonality

The considerable cross-cluster sharing suggests that clonality is not directly related to gene expression. To more systematically assess the relationship between clonal identity and transcriptomic signature, I performed Clonotype Neighbor Graph Analysis (CoNGA), an

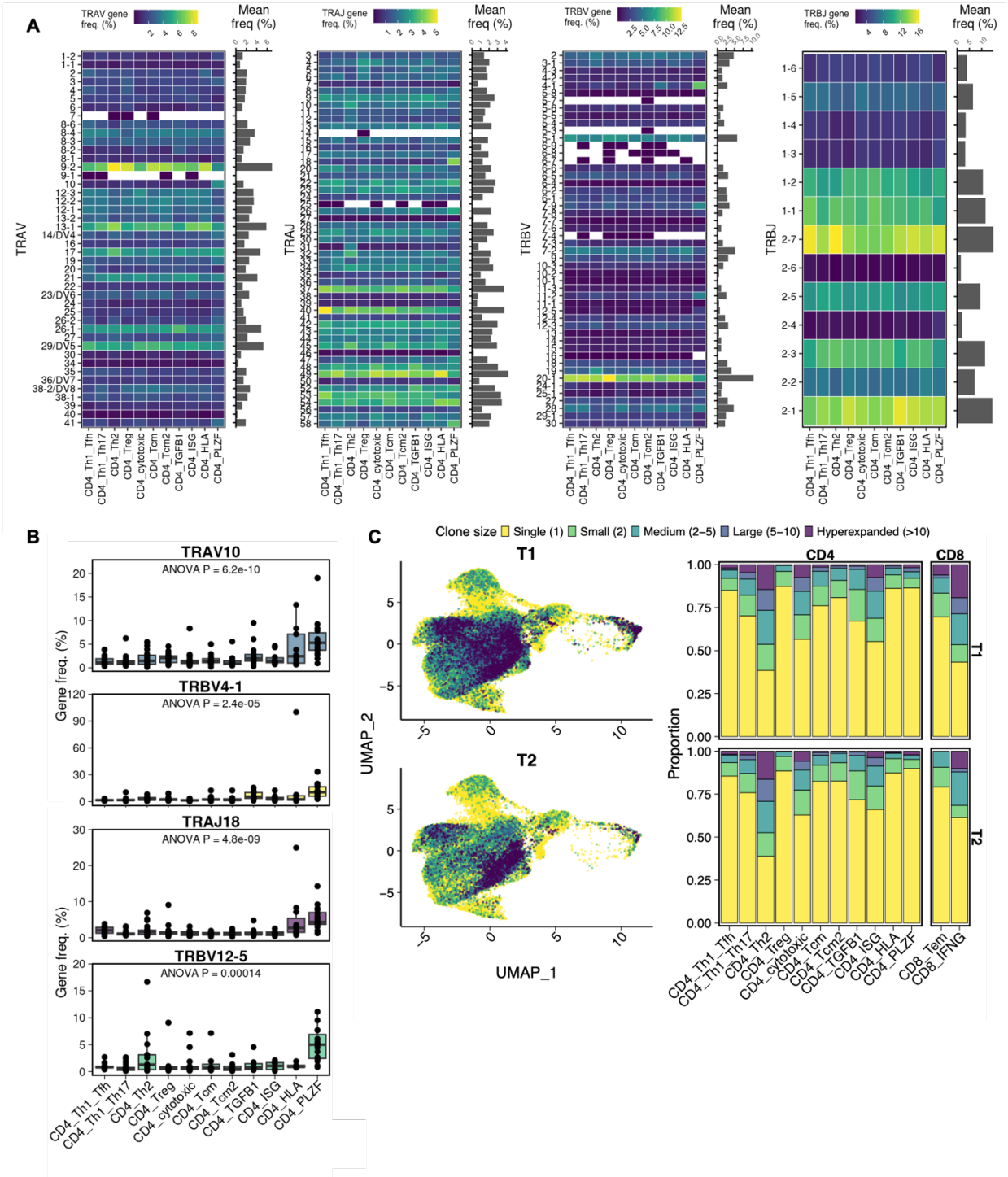

Fig. 4.7 The SARS-CoV-2 spike responsive TCR repertoire is diverse and includes large, expanded clones

A) *TRAJ*, *TRAV*, *TRBJ* and *TRBV* frequencies within spike-responsive CD4⁺ cell populations.

B) Gene usages with most significant differences in variation across cell clusters measured by ANOVA. Benjamini-Hochberg adjusted P value presented.

C) Proportion of cells within expanded or singlet clones per cluster and timepoint projected onto gene expression UMAP (left) or as proportion of cluster (right). Clones defined as an identical paired αβ CDR3 amino acid sequence within an individual/timepoint.

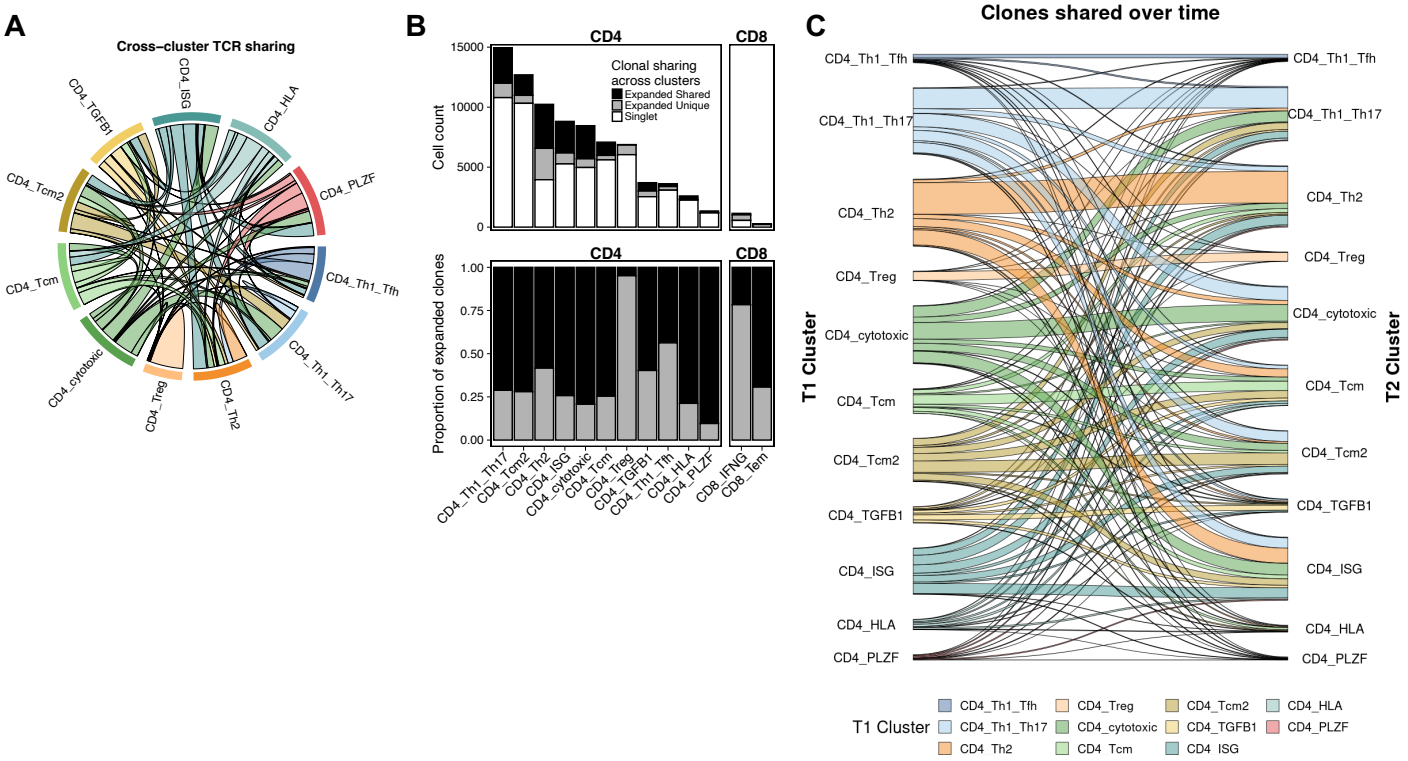

Fig. 4.8 SARS-CoV-2 spike responsive T cell clones are shared between clusters and their phenotype is altered with a boosting dose

A) Sharing of expanded CD4⁺ T cell clones (clone size >1) across transcriptional phenotype. Chord sizes reflect the relative proportion of each cluster that has shared clones.

B) Number and proportion of clones that are singlets; or expanded clones that are unique to a given cluster or shared across clusters.

C) Overlap of paired αβ CDR3 amino acid sequence clones between spike-responsive CD4⁺ T cell populations across timepoints

approach which integrates TCR distance metrics with gene expression values to find associations between T cell functionality and specificity (**Section 4.5.4**)(*323*). As expected, this approach identified a strong correlation between gene expression and TCR specificity in both MAIT populations **(Fig. 4.9A&B)**. However, other AIM⁺ clonotypes showed mostly low or no relationship between gene expression and TCR specificity. The CD4_PLZF and CD8_IFNG clusters had the highest proportion of clones with significant enrichment of gene expression and TCR clonality, including groups of highly enriched clones **(Fig 4.9C)**. Further analysis of these enriched clonotypes identified groups of T cell clones with restricted TCR gene usage (**Fig. 4.9D**). Clones within the PLZF⁺ CD4⁺ T cell cluster were restricted to *TRBV4-1* and had diverse *TRAV/TRAJ* gene usages **(Fig. 4.9D)**. The semi-invariant TCR chain in combination with *PLZF* expression in this population align with previously described CD1c auto-reactive CD4⁺ T cells (*336*). A search of VDJdb (vdjdb.cdr3.net) indicated that one of the

enriched CD8⁺ CDR3b amino acid sequences (CASQETNTGELFF) matched a previously published SARS-CoV-2 spike specific clone, suggesting this likely represents a public SARS-CoV-2 spike specific clonotype.

This analysis suggested that when looking at clones across the entire dataset, TCR specificity was not related to T cell gene expression, likely because of the cross-cluster clonal sharing previously observed (**Fig. 4.8A)**. I next assessed if measures of T cell activity were associated with clonal expansion within a given cell type. In contrast to the CoNGA analysis, expanded clones within IFNγ⁺ CD8⁺ and T_H1/T_{FH} clusters were associated with increased cytotoxicity

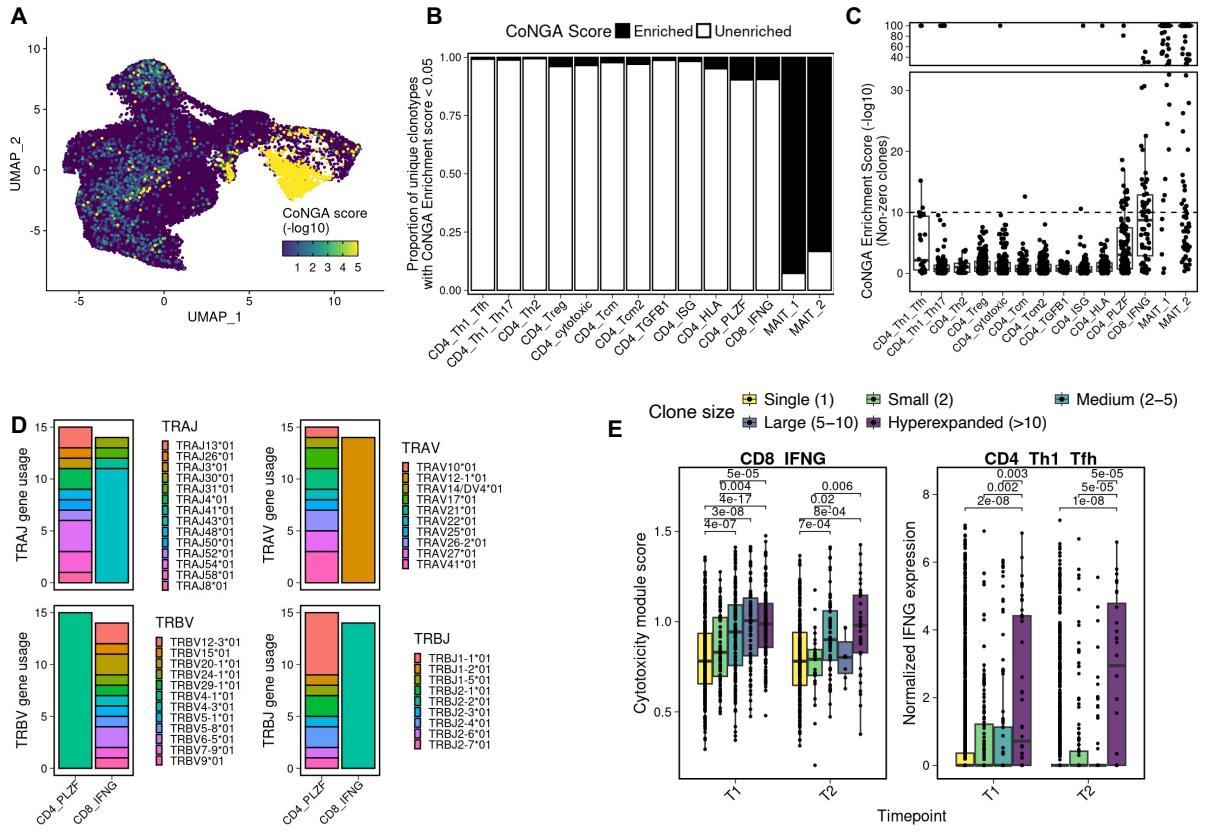

Fig. 4.9 The clonality and functionality of SARS-CoV-2 spike responsive T cells are related

CoNGA analysis of TCR x Gene expression. All data represent cells condensed into single unique clonotypes (n=61,375) as per **Section 4.5.4** and Schattgen *et al.* 2022.

A) Gene expression UMAP embedding coloured by CoNGA score. Score capped at 10^{-5} to aid visualization.

B) Proportion of unique clonotypes with CoNGA enrichment score <0.05 (enriched).

C) Enrichment score for individual CoNGA enriched clonotypes, dotted line represents cut-off used to select clonotypes for further analysis.

D) Analysis of gene usage from top CoNGA enriched clones within CD4_PLZF and CD8_IFNG clusters.

E) Per cell effector CD8⁺ cytotoxicity module score (left) and effector CD4⁺ normalized *IFNG* transcript expression (right) as a function of clonal size (Mann-Whitney U test, Bonferroni adjusted).

(published geneset from (*246*)) and *IFNG* production respectively (**Fig. 4.9E**). Therefore, for a given effector state, clonal expansion is associated with T cell functionality.

4.6.9 Antigen-enriched meta-clonotypes are enriched in certain AIM$^+$ T cell clusters

On the basis that TCR clones with similar physiochemical and sequence properties are likely to bind to similar antigen (*337*), TCR distancing metrics which quantify these properties can be used to cluster highly physiochemically similar, but non-identical, TCRs together into "meta-clonotypes". Such meta-clonotypes are informative as the high potential variation in the TCR repertoire (estimated number of clones in the human body is between 10^8-10^{10} (*338*), with a theoretical limit of 10^{61} possible clones (*339*)) makes it challenging to identify expanded clones with limited sample sizes, even within antigen-enriched T cell populations as in this study.

To test whether each meta-clonotype was likely to be antigen enriched, I performed TCR clumping analysis using the CoNGA package (**Section 4.5.4**). This analysis identified multiple antigen-enriched meta-clonotypes in both CD4$^+$ and CD8$^+$ T cell clusters and accounted for 0-2.5% of clonotypes within each conventional T cell population (**Fig. 4.10A&B**). Notably, none of the 6,001 unique clonotypes identified in the CD4$^+$ T_{reg} cluster were predicted to belong to an antigen-enriched meta-clonotype (**Fig. 4.10B**). Furthermore, CD4$^+$ T cells associated with the AIM$^+$ background (CD4_Tcm, **Fig. 4.3C**) or with a more resting gene expression phenotype (CD4_TGFB1 and CD4_HLA, **Fig. 4.5A**) had lower frequencies of antigen-enriched clonotypes compared with other CD4$^+$ T cell populations (**Fig. 2F**).

173 distinct meta-clonotypes were predicted to be antigen-enriched, including 11 with more than 10 unique participating clonotypes (**Fig. 4.10C-F**). The antigen-enriched meta-clonotypes included cells from several cell types (**Fig. 4.10C**). Interestingly, based on TCR gene usage, the largest antigen-enriched meta-clonotype matched the description of a CD1d restricted invariant NKT TCR (*340*). This aligned with the CoNGA clonotype analysis, which independently identified clones within the PLZF$^+$ CD4$^+$ T cell cluster that were restricted to *TRBV4-1* gene usage (**Fig 4.9D)**. These TCR characteristics, combined with *PLZF* expression

in this cluster, suggests that CD1c, CD1b and CD1d auto-reactive CD4+ T cells may additionally be captured in this assay (*336, 341*). The presence of these cells in the AIM+ T cell population is likely caused by the same processes of bystander activation that result in identification of MAIT cells, as discussed above (**Fig. 4.4)**.

Other predicted antigen-enriched meta-clonotypes represent undescribed clusters of likely SARS-CoV-2 spike-specific T cell clones with similar TCR properties, the largest of which are characterized in **Fig. 4.10C-F.**

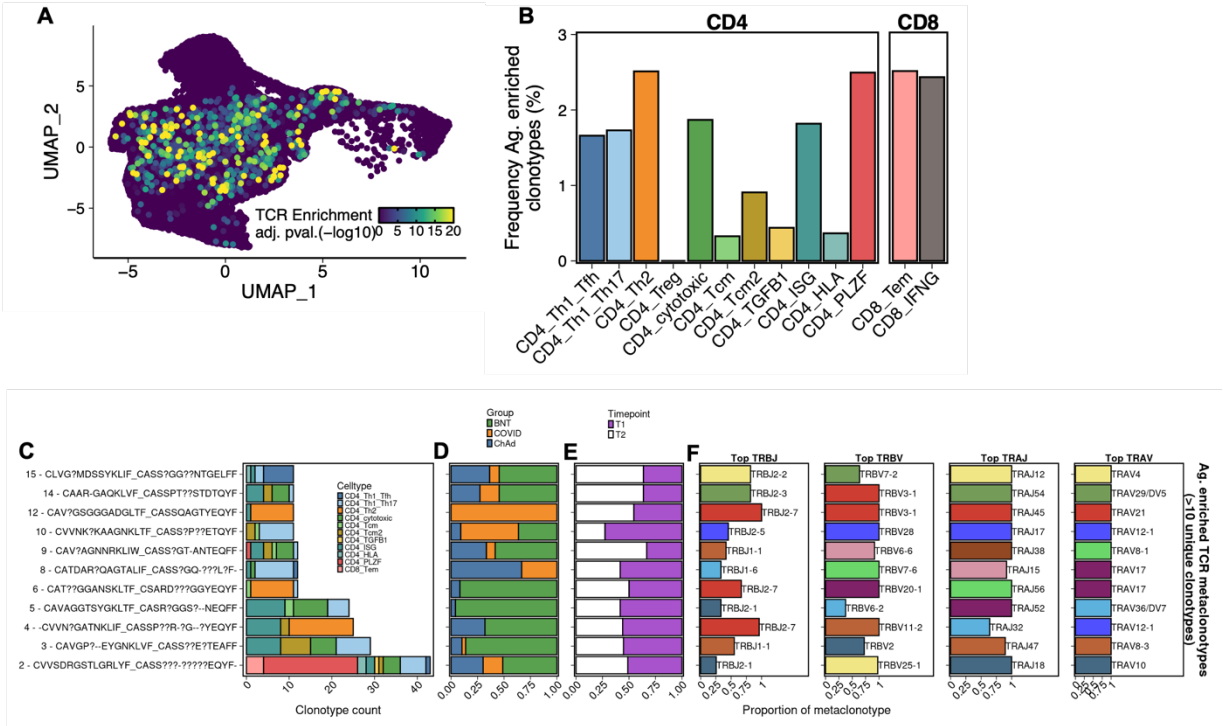

Fig. 4.10 Meta-clonotype analysis identifies SARS-CoV-2 spike responsive T cell clones that are antigen enriched

A) Gene expression UMAP colored by the statistical significance of TCR neighborhood (meta-clonotype) antigen enrichment compared with the simulated expected VDJ background.

B) Frequency of clonotypes within each T cell cluster that are predicted to be within an antigen-enriched TCR meta-clonotype (adjusted p value <0.05).

C-F) Antigen-enriched TCR meta-clonotypes with >10 participating unique clonotypes detected using TCR enrichment programme within CoNGA package, includes paired αβ CDR3 consensus sequences and cell type (C), vaccine (D), timepoint (E), and TCR gene usage proportions (F).

4.6.10 AIM+ Treg cells suggest an immune promoting phenotype

The TCR analysis suggests that the T_{reg} population is not a clonally-restricted antigen-specific population (**Fig. 4.10**). However, prior optimization studies have suggested that AIM+ T_{reg} cells are activated in a manner dependent on antigen stimulation (*317, 342*). Consistent with this,

our baseline analysis found only a minor contribution of T_{reg} cells to the background (**Fig. 4.3**). Therefore, I was interested in understanding the function of these antigen-responsive T_{reg} cells. Sub-clustering identified multiple clusters with graded expression of CCR7, CD278 (ICOS), *LEF1* and *CTLA4*, suggesting the presence of both effector T_{reg} cells (CTLA-4^{+} ICOS^{+} FoxP3^{int} CD25^{lo}) and memory T_{reg} cells (LEF1^{+} CCR7^{+} FoxP3^{hi} CD25^{hi}) (**Fig. 4.11A-C**)(*343*). *FOXP3*, *IL2RA* and moderate levels of *IKZF2* (HELIOS) were expressed by all clusters (**Fig. 4.11B**). All T_{reg} cell clusters had minimal production of canonical T_{reg} effector cytokines *IL10*,

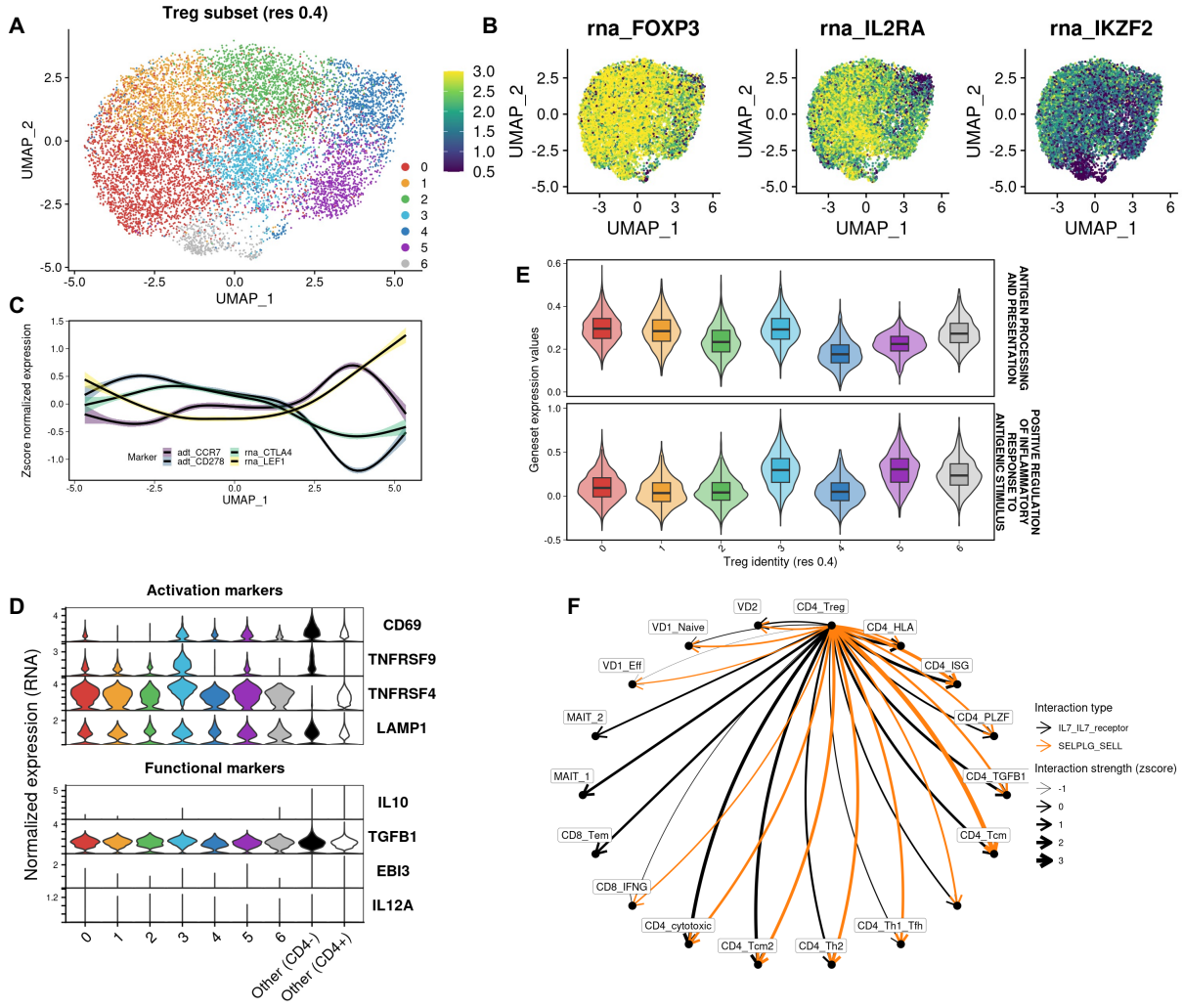

Fig. 4.11 AIM^{+} Regulatory T cells have an immune promoting phenotype

A) UMAP and Louvain clustering of CD4_Treg subset.

B) Scaled expression of T_{reg} associated genes.

C) Scaled surface protein or gene expression of markers associated with effector and memory T_{reg}s.

D) Expression of activation induced marker associated and T_{reg} functionality associated genes in T_{reg} clusters and other CD4^{+} and CD4^{-} spike-responsive T cells.

E) Aggregate gene expression for gene ontology biological pathway (GOBP) modules associated with antigen processing and response to antigen.

F) Selected unique or enriched CellphoneDB derived significant interactions made from T_{reg}s to other spike-responsive T cell clusters.

TGFB, *IL12A* and *EBI3* (**Fig. 4.11D**). In contrast to a suppressive response, the T_{reg} populations appeared to have an immune promoting phenotype. Multiple effector T_{reg} clusters (clusters 0-3) had elevated expression of gene sets associated with antigen presentation and positive regulation of inflammatory responses to antigen stimulation (cluster 3), compared with other T_{reg} populations (**Fig. 4.11E**). A putative reciprocal interaction between the T_{reg} cluster and nearly all populations involved cell-cell interaction via CD62L (*SELL*) binding to the receptor PSGL-1 (*SELPLG*). Additionally, T_{reg} cells uniquely produced *IL7* (**Fig. 4.11F**). In sum, this suggests that although AIM^+ T_{reg}s are clonally unrelated to the other $CD4^+$ AIM^+ T cells, they have a unique immune-promoting role.

4.6.11 Pre-existing SARS-CoV-2-reactive T cells are detectable prior to COVID-19 vaccination

Having broadly described the phenotype, functionality and clonality of AIM^+ T cells after vaccination, I next aimed to assess the impact of pre-existing T cell clones on the development of SARS-CoV-2 spike-specific T cell responses.

To address this, I analysed a dataset of spike-specific T cells generated by Dr Nicholas Provine using a seven-day cell proliferation assay at the pre-vaccine timepoint ("T0") (*231*) (**Fig. 4.12A&B**). The CTV-dilution cell proliferation assay was selected due to its high sensitivity (*309*), and because the main aim of this analysis was to assess the recall of pre-existing T cell clones over vaccination, rather than to investigate the functionality of pre-existing clones (which is altered over the 7-day stimulation period).

After QC, 1,050 pre-vaccination SARS-CoV-2 responsive T cells were recovered comprising $CD4^+$ and $CD8^+$ T cell populations with naïve and effector phenotypes (**Fig. 4.12C-E**). Unconventional T cells were also recovered (**Fig. 4.12C-E**). Reference mapping the T0 dataset to the T1/T2 AIM dataset found that only a portion of the populations described in the AIM^+ data mapped to the T0 data, but there was logical concordance between annotations (**Fig. 4.12F**). The relative frequency of T cell populations captured from individuals in BNT and

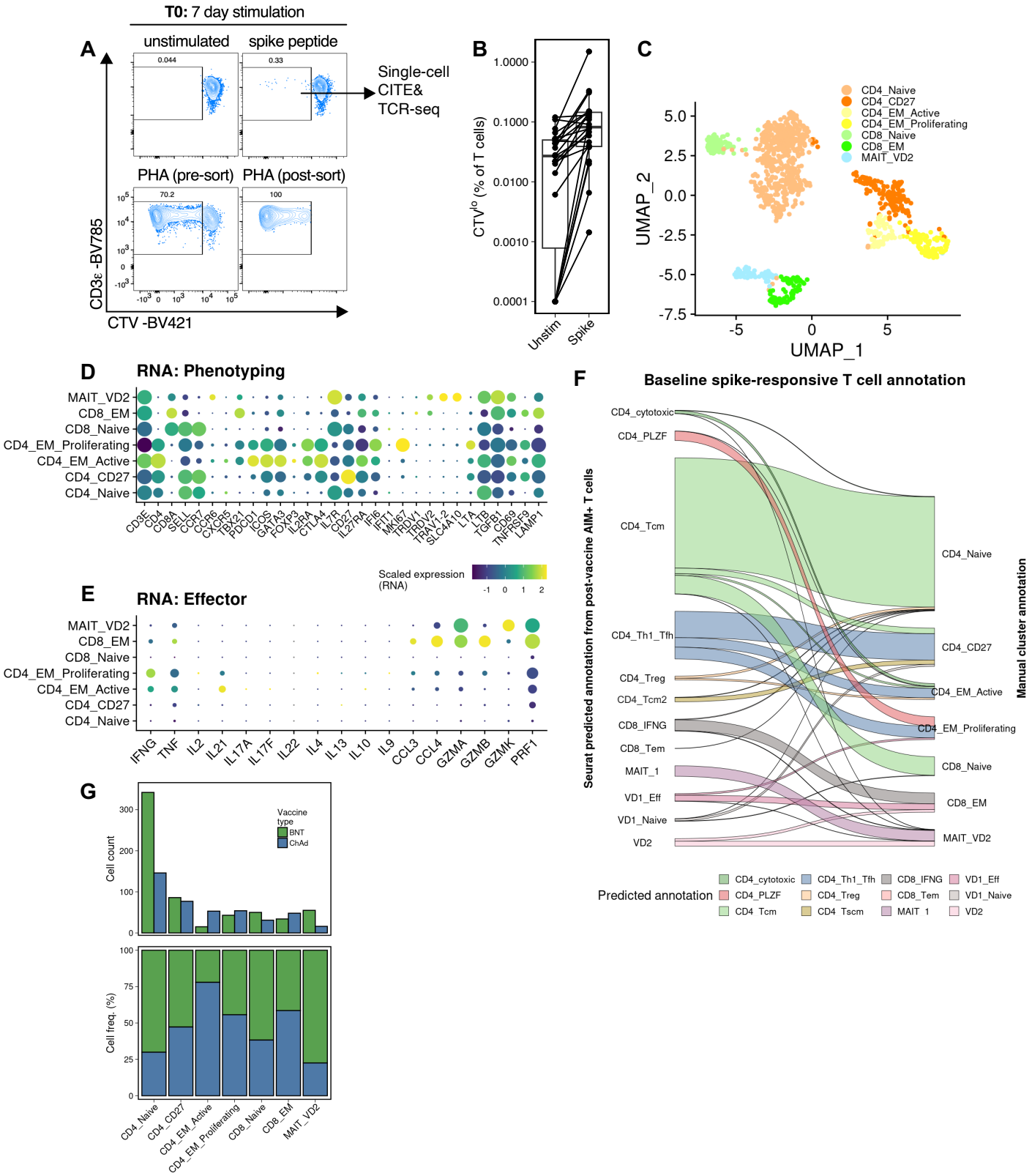

Fig. 4.12 Proliferative SARS-CoV-2-reactive T cells are detectable prior to COVID-19 vaccination

A) Representative flow cytometric staining of cell trace violet (CTV) dilution assay to detect SARS-CoV-2 spike reactive T cells prior to vaccination.

B) Frequency of CTV^{lo} T cells after 7 days with or without SARS-CoV-2 peptide stimulation.

C) UMAP embedding of pre-vaccination spike-responsive T cells.

D&E) Scaled gene expression of phenotyping (D) and effector (E) genes in pre-vaccination spike-responsive T cells.

F) Comparison of manual annotation of pre-vaccination spike-responsive T cells with annotations mapped onto pre-vaccination spike-responsive T cell dataset from post-vaccination AIM^+ spike-responsive T cells.

G) Proportion of cells from each vaccination group in each pre-vaccination T cell cluster.

ChAd groups were broadly similar, however more cells within naive CD4+ and the mixed MAIT/ Vδ2 γδT cell population were captured prior to vaccination in individuals in the BNT group **(Fig. 4.12G)**.

4.6.12 Recall of pre-existing SARS-CoV-2 reactive T cell clones has little impact on the function of vaccine-induced T cells.

I next assessed the recall of T0 clones at T1 and T2 timepoints. 756 unique paired TCR clonotypes were detected at T0. Only 21 (2.8%) of these overlapped with either of the post-vaccine timepoints and only eight (1.1%) were found at both timepoints **(Fig. 4.13A)**. Strikingly, pre-existing spike-reactive T cells were found post-vaccination only in the BNT group (0 out of 22,368 cells in pre-existing clones ChAd vs 94 out of 40,569 cells in pre-existing clones BNT, $p = 1.46x10^{-18}$, Fisher's exact test) (**Fig. 4.13B**). Baseline clones identified at post-vaccine timepoints were mostly found in CD8+ T cell clusters (**Fig. 4.13C**). Post-vaccination, pre-existing clonotypes were not more cytotoxic than ones only identified after vaccination (**Fig. 4.13D**). Collectively, these data suggest that pre-existing cross-reactive T cells make only a minor contribution to the overall vaccine-induced response and recall of pre-existing clones does not alter the cytotoxic function of vaccine-induced CD8+ T cells.

4.6.13 CD4+ T cells that are recalled upon second vaccination have an altered phenotype compared to the *de novo* response.

I next examined if clones induced by the primary vaccine and recalled by the second dose (detected at T1 and T2; "recalled clones") were different from clones only detected at T2 (and thus more likely to be a *de novo* response of vaccine dose 2). Differential expression analysis revealed a limited set of genes in each cluster between recalled and *de novo* clones, with the largest number of differences in the T_H1/T_{FH}, T_H1/T_H17, cytotoxic and ISG^{hi} CD4+ T cell clusters (**Fig. 4.14A**). No genes were significantly differentially expressed between recalled and *de novo* clones in IFNγ+ CD8+ T cells. Cytolytic components such as *GZMA*, *GZMB* (Granzyme A & B), *GNLY* and *LGALS1* were amongst the most upregulated genes in recalled versus *de novo* clones in CD4+ populations (**Fig. 4.14B**). In T_H1/T_{FH} cells but not T_H1/T_H17 cells, this

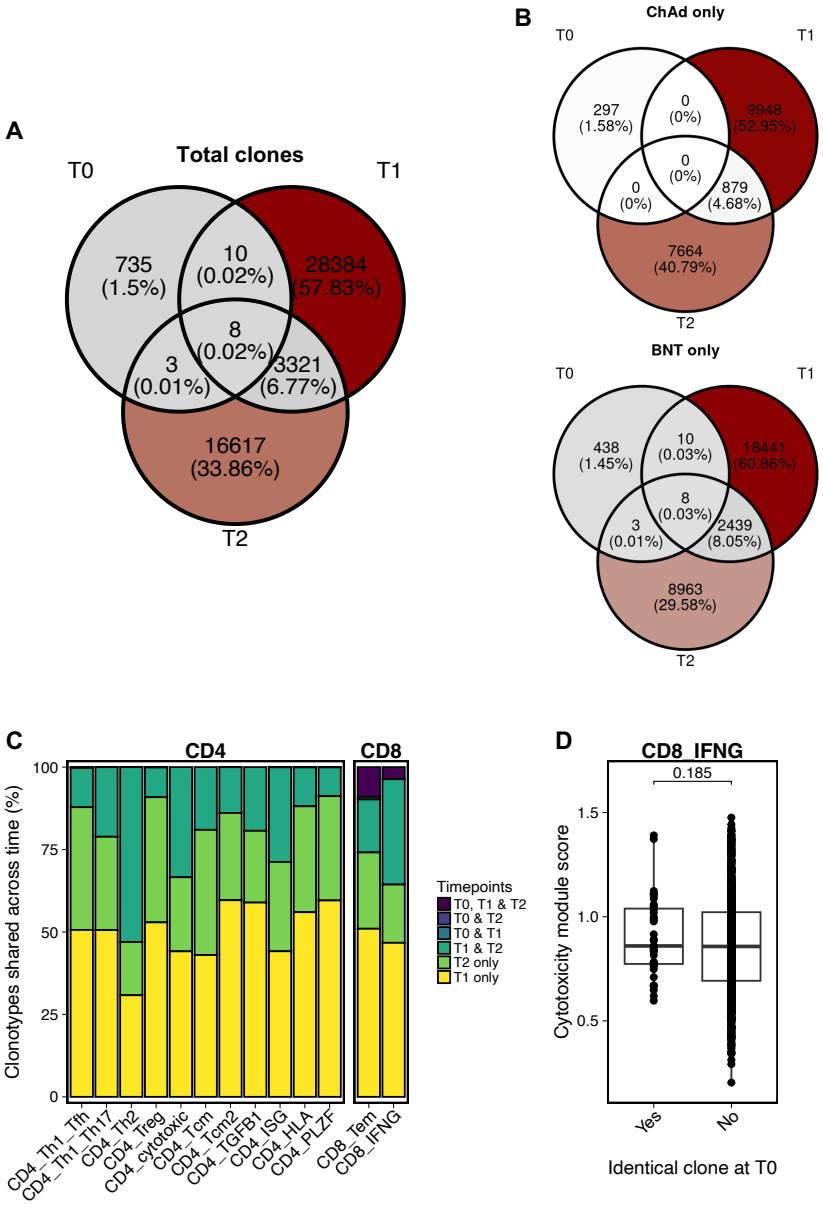

Fig. 4.13 Pre-existing clones are recalled after vaccination with BNT162b2 but not ChAdOx1 nCoV-19, but have little impact on SARS-CoV-2 specific response

A) Number of unique paired αβ TCR clones that are shared across study timepoints in conventional spike-responsive T cells.

B) Number of unique paired TCR clones that are shared across study timepoints in conventional spike-responsive T cells, split by vaccine type.

C) Proportion of post-vaccine spike-responsive conventional T cell clones that are shared across timepoints within an individual donor.

D) Cytotoxicity module score of post-vaccination effector $CD8^+$ cells that shared or did not share clonality with a pre-vaccination spike-responsive T cell (students T-test).

corresponded with a more effector-like phenotype, with decreased protein expression of CCR7 and CD45RA (**Fig. 4.14C)**. Thus, effector function and memory phenotype differ across

recalled and *de novo* clones in CD4⁺ populations, but not in CD8⁺ T cells.

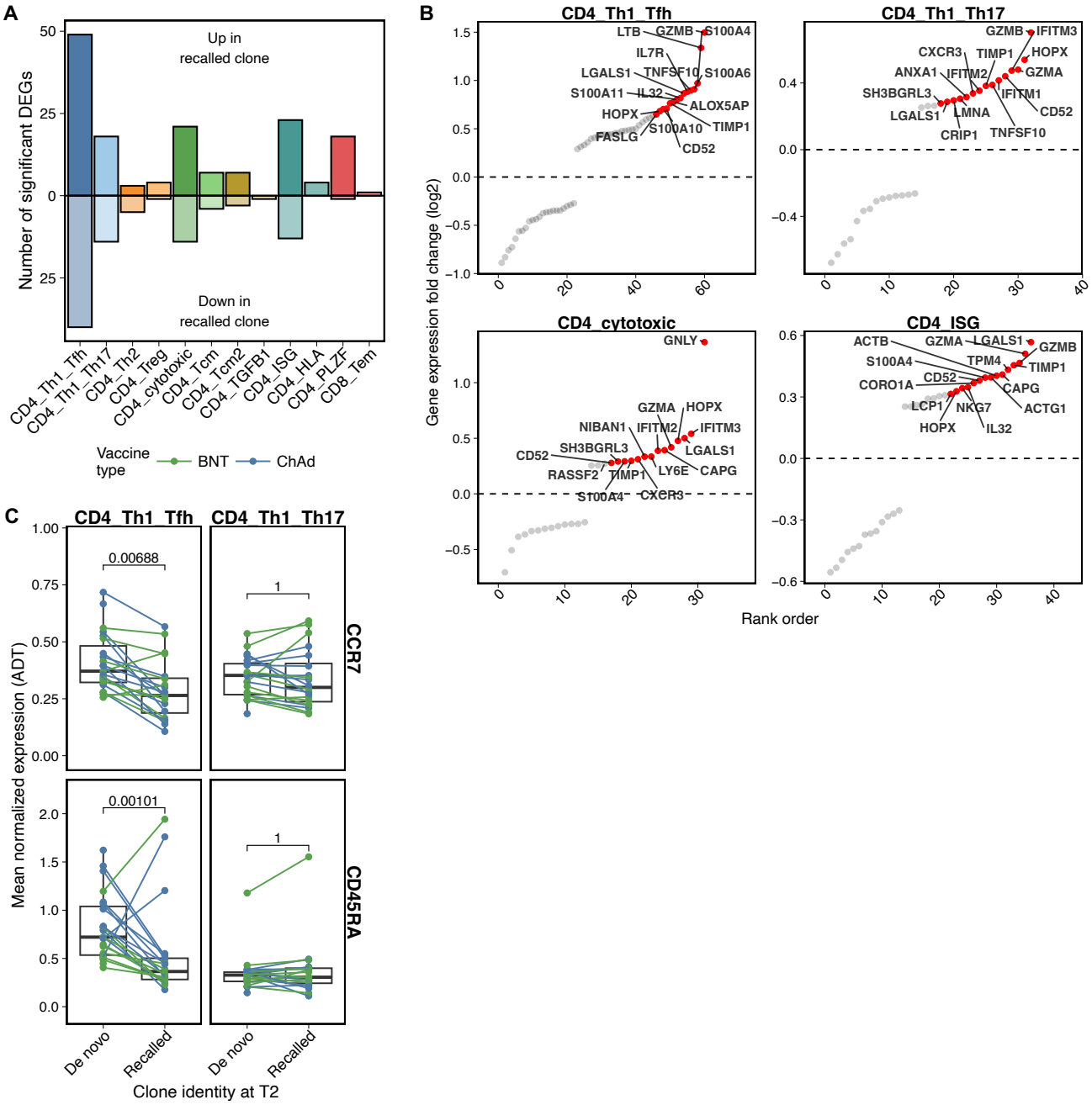

Fig. 4.14 CD4⁺ T cells that are recalled upon second vaccination have an altered phenotype compared to *de novo* responses

A) Number of within-cluster differentially expressed genes (DEGs, average $\log_2$ fold change >0.25 and adjusted p <0.05) between post-second dose (T2) T cells with (recalled) or without (de novo) a shared identical paired TCR at an earlier study timepoint.

B) Significantly differentially expressed genes (as in F) from selected CD4⁺ T cell clusters with highest frequencies of DEGs.

C) Mean per person normalized surface protein (ADT) expression of T cell memory markers in selected T2 CD4⁺ T cell clusters (Mann-Whitney U test, Bonferroni adjusted).

4.6.14 Distinct T cell responses are induced by ChAdOx1 nCoV-19 and BNT162b2 vaccines

Analysis of the overall AIM dataset identified T cells of varied phenotype, with a potential effect of T cell recall on the vaccine induced response. I next assessed the impact of the SARS-CoV-2 stimulus (e.g. COVID vs vaccine, BNT vs ChAd) on spike-responsive T cells.

I first compared ChAd with BNT responses. ChAd vaccination induced a significantly greater proportion of T_H1/T_{FH} $CD4^+$ T cells at both the T1 and T2 timepoints compared with BNT, in addition to select unconventional T cell populations (MAIT_1 and naive $V\delta1^+$ γδT cell clusters) (**Fig. 4.15A**). The frequency of the HLA^{hi} $CD4^+$ T cell cluster was lower in ChAd compared with BNT at both timepoints. Differential gene expression analysis per cluster revealed only minor differences between ChAd and BNT vaccination, with the majority of differences in the $IFN\gamma^+$ $CD8^+$ population (**Fig. 4.15B**). Differential expression of AIMs at the protein level were also observed between groups. CD107a, ICOS and CD279 (PD-1) expression was significantly increased in the $IFN\gamma^+$ $CD8^+$ T cell population in ChAd compared with BNT (**Fig. 4.15C**). PD-1 expression was also increased across most of the $CD4^+$ T cell populations in ChAd compared with BNT (**Fig. 4.15C**).

The difference in both transcriptional and surface AIMs on the $IFN\gamma^+$ $CD8^+$ population was intriguing, as it suggests differing activation of $CD8^+$ effector T cells by ChAd and BNT vaccination. Examination of a signature of cytotoxic function found discordant differential expression based on vaccine type (**Fig. 4.15D**). *IFNG* expression was significantly higher in response to ChAd vaccination, while BNT induced significantly greater levels of cytotoxic granule molecules (*GZMA* and *GNLY*) (**Fig. 4.15D**). Differential gene expression in the CD8_IFNG cluster was largely concordant at both timepoints, however a signature of increased ISG expression (*IRF7*, *OAS3*, *IFIT2*, *IFI6*) was identified in BNT vaccinees at T2 only (**Fig. 4.15E**). These differences corresponded to a more T_{EMRA} phenotype in $CD8^+$ T cells induced by BNT compared with a mixed T_{EM}/T_{EMRA} phenotype induced by ChAd

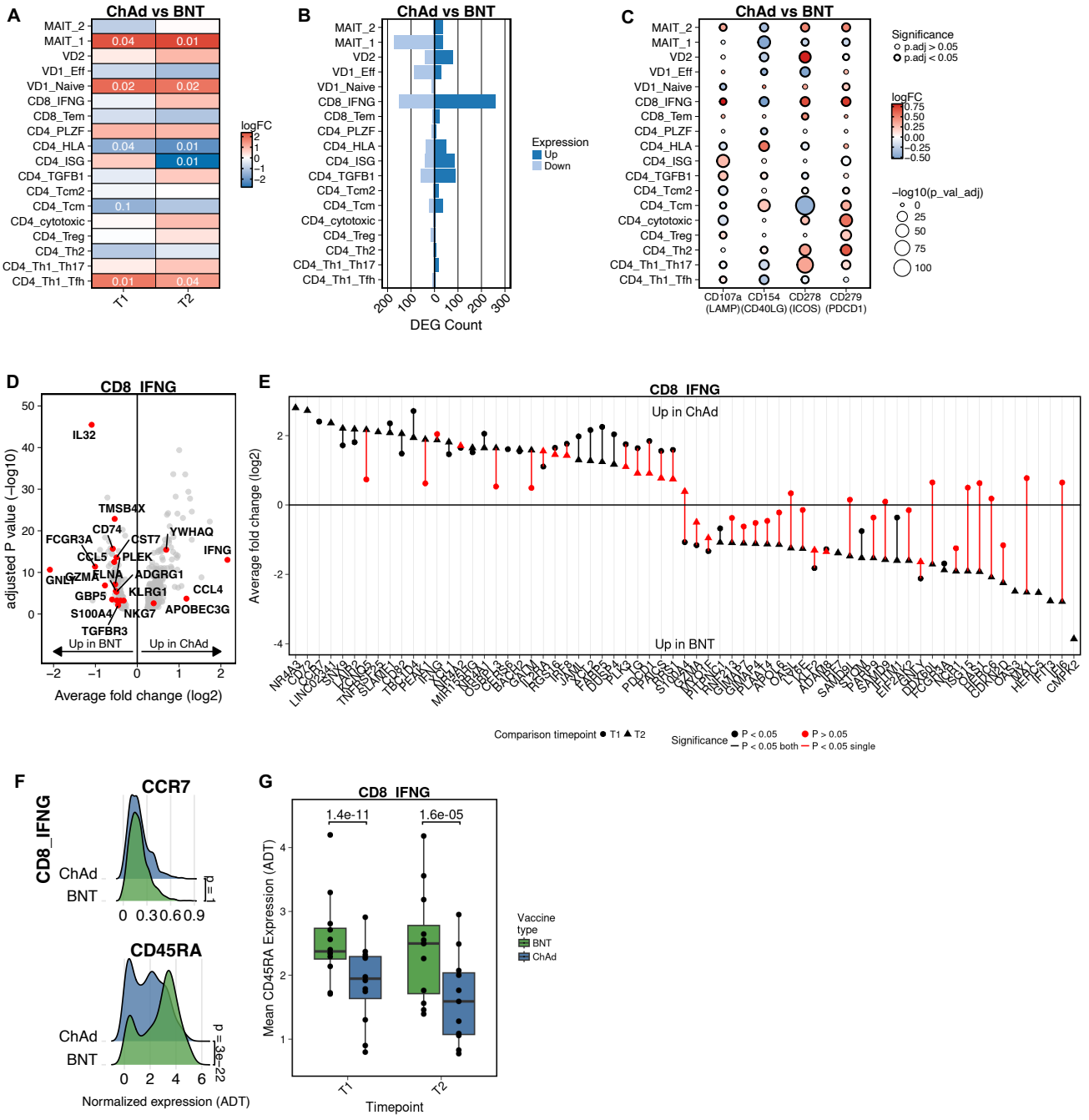

Fig. 4.15 Distinct T cell responses are induced by ChAdOx1 nCoV-19 and BNT162b2 vaccines

A) Log_2 fold change (FC) in abundance of spike-responsive T cell clusters at pre- (T1) and post- (T2) second vaccine timepoints. Benjamini-Hochberg derived false discovery rate (FDR) values for comparisons with an FDR < 0.1 are denoted.

B) Number of significantly differentially expressed genes with an average log_2 fold change >0.25 and adjusted p <0.05 across study group comparisons.

C) Average log_2 fold change of activation induced marker surface protein (ADT) expression.

D) Average log_2 fold change in gene expression between spike-responsive $CD8^+$ effector T cells of ChAdOx1 nCoV-19 (ChAd) and BNT162b2 (BNT) vaccinees. Labelled genes are those included within the Watson *et al.* cytotoxicity-associated geneset.

E) Top 40 most significantly up and down regulated genes between ChAd and BNT vaccinees at T1 and T2 in the CD8_IFNG cluster.

F) Normalized expression of selected surface proteins within spike-responsive effector $CD8^+$ T cells.

G) Mean per person CD45RA surface protein normalized expression in CD8_IFNG cluster at each timepoint.

(**Fig. 4.15F&G**).

Comparison of putative cell-cell interactions between vaccine types indicated that most signalling pathways were shared by vaccine type (**Fig. 4.16A**), with a small number of interesting differences. PD-L1/PD-1 signalling was differential based on vaccine type, with a greater number of involved cell types and cell-cell interactions in ChAd vaccination relative to BNT – corresponding to its increased surface protein expression (**Fig. 4.16B**). CD160, a co-inhibitory receptor (*344*), was uniquely expressed by IFNγ^{+} CD8^{+} T cells and effector Vδ1^{+} γδT cells from ChAd vaccinated individuals (**Fig. 4.16C**). Interaction with its receptor HVEM (*TNFRSF14*), expressed on all clusters, represented a broad and distinct feedback mechanism (**Table 4.2**).

4.6.15 Differing recall of T cell clones induced by ChAdOx1 nCoV-19 and BNT162b2 vaccines

The finding that only BNT vaccinees recalled pre-existing T cell clones **(Fig. 4.13B)** was surprising and suggests that ChAd and BNT may have different memory recall dynamics. To further explore this, I examined the impact of vaccine type on the TCR repertoire. A substantially larger proportion of the top expanded CD4^{+} clonotypes at T2 were also identified at T1 following BNT as compared with ChAd vaccination (**Fig. 4.17A**). Amongst the top expanded clonotypes at T2, clonotypes found at both timepoints (i.e. "recalled" clones) significantly increased as a proportion of total cells at T2 compared with T1 within BNT and ChAd vaccinees (**Fig. 4.17B)**. Compared with top clones only found at T2 ("*de novo"* clones), there was an increased proportion of clones with a T_H2 phenotype in the recalled clones in individuals in all groups (Bonferroni adjusted $p<0.001$, Fisher's exact test) (**Fig. 4.17C**). Notably, there was a significantly higher proportion of CD4^{+} T cells with an ISG^{hi} phenotype in top recalled clones in BNT compared with ChAd vaccinees (**Fig. 4.17D**), highlighting the important contribution of this interferon-driven cell type to the recall response, singularly in BNT vaccination. Interestingly, clones that were expanded at T2 made up a higher average

proportion of T1 clones per person and were more likely to be expanded (**Fig. 4.17E&F**).

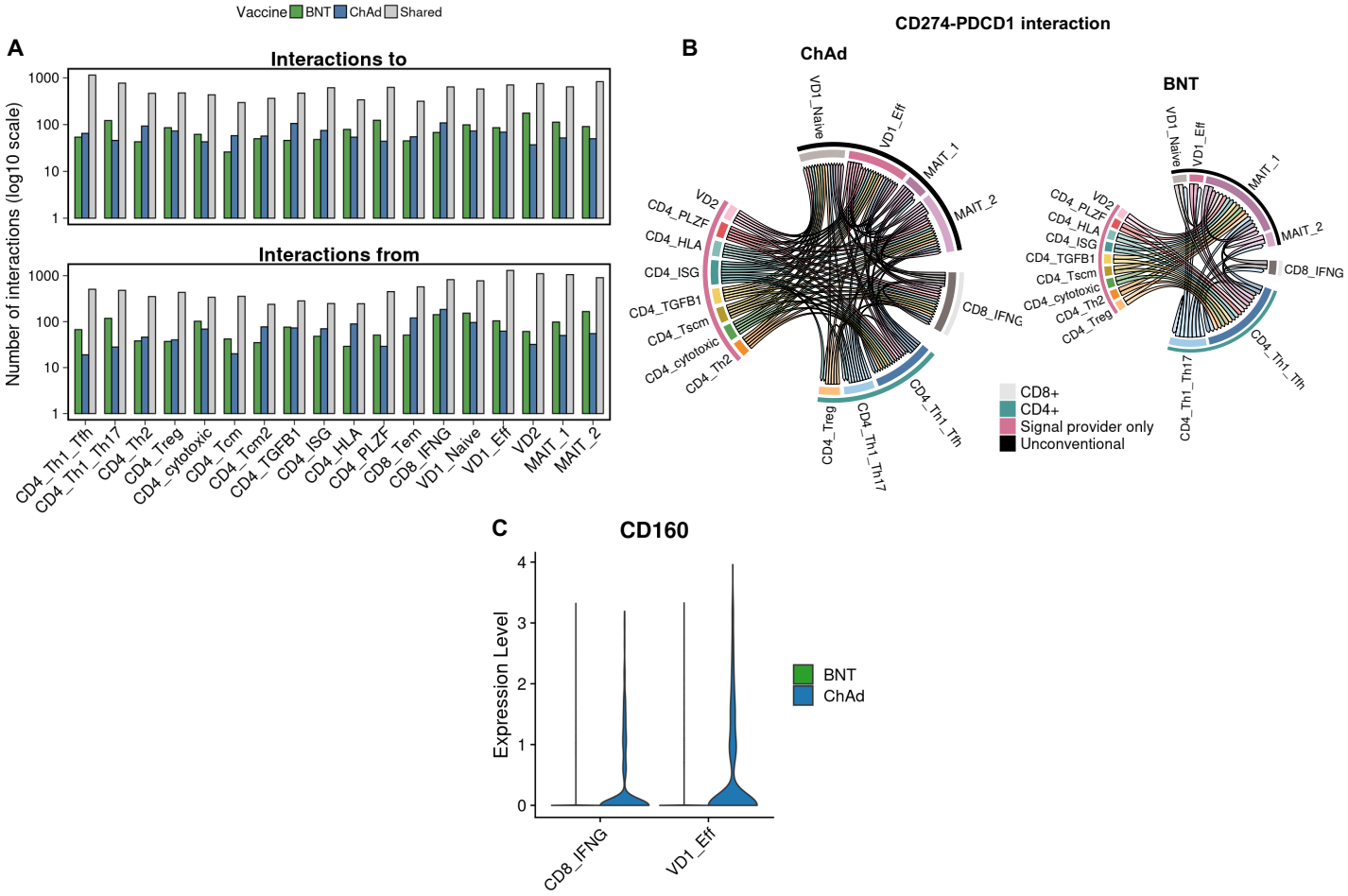

Fig. 4.16 Interaction analysis identifies few differing interaction pathways induced by BNT compared to ChAd.

A) Number of significant CellphoneDB derived interactions to the given cell type that are unique in spike-responsive T cells derived from given vaccine type.

B) Number of significant *CD274-PDCD1* interactions between each cell type. Size of plot is scaled to total number of significant interactions, the arrow and distance of the chord end to the circle edge denotes the directionality of the interaction.

C) Scaled gene expression of CD160 in selected spike-responsive T cell subsets.

4.6.16 The activation dynamics of COVID-19 infection-induced spike-responsive T cells are different to COVID-19 vaccine-induced T cells

Having compared vaccine-induced responses, I next compared vaccine-induced with SARS-CoV-2 infection-induced spike-specific T cells at T1-Short and T1-Long timepoints. Proportions of $CD4^{+}$ HLA^{Hi} AIM^{+} T cells were significantly lower in COVID vs vaccine groups at both T1-Short and T1-Long timepoints and CD8_Tem and effector VD1 T cells proportions were also significantly reduced at the T1-Long timepoint **(Fig 4.18A)**. Differences were largely

consistent when comparing COVID with either ChAd or BNT **(Fig 4.18A)**. Comparison of gene expression profiles between COVID and vaccinees revealed a large number of significantly upregulated genes in COVID, particularly compared to BNT vaccinees and especially at the T1-short timepoint **(Fig 4.18B)**. The number of differentially expressed genes between COVID and vaccines was far greater than the number found when comparing BNT and ChAd

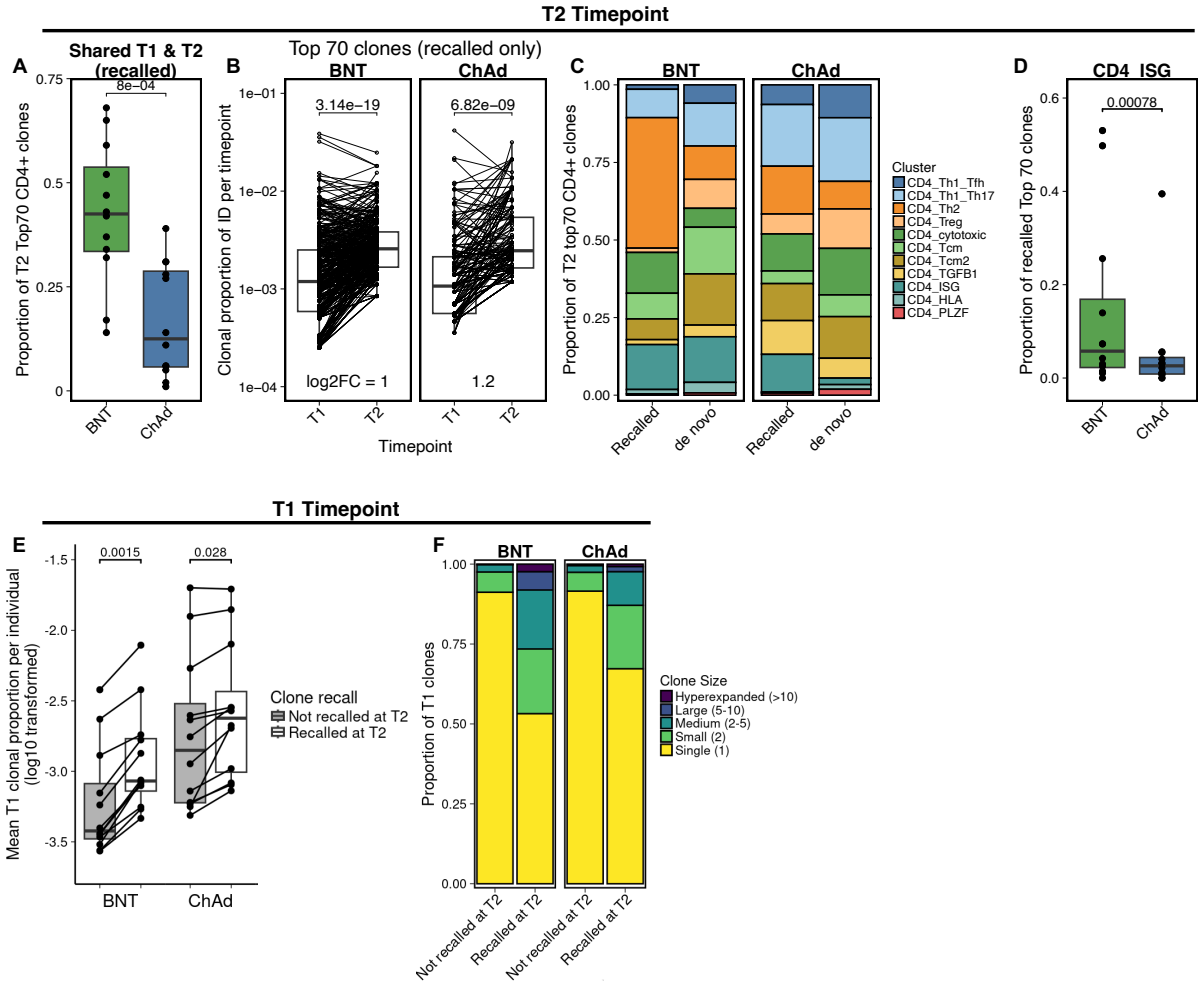

Fig. 4.17 Differing recall of T cell clones induced by ChAdOx1 nCoV-19 and BNT162b2 vaccines

A) Proportion of the top 70 largest paired CD4+ T cell clones at T2 that share an identical clone at the T1 timepoint (recalled T cell).

B) Proportion of total cells per individual/timepoint of each clone in G. (Paired t-test, Bonferroni adjusted)

C) T cell phenotype of recalled clones, or clones which are only found at T2 (de novo) within the top 70 CD4+ T cell clones.

D) Proportion of recalled top 70 clones that have a CD4_ISG phenotype at T2. G & J, Mann-Whitney U test, Bonferroni adjusted. COVID, individuals sampled post-SARS-CoV-2 infection; BNT, BNT162b2 vaccinees; ChAd, ChAdOx1 nCoV-19 vaccinees.

E) Mean proportion of T1 clones per donor that are recalled or not recalled at T2. For COVID group, T2 timepoint = T1-Long (Mann-Whitney U-test, Bonferroni adjusted).

F) Proportion of T1 clones of given clone size, split based on clones that are recalled at T2 and those that aren't. Clones are called on a per donor basis.

vaccinees **(Fig. 4.15B)**.

Geneset enrichment analysis of the differentially expressed genes found multiple genesets significantly positively enriched in the COVID-induced T cells at the T1-Short timepoint **(Fig 4.18C).** These genesets were independently enriched in multiple different T cell clusters, for instance genesets relating to type I and type II interferon signalling (HALLMARK_INTERFERON_GAMMA/ALPHA_RESPONSE), TNF signalling and IL2 signalling were each enriched in most of the T cell clusters at the T1-Short timepoint **(Fig 4.18C)**. At the T1-Long timepoint, expression enrichment had reversed – many of the genesets that were positively enriched in COVID-induced T cells at the T1-Short timepoint were instead enriched in vaccine-induced T cells **(Fig 4.18C)**. Thus, SARS-CoV-2 infection induces T cells that have increased early T cell activation compared to COVID-19 vaccines, but vaccine-induced T cell activation persists for longer than COVID-19 induced T cell activation.

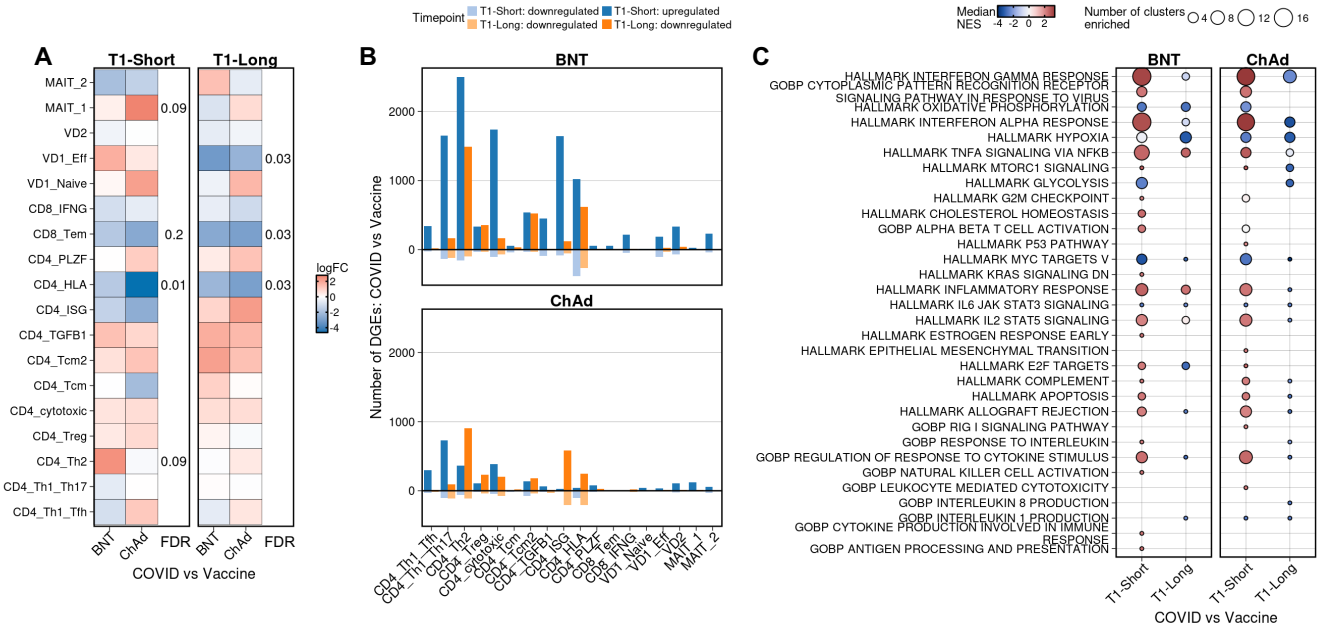

Fig. 4.18 The activation dynamics of COVID-19 infection-induced spike-responsive T cells are different to COVID-19 vaccine-induced T cells

A) Differential abundance analysis of COVID with vaccines at T1-short (early) and T1-long (late) sampling timepoints. False discovery rate (FDR) next to each cell type represents adjusted P of comparison at each timepoint (EdgeR F-test).

B) Number of differentially expressed genes with average $\log_2$ fold change >0.25 in spike-responsive T cells at T1-short and T1-long timepoints in COVID compared to vaccines.

C) Geneset enrichment analysis of differentially expressed genes in COVID compared to vaccines.

4.6.17 Time interval between vaccine dose 1 and dose 2 impacts on the T cell response

I next examined the impact of dose number on the vaccine-induced T cell response. Despite the boosting dose, a comparison of T1 versus T2 revealed only minor differences in the relative abundance of different cell populations (**Fig. 4.19A**). TGFB1^{+} CD4^{+} and Vδ2^{+} γδ T cells decreased at T2 compared with T1 in BNT vaccinees, but no significant differences were observed between timepoints in ChAd vaccinees. Correspondingly, few genes were differentially expressed by timepoint, and increased gene expression at T2 compared with T1 was primarily associated with BNT vaccination (**Fig. 4.19B**).

However, when T2 was separated based on the interval between first and second vaccine dose, substantial differences were observed – many of these were in opposite directions based on interval and thus masked the observations when T2 was analysed in aggregate **(Fig. 4.19C)**. The long interval was associated with increased abundance of T_{EM} CD8^{+} T cells and HLA^{hi} CD4^{+} T cells in ChAd vaccinees, a phenomenon not observed in BNT vaccinees.

Across clusters, surface effector molecule expression was differentially impacted by vaccine type and interval. CD154 (CD40L) was significantly upregulated in short compared with long BNT, but the opposite was seen for ChAd. This pattern was flipped with CD278 (ICOS), which was upregulated specifically in short ChAd **(Fig. 4.19D)**. Differential gene expression analysis revealed major differences based on interval for both the CD4^{+} T cell and unconventional T cell clusters **(Fig. 4.19E)**. Strikingly most of these genes were unique to ChAd or BNT, with relatively little overlap. Overrepresentation analysis highlighted broad differences in the strength of geneset enrichment across the clusters in short versus long interval for both BNT and ChAd **(Fig. 4.19F)**. Genesets related to IFNα and IFNγ were more significantly overrepresented in multiple cell types in the short BNT group but less so in short ChAd; whereas processes related to mTOR signalling, hypoxia and glycolysis were more strongly increased in short compared with long ChAd **(Fig. 4.19F)**.

Fig. 4.19 The dosing interval impacts the vaccine-induced SARS-CoV-2-spike responsive T cell response

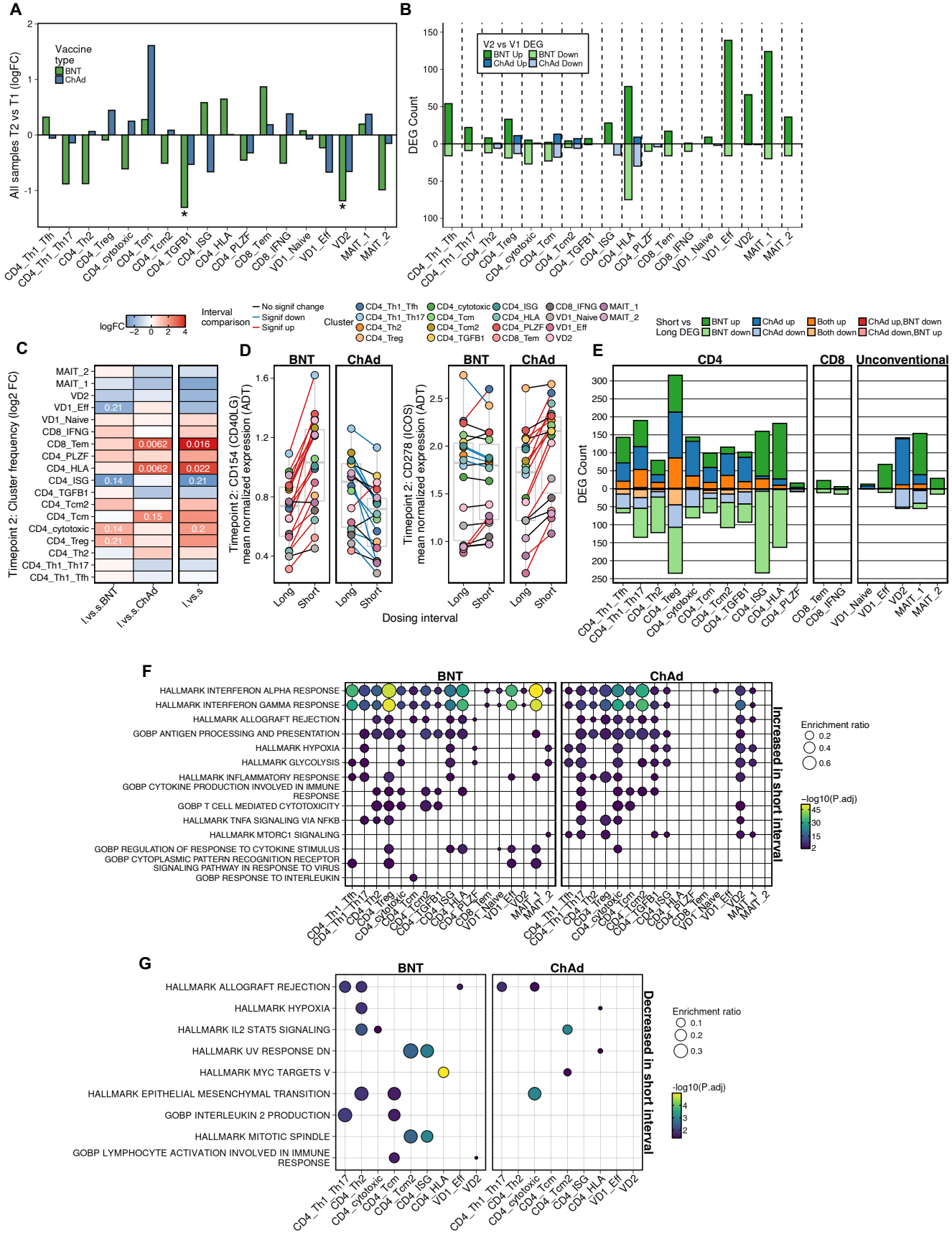

Fig. 4.19 The dosing interval impacts the vaccine-induced SARS-CoV-2 spike-responsive T cell response

A) Log_2 fold change of cell type frequencies at timepoint T2 compared to T1. FDR < 0.05 is marked with an *.

B) Number of differentially expressed genes with average log2 fold change >0.25 in spike-responsive T cells.

C) Log_2 fold change (FC) of post- (T2) second vaccine spike-responsive T cell clusters. Benjamini-Hochberg derived false discovery rate (FDR) values for comparisons with an unadjusted p value <0.1 are denoted. l, long interval; s, short interval.

D) Mean normalized surface protein expression (ADT) of activation induced markers in T2 spike-responsive T cell clusters (Wilcoxon signed-rank test, signif = Bonferroni adjusted p <0.05).

E) Number of significantly differentially expressed genes (DEG) with an average log_2 fold change >0.25 and adjusted p <0.05 within T2 spike-responsive T cell clusters.

F) Overrepresentation of genesets in upregulated genes identified in panel E.

G) Overrepresentation of genesets in downregulated genes identified in panel E

Conversely, when assessing long interval boosting for either vaccine platform, relatively few annotated biologic processes were enriched for the upregulated genes **(Fig. 4.19G)**.

Based on these findings, short interval and long interval were compared head-to-head for the two vaccines. GSEA analysis identified few differences in the cell processes or signalling pathways induced by long BNT versus long ChAd (**Fig. 4.20A**). In contrast, short BNT more strongly induced type I and II interferon signatures across the majority of cell types compared with short ChAd (**Fig. 4.20A**). Examining this in detail in the IFNγ-producing conventional T cell clusters revealed different patterns based on cell type (**Fig. 4.20B**). For the T_H1/T_{FH} and T_H1/T_H17 $CD4^+$ T cell clusters, there was stronger induction of this pathway in both vaccine types by the short interval and downregulation in the long interval, but it was more strongly induced in short BNT compared with short ChAd (**Fig. 4.20B**). For $IFN\gamma^+$ $CD8^+$ T cells, it was uniquely induced by short BNT at T2, with decreased signalling for all other regimens at T2 relative to T1 (**Fig. 4.20B**). This could be seen as coordinated induction of genes in this biologic pathway specifically in this vaccine condition (**Fig. 4.20C**). In contrast, a hypoxia pathway, known to regulate effector T cell function (*345*), was more strongly induced in nearly all $CD4^+$ T cell clusters in short ChAd relative to short BNT (**Fig. 4.20A**). Together, these data highlight the critical role that interval between first and second dose of vaccine has on resultant T cell functionality, and suggest that the biology is not concordant between vaccine types.

4.6.18 A short interval between BNT162b2 doses induces a more inflammatory recall T cell phenotype

A particular characteristic of the short interval is that the time since last dose at T1 and T2 sampling timepoints is the same (28 days). Thus, I next sought to determine how the T cell phenotype changed in the between first and second dose depending on the interval, first focussing on BNT participants. In the short but not long BNT interval, type I and II IFN signalling were elevated across all cell types at T2 relative to T1 **(Fig. 4.21A&B)**. The short interval between doses also led to sustained TNF signalling between T1 and T2, while the long dose resulted in reduced induction of this pathway post-boost **(Fig. 4.21A&B)**. At an

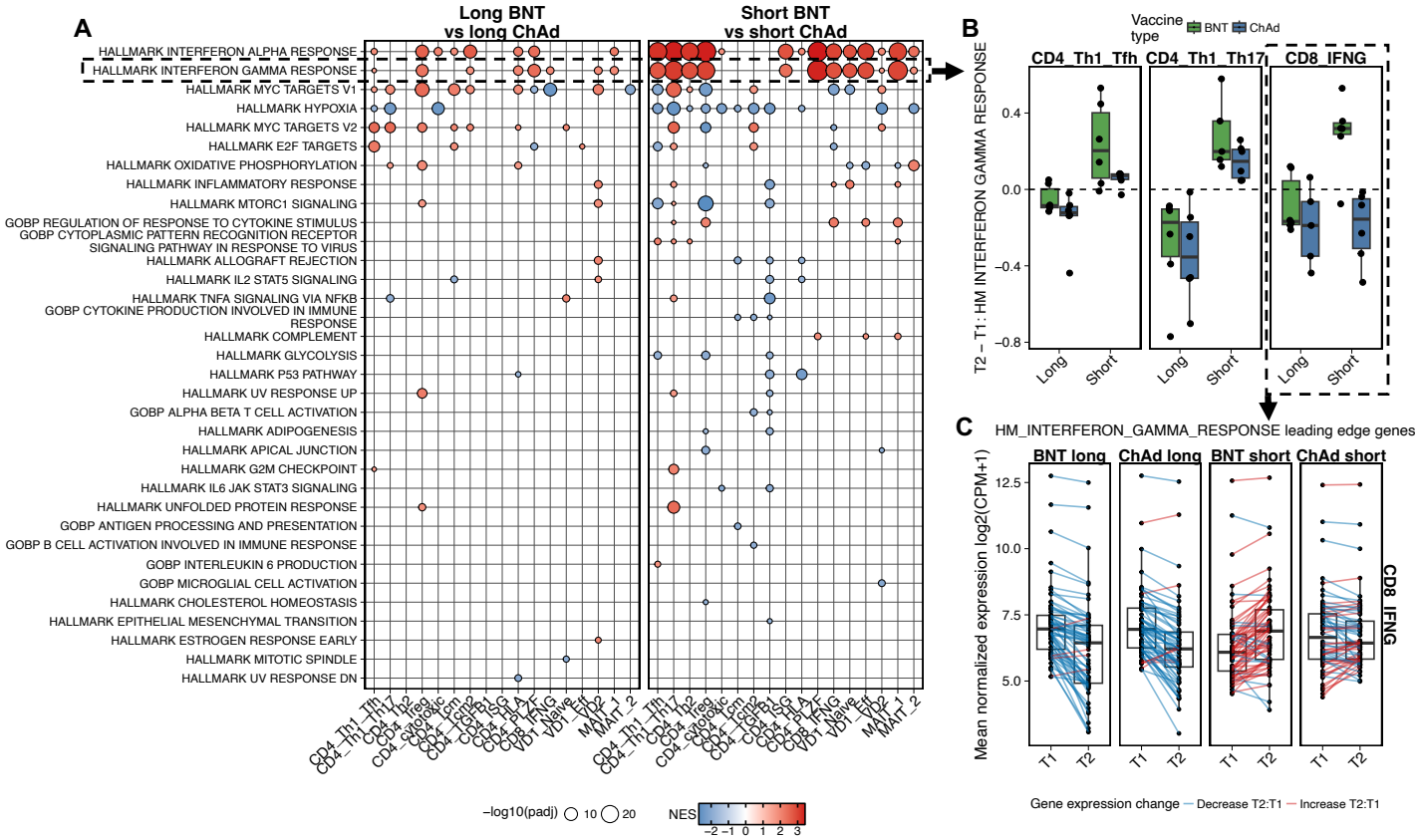

Fig. 4.20 A short dosing interval of BNT162b2 induces a more inflammatory recall T cell phenotype than ChAdOx1 nCoV-19

A) Enrichment of genesets in genes ranked based on the strength of association of their expression with the given comparison at T2, using a mixed-linear models (**Section 4.5.5**). Only enrichments with adjusted p value <0.01 are shown.

B) Difference between T2 and T1 in the aggregate expression of genes (measured by geneset variation analysis; GSVA) within the Hallmark Interferon Gamma Response (M5913) geneset in selected spike-responsive T cell subsets.

C) Mean normalized expression of genes within the Hallmark Interferon Gamma Response geneset in spike-responsive CD8⁺ effector T cells.

individual gene level, this reflected coordinated changes in expression of nearly all genes in the signature, with little overlap of the two signatures, suggesting multiple parallel inflammatory pathways **(Fig. 4.21C)**. Unlike BNT vaccination, the short dosing interval in ChAd vaccinees induced a less dramatic IFN and TNF response at T2 relative to T1 (**Supp Fig. S4.1**).

Interestingly, there was less expansion of recalled clones in individuals vaccinated with a short dosing interval of either vaccine (**Fig. 4.21D**). Thus, increasing the time between doses of mRNA vaccines results in a secondary response that is less inflammatory with lower production of effector molecules, such as *TNF, GZMA, CCL20, CXCL10* (**Fig. 4.21C**) and a larger average expansion of recalled clones.

On the basis that T1 is immediately before the boosting dose, differences in stem-like properties, or markers related to long-term potentiation at T1-Long compared to T1-Short may explain the readiness of the cells to recall upon antigen recall (*346*). Interestingly, several T cell clusters in the T1-Long group had significantly higher expression of T stem cell memory-associated markers including *TCF7*, *SELL* (CD62L), *IL7R* and *CCR7* **(Fig. 4.21E)**. In addition, the CD4+ Tcm2 population, which

was characterised by high expression of markers associated with long-term potentiation (**Fig. 4.2E**), was also enriched at the T1-Long compared with T1-short timepoint. Taken together, this suggests that T cells at the long dosing interval are enriched for stem-cell like properties and therefore have increased potential for memory recall and clonal expansion upon boosting.

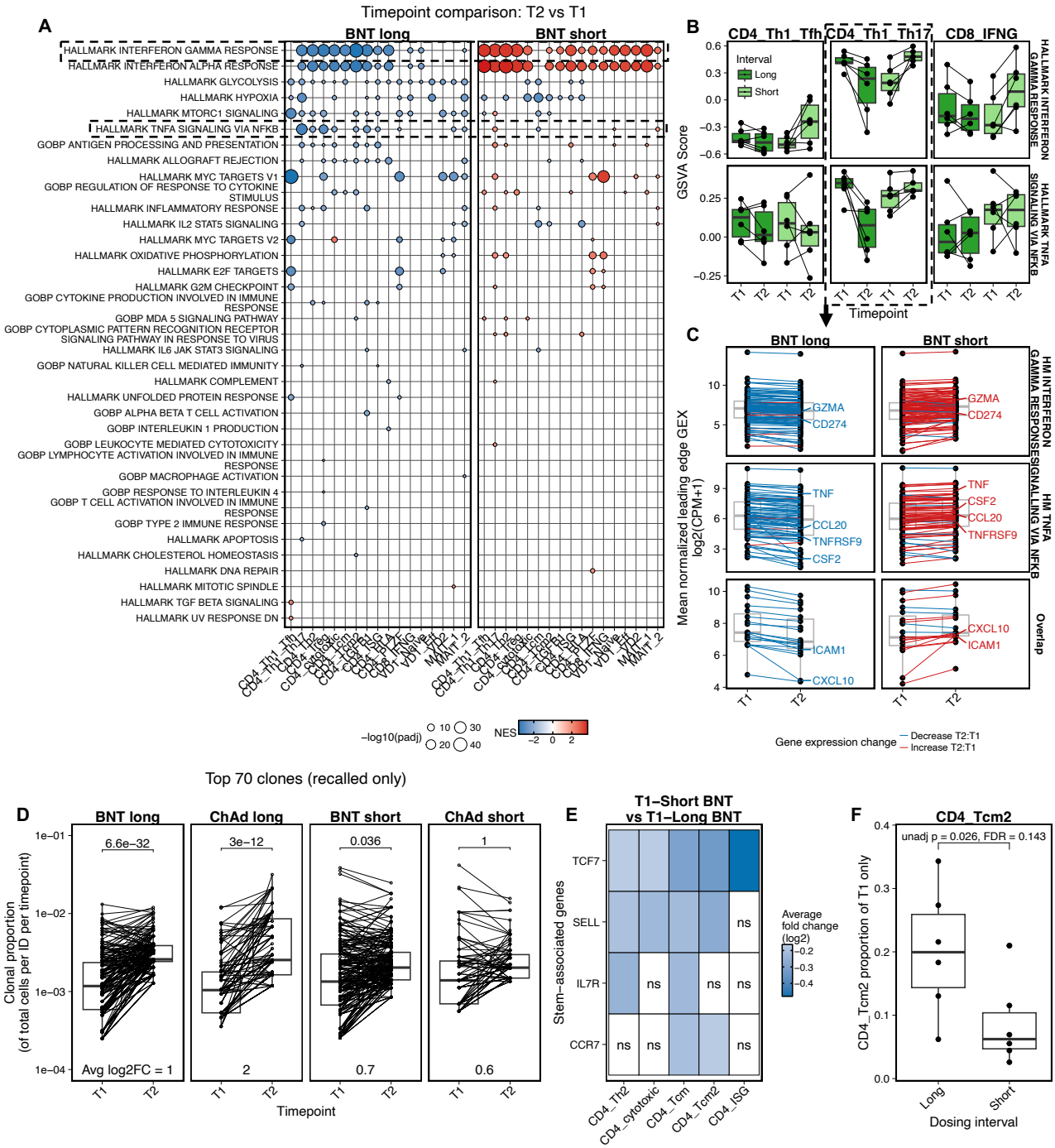

Fig. 4.21 An extended BNT162b2 vaccine dosing interval induces spike-responsive T cells with reduced inflammatory functionality

A) Enrichment of genesets in genes ranked based on the strength association of their expression with the given comparison (**Section 4.5.5**). Comparisons are made between paired timepoints, controlling for variation across individuals. Only enrichments with adjusted p value <0.01 are shown.

B) Geneset variation analysis (GSVA) scoring of aggregate expression of genes within the Hallmark Interferon Gamma Response (M5913) and Hallmark TNFA signaling via NFKB (M5890) genesets.

C) Mean normalized expression of genes within the Hallmark Interferon Gamma Response geneset in spike-responsive CD4+ T_H1/T_H17 effector T cells.

D) Proportion of total cells per individual/timepoint of each clone that is shared within an individual at T2 and T1 (recalled) and within the top 70 largest clones at T2 (Paired t-test, Bonferroni adjusted).

E) Average log_2 fold change of gene expression of selected stem-associated genes. Genes with log_2 fold change <0.25 or adjusted p >0.05 denoted by ns.

F) Proportion of T1 AIM+ T cells represented by CD4_Tcm2, a stem-associated T cell cluster. Unadjusted p value and false discovery rate (FDR) presented. EdgeR comparison. BNT, BNT162b2 vaccinees; ChAd, ChAdOx1 nCoV-19 vaccinees.

4.7 Discussion

This chapter demonstrates that the AIM assay is an unbiased approach to capture spike-specific T cells with broad functional heterogeneity. Combining the AIM-assay with scRNA-seq and scTCR-seq (AIM-seq), I characterised multiple distinct T cell populations, including not only the expected IFNγ$^+$ CD4$^+$ and CD8$^+$ T cells but also CD4$^+$ T_H2, CD4$^+$ T_H17 cells and unconventional T cells. Some of these populations were enriched for cells that appear activated at rest, and others that are likely captured due to non-specific bystander activation. Surprisingly, I observed that the interval between vaccine doses had more of a difference on the post-boost SARS-CoV-2 responsive T cell phenotype than the type of COVID-19 vaccine, with a short 3–4-week interval between doses resulting in a markedly more pro-inflammatory T cell response than a long dosing interval. This phenotype was associated with increased expansion of recalled clones in the long compared to short dosing interval. Pre-existing SARS-CoV-2 responsive T cells had little impact on the subsequent vaccine induced response. Overall, these data reveal unexpected functional heterogeneity in vaccine-induced T cell responses and a significant impact of the vaccine type and dosing interval on T cell function.

4.7.1 Characterisation of AIM$^+$ T cell populations

Comprehensive analysis of CD4$^+$ T cell responses is complicated by both functional heterogeneity and HLA genetic diversity, which limits the use of ICS and MHC tetramer-based approaches (*347, 348*). The AIM assay is an increasingly commonly used assay to measure vaccine-induced T cell responses (*63, 315-317*), and is appealing because it identifies cells responsive to a specific antigen in a function-independent and HLA-agnostic manner. The most pressing issue to generate robust data from AIM-seq is that background AIM$^+$ T cells cannot be removed (i.e., background subtraction) if cells are being isolated by flow cytometric cell sorting for sequencing. Thus, understanding the phenotype of contaminating cells is critical for subsequent data interpretation. Reanalysis of published CITE-seq data (*327*) revealed that “background” cells are associated with very specific transcriptional states,

namely CD4+ T_{CM} cells and unconventional T cell populations (**Fig. 4.3**). The relatively low levels of transcriptional activation and paucity of enriched meta-clones observed in CD4+ T_{CM} cells aligned well with this observation. The HLA^{hi} CD4+ T cell cluster had an identical "background" phenotype. Encouragingly, none of the other effector CD4+ or CD8+ T cell clusters mapped to background AIM+ T cells, supporting their identification as true antigen-responsive cells.

Identification of unconventional T cells (MAIT cells and γδT cells) by AIM-seq appears to be driven by two processes. Firstly, unconventional T cells were contributors to background AIM+ populations, suggesting even unstimulated unconventional T cells may be captured using AIM markers. Secondly, unconventional T cells, particularly MAIT cells and Vδ2+ γδT cells, are cytokine responsive (*349, 350*). Feed-forward signalling over 24 hours, the length of this assay, can drive activation of these cells in a cytokine-dependent manner, by combinations of IL-12, IL-18 (*351*) and/or IFNγ (*352*). Consistent with this, there was clear evidence of cytokine signalling in these cells. In unpublished work, activation of unconventional cells by BNT162b2 vaccination was associated with vaccine reactogenicity (Amini et al, data unpublished). Thus, including these cells in future analyses may reveal intriguing biology. It is possible that the T_{reg} population identified in this study may also be induced by a similar bystander effect driven by IL-2 signalling independent of TCR engagement (*314*).

The functional heterogeneity of AIM+ CD4+ T cells was striking; AIM+ CD4+ T cells were not simply IFNγ-producing T_H1 cells. With the exception of TNF, cells within each cluster were not necessarily producing cytokines associated with the cluster phenotype (e.g., IFNγ and T_H1), possibly due to the suboptimal for cytokine capture (*353*). Regardless, identification of IL-4/IL-13-producing CD4+ T_H2 cells is consistent with prior ICS-based analysis (*65, 354*). IL-17 production was also observed as a hybrid T_H1/T_H17 population. It is unclear if this reflects conversion of T_H17 into T_H1 cells over time after vaccination, or a true hybrid phenotype. The TCR analysis revealed considerable clonal overlap between CD4+ T cell clusters and evidence

of interconversion over subsequent vaccine doses. Interconversion of T cell polarization states is an increasingly well-understood phenomenon (*355*), but the underlying cause for such functional heterogeneity and why cells would change polarization states from one vaccine dose to the next remains to be determined.

4.7.2 Differences in spike-responsive T cells induced by ChAdOx1 nCoV-19 and BNT162b2 vaccines and by SARS-CoV-2 infection

Previous studies have reported increased frequencies of IFNγ$^+$ T cells after ChAdOx1 nCoV-19 vaccination compared with BNT162b2 (*68-70*)**,** particularly after the first dose. Consistent with this, I observed that the predominant IFNγ$^+$ CD4$^+$ T_H1/T_{FH} cluster was more abundant following ChAdOx1 vaccination, while the numerically more abundant CD4$^+$ T_H1/T_H17 trended towards an increased frequency in BNT162b2 vaccinees. Transcriptionally, the IFNγ$^+$ CD8$^+$ T cell was most distinct between BNT and ChAd vaccinees. Various cytotoxic and inflammatory genes were differentially expressed, indicating broad differences in programmes of effector function within this population. Notably, the IFNγ$^+$ CD8$^+$ T cell cluster had elevated *IFNG* transcripts in the ChAd group relative to BNT.

Comparison of T cells induced by COVID-19 vaccines and mild COVID-19 provides an understanding of how the vaccine-induced T cell response relates to the T cell response induced in resolved, mildly symptomatic, SARS-CoV-2 infection. Peak SARS-CoV-2 T cell responses (3-4weeks post infection/vaccine) induced by SARS-CoV-2 infection were significantly more inflammatory than those induced by vaccines and were characterised by high type I and type II IFN signalling. By the 8-12week timepoint the T cells induced by infection more closely resembled those induced by vaccination. This is consistent with data suggesting COVID-19 infection primes higher IFNγ T cell responses than mRNA vaccines (*356*) but that AIM$^+$ T cell frequencies are similar at around 6 months after infection or vaccination (*321*).

The identification of pre-existing SARS-CoV-2 responsive T cells that cross-react between seasonal “common cold” coronaviruses and SARS-CoV-2 prompted interest into their role in

the vaccine-induced T cell response (*79*). In this study, only a small proportion of post-vaccine spike-reactive clones corresponded to pre-existing clones. This supports the existing evidence that pre-existing clones make only a minor contribution to the vaccine response (*357*), and is not entirely surprising given their low frequency. Consistent with a larger study of a single cross-reactive T cell epitope ($S_{816-830}$) (*70*), only vaccination with BNT162b2 and not ChAdOx1 nCoV-19 appeared to recall pre-existing clones. In our study, the BNT groups also had greater recruitment of T cells induced by dose 1 into the recall response following dose 2. Thus, while pre-existing cross-reactive immunity makes only a minor contribution to the overall vaccine T cell response, there appears to be a fundamental difference in how these two vaccine vectors engage cellular immunity, and in particular recall of memory T cell populations.

4.7.3 Differences in vaccine dosing interval

Regardless of vaccine platform, extending the interval between first and second dose of vaccine increases post-boost antibody titres, but is associated with a modest expansion of IFNγ$^+$ T cell frequencies (*66, 71*). Thus, only minor differences in T cell phenotype after dose 2 based on interval were expected. However, interval had a large impact on T cell phenotype and the effect varied by vaccine platform. Increased innate inflammatory signalling after mRNA vaccine dose 2 has been demonstrated, which appears strongly driven by reactivation of memory T cell responses (*208, 222, 223, 358*). Increasing the interval between doses dampens this response (Amini et al, data unpublished). We therefore hypothesize that after short BNT162b2 vaccination the elevated inflammatory environment induced by the second dose leads to a recall T cell response with increased IFNγ and TNF signalling. By contrast, inflammation induced by Ad vectors is driven primarily by engagement of innate pDCs and myeloid cells (*351, 359*) and thus would vary less between priming and boosting – explaining the smaller difference between intervals observed in ChAdOx1 compared to mRNA vaccination.

The functional implications of this altered T cell phenotype for immunity remain unclear. However, since heightened inflammatory signalling can drive $CD4^+$ T cells away from a T_{FH} polarization state (*360*), the lower inflammatory T cell response after a longer dosing interval may contribute to the enhanced antibody responses observed with this regimen. Conversely, the stronger interferon signalling in activated T cells following a short-interval boost may help explain the high efficacy of this approach against severe COVID-19, despite the significantly lower antibody titres compared to long-interval boosting (*305*).

Inflammatory signalling in T cells is associated with increased effector polarization at the expense of long-lived proliferative memory differentiation (*361*). Given the elevated inflammatory phenotype of short-interval mRNA vaccination, we hypothesize T cells induced by this regimen would have reduced proliferative potential after boosting. Consistent with this, IFNγ T cell responses generated by two doses of mRNA vaccination given in a long-interval increased in magnitude following an additional (third) dose, whereas those generated by a short-interval mRNA regimen did not (*284*). In this chapter, I observed an expansion of recalled clones after two doses of vaccine given in a long-interval vaccine regimen, but no expansion of recalled clones after a short-interval regimen. Thus, the dosing interval for a primary vaccination regimen has a long-term impact on the anamnestic potential of vaccine induced T cells.

4.7.4 Limitations

The primary limitation of this study is the sample size per experimental group. While the overall dataset includes 60 samples for the AIM-seq assay (30 individuals at two timepoints) the inclusion of five different experimental groups limits the power of comparisons when performed at the level of individuals. In addition, the number of cells captured per individual is variable and relatively limited for analysis of T cell clonality. This is a general concern in analyses of T cell clonality where under sampling likely leads to overestimation of the number of singlet clones (*338*), even when antigen-enrichment has been performed, as in this study.

Another important limitation is the fact that this study is limited to the analysis of two COVID-19 vaccine doses, and only infection with the ancestral strain of SARS-CoV-2, and so is not representative of the current COVID-19 immunological landscape. Nevertheless, this study gives important insight into human T cell responses to a prime-boosting regimen of mRNA and ChAdOx1 vaccines against a novel antigen – which is of relevance to ongoing studies using these platforms to vaccinate against cancer (*25, 362, 363*) and emergent pathogens (*22, 364*).

Finally, the use of 15mer peptide pools may bias towards the detection of $CD4^+$ T cells, and optimisation of peptide pools to capture both $CD4^+$ and $CD8^+$ T cells may increase the detection of $CD8^+$ T cells (*78*).

4.8 Conclusions

In conclusion, ChAdOx1 and mRNA COVID-19 vaccines induce T cells that are highly heterogenous and include putative effector populations and bystander-activated T cells. The interval between prime and boosting doses of mRNA vaccination has a large impact on the functionality of T cells induced after boost. A short (3-4week) dosing interval induces T cells that are more inflammatory and include fewer recalled memory T cells. Recall of pre-existing T cells that are cross-reactive to SARS-CoV-2 does not impact the subsequent vaccine-induced T cell response but recall of these pre-existing cells is observed only after vaccination with mRNA and not ChAdOx1 COVID-19 vaccines.

4.9 Tables

Table 4.1 Study group demographics

Characteristic	BNT		ChAd			
	l_BNT, N = 6[1]	s_BNT, N = 6[1]	l_ChAd, N = 6[1]	s_ChAd, N = 6[1]	COVID, N = 6[1]	p-value[2]
Age	38 (33, 45)	42 (35, 52)	26 (22, 34)	30 (26, 34)	36 (31, 37)	0.10
Sex						>0.9
F	4 (67%)	3 (50%)	4 (67%)	3 (50%)	2 (33%)	
M	2 (33%)	3 (50%)	2 (33%)	3 (50%)	4 (67%)	

[1] Median (IQR); n (%)

[2] Kruskal-Wallis rank sum test; Fisher's exact test

Table 4.2 Vaccine-specific cell-to-cell interactions (CellphoneDB)

Significant CellphoneDB derived interactions which are unique to the given vaccine type, with breakdown of the type of interaction and the uniquely interacting cell types.

Interaction pair	Vaccine	No. interacting cell pairs	Interaction from	Interaction to
Adenosine_byNT5E_and_SLC29A1_ADORA2B	ChAd	1	CD4_Th1_Tfh	VD1_Naive
Adenosine_byNT5E_and_SLC29A2_ADORA2A	ChAd	2	CD4_Th1_Tfh	VD1_Naive, MAIT_2
Adenosine_byNT5E_and_SLC29A3_ADORA2A	ChAd	2	CD4_Th1_Tfh	VD1_Naive, MAIT_2
CD160_TNFRSF14	ChAd	18	CD8_IFNG	VD1_Naive, MAIT_2, CD4_HLA, CD4_PLZF, CD4_ISG, CD4_TGFB1, CD4_Tcm, CD4_Th1_Th17, CD4_Th1_Tfh, CD4_Th2, CD4_Treg, CD4_Tscm, CD4_cytotoxic, CD8_IFNG, CD8_Tem, MAIT_1, VD1_Eff, VD2
CD160_TNFRSF14	ChAd	18	VD1_Eff	VD1_Naive, MAIT_2, CD4_HLA, CD4_PLZF, CD4_ISG, CD4_TGFB1, CD4_Tcm, CD4_Th1_Th17, CD4_Th1_Tfh, CD4_Th2, CD4_Treg, CD4_Tscm, CD4_cytotoxic, CD8_IFNG, CD8_Tem, MAIT_1, VD1_Eff, VD2
CD248_IL6R	BNT	1	VD1_Naive	CD4_Treg
CD80_CD28	ChAd	1	CD4_Th1_Th17	MAIT_1
CD80_CD28	ChAd	1	CD4_Treg	MAIT_1
DLL3_NOTCH1	BNT	1	CD4_Th1_Tfh	VD1_Eff
Dehydroepiandrosterone_bySTS_ESR1	ChAd	1	CD4_Th1_Tfh	CD4_PLZF
Dehydroepiandrosterone_bySTS_ESR1	ChAd	1	CD8_IFNG	CD4_PLZF
Dehydroepiandrosterone_bySTS_ESR1	ChAd	1	VD1_Naive	CD4_PLZF
EFNB1_EPHA4	BNT	1	CD4_Th1_Tfh	CD4_Tcm
ENTPD1_ADORA2B	ChAd	1	CD4_Treg	VD1_Naive
IL21_IL21_receptor	BNT	8	CD4_Th1_Tfh	VD1_Naive, MAIT_2, CD4_Th1_Tfh, CD4_Treg, CD8_IFNG, MAIT_1, VD1_Eff, VD2
L1CAM_integrin_a5b1_complex	ChAd	4	CD4_TGFB1	CD4_TGFB1, CD4_Th2, CD4_Treg, MAIT_1
L1CAM_integrin_aVb1_complex	ChAd	3	CD4_TGFB1	CD4_TGFB1, CD4_Th2, CD4_Treg
NCR3LG1_NCR3	ChAd	3	CD8_IFNG	MAIT_2, MAIT_1, VD2
NCR3LG1_NCR3	ChAd	3	VD1_Naive	MAIT_2, MAIT_1, VD2
ProstaglandinD2_byAKR1C3_PTGDR	BNT	1	VD2	CD8_IFNG
THBS1_integrin_a3b1_complex	ChAd	1	CD4_HLA	CD4_TGFB1
THBS1_integrin_a3b1_complex	ChAd	2	CD8_Tem	MAIT_2, CD4_TGFB1
THBS1_integrin_a3b1_complex	ChAd	1	MAIT_1	CD4_TGFB1
TNFSF9_TNFRSF9	ChAd	5	CD8_IFNG	VD1_Naive, CD4_Th1_Tfh, CD8_IFNG, MAIT_1, VD1_Eff
ULBP2_NKG2D_II_receptor	ChAd	7	CD4_Th1_Th17	VD1_Naive, MAIT_2, CD8_IFNG, CD8_Tem, MAIT_1, VD1_Eff, VD2

4.10 Supplementary Figures

Fig. S4.1 Comparison of long and short dosing intervals in ChAd vaccinees

Enrichment of genesets in genes ranked based on the strength association of their expression with the given comparison (Section 4.5.5). Comparisons are made between paired timepoints, controlling for variation across individuals. Only enrichments with adjusted P value < 0.01 are shown.

5 Results: Multi-omic assessment of the pre- vaccine immunophenotype and its association with immunosuppressive conditions and mRNA vaccine-induced antibody and T cell responses

5.1 Introduction

In chapter 3, I established that certain clinical and demographic factors were associated with reduced SARS-CoV-2 specific antibody and T cell responses to up to three doses of COVID-19 vaccines in individuals with immune-suppressive diseases. Specific diseases, immunosuppressive therapeutics and demographic factors were associated with reduced vaccine immunogenicity. However, the complexity and variability of immunosuppressive therapeutic regimens (dose and combination of therapeutics), diseases (severity, duration since diagnosis, disease burden), and human demographics means that even within a single immunosuppressive disease there is large variation in immune responses to vaccines. Even within healthy populations, although generally higher, vaccine-induced immune responses are subject to large variation between individuals, depending on genetic (*12, 301*), epigenetic (*365*) and other host factors (*366*). This variation is increased further within and between immunosuppressive conditions (**Fig. 3.2A)**. Therefore, assessing vaccine immunogenicity simply from the viewpoint of clinical/demographic variables gives only limited insight into the biology underlying variation in vaccine responsiveness.

One approach to assess the variability underlying vaccine immunogenicity is to use “systems immunology” methodologies to broadly phenotype immunological parameters prior to or early after vaccination. In healthy individuals, multiple immune signatures have been identified that are related to peak (e.g. 21-28d post vaccine) (*367-369*) or long-lived (*370*) antibody responses after vaccination. These signatures include features such as baseline inflammation (*367, 371*) and day-7 post-vaccination plasmablast frequency (*369*). While informative, because they are derived in healthy individuals these signatures only provide insight into a spectrum of antibody-induced immune responses ranging from ‘moderate’ to ‘high’ and

therefore do not resolve features related to complete or partial vaccine failure (that is, 'low or no' vaccine response). Understanding the factors that lead to 'low or no' response in COVID-19 vaccination is clinically relevant, as individuals with low or no V2+28d anti-RBD Ig titres had reduced protection against subsequent severe COVID-19 (**Section 3.6.12**). The ability to predict vaccine non-responsiveness based on easily assessable measures (i.e. protein concentration in blood) before vaccination is also attractive, so that individuals that are not likely to respond to vaccines can be targeted for alternative therapies. In addition, by measuring how immune dysfunction impacts the vaccine-induced response, we gain a unique opportunity to identify the biological pathways required for optimal vaccine immunogenicity.

Considering this, it is important to first survey the effect of disease and different therapeutics on the immune system and compare these to HCs. Immunosuppressive medications have various mechanisms of action (**Section 1.11**) and therefore differently impact the immune landscape. Chronic diseases may also impair different facets of the immune system (**Section 1.12**). Several studies have previously explored the impact of immunosuppressive medications and diseases on the immunophenotype, but these studies have mostly not been in the context of vaccination, have largely focussed on single diseases, and have not applied modern immune-phenotyping techniques (**Section 1.11)**. In addition, studies that investigated baseline factors associated with vaccine immunogenicity in healthy people have focussed primarily on the vaccine-induced antibody response and few have investigated features predictive of T cell responses (*205, 372, 373*). As reported in chapter 3, both antibody titres and frequencies of SARS-CoV-2 spike responsive IFNγ T cells are associated with post-vaccine COVID-19 severity outcomes but are weakly correlated with each other. Therefore, understanding baseline variables associated with both vaccine-induced antibody and T cell responses is relevant to understanding important outcomes of vaccine immunogenicity.

Furthermore, baseline predictors of vaccine immunogenicity likely depend upon the vaccine platform itself. Some baseline predictors, such as such as baseline B cell frequency, have

been identified over several vaccine platforms (*204, 212*); however, generally, markers that are predictive of the immunogenicity of one vaccine type are not accurate in others (*367*). Indeed, application of inflammation-associated genesets identified as positively predictive for increased antibody responses after inactivated (*367*) or protein subunit influenza vaccines (*212*) were strongly negatively associated with antibody responses to a modified vaccinia Ankara (MVA) Mpox vaccine (*374*). This is likely due to differing sensitivities of the vaccine platforms to interferon (*375*). The relatively low overlap of predictive factors across platforms suggests that it is important to define predictors for each vaccine platform. Due to their relative novelty, little work has been done so far to understand predictors of mRNA vaccine immunogenicity in humans. However, given their proven efficacy as vaccines in infectious disease (*304, 305*) and nascent use as cancer vaccines (*25*), understanding the factors associated with immune responsiveness to these platform is highly relevant. This is especially true in the context of immunosuppressive disease, where individuals are at increased vulnerability to both severe infectious disease (*5, 252, 376*) and cancer (*377, 378*).

5.2 Summary of chapter rationale

Understanding human variation related to vaccine immunogenicity is challenging due to the complexity of underlying genetic, epigenetic and environmental factors that influence the immune response. This is especially the case in immunosuppressive diseases where disease and therapy combinations severely and distinctively impact the immune response to vaccines. Given the broad dysregulation caused by some immunosuppressive conditions, systems immunology approaches provide a method to quantify immune pathways that are related to vaccine immunogenicity. Furthermore, application of these approaches across immunosuppressive conditions provides the opportunity to identify shared or unique pathways of immune dysregulation across disease. Providing insight into the immunogenicity of mRNA vaccines in immunocompromised individuals has potential broad future relevance, given their growing use as vaccine platforms for cancer and infectious diseases.

5.3 Hypotheses and aims

The central hypotheses of this chapter are as follows:

1) The immunophenotype of individuals with different immunosuppressive diseases vary depending on disease type and are different to healthy individuals.
2) The pre-vaccination ("baseline") immunophenotype is associated with peak (i.e. 21-28d post) mRNA vaccine-induced immunogenicity.

To address the hypotheses, in this chapter I aim to:

1) Assess the baseline (pre-vaccine) immunophenotype of individuals with immune-suppressive conditions and healthy individuals using "systems" approaches:
    a. Assess the whole-blood transcriptome
    b. Assess the serum inflammatory proteome
    c. Assess peripheral blood immune-cell phenotype
    d. Assess peripheral blood adaptive immune cell functionality/phenotype (antigen-specific and non-antigen specific)
2) Compare the baseline immunophenotype between immunosuppressive disease groups and with healthy individuals
3) Identify associations between the baseline immunophenotype and vaccine-induced antibody and T cell responses
4) Generate machine learning models to identify baseline features that are predictive of the vaccine-induced antibody and T cell response

5.4 Chapter overview

To address these aims, I performed bulk-RNA sequencing, Olink proteomics and spectral flow cytometry on pre-vaccine blood samples from immunocompromised individuals in the OCTAVE DUO study and healthy individuals from the PITCH study. OCTAVE DUO was a clinical trial to investigate the immunogenicity of a third dose of mRNA COVID-19 vaccines in immunocompromised individuals that had low or no antibody responses to two doses of

COVID-19 vaccines. I contributed significantly to the initial grant proposal for this work and the publication of primary and secondary outcomes from the trial (*379*).

I associated the pre-vaccine transcriptomic, proteomic and cellular data with clinical/demographic and vaccine immunogenicity data generated as part of the trial to identify features associated with immune-suppressive diseases and with vaccine outcome.

5.5 Chapter specific methods

5.5.1 Cohort recruitment and definitions

OCTAVE-DUO was an open-label, multicentre, randomised, controlled, phase 3 trial, conducted in 11 UK hospitals, recruiting patients who were over 18 years of age, immunocompromised, and had inadequate or no response to two COVID-19 vaccine doses. All patients gave informed consent, and the study was approved by an ethics committee, funded by UKRI/DHSC, and sponsored by the University of Birmingham (*379*). The University of Birmingham statistics team performed data cleaning and performed the primary analysis for the trial. Low or no response was defined as <380AU/mL anti-SARS-CoV-2 RBD Ig titre by Roche Elecsys or <700AU/mL by Abbott AdviseDx SARS-CoV-2 IgG II assay. Full inclusion and exclusion criteria are listed in **Table S5.1**.

World Health Organisation (WHO) performance status is measure of physical activity and is defined: 0: able to carry out all normal activity without restriction, 1: restricted in strenuous activity but ambulatory and able to carry out light work, 2: ambulatory and capable of all self-care but unable to carry out any work activities; up and about more than 50% of waking hours, 3: symptomatic and in a chair or in bed for greater than 50% of the day but not bedridden, 4: completely disabled; cannot carry out any self-care; totally confined to bed or chair (*380*).

5.5.2 GLMnet and Random Forest to predict vaccine immunogenicity

Models were generated based on scaled plasma protein NPX values. Cohorts were randomly separated 70:30 into train and test datasets. Clinical group was included as a covariate in all models. GLMnet (*381*) and random forest models were independently trained on train datasets

using 20 repeats of 10 fold cross-validation to optimise hyperparameter selection (Caret package). Hyperparameter values that minimised the classification accuracy within the train dataset were selected. The caretEnsemble package was used to stack trained predictive models using generalised linear models. The specificity and sensitivity of the predicted compared to real values were calculated using independent and combined models on the with-held test dataset.

5.5.3 Dimensional reduction of spectral flow cytometry data

Flow cytometric data was pre-processed in FlowJo (v10.10.0) remove doublets and only include live, $CD45^+$ cells and randomly down-sampled to 2000 cells per donor. Flow Cytometry Standard (FCS) files were loaded and data were transformed using negative value pruned inverse hyperbolic sine transformation (cytofAsinh, CytoTree package). PCA was performed, using all flow cytometry measurements except Live/Dead staining. Unsupervised clustering with Phenograph and uniform manifold embedding and projection (UMAP) was performed on the top 20 principal components. Phenograph clusters were manually annotated by assessing the expression of canonical immune cell phenotypic markers.

5.5.4 Variance of RNA-sequencing data explained by cell frequency

The variance in geneset module scores explained by cell frequency was assessed by fitting linear models of geneset module score, using scaled frequencies of selected major immune cell subsets, age and sex. T cells and monocytes were not included together in models due to collinearity between these measures. The variance explained was calculated by taking the simple unweighted averages of the sums of squares of each variable, using the realimpo package lmg function (*382*). Coefficients were deemed significantly positive or negative if p was <0.05 and the linear coefficient was above or below 0, respectively.

5.6 Results

5.6.1 OCTAVE DUO: Study design and cohort overview

Pre- (pre-V3) and 21-28 days-post (V3+21d) third COVID-19 mRNA vaccine (BNT162b2 or

mRNA-1273) peripheral blood from immunocompromised individuals was sampled in the OCTAVE DUO study (**Fig. 5.1A**). All individuals had low or no (**Section 5.5.1**) anti-RBD Ig titres 28 days post second vaccine. Individuals were recruited across several clinical groups, including inflammatory bowel disease (IBD), rheumatoid arthritis (RA), ANCA-associated vasculitis (AAV), haematological malignancies (HM), haematological stem cell transplants (HSCT), primary immunodeficiencies (PID), cirrhosis (Cirr), liver transplant (LT) and renal transplant (RT) (**Fig. 5.1B**). Healthy individuals (healthy controls; HC) with no known SI were sampled in parallel in the PITCH study and analysed as 'optimal' immune response controls **(Fig. 5.1A)**. Peripheral blood samples at the pre-vaccine timepoint from different disease groups were assessed for phenotype and function using 'omic approaches (**Fig. 5.1C)**

All individuals were naive for COVID-19 and previously received two doses of AZD1222 or BNT162b2 vaccine, except one HC that received mRNA-1273 **(Table 5.1)**. Factors such as age, sex and comorbidities, BMI and WHO performance status (a donor-reported classification of how able participants are to carry out day-to-day activities) varied between groups **(Fig. 5.1D, Table 5.1).** The inter-group variation largely aligned with the different demographic risk-profiles for each disease, i.e. RA patients were predominantly female (*383*); solid organ transplant recipients patients were predominantly males (*384, 385*); HM patients had increased age and were predominantly male (*386*). As HC individuals were recruited from a health care work study (PITCH), they were younger and predominantly female. 214 of 244 (89%) of individuals were white, 80 of 244 (32%) individuals currently or previously smoked, and 172 of 244 (70%) individuals had at least one comorbidity **(Table 5.1).** The commonest comorbidities were hypertension (82 of 244; 34%, including 34 of 37 (92%) in RT) and type 2 diabetes (44 of 244; 18%, highest in cirrhosis, LT and RT groups). Immunosuppressive therapy use varied by clinical group (**Fig. 5.1E**, **Table 5.1**). aCD20 therapy was used in AAV (12 of 15; 80%), RA (11 of 49; 22%), HSCT (2 of 14; 14%) and lymphoma groups

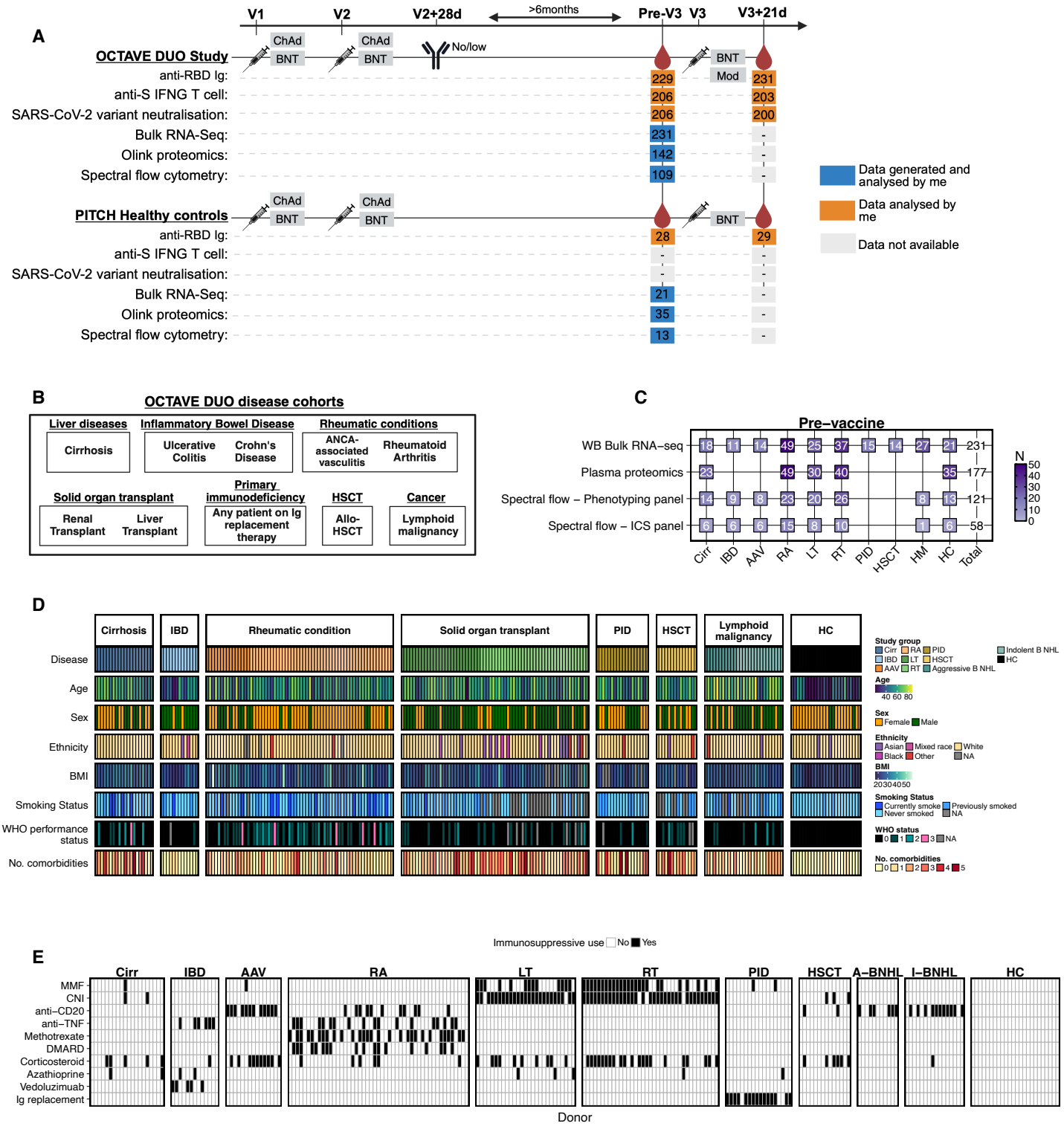

Fig. 5.1 OCTAVE DUO study overview and demographics

A) Sampling timepoints and vaccine regimen for individuals in the OCTAVE DUO and PITCH studies included in chapter 5. Individuals in OCTAVE DUO study were selected to have low or no antibody titre at V2+28d (Methods). The number indicated is the number of individuals included for the given analysis/study. The vaccine types given at each dose is indicated for each study/timepoint. Red droplet indicates peripheral blood sampling timepoints. Colours at each timepoint represents my contribution to the data presented in this analysis.

B) Disease cohorts included in chapter 5

C) Number of individuals included per assay/disease group in chapter 5

D) Per person demographic breakdown of individuals included in chapter 5, associated with Table 5.1

E) Per person immunosuppressive therapies included in chapter 5, associated with Table 5.1

(6 of 11 [55%] aggressive B NHL, 11 of 16 [69%] indolent B NHL). CNI and MMF were predominantly used in solid organ transplant recipients, 92% of RT and 93% of LT received CNI which was used in combination with MMF in 68% of RT and 48% of LT. Corticosteroids were additionally used in 37% of LT and 57% of RT, as well as in AAV (67%), cirrhosis (25%), RA (12%), IBD (7.7%), HSCT (43%) and aggressive B NHL (6.3%). Anti-TNF monoclonal antibody therapy was used in IBD (46%) and RA (37%). Disease modifying anti-rheumatic drugs (including methotrexate and hydroxychloroquine and sulfasalazine; DMARD) were used in varying combinations in 37 of 49 (76%) of RA patients.

5.6.2 COVID-19 vaccine immunogenicity in OCTAVE DUO cohort

Anti-RBD Ig binding, SARS-CoV-2 neutralisation and IFNγ T cell immunogenicity data was available at pre- and 21d-post V3 timepoints in the OCTAVE DUO cohort (*379*). HCs had anti-RBD Ig data only, available pre- and 21d post-V3 **(Fig. 5.1A)**. Reanalysis of this data demonstrated that there was a significant increase in anti-RBD Ig binding titres with a third vaccine dose in most clinical groups and HCs **(Fig. 5.2A).** However, all groups still had significantly lower anti-RBD Ig responses at V3+21d than the HC group and some groups remained enriched for vaccine immune non-responsiveness **(Fig. 5.2A)**. Live neutralisation assays against ancestral (wild-type), delta and omicron BA.1 SARS-CoV-2 variants at V3+21d demonstrated reduced neutralising IC_{50} to SARS-CoV-2 variants compared to wildtype **(Fig. 5.2B)**. While some groups had high neutralising titres to all variants (Cirr, IBD), most groups did not – especially against omicron BA.1 **(Fig. 5.2B)**. There was strong positive correlation between (ancestral) anti-RBD Ig binding titres and neutralising antibody IC_{50} to all SARS-CoV-2 variants, but notably individuals with anti-RBD Ig binding titres below 1000AU/ml were largely unable to neutralise omicron BA.1 **(Fig. 5.2C-E)**. Stratifying the cohort by the manufacturer recommended threshold of 0.8AU/mL to define non- responsiveness ('no' response), and the threshold defined for omicron BA.1 neutralisation (1000AU/mL; 'low' response), there were certain clinical groups clearly enriched for low or no anti-RBD Ig

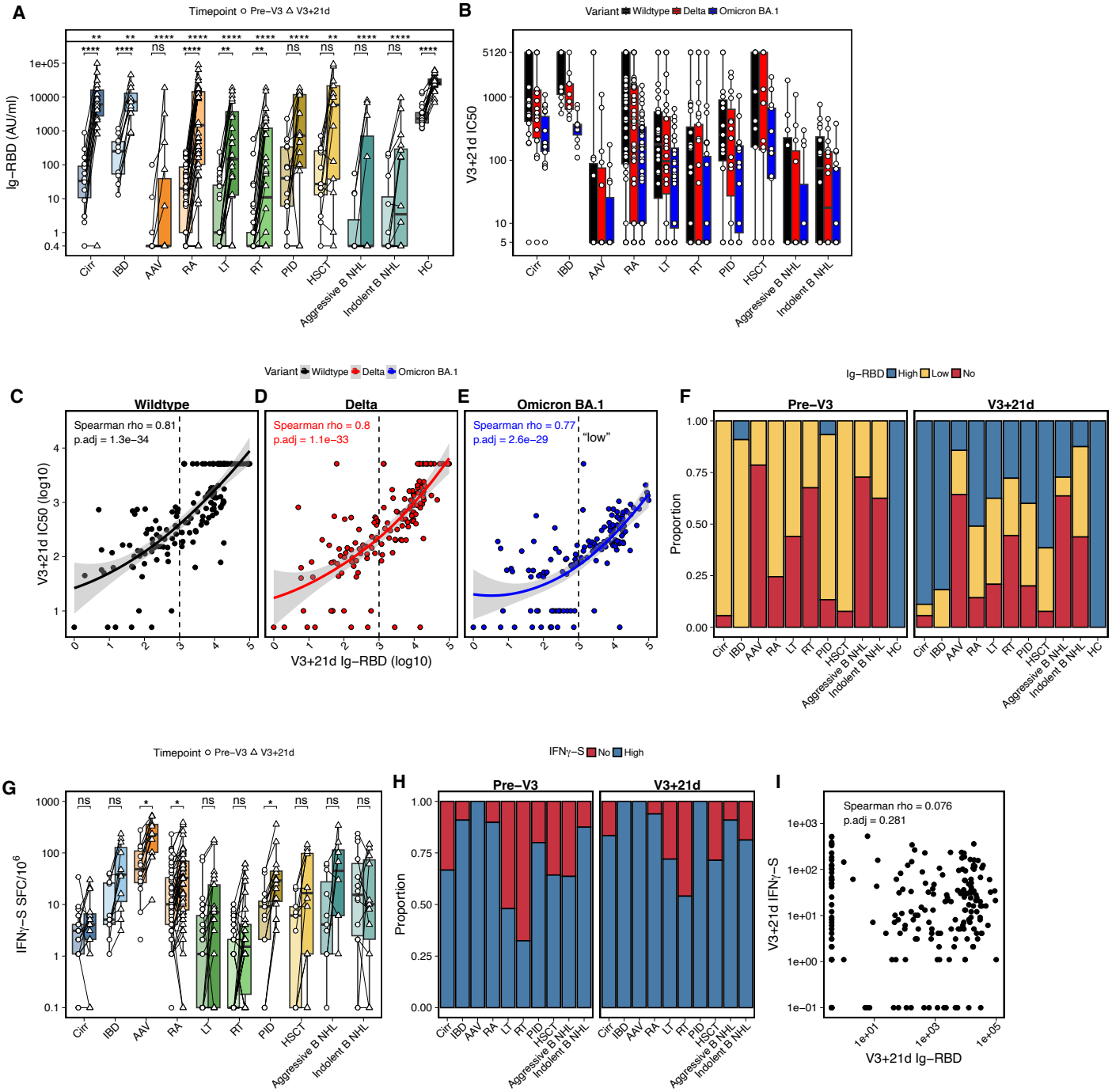

Fig. 5.2 SARS-CoV-2 spike responses are increased by a third COVID-19 vaccine but reduced compared to healthy controls

A) Total binding immunoglobulin (Ig) to receptor binding domain (RBD) before (pre-V3) and 21d post (V3+21d) a third mRNA COVID-19 vaccine dose. Symbols above solid line represent comparisons with healthy controls.

B) V3+21d microneutralisation 50% inhibitory concentration titre (IC50) of live SARS-CoV-2 variants by donor serum.

C-E) Correlation of V3+21d SARS-CoV-2 ancestral (wildtype, C), delta (D) or omicron BA.1 (E) microneutralisation IC50 with V3+21d anti-RBD Ig. Spearman correlation and loess curve for each variant displayed. 1000AU/mL marked as low antibody titre.

F) anti-RBD Ig stratified by no (<0.8AU/mL), low (0.8-1000AU/mL) and high (>1000AU/mL) response per group.

G) IFNγ ELISpot to peptide pools covering full SARS-CoV-2 spike (IFNγ-S)

H) IFNγ-S stratified by no (<1 SFC/10^6) and high response per group.

I) Correlation of V3+21d anti-RBD Ig and V3+21d anti-S IFNγ response. Spearman correlation displayed.

Reanalysis of data generated in OCTAVE DUO study.

* P <0.05; ** P < 0.01; *** P <0.001; **** P < 0.0001.

responsiveness after a third vaccine dose **(Fig. 5.2F)**. More than 50% of patients in AAV, NHL, LT, RT and PID groups had low or no anti-RBD Ig titre at V3+21d **(Fig. 5.2F)**.

Healthy control data was not available for V3+21d IFNγ T cell responses, however amongst immunocompromised individuals only AAV, RA and PID groups had anti-S IFNγ T cell responses that increased significantly between pre-V3 and V3+21d **(Fig. 5.2G)**. Notably, AAV recipients had the highest V3+21d IFNγ T cell responses of all disease groups, despite having amongst the lowest anti-RBD Ig titres. Individuals in cirrhosis, LT and RT groups had the lowest V3+21d anti-S IFNγ T cell magnitudes and the highest proportions of T cell non-responsiveness before and after a third vaccine **(Fig. 5.2G&H)**. In the whole cohort, there was no correlation between anti-RBD Ig titres and anti-S IFNγ T cell responses (**Fig. 5.2I)** - highlighting the importance of measuring both antibody and T cell responses to vaccines in immunocompromised individuals.

5.6.3 Geneset modules identify biologically relevant differences between clinical groups in bulk RNA-sequencing data

To assess broad transcriptomic differences associated with clinical groups and immunosuppressive therapies, I used bulk RNA-sequencing of whole blood in 231 immunocompromised and healthy individuals at a pre-vaccine timepoint. A total of 24,866 genes passed QC and were captured across all individuals. A challenge of RNA-sequencing data is to interpret the high-dimensional output of thousands of genes in a meaningful and unbiased way. To address this, I first used geneset variation analysis (GSVA) to aggregate the normalised per-person expression of genes into genesets, using a library of annotated genesets derived from whole blood (*238*). This organised groups of genes into biologically meaningful units and reduced the number of measurements from the 24,866 genes captured to 263 genesets. Principal component analysis (PCA) based on the geneset scores for each individual demonstrated that this approach captured enough variation to identify differences between disease groups and demographic factors (**Fig. 5.3)**.

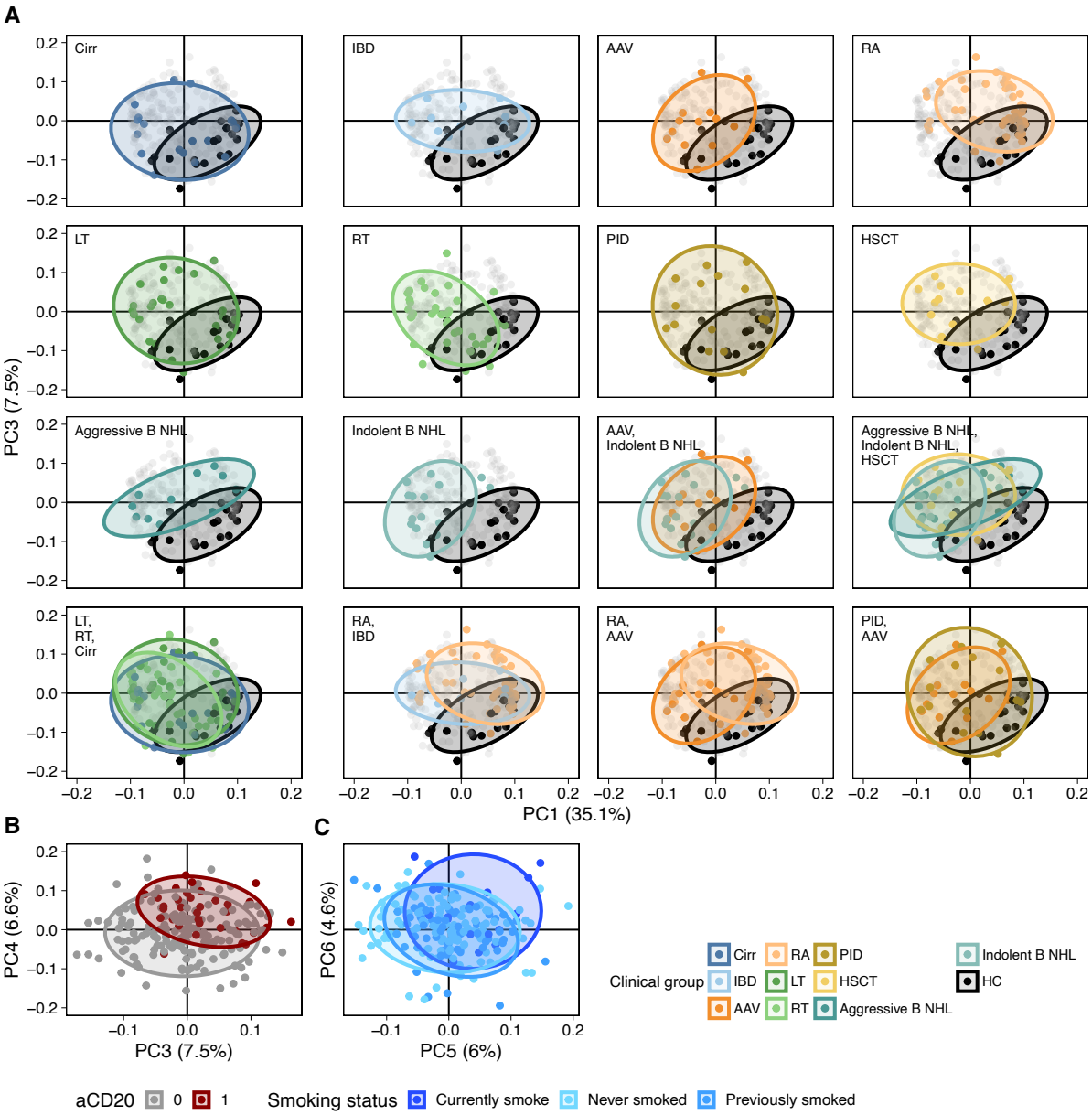

Fig. 5.3 Principal components of geneset expression distinguish transcriptomic phenotypes

A-C) Principal component analysis using geneset expression values from geneset variation analysis. Loadings of principal component one and three shown, coloured with relevant disease groups and healthy individuals (A), by anti-CD20 therapy use (0 = none, 1 = in use) (B) or by smoking status (C). 95% confidence interval ellipse is shown

To further reduce the data, I developed a semi-unsupervised approach to generate modules of related genesets (**Fig. 5.4**). I filtered genesets with low variation across the dataset (**Fig. 5.4A)** and used k-means clustering to identify clusters of genesets with similar expression profiles, using 10 k-means clusters (k) as a first pass. I calculated the within cluster correlation of each cluster and removed one cluster that had low internal correlation (Pearson r^2 of 0.13) (**Fig. 5.4B)**, resulting in 104 genesets. Finally, I performed repeated kmeans and selected an

optimal k value for clustering, where each cluster had a minimum cluster size of 4 and lowest internal variation (**Fig. 5.4C&D)**; then manually annotated geneset modules based on the

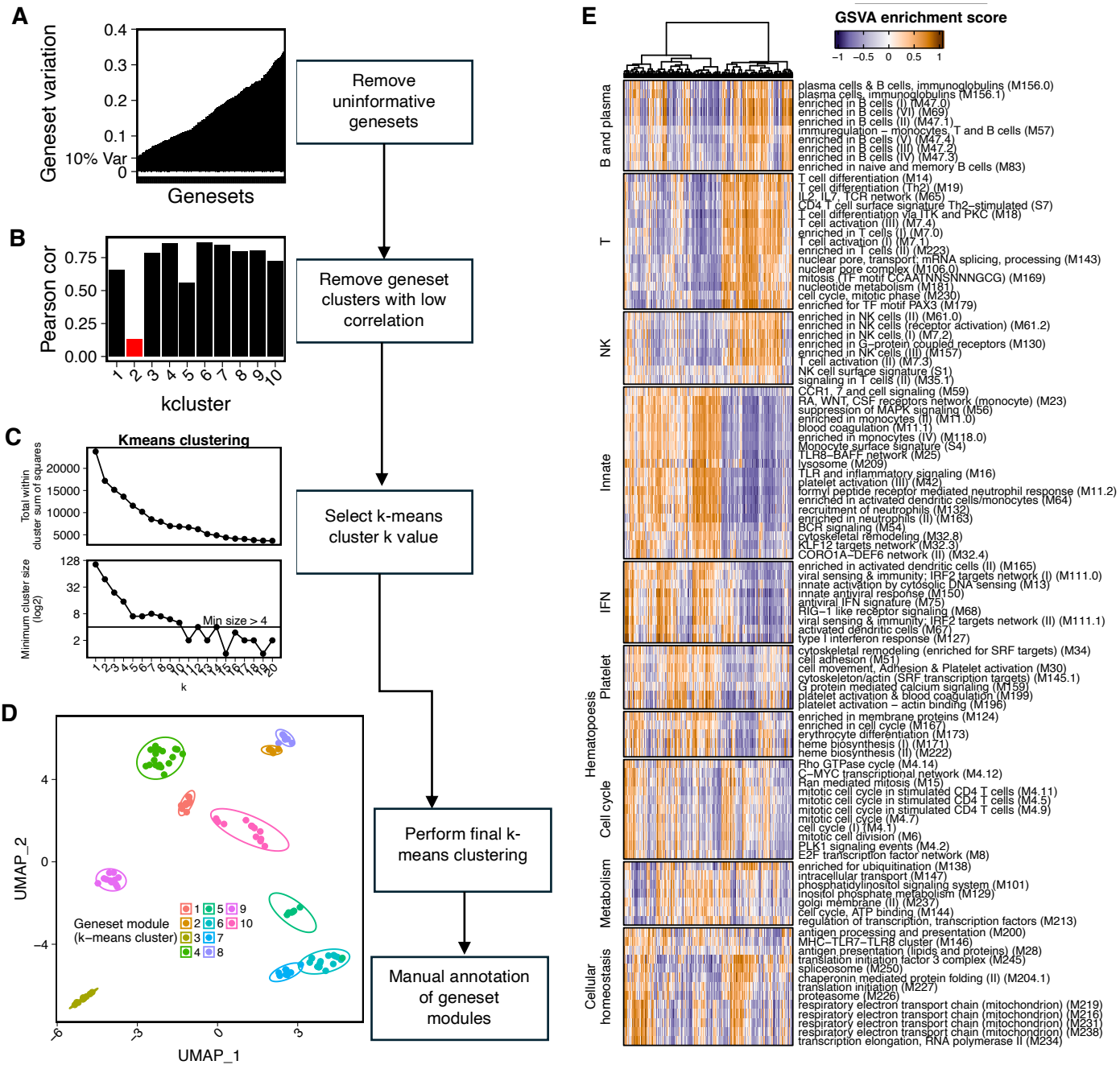

Fig. 5.4 Clustering of genesets to identify broad biologically relevant geneset modules

A-C) Process to identify geneset modules. The genesets with the lowest variance (<10% of the maximum variance of any geneset) were removed (A). Genesets were then clustered based on expression similarity across individuals and filtered to remove geneset clusters with low internal correlation (B). The remaining genesets were clustered again after selection of the optimal number of k-means centres (C).

D) Uniform manifold approximation and embedding (UMAP) of the expression of genesets, clustered into the geneset modules from A-C. 95% confidence interval ellipse is shown.

E) Geneset variation analysis scores for the entire dataset, with genesets clustered into geneset modules manually annotated based on their geneset composition.

constituent genesets **(Fig. 5.4E)**. This resulted in 10 clusters related to B and plasma cells, T cells, NK cells, monocyte and neutrophils (innate), interferon signalling (IFN), platelets, haematopoiesis, cell cycling, metabolic processes and cellular homeostasis. The mean GSVA enrichment score of genesets within each module for each donor was derived as the 'geneset module score'.

Significant differences in geneset module scores were observed between disease groups in all geneset modules except the NK module, when adjusted for age and sex **(Fig. 5.5A)**. As expected, individuals in the AAV and NHL groups, which were enriched for use of aCD20 therapy (**Fig. 5.1E)**, had lowest expression of the B and plasma module **(Fig. 5.5A)**. The solid organ transplant, HSCT and aggressive B NHL groups had lowest expression of the T cell module **(Fig. 5.5A)**. Interferon-signalling was lowest in RA and HC, and this corresponded with lower innate cell signalling in these groups.

To assess the relative contribution of immunosuppressive therapeutics, diseases and demographic factors to the geneset module scores, I fitted multivariable linear models for each geneset module score to compare specific therapy and disease combinations with HCs while accounting for age, sex and obesity and diabetes status **(Fig. 5.5B)**. There were several unique interactions between drug type and disease group, for instance aTNF use in individuals with IBD was associated with significantly reduced B and plasma cell geneset module score compared to HC, but there was no significant difference in this module score between RA patients on aTNF and HCs **(Fig. 5.5B)**. While all individuals on aCD20 therapy had reduced B and plasma cell module score compared with HC, individuals with indolent B NHL on aCD20 therapy also had significant upregulation of innate, interferon, platelet and haematopoiesis genesets modules. This was not seen in RA, AAV or aggressive B NHL patients – suggesting that the indolent B NHL group had additional immune dysregulation attributable to disease **(Fig. 5.5B)**. In individuals with cirrhosis, corticosteroid use was associated with significant differences in in B and plasma, NK, innate and interferon related genesets compared to HCs

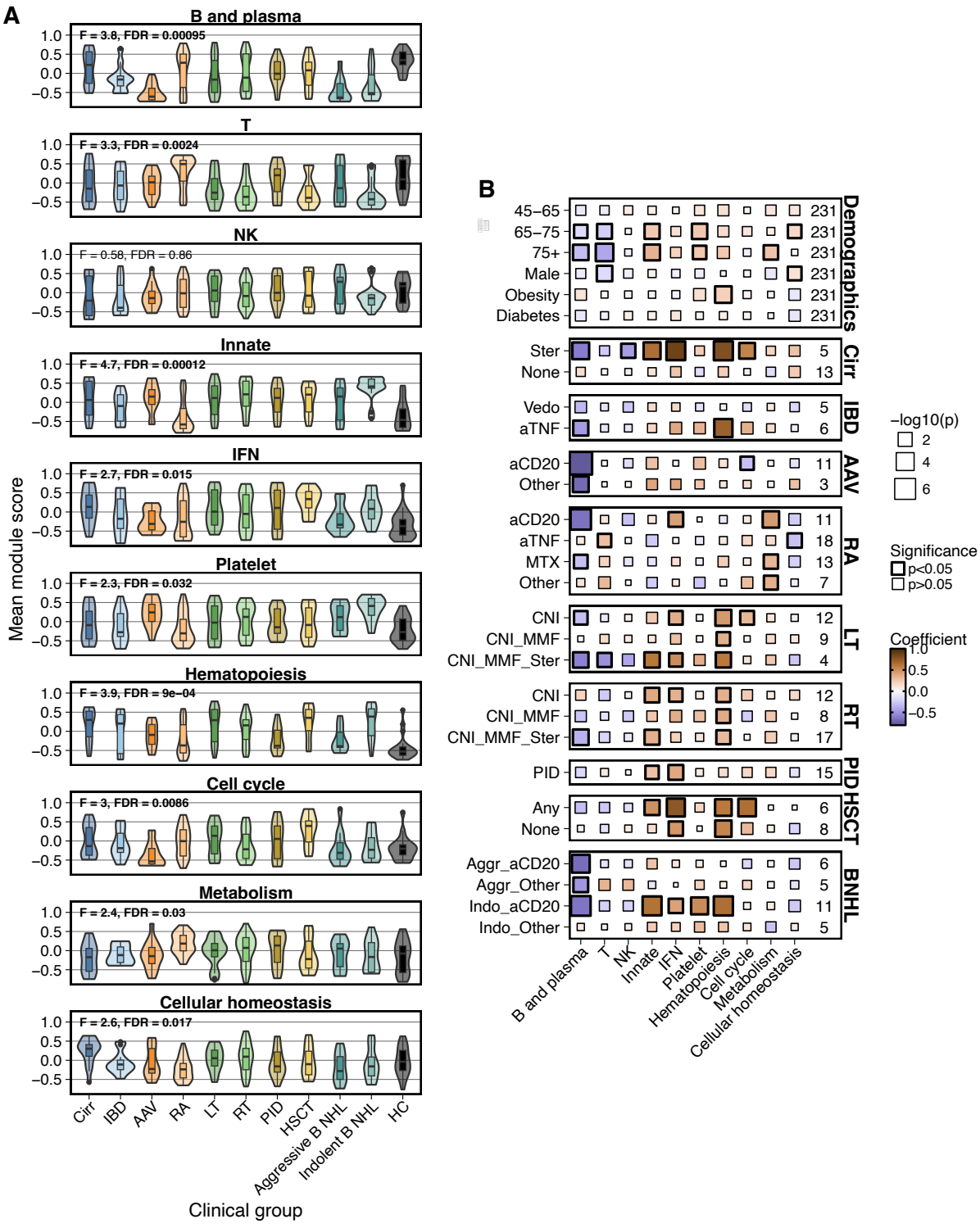

Fig. 5.5 Clinical and demographic phenotype is associated with geneset module scores

A) The geneset module score (the mean geneset variation analysis score of all genesets within the module) across clinical groups. F-statistic and Benjamini-Hochberg false-discovery rate (FDR) from ANCOVA, adjusted for age and sex.

B) Multivariate linear models fit to each geneset module score. An independent model was fitted for each geneset module, with all other variables as covariates. Age is compared to individuals 26-45years old, all disease group and immunosuppression combinations are compared to healthy individuals. P values from each model (10 in total) were adjusted using Benjamini-Hochberg false-discovery rate (FDR). Thick lines around a square indicate FDR < 0.05.

that were not observed in cirrhosis patients without immunosuppression, suggesting that immunosuppression exacerbates the dysregulated phenotype in this group **(Fig. 5.5B)**.

5.6.5 Shared transcriptomic signatures span across multiple clinical phenotypes

The analysis in **Figure 5.5B** suggested that in some cases, there were unique interactions between diseases and immunosuppressive therapeutics. However, it is likely that some of the immune signatures at baseline are shared across multiple disease groups – especially those with shared use of immunosuppressive therapies. To investigate this, I grouped individuals into clusters based on their baseline geneset expression profiles. To produce robust and reproducible clusters, I performed two rounds of k-means clustering and unsupervised hierarchical clustering. The first round included 1000 iterations of k-means clustering with k values from 4 to 10 (**Fig. 5.6A)**. Based on the resultant matrices, I performed k-means clustering again with k values from 1 to 10 and selected the k values from both rounds of clustering that had the lowest within cluster sums of squares (**Fig. 5.6B)**. This resulted in four clusters which accurately grouped individuals into distinct clusters **(Fig. 5.6C)**. Cluster number three had the most overlap with other clusters **(Fig. 5.6C).**

The expression of all geneset modules differed significantly across the modules (ANOVA $p < 0.05$ for all) (**Fig. 5.6D&E)**. Cluster 1 had low expression of T and metabolism modules; cluster 2 had low expression of B and plasma, T, and NK modules; cluster 3 had intermediate expression of all immune related clusters and low expression for cell cycling modules and cluster 4 had low expression for innate and interferon related genes (**Fig. 5.6D&E)**. Each cluster contained individuals from different immunocompromised groups with notable skewing: clusters 3 and 4 were enriched for HC individuals, with cluster 2 containing no HC individuals (**Fig. 5.7A&B)**. RA patients were heavily enriched in cluster 4, but this cluster had few individuals from solid organ and haematopoietic stem cell transplant, AAV, and NHL groups (**Fig. 5.7A&B)**. Demographic and clinical factors also varied significantly across groups, including age, sex and number of comorbidities and immunosuppressive therapies

Fig. 5.6 Robust and reproducible clustering of individuals by geneset signatures

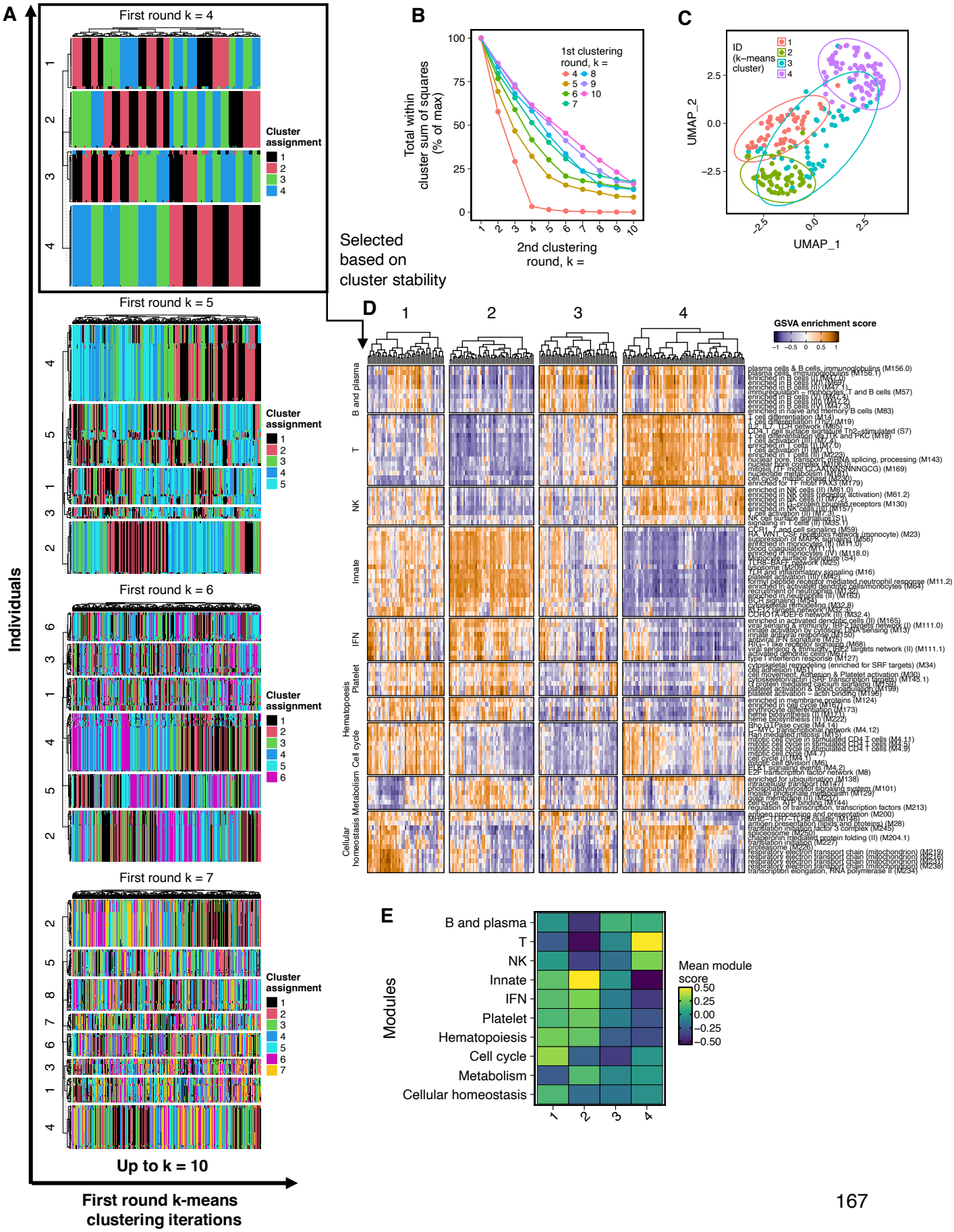

Fig. 5.6 Robust and reproducible clustering of individuals by geneset signatures

A&B) Individuals were clustered based on similarity of geneset variation analysis expression score similarity 1000 times (with each round of clustering using a random seed) with a k value ranging from four to 10 (k value from 4 to 7 depicted) Heatmaps are hierarchically clustered for visualisation (A). The 1000 iterations of the initial clustering was then used for a second round of k-means clustering using an optimised k-means threshold (B), resulting in the row clusters used to split rows in A.

C) Uniform manifold approximation and projection (UMAP) representation of the geneset signatures of each individual, coloured by k-means cluster derived from A&B. 95% confidence interval ellipse is shown.

D) Geneset variation analysis expression scores of each individual in the cohort, with genesets (y axis) grouped into geneset modules and individuals (x axis) grouped into clusters derived from A&B. Individuals within clusters are hierarchically clustered based on Euclidean distance.

E) The mean geneset module score for each cluster of individuals.

(Fig. 5.7C-J). Notably, these changes are confounded by the biases of demographic factors between disease groups. Together, this suggests that unsupervised clustering of transcriptomic measurements can broadly discern immunologically 'healthy' individuals from immunocompromised individuals, but that immunocompromised transcriptomic signatures are shared across different clinical phenotypes.

5.6.6 The baseline transcriptome is associated with vaccine-induced antibody responsiveness.

There are clear differences between the transcriptomes of individuals with different SIs, however it is not clear how these differences relate to functional responses to vaccination. To assess this, I first compared V3+21d anti-RBD Ig binding responses between individuals stratified by transcriptomic clusters (**Fig. 5.6).** Individuals in cluster 2, which was associated with low adaptive immune module expression, had significantly lower anti-RBD Ig and was enriched for anti-RBD non-responsiveness compared with individuals in cluster 4 **(Fig. 5.8A)**. To identify specific geneset modules that were associated with anti-RBD Ig titres, I next directly compared the expression of each geneset module score with anti-RBD Ig titres. B and plasma, T, innate, IFN and platelet geneset modules were significantly correlated with antibody responses **(Fig. 5.8B)**. There was a sigmoidal relationship between the T module and anti-RBD Ig which was mirrored by the innate module. The B and plasma cell module was most strongly associated with anti-RBD Ig and exhibited an asymptotic relationship with an exponential increase followed by a plateau – indicating that once B and plasma cell-related

Fig. 5.7 Clinical and demographic features associated with transcriptomic clustering

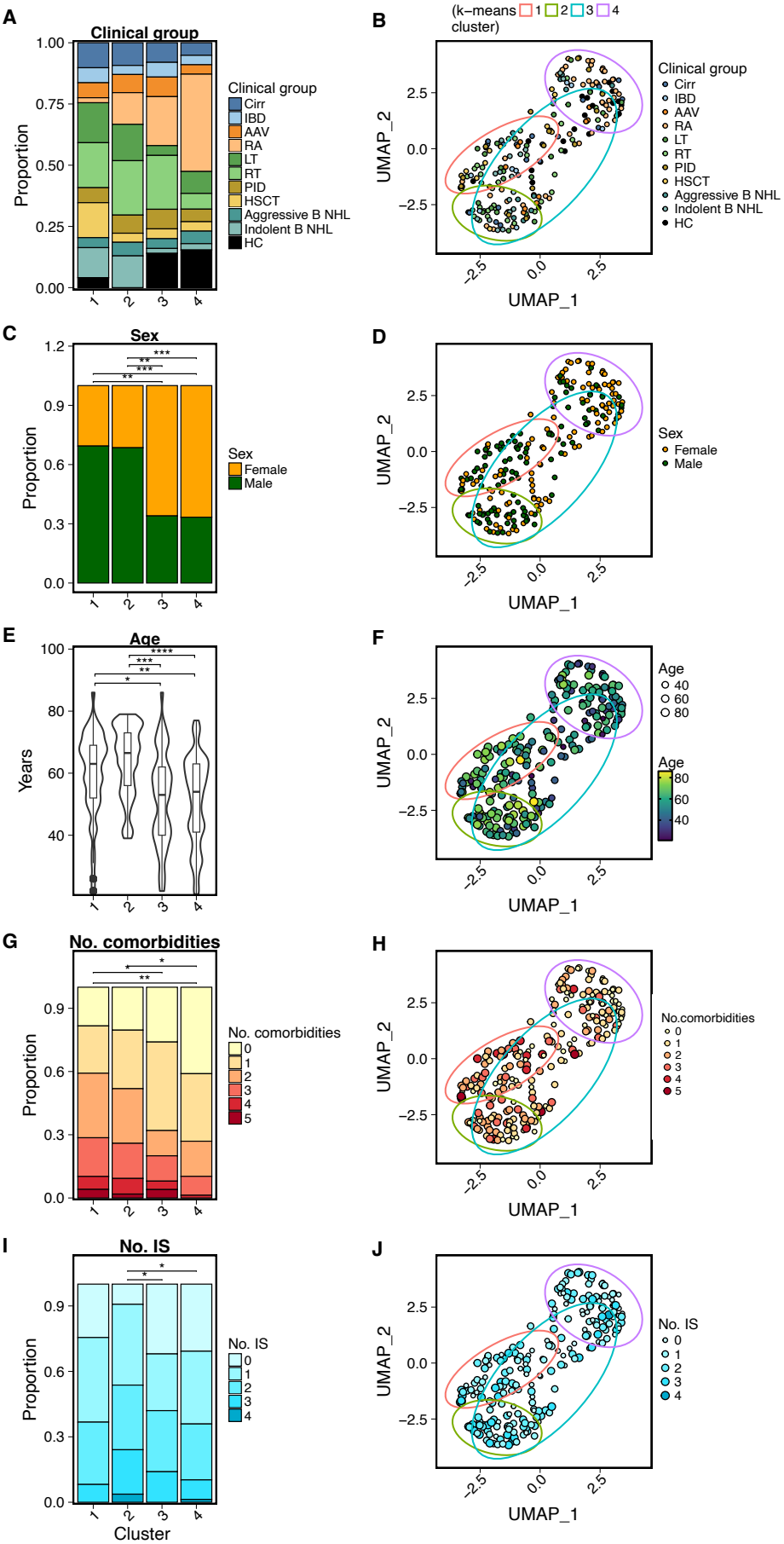

Fig. 5.7 Clinical and demographic features associated with transcriptomic clustering

A-J) Proportions (A,C,E,G,I) and uniform manifold approximation and projection (UMAP) (B,D,F,H,J) representations of clinical and demographic features of the transcriptional phenotypes. Disease group (A&B), Sex (C&D), Age (E&F), number of comorbidities (G&H) and combined number of immunosuppressive therapies (I&J) depicted. C, G and I statistical tests are Fisher's exact tests with Bonferroni correction. G is comparison o proportion with >1 comorbidities. I is comparison of proportion >0 immunosuppressive therapies. E is Mann-Whitney U test with Bonferroni correction. * P <0.05; ** P < 0.01; *** P <0.001; **** P < 0.0001.

expression reached a certain threshold, it was no longer beneficial to vaccine-induced antibody responses **(Fig. 5.8B)**.

Contrary to the overall trend, some individuals had high expression of the B and plasma geneset module but had low or no anti-RBD Ig titres (**Fig. 5.8B,** indicated in black box). To identify which groups of individuals these were, I separated the dataset based on a threshold of B and plasma module expression optimised to maximally segregate the dataset based on V3+21d anti-RBD Ig responsiveness **(Fig. 5.8C)**. Using only this binary threshold (-0.28) of B and plasma geneset module score was sufficient to accurately classify individuals from most clinical groups by antibody responsiveness (180 of 228 (78%) correctly classified; specificity = 0.8, sensitivity = 0.78). However, participants from the solid organ transplant groups made up the largest proportion of false positive individuals **(Fig. 5.8D)** – suggesting that the B and plasma geneset module had a different relationship with anti-RBD Ig depending on the clinical phenotype. Stratification by clinical group revealed that the positive correlation between B and plasma module expression and V3+21d anti-RBD Ig titre was largely only present in groups where aCD20 therapy was in use (**Fig. 5.8E)**. To explore whether the lack of correlation within some groups was due to differential expression of genesets within the geneset modules, I fitted linear models of $\log_{10}$ transformed V3+21d anti-RBD Ig using genesets that made up the geneset modules that were significantly correlated with V3+21d anti-RBD Ig titre (**Fig. 5.8B)**. I included an interaction term between the geneset score and the clinical group, and additionally controlled for sex, age and third vaccine type. Most genesets within B and plasma, IFN and innate geneset modules were significantly independently associated with anti-RBD Ig titre across the groups on aggregate (**Fig. 5.8F)**.

Fig. 5.8 Baseline transcriptional signature is associated with V3+21d anti-RBD antibody titre

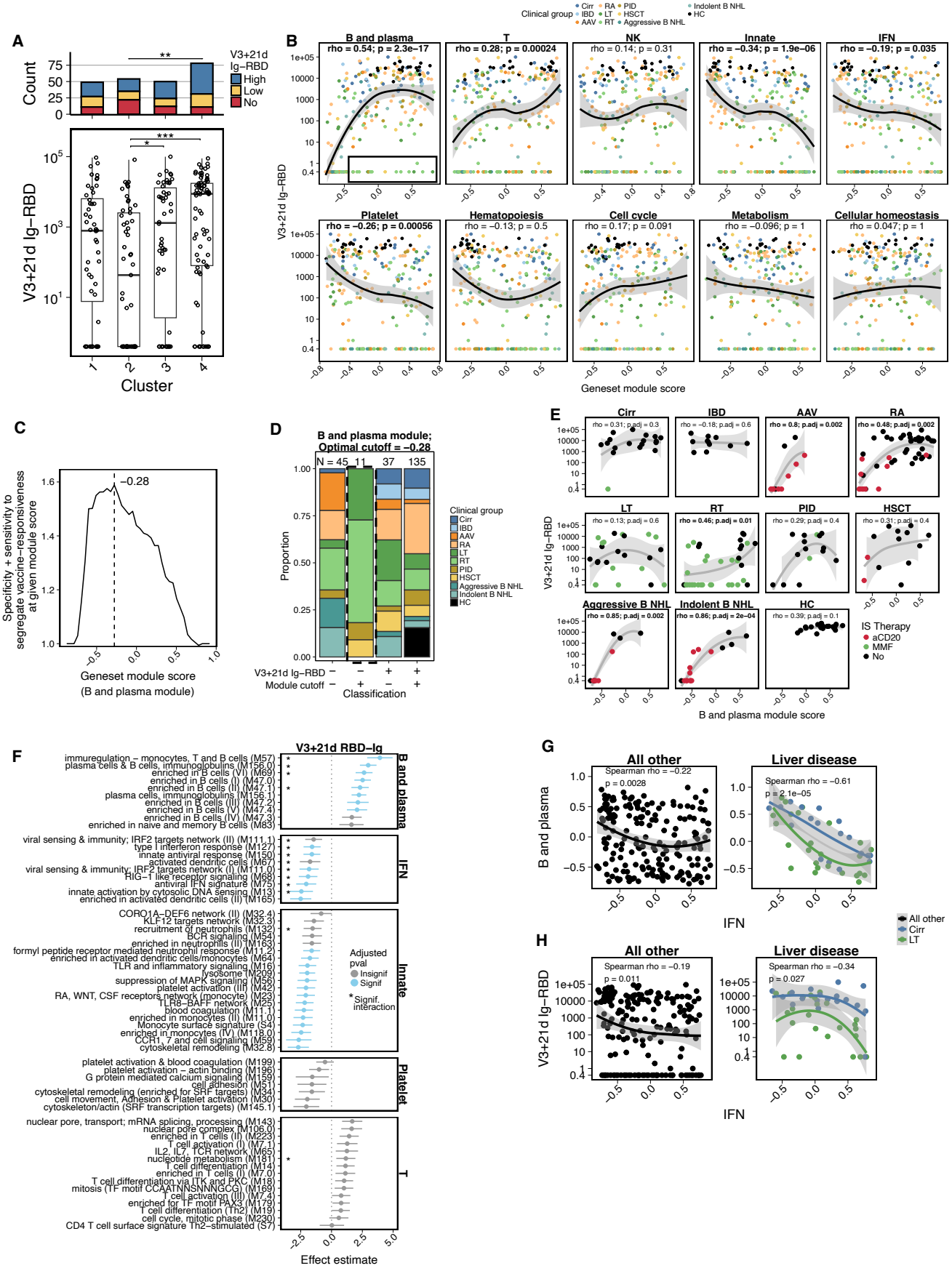

Fig. 5.8 Baseline transcriptional signature is associated with V3+21d anti-RBD antibody titre

A) SARS-CoV-2 receptor binding domain (RBD) binding Ig responses 21days after third vaccine (V3+21d) in individuals stratified by transcriptomic clusters. Top bars are counts of individuals with V3+21d anti-RBD Ig titres stratified by no (<0.8AU/mL), low (1000AU/mL) or high (>1000AU/mL). Magnitudes compared with Mann-Whitney U test, Bonferroni corrected. Counts compared with Fisher's exact test, Bonferroni corrected.

B) Spearman's correlation and loess regression curves of the pre-vaccine geneset module score for each geneset module with V3+21d anti-RBD Ig titre. P is Benjamini-Hochberg false-discovery rate.

C) Cumulative specificity and sensitivity of classifying anti-RBD Ig responsiveness (no response (<0.8AU/mL versus response (>0.8AU/mL)) at different threshold values of B and plasma geneset module score. The maximum cumulative specificity and sensitivity is marked with dashed line (geneset module score of -0.28)

D) Stratification of clinical groups based on anti-RBD Ig response above (+) or below 0.8AU/mL (-) and B and plasma module score expression above (+) or below -0.28 (-).

E) Spearman's correlation of B and plasma module score with V3+21d anti-RBD Ig, separated by clinical groups and coloured by key immunosuppressive therapies. aCD20, anti-CD20 therapy. MMF, mycophenolate mofetil. P.adj is Benjamini-Hochberg false-discovery rate.

F) Linear models of $\log_{10}$ transformed V3+21d anti-RBD Ig titres with genesets within geneset modules that were correlated with V3+21d anti-RBD Ig (B). A model was fitted independently for each geneset, with an interaction term between geneset and clinical group (with the healthy control group as the null), and age and sex as covariates. Significant geneset terms (Benjamini-Hochberg FDR <0.05) are marked in blue. Significant interactions between the geneset expression and clinical group are marked with *. The point and lines represent the geneset variable coefficient and standard error.

G&H) Spearman's correlations of pre-vaccine B and plasma score (G) and anti-RBD Ig titre (H) with the IFN geneset module score.

As expected, there were significant interactions between expression of genesets within the B and plasma module and the clinical group (**Fig. 5.8F)**. There were also significant interactions between expression of genesets within the interferon geneset module and clinical group – due to a differing relationship between the expression of these genesets and anti-RBD Ig titre in the LT and cirrhosis groups (liver disease groups) compared to other groups in the analysis (**Fig. 5.8F&G)**. Further inspection of this interaction identified that there was a strong negative correlation between the IFN and B and plasma modules specifically in individuals with liver disease (**Fig. 5.8G)**. Interestingly, although B and plasma module expression alone was not significantly associated with anti-RBD Ig responses in individuals in LT or cirrhosis groups (**Fig. 5.8E)**, expression of the IFN module was significantly negatively correlated with anti-RBD Ig **(Fig. 5.8H)**. Suggesting a unique interaction of interferon signalling and reduced B cell expression with anti-RBD Ig titre in these groups and a crucial link between baseline inflammation and vaccine-induced antibody responses.

5.6.7 Baseline transcriptomic signatures that are associated with anti-RBD Ig

responses are distinct from the signature associated with vaccine-induced anti-S IFNγ T cell responses.

I next assessed the relationship of the baseline transcriptome with vaccine-induced IFNγ T cell responses. Comparison of V3+21d anti-S IFNγ T cell responses between individuals in different transcriptomic clusters identified reduced T cell magnitude and responsiveness associated with cluster 1 compared to cluster 3 (FDR = 0.054) and 4 (FDR = 0.03) (**Fig. 5.9A)**. Thus, while cluster 2 was associated with reduced vaccine-induced antibody responses, cluster 1 was the predominant cluster associated with reduced T cell responses. Baseline expression of B and plasma, T, cell cycling and cellular homeostasis modules were weakly but significantly correlated with V3+21d anti-S IFNγ T cell responses (**Fig. 5.9B)**.

Analysis of the association between the expression of genesets within the geneset modules and V3+21d anti-S IFNγ identified that only 4 genesets within the T module were significantly associated with vaccine-induced T cell response, namely: "*T cell differentiation", "CD4 T cell surface signature Th2-stimulated', "T cell activation (III)"* and *"T cell differentiation (Th2)"* (**Fig. 5.9C)**. Geneset enrichment analysis also identified T cell genesets upregulated in individuals with detectable V3+21d T cell responses compared to those with no V3+21d T cell response (**Fig. 5.9D)**. Several B cell genesets were significantly negatively associated with T cell responses, likely primarily driven by the increased T cell magnitude observed in the AAV group which has low B cell module expression (**Fig. 5.2G & 5.6A).** Interestingly, increased expression of TLR signalling-related genes (*"MHC-TLR7-TLR8 cluster"* and "*TLR and inflammatory signalling"*), which is involved in mRNA vaccine sensing and associated inflammation (*387*), was associated with reduced T cell responses to vaccination (**Fig. 5.9C & 5.9D)**. Thus, the baseline transcriptomic profile was associated with V3+21d anti-S IFNγ T cell responses – however the association differed and was less strong compared to the baseline signature associated with V3+21d anti-RBD Ig responses after vaccination

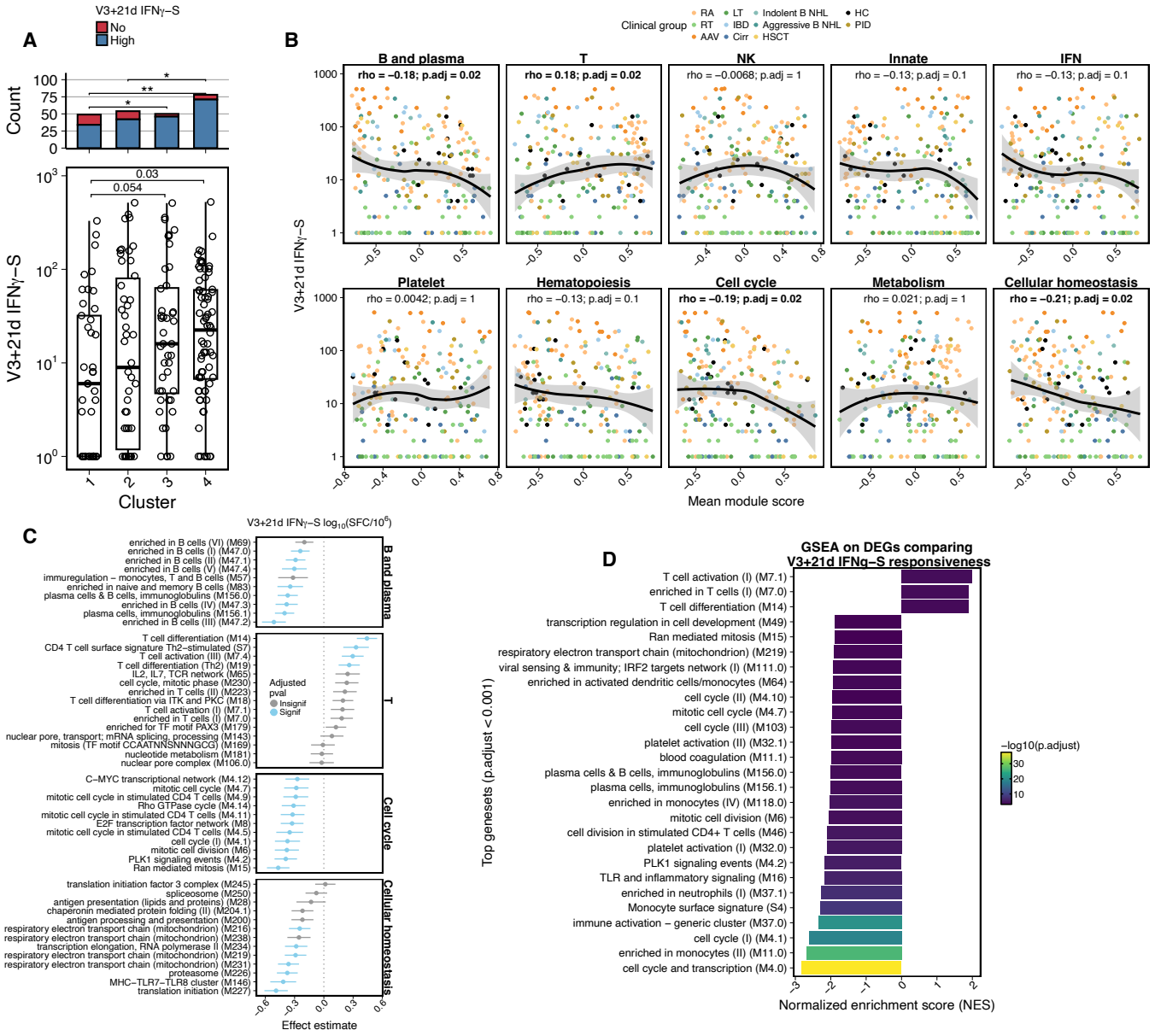

Fig. 5.9 Baseline transcriptional signature is associated with V3+21d anti-SARS-CoV-2 spike IFNγ T cell responses

A) SARS-CoV-2 spike IFNγ T cell (anti-S) responses 21 days after third vaccine (V3+21d) in individuals stratified by transcriptomic clusters. Top panel are counts of individuals with V3+21d anti-S IFNγ T cell responses stratified by no (< 1 SFC/10^6 PBMC) or high (>0 1 SFC/10^6 PBMC). Comparison of magnitudes using Mann-Whitney U test, with Bonferroni correction. Counts compared with Fisher's exact test, with Bonferroni correction.

B) Spearman's correlation and loess regression curves of the pre-vaccine geneset module score for each geneset module with V3+21d anti-S IFNγ T cell response. P is Benjamini-Hochberg false-discovery rate.

C) Linear models of $\log_{10}$ transformed V3+21d anti-S IFNG T cell response with genesets within geneset modules that were correlated with V3+21d anti-S IFNγ T cell response (B). A model was fitted independently for each geneset, with clinical group (with the healthy control group as the null), age and sex as covariates. Significant geneset terms (Benjamini-Hochberg FDR <0.05) are marked in blue. The point and lines represent the geneset variable coefficient and standard error.

D) Geneset enrichment analysis of differentially expressed genes (calculated using DESeq2, with age and sex as covariates) between individuals with anti-S IFNγ T cell responses above compared with below 1 SFC/10^6 PBMC. Only genesets with an adjusted p value below 0.001 are shown.

5.6.8 The baseline inflammatory proteome is associated with transcriptomic signatures and identifies differences between clinical groups.

The transcriptomic data indicated that inflammatory signalling was associated with different clinical phenotypes and with vaccine-induced antibody and T cell responses. To assess whether transcriptomic differences in inflammatory signalling were also detectable at the protein level, I used the Olink Inflammatory panel I to measure the concentration of 368 inflammatory-related proteins in serum taken at the pre-V3 timepoint **(Table 5.2 Fig. 5.1C)**. 176 individuals from the cirrhosis, LT, RT, RA and HC groups were included in this analysis. These groups were selected based on their inclusion of individuals with and without vaccine-induced T and antibody responses, and sample availability. The inflammatory blood proteome distinguished healthy individuals from individuals in disease groups, particularly the LT and cirrhosis groups (**Fig. 5.10A).** There was a total of 205 differentially expressed proteins (DEP) in one or more disease group compared to HCs (**Fig. 5.10B).** Cirrhosis and LT groups had the most differentially expressed proteins compared to HCs (Cirrhosis = 149 of 368; 40%, LT = 138 of 368; 38%), RT had the next most with 82 DEPs (22%) and only 19 proteins (5.2%) were differentially expressed in the RA group compared to HC (**Fig. 5.10B)**. Of the total DEPs between clinical groups and HCs, the groups that shared the most DEPs were cirrhosis, LT and RT groups (52 DEPs) and cirrhosis and LT groups (51 DEPs) (**Fig. 5.10B&C)**. Only one protein (CCL11) was differentially expressed between HC and all disease groups. Of the 19 DEPs between RA and HC, 12 (63%) were uniquely differentially expressed in RA compared to HC. Therefore, the RA group has a different inflammatory proteome compared to cirrhosis, LT and RT groups and is more similar to HC.

DEPs were almost ubiquitously upregulated compared to HCs (**Fig. 5.10C)** and included various important immune regulating and pro-inflammatory proteins. The top five overexpressed proteins compared with HCs in cirrhosis were CCL20, CMKT1A_1B, IL6, FABP1 and CXCL8 (**Fig. 5.10D)**. FABP1 was also a top upregulated protein in LT and RT

Fig. 5.10 384-plex inflammatory proteomics identifies unique and shared features of inflammation in the plasma of different immunosuppressive diseases

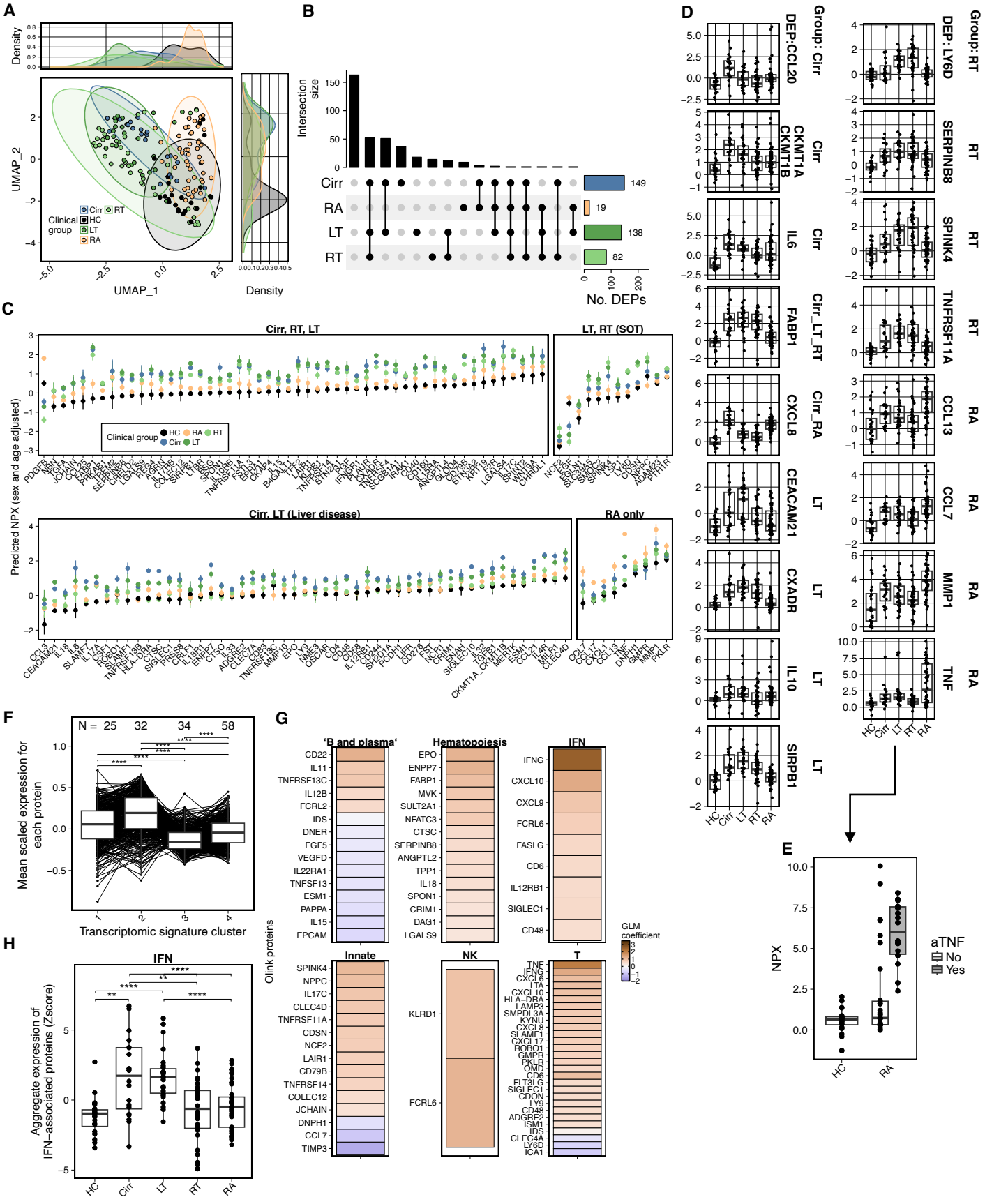

Fig. 5.10 384-plex inflammatory proteomics identifies unique and shared features of inflammation in the plasma of different immunosuppressive diseases

A) Uniform manifold approximation and projection (UMAP) dimensional reduction of Olink Inflammatory proteomics across disease groups. Ellipses represent 95%CI

B) Number of differentially expressed proteins between healthy controls and each disease group. Total number of differentially expressed proteins per group on right panel. Number of differentially expressed proteins shared between different disease groups in comparison to healthy controls on top.

C) Predicted NPX from linear models fit to each Olink protein adjusted for age and sex. Proteins in each panel are those that are differentially expressed compared to healthy controls in each of the groups in the panel title. Point is mean NPX, lines are standard deviation.

D) Expression of the top five differentially expressed proteins from each disease group compared to healthy controls. For each protein, the disease groups that are significantly compared to healthy control is labelled.

E) Expression of TNF protein in healthy controls and patients with rheumatoid arthritis, separated by anti-TNF therapeutic use.

F) The mean scaled expression of each of the 384 proteins in the Olink Inflammatory I panel for individuals stratified by transcriptomic cluster. Each point represents a protein.

G) Linear models (with age and sex as covariates) of the NPX value of each Olink protein with each geneset module score defined in transcriptomic data. Only significantly associated proteins (Benjamini-Hochberg false discovery rate <0.05) are shown.

H) The aggregate expression (average zscore of NPX values) of proteins identified in G that were significantly associated with the IFN geneset module.

F&H) Mann-Whitney U test with Bonferroni adjustment. * P <0.05; ** P < 0.01; *** P <0.001; **** P < 0.0001.

recipients, alongside CEACAM21, CXADR, IL10 and SIRPB1 in LT and LY6D, SERPINB8, SPINK4 and TNFRSF11A in RT recipients (**Fig. 5.10D)**. Individuals in the RA group had upregulation of CXCL8, CCL13, CCL7, MMP1 and TNF (**Fig. 5.10D)**. Interestingly, anti-TNF medication use within the RA group was associated with the increased plasma TNF concentrations observed within this group (**Fig. 5.10E).**

When individuals were clustered based on the baseline transcriptome, individuals in clusters 1 and 2 appeared to have increased inflammatory and innate signalling (**Section 5.6.5**). To test if this was also observed at the protein level, I stratified the Olink dataset based on transcriptomic clusters. Consistent with the transcriptomic signatures, individuals in cluster 1 and 2 had the highest overall expression of inflammatory proteins in plasma **(Fig. 5.10F)**. Direct comparison of the geneset module scores with inflammatory proteome concentrations identified several proteins measurable in the blood that were significantly associated with geneset modules scores from the B and plasma, haematopoiesis, IFN, innate, NK and T modules **(Fig. 5.6G)**. The aggregate expression of proteins that were associated with

expression of the IFN module (IFNγ, CXCL10, CXCL9, FCRL6, FASLG, CD6, IL12RB1, SIGLEC1 and CD48) was upregulated in the cirrhosis and LT groups, consistent with transcriptomic expression (**Fig. 5.6 & 5.10H)**.

5.6.9 The inflammatory proteome demonstrates that baseline inflammation is negatively associated with serological responses to mRNA COVID-19 vaccines.

The transcriptomic data demonstrated that increased baseline inflammation was negatively associated with V3+21d anti-RBD Ig titres. Consistent with this, V3+21d anti-RBD Ig titres were negatively associated with several inflammatory proteins at baseline **(Fig. 5.11A),** after controlling for disease group, sex and age. Many of the proteins that were associated with V3+21d anti-RBD Ig were also significantly associated with expression of transcriptomic geneset modules **(Fig. 5.11A)**. Notably, B and plasma cell module related proteins IL15, TNFSF13 (both negatively associated with B and plasma module expression), and CD22 (positively associated with B and plasma module expression) were most significantly associated with antibody immunogenicity. Several proteins related to interferon or T cell signalling were negatively associated with anti-RBD Ig responses, including IFNγ, CXCL9, CXCL10, CXCL17, LY6D and FLT3LG **(Fig. 5.11A)**. Individuals with low or no vaccine-induced anti-RBD Ig response had higher average expression of each protein compared to individuals **(Fig. 5.11B)**.

To identify baseline protein features that were predictive of anti-RBD Ig low and no versus high responsiveness, classification models were trained using Olink data with clinical group as a covariate (**Section 5.5.2)**. Both glmnet and random forest classifiers were able to accurately predict low vaccine-induced anti-RBD Ig (area under the receiver operating characteristic curve (auROC) of 0.83 and 0.86 respectively) (**Fig. 5.11C)**. Stacking both models together improved the auROC to 0.87 (**Fig. 5.11C)**. The tuned glmnet model contained 11 proteins, nine of which were also found within the top 50 most important variables of the random forest model (**Fig. 5.11D&E).** The top most important variables (those with the highest

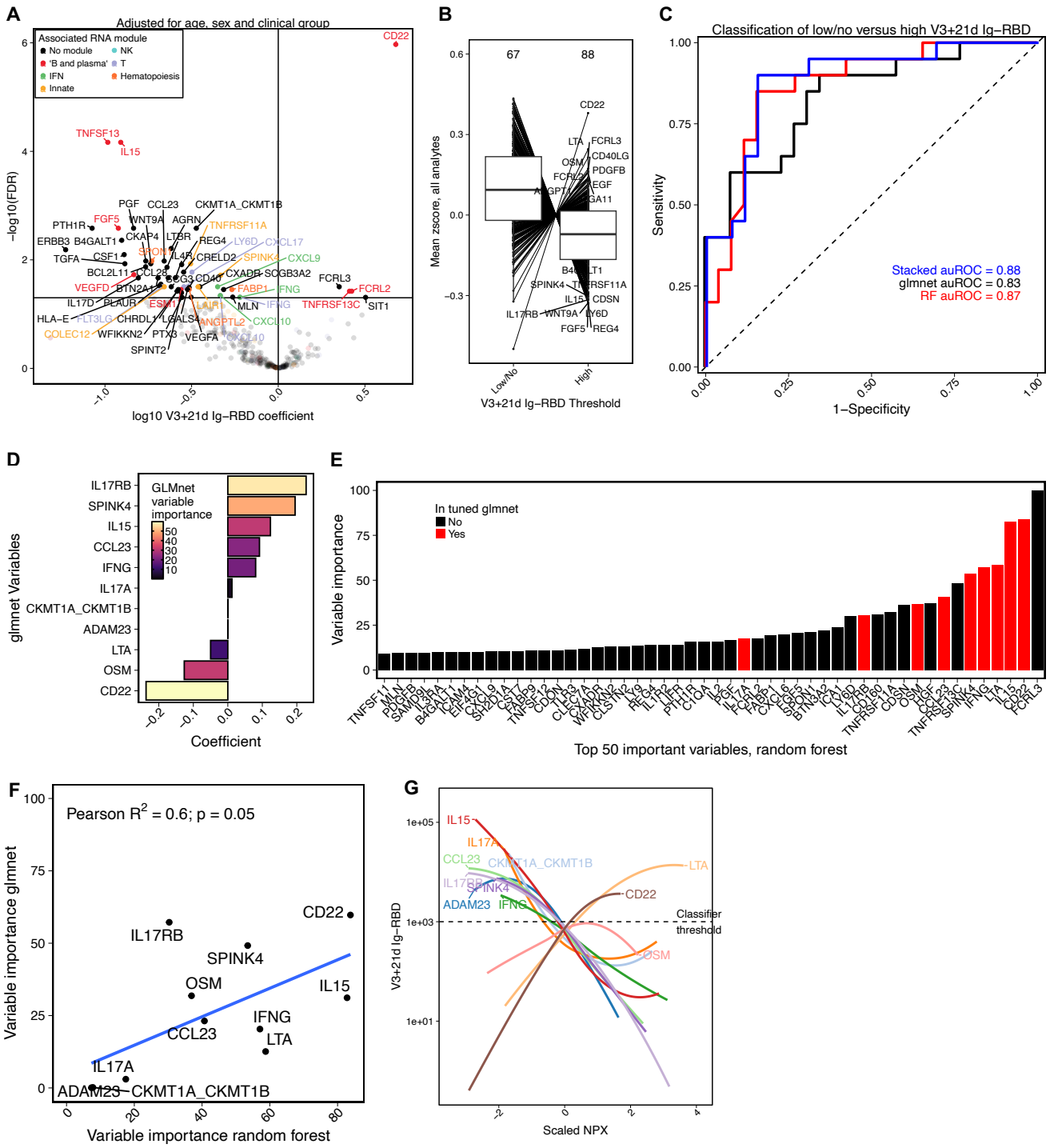

Fig. 5.11 The baseline inflammatory proteome can predict vaccine-induced SARS-CoV-2 receptor binding domain binding antibody responses

A) Linear regression model of $\log_{10}$ transformed V3+21d anti-RBD Ig fit using individual pre-V3 protein concentrations, adjusted for age, sex and clinical group. Proteins are coloured by their association with given geneset module.

B) The mean scaled expression of each of the 384 proteins in the Olink Inflammatory I panel for individuals stratified by anti-RBD Ig responsiveness. Each point represents a protein. Top and bottom 10 expressed proteins are labelled.

C) Receiver operating characteristic curves of classifier models on test data, trained on baseline Olink data to classify no/low V3+21d anti-RBD Ig (<1000AU/ml) versus high V3+21d anti-RBD Ig response.

D) Variables included in the glmnet classifer model in C.

E) Top 50 variables contributing to the random forest classifier model in C.

F) Correlation of contribution scores in the glmnet and random forest classifier models in C.

G) Loess curves of Olink protein expression (NPX) and V3+21d anti-RBD Ig titre. Only Olink proteins included in the glmnet classifier model are shown.

coefficients in the tuned model) in the glmnet model were CD22, IL17-RB, IL15, OSM and SPINK4. There was a moderate positive correlation between the variable importance in the optimised glmnet and random forest models, but FCRL3, which was the most important variable in the random forest model did not appear in the glmnet model (**Fig. 5.11E&F).** Visualisation of loess regression curves showed that the glmnet selected models changed as expected with respect to V3+21d anti-RBD Ig tires (**Fig. 5.11G)**.

5.6.10 A small number of baseline inflammatory proteins can predict mRNA COVID-19 vaccine-induced T cell responses

I next investigated the relationship of baseline inflammatory proteins with V3+21d anti-S IFNγ T cell responses. Using the same methods as in **Figures 5.11C-F**, glmnet and random forest models trained on baseline inflammatory protein concentrations accurately predicted individuals with and without V3+21d IFNγ T cell responses **(Fig. 5.12A)**. The glmnet model outperformed the random forest model and the stacked random forest + glmnet models (glmnet auROC = 0.85, random forest = 0.76, stacked = 0.82) **(Fig. 5.12A)**. The final optimised glmnet model only included seven proteins: JCHAIN, SCFB3A2, CCL26, AGRP, CXCL6, CDON and CXCL3 **(Fig. 5.12B&C)**. JCHAIN was the only one of these proteins not also included in the top 50 most important variables of the random forest model, but there was less agreement between variable importance in the models than was observed when predicting anti-RBD Ig immune responses **(Fig. 5.12D&E)**. Thus, compared to the predictors of antibody responsiveness a small number of proteins could accurately predict vaccine-induced T cell immunogenicity, and predictive proteins for each immunogenicity measure were non-overlapping.

5.6.11 The impact of clinical phenotype on immune cell composition determined by spectral flow cytometry

Broad differences in immune cell composition can be inferred using bulk RNA-sequencing data, but RNA-sequencing data cannot accurately resolve differences between cell frequency and cell function. The frequency of cells in peripheral blood has a major impact on the capacity of individuals to respond to vaccine (*206*) and so is likely of importance here. Therefore, I used flow cytometry to quantify the frequencies of immune cells in peripheral blood mononuclear cells from 121 individuals at the pre-vaccine timepoint **(Fig. 5.1C)**. Manual gating and unsupervised hierarchical clustering demonstrated the detection of most major immune cell

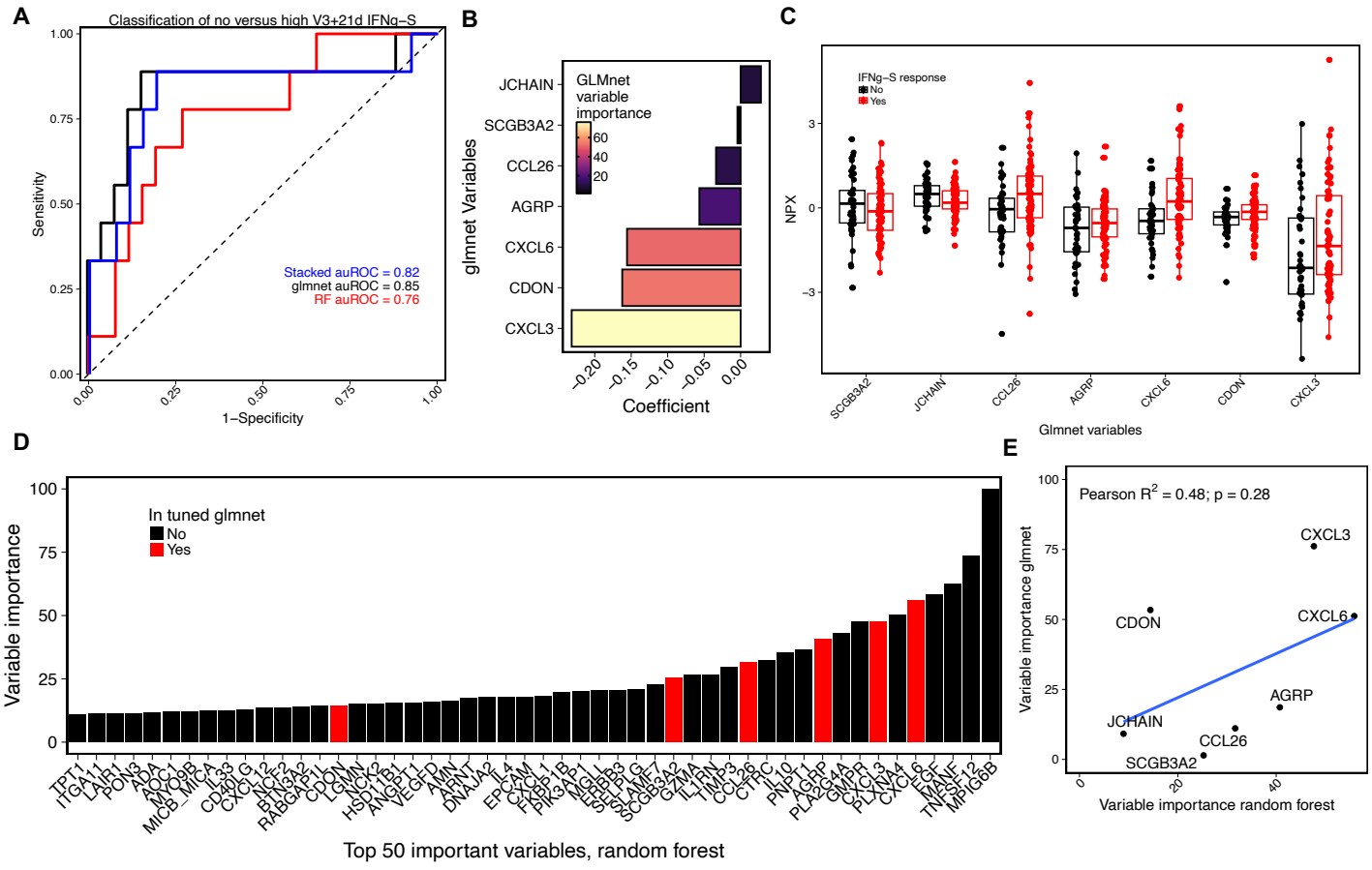

Fig. 5.12 The baseline inflammatory proteome can predict vaccine-induced SARS-CoV-2 spike IFNγ T cell responses

A) Receiver operating characteristic curves of classifier models on test data, trained on baseline Olink data to classify IFNG T cell non-response (< 1 SFC/10^6) versus response.

B) The model coefficient of the variables included in the glmnet classifer model in A.

C) Olink expression values of proteins included in glmnet classifier model in A, stratified by V3+21d IFNG T cell responsiveness.

D) Top 50 variables contributing to the random forest classifier model in C.

E) Correlation of contribution scores in the glmnet and random forest classifier models in C.

populations in PBMC (**Figs. 5.13 & 5.14A&B).**

Whole blood RNA-sequencing is confounded by changes in cell frequency (*206*), therefore I first assessed what proportion of the variation in the bulk transcriptomic data could be attributed to changes in cell frequency in the blood. This analysis is limited by the fact that neutrophil related genes were captured in the whole-blood transcriptomic data, but not in the flow cytometry data of PBMC. 65.6% of variance in expression of the B and plasma cell

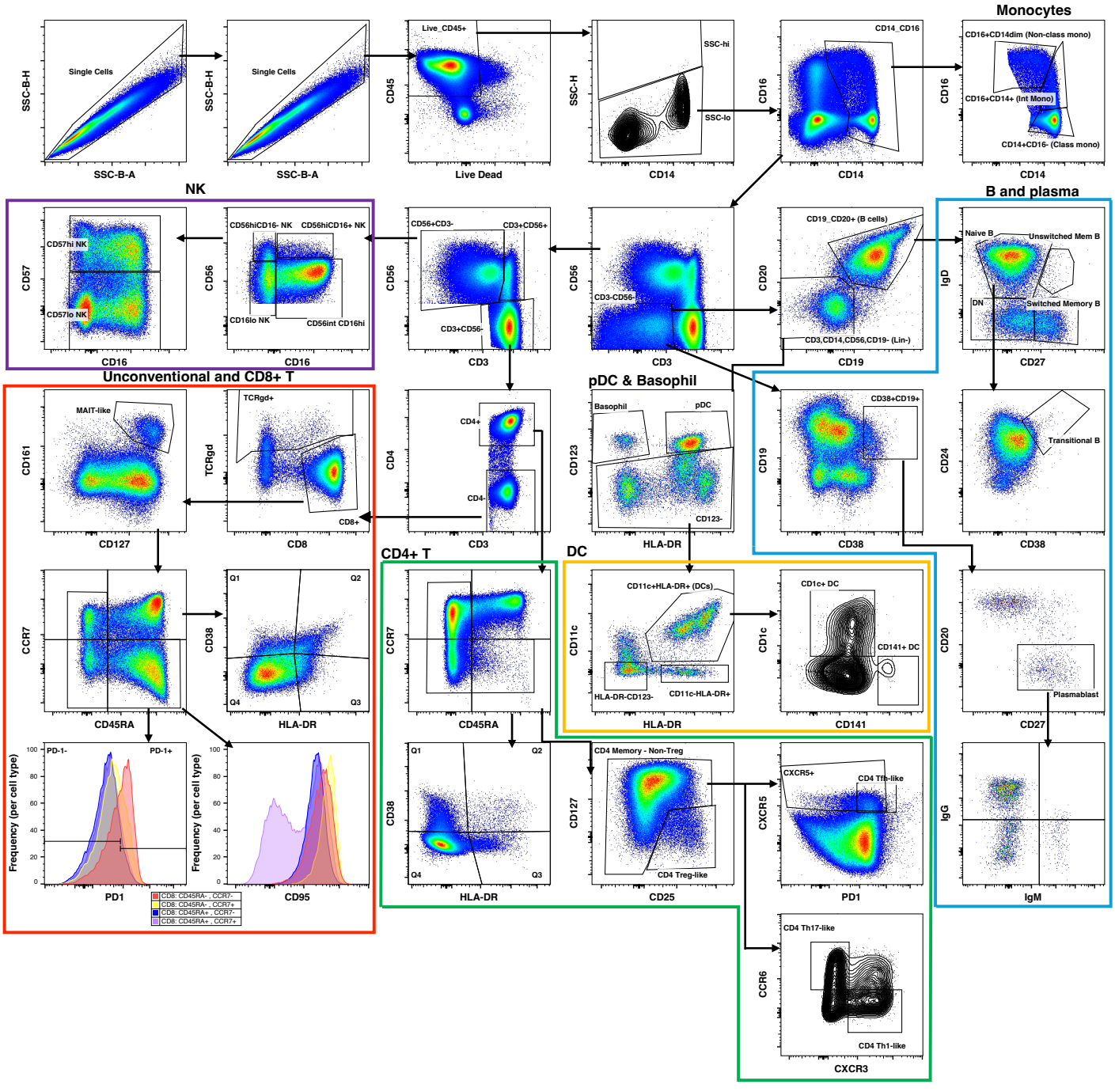

Fig. 5.13 Gating scheme for Cytek Aurora immunophenotyping panel.

geneset module was explained by changes in frequency of B cells, plasma cells and monocytes (**Fig. 5.14C)**. 37% of the variance of expression of the T module and 34% of the innate module was explained by total T and classical monocyte frequencies, respectively (**Fig. 5.14C)**. Variation in NK geneset module expression was partially explained by T and NK cell frequencies, highlighting the overlapping gene expression of these two cell subsets (*388*). All other geneset modules were poorly explained by flow cytometry derived cell frequencies, indicating that these genesets capture information independent of immune cell frequency (**Fig. 5.14C)**.

To understand the effect of clinical phenotypes and immunosuppressive medications on immune cell frequencies, I assessed the relationship between the frequencies of immune cell populations with the clinical phenotype and demographic data (**Fig. 5.14D)**. As the unsupervised approach was unable to resolve unconventional T cell populations and more rare cell subsets without additional sub clustering (such as DC subsets, B cell subsets), I focussed on the manually annotated clusters. Consistent with bulk-RNA sequencing data (**Fig. 5.6B)**, there were significantly reduced B cell frequencies in individuals on anti-CD20 therapies and solid organ transplant recipients on CNI + MMF + corticosteroid, and broad increases in innate cell frequencies across several groups compared to healthy individuals (**Fig. 5.14D)**. The flow cytometry data provided additional resolution into the cell type differences: aCD20 therapy patients had reduced frequencies of all B cells whereas solid organ transplant recipients on CNI + MMF + corticosteroids only had reduced plasmablast frequencies (**Fig. 5.14D)**. Amongst innate cells, classical and nonclassical monocytes were the predominant cell type increased in frequency and dendritic cells were decreased in frequency in several groups compared to HCs (**Fig. 5.14D)**. Interestingly, basophils were increased in frequency in several groups, but particularly in individuals with rheumatic conditions (RA and AAV) (**Fig. 5.14D&E)**. There was also a strong association between increased age and reduced naive CD4 and CD8 T cell frequency and reduced overall frequencies of $CD8^+$ effector and central memory

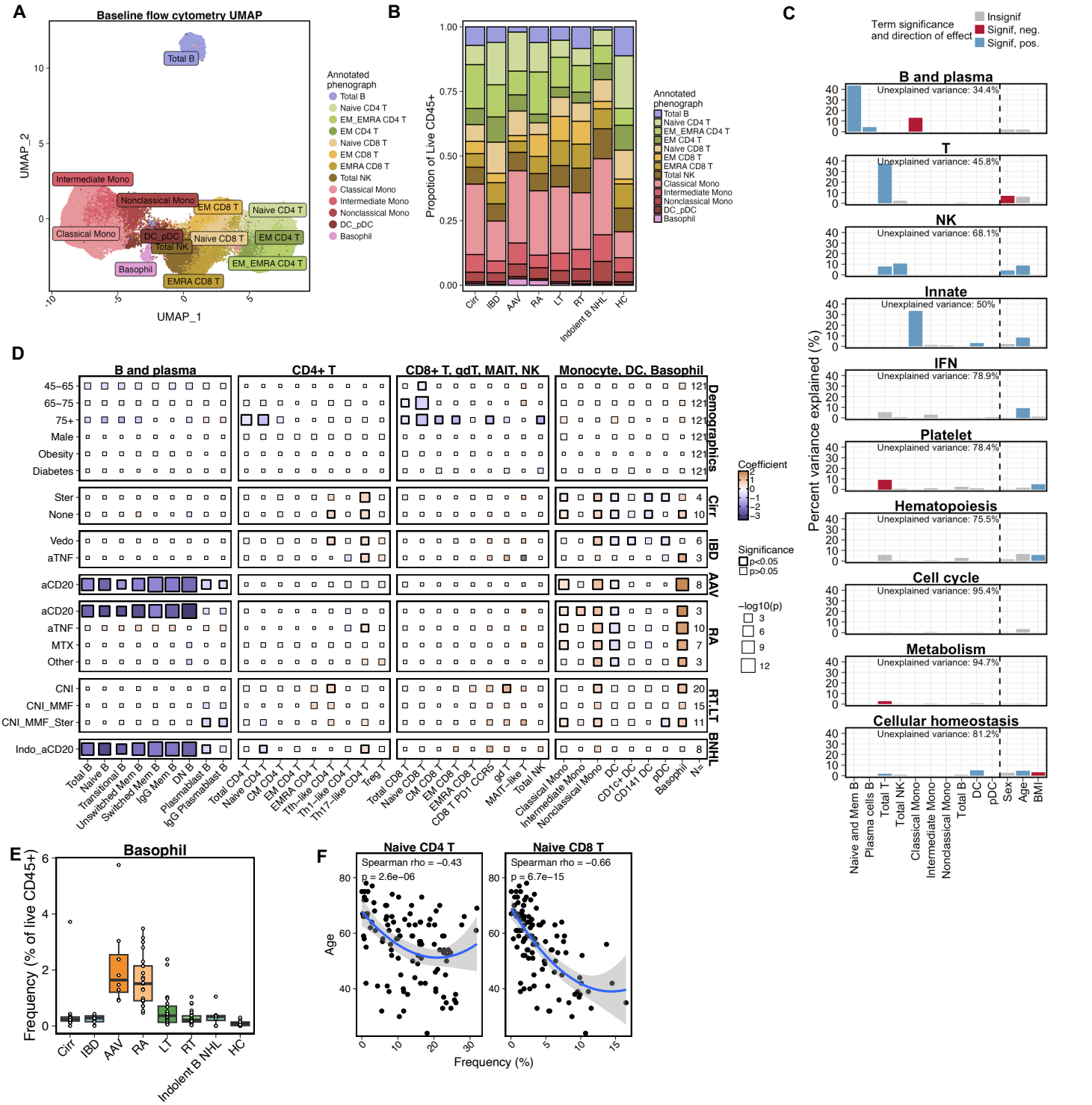

Fig. 5.14 The baseline cellular immunophenotype differs between immunosuppressive groups and healthy individuals

A) Uniform manifold embedding and projection (UMAP) depiction of peripheral blood mononuclear cells from flow cytometric immunophenotyping, coloured by annotated phenograph clustering.

B) Mean immune cell composition (annotated phonograph clusters) of individuals in different immunosuppressive groups and healthy controls.

C) The relative importance of immune cell frequencies to geneset module scores identified using bulk transcriptomic data. Variance explained is the R2 partitioned by averaging over orders (Section 5.5.4). Significance and the coefficient direction is denoted by colour and is calculated using an ANCOVA-like test. Blue denotes significant coefficients which are positively associated with the geneset module of interest, red are negatively associated significant coefficients.

D) Multivariate linear models fit to each manually annotated cell type frequency. Frequencies were $\log_{10}$ transformed with a prior of $1x10^{-3}$. An independent model was fitted for each cell type, with all demographic variables as covariates. Age is compared to individuals 26-45years old, all disease group and immunosuppression combinations are compared to healthy individuals. P values from each model were adjusted using Benjamini-Hochberg false-discovery rate (FDR). Thick lines around a square indicate FDR < 0.05.

E) Frequency of manually annotated basophils

F) Correlation of frequency of naive CD4 and CD8 T cells (of $CD45^+$ $Live^+$ singlets) with subject age.

populations, as previously reported (*389*), which was still observed with healthy individuals removed (**Fig. 5.14F**).

5.6.12 B cell functionality is impaired in liver and renal transplant recipients

Transcriptional signatures related to B cell signalling were clearly linked to vaccine-induced antibody responses across the entire cohort, but there were certain clinical groups where this was not the case (**Fig. 5.8E)**. To assess whether this was due to differences in B cell phenotype - which was not resolvable by bulk-RNA sequencing - I used the flow cytometry data to assess B cell phenotypes across disease groups. Within the entire cohort, baseline B cell subset frequencies were significantly associated with V3+21d anti-RBD Ig titre (**Fig. 5.15A)**. AAV and indolent B NHL patients on aCD20 therapy had the lowest frequencies of B cells and were enriched for naive and transitional B cells, with very low frequencies of memory B cells on average (**Fig. 5.15B).** This was consistent with their low rates of V3+21d anti-RBD Ig responsiveness (**Fig. 5.15B, top).** In contrast, RT and LT recipients, which also had low rates of vaccine responsiveness (**Fig. 5.15B, top),** had B cells of a similar overall frequency and similar phenotype as HC individuals that had high antibody response rates **(Fig. 5.15B).** This indicated that unlike individuals on aCD20 therapy, LT and RT recipients had normal frequencies of B cells but they were still unable to successfully generate antibodies in response to vaccine. In the overall cohort there was a positive correlation between pre-V3 B and plasma cell frequencies with V3+21d anti-RBD Ig (**Fig. 5.15C)**, similar to the trend observed in the bulk RNA-sequencing data (**Fig. 5.8B).** However, the relatively high frequencies of memory B cells and plasmablasts observed in RT and LT was not associated with high anti-RBD Ig titres and there was overall a low correlation between pre-V3 B and plasma cell subset frequencies with V3+21d anti-RBD Ig in these groups (**Fig. 5.15C)**. To assess if the reduced V3+21d anti-RBD Ig in solid organ transplant recipients was due to reduced pre-existing antigen-specific B cells, I assessed the frequencies SARS-CoV-2 S1-specific B cells in pre-vaccination samples of a subset of the cohort using S1-specific

Fig. 5.15 Association of baseline bulk and antigen-specific B cell frequency and phenotype with vaccine-induced antibody response

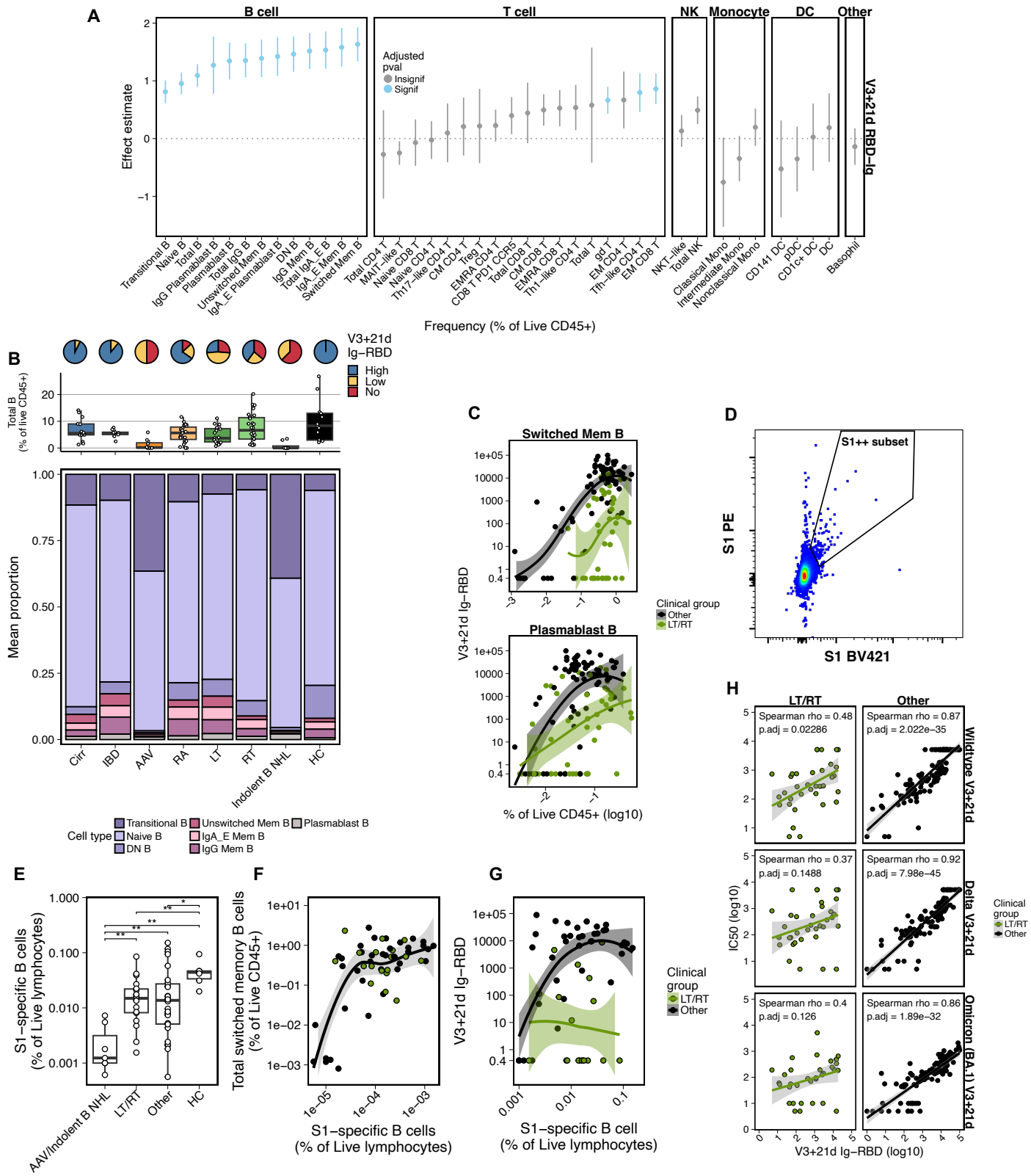

Fig. 5.15 Association of baseline bulk and antigen-specific B cell frequency and phenotype with vaccine-induced antibody response

A) Linear models of log_{10} transformed V3+21d anti- receptor binding domain (RBD) binding antibody (Ig) titres with log_{10} transformed cell frequency (with a $1x10^{-3}$) prior. A model was fitted independently for each cell type with clinical group, age and sex as covariates. Significant geneset terms (Benjamini-Hochberg FDR <0.05) are marked in blue. The point and lines represent the geneset variable coefficient and standard error.

B) The mean proportion of manually annotated B cell subtypes amongst total B and plasma cells per disease group (bottom panel).Total B cell frequency within all live CD45+ singlets is shown (middle panel) and the proportion of individuals with no (<0.8AU/mL) low (0.8-1000AU/mL) and high (>1000AU/mL) V3+21d anti-RBD Ig (top panel).

C) Correlation of pre-vaccination class-switched memory B (top) and plasma cell (bottom) frequencies and V3+21d anti-RBD Ig titres stratified by liver transplant (LT) and renal transplant (RT) versus all other groups.

D) Exemplar flow cytometric gating scheme for SARS-CoV-2 S1 specific B cells.

E) Frequency of pre-vaccine S1-specific B cells as a percentage of live lymphocytes. Mann-Whitney U test with Benjamini- Hochberg false discovery rate. * = FDR < 0.05, ** = FDR <0.01

F) Frequency of pre-vaccine S1-specific B cells and total switched memory B cells with loess regression curve.

G) Frequency of pre-vaccine S1-specific B cells against V3+21d anti-RBD Ig titres

H) Correlation of V3+21d neutralisation 50% inhibitory concentration (IC_{50}) of ancestral SARS-CoV-2 (wildtype), SARS-CoV-2 delta and omicron BA.1 variants with V3+21d anti-RBD Ig titres, stratified by LT/RT versus all else. Healthy controls not included. Bonferroni adjusted P value shown.

B cell "baits" (**Fig. 5.15D)**. The frequency of S1-specific B cells as a proportion of overall lymphocytes was similar in LT and RT recipients compared to the rest of the cohort and significantly increased compared to aCD20 recipients, but lower than HCs (**Fig. 5.15E)**. The relationship between total memory B cell frequency and S1-specific B cells was similar in the LT and RT groups compared to the rest of the cohort (**Fig. 5.15F)**. However, LT and RT recipients with comparatively high pre-existing S1-specific B cell frequencies were unable to produce high titres of antibody in response to vaccine (**Fig. 5.15G)**. Additionally, the neutralising capacity of vaccine-induced anti-RBD Ig was reduced in LT and RT compared to the rest of the cohort: there was only weakly positive or no significant correlation between V3+21d anti-RBD Ig binding titres and neutralising IC_{50} in the RT and LT groups compared with strong positive correlation in the rest of the cohort (**Fig. 5.15H).** Therefore, RT and LT recipients may generate B cells to SARS-CoV-2 vaccine, but they produce reduced quantities of binding Ig with lower neutralising capacity than other immunocompromised patient groups.

5.6.13 The baseline T cell phenotype, assessed using flow cytometry, is associated with disease and vaccine T cell non-responsiveness

I next assessed the relationship of the baseline cellular immunophenotype with T cell responsiveness using flow cytometry. To facilitate detection of T cell features associated with vaccine non-responsiveness, while controlling for differences in T cell phenotype between different diseases I stratified the cohort into four groups: (1) individuals with AAV, who had notably high magnitudes of V3+21d IFNγ-S T cell responses (**Fig. 5.2G)**; (2) LT and RT recipients and cirrhosis patients with no V3+21d IFNγ T cell response; (3) LT and RT recipients with V3+21d IFNγ T cell response and (4) all others (RA, indolent B NHL and IBD). The LT, RT and cirrhosis groups contained all individuals with no V3+21d IFNγ T cell response in the flow cytometry sub cohort and were amongst the clinical groups most enriched for T cell non-responsiveness overall (**Fig. 5.2H)**.

T cell frequencies at baseline were significantly lower in LT, RT and cirrhosis groups compared to other disease groups in the cohort and there was a significant interaction between the LT, RT and cirrhosis group and V3+21d T cell non-responsiveness (**Fig. 5.16A)**. This was largely due to reduced naive T cell frequencies in LT, RT and cirrhosis patients **(Fig. 5.16B&C).** Naive $CD4^+$ T cells were significantly reduced in LT, RT and cirrhosis compared to other groups and further reduced in LT, RT and cirrhosis T cell non-responders regardless of age (**Fig. 5.16B)**. The frequency of naive $CD8^+$ T cells exhibited a similar pattern as the naive $CD4^+$ T cells, but between group comparisons were confounded by age **(Fig. 5.14F)** and there were no significant differences when participant age was adjusted for **(Fig. 5.16C)**. Consistent with this, across the entire cohort increasing age was weakly, but significantly, negatively correlated with V3+21d IFNγ-S **(Fig. 5.16D)**. The decreased overall frequency of naive T cells was associated with altered compositions of naive, central (CM), effector (EM), and effector memory re-expressing CD45RA (EMRA) within $CD4^+$ and $CD8^+$ T cell populations in the LT, RT and cirrhosis groups compared to other groups **(Fig. 5.16E&F).** There were proportionally more $CD4^+$ CM T cells and $CD8^+$ EMRA T cells amongst $CD4^+$ and $CD8^+$ T cell populations

Fig. 5.16 The baseline T cell phenotype is associated with vaccine-induced IFNγ T cell responsiveness

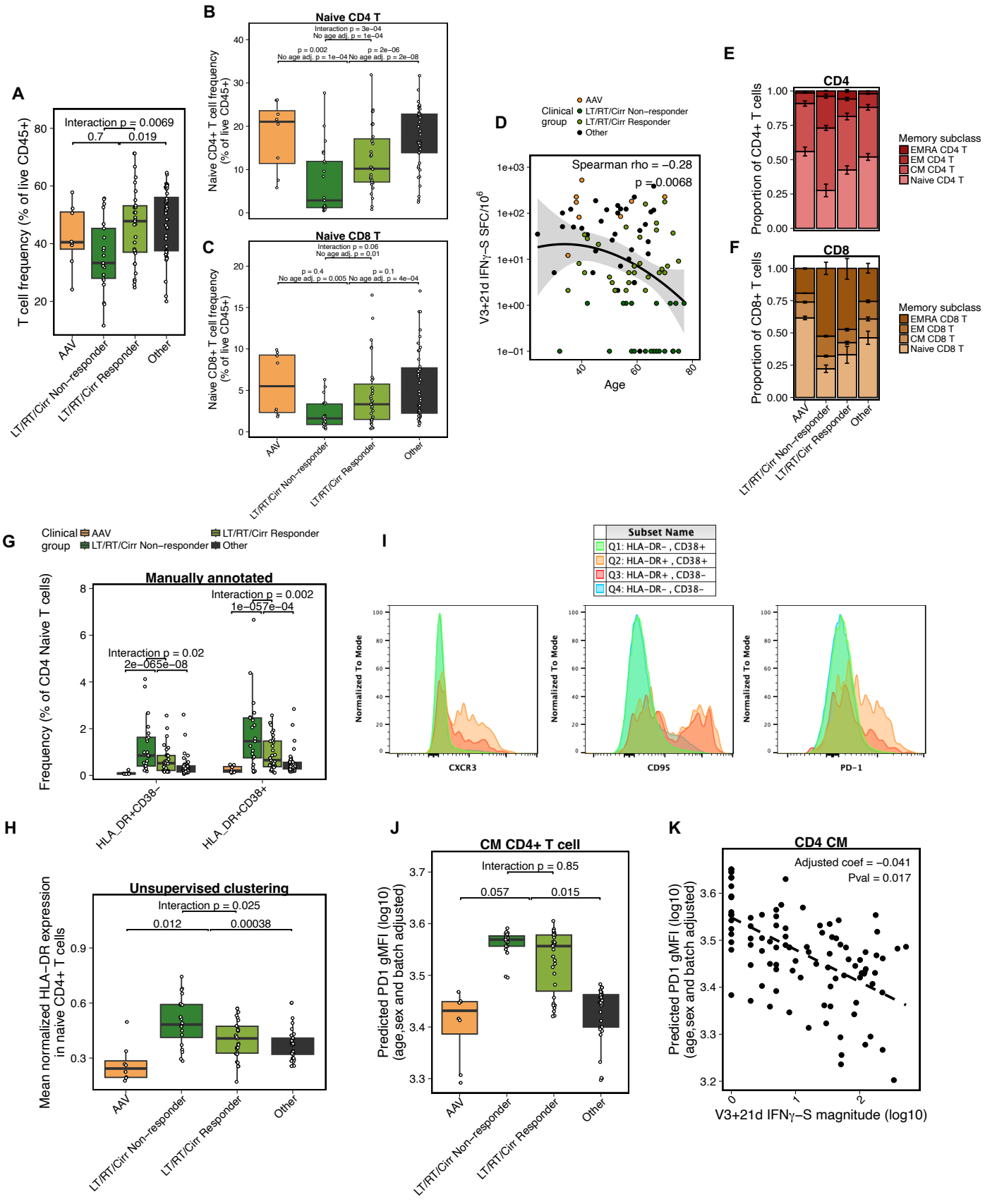

Fig. 5.16 The baseline T cell phenotype is associated with vaccine-induced IFNγ T cell responsiveness

A) Baseline (pre-vaccination) T cell frequencies of live $CD45^+$ singlets. Individuals are grouped into ANCA-associated vasculitis (AAV), liver transplant (LT) and renal transplant (RT) or cirrhosis (Cirr) with or without a V3+21d T cell response (< / > $1SFC/10^6$) and all other participants. All individuals in AAV and other groups were positive for V3+21d T cell responses.

B&C) Baseline naive $CD4^+$ (B) T cell frequencies and $CD8^+$ (C) T cell frequencies, p values provided indicate linear model with or without inclusion of age as a covariable. Grouped as in A.

D) Correlation of V3+21d IFNγ T cell $SFC/10^6$ to SARS-CoV-2 spike and subject age.

E&F) $CD4^+$ (E) and $CD8^+$ (F) T cell memory subclasses grouped as in A. Includes naive, effector memory (EM), central memory (CM) and effector memory re-expressing CD45RA (EMRA) populations. Error bars are standard error.

G) HLA-DR and CD38 cell type frequencies within $CD4^+$ naive T cells. Grouped as in A.

H) Mean normalised HLA-DR expression in naive $CD4^+$ T cells identified by phenograph unsupervised clustering

I) Surface expression histograms of CXCR3, CD95 and PD-1 in each HLA-DR/CD38 $CD4^+$ naive T cell subpopulation.

J) Predicted $\log_{10}$ transformed PD-1 geometric mean fluorescence intensity (gMFI) on central memory $CD4^+$ T cells after adjusting for age, sex and batch.

K) Correlation of predicted $\log_{10}$ transformed PD-1 gMFI on central memory CD4+ T cells (as in J) with V3+21d IFNγ T cell $SFC/10^6$ to SARS-CoV-2 spike

respectively, in individuals in LT, RT and cirrhosis groups - especially LT, RT and cirrhosis T cell non-responders – compared with other groups **(Fig. 5.16E&F)**.

In addition to different T cell memory phenotypes across disease groups and T cell response status, $CD4^+$ T cell activation status at baseline was also altered. There were significantly increased frequencies of HLA-DR^+ $CD38^-$ and HLA-DR^+ $CD38^+$ naive $CD4^+$ T cells in individuals in LT, RT and cirrhosis groups compared with other clinical groups and there was a significant interaction of the LT, RT and cirrhosis group with V3+21d IFNγ-S T cell response status **(Fig. 5.16G)**. A similar pattern was observed when comparing normalised HLA-DR expression within naive $CD4^+$ T cells identified through unsupervised clustering (**Fig. 5.16H)**. The HLA-DR^+ populations were notable for their increased surface expression of CD95, PD-1 and CXCR3, markers related to sensitivity to apoptosis (*390*), exhaustion (*391*), and inflammatory tissue entry (*392*), respectively (**Fig. 5.16I),** compared to HLA-DR^- $CD4^+$ naive T cells. $CD4^+$ CM T cells also exhibited differences in functional surface markers, with significantly increased geometric mean fluorescence intensity (gMFI) of PD-1 expression in LT, RT and cirrhosis groups compared with other groups (**Fig. 5.16J)** in a manner that was negatively correlated with IFNγ-S T cell response magnitude (**Fig. 5.16K)**. Thus, $CD4^+$ naive

T cell maturity and activation (*389*) and CM CD4$^+$ T cell exhaustion phenotypes were altered between groups and with T cell responses status.

5.6.14 Antigen-specific, but not global T cell function is impaired in immunocompromising conditions and vaccine T cell non-responders.

One possible explanation for the reduced T cell response to vaccine in individuals in the renal and LT and cirrhosis groups is that their T cells are hyporesponsive to any stimulus – not only the vaccine, because of immunosuppressive therapies and inflammation (*132*). To test this hypothesis, I used intracellular cytokine staining (ICS) to detect T cell responses in pre-vaccination PBMC after overnight stimulation with anti-CD3, anti-CD28 and anti-CD49d (representative gating in **Fig. S5.1)**. There were no significant differences in the frequency of CD69$^+$ cytokine (IFNγ, IL-2, TNF, IL-4 or IL-17A) or surface activation (CD71 and CD107a) positive T cell subsets between AAV, LT, RT and cirrhosis, or other disease groups (**Fig. 5.17A)**. The only exception was IL-2 in combination with TNF, which was reduced in frequency amongst CD8$^+$ EMRA cells in the LT, RT and cirrhosis groups compared with all the combined group of other (none AAV) disease groups (**Fig. 5.17A)**. Contrary to the aCD3 stimulus, there were significant differences between groups when comparing cytokines and surface markers after overnight stimulation with SARS-CoV-2 spike peptide pools (**Fig. 5.17B).** The T cell phenotype with the largest difference in frequency between groups in response to spike peptide pools was polyfunctional (IFNγ$^+$IL2$^+$TNF$^+$) CD4$^+$ EM T cells, which were significantly reduced in LT, RT and cirrhosis groups compared to AAV or combined non-AAV groups, and were further reduced in LT and RT and cirrhosis V3+21d T cell non-responders (**Fig. 5.17B-D)**. The AAV group also had increased frequencies of CD107a$^+$ CD4$^+$ T cells, including naive and CM subtypes, compared to individuals in LT, RT and cirrhosis groups (**Fig. 5.17B)**. The differences in pre-V3 cytokine production in response to SARS-CoV-2 peptides was consistent with the V3+21d IFNγ ELISpot assay results - SARS-CoV-2 spike responsive IFNγ$^+$IL2$^+$TNF$^+$ CD4$^+$ EM T cells were the pre-vaccine functional T cell type with the strongest correlation with

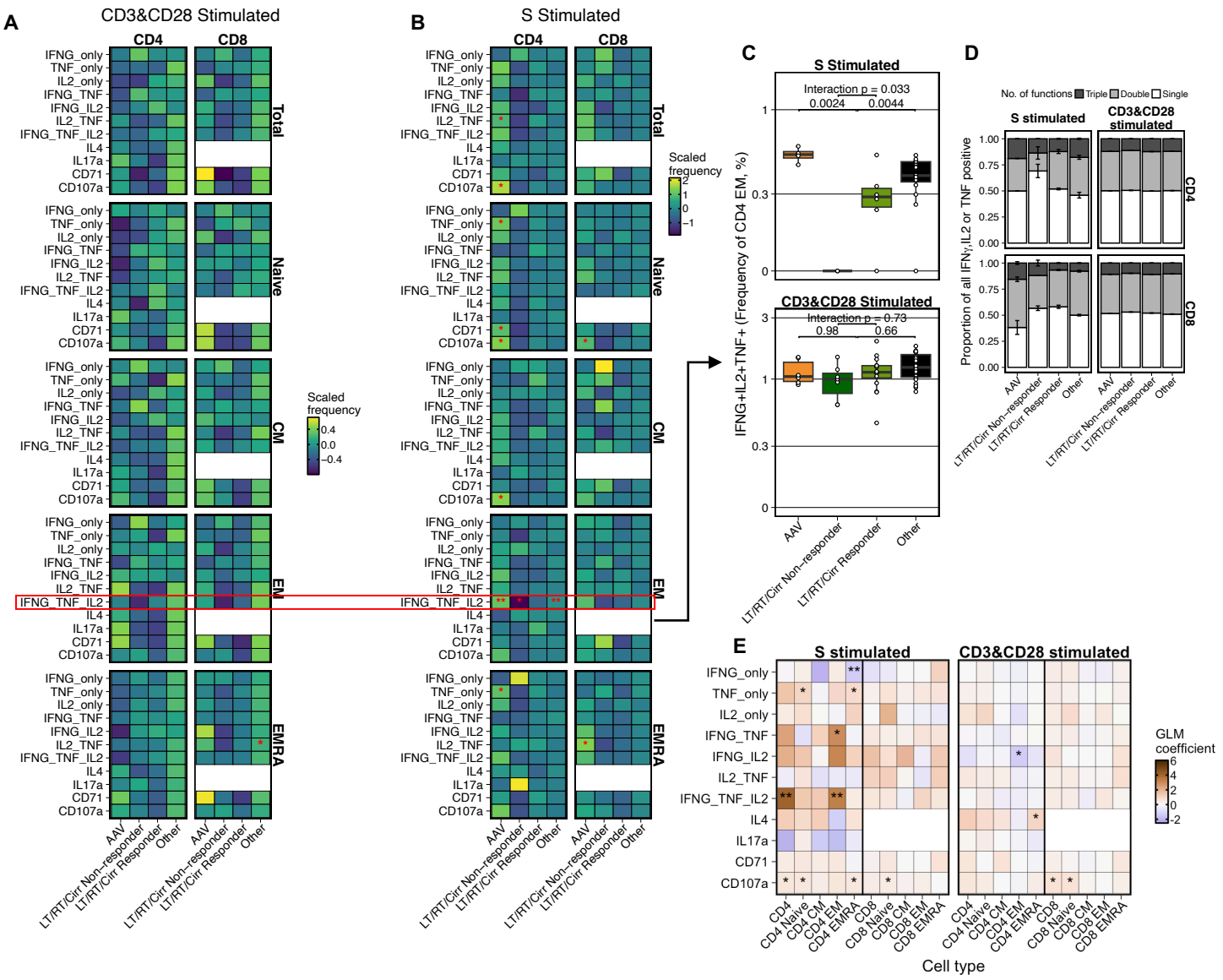

Fig. 5.17 Functionality of pre-vaccination antigen-specific and non-antigen specific T cells

A&B) The mean scaled frequency of cells (scaled percent of live lymphocytes) producing the given cytokine combination within CD4⁺ (left) and CD8⁺ (right) CD69⁺ T cell populations. Cells were stimulated with either anti-CD49d, anti-CD28 and anti-CD3 (A) or anti-CD49d, anti-CD28 and a peptide pool covering the entire SARS-CoV-2 spike protein (B) (Section 2.4.4). Separated into total CD4/CD8⁺ T cells, naive, central memory (CM), effector memory (EM), or effector memory re-expressing CD45RA (EMRA) T cell types. Frequency is scaled for the given cell type/ cytokine function. * or ** in AAV or other column is statistically significantly (Benjamini-Hochberg false discovery rate < 0.05 or <0.01, respectively) different compared to liver or renal transplant (LT/RT) or cirrhosis (Cirr). * in LT/RT/Cirr non-responder group represents significant interaction with V3+21d anti-IFNG T cell responsiveness.

C) Frequency of CD4+ effector memory CD69+IFNG+IL2+TNF+ T cells after overnight stimulation with SARS-CoV-2 spike peptides (top) or anti-CD3 (bottom), plus anti-CD28 and anti-CD49d.

D) The mean proportion of cells producing one, two or three cytokines (out of IFNγ, IL2, or TNF) amongst all CD69⁺IFNG⁺, CD69⁺IL2⁺ or CD69⁺TNF⁺ CD4⁺ (top) or CD8 ⁺ (bottom) T cells. Bars are standard error.

E) Linear models of pre-vaccination $\log_{10}$ transformed (with a prior of 10^{-3}) CD69⁺ cytokine +ve (as in A/B) CD4⁺ and CD8⁺ T cell frequencies with $\log_{10}$ transformed V3+21d IFNγ T cell response, adjusted for age and sex. Frequencies are measured as percentage of live lymphocytes.

V3+21d IFNγ T cell responses (**Fig. 5.17E)**. Thus, individuals in disease groups enriched for vaccine non-responsiveness have T cells with equivalent capacity to respond to non-antigen specific stimulus, suggesting that impairment of the generation or boosting of new antigen-specific responses is the limitation to vaccine-induced responses in these individuals.

5.7 Discussion

In this chapter, I characterised the pre-vaccination immunophenotype across various SIs and HCs. By correlating these profiles with vaccine-induced antibody and T cell responses, I identified immune features linked to vaccine outcomes. Using pre-vaccine transcriptomic data, an unsupervised approach uncovered immune signatures that spanned multiple diseases and was associated with subsequent vaccine immunogenicity. I also derived biologically relevant gene expression modules, reducing data complexity and highlighting disease- and therapy-specific differences. These modules revealed baseline pathways related to vaccine immunogenicity, including B cell- , T cell- , innate- and interferon-related transcriptomic modules. I validated the inflammatory transcriptional signature at the protein level by demonstrating that baseline inflammatory protein signalling was negatively correlated with antibody responses to vaccination. Classification models trained on the baseline inflammatory proteome accurately predicted vaccine immune responsiveness using few protein measurements. Lastly, high-dimensional flow cytometry identified key immune cell populations associated with vaccine responsiveness. This included the relationship of specific B cell subsets with vaccine-induced antibody responsiveness, and association of naive and activated naive T cells with subsequent vaccine-induced T cell response.

5.7.1 Immunophenotyping between clinical groups

Immunosuppressive diseases and therapeutics act to disrupt immune processes through various mechanisms, targets, and intensities of action. In combination with the demographic risk factors for SIs which may impact the immune response independently of disease (such as increasing age), there is a highly heterogenous range of immune phenotypes. Studies of

vaccine immunogenicity illustrate this variation, as both antibody and T cell responses to vaccines vary considerably both between and within broad SIs. In this chapter I used systems approaches to provide a broad view of the impact of various SIs on the immunophenotype.

Unsupervised clustering of the cohort into clusters based only on transcriptomic signatures demonstrated that individuals from different drug/disease groups had similar overall immune signatures. Of note, in the transcriptomic clusters identified, 19 of 21 (90%) healthy individuals appeared in two of four clusters and co-clustered with immunocompromised people that were on average younger and had fewer immunosuppressive therapies and comorbidities, suggesting that these clusters may be associated with immune health. This supports data from a recent compendium of monogenic diseases that suggests signatures of 'immune health' are shared across diseases and can be used to broadly differentiate individuals with disease from healthy individuals (*393*). Unlike this publication however, the work presented here demonstrates the direct association of these transcriptomic signatures with vaccine-induced antibody and T cell responses demonstrating the capacity of the baseline transcriptome to distinguish functionally relevant features of immune health.

Analysis of the inflammatory proteome in plasma from four immunocompromised conditions and healthy individuals revealed both shared and disease-specific immune disruptions. Cirrhosis, LT and RT groups showed broad overexpression of inflammatory proteins compared to HCs, whereas RA patients had comparatively few differentially expressed proteins. The RA cohort was also clearly distinct from cirrhosis, LT and RT groups.

Examining the top differentially expressed proteins in each condition provides insight into these patterns. Fatty acid binding protein 1 (FABP1), highly upregulated in cirrhosis, LT, and RT, is expressed in hepatocytes and kidney tubular cells and is associated with metabolic syndromes and acute kidney injury (*394, 395*). This suggests that liver and kidney dysfunction in these conditions contributes to its elevated expression. In comparison, the top upregulated proteins of RA are all associated with neutrophil and monocyte recruitment in the inflamed

synapse (*396-400*). TNF, which was uniquely upregulated compared to HC in the plasma of RA patients is a central mediator of inflammation in RA (*401*) and as such TNF inhibitors are key anti-rheumatic drugs. TNF is also essential to T cell function (*402*). The paradoxical observation that plasma TNF concentration is increased in individuals on aTNF therapeutics has been demonstrated previously (*403-406*). Proposed mechanisms for this observation suggest that TNF inhibitors may stabilise and increase the half-life of TNF in the plasma of patients, thereby reducing its clearance and increasing concentrations.

Bulk blood transcriptome measurements capture both immune cell frequency and function but cannot distinguish their relative contributions. To address this, I used high-dimensional spectral flow cytometry to analyse immune phenotype and function at the single-cell level. Comparing whole-blood transcriptomic signatures with PBMC cellular frequencies revealed that immune cell frequency explained 19% (NK cells) to 65% (B and plasma cells) of immune-related transcriptomic variation. However, non-immune cell transcriptomic signatures (e.g., IFN, platelet, haematopoiesis, metabolism) were largely independent of immune cell frequencies, highlighting the ability to capture broader biological variation using transcriptomics. Nevertheless, flow cytometry provided additional resolution of cellular phenotypes, identifying group-specific differences not apparent from transcriptomic data alone. For example, while transcriptomic analysis showed reduced B and plasma gene module expression across multiple SIs, flow cytometry revealed that plasma cells were specifically reduced in RT and LT groups, whereas global B cell frequencies were lower in aCD20 therapy. This distinction is difficult to resolve in bulk RNA sequencing, as B and plasma cells share many key transcripts, particularly Ig genes, and while B cells are more abundant, plasma cells are more transcriptionally active (*407*).

Resolution of T cell phenotypes using whole-blood transcriptomics is also challenging due to the relative similarities in transcriptional programmes of different T cell phenotypes. Flow cytometric analysis of bulk T cells demonstrated broad differences in the frequencies of

memory T cell subsets across group, with decreased $CD4^+$ and $CD8^+$ naive T cell frequencies with increasing age, as is expected due to thymic involution (*408*). Within $CD8^+$ T cells, age was the dominant factor associated with reduced naive cell frequency. For $CD4^+$ T cells however, the effect of being within liver, renal and cirrhosis transplant groups – which were all enriched for vaccine T cell non-responsiveness compared to other groups – was larger than that of increasing age. Specifically, within the LT, RT and cirrhosis groups, individuals with the lowest pre-vaccine naive $CD4^+$ T cell frequencies were those that would were unable to go on to generate a T cell response to vaccination irrespective of age. A similar, age dependent, pattern was observed in $CD8^+$ T cells, highlighting the overall importance of a maintained naive T cell compartment to vaccine responsiveness.

Interestingly, there were increased frequencies of HLA-DR^+CD38^- or HLA-DR^+CD38^+ $CD4^+$ naive T cells and an overall increase in HLA-DR expression on naive $CD4^+$ T cells in individuals in the LT, RT and cirrhosis group compared with disease groups not enriched for T cell non-responsiveness. Both HLA-DR and CD38 are considered markers of recent T cell activation on EM T cells, but are not usually associated with naive T cells (*409*). CD38 and HLA-DR expression is significantly increased on naive T cells in settings of acute inflammation (e.g. after influenza and COVID-19 infection) (*389, 409, 410*) due in part to interferon or TNF signalling (*411, 412*). Bystander activation of cells by cytokines (including IL-12, IL-15, IL-18, IFNγ (*311*)) resulted in increased frequencies of $CD38^+$HLA-DR^+CXCR3^+ after COVID-19 infection in a manner positively correlated with increasing age (*413*). This age associated increase in bystander activation is proposed to be due to the increased low-grade inflammation observed with increased age (*413*). It is possible that the increased frequencies of HLA-DR^+ $CD38^+$ naive T cells enriched in T cell non-responders in this work represent bystander activated T cells enriched as a result of the high systemic inflammation observed in individuals in the LT, RT and cirrhosis groups. The upregulation of PD-1 on the surface of the HLA-DR^+ naive CD4 T cells suggests they are less likely to undergo proliferation/expansion following

subsequent stimulus (e.g. vaccination) (*414*). Furthermore, due to its function as a nicotinamide adenine dinucleotide (NAD) hydrolase, upregulation of CD38 on the T cell surface reduces T cell activation capacity by reducing mitochondrial function in the cell (*415*). Further *in vitro* studies of the capacity of the $CD38^+$ $HLA\text{-}DR^+$ naive T cells to directly respond upon antigen stimulation are required to understand their negative association with vaccine-induced T cell responsiveness.

Taken together, these observations suggest a model of reduced vaccine-induced T cell responsiveness due to a reduced pool of possible responding naive T cells through two pathways: firstly, reduced overall frequencies of naive $CD4^+$ T cells due to advancing age which is enhanced by disease/immunosuppression; secondly because of increased frequencies of pre-activated naive T cells that are unresponsive to vaccine, possibly due to increased systemic inflammation.

5.7.2 Predicting vaccine immunogenicity

Much work has been done to identify phenotypic markers, measurable prior to vaccination, that predict vaccine immunogenicity in healthy individuals. There are some limitations to this work however: 1) there is relatively low heterogeneity in the vaccine-induced response in healthy individuals, therefore arbitrary thresholds are used to classify vaccine responsiveness – often with unknown relevance to vaccine efficacy (*207*); 2) in the case of commonly circulating pathogens (such as influenza) pre-existing immunity to the vaccine immunogen variably impacts the vaccine-induced response. Challenges in delineating recalled memory responses from *de novo* vaccine-induced immune responses therefore limit the robustness of conclusions (*369*); 3) large studies to understand mRNA vaccine immunogenicity have not yet been performed; 4) studies in healthy individuals do not give insight into vaccine immunogenicity in populations most at-risk from severe disease due to SIs.

The work in this chapter overcomes these limitations by studying pre- and post- third dose mRNA vaccine in immunocompromised and healthy individuals. In the studied individuals,

there was high heterogeneity in antibody and T cell response following the third vaccine dose – allowing the comparison of extreme differences in vaccine immunogenicity. Even after third vaccine dose, some individuals in the immunocompromised cohort had no antibody or T cell response to vaccine, in comparison to almost 100% of healthy individuals with an antibody response at V3+21d and 99% of healthy individuals generating an antibody response after just two doses of COVID-19 vaccine (**Fig. 3.2B)**. By comparing binding anti-RBD Ig titres with neutralising IC_{50}, I identified a biologically relevant threshold to classify antibody 'low' responders, who generated antibodies to vaccine but at insufficient titres to neutralise omicron BA.1. Vaccine-induced binding Ig titres to SARS-CoV-2 RBD and live SARS-CoV-2 neutralisation, are both strongly associated with vaccine efficacy against symptomatic COVID-19 (*267, 298, 299*). Low magnitudes of T cells and T cell non-responsiveness after vaccination have additionally been associated with severe COVID-19 outcomes in immunocompromised individuals (**Fig. 3.13J)** (*416*). Therefore, features associated with these immunogenicity outcomes are relevant to protection against COVID-19.

We chose to study predictors of vaccine immunogenicity at the pre- third vaccine timepoint for multiple reasons. Practically, sample availability in our immunocompromised cohorts prior to first COVID-19 vaccination was limited due to the relative speed at which COVID-19 vaccines were rolled out in immunocompromised populations compared to how quickly our studies could be set up and samples collected. In contrast, the OCTAVE DUO study was set up early, before third vaccines were nationally recommended. Indeed, preliminary findings of the OCTAVE DUO study were provided as integral evidence to the UK Joint Commission on Vaccination and Immunisation (JCVI) for the recommendation of national deployment of a third vaccine dose in immunocompromised individuals. In studies aiming to identify baseline predictors of influenza vaccine response, the outcomes are confounded by pre-existing immunity to circulating influenza virus (*204, 206, 207, 369*). However, because the OCTAVE DUO study only included individuals with low or no antibody response after two doses of

COVID-19 vaccine, the effect of pre-existing immunity was largely mitigated, despite this study identifying predictors of responsiveness to a third vaccine dose. Furthermore, the majority of (75%) of individuals in this study had two doses of ChAdOx1 nCoV-19 vaccine and no evidence of previous COVID-19 infection, ensuring uniform past exposure across most of the cohort. All participants included in this study were sampled at least six months after their previous COVID-19 vaccine dose. Since most vaccine-induced transcriptional changes in blood become undetectable 28–70 days post-vaccination (*208, 369*), this interval was sufficient to reflect the 'resting' pre-vaccine immunophenotype. Notably, there is temporal variation in the resting phenotype, which can be resolved by sampling multiple pre-vaccine timepoints (*369*) – however this was impracticable in this study and temporal variation represents only a small amount of the overall variation in the baseline transcriptome (*369, 393*).

5.7.3 Predictors of immunogenicity in immunocompromised individuals

Within the entire cohort, the transcriptomic analysis identified a strong positive association between B and plasma module expression and V3+21d anti-RBD Ig titres, up to a plateau above which anti-RBD Ig titres no longer increased. This was consistent with flow cytometry data which identified a similar pattern of B and plasma cell/plasmablast frequencies and V3+21d anti-RBD Ig titres. However, when studied within immunosuppressive groups, the pattern was only observed in groups that included recipients of aCD20 therapy - suggesting that low B cell frequency limits vaccine-induced antibody responses only up to a certain threshold, consistent with other studies in healthy individuals with different vaccines (*212, 367*).

In transplant recipients, low antibody titres despite high B cell frequency suggests impaired B cell function, rather than frequency. Baseline antigen-specific B cell frequency was also equivalent in transplant recipients compared to other groups in the cohort but had a less strong association with vaccine-induced anti-RBD Ig responses. The anti-RBD Ig response induced

in LT and RT groups also had lower neutralisation potency compared to the rest of the cohort. This is in line with reports of reduced class-switching in antigen-specific B cells in LT and RT in response to COVID-19 vaccination (*417*) and impaired GC functionality in the lymph nodes of RT recipients (*279*). Further assessment of the BCR sequences and gene expression of antigen-specific B cells using single-cell RNA-sequencing is required to give further insight into the impaired B cell function of transplant recipients **(Chapter 6).**

In individuals with liver diseases (cirrhosis and LT), IFN module expression was significantly negatively correlated with B and plasma cell expression and anti-RBD Ig titre indicating that increasing inflammation may be important in reduced vaccine-responsiveness in these individuals. Concordantly, Olink proteomics identified that low/no V3+21d anti-RBD Ig response was associated with increased baseline systemic inflammation, including proteins associated with interferon signalling (IL-15, IFNγ, CXCL9, CXCL10). Interestingly, a study in healthy individuals identified that increased IFNγ and IL-15 expression at day 1 *after* vaccination was associated with increased antibody responsiveness to mRNA vaccines (*223*). This suggests that a pre-activated immune state is negatively associated with vaccine responsiveness in immunocompromised individuals. IFNγ and IL-15 can alter or inhibit B cell differentiation (*418, 419*), reduce B cell frequencies (*420*) and skew class-switch recombination away from an IgG1 sub-type which are the predominant subclass required to neutralising SARS-CoV-2 (*421, 422*). Importantly, both IFNγ and IL-15 were variables selected in a model of 11 proteins with high predictive efficacy (auROC of 0.83) at classifying no/low compared with high vaccine responses – suggesting that these are important biomarkers of the vaccine-induced antibody response.

The baseline protein with the highest positive predictive capacity for vaccine responsiveness was CD22. CD22 is a surface protein expressed on mature B cells and the concentration of soluble CD22 in plasma can be used as a diagnostic tool for leukaemia (*423*). CD22 is required for the proper formation of germinal centres and memory B cells (*424*), and so it is plausible

that the measurement of soluble CD22 is an indirect measure for this process. Interestingly, lymphotoxin-α (LTA) – also positively predictive of vaccine-induced antibody responses – is similarly involved in germinal centre formation through maintenance of follicular dendritic cells (*425*). Considering the strong predictive capacity for soluble CD22 and that it can easily be measured in blood, this is a promising candidate for baseline prediction of vaccine-induced antibody responsiveness. Validation of the predictive capacity of the protein signatures identified here in external cohorts is required to prove its robustness in other cohorts/SI conditions.

5.7.4 Limitations

There are several limitations to this chapter. Firstly, the HCs included are not age or sex matched to the rest of the cohort and instead represent 'optimal' immune response controls. Because of this, deconvoluting the specific contributions of age compared with immunocompromising conditions to the observations is challenging. However, age and sex were included as covariates in all analyses and comparisons between disease groups, rather than against HCs, provides insight into the effect of specific immunocompromising conditions on outcomes while better controlling for age.

Second, not all immunophenotyping methods were used on all patients in the cohort. For flow cytometry, a minimum of eight individuals per disease group were randomly selected from the group of individuals that had bulk RNA-sequencing data available. For the ICS analysis, only individuals with enough cells left after performing the immunophenotyping panel were included – biasing sampling toward those without lymphopenia. HC individuals were recruited in a separate cohort and did not have comparable IFNγ ELISpot immunogenicity data at the pre-V3 or V3+21d timepoint. Finally, absolute frequencies of immune cells were not captured.

5.8 Conclusions

In conclusion, the pre-vaccination transcriptomic, proteomic and cellular phenotype can be used to identify differences between SIs which are associated with mRNA COVID-19 vaccine-

induced antibody and T cell responses. Functionally impaired or low B cell frequencies and increased systemic inflammation, measured prior to vaccination, are associated with low or no antibody response to subsequent COVID-19 vaccine. Low frequencies of naive T cells, and increased frequencies of activated naive T cells, was associated with reduced IFNγ T cell responsiveness to subsequent vaccination.

5.9 Tables

Table 5.1 Demographic and clinical information for individuals included in chapter 5

	Cirr N = 20[1]	IBD N = 13[1]	AAV N = 15[1]	RA N = 49[1]	LT N = 27[1]	RT N = 37[1]	PID N = 18[1]	HSCT N = 14[1]	Aggr B NHL N = 11[1]	Indo B NHL N = 16[1]	HC N = 24[1]	Overall N = 244[1]
Sex												
Female	12 (60%)	2 (15%)	7 (47%)	42 (86%)	7 (26%)	9 (24%)	11 (61%)	6 (43%)	6 (55%)	3 (19%)	21 (88%)	126 (52%)
Male	8 (40%)	11 (85%)	8 (53%)	7 (14%)	20 (74%)	28 (76%)	7 (39%)	8 (57%)	5 (45%)	13 (81%)	3 (13%)	118 (48%)
Age	62 (51, 69)	43 (33, 51)	56 (39, 71)	58 (50, 64)	63 (54, 68)	59 (50, 67)	62 (43, 68)	55 (50, 70)	74 (60, 77)	70 (54, 76)	33 (26, 44)	58 (44, 67)
Ethnicity												
Asian	0 (0%)	1 (7.7%)	0 (0%)	0 (0%)	1 (3.7%)	8 (22%)	0 (0%)	1 (7.1%)	0 (0%)	1 (6.3%)	2 (8.3%)	14 (5.8%)
Black	0 (0%)	0 (0%)	0 (0%)	0 (0%)	1 (3.7%)	3 (8.1%)	0 (0%)	0 (0%)	0 (0%)	0 (0%)	0 (0%)	4 (1.7%)
Mixed race	0 (0%)	1 (7.7%)	0 (0%)	0 (0%)	0 (0%)	0 (0%)	0 (0%)	0 (0%)	0 (0%)	0 (0%)	0 (0%)	1 (0.4%)
Other	0 (0%)	0 (0%)	0 (0%)	2 (4.3%)	0 (0%)	2 (5.4%)	1 (5.6%)	1 (7.1%)	1 (9.1%)	0 (0%)	0 (0%)	7 (2.9%)
White	20 (100%)	11 (85%)	13 (100%)	45 (96%)	25 (93%)	24 (65%)	17 (94%)	12 (86%)	10 (91%)	15 (94%)	22 (92%)	214 (89%)
Unknown	0	0	2	2	0	0	0	0	0	0	0	4
BMI	30.2 (26.4, 32.5)	24.4 (21.0, 28.4)	32.3 (26.7, 37.6)	25.5 (24.1, 32.5)	26.5 (23.3, 32.2)	26.4 (25.0, 30.0)	24.5 (23.8, 28.4)	26.3 (24.3, 27.4)	27.0 (24.1, 30.1)	27.2 (25.3, 28.9)	24.2 (20.6, 26.0)	26.5 (24.2, 30.4)
Unknown	0	0	0	1	0	7	5	2	0	0	0	15
WHO Performance status												
0	12 (60%)	11 (92%)	6 (40%)	14 (29%)	18 (67%)	20 (67%)	14 (82%)	6 (50%)	9 (82%)	11 (69%)	24 (100%)	145 (62%)
1	2 (10%)	1 (8.3%)	7 (47%)	19 (39%)	8 (30%)	9 (30%)	2 (12%)	5 (42%)	2 (18%)	3 (19%)	0 (0%)	58 (25%)
2	5 (25%)	0 (0%)	1 (6.7%)	12 (24%)	1 (3.7%)	1 (3.3%)	1 (5.9%)	1 (8.3%)	0 (0%)	2 (13%)	0 (0%)	24 (10%)
3	1 (5.0%)	0 (0%)	1 (6.7%)	4 (8.2%)	0 (0%)	0 (0%)	0 (0%)	0 (0%)	0 (0%)	0 (0%)	0 (0%)	6 (2.6%)
Unknown	0	1	0	0	0	7	1	2	0	0	0	11
Smoking status												
Currently	4 (20%)	1 (7.7%)	2 (15%)	8 (16%)	1 (3.7%)	0 (0%)	0 (0%)	0 (0%)	1 (11%)	0 (0%)	0 (0%)	17 (8.3%)
Previously	5 (25%)	3 (23%)	4 (31%)	16 (33%)	10 (37%)	3 (21%)	6 (33%)	3 (43%)	3 (33%)	7 (58%)	3 (13%)	63 (31%)
Never	11 (55%)	9 (69%)	7 (54%)	25 (51%)	16 (59%)	11 (79%)	12 (67%)	4 (57%)	5 (56%)	5 (42%)	21 (88%)	126 (61%)
Unknown	0	0	2	0	0	23	0	7	2	4	0	38
Comorbidities												
CVD	2 (10%)	0 (0%)	3 (20%)	4 (8.3%)	2 (7.4%)	14 (38%)	1 (6.3%)	0 (0%)	4 (36%)	4 (25%)	0 (0%)	34 (14%)
Stroke	0 (0%)	0 (0%)	1 (7.1%)	3 (6.3%)	1 (3.7%)	2 (5.4%)	0 (0%)	0 (0%)	3 (27%)	0 (0%)	0 (0%)	10 (4.2%)
Diabetes	11 (55%)	0 (0%)	3 (20%)	6 (13%)	11 (41%)	16 (43%)	1 (6.3%)	3 (21%)	2 (18%)	2 (13%)	0 (0%)	55 (23%)
Type 1	0 (0%)	0 (NA%)	0 (0%)	2 (33%)	0 (0%)	2 (13%)	0 (0%)	2 (67%)	0 (0%)	0 (0%)	0 (0%)	6 (11%)
Type 2	11 (100%)	0 (NA%)	2 (100%)	4 (67%)	10 (100%)	11 (69%)	1 (100%)	1 (33%)	2 (100%)	2 (100%)	0 (0%)	44 (83%)
Asthma	3 (15%)	1 (7.7%)	1 (6.7%)	6 (13%)	1 (3.7%)	1 (2.7%)	5 (31%)	3 (21%)	0 (0%)	0 (0%)	2 (9.1%)	23 (9.6%)
COPD	0 (0%)	0 (0%)	0 (0%)	1 (2.1%)	1 (3.7%)	1 (2.7%)	0 (0%)	0 (0%)	0 (0%)	0 (0%)	1 (4.2%)	4 (1.7%)
Hypertension	11 (55%)	0 (0%)	6 (40%)	10 (21%)	8 (30%)	34 (92%)	4 (25%)	2 (14%)	2 (18%)	4 (25%)	1 (4.2%)	82 (34%)
Unknown	0	0	0	1	0	0	2	0	0	0	0	3
Number of comorbidities												
0	3 (15%)	10 (77%)	3 (20%)	16 (33%)	5 (19%)	1 (2.7%)	6 (33%)	2 (14%)	4 (36%)	4 (25%)	18 (75%)	72 (30%)
1	5 (25%)	3 (23%)	4 (27%)	20 (41%)	9 (33%)	13 (35%)	5 (28%)	4 (29%)	2 (18%)	5 (31%)	6 (25%)	76 (31%)
2	5 (25%)	0 (0%)	6 (40%)	8 (16%)	7 (26%)	7 (19%)	1 (5.6%)	4 (29%)	3 (27%)	7 (44%)	0 (0%)	48 (20%)
3	3 (15%)	0 (0%)	2 (13%)	3 (6.1%)	3 (11%)	13 (35%)	3 (17%)	3 (21%)	2 (18%)	0 (0%)	0 (0%)	32 (13%)
4	3 (15%)	0 (0%)	0 (0%)	2 (4.1%)	3 (11%)	2 (5.4%)	1 (5.6%)	0 (0%)	0 (0%)	0 (0%)	0 (0%)	11 (4.5%)
5	1 (5.0%)	0 (0%)	0 (0%)	0 (0%)	0 (0%)	1 (2.7%)	2 (11%)	1 (7.1%)	0 (0%)	0 (0%)	0 (0%)	5 (2.0%)
Prior vaccine type												
AZD1222	18 (90%)	13 (100%)	15 (100%)	45 (92%)	24 (89%)	21 (57%)	12 (67%)	7 (50%)	4 (36%)	9 (56%)	0 (0%)	168 (69%)
BNT162b2	2 (10%)	0 (0%)	0 (0%)	4 (8.2%)	3 (11%)	16 (43%)	6 (33%)	7 (50%)	7 (64%)	7 (44%)	23 (96%)	75 (31%)
mRNA-1273	0 (0%)	0 (0%)	0 (0%)	0 (0%)	0 (0%)	0 (0%)	0 (0%)	0 (0%)	0 (0%)	0 (0%)	1 (4.2%)	1 (0.4%)
V2+28d antibody response status												
High	0 (0%)	0 (0%)	0 (0%)	0 (0%)	0 (0%)	0 (0%)	0 (0%)	0 (0%)	0 (0%)	0 (0%)	24 (100%)	24 (9.8%)
Low	19 (95%)	13 (100%)	4 (27%)	33 (67%)	13 (48%)	4 (11%)	5 (28%)	9 (64%)	2 (18%)	2 (13%)	0 (0%)	104 (43%)
None	1 (5.0%)	0 (0%)	11 (73%)	16 (33%)	14 (52%)	33 (89%)	13 (72%)	5 (36%)	9 (82%)	14 (88%)	0 (0%)	116 (48%)
V3 vaccine type												
BNT162b2	10 (50%)	6 (46%)	8 (53%)	26 (53%)	13 (48%)	20 (54%)	11 (61%)	7 (50%)	6 (55%)	6 (38%)	21 (88%)	134 (55%)
mRNA-1273	10 (50%)	7 (54%)	7 (47%)	23 (47%)	14 (52%)	17 (46%)	7 (39%)	7 (50%)	5 (45%)	7 (44%)	3 (13%)	107 (44%)
Immunosuppressive therapy												
MMF	1 (5.0%)	0 (0%)	1 (6.7%)	0 (0%)	13 (48%)	25 (68%)	2 (11%)	0 (0%)	0 (0%)	0 (0%)	0 (0%)	42 (17%)
CNI	2 (10%)	0 (0%)	0 (0%)	0 (0%)	25 (93%)	34 (92%)	0 (0%)	3 (21%)	0 (0%)	0 (0%)	0 (0%)	64 (26%)
Anti-CD20	0 (0%)	0 (0%)	12 (80%)	11 (22%)	0 (0%)	0 (0%)	0 (0%)	2 (14%)	6 (55%)	11 (69%)	0 (0%)	42 (17%)
Anti-TNF	0 (0%)	6 (46%)	0 (0%)	18 (37%)	0 (0%)	0 (0%)	0 (0%)	0 (0%)	0 (0%)	0 (0%)	0 (0%)	24 (9.8%)
Methotrexate	0 (0%)	0 (0%)	0 (0%)	29 (59%)	0 (0%)	0 (0%)	0 (0%)	0 (0%)	0 (0%)	0 (0%)	0 (0%)	29 (12%)
DMARD	0 (0%)	0 (0%)	0 (0%)	18 (37%)	0 (0%)	0 (0%)	0 (0%)	0 (0%)	0 (0%)	0 (0%)	0 (0%)	18 (7.4%)
Corticosteroid	5 (25%)	1 (7.7%)	10 (67%)	6 (12%)	10 (37%)	21 (57%)	0 (0%)	6 (43%)	0 (0%)	1 (6.3%)	0 (0%)	60 (25%)
Azathioprine	2 (10%)	2 (15%)	0 (0%)	0 (0%)	3 (11%)	1 (2.7%)	1 (5.6%)	0 (0%)	0 (0%)	0 (0%)	0 (0%)	9 (3.7%)
Vedolizumab	0 (0%)	5 (38%)	0 (0%)	0 (0%)	0 (0%)	0 (0%)	0 (0%)	0 (0%)	0 (0%)	0 (0%)	0 (0%)	5 (2.0%)
Ig therapy	0 (0%)	0 (0%)	0 (0%)	0 (0%)	0 (0%)	0 (0%)	15 (83%)	0 (0%)	0 (0%)	0 (0%)	0 (0%)	15 (6.1%)
Number of immunosuppressive therapeutics												
1	1 (5.0%)	9 (69%)	7 (47%)	20 (41%)	6 (22%)	8 (22%)	13 (72%)	2 (14%)	6 (55%)	10 (63%)	0 (0%)	82 (34%)
2	3 (15%)	3 (23%)	8 (53%)	15 (31%)	18 (67%)	14 (38%)	3 (17%)	4 (29%)	0 (0%)	0 (0%)	0 (0%)	68 (28%)
3	1 (5.0%)	0 (0%)	0 (0%)	7 (14%)	3 (11%)	15 (41%)	1 (5.6%)	1 (7.1%)	0 (0%)	1 (6.3%)	0 (0%)	29 (12%)
4	0 (0%)	0 (0%)	0 (0%)	3 (6.1%)	0 (0%)	0 (0%)	0 (0%)	0 (0%)	0 (0%)	0 (0%)	0 (0%)	3 (1.2%)

[1]n (%); Median (Q1, Q3)

Table 5.2 Proteins included in the Olink Inflammatory I panel

UniProt ID	Gene name	UniProt ID	Gene name	UniProt ID	Gene name	UniProt ID	Gene name
P60568	IL2	P10144	GZMB	Q06520	SULT2A1	P55773	CCL23
Q13651	IL10RA	P24001	IL32	O60575	SPINK4	Q14116	IL18
Q13219	PAPPA	P42702	LIFR	Q9Y5A7	NUB1	P13236	CCL4
Q9UHF4	IL20RA	Q9UIB8	CD84	O60542	PSPN	Q08334	IL10RB
P63241	EIF5A	P20340	RAB6A	P30838	ALDH3A1	P02778	CXCL10
P05412	JUN	Q8WXI8	CLEC4D	O43521-2	BCL2L11	P01133	EGF
Q96AX2	RAB37	P10147	CCL3	O60880	SH2D1A	O75462	CRLF1
P05112	IL4	P50591	TNFSF10	Q12778	FOXO1	P18510	IL1RN
P01584	IL1B	O15455	TLR3	Q7L8A9	VASH1	Q9NZV1	CRIM1
O95760	IL33	P80162	CXCL6	P55957	BID	O14836	TNFRSF13B
Q8NHJ6	LILRB4	Q08174	PCDH1	Q6UB28	METAP1D	Q9BY76	ANGPTL4
P35225	IL13	P37235	HPCAL1	P01903	HLA-DRA	O76096	CST7
P22301	IL10	P29965	CD40LG	Q92609	TBC1D5	P21860	ERBB3
P27540	ARNT	Q07065	CKAP4	P01588	EPO	Q99435	NELL2
O95379	TNFAIP8	P68106	FKBP1B	P80098	CCL7	P55145	MANF
Q8WV07	LTO1	P22304	IDS	Q9UN19	DAPP1	Q14210	LY6D
O43707	ACTN4	O00273	DFFA	Q9UNE0	EDAR	P29279	CCN2
P28838	LAP3	P01137	TGFB1	Q9C035	TRIM5	Q9HC38	GLOD4
Q9NP70	AMBN	Q6UXB2	CXCL17	Q8N608	DPP10	Q99685	MGLL
Q6UXK5	LRRN1	Q9Y266	NUDC	P23229	ITGA6	Q8NFT8	DNER
Q9HCU5	PREB	O43508	TNFSF12	Q6DN72	FCRL6	Q7KYR7	BTN2A1
Q13007	IL24	Q04637	EIF4G1	P33241	LSP1	P34896	SHMT1
Q9UPV0	CEP164	P35613	BSG	Q9UNK0	STX8	O95750	FGF19
O60934	NBN	O60884	DNAJA2	P13747	HLA-E	P19256	CD58
Q96P31	FCRL3	Q9BZW8	CD244	P19474	TRIM21	P29350	PTPN6
Q9Y478	PRKAB1	Q12918	KLRB1	O75475	PSIP1	P0DMV8	HSPA1A
Q8TCS8	PNPT1	P50452	SERPINB8	P13232	IL7	P09603	CSF1
Q5T4W7	ARTN	P10145	CXCL8	Q8IVG5	SAMD9L	O43291	SPINT2
Q5R372	RABGAP1L	Q13241	KLRD1	Q96LC7	SIGLEC10	P12532	CKMT1A_CKMT1B
Q969V3	NCLN	Q14005	IL16	B1AKI9	ISM1	Q9Y3D6	FIS1
Q8N6P7	IL22RA1	O94856	NFASC	Q6ZMH5	SLC39A5	Q96PL1	SCGB3A2
P14784	IL2RB	P40259	CD79B	P78410	BTN3A2	P25942	CD40
Q13459	MYO9B	Q9BXN2	CLEC7A	P12872	MLN	Q99983	OMD
P19801	AOC1	P20273	CD22	Q12765	SCRN1	Q9UKU9	ANGPTL2
Q9NYY1	IL20	Q9UQV4	LAMP3	P58294	PROK1	P22466	GAL
P57771	RGS8	Q96LA5	FCRL2	Q9Y6K9	IKBKG	Q8WXD2	SCG3
P20809	IL11	O43561	LAT	O95644	NFATC1	Q9NR12	PDLIM7
Q96PD4	IL17F	P36959	GMPR	Q9Y258	CCL26	Q9H3U7	SMOC2
O76038	SCGN	Q15661	TPSAB1	Q8WTT0	CLEC4C	Q9NZC2	TREM2
O95715	CXCL14	Q96SB3	PPP1R9B	Q3KPI0	CEACAM21	Q8WU39	MZB1
Q03426	MVK	P30044	PRDX5	Q9BT73	PSMG3	O75888	TNFSF13
O14904	WNT9A	P00813	ADA	P20849	COL9A1	Q9Y6N7	ROBO1
P26951	IL3RA	Q9Y6Q6	TNFRSF11A	Q9HD26	GOPC	O00300	TNFRSF11B
Q9Y3P8	SIT1	O95971	CD160	P52564	MAP2K6	Q9UJA9	ENPP5
Q96DB9	FXYD5	P14317	HCLS1	Q9H0P0	NT5C3A	Q6GTX8	LAIR1
P48061	CXCL12	P30203	CD6	Q9NZN5	ARHGEF12	Q5KU26	COLEC12
Q99748	NRTN	P15692	VEGFA	P42575	CASP2	O00241	SIRPB1
Q13574	DGKZ	O75077	ADAM23	Q9UHC6	CNTNAP2	Q15389	ANGPT1
Q9Y2J8	PADI2	Q13478	IL18R1	P45984	MAPK9	P01127	PDGFB
Q04759	PRKCQ	P43489	TNFRSF4	P11274	BCR	P46109	CRKL
Q16552	IL17A	P02745	C1QA	Q9UDT6	CLIP2	P16422	EPCAM
Q12968	NFATC3	Q99616	CCL13	Q14242	SELPLG	O43598	DNPH1
Q14435	GALNT3	P14210	HGF	P78310	CXADR	Q92583	CCL17
P05113	IL5	Q12866	MERTK	P40933	IL15	Q96KG7	MEGF10
P01375	TNF	O00253	AGRP	P05231	IL6	P24387	CRHBP
Q92844	TANK	P43234	CTSO	P24071	FCAR	P56470	LGALS4
O43597	SPRY2	P49771	FLT3LG	Q01151	CD83	Q9H008	LHPP
P13693	TPT1	O43915	VEGFD	O76036	NCR1	O14773	TPP1
Q9P0M4	IL17C	P12544	GZMA	P19878	NCF2	Q6UXH1	CRELD2
Q7Z739	YTHDF3	Q9H4D0	CLSTN2	P23582	NPPC	Q99895	CTRC
P42768	WAS	P48023	FASLG	Q9NRJ3	CCL28	Q9NQ76	MEPE
Q96RJ3	TNFRSF13C	P29460	IL12B	P26022	PTX3	Q4KMG0	CDON
Q8TAD2	IL17D	Q15517	CDSN	Q03431	PTH1R	Q9UHX3	ADGRE2
Q7Z6M3	MILR1	P51671	CCL11	Q9GZT9	EGLN1	Q15109	AGER
P30048	PRDX3	Q16719	KYNU	Q9UMR7	CLEC4A	P27930	IL1R2
Q05084	ICA1	Q9HBG7	LY9	P13725	OSM	Q9NQ30	ESM1
P51617	IRAK1	P78556	CCL20	P28845	HSD11B1	Q9HCB6	SPON1
P42701	IL12RB1	P03956	MMP1	P24394	IL4R	Q9UII2	ATP5IF1
Q9HB29	IL1RL2	P49763	PGF	Q9NWZ3	IRAK4	O75563	SKAP2
P01583	IL1A	O15444	CCL25	Q14773	ICAM4	P09341	CXCL1
P32456	GBP2	Q07325	CXCL9	Q16698	DECR1	Q16651	PRSS8
P12034	FGF5	Q92484	SMPDL3A	O60449	LY75	Q03405	PLAUR
P09919	CSF3	P21709	EPHA1	Q9UKX5	ITGA11	O00626	CCL22
Q9BXJ7	AMN	P15260	IFNGR1	O15169	AXIN1	P51888	PRELP
P18564	ITGB6	P53634	CTSC	P50995	ANXA11	O00339	MATN2
P01591	JCHAIN	Q5ZPR3	CD276	P01730	CD4	P36941	LTBR
P01579	IFNG	Q9UJU6	DBNL	Q9NRM6	IL17RB	Q16363	LAMA4
Q13291	SLAMF1	P30613	PKLR	P01374	LTA	P19883	FST
Q8N8S7	ENAH	O43639	NCK2	Q6ZUJ8	PIK3AP1	Q9BU40	CHRDL1
Q13261	IL15RA	P35625	TIMP3	P16455	MGMT	O00175	CCL24
P09874	PARP1	P47712	PLA2G4A	O94992	HEXIM1	Q99538	LGMN
Q0Z7S8	FABP9	O00585	CCL21	Q6UXB4	CLEC4G	Q14118	DAG1
P78362	SRPK2	P09238	MMP10	P20783	NTF3	P54317	PNLIPRP2
P09038	FGF2	P11684	SCGB1A1	O14788	TNFSF11	Q8IYS5	OSCAR
O43736	ITM2A	Q6UWV6	ENPP7	Q29980_Q29983	MICB_MICA	Q15166	PON3
O14867	BACH1	Q9BZZ2	SIGLEC1	Q8NDB2	BANK1	P07148	FABP1
Q8IU57	IFNLR1	P25116	F2R	Q8TD46	CD200R1	O95866	MPIG6B
Q12933	TRAF2	P09326	CD48	P08727	KRT19	P15291	B4GALT1
Q01344	IL5RA	Q8TEU8	WFIKKN2	Q9HCM2	PLXNA4	O00182	LGALS9
Q9NQ25	SLAMF7	O00468	AGRN	P28827	PTPRM	O95633	FSTL3
P41217	CD200	Q03403	TFF2	P32970	CD70	Q92956	TNFRSF14
Q13232	NME3	P19876	CXCL3	P01135	TGFA	Q9BYZ8	REG4

5.10 Supplementary Figures

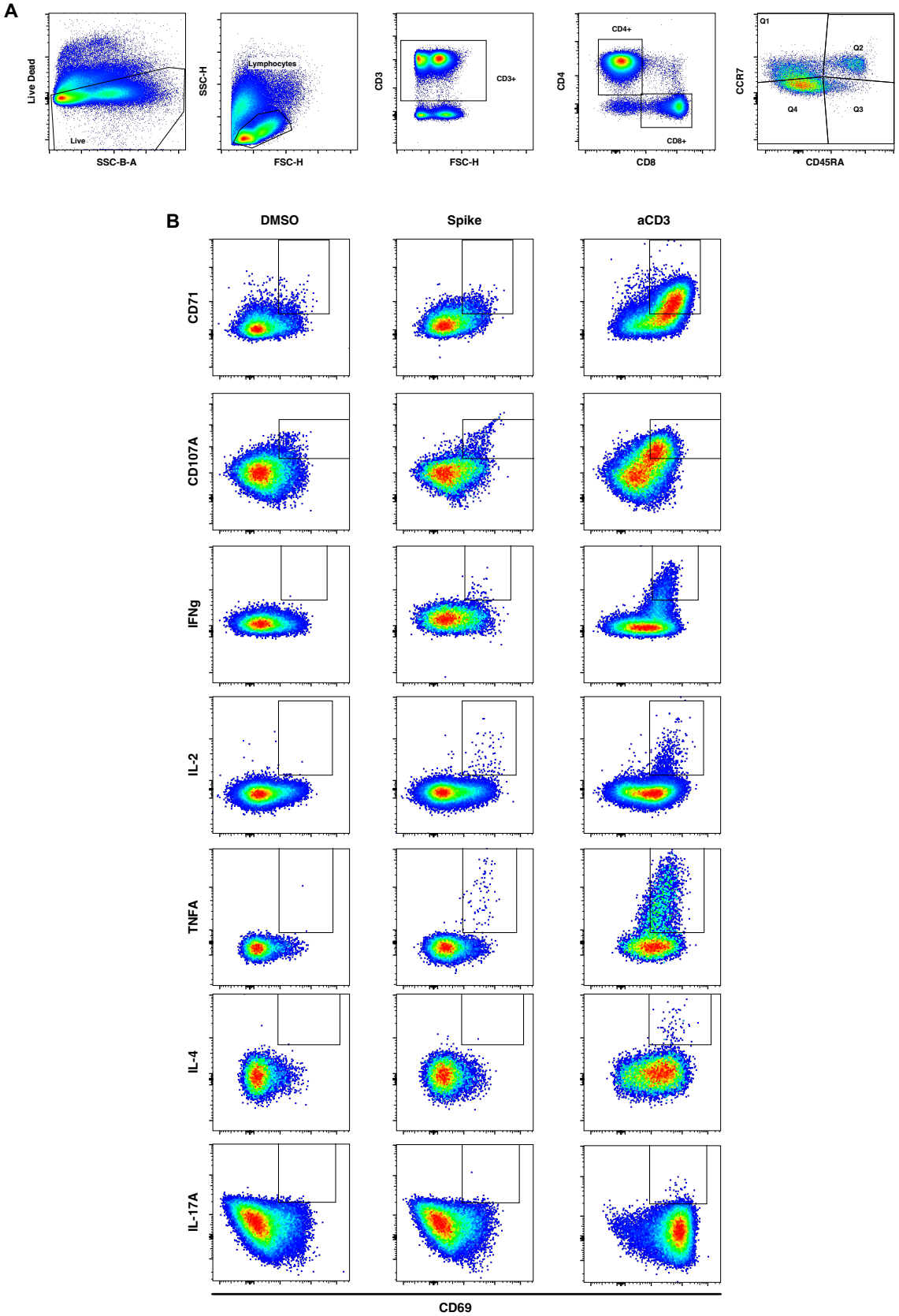

Fig. S5.1 Exemplar flow cytometric gating of Cytek Aurora intracellular cytokine staining panel

A) T cell memory subset gating

B) Example flow cytometric gating for cytokines in DMSO, SARS-CoV-2 and anti-CD3 (aCD3) stimulation conditions

Table S5.1 OCTAVE DUO Study eligibility criteria

Inclusion Criteria
Aged ≥18 years.
Have an inadequate response to two doses of SARS-CoV-2 vaccine measured at least 14 days after receipt of the second vaccine, defined by SARS-CoV-2 spike antibody response. An inadequate response is defined as: - Antibody non-response: SARS-CoV-2 anti-spike antibodies below the level of detection using the PHE Roche platform [or equivalent assay, see appendix p 5] <0.8 Arbitrary Units (AU)/ml; or - Antibody low-response*: SARS-CoV-2 anti-spike antibodies <0.8 and <400 AU/mL using the Roche platform [or equivalent assay, see appendix p 5]).
Anticipated life expectancy of 6 months or greater.
Fall into one (or more) of the patient cohorts listed in appendix p 4 who will meet disease relevant classification, disease state, and staging according to established international standards.
Participant is willing and able to comply with trial requirements.
For the randomised sub-study only, female participants of childbearing potential* must be willing to ensure that they or their partner use acceptable effective contraceptive methods^ until 3 months after the re-boost immunisation. * Defined as a fertile woman, following menarche and until becoming post-menopausal unless permanently sterile. Permanent sterilisation methods include hysterectomy, bilateral salpingectomy and bilateral oophorectomy. Postmenopausal is defined as no menses for 12 months without an alternative medical cause. ^ Acceptable birth control methods include: - Combined (oestrogen and progestogen containing) hormonal contraception associated with inhibition of ovulation - Progestogen-only hormonal contraception associated with inhibition of ovulation - Intrauterine device (IUD) - Intrauterine hormone-releasing system (IUS) - Bilateral tubal occlusion - Vasectomised partner - Sexual abstinence - Progestogen-only oral hormonal contraception, where inhibition of ovulation is not the primary mode of action - Male or female condom with or without spermicide - Cap, diaphragm or sponge with spermicide Note: Haematopoetic stem cell transfer (HSCT) and chimeric-antigen receptor (CAR)-T cell recipients who have received any SARS-CoV-2 vaccine pre-procedure and are receiving a re-vaccination course post HSCT/CAR-T are eligible for recruitment.
Exclusion Criteria
Receipt of any vaccine within 30 days before trial entry, with the exception of: a SARS-CoV-2 vaccine which is allowed ≥14 days prior; or a flu vaccination which is allowed ≥7 days prior.
For aggressive B-cell non-Hodgkin's lymphoma (B-NHL) or Hodgkin lymphoma only, participants on active systemic treatment or within 4 weeks of completion of systemic treatment.
Any known contraindications as specified in the applicable product information including but not limited to: - Known allergy or hypersensitivity to any of the trial IMPs or any of the trial drug excipients; and - History of anaphylaxis to prior COVID-19 vaccinations, or any component of the vaccine.
In the judgement of the Investigator, the patient is unsuitable to participate in the trial or is unlikely to comply with trial procedures.
For the randomised sub-study only, patients who are pregnant or lactating at trial entry or planning to become pregnant within 3 months after re-vaccination.

6 Results: Single-cell transcriptomic analysis of bulk immune cells and vaccine-induced spike specific B and T cells in individuals with secondary immunodeficiencies

6.1 Introduction

In chapter 5, I identified several immunophenotypic features which differed between SIs at baseline and were associated with mRNA COVID-19 vaccine-induced antibody and T cell responses. This included transcriptomic differences, such as in the expression of genesets relating to B and T cells, monocytes and inflammatory signalling pathways. Analysis of immune cell subsets demonstrated that these transcriptomic differences could partially be explained by differences in the frequency of immune cell subsets and that bulk and antigen-specific T and B cell function was impaired in certain SI groups. Analysis of the inflammatory proteome in plasma demonstrated that increased systemic inflammation was associated with reduced antibody and T cell responsiveness to vaccination and identified specific markers of this. Immunosuppressive conditions therefore had a significant impact on immune cell composition, functionality and inflammation – however, questions remained as to the relative contribution of each of these factors on the vaccine-induced response. In particular, the impact of SIs on the phenotype and function of antigen-specific T and B cells, induced by mRNA vaccines, remains largely unexplored.

In chapter 4 I demonstrated the utility of combining scRNA-sequencing with flow cytometric sorting to assess the function of activation induced marker (AIM) positive SARS-CoV-2 spike-responsive T cells after COVID-19 vaccination or SARS-CoV-2 infection in healthy individuals. This work identified that SARS-CoV-2 specific T cells induced by vaccines were highly heterogenous and varied depending on vaccine platform and dosing regimen. Applying this approach to samples from immunocompromised populations may give insight into the effect of SIs on T cell responses beyond IFNγ release. At baseline in immunocompromised groups, I identified that the frequency and phenotype of naive $CD4^+$ T cells was associated with reduced vaccine-induced IFNγ T cell responses, but questions remained as to how and why

the pre-vaccine naive T cell phenotype impacted the vaccine-induced T cell response. It is possible that the capacity for T cells to differentiate into functional effector T cells was impaired in these participants (*131-133*), or that reduced diversity of the TCR repertoire led to dysfunctional T cell induction (*426, 427*). However, this remained unclear.

In addition to impaired T cell functionality, in chapter 5 I observed that liver and renal transplant recipients generated reduced magnitudes and quality of RBD-binding Ig, despite having equivalent frequencies of total and SARS-CoV-2 specific B cells compared to healthy individuals at baseline. This indicated some impairment in the function rather than generation of memory B cells. Exactly how vaccine-induced memory B cells were impaired was unclear, with several possible explanations including reduced maturation of memory B cells (*428*), reduced somatic hypermutation and affinity maturation (*429, 430*), reduced B cell class-switch recombination (*430*). Previous publications have suggested that solid organ transplant recipients produce fewer IgG antibodies in response to vaccination (*417*). However, the relative contribution of each of these factors to the resultant vaccine-induced antibody response was unknown.

6.2 Summary of chapter rationale

In chapter 5 I identified significant differences in the underlying immunophenotype of individuals with different SIs, relating to vaccine-induced immune responses. High systemic inflammation at baseline was associated with reduced vaccine-induced antibody responses, however the source of this inflammation, and possible mechanisms of its impact on vaccine-induced immune responses was unclear. Flow cytometric and transcriptomic analysis indicated that specific defects in antigen specific B cells and T cells were present in certain SIs, however the exact phenotype of these defects was unknown. In this chapter, I use scRNA-sequencing of PBMC and antigen-specific B and T cells to further investigate the impact of SIs on vaccine-induced immune responses.

6.3 Hypothesis and aims

Based on my findings in chapter 5, I hypothesised the following:

1) Immunocompromising diseases and immunosuppressive drugs would specifically impact the transcriptional programmes of immune cells, in particular, monocytes, dendritic cells, and T and B lymphocytes
2) Vaccine-induced antigen-specific B cells in individuals on aCD20 therapies and in transplant recipients are altered in frequency and functionality, respectively.
3) Vaccine-induced antigen-specific T cells are significantly impaired in cirrhosis, liver transplant and renal transplant recipients due to the impairment of T cell maturation from naive to effector T cells.
4) Single-cell transcriptional phenotypes of bulk and antigen-specific immune cells are associated with conventional measures (IFNγ ELISpot, binding Ig) of vaccine-induced adaptive immune responses.

To assess these hypotheses, I aim to:

1) Assess and compare the transcriptomic and cell surface phenotype of peripheral blood immune cells from individuals with secondary immunodeficiencies at a single cell resolution.
2) Assess and compare the transcriptomic and BCR-sequence phenotype of COVID-19 vaccine-induced antigen-specific B cells in individuals with secondary immunodeficiencies.
3) Assess and compare the transcriptomic and TCR-sequence phenotype and functionality of COVID-19 vaccine-induced antigen-responsive T cells in individuals with secondary immunodeficiencies.
4) Associate the single-cell transcriptomic phenotypes with vaccine-induced binding antibody and IFNγ T cell responses.

6.4 Chapter overview

To address these aims, I generated and analysed a single-cell RNA, surface protein and TCR and BCR sequencing dataset of $CD45^+$ PBMC across 80 individuals with several different SIs. In the same individuals, I also generated and analysed single-cell RNA- and V(D)J-sequencing datasets of sorted SARS-CoV-2 spike specific B and T cells 21 days after a third COVID-19 vaccine.

Through integration and analysis of these datasets, in combination with the pre-vaccination

data generated in chapter 5, I identify transcriptomic differences in peripheral blood and vaccine-specific responses across diseases. I associate these transcriptional differences with relevant immune measures related to vaccine efficacy.

6.5 Chapter specific methods

6.5.1 Study samples

Samples were obtained from the OCTAVE DUO study. All patients gave informed consent, and the study was approved by an ethics committee, funded by UKRI/DHSC, and sponsored by the University of Birmingham (*379*) (**Section 5.5.1**).

6.5.2 Pre-processing of antibody derived tag (ADT) data

Cell surface protein staining for antibody-derived tags (ADT) for cellular indexing of transcriptomes and epitopes (CITE) sequencing was performed using the DSBNormalizeProtein function from the denoised and scaled by background (dsb) package with default settings (*431*). ADT sequencing data from empty droplets from one batch of one experiment was selected for normalization.

6.5.3 Weighted nearest-neighbour analysis for dimensionality reduction

Pre-processed transcriptional and dsb ADT data were normalised to library size and log2 transformed, scaled, and principal components were calculated for each data type. The top 30 principal components from the transcript data and top 50 principal components from the dsb data were integrated using the FindMultiModalNeighbors function in the Seurat package. Louvain clustering and uniform manifold approximation and projection (UMAP) was performed on the weighted nearest neighbours.

6.5.4 Antigen-specific B and T cell integration and annotation prediction

SARS-CoV-2 specific B cells and SARS-CoV-2 responsive AIM^+ T cells (derived from PBMC, **Section 2.4**) were each separately integrated with bulk B and T cells, respectively. Each dataset was separately normalised using SCTransform (v2) and integrated using reciprocal PCA in Seurat (V4.1) based on experimental condition. For prediction of annotations for B

cells, an annotated pan-B cell dataset was downloaded from (*432*), normalised using SCTransform and then used for reference mapping (FindTransferAnchors and TransferData functions, Seurat), using PCA as the reference reduction.

6.5.5 BCR analysis

BCR analysis was performed using the Immcantation BCR analysis pipeline. Filtered_contig.fasta and filtered_contig_annotations outputs generated by CellRanger vdj were used to assign V(D)J genes using IgBLAST (*433*) and formatted to be Adaptive Immune Receptor Repertoire (AIRR) compatible for downstream analysis. AIRR formatted BCR calls were read into R and filtered to remove non-productive sequences. For further BCR analysis, cells with no or with multiple heavy gene calls were removed. Paired heavy and light chain BCR calls were integrated with gene expression and ADT data. B cell clones were identified for each individual separately by spectral clustering of BCR heavy and light chains from the SCOPer (v1.3.0) package (*434, 435*). Germline sequences for the heavy chain of each clone were reconstructed using reference germline V and J sequences from the international ImMunoGeneTics information (IMGT) database. By comparing the observed VDJ sequence with the inferred germline VDJ sequence, the frequency of mutated nucleotides was calculated using SCOPer. This frequency is referred to as the somatic hypermutation (SHM) rate. Due to redundancy in the translation of nucleotides into amino acids, some nucleotide substitutions do not cause difference in the amino acid sequence of the encoded VDJ (*436*). Such mutations are referred to as synonymous mutations. Synonymous and non-synonymous mutations were assessed separately. Finally, clonal trees were generated using the dowser (v2.3.0) package

6.5.6 Pseudotime analysis using Monocle3 and Lamian

Antigen specific $CD4^+$ T cells in all clusters except CD4_Th1_Tfh and CD4_Treg were included for pseudotime analysis using monocle3. Subsetted cells were normalised, 3000 top variable genes were selected and scaled, then PCA and UMAP analysis was performed. Monocle3 learn_graph function was used to calculate a pseudotime trajectory, using a manually selected

root node within the CD4_Naive cluster as the base of the pseudotime. A Moran's I test was used to identify genes with expression that was spatially associated with the pseudotime trajectory. The top 250 correlated genes (based on Morans I statistic) were plotted and the top 100 labelled.

The Lamian package was used to calculate genes that were differentially expressed with respect to the pseudotime trajectory based on clinical group. 200 cells from each individual were randomly subsampled from the cells used in the Monocle3 pseudotime analysis, and subsampled data was reprocessed and UMAP analysis performed. Individuals with <50 cells in total were filtered out (12 individuals in total). Pseudotime was recalculated on the down sampled object using Monocle3 and converted into integers by ranking, and the lamian_test was used with analysis group (RT, LT and Cirr versus all others) as a covariate with 100 permutations. Genes with an FDR <0.05 were selected and clustered based on expression using lamian clusterGene with a k of 4.

6.5.7 MiloR differential abundance analysis

Differential abundance analysis was performed at a sub-cluster resolution by identification of cell 'neighbourhoods' using MiloR (v2.0.1) (*437*). A graph was built using all $CD8^+$ AIM^+ T cells with k=30, d=30 and neighbourhoods calculated using k=30, d=30 using a graph-based refinement scheme based on PCAs. Comparison was performed between analysis groups, using sex, age and batch as covariates.

6.6 Results

6.6.1 OCTAVE DUO Cohort and study design

72 individuals from the OCTAVE DUO cohort that were included in the baseline immunophenotyping project (Chapter 5) were selected for analysis **(Fig. 6.1A)**. Individuals from liver disease, inflammatory bowel disease, rheumatic condition, solid organ transplant and lymphoma disease groups were included **(Fig. 6.1B)**. Participants were selected based on their underlying disease aetiology and immunosuppressive regimen, and sample availability. Selected disease-drug combinations included: AAV on aCD20 (n = 8), indolent B

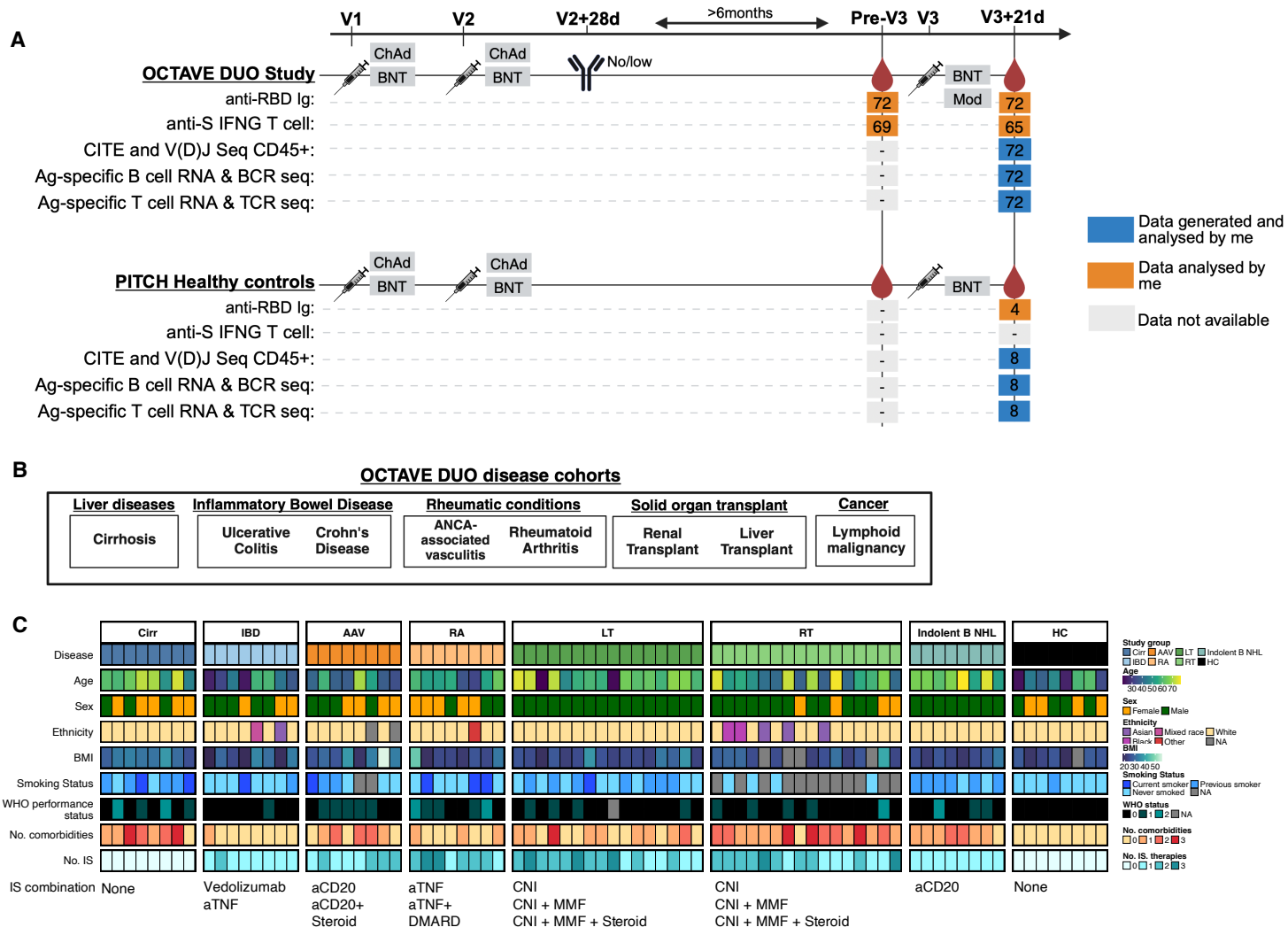

Fig. 6.1 OCTAVE DUO study overview and demographics

A) Sampling timepoints and vaccine regimen for individuals in the OCTAVE DUO and PITCH studies included in chapter 5. Individuals in OCTAVE DUO study were selected to have low or no antibody titre at V2+28d (Methods). The number indicated is the number of individuals included for the given analysis/study. The vaccine types given at each dose is indicated for each study/timepoint. Red droplet indicates peripheral blood sampling timepoints. Colours at each timepoint represents my contribution to the data presented in this analysis.

B) Disease cohorts included in chapter 6

C) Per person demographic breakdown of individuals included in chapter 6, associated with Table 6.1. Immunosuppressive therapy combinations used in each disease group are listed.

NHL on aCD20 (n = 8), RA on aTNF (n = 8), IBD on aTNF (n = 4), IBD on Vedolizumab (n = 4), RT on CNI + MMF +/- corticosteroid (n = 8), RT on CNI only (n = 8), LT on CNI + MMF +/- corticosteroid (n = 8), LT on CNI only (n = 8), and cirrhosis on no immunosuppression (n = 8). Within disease-drug combinations, individuals were selected that were broadly representative of the age and sex status of the disease group in the overall cohort (**Table 6.1, Table 5.1)**. Healthy control participants from the PITCH study were selected by the same criteria (n = 8) (**Fig. 6.1C)**.

6.6.2 The peripheral blood single-cell transcriptome differs between immunocompromising conditions and healthy controls

Baseline immunophenotyping (Chapter 5) identified that there were broad differences in the transcriptional composition of peripheral blood immune responses between individuals with different SIs, however bulk RNA-sequencing and flow cytometry cannot resolve transcriptomic differences at a single cell level. To assess if there were differences in the function or phenotype of immune cells, I used single cell RNA-sequencing to profile live $CD45^+$ immune cells sampled at the V3+21d timepoint. I additionally quantified expression of 138 immune-related surface proteins using oligomer-tagged antibodies (**Table 6.2**). In total 175,630 cells passed QC across 80 participants (**Fig. 6.2A**). Integration of both transcriptomic and surface protein expression profiles (using weighted-nearest neighbour; WNN, **Section 6.5.3**) for dimensionality reduction and Louvain clustering identified all major immune cell populations found in peripheral blood (**Fig. 6.2A&B**). Manual annotation of the clusters using lineage defining transcriptional and protein markers identified four $CD4^+$ T cell clusters (T_CD4_Naive, T _CD4_Mem, T_CD4_reg, T_CD4_Cytotoxic), two $CD8^+$ T cell clusters (T_CD8_Naive, T_CD8_Mem), a mixed unconventional T cell cluster (T_MAIT_Vd2) , three NK cell clusters (NK, NK_CD16, NK_proliferating), two monocyte populations (Mono_Classical, Mono_Nonclassical), a mixed $CD1c^+$, $CD141^+$ DC population (Mono_DC), a plasmacytoid

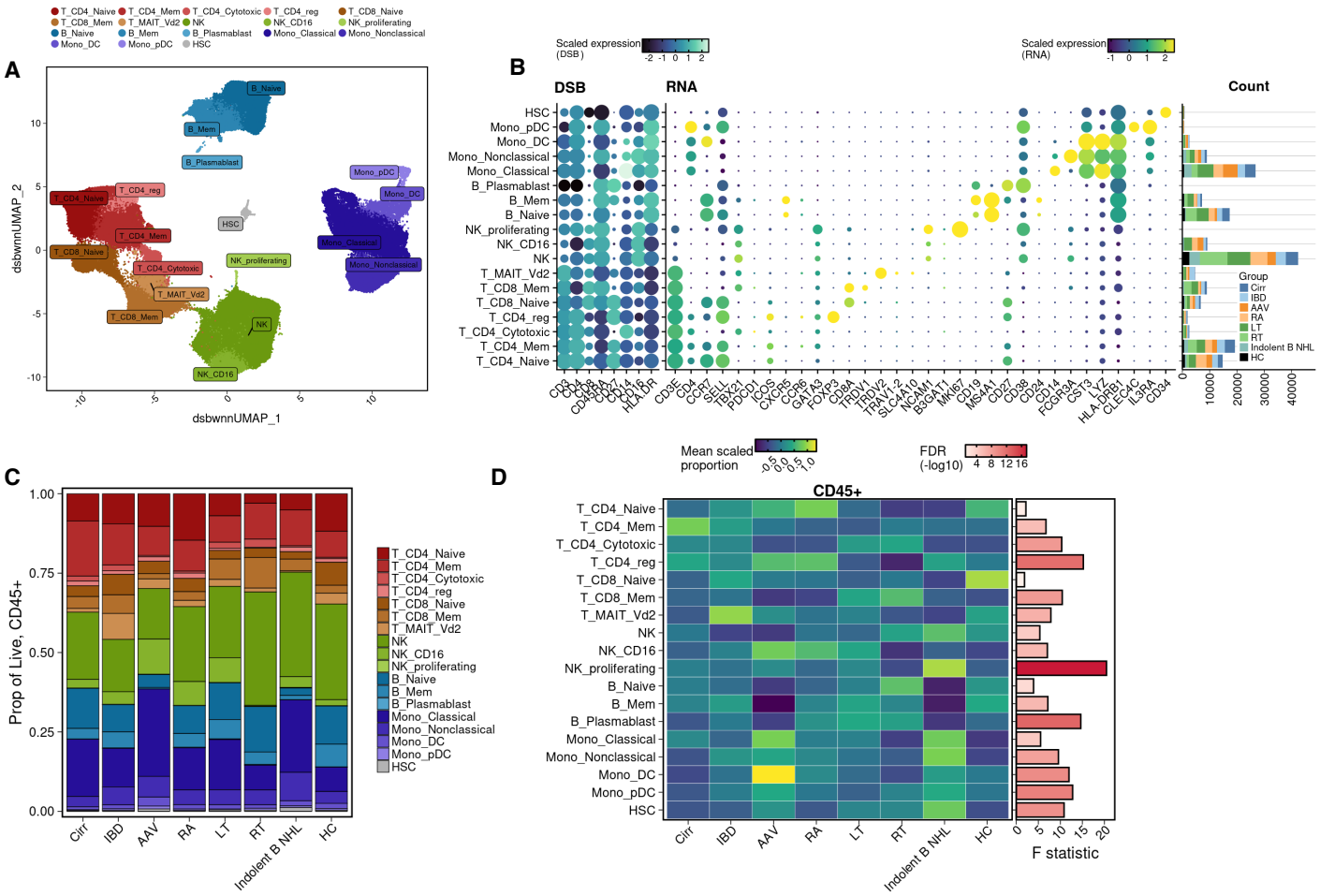

Fig. 6.2 The CD45⁺ single cell transcriptomic immunophenotype of individuals with immunosuppressive conditions and healthy controls

A) Uniform manifold approximation and projection (UMAP) of CD45⁺ live peripheral blood mononuclear cells from n = 80 individuals in OCTAVE DUO study and healthy controls. Manually annotated Louvain clusters.

B) Scaled surface expression of selected phenotypic denoised surface protein (DSB) and RNA markers. Absolute count of each cell type broken down by clinical group.

C) Mean proportion of cell type per clinical group.

D) The mean of the scaled proportion of each cell type per clinical group (left panel). EdgeR quasi-likelihood F test false discovery rate (FDR) comparing proportions across groups (right panel).

dendritic cell population (pDC), two B cell populations (B_Mem, B_Naive) and a plasma blast / plasma cell population (B_plasmablast) (**Fig. 6.2A&B)**. The cell composition of each group broadly aligned with that observed in the flow cytometry data (**Fig. 5.15B**), but the scRNA-sequencing data captured higher relative frequencies of NK cells compared to flow cytometry (**Fig. 6.2C**). The cell type with the greatest degree of variation between disease groups was the NK proliferating cell type, which was enriched in indolent B NHL patients (**Fig. 6.2D),** but was likely biased by the small number of cells in the cluster. Consistent with baseline, the AAV

and indolent B NHL patients on aCD20 therapies had reduced frequencies of naive and memory B cells and plasmablast/plasma cells and relatively increased monocyte and DC populations (**Fig. 6.2D)**. The mixed unconventional T cell population was highest frequency in IBD patients, as demonstrated previously (*438, 439*).

To assess transcriptional differences between clusters, I aggregated gene expression values of all cells within a given cluster for each donor and performed geneset variation analysis (GSVA) upon the aggregate (pseudobulk) expression values (**Fig. 6.3A**). I used the same blood transcriptomic module (BTM) genesets as were used to phenotype the baseline bulk-RNA sequencing data as well as Hallmark gene ontology genesets (*440*). There was significant variation in the expression of different genesets across cell types (**Fig. 6.3B**), and this was broadly consistent with the aggregate geneset modules derived in Chapter 5 (**Fig. 6.3C**). While some genesets were highly specific to certain clusters (e.g. plasma cells, immunoglobulins (M156.1) and B cells; enriched in monocytes (I) (M4.15) and monocytes and DCs) genesets relating to T and NK cells were less specific to those cell types (**Fig. 6.3B&C**).

There were significant differences in geneset expression values between immunocompromised groups and healthy controls for all clusters except T_CD4_Cytotoxic, T_MAIT_VD2, NK_CD16 and NK_proliferating **(Fig. 6.3D)**. Monocyte clusters had the largest differences, including in antigen presentation and monocyte signalling **(Fig. 6.3D&E, Fig. 6.4)**. There were significant differences in T cell differentiation pathways between healthy controls and immunocompromised individuals in $CD4^+$ and $CD8^+$ T memory **(Fig. 6.3D and Fig. 6.4)**. Memory B cells were broadly similar between groups, but AAV patients had increased expression of inflammatory signalling and genesets associated with adaptive immune activation **(Fig. 6.4).**

6.6.3 Pro-inflammatory monocyte signalling is associated with vaccine non-responsiveness in solid organ transplant recipients

Fig. 6.3 Differential geneset expression across immunocompromised states, within cell types

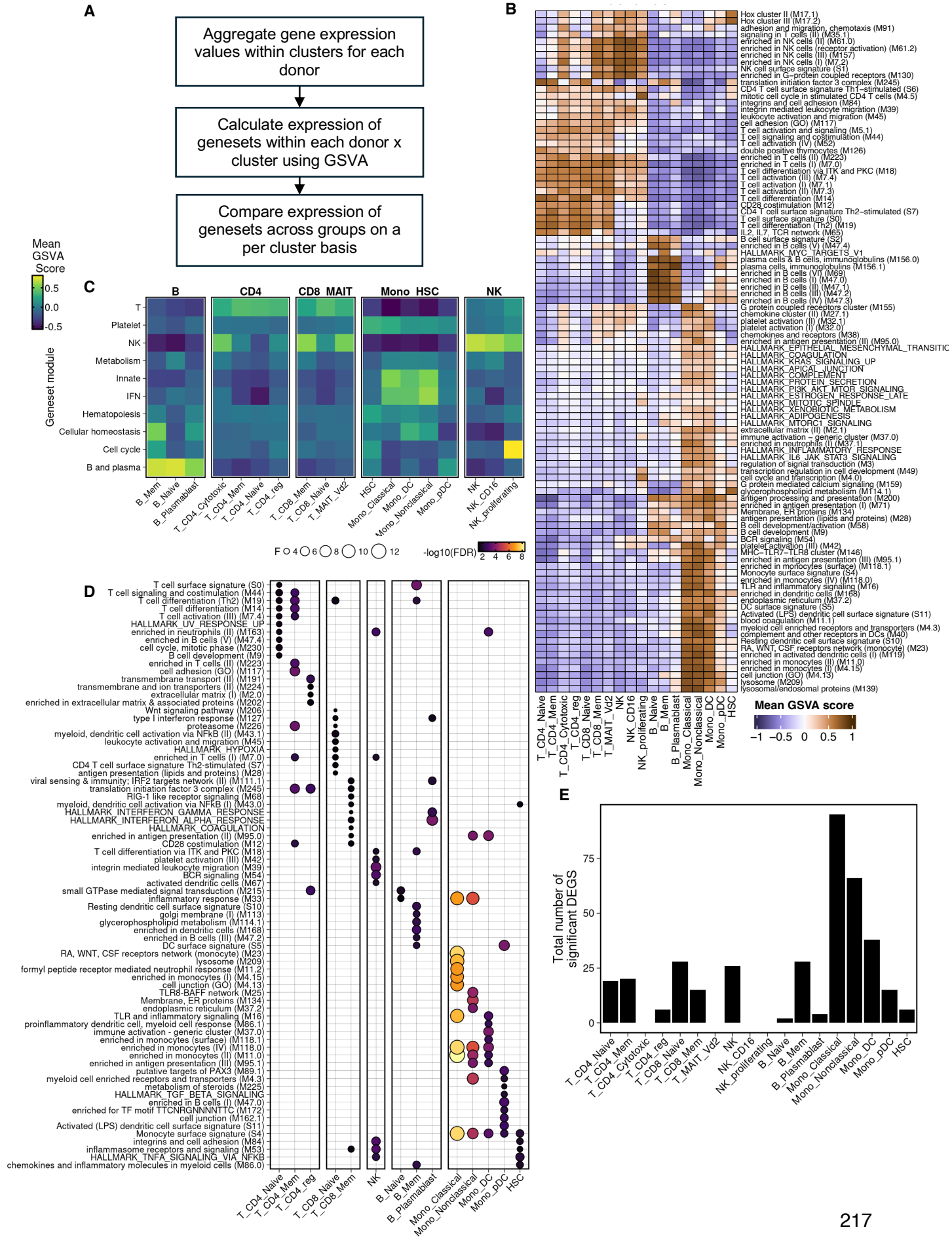

Fig. 6.3 Differential geneset expression across immunocompromised states, within cell types

A) Analysis scheme

B) Mean geneset variation analysis (GSVA) score across individuals, per geneset per cluster

C) The mean GSVA score for genesets within geneset modules identified in Chapter 5

D) The top 10 most significantly differentially expressed genesets within each cluster, using a quasi-likelihood F-test to compare GSVA score in healthy controls with individuals in all analysis groups. Adjusted for age, sex and batch.

E) The total number of differentially expressed genesets in immunocompromised groups compared to healthy controls (as in D).

In chapter 5 I observed that increased inflammation was associated with reduced vaccine-induced antibody responses in RT and LT recipients. Monocytes and dendritic cells are a major source of inflammatory proteins in the blood (*441-443*) and had the highest expression of inflammation related genesets **(Fig. 6.3B&C).** Importantly, monocytes, dendritic cells and macrophages are also the main cell type to uptake and express mRNA vaccine delivered protein (*293*), so altered functionality of these populations may reduce expression and antigen presentation of the antigen itself – reducing immunogenicity.

To assess differences in the phenotype/functionality of monocytes and dendritic cells, I analysed these cells separately from the overall dataset (39,127 cells). To avoid biasing of differential gene expression analysis by using transcriptomic data to cluster cells (*212*), I used only the 138 surface proteins for dimensional reduction and clustering. This method identified the same broad monocyte/DC types as the WNN analysis (**Fig. 6.5A-C)**. There was a clear distinction between $CD16^{+}CD14^{mid}$ non-classical monocytes and $CD14^{hi}CD16^{lo}$ classical monocytes and the cells had distinct overall surface protein profiles **(Fig. 6.5B&C)**. These profiles were consistent with previous phenotypic descriptions (*444*). No clear 'intermediate' monocyte population was identified.

Because non-classical monocytes are associated with inflammatory function (*445, 446*), I first compared the relative frequency of non-classical to classical monocytes in the overall dataset. The log ratio of non-classical to classical monocytes was increased in patients on aCD20 therapy compared to LT and RT, but there was no significant interaction within the LT and RT group with vaccine-induced antibody responses **(Fig. 6.5D)**. There was also no significant

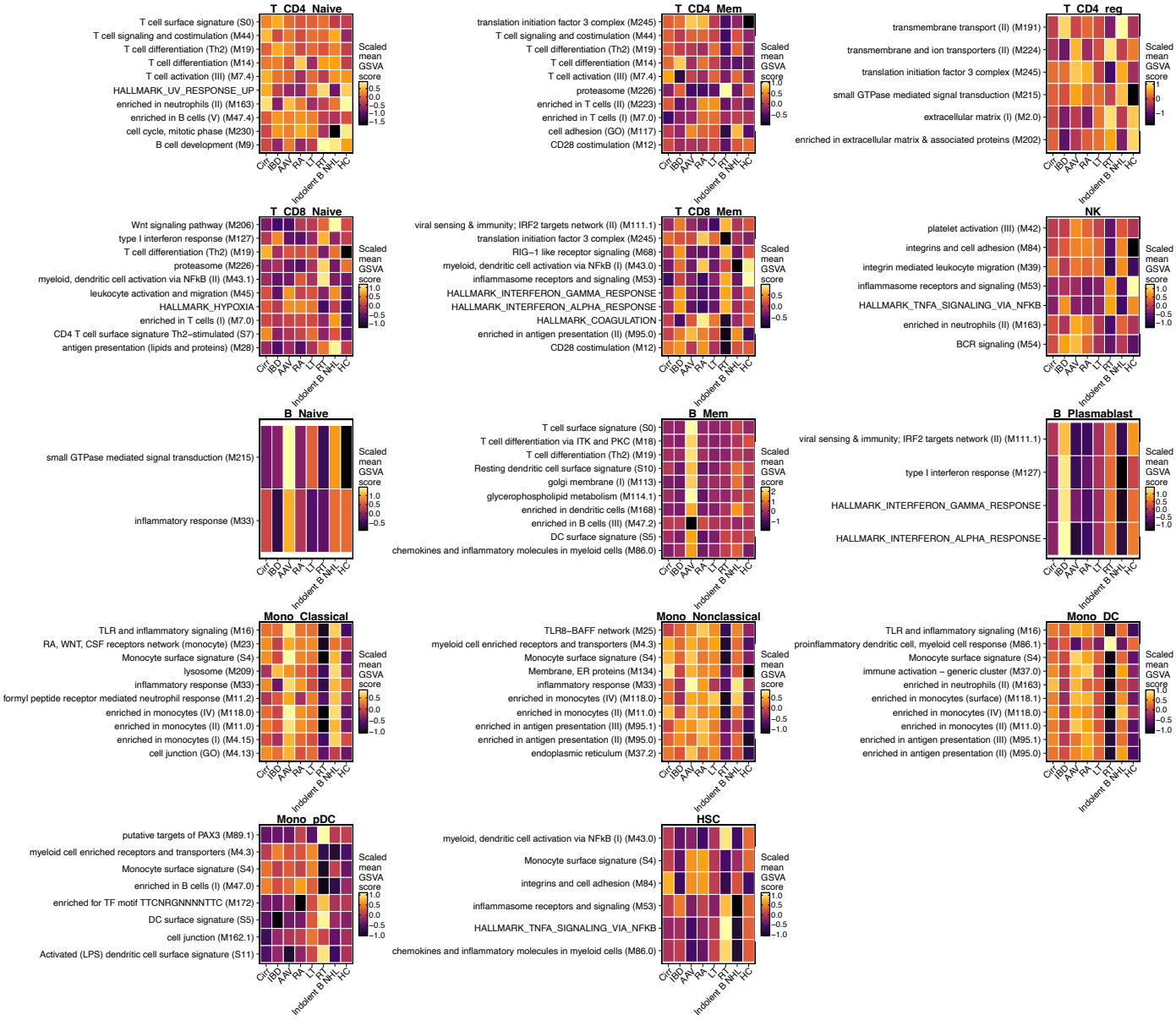

Fig. 6.4 Differential geneset expression in immunocompromised groups compared to healthy controls

Mean geneset variation analysis (GSVA) expression score for individuals within each immunosuppressive group of the top 10 differentially expressed genes between healthy controls and immunocompromised groups as in **Fig. 6.3D**

difference between the LT and RT group and other individuals in the cohort, suggesting that there was no overall skewing toward an inflammatory monocyte phenotype in this group. I next used the pseudobulk GSVA scores of each cluster and individual (as in **Fig. 6.3A)** to fit linear models comparing LT and RT with aCD20 therapy patients and other immunocompromised groups, with an interaction term between analysis group and no/low serological response. There were a large number of differentially expressed genesets

between aCD20 therapy patients and RT and LT patients, particularly in classical and non-classical monocyte populations which shared many differentially expressed genesets (**Fig. 6.6A)**. There were few differentially expressed genesets when comparing LT/RT and

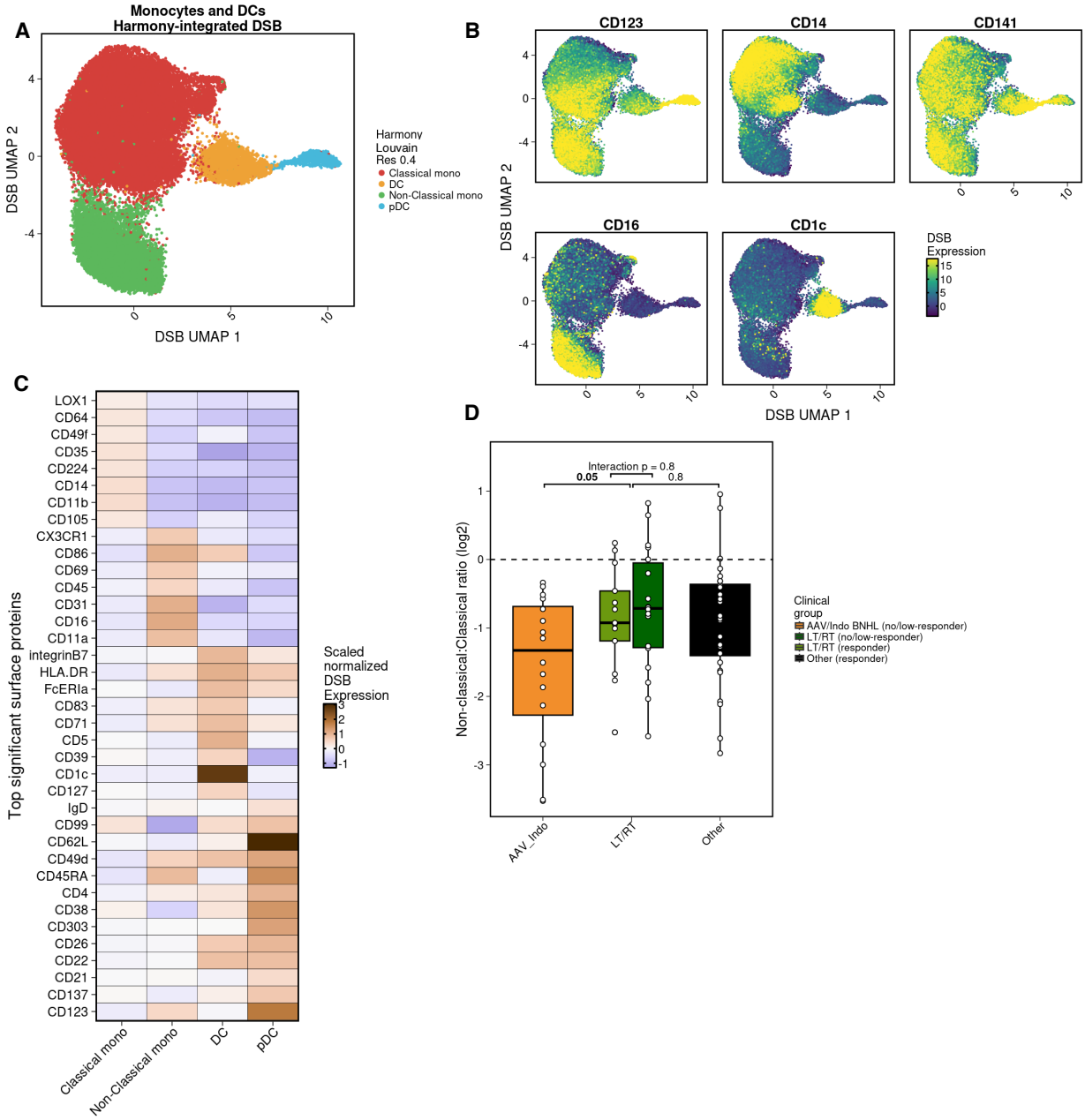

Fig. 6.5 Monocyte and dendritic cell phenotypes

A) Harmony integrated (across experimental batches) UMAP of monocyte and dendritic cells (DC) subsets, based on denoised surface protein expression (DSB). Annotated Louvain clusters.

B) Normalised DSB expression of monocyte and dendritic cell related surface proteins on monocyte and DCs.

C) Mean scaled normalised expression of top 10 differentially expressed DSB across cell types.

D) Log_2 ratio of non-classical to classic proportions. P values from linear model based on log_2 ratio, comparing LT and RT with aCD20 therapy recipients (AAV_Indo) and other immunocompromised and healthy individuals, including an interaction term for V3+21d antibody responsiveness (anti-RBD Ig <1000AU/mL vs >1000AU/mL) and age, sex and batch as covariates.

individuals other than aCD20 recipients, only three significantly different genesets within classical monocytes, one within non-classical monocytes and three within the pDC population (**Fig. 6.6A)**. In addition to increased relative frequency (**Fig. 6.5D)**, classical and inflammatory monocytes in the aCD20 treated groups had higher expression of several activation and inflammatory genesets compared to the RT and LT groups **(Fig. 6.6A)**.

Within the LT and RT group there were significant interactions between anti-RBD Ig response status (no/low versus high) and geneset expression for several genesets in classical and non-classical monocytes **(Fig. 6.6A)**. The strongest interaction occurred in the non-classical monocytes with the 'antiviral IFN signature' significantly enriched in no/low responders **(Fig. 6.6A&B).** There were some genesets with interactions between disease group and vaccine-induced antibody responsiveness in both classical and non-classical monocytes, including 'TLR and inflammatory signalling' and 'enriched in antigen presentation and immune response' **(Fig. 6.6A,C&D).** Differential gene expression analysis between monocyte subsets from RT and LT individuals with no/low compared with high antibody responses identified significant overexpression of many genes relating to interferon signalling, chemokine production and TLR signalling **(Fig. 6.6E&F).** Interestingly, transcripts for *CXCL9* and *CXCL10*, whose pre-vaccination plasma protein concentration was negatively associated with anti-RBD Ig responsiveness **(Fig. 5.12A),** were significantly upregulated in the classical monocytes and DCs of no/low antibody responsive RT and LT recipients **(Fig. 6.6E-G)**. Intriguingly, *TMEM176A* and *TMEM176B* which is overexpressed in immature dendritic cells (*447*), were also significantly enriched in monocytes and DCs from individuals with no/low vaccine-induced antibody response (**Fig. 6.6F&G).** Together this suggests that increased inflammatory signalling and a less mature transcriptional phenotype in monocytes is associated with vaccine non-responsiveness in LT and RT recipients.

6.6.4 Vaccine-induced antigen specific B cells are predominantly activated memory phenotype

Fig. 6.6 Inflammatory monocyte signaling associated with vaccine antibody non-responsiveness

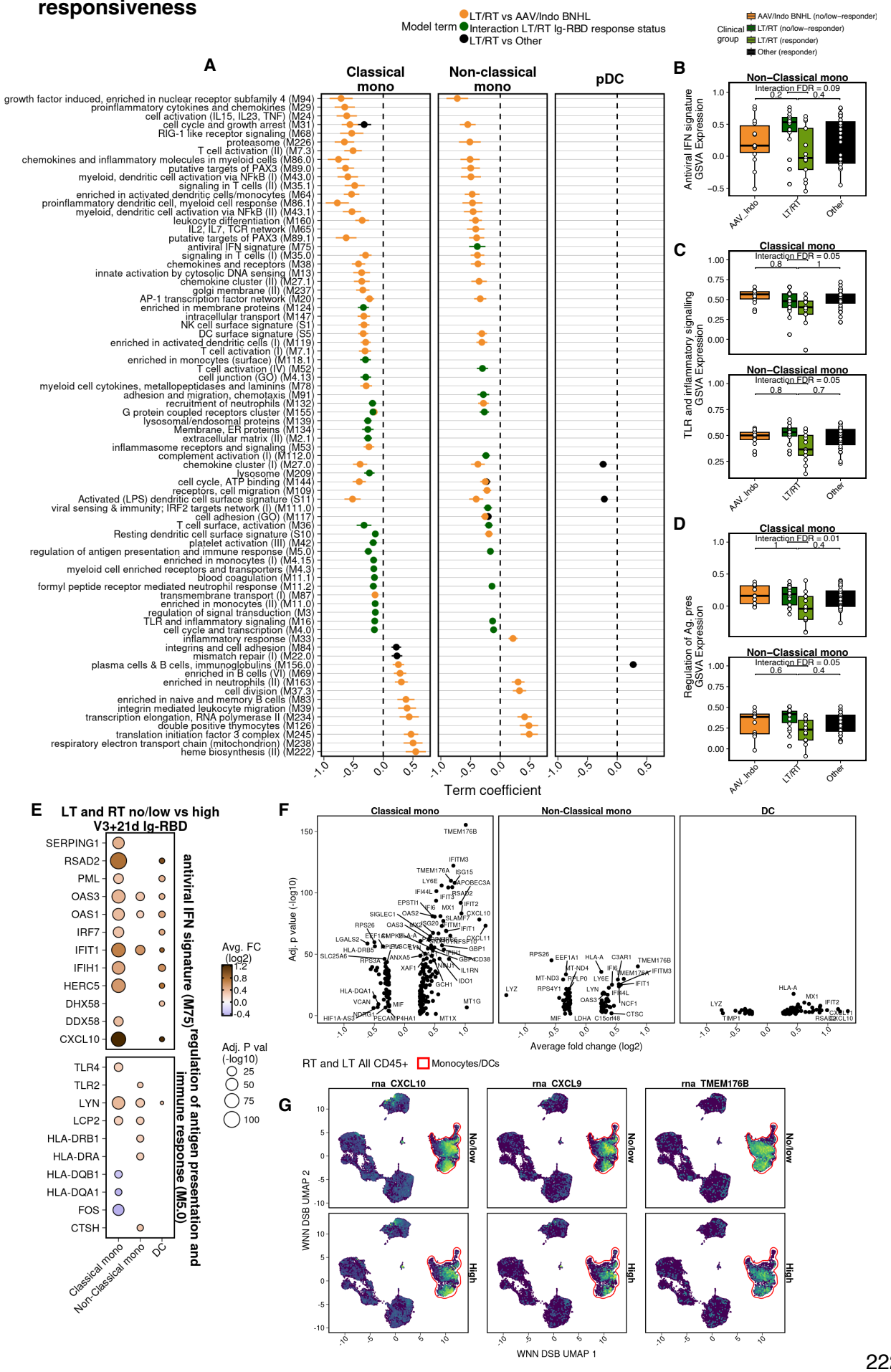

Fig. 6.6 Inflammatory monocyte signaling associated with vaccine antibody non-responsiveness

A) Models were fit on the geneset variation expression analysis (GSVA) score for each geneset within given cell type. The coefficient for the given term comparing LT and RT with aCD20 therapy recipients (AAV_Indo) and other immunocompromised and healthy individuals, including an interaction term for V3+21d antibody responsiveness (anti-RBD Ig <1000AU/mL vs >1000AU/mL) and age, sex and batch as covariates. All comparisons with FDR <0.1 are shown. Point is coefficient, lines are standard error.

B-D) GSVA score for cell type and comparison, with p values as in A. Antiviral IFN signature (M75) expression in non-classical monocytes (B), TLR and inflammatory signalling (M16) in classical and non-classical monocytes (C) and regulation of antigen presentation and immune response (M5.0) in classical and non-classical monocytes (D).

E) Average $\log_2$ fold change of genes from genesets in B-D, comparing no/low V3+21d anti-RBD Ig versus high V3+21d anti-RBD Ig in LT and RT groups.

F) All differentially expressed genes in all cell types, comparing no/low V3+21d anti-RBD Ig versus high V3+21d anti-RBD Ig in LT and RT groups.

G) Scaled normalised RNA expression of selected genes across entire $CD45^+$ dataset, split by anti-RBD Ig responsiveness.

Baseline immunophenotyping demonstrated the association of bulk and antigen-specific B cells with the vaccine-induced antibody response, however some questions about the quality of the induced cells remained. There were 24,740 B cells amongst the live $CD45^+$ PBMC after final QC. To phenotype SARS-CoV-2 spike-specific B cells, I additionally sorted SARS-CoV-2 S1 binding $CD19^+$ B cells (**Fig. 6.7A)** from all 80 donors and performed scRNA- and BCR-sequencing, capturing 1,784 SARS-CoV-2 spike specific B cells after QC. To assess the relative phenotype of antigen-specific and bulk B cells, I integrated the two datasets (**Section 6.5.4**) and performed a joint analysis **(Fig. 6.7B)**.

After integration, I projected the annotations from a previously published B cell dataset to identify major B cell populations (**Section 6.5.4**, **Fig. 6.7C)**. Although the reference dataset included annotations for germinal centre B cells (*432*), only naive, memory and atypical B cell and plasma cell subsets were identified in this dataset, consistent with the expected composition of B cells in peripheral blood (*432*). Louvain clustering was also performed and demonstrated that although there were some sub-clusters within the predicted annotated B cell compartments, the predicted annotations broadly overlapped with the unsupervised clusters (**Fig. 6.7D)**. Spike-specific B cells co-clustered with bulk B cells, suggesting that they are not transcriptionally dissimilar and that potential batch effects caused by the experimental conditions were sufficiently overcome through integration **(Fig. 6.7E)**. While the majority of the

Fig. 6.7 SARS-CoV-2 spike-specific B cells are predominantly of an activated memory phenotype

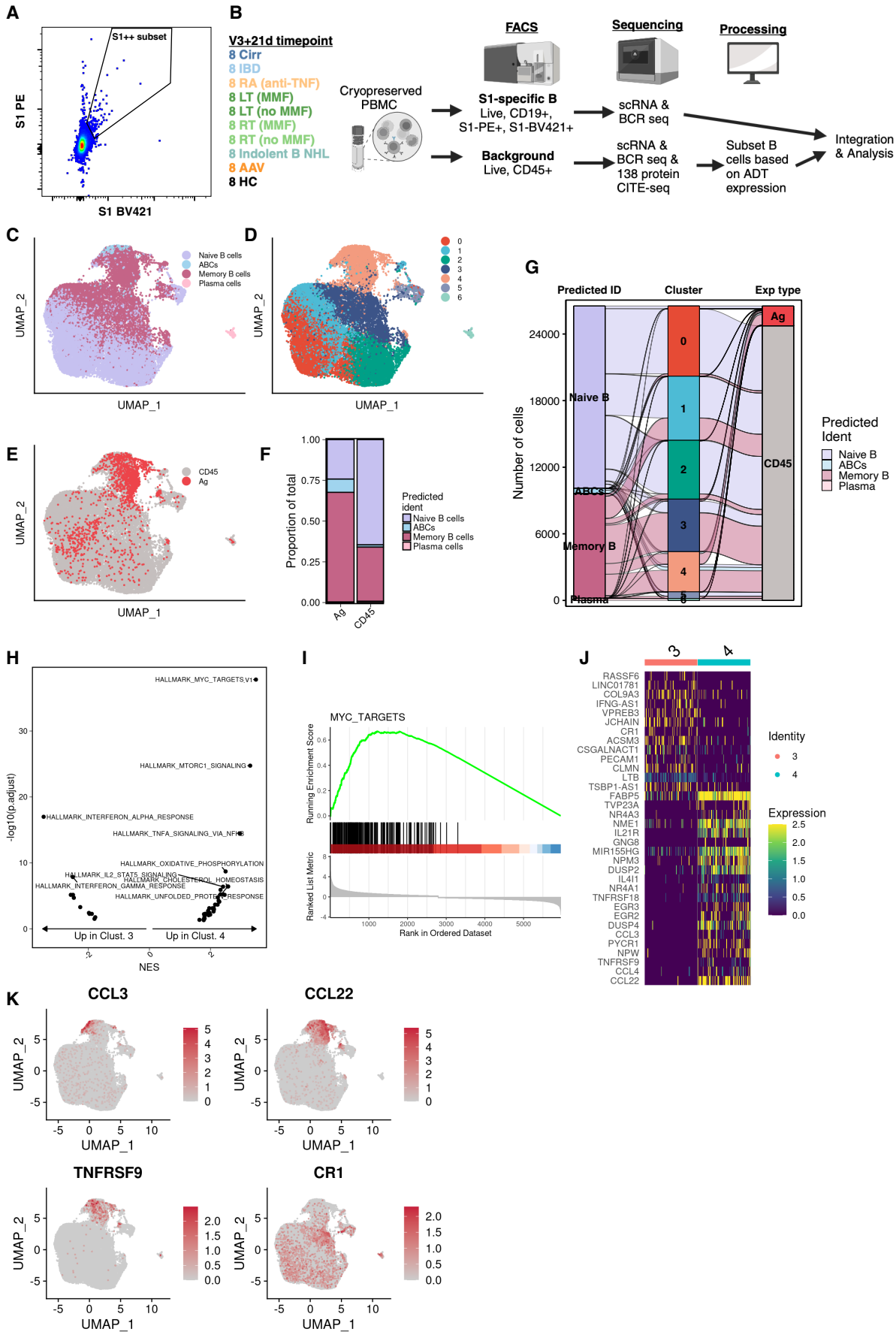

Fig. 6.7 SARS-CoV-2 spike specific B cells predominantly have an activated memory phenotype

A) Example gating of SARS-CoV-2 S1-protein B cell gating for fluorescence-activated cell sorting (FACS). Gated on $CD19^+$ $CD45^+$ live lymphocytes.

B) Experimental overview

C-E) UMAP representation of integrated normalised RNA expression, grouped by predicted annotated phenotype (C), Louvain clusters (D) or experimental condition: background (CD45) or S1-specific (Ag).

F) Proportion of S1-specific or background B cells by predicted phenotype

G) Alluvial plot of integrated B cells, showing proportion sharing across groups as in C-E.

H) Geneset enrichment analysis of differentially expressed genes (Limma) comparing Louvain clusters 3 and 4. Normalised enrichment score (NES) shown.

I) Example running enrichment score of the HALLMARK_MYC_TARGETS_V1 geneset as in H.

J) Scaled normalised expression of top 20 genes differentially expressed in each of cluster 3 compared to cluster 4. Randomly down sampled to 50 cells per cluster.

K) Scaled normalised RNA expression of selected genes

antigen-specific B cells were memory B cells, a notable minority (432 of 1,784 cells; 24%) were phenotypically naive (**Fig. 6.7E&F)**. Very few antigen-specific or bulk plasma cells were identified (7 of 1,784 S-specific; 0.4%, 194 of 27,740 background; 0.8%) likely due to inefficient capture of S-specific plasma cells due to reduced surface BCR expression (*448*) and their low frequency in blood, especially 21 days after vaccination (plasma cell frequency peaks at 7-days post-vaccine (*449, 450*)). Compared to the bulk B cells, there was relative enrichment of both memory and atypical B cells in the spike-specific populations (**Fig. 6.7F)**. Interestingly, the unsupervised cluster 4 was enriched for spike-specific B cells compared to cluster 3, despite both being phenotypically memory B cells **(Fig. 6.7G)**. Cluster 4 also contained cells from the bulk B cell experiment, suggesting that the enrichment in this cluster was not solely due to differences between experiments **(Fig. 6.7G)**.

Compared to the other predominant memory B cell cluster (cluster 3), cluster 4 was enriched for c-Myc and mTORC1 signalling, both of which are critical for B cell activation and primary and secondary responses to T-dependent B cell antigens (*451-454*) – whereas cluster 3 was enriched for interferon signalling **(Fig. 6.7H&I)**. Cluster 4 was also enriched for the expression of genes relating to BCR signalling (*CCL4*, *CCL3*) (*455*), B cell activation (*TNFRSF9) (456),* T cell chemoattraction (*CCL22)* (*457*) and had reduced expression of genes relating to inhibitory receptors such as *CR1* (*458*) **(Fig. 6.7J&K)**. Therefore, the majority of spike-specific B cells

are of an activated memory phenotype.

6.6.5 Vaccine-induced antigen specific B cells are enriched for immunoglobulin class-switching but not somatic hypermutation

The BCR repertoire is central to B cell functionality (*430*) and immunoglobulin class-switch recombination and somatic hypermutation (SHM) are critical processes in defining the BCR repertoire (*459, 460*). B cells of all Ig isotypes except IgE (IgA1, IgA2, IgD, IgG1, IgG2, IgG3, IgG4, IgM) were observed in the dataset (**Fig. 6.8A)** and there was a diverse range of somatic hypermutation rates **(Fig. 6.8B)**. IgM and IgD are usually co-expressed on naive B cells (*459*), therefore IgM is used to denote IgM+IgD$^+$ or IgM$^+$ B cells, and IgD are IgD$^+$ only. As expected, there were low frequencies of class-switched Ig within S-specific or bulk B cell populations that were phenotypically naive, and most naive cells expressed IgM or IgD BCRs (385 of 393 naive S-specific; 98%, 14,651 of 14,777; 99% naive bulk B) (**Fig. 6.8A&C)**. Compared to naive B cells, ABCs and memory B cells were enriched for class-switched BCRs **(Fig. 6.8C)**. The commonest Ig subclasses within these cell types were IgG1, followed by IgG2 and IgA1**,** however there was a substantial proportion of IgM$^+$ S-specific memory B cells (**Fig. 6.8C).** All identified antigen-specific and 154 of 172 (90%) of plasma cells were class-switched. The majority of S-specific and bulk plasma cells were IgA1 subclass - consistent with earlier reports (*461*).

Rates of complementarity determining region (CDR) SHM were lowest in naive B cells (**Fig. 6.8D)**, concomitant with their enrichment for non-class switched BCRs which had the lowest frequencies of SHM **(Fig. 6.8E)**. S-specific naive B cells had higher frequencies of CDR SHM compared to bulk B cells due to increased SHM rate in naive IgM$^+$ cells, but overall, only the IgD subclass exhibited different rates of CDR SHM in bulk compared to S-specific B cells **(Fig. 6.8D-F)**. Interestingly, IgM$^+$ memory B cells had higher rates of SHM compared to IgM$^+$ naive B cells and the SHM rate of IgM$^+$ memory B cells did not differ between S-specific and bulk B cells (**Fig. 6.8F)**. IgG2 subclass S-specific memory B cells had reduced rates of SHM

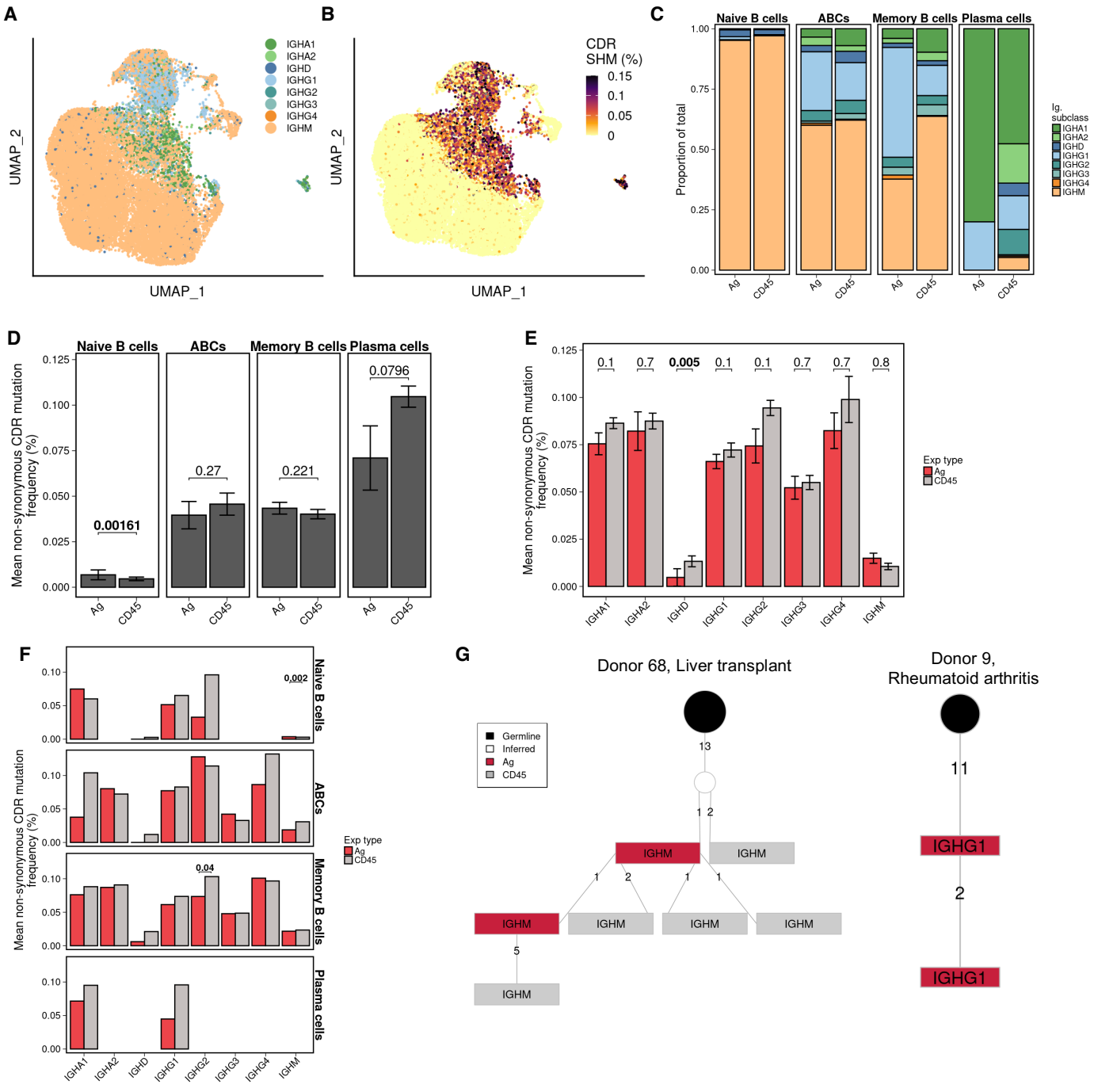

Fig. 6.8 The B cell receptor (BCR) repertoire of SARS-CoV-2 S1 specific and bulk B cells

A&B) UMAP representation of integrated normalised RNA expression, grouped by immunoglobulin (Ig) subclass (A) or by the non-synonymous somatic hypermutation (SHM) frequency of the complementarity determining region (CDR) 3 of the heavy chain of B cells with paired BCR sequences.

C) The proportion of Ig subclasses within each of the predicted cell types in S1-specific (Ag) or background (CD45) B cells.

D-F) The mean non-synonymous CDR3 SHM frequency within predicted cell types (D), each Ig subclass (E) or combination of predicted cell type and Ig subclass (F) in S1-specific or background B cells. Error bars are per person standard error of mean.

G) Example clonal trees of expanded paired B cell clones. The number on each branch is the number of cells in the next branch of the tree. Ig subclass given. Associated with Table 6.2.

D-F) Benjamini-Hochberg adjusted FDR from Mann-Whitney U test is presented. For F, only FDR with value < 0.1 are presented.

compared to bulk IgG2 subclass memory B cells (**Fig. 6.8F).** Finally, I assessed the expansion of clones in the dataset (**Section 6.5.5**). In total, there were 23 B cell clones containing more than one B cell (**Table 6.3)**. The expanded clones were identified in only nine of 80 donors, all of which were in the LT, Cirr and RA clinical groups. Some clones included S-specific cells, or a mixture of cells detected in S-specific and bulk B cells **(Table 6.2, Fig. 6.8G)**. Most expanded clones were of memory phenotype, but a large number of the clones included naive phenotype B cells, and the majority were of IgM subclass **(Table 6.3)**.

6.6.6 Reduced class-switch recombination is associated with reduced antibody frequency and B cell functionality in renal and liver transplant recipients.

At the pre-V3 timepoint I used flow cytometry to identify a unique association of B cell frequency and vaccine-induced antibody responses in LT and RT compared to other immunocompromised groups and healthy controls, which suggested that LT and RT recipients had S-specific B cells with impaired functionality **(Fig. 5.16)**. This pattern was also observed at the V3+21d timepoint, whereby LT and RT had similar frequencies of S1-specific B cells compared with other immunocompromised groups, but exhibited a different pattern of association between S1-specific B cell frequency and anti-RBD Ig titres compared to the rest of the cohort **(Fig. 6.9A&B)**. Participants on aCD20 therapies had the lowest S1-specific B cell frequencies, also consistent with the pre-vaccine results **(Fig. 6.9A)**.

Having confirmed that the observations made using flow cytometry at pre-vaccine and V3+21d timepoints were consistent, I assessed the impact of SIs on the phenotype of bulk and S-specific B cells in the V3+21d scRNA-sequencing dataset. Within S-specific B cells, there was significant skewing of B cells toward a transcriptionally naive phenotype in LT and RT recipients compared with other individuals in the cohort (**Fig. 6.9C).** This was not observed in the bulk B cells (**Fig. 6.9C).** Differential gene expression of S-specific B cells from LT and RT compared with individuals in RA, IBD, Cirr (other group) demonstrated that several genes relating to BCR activation were downregulated in LT and RT B cells, including *CCL22* and

ZBTB32 (462) **(Fig. 6.9D)**. The downregulated genes were notably enriched for genesets associated with IL2 signalling, cell cycling and c-Myc related signalling – suggesting reduced proliferation and differentiation of LT and RT antigen-specific B cells (**Fig. 6.9D-F)**. LT and RT S-specific B cells were enriched for expression of *NIBAN3,* (B-cell novel protein-1) implicated in negative regulation of mature B cell activation (*463*), *CXCR4*, *CD79A* and *TCL1A* a proto-oncogene associated with naive B cells (*462*). Therefore S-specific B cells induced by vaccine in LT and RT groups are transcriptionally less differentiated and less active than those from other immunocompromised groups.

Across the entire dataset I observed that S-specific memory B cells were enriched for IgG1 expression compared to bulk B cells but still contained a large proportion of IgM^+ B cells (**Fig. 6.8C)**. On the basis that S-specific B cells in LT and RT were less differentiated than other groups, I reasoned that class-switch recombination of S-specific B cells may also be impaired. Consistent with this, LT and RT had similar frequencies of class-switched bulk memory B cells compared to other groups, but, unlike RA, IBD and cirrhosis groups or HC, there was no enrichment for class-switched Ig in the S-specific memory B cells compared to bulk memory B cells of LT and RT recipients (**Fig. 6.9G&H)**. Notably, within the S-specific B cells of LT and RT recipients (**Fig. 6.9H)** there appeared to be two distinct trajectories of class-switch recombination – one group that had increased class-switching in S-specific B cells compared to bulk B cells, and one group that had no relative increase in S-specific compared to bulk B cells. Interestingly, these groups broadly corresponded with V3+21d anti-RBD Ig responsiveness **(Fig. 6.9I).** Despite reduced class-switch recombination of memory B cells in LT and RT, SHM frequency was not reduced compared to other groups in either S-specific or bulk memory B cells (no significant differences, **Fig. 6.9J**). There were no specific demographic/clinical factors associated with an inability of RT and LT recipients to switch Ig sub-classes (**Fig. 6.9K)**. Thus, LT and RT recipients have impaired differentiation and class-switch recombination of memory B cells in response to vaccine, and this is associated with

Fig. 6.9 Low vaccine-induced antibody titres are associated with IgM+ S1-specific memory B cells in solid organ transplant recipients

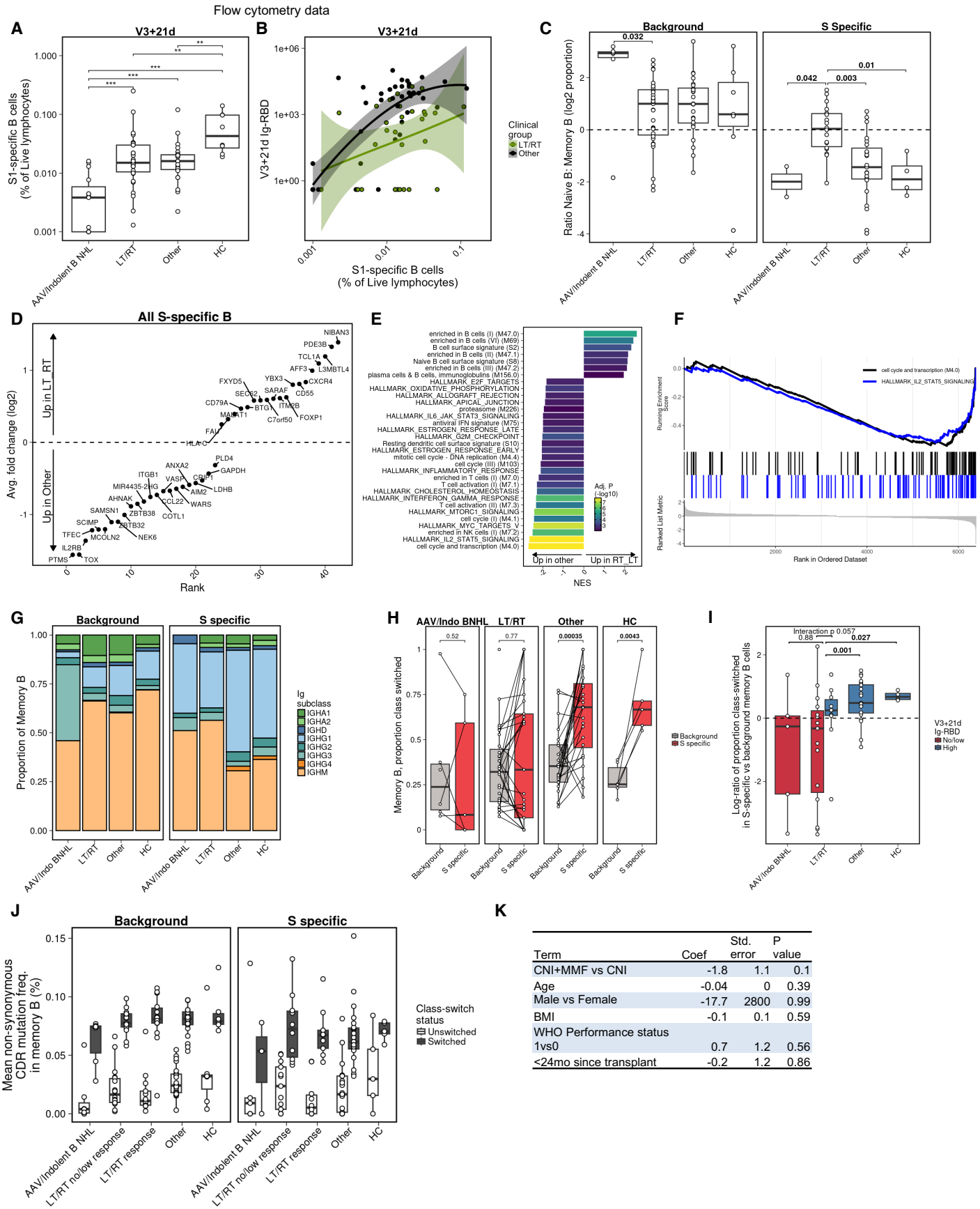

K

Term	Coef	Std. error	P value
CNI+MMF vs CNI	-1.8	1.1	0.1
Age	-0.04	0	0.39
Male vs Female	-17.7	2800	0.99
BMI	-0.1	0.1	0.59
WHO Performance status 1vs0	0.7	1.2	0.56
<24mo since transplant	-0.2	1.2	0.86

Fig. 6.9 Low vaccine-induced antibody titres are associated with IgM$^+$ S1-specific memory B cells in solid organ transplant recipients

A) Frequencies of S1-specific B cells captured in flow cytometry experiment at V3+21d

B) Loess curves of S1-specific B cell against V3+21d anti-RBD antibody response, separated by RT and LT compared with all other groups.

C) Log_2 ratio of predicted naive to memory B cell proportions amongst background and S1-specific B cells.

D) Differential gene expression analysis (MAST, age, sex and batch covariates) comparing all S1-specific B cells in LT and RT vs all other groups. Only significant genes (Bonferroni adjusted $p < 0.05$) shown.

E) Geneset enrichment analysis (GSEA) of ranked differentially expressed genes from comparison as in D. Normalised enrichment score (NES) shown.

F) Example running enrichment scores of cell cycle and transcription (M4.0) and HALLMARK_IL2_STAT5_SIGNALING genesets from E.

G) Immunoglobulin (Ig) subclass proportions of predicted memory B cells split by clinical groupings in background and S1-specific B cells.

H) Per person proportions of class-switched (IGHA1-2, IGHG1-4) and non-class-switched (IGHD and IGHM) background and S1-specific predicted memory B cells.

I) Log_2 ratio of the proportion of class-switched memory B cells in S1-specific compared to background memory B cells. P values are from linear model comparing LT and RT with other groups, including an interaction for V3+21d anti-RBD Ig responsiveness (<1000AU/mL versus >1000AU/mL) and age, sex and batch as covariates.

J) The mean non-synonymous complementarity determining region 3 (CDR3) somatic hypermutation rate (SHM) of background and S1-specific B cells in class-switched and non-class-switched B memory B cells. Mann-Whitney U test performed but there were no significant comparisons, so none are shown.

K) Linear model of log_2 ratio of the proportion of class-switched memory B cells in S1-specific compared to background memory B cells (as in I) within LT and RT recipients.

D-F) Benjamini-Hochberg adjusted FDR from Mann-Whitney U test is presented**.** Only FDR with value < 0.1 are presented.

reduced vaccine-induced antibody titres. Unlike aCD20 therapy recipients, the overall bulk B cell frequencies and phenotype was similar in LT and RT groups compared to other immunocompromised groups that generate robust antibody responses to vaccination. This suggests that the B cell deficiencies in LT and RT groups are intrinsic to the *de novo* response to vaccination.

6.6.7 The antigen specific CD4$^+$ T cell response to vaccine in immunocompromised individuals

In chapter 5 I identified that there were baseline differences in T cell immunophenotype which related to functional differences in vaccine-induced T cell responses. To gain further insight into the impact of SIs on antigen-specific T cells, I applied the AIM assay with scRNA- and TCR-sequencing to the V3+21d samples in the 80 individuals included in this chapter (**Fig. 6.10A&B)**. I used the same experimental procedure as in chapter 4 (**Section 2.4.1**). In total, 137,759 AIM$^+$ T cells were captured and passed scRNA-sequencing QC. As in chapter 4 (**Fig.**

4.2A), CD4+, CD8+, Vδ1 and Vδ2 γδT cells and mucosal-associated invariant T (MAIT) cell populations were captured. To make use of the paired unstimulated and stimulated SARS-CoV-2 spike-specific T cell scRNA-sequencing data, I subsetted CD4+ T cells from the CD45+ dataset and integrated them with the CD4+AIM+ T cells (**Fig. 6.10A&C)**.

Dimensionality reduction and unsupervised clustering of the integrated CD4+ T cell populations identified nine CD4+ T cell clusters (**Fig. 6.10C).** The clusters identified were similar to those identified in chapter 4 **(Fig. 4.2D)** and were annotated by expression of canonical CD4+ T cell lineage markers (**Fig. 6.10D).** The identified clusters included: a naive population (CD4_Naive), a resting Tcm population (CD4_Tcm), a relatively more active stem-cell memory like population (CD4_Tscm), an effector like interferon stimulated gene (ISG) high population (CD4_ISG), a regulatory T cell population expressing *FOXP3* and *IL2RA* (CD25) (CD4_Treg), an undifferentiated effector memory population (CD4_Tem), two differentiated effector memory populations including a T_H2-like population expressing *GATA3* (CD4_Th2) and a mixed T_H1/T_H17 effector population expressing *TBX21* (Tbet), *RORC*, *CCR6* (CD4_Th1_Th17) and a terminally differentiated population that expressed T_H1 and T_{FH}-type markers (*TBX21, CXCR5*; CD4_Th1_Tfh) **(Fig. 6.10C&D)**. Many of the populations contained a mixture of unstimulated (background) and AIM+ T cells except for the CD4_Th1_Tfh and CD4_Th1_Th17 populations which were each more than 99% AIM+ **(Fig. 6.10E&F)**. The CD4_Tcm and CD4_Naive populations were predominantly unstimulated **(Fig. 6.10E&F)**.

Having defined populations based on canonical CD4+ T cell genes, I next investigated genes commonly associated with CD4+ T cell function **(Fig. 6.10G)**. The Th1_Tfh and Th1_Th17 populations expressed most *IFNG* and *TNF* and the Th1_Tfh population was the only *IL2* expressing cell type observed **(Fig. 6.10G)**. Consistent with their lineage-defining markers, the Th1_Tfh population expressed *IFNG* and *IL21*, the Th1_Th17 population expressed *IFNG*, *IL17A*, *IL17F* and *IL22,* and the Th2 population expressed *IL13* but did not express *IL4* **(Fig. 6.10G)**. The chemokines *CCL3 and CCL4,* which are produced after TCR stimulation by CD4+

Fig. 6.10 Heterogenous vaccine-induced spike-responsive CD4+ T cells are detected in immunocompromised individuals

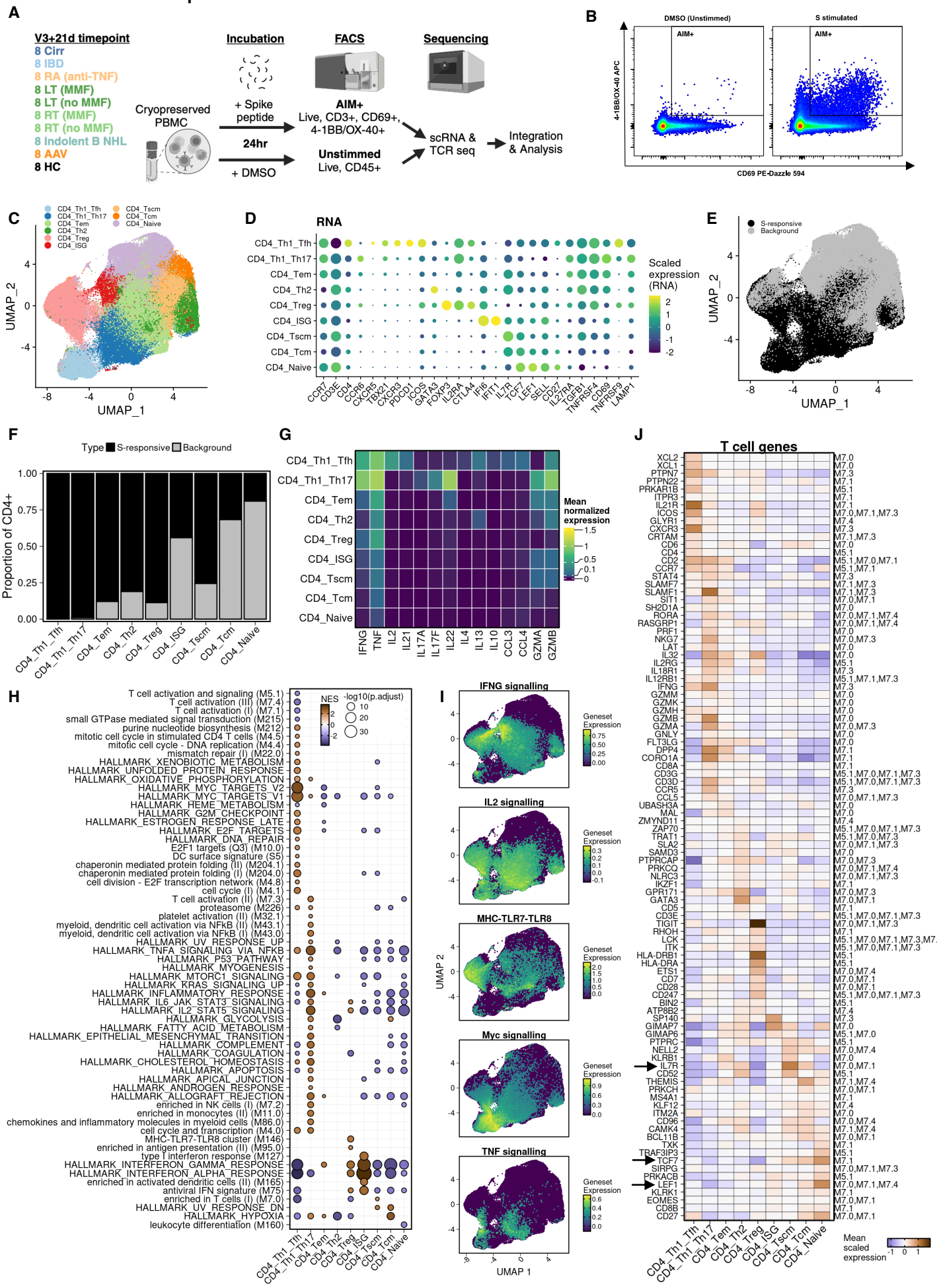

Fig. 6.10 Heterogenous vaccine-induced spike-responsive CD4⁺ T cells are detected in immunocompromised individuals

A) Experimental overview

B) Example gating of SARS-CoV-2 spike-peptide stimulated activation induced marker (AIM) positive cells for fluorescence-activated cell sorting (FACS). Gated on $CD3^+$ $CD45^+$ live lymphocytes.

C) UMAP representation of integrated RNA expression values from SARS-CoV-2 spike stimulated $CD4^+$ AIM^+ and background unstimulated $CD4^+$ T cells. Manually annotated Louvain clusters.

D) $CD4^+$ phenotypic markers used for manual annotation of C.

E) As in C, but grouped by experimental condition: unstimulated $CD4^+$ (background) or $CD4^+$ AIM^+ after spike-peptide pool stimulation (S-responsive).

F) Proportion of background and S-responsive cells per annotated cluster.

G) Mean log_2 normalised RNA expression of selected $CD4^+$ T cell functional genes

H) Geneset enrichment analysis of genes ranked based on log_2 fold change in given cluster compared to all other clusters.

I) Aggregate expression of given geneset projected onto UMAP visualization

J) Mean scaled RNA expression of genes from selected T cell related genesets in H. Geneset ID value is listed.

T cells to recruit naive $CD8^+$ T cells (*464*) were uniquely expressed by the Th1_Tfh population. Cytotoxic granules (granzyme A; *GZMA*, granzyme B; *GZMB*) were produced by most of the AIM^+ T cell populations, except for the CD4 T_{reg} population. Notably, as defined in chapter 4, the $CD4^+$ T_{reg} population did not express *IL10* and only low expression of *TNF* and *IFNG* transcripts were detectable in this population (**Fig. 6.10G)**.

Differential gene expression of each cluster versus all other clusters followed by geneset enrichment analysis identified several genesets that were characteristic of each cluster **(Fig. 6.10H)**. The CD4_Th1_Tfh population was positively enriched for genesets relating to c-Myc signalling, proliferation and metabolism, but was negatively enriched for some T cell activation associated genesets (**Fig. 6.10H&I)**. The CD4_Th1_Th17 cluster was notably enriched for cytokine signalling pathways, including IL2, IL6 and NFκB signalling through TNF (**Fig. 6.10H&I)**. The CD4_Tem and CD4_Th2 cell types were enriched for comparatively few genesets, likely due to their relatively less transcriptionally active/differentiated states. The CD4_T_{reg} population was positively enriched for genes relating to MHC, TLR7 and TLR8, antigen-presentation and IFNG signalling (**Fig. 6.10H&I)**. CD4_Tscm, CD4_Tcm and CD4_Naive populations had notably lower expression of cytokine signalling related pathways, indicative of their lack of differentiation.

Interestingly, there were unique enrichment patterns for T cell activation/differentiation related genesets across different cell types (**Fig. 6.10H)**. To gain further insight into the contributing genes in each enrichment, I assessed the mean expression of the genes within each geneset across the clusters. There was considerable overlap in the genes included in each geneset, but this method identified clear differences in T cell related gene expression across the clusters (**Fig. 6.10J)**. There was a gradient of differentiation and effector functionality, whereby cells in the CD4_Th1_Tfh and CD4_Th1_Th17 cluster had highest expression of several genes associated with $CD4^+$ T cell cytotoxicity and TCR activation and CD4_Tcm, CD4_Tscm and CD4_Naive clusters exhibited expression of genes relating to early activation and naivety (*LEF1*, *IL7R*, *TCF7*) (**Fig. 6.10J)**.

6.6.8 The vaccine-induced AIM^+ T cell phenotype is functionally associated with the vaccine-induced IFNγ ELISpot response

To better understand how the populations captured in the AIM assay relate to a common functional T cell assay for vaccine immunogenicity studies – the IFNγ ELISpot – I assessed the association of AIM^+ $CD4^+$ T cell frequencies and function in 65 of 72 individuals in OCTAVE DUO with paired V3+21d IFNγ ELISpot data. There was a moderate positive correlation (Spearman's ρ= 0.48) between the overall frequencies of AIM^+ $CD3^+$ T cells detected by flow cytometry and IFNγ ELISpot magnitudes (**Fig. 6.11A)**. Within the AIM^+ $CD4^+$ cell subsets, there was weak positive correlation of CD4_Tem and CD4_Th1_Th17 frequencies with IFNγ T cell magnitudes, which corresponded with negative correlation in the CD4_Tscm and CD4_Naive populations **(Fig. 6.11B).** These reciprocal compositional changes suggest a possible differentiation trajectory relating to IFNγ production between naive, Tscm, Tem and Th1_Th17 populations.

Correlation analysis of pseudobulk geneset expression values for each cell type identified a number of functional programmes that were significantly correlated between the AIM^+ populations and IFNγ ELISpot magnitudes (**Fig. 6.11C)**. Various genesets related to IFNγ

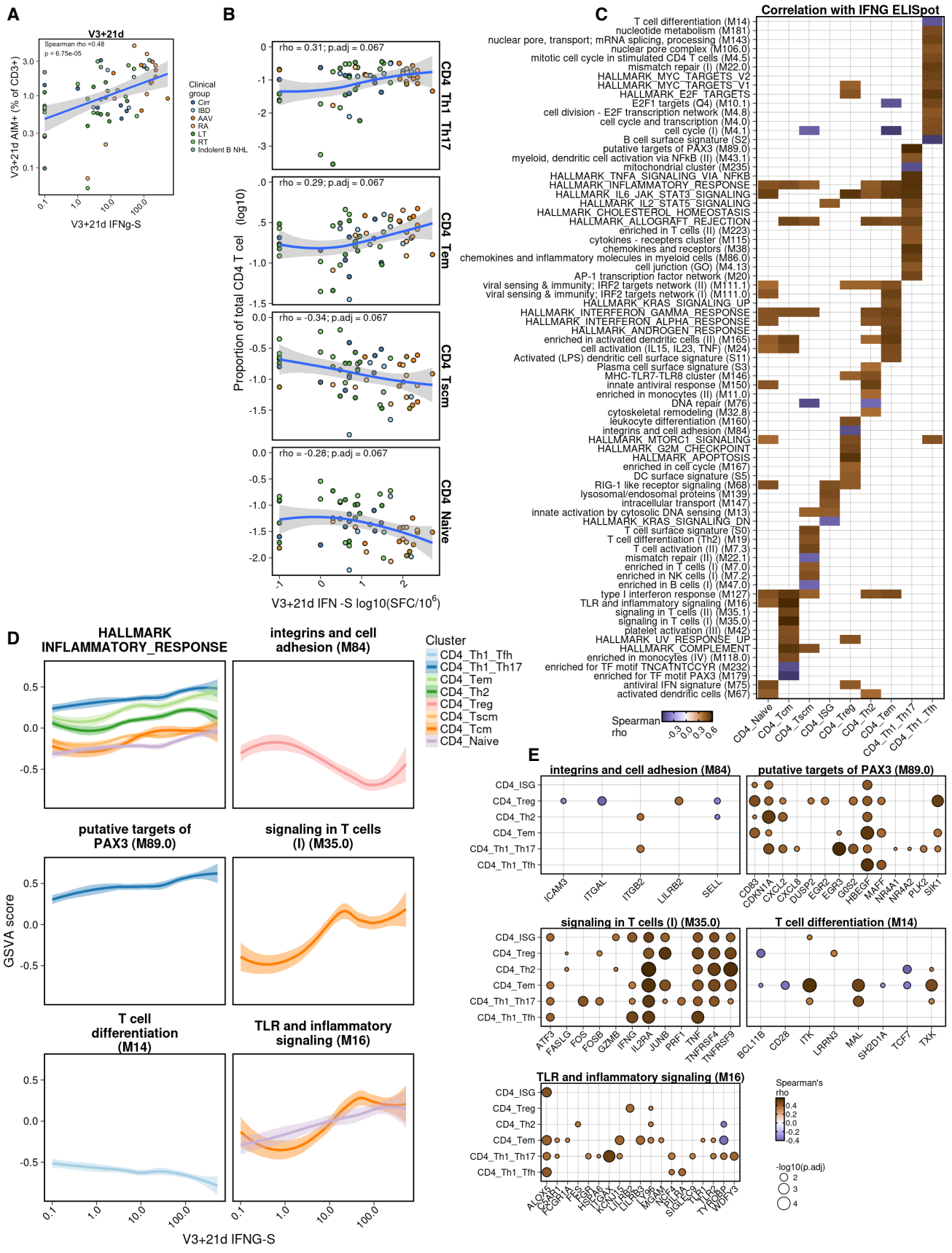

Fig. 6.11 AIM⁺ CD4⁺ T cells are associated with IFNγ ELISpot magnitudes

A&B) Correlation of V3+21d AIM⁺ CD3⁺ T cells (A) and CD4⁺ AIM⁺ subpopulations with (B) V3+21d IFNγ T cell responses to peptide pools covering SARS-CoV-2 spike. Only correlations with Benjamini-Hochberg false discovery rate < 0.1 shown.

C) Correlation of the geneset variation analysis (GSVA) score of each geneset within AIM⁺ CD4⁺ T cell clusters with V3+21d IFNγ T cell responses. Spearmans correlation, only correlations with Benjamini-Hochberg false discovery rate < 0.05 shown.

D) Association of selected geneset expression scores (from C) with V3+21d IFNγ T cell responses.

E) Mean expression of each gene within the genesets in D, correlated with V3+21d IFNγ T cell responses. Only correlations with Benjamini-Hochberg false discovery rate < 0.05 shown.

signalling were significantly correlated with IFNγ ELISpot magnitudes across multiple AIM$^+$CD4$^+$ cell types, including transcriptionally naive AIM$^+$ T cells with relatively low overall inflammatory signalling (**Fig. 6.11C&D)**. As expected, expression of HALLMARK_INTEFERON_GAMMA and HALLMARK_INFLAMMATORY_RESPONSE genesets correlated with IFNγ ELISpot across multiple cell types. The geneset expression in AIM$^+$ T cells that was most significantly correlated with IFNγ ELISpot responses was: '*putative targets of PAX3 (M89.0)'* in CD4_Th1_Th17, '*signaling in T cells (I) (M35.0)'* and '*TLR and inflammatory signaling (M16)'* in CD4_Tcm (each with Spearman's ρ = 0.63, FDR < 0.0001) (**Fig. 6.11C&D).** Interestingly, the Th1_Tfh population appeared to be distinctly related to IFNγ ELISpot responses compared to the rest of the AIM$^+$ populations: unlike the other *IFNG* producing population (Th1_Th17), its overall frequency was not associated with IFNγ ELISpot magnitudes (**Fig. 6.11B**) and instead within the Th1_Tfh population expression of genesets related to proliferation and metabolism were most correlated with IFNγ ELISpot responses (**Fig. 6.11C)**. The expression of some genesets was negatively associated with IFNγ ELISpot response, including *'T cell differentiation (M14)'* in Th1_Tfh and '*integrins and cell adhesion (M84)'* expression in CD4_Treg cells (**Fig. 6.11C&D)**.

Further correlation analysis of the mean expression of each gene within the given genesets identified specific genes whose expression was significantly correlated with IFNγ ELISpot response. In particular, expression of *IL2RA, IFNG, TNF, TNFRSF4* (OX-40) and *TNFRSF9* (4-1BB) in the '*signaling in T cells (I)'* geneset was significantly correlated with IFNγ ELISpot response (**Fig. 6.11E)**. *HBEGF,* a gene upregulated early after CD4$^+$ T cell activation which reduces T_H17 differentiation in favour of T_H1 differentiation (*465*) was significantly associated with IFNγ ELISpot response (**Fig. 6.11E)**.

6.6.9 The effect of immunosuppressive conditions on spike-responsive CD4$^+$ T cell phenotype and functionality.

Having identified functionally relevant features of the CD4$^+$ AIM$^+$ T cells, I next compared their

phenotype across SIs. The frequencies of AIM+ T cells varied by clinical group but were unexpectedly low in the healthy control individuals (**Fig. 6.12A)**. Compared to the background unstimulated CD4+ T cell phenotypes, Th1_Th17, Th1_Tfh, Tem and T_{reg} populations were significantly increased in proportion in the AIM+ CD4+ T cells, whereas naive, ISG and Tcm populations were significantly decreased (**Fig. 6.12B)**. This was broadly consistent across groups (**Fig. 6.12B)**, however the proportions of CD4+ AIM+ T cell subtypes varied by clinical group (**Fig. 6.12C)**. The cell type with the most significant difference in proportion across AIM+ CD4+ T cells was the naive CD4+ population which was highest in the LT and RT groups. CD4_ISG and CD4_Tregs had the next largest difference between groups, with CD4_ISG being particularly enriched in IBD and HC and a notably low frequency of CD4_Tregs in the RT group (**Fig. 6.12C).**

I next compared the functionality of the clusters between clinical groups using pseudobulk geneset expression. Using an ANOVA-like test controlling for age, sex and batch as covariates, I identified a large number of genesets that were significantly different across groups in each cluster (**Fig. 6.12D&E)**. In particular, genesets relating to interferon, TNF and IL2 signalling were amongst the most significantly differently expressed across Th1_Th17, Tem, Th2, Tscm, Tcm and naive AIM+ CD4+ T cell populations (**Fig. 6.12E)**. The differences in expression of these genesets were broadly consistent with the patterns identified in the IFNγ ELISpot data **(Fig. 5.12G)**: there was high expression of cytokine signalling genesets in activated T cells in the AAV, RA and IBD groups which had high IFNγ ELISpot responses and low expression of these genesets in LT, RT and Cirrhosis patient groups that were enriched for vaccine IFNγ non-responsiveness (**Fig. 6.12E)**. Interestingly, as well as having increased frequencies of phenotypically naive AIM+ CD4+ T cells, the naive T cells in LT and RT were also significantly less transcriptionally active in terms of T cell and cytokine signalling compared to the other groups (**Fig. 6.12E)**. The low frequencies of AIM+ T cells (**Fig. 6.12A)** and relatively low

Fig. 6.12 Distinct patterns of inflammatory signaling in vaccine-induced spike-responsive CD4+ T cells across immunosuppressive conditions

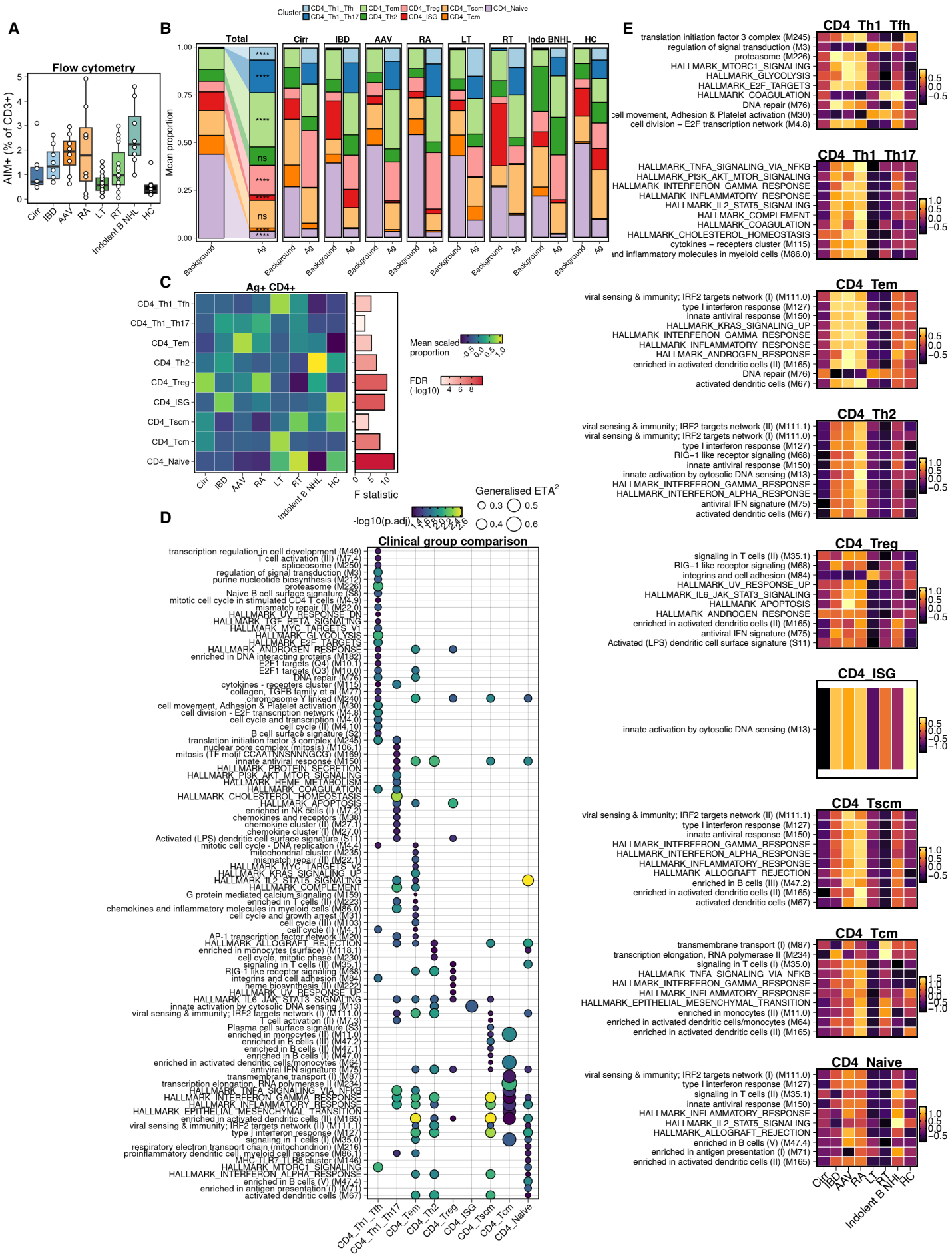

Fig. 6.12 Distinct patterns of inflammatory signaling in vaccine-induced spike-responsive CD4⁺ T cells across immunosuppressive conditions

A) AIM⁺ CD3⁺ T cell frequencies in different immunosuppressive conditions

B) The composition of unstimulated (background) CD4⁺ T cells and SARS-CoV-2 spike responsive AIM⁺ CD4⁺ T cells (Ag). Statistical comparisons are EdgeR paired comparisons of composition. **** is false discovery rate of <0.0001.

C) Mean scaled proportion of SARS-CoV-2 responsive AIM⁺ CD4⁺ T cell subsets. Statistical comparison is EdgeR quasi-likelihood F test comparing differential frequency across clinical groups, including age, sex and batch as covariates. All comparisons are FDR < 0.05.

D) ANOVA test of differential expression of geneset variation analysis scores for each cell type, comparing across clinical groups, including age, sex and batch as covariates. Only comparisons with FDR < 0.05 are shown.

E) Mean scaled GSVA expression values for top 10 differentially expressed genesets in each cluster (as in D).

expression of activation related genesets (**Fig. 6.12E)** suggested that the PBMC samples from healthy control samples in this study were of too low quality to accurately study T cell functionality. Unlike the PBMC in the OCTAVE DUO study, healthy control PBMC were stored in suboptimal conditions (-80°C rather than liquid nitrogen) for a long duration of time, likely leading to this reduction in quality (*466*). Nevertheless, there were clear differences across the cohort in the functionality of the AIM⁺ T cells, in a manner consistent with alternative measures of vaccine-induced T cell functionality.

6.6.10 Expanded T cell clones span across the spectrum of T cell differentiation

The AIM⁺ and IFNγ ELISpot correlation analysis suggested that there was a pathway of differentiation within the AIM data that was related to IFNγ production. Expansion and differentiation of CD4⁺ T cells clones is central to their functionality (*467*), therefore I next assessed if expanded TCR clones could be tracked across this differentiation trajectory. As in healthy individuals after one and two doses of COVID-19 vaccines (**chapter 4**), the majority of CD4⁺ AIM⁺ T cells were not measurably expanded (**Fig. 6.13A).** However, compared to non-antigen enriched CD4⁺ T cells there was evidence of expansion in CD4⁺ AIM⁺ T cells in all diseases, with the lowest proportion of expanded clones observed in LT and AAV groups (**Fig. 6.13A)**. Analysis of clonal sharing across cell types identified that the majority of expanded clones in the Th1_Th17, Th2, Tem, Tscm, ISG^{hi}, Tcm and naive CD4⁺ AIM⁺ populations were shared between cell types (**Fig. 6.13B)**. The T_{reg} and Th1_Tfh population were more clonally

distinct, with the majority of expanded clones in those populations not shared with other cell types (**Fig. 6.13B)**. Notably, the cell types with the highest proportion of shared clonotypes was Tscm and Tem and Tem and Th1_Th17, suggesting a trajectory of expansion and differentiation within clones (**Fig. 6.13B)**. To investigate whether the clones were shared between more than two cell types, I investigated the phenotype of all hyperexpanded clones (>10 identical paired $\alpha\beta$TCR amino acid sequences). 15 individuals had hyperexpanded clones, and one individual (patient 92) had 21 unique hyperexpanded clones (**Fig. 6.13C)**. In most individuals with hyperexpanded clones, there was a clear pattern of clonal expansion across the Tscm, Tem and Th1_Th17 (e.g., patient 9, or 218). Others had distinct hyperexpanded clones solely within T_H2, T_{reg} or Th1_Tfh cell types (e.g., patient 569) (**Fig. 6.13C)**.

6.6.11 The pseudotime trajectory of individuals with poor T cell vaccine responsiveness is altered

Evidence of clonal expansion across clusters suggests that the captured T cells maybe at a different point of differentiation along a given trajectory. To assess if this was the case, I used transcriptomic data to fit pseudotime trajectories across the $CD4^+$ AIM^+ T cells clusters that had evidence of clonal sharing (**Fig. 6.14A)**. Using naive $CD4^+$ T cells as the root of the pseudotime, there was a clear difference in the distribution of cells across pseudotime in groups enriched for poor vaccine responsiveness (RT, LT and Cirr) compared to the rest of the cohort (**Fig. 6.14B).** The majority of the cells in the RT, LT and cirrhosis groups appeared early in the pseudotime trajectory, coinciding with naive and Tscm annotations, compared to the other groups in the cohort (**Fig. 6.14B)**. This was particularly notable in RT, LT and cirrhosis patients with no IFNγ T cell response to vaccination.

To identify genes associated with this reduced differentiation, I first identified genes which were significantly correlated with the pseudotime trajectory (**Fig. 6.14C).** In total, 2076 of 3000

Fig. 6.13 Hyperexpanded T cell clones are shared across a CD4+ T cell trajectory

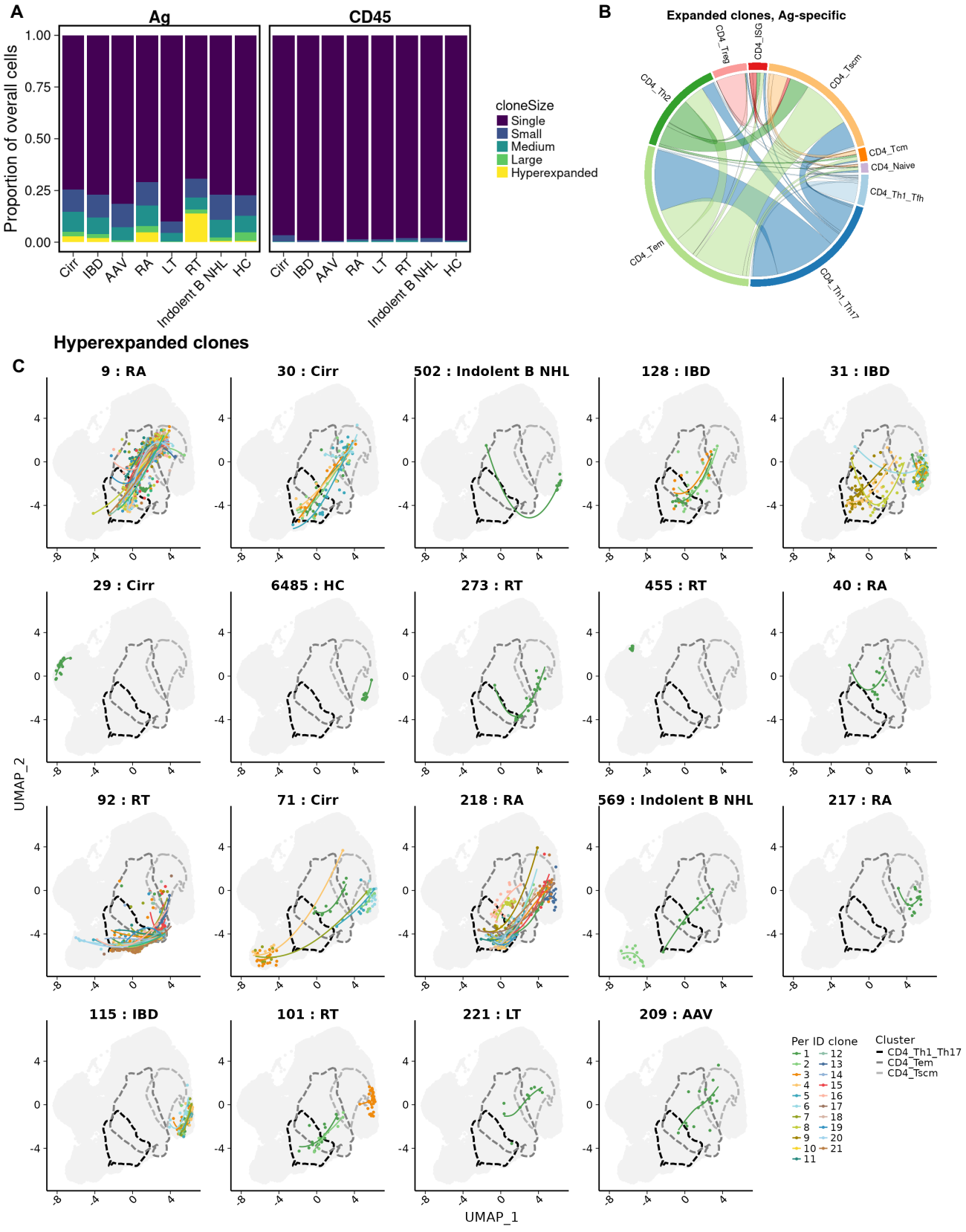

Fig. 6.13 Hyperexpanded T cell clones are shared across a CD4⁺ T cell trajectory

A) The proportion of paired αβ TCR clones of given expansion sizes within individuals within AIM⁺ CD4⁺ T cells. Single = 1 clone, Small = 2 identical clones, Medium = 3-5 identical clones, Large = 6-10 identical clones, Hyperexpanded >10 identical clones.

B) Sharing of expanded SARS-CoV-2 responsive CD4⁺ T cell clones (clone size >1) across transcriptional phenotype. Chord sizes reflect the relative proportion of each cluster that has shared clones.

C) Visualisation of cells within hyperexpanded clones on the CD4⁺ AIM⁺ RNA UMAP representation. Hyperexpanded clones are unique to each donor and coloured individually. Each donor and the clinical group they are part of is labelled above each panel. Outlines of CD4_Th1_Th17, CD4_Tem and CD4_Tscm were generated from 2-dimensional density statistics. Loess curves were generated on the UMAP coordinates for cells within each clone.

variable genes were significantly associated with the pseudotime trajectory. The top 100 genes most associated with the pseudotime trajectory included genes related to T cell activation (e.g: *IL2RA*, *TNFRSF9*, *TNFRSF18, CD40LG*), cytotoxicity (e.g. *GZMB, GZMA),* cytokine production (*IFNG, TNF, IL22, LTB)* and interferon stimulated genes (*IFIT1, IFIT2, IL1B, IFITM)* (**Fig. 6.14C)**.

I next assessed if the relationship between gene expression and pseudotime was altered in the RT, LT and cirrhosis groups compared to the other groups in the dataset (**Section 6.5.6**). In total, 50 genes were significantly differentially associated with pseudotime in RT, LT and cirrhosis groups compared to the rest of the cohort (**Fig. 6.14D).** Clustering of these genes based on their expression across the dataset identified five clusters of genes with shared expression and two independently associated genes (**Fig. 6.14D)**. The clusters included two enriched for interferon stimulated genes (Cluster 3&7) which were consistently significantly reduced across pseudotime in the RT, LT and cirrhosis group compared to other groups (**Fig. 6.14D&E)**. This included *IL2RA* (CD25), an important activation marker on T cells (*468*). *MCM6,* a gene associated with cell cycle regulation regulated by E2F (*469*) was increased in expression in RT, LT and Cirrhosis patients across the pseudotime trajectory. Cluster one contained lymphotoxin-α (*LTA*), a TNF family cytokine (*470*), and genes relating to NFκB signalling (*TNFAIP3 (471), MIR155HG* (miR-155) (*472*)) which were increased in RT, LT and cirrhosis compared to other groups **(Fig. 6.14D)**. Cluster four included integrin alpha-4 (*ITGA4*, CD49d)

Fig. 6.14 Pseudotime trajectory of SARS-CoV-2 responsive CD4+ T cells reveals impaired signalling pathways in solid organ transplant recipients and cirrhosis patients

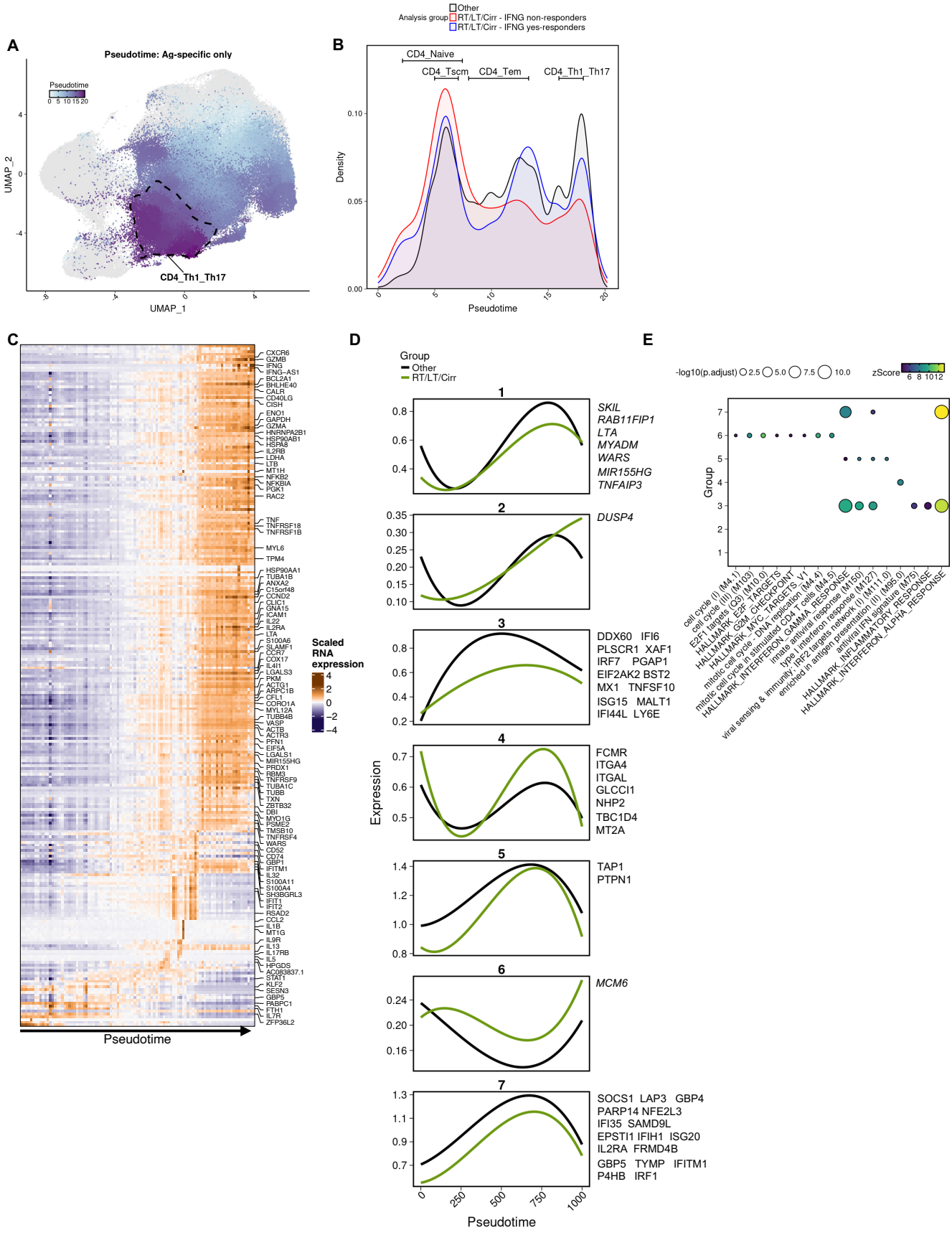

Fig. 6.14 Pseudotime trajectory of SARS-CoV-2 responsive CD4+ T cells reveals impaired signalling pathways in solid organ transplant recipients and cirrhosis patients

A) UMAP dimensional reduction of all CD4+ T cells, with pseudotime trajectory generated only in AIM+ T cells with CD4_Th1_Tfh and CD4_Treg clusters removed. A node within phenotypically naive AIM+ T cells was used as the root of the trajectory.

B) Density of AIM+ cells across pseudotime trajectory in clinical groups and based on V3+21d IFNγ T cell responsiveness (<1SFC/10^6 peripheral blood mononuclear cells) to peptide pools covering SARS-CoV-2 spike. The interquartile range of the pseudotime for each of the annotated AIM+ CD4+ T cell clusters is labelled.

C) The scaled RNA expression of the top 250 genes with expression that significantly associated with pseudotime distance (Morans I value, **Section 6.5.6**). The top 100 most associated genes are labelled. The expression is the mean RNA expression of cells within 100 pseudotime bins.

D) Loess curves of mean expression of clusters of genes that were differentially expressed in RT, LT and cirrhosis patients compared to other individuals with respect to pseudotime (derived from Lamian package, **Section 6.5.6**). Constituent genes of each cluster are labeled.

E) Geneset enrichment of genes within each module compared to the 3000 variable genes included in the Lamian analysis. Only genesets with FDR <0.05 are shown.

and integrin alpha ligand (*ITGAL*, CD11A) which are important for T cell trafficking and interaction with antigen-presenting cells (*473, 474*) and were reduced on more differentiated cells in the LT, RT and cirrhosis groups **(Fig. 6.14D)**.

In conclusion, SARS-CoV-2 spike responsive CD4+ T cells in LT, RT and cirrhosis are less differentiated and have different gene expression programmes compared to other individuals, including reduced interferon signalling and integrin expression.

6.6.12 The antigen specific CD8+ T cell response to vaccine in immunocompromised individuals

In addition to CD4+ T cells, unconventional T cells, including MAIT, Vδ1 and Vδ2 $\gamma\delta$T populations, and conventional CD8+ T cells were identified in background and AIM+ conditions (**Fig. 6.15A&B)**. As described in chapter 4, the unconventional T cells likely represent bystander activated cells that are not directly SARS-CoV-2 peptide responsive. Therefore, I next focussed on the analysis of conventional CD8+ T cells. A total of 17,045 background and AIM+ CD8+ T cells were captured and passed QC. Louvain clustering with manual annotation based on canonical T cell marker expression identified six conventional CD8+ T cell populations in the integrated background and AIM+ datasets, including a naive population (CD8_Naive); resting central and effector memory (CD8_Tcm, CD8_Tem) and ISG^{hi} effector

memory populations (CD8_Tem_ISG) and early and late activated CD8+ effector populations (CD8_Early_Active, CD8_Tem_Active) (**Fig. 6.15C-E)**. The early and late activated effector populations were enriched for AIM+ CD8+ T cells (CD8_Early_Active: 2006 of 2692 cells; 74.5%, CD8_Tem_Active 2056 of 2066 cells; 99.5%) **(Fig. 6.15D&E)**.

Compared to other AIM+ CD8+ T cell populations, the early activated CD8+ effector population was enriched for genesets relating to TNF signalling and cellular activation (**Fig. 6.15F)**. The late activated effector CD8+ population was also enriched for TNF signalling, but additionally IL-2, cell-cycling and T cell signalling pathways (**Fig. 6.15G)**. The resting populations were less distinct and enriched for few genesets overall (**Fig. 6.15F)**. Because the T and NK cell related genesets were differentially expressed across the populations, I assessed the expression of the genes within these genesets across the cell subsets. The CD8+ late active population expressed several genes related to CD8+ T cell cytotoxicity, including *PRF1, GZMB* and *GZMH* (but not *GZMA*), effector cytokine and cytokine receptor genes such as *IFNG, TNF, IL2RB, IL12RB1, IL21R, IL18R1* and chemokines and chemokine receptor genes *XCL1, XCL2, CCR5, CXCR3* (**Fig. 6.15G).** Thus, this population represents a highly activated effector CD8+ population. Consistent with the high expression of *IFNG* transcript in the CD8_Tem_Active population, an increased proportion of this cell type compared to the less activated CD8_Early_Active population was significantly correlated with increasing V3+21d IFNγ ELISpot magnitudes (**Fig. 6.15H)**.

6.6.13 The effect of immunosuppressive conditions on spike-responsive CD8+ T cell phenotype and functionality

I next assessed the composition of background and AIM+ CD8+ T cells across SIs. Due to the low quality of healthy control AIM+ T cells observed in the S-specific CD4+ T cell data, comparisons were made between immunosuppressive groups. AAV patients had the highest frequencies of AIM+ CD8+ T cells relative to background CD8+ T cells of all groups, especially compared to LT, RT and cirrhosis patients which had

Fig. 6.15 Spike-responsive and background CD8+ T cells have distinct phenotypes

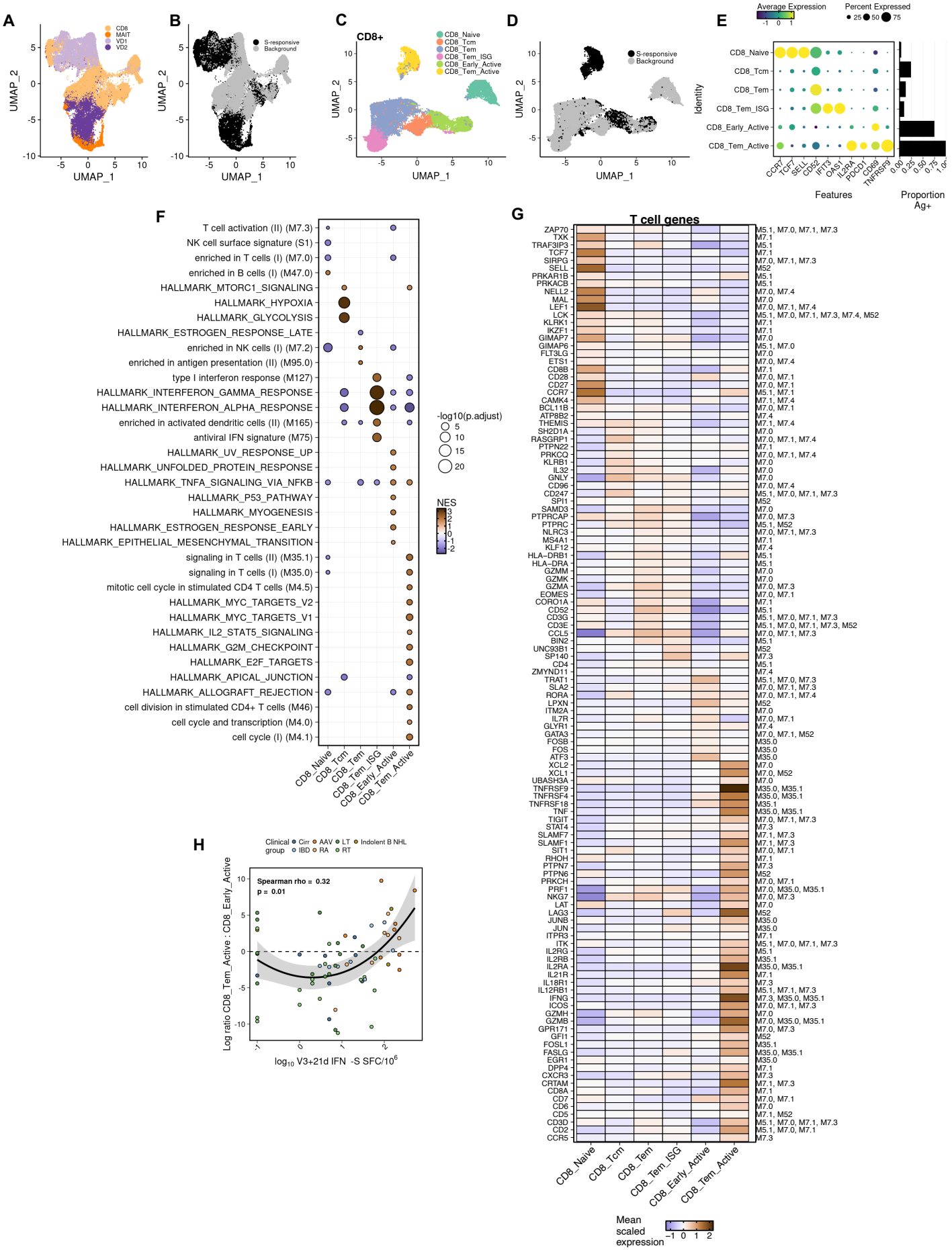

Fig. 6.15 Spike-responsive and background CD8⁺ T cells have distinct phenotypes

A&B) UMAP representation of integrated background and SARS-CoV-2 spike responsive (S-responsive) unconventional and conventional CD8⁺ T cells. Grouped by broad manual annotation (A) or experimental condition (B).

C&D) UMAP representation of integrated CD8⁺ T cells grouped by manually annotated Louvain clustering (C) or experimental condition (D).

E) Selected RNA values used for manual annotation (right panel) and the proportion of each cluster that is from the S-responsive condition (left panel, related to D).

F) Geneset enrichment analysis of genes ranked based on log fold change in given cluster compared to all other clusters.

G) Mean scaled RNA expression of genes from selected T cell related genesets in F. Geneset ID value is listed.

H) Correlation between the log_2 ratio of AIM⁺ CD8⁺ Tem_Active compared to AIM⁺ CD8⁺ Early_Active proportions with V3+21d IFNγ T cell responses to peptide pools covering SARS-CoV-2 spike.

reduced relative frequencies (FDR; LT = 0.027, RT = 0.059, cirrhosis = 0.066) (**Fig. 5.16A)**. All CD8⁺ T cell subpopulations had significantly different proportions in the AIM⁺ condition compared to the background condition: the early and late active populations were significantly increased in proportion and all other populations were significantly decreased (**Fig. 5.16B)**. Within AIM⁺ populations, AAV patients had highest frequencies of highly activated effector populations compared to early active CD8⁺ T cells of all immunocompromised groups, especially compared to RT and cirrhosis (FDR; RT = 0.005, cirrhosis = 0.045) (**Fig. 5.16B&C).** Therefore, AAV recipients have increased total frequencies of spike-responsive CD8⁺ T cells and they are of a more highly activated phenotype than other immunocompromised groups – especially LT, RT and cirrhosis groups.

To further assess the impact of SIs on SARS-CoV-2 spike-responsive CD8⁺ T cells, I compared geneset expression profiles within the AIM⁺ CD8⁺ T cell clusters. Clear patterns of differential expression emerged with two groupings: 1) individuals in the IBD, AAV and RA groups were similar, and 2) individuals in the LT, RT, cirrhosis and indolent B NHL groups had similar expression patterns within cell types (**Fig. 5.16D)**. Individuals in IBD, RA and AAV groups had significantly higher expression of genes relating to T cell proliferation and metabolism in the CD8_Tem_Active cluster compared to LT, RT, cirrhosis and indolent B NHL. In the CD8_Early_Active cluster individuals in the IBD, RA and

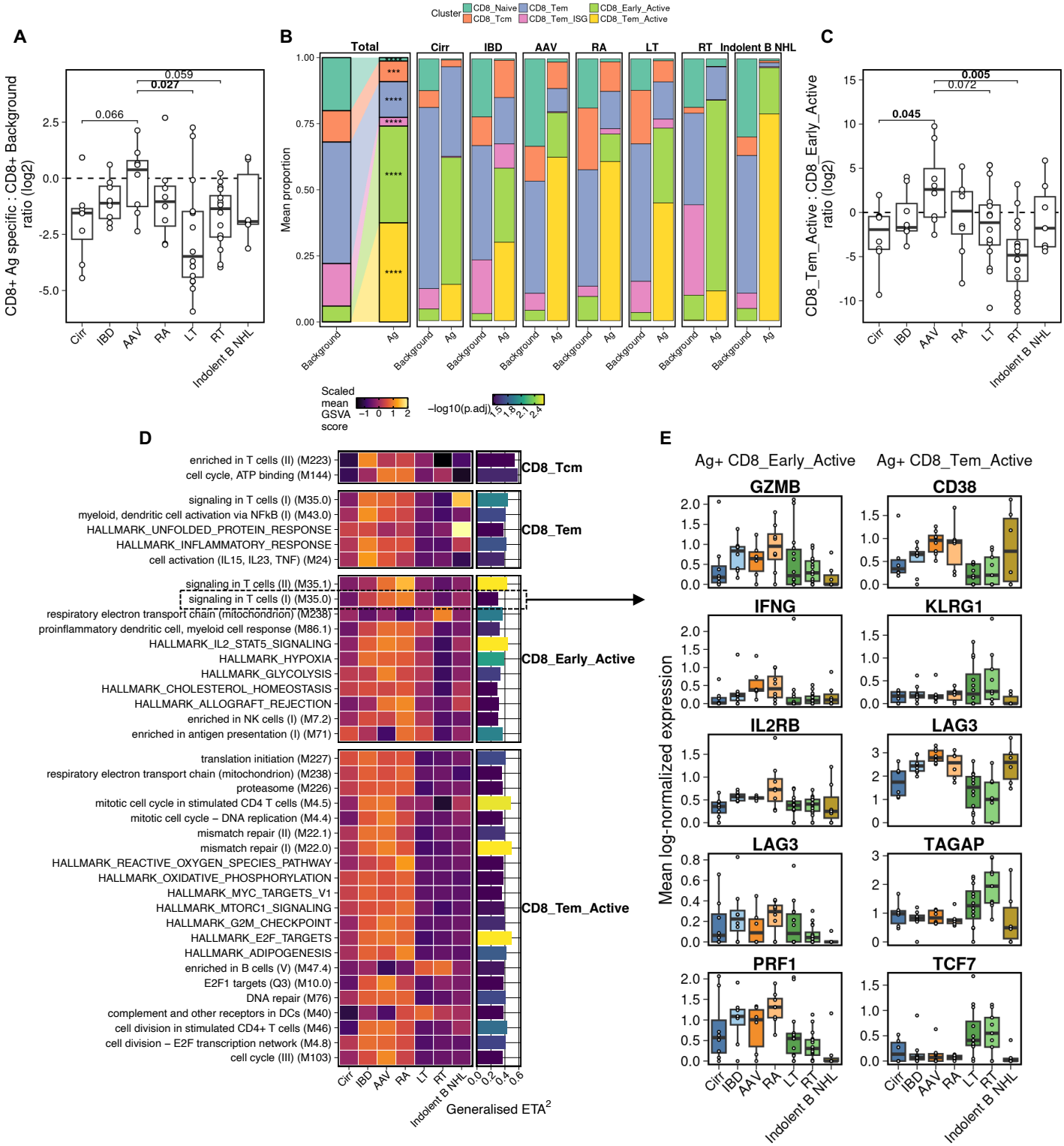

Fig. 6.16 Distinct patterns of inflammatory signaling in spike-responsive CD8⁺ T cells after vaccination in different immunosuppressive conditions

A) Log_2 ratio of spike-responsive CD8⁺ T cells to background CD8⁺ T cells amongst all CD8⁺ T cells. False discovery rate values from Benjamini-Hochberg corrected Mann-Whitney U test, only FDR < 0.1 is shown.

B) The composition of unstimulated (background) CD8⁺ T cells and SARS-CoV-2 responsive AIM⁺ CD8⁺ T cells (Ag). Statistical comparisons are EdgeR paired comparisons of composition. **** is false discovery rate of <0.0001.

C) Log_2 ratio of spike-responsive CD8⁺ Tem active to spike-responsive CD8⁺ early active populations across clinical groups. False discovery rate values from Benjamini-Hochberg corrected Mann-Whitney U test, only FDR < 0.1 is shown.

D) Mean scaled expression of all genesets with significant difference (FDR <0.05) between clinical groups, measured by ANOVA including age, sex and batch as covariates. ETA^2 effect size an test significance depicted.

E) Mean RNA expression values for selected genes in the 'signaling in T cells (I) (M35.0)' geneset in AIM⁺ CD8⁺ T cell populations.

AAV groups had higher expression of T cell signalling, IL2 and NK-functionality related genesets (**Fig. 5.16D)**. Underlying the differential expression of these genesets was the differential expression of several important genes related to T cell functionality (**Fig. 5.16E).**

6.6.14 Distinct populations of exhausted SARS-CoV-2 specific CD8+ T cells in solid organ transplant recipients

The evidence of such distinct gene expression patterns within the active effector cluster between immunosuppressive groups suggested that there were broad differences in the T cell signalling programmes within the cluster. To assess if there were possible subclusters of cells within clusters, I used MiloR which detects differential abundance of sub-cluster cell neighbourhoods (**Section 6.5.7**). There were two clear groups of neighbourhoods within the CD8_Tem_Active cluster, one positively enriched for LT and RT recipients and one negatively enriched (**Fig. 6.17A)**. Sub-clustering of the CD8_Tem_Active cluster using Louvain clustering identified three distinct populations, including one which included almost all CD8_Tem_Active cells in the RT and LT groups (LT = 398 of 432 CD8_Tem_Active cells; 92%, RT = 87 of 106 CD8_Tem_Active cells; 82%) and was predominantly composed of cells from LT and RT recipients (85%) (**Fig. 6.17B&C)**. Differential gene expression analysis between the LT and RT enriched cluster (cluster 2) and the other CD8_Tem_Active clusters identified a large number of significantly differentially expressed genes (3882 genes) between clusters (**Fig. 6.17D)**. This included a number of T cell signalling related genes. Notably, the LT and RT enriched cluster was enriched for expression of transcription factors *TCF7*, *EOMES* and had downregulated *MYC* expression (**Fig. 6.17D)**. This, alongside expression of *CD96* and *TIGIT* and reduced expression of cytotoxic and cytokine genes *IFNG, GZMB* and *PRF1* and cell cycling genesets **(Fig. 6.17D&E),** suggest the active CD8 populations have a more exhausted phenotype in LT and RT compared to other immunosuppressive groups (*475-478*). All clusters in the CD8_Tem_Active cluster had elevated expression of inhibitory markers *PDCD1* (PD-1), and *CTLA4,* but unlike other the other cell types the LT and RT related cluster did not have

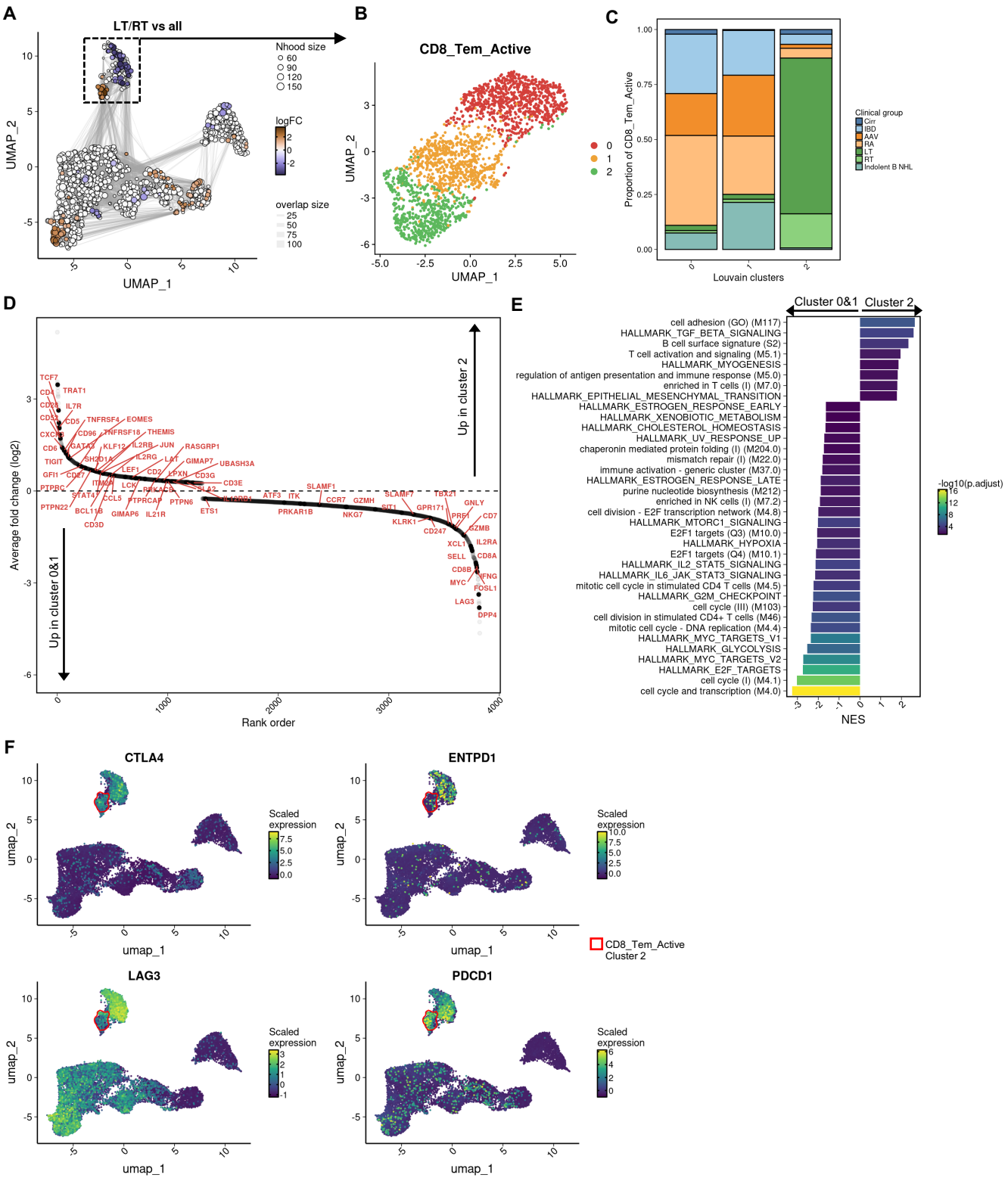

Fig. 6.17 Unique highly active SARS-CoV-2 specific CD8⁺ T cell phenotype in response to mRNA vaccine in solid organ transplant recipients

A) MiloR differential abundance analysis of LT and RT versus all other groups (Section 6.6.6). Sex, Age and batch included as covariates.

B) Louvain clustering of AIM⁺ CD8_Tem_Active cluster.

C) Proportion of clinical phenotypes within each CD8_Tem_Active Louvain sub-cluster

D) Differential gene expression analysis (MAST, age, sex and batch as covariates) comparing CD8_Tem_Active Louvain sub-cluster 2 with sub-clusters 0 and 1. Only significant genes are shown, and only genes in T cell related genesets are labelled.

E) Geneset expression analysis of genes ranked as in D. Normalised enrichment score is shown, only genesets with enrichment FDR < 0.05 are depicted.

F) Scaled normalised expression of selected exhaustion-related genes in all CD8s. CD8_Tem_Active Louvain sub-cluster 2 is labelled.

expression of exhaustion markers *ENTPD1* (CD39) and *LAG3* (**Fig. 6.17D&F)**. Thus, solid organ transplant recipients have reduced general CD8$^+$ T cell activation and have a unique activated CD8$^+$ T cell phenotype compared to other immunosuppressive groups.

6.7 Discussion

In this chapter, I used single cell RNA-, TCR-, BCR- and surface protein-sequencing approaches to comprehensively assess the phenotype of COVID-19 vaccine-induced antigen-specific B and T cells and broader peripheral blood immune cells of individuals across a range of SIs. scRNA-sequencing analysis of monocytes identified a signature of high ISG expression associated with no or low antibody response to vaccination, consistent with the pro-inflammatory protein signature observed in blood at baseline. Through integration of bulk and SARS-CoV-2 specific B cells, I identified a pathway of reduced antibody responsiveness in solid organ transplant recipients through decreased B cell differentiation and impaired class-switch recombination. Analysis of integrated unstimulated and SARS-CoV-2 spike responsive CD4$^+$ T cells revealed an IFNγ-related differentiation trajectory that was impaired in solid organ transplant and cirrhosis patients. Similarly to the antigen-specific B cells, solid organ transplant recipients were enriched for a naive-like phenotype and had reduced effector functions, revealing the parallel impairment of differentiation in both B and T cells. In contrast, immunocompromised groups such as RA, IBD and AAV groups had heterogenous populations of highly active SARS-CoV-2 spike responsive CD4$^+$ T cells – corresponding to high IFNγ ELISpot responses after vaccination in these groups. Finally, I demonstrated that vaccine-induced SARS-CoV-2 spike responsive CD8$^+$ T cells varied significantly in functionality across immunosuppressive groups. AAV patients, who had the highest IFNγ ELISpot responses after three COVID-19 vaccine doses, had higher frequencies of highly activated CD8$^+$ effector T cells. In contrast, LT and RT recipients had low frequencies of highly activated CD8$^+$ effector T cells with a unique exhausted phenotype. This analysis provides new insight into the impact of SIs on mRNA vaccine-induced antigen-specific B and T cells.

6.7.1 Monocytes and dendritic cells

Monocytes and dendritic cells are central to the vaccine response as the main transduced populations by mRNA vaccine (*293*), important antigen presenting cells (*479, 480*) and mediators of inflammatory responses to infections (*481*) and in conditions of chronic inflammation (*444*). Pre-vaccination, I identified that high levels of inflammatory signalling was negatively associated with vaccine-induced antibody responsiveness. Given that monocytes are both sensitive to inflammation (*444*) and producers of inflammatory molecules, including TNF, IL-1β and IL-6 (*482*) I investigated their phenotype in SIs. Monocytes respond to mRNA vaccination by producing interferon and interferon stimulated genes, however this early response was shown to subside two days after vaccination (*208*) – therefore we used the V3+21d timepoint to assess 'steady state' monocytes and dendritic cells in immunocompromised individuals (*208*). Monocyte and DC subsets in solid organ transplant recipients with low/no V3+21d anti-RBD Ig titre had consistently increased expression of genesets relating to inflammatory signalling, including ISGs and TLR signalling. This included *CXCL9* and *CXCL10,* proteins which were upregulated in the baseline plasma of individuals with low/no V3+21d anti-RBD Ig titre (**Fig. 5.12A)**. Out of all CD45$^+$ immune cell populations, monocytes were the primary producers of *CXCL9* and *CXCL10,* implicating them as the primary immune source of the increased protein production at baseline. mRNA vaccines and subsequent immunogenicity are highly susceptible to interferon and TLR signalling due to reduced cellular protein production (*483*) and increased degradation of mRNA – including through 2′-5′-oligoadenylate synthetase (OAS) (*484*) which was upregulated in monocytes of antibody non-responsive vaccinees.

This presents a model of reduced mRNA vaccine antibody responsiveness within immunocompromised individuals whereby high levels of baseline inflammation and increased interferon signalling in monocytes and DCs leads to reduced immunogen production and/or impaired efficacy of antigen presentation, in turn leading to reduced antibody production.

Further studies are required to test this hypothesis. Validation of the hypothesis that the increased inflammation/interferon signalling observed in monocytes in this study leads to reduced SARS-CoV-2 spike protein production after vaccination *in vitro*. Further *in vitro* studies whereby monocytes and DCs are pre-conditioned with select inflammatory mediators may additionally identify which mediators are important in driving this condition. Considering the majority of mRNA vaccine derived antigen production occurs in the lymph node after intra-muscular injection (*293*), and the lymph node is the main site of antigen-presentation (*479*), the impact of inflammation on monocytes/macrophage should be studied in the lymph node, either in mice models, or in lymph node fine needle aspirate samples from human donors.

6.7.2 SARS-CoV-2 spike-specific B cells

In addition to altered monocyte functionality, there were striking differences in the phenotype of S-specific B cells after COVID-19 vaccination in immunocompromised individuals. As expected, patients on aCD20 therapies had few or no S1-specific B cells even after three doses of COVID-19 vaccine, consistent with their non-existent or low antibody response at this timepoint. On the other hand, solid organ transplant recipients had detectable S1-specific B cells but they were enriched for a naive phenotype, and memory S1-specific B cells exhibited reduced class-switch recombination compared to other (non-aCD20 therapy) immunocompromised groups and healthy controls. Interestingly, the proportion of class-switched memory B cells in background memory B cells was not reduced in solid organ transplant recipients compared to other groups – suggesting a specific impairment in the ability to generate class-switched memory B cells to the vaccine stimulus. Whether this represents a defect related specifically to mRNA vaccine responsiveness, or any novel antigen or vaccine platform, is not known. The fact that ChAdOx1 nCoV-19 also does not induce robust antibody responses in solid organ transplant recipients (Chapter 3, and (*485*)) suggests a general inability to respond to vaccine. Notably however, solid organ transplant recipients that are infected with SARS-CoV-2 generate equivalent RBD-specific IgG^+ memory B cells compared

to healthy individuals (*486*) and all previously SARS-CoV-2 infected LT recipients induced high anti-RBD Ig titres (**Chapter 3**). This suggests that although COVID-19 vaccines cannot induce class-switched Ig, SARS-CoV-2 infection can do so.

Nevertheless, the generation of high frequencies of IgM^+ S1-specific B cells in this cohort was initially surprising. Subsequent work to clone and produce monoclonal antibodies from the BCR sequences of IgG^+ and IgM^+ B cells in this study has validated that the BCRs from these B cells generate antibodies that bind to SARS-CoV-2 spike (data unpublished). However, interestingly, monoclonal antibodies generated from IgG^+ B cells from LT and RT recipients were able to neutralise SARS-CoV-2 pseudoviruses, but monoclonal antibodies generated from IgM^+ memory B cells were generally not able to neutralise SARS-CoV-2 pseudoviruses (data unpublished) – consistent with the reduced neutralisation capacity of vaccine-induced antibodies in RT and LT (**Fig. 5.16H**). Further work to quantify the overall proportion of IgG/IgM antibodies in the solid organ transplant recipients in this study is ongoing, however a previous study suggests the IgG/IgM ratio is reduced after two doses of COVID-19 vaccination in kidney transplant recipients compared to healthy controls (*417*). Somatically mutated memory IgM^+ B cells have been described previously (*487, 488*), and are thought to derive from either 1) a normal GC response, 2) an antigen independent pathway and/or 3) T cell-independent B cell stimulation (reviewed in detail in (*489*)). IgM^+ memory B cells are increased in ICOS deficient patients because of reduced ability to form germinal centres (GC) (*489-491*). Studies of lymph node FNAs in kidney transplant recipients suggest they have a similar inability to form proper GCs, due in part to reduced frequencies of $CD4^+$ T_{FH} cells (*279*) – suggesting these cells are unlikely to originate through a GC mediated reaction.

It is most plausible that vaccine-induced IgM^+ memory B cells are generated independently of the GC through T independent means. mRNA vaccination of T_{FH} (*Bcl6*$^{fl/fl}$*Cd4*^{Cre}) or $CD4^+$ T cell (*Ciita*$^{-/-}$) knockout mice demonstrated that somatically hypermutated and class-switched antibodies could be generated without T_{FH} cells, but with reduced affinity compared to wild-

type animals, supporting a possible T-independent mechanism of antibody generation after mRNA vaccine. Reduced T cell help due to use of T cell targeting calcineurin inhibitors and anti-proliferative immunosuppressive medications (**Section 1.11**) is likely responsible for the increased reliance on IgM^+ memory B cells and reduced class-switching in solid organ transplant recipients. The S-specific B cells of solid organ transplant recipients also had reduced cell cycling and Myc-related signalling – consistent with prior studies (*492*), suggesting that vaccine-induced B cells are impaired through both direct inhibition of B cell activation/proliferation and through reduced T cell help.

6.7.3 SARS-CoV-2 specific $CD4^+$ T cells

In chapters 3 and 5, I identified that IFNγ T cell ELISpot responses to vaccines were impaired in certain groups of immunocompromised individuals, particularly individuals with cirrhosis, and solid organ transplant recipients. However, the IFNγ T cell response is only a single measure of T cell vaccine responsiveness and does not give insight into pathways associated with non-responsiveness (**Chapter 4**). Applying the same approach as in chapter 4, I identified similar SARS-CoV-2 responsive AIM^+ T cell populations after at V3+21d in immunocompromised individuals as after COVID-19 vaccination in healthy individuals. This demonstrated the consistency of the approach to identify similar populations across cohorts and experiments. Furthermore, by performing scRNA-sequencing of unstimulated cells from the same donors in the same experimental batch, I could accurately confirm which populations were unique to the stimulated condition and not background activated.

Through tracking of T cell clones based on paired TCR sequences, I observed that T cells with identical clones were present across CD4_Tscm, CD4_Tem and CD4_Th1_Th17 populations – indicative of an axis of differentiation along these T cell phenotypes. Further evidence in support of this trajectory was its clear association with IFNγ ELISpot responses. RNA trajectory analysis can give spurious results because it finds relationships between cells based on RNA expression similarity regardless of biological/developmental feasibility (*493*).

However, due to the shared TCR clonality, relationship with a relevant alternative T cell functionality measure and the presence of a biologically relevant pseudotime 'root' (naive T cells), the use of pseudotime to identify a trajectory of cell state relatedness was appropriate. There are now over 70 single cell RNA trajectory inference tools available (*494*), so I selected Monocle3 based on its comparatively high accuracy (Monocle benchmarked in (*494*)) and its scalability (*495*). Using this method, I observed that individuals in groups enriched for vaccine non-responsiveness – RT, LT and cirrhosis – had T cells that were less differentiated than other individuals and RT and LT recipients were enriched for AIM^+ T cells that were phenotypically naive. Interestingly, increased frequencies of phenotypically naive SARS-CoV-2 specific B cells were also identified in these populations – indicating that this is a feature that is applicable to both arms of adaptive immune responses in these groups. Tacrolimus, the calcineurin inhibitor that all RT and LT recipients in this study received, has been demonstrated *in vitro* to reduce T_{FH} (*496*), T_H1, T_H17 and T_H2 $CD4^+$ T cell differentiation and cytokine production (*132*) – supporting the observed phenotype and demonstrating its relevance to vaccine-induced T cell responses.

6.7.4 SARS-CoV-2 specific $CD8^+$ T cells

Compared to the continuum of differentiation observed in $CD4^+$ T cells, AIM^+ $CD8^+$ T cell populations were more transcriptionally distinct and less functionally heterogenous – containing only two distinct populations. The ratio of highly activated to early activated AIM^+ $CD8^+$ T cells was positively associated with IFNγ ELISpot response and concordantly was significantly increased in AAV patients, who had notably high IFNγ ELISpot responses. Recipients of aCD20 therapies have consistently been identified to induce higher T cell cytokine responses to COVID-19 mRNA vaccines compared to healthy donors, including in patients with multiple sclerosis (*228, 497*) and AAV and RA (*416*). Previous studies have suggested that this reduced response may partially be due to increased naive $CD8^+$ T cell frequencies in aCD20 recipients (*416*). However, there was no evidence for that in my work,

and instead I observed higher frequencies of activated CD8+ T cells with increased expression of cytokines and activation markers in AAV patients on aCD20. This phenotype was not observed indolent B NHL patients who also received aCD20 therapies, but were notably older than AAV patients (AAV median age = 40, indolent B NHL median age = 66) and had reduced naive T cell frequencies at baseline (**Chapter 5**). Thus, the T cell enhancing effect of aCD20 therapy requires an intact T cell compartment. Despite the globally high activation of vaccine-responsive cells, there was no evidence of unique vaccine-responsive CD8+ T cell populations in AAV. Possible explanations for the increased activation of T cells to vaccination in aCD20 recipients with intact T cell compartments include increased T cell CD27 expression and activation potential (possibly due to reduced CD70 mediated cleavage of CD27 (*498*)) increased retention and relative proportion of CCR7+ T cells in secondary lymphoid organs leading to increased immune activation to novel antigen (*499*) or reduction of CD20+ CD8+ T cells which negatively regulate the cytotoxic CD4+ and CD8+ T cells through an unknown mechanism (*416, 500*). Further study of the effect of aCD20 therapy on the lymph node architecture and T cell response is required to elucidate these mechanisms.

Detailed analysis of highly activated CD8+ T cells identified that there was a subset of active CD8+ T cells that was enriched for cells from LT and RT recipients. This subset had reduced expression of *IFNG* and cytotoxic molecules compared to the active CD8+ T cells from other groups, and increased signalling of genes associated with T cell exhaustion, including *EOMES, TIGIT, CD96*. Development of exhausted progenitor cells through a process initiated by TCF-1 (*TCF7)* and maintained by Eomes (*EOMES)* has previously been described in lymphocytic choriomeningitis virus (LCMV) chronic infection models in mice (*501*). The solid organ transplant recipient CD8+ T cells were not specifically enriched for expression of canonical exhaustion/inhibitory markers such as CTLA-4 or PD-1, but all cells in the CD8_Tem_active cluster had higher expression of these markers compared to other CD8+ cells. It is possible that the chronic and high levels of systemic inflammation in solid organ

transplant recipients lead to dysregulation of $CD8^+$ activation (*502, 503*). Solid organ transplant recipients, particularly RT, had reduced frequencies of baseline and S-responsive $CD4^+$ T_{reg}s - which have been shown to induce the trafficking of $Eomes^+$ $CD8^+$ T cells to become tissue resident memory $CD8^+$ T cells in mice and thus reduce the circulating exhausted phenotype (*504*). It is likely that a unique interaction of inhibited T cell signalling pathways by the immunosuppressive therapeutics used in solid organ transplant led to this unique population. However, further work is required to understand the mechanisms leading to this previously undescribed $CD8^+$ T cell population.

6.7.5 Limitations

There are several limitations to the work presented in this chapter. Firstly, due to experimental constraints, peripheral blood samples were rested overnight before scRNA-sequencing which may lead to some alteration to the phenotype of resting immune cells. Secondly, the healthy control samples had poor T cell responsiveness and therefore could not be accurately compared to the rest of the group. This is possibly due to their long-term storage at -80°C instead of below -150°C, which impairs T cell responsiveness (*466*). Samples from immunocompromised individuals were stored separately in liquid nitrogen, so were not impacted by this phenomenon. S-specific B cell quality did not appear to be impaired in healthy individuals as they were selected based on expression of the S1-specific BCR, not on activation capacity. Experimental batch effects can greatly impact the outcome of scRNA sequencing studies (*505*). To reduce the effect of batch effects on my conclusions, I performed the entire experiment in four batches of 20 individuals, where each experiment included 2 of 8 individuals from each of the immunosuppressive disease groups. Despite including a large number of donors, the number of cells per donor was low for some donors due to the low frequency of detectable S-specific B cells in blood and cell loss during the scRNA-sequencing experimental pipeline. As discussed, peripheral blood in this study was phenotyped 21 days after vaccination, therefore I cannot conclude with certainty that the observed phenotypes are

representative of the pre-vaccine timepoint, and few residual genes may remain altered by vaccination. Finally, because only one timepoint was included, the phenotype of the antigen-specific response after the preceding vaccine doses remains unknown.

6.8 Conclusions

In conclusion, differences in innate-inflammatory signalling and generation of antigen-specific class-switched memory B cells are associated with mRNA vaccine-induced antibody titres in immunocompromised individuals. The differentiation and activation of COVID-19 vaccine-induced $CD4^+$ and $CD8^+$ T cells is impaired in individuals with cirrhosis and liver and renal transplant recipients, and this is associated with unique $CD8^+$ T cell populations. Other immunocompromised groups, such as ANCA-associated vasculitis patients on aCD20 therapies generate no or low antigen-specific antibodies or memory B cells, but generate highly activated $CD8^+$ T cells in response to vaccination. Thus, this chapter uses high-resolution techniques to identify novel phenotypes of mRNA vaccine induced immune responses in immunocompromised individuals.

6.9 Tables

Table 6.1 Demographics for donors included in chapter 6

	Cirr N = 8[1]	**IBD** N = 8[1]	**AAV** N = 8[1]	**RA** N = 8[1]	**LT** N = 16[1]	**RT** N = 16[1]	**Indolent B NHL** N = 8[1]	**HC** N = 8[1]	**Overall** N = 80[1]
Sex									
Female	5 (63%)	3 (38%)	4 (50%)	5 (63%)	0 (0%)	4 (25%)	0 (0%)	4 (50%)	25 (31%)
Male	3 (38%)	5 (63%)	4 (50%)	3 (38%)	16 (100%)	12 (75%)	8 (100%)	4 (50%)	55 (69%)
Age	63 (55 – 71)	40 (30 – 51)	40 (38 – 56)	54 (45 – 58)	60 (57 – 68)	54 (41 – 69)	66 (58 – 71)	42 (30 – 54)	56 (41 – 65)
Ethnicity									
Asian	0 (0%)	1 (13%)	0 (0%)	0 (0%)	0 (0%)	3 (19%)	0 (0%)	0 (0%)	4 (5·1%)
Black	0 (0%)	0 (0%)	0 (0%)	0 (0%)	0 (0%)	2 (13%)	0 (0%)	0 (0%)	2 (2·6%)
Mixed race	0 (0%)	1 (13%)	0 (0%)	0 (0%)	0 (0%)	0 (0%)	0 (0%)	0 (0%)	1 (1·3%)
Other	0 (0%)	0 (0%)	0 (0%)	1 (13%)	0 (0%)	0 (0%)	0 (0%)	0 (0%)	1 (1·3%)
White	8 (100%)	6 (75%)	6 (100%)	7 (88%)	16 (100%)	11 (69%)	8 (100%)	8 (100%)	70 (90%)
Unknown	0	0	2	0	0	0	0	0	2
BMI	31·7 (29·4 – 33·1)	27·1 (19·3 – 31·8)	31·6 (26·5 – 35·4)	24·5 (23·0 – 29·4)	24·9 (23·5 – 28·1)	26·2 (24·7 – 29·8)	25·2 (23·2 – 27·2)	26·8 (21·0 – 27·5)	26·5 (24·2 – 31·2)
Unknown	0	0	0	0	0	4	0	1	5
WHO Performance status									
0	4 (50%)	7 (88%)	3 (38%)	3 (38%)	11 (73%)	11 (69%)	5 (63%)	8 (100%)	52 (66%)
1	2 (25%)	1 (13%)	5 (63%)	3 (38%)	4 (27%)	4 (25%)	2 (25%)	0 (0%)	21 (27%)
2	2 (25%)	0 (0%)	0 (0%)	2 (25%)	0 (0%)	1 (6·3%)	1 (13%)	0 (0%)	6 (7·6%)
Unknown	0	0	0	0	1	0	0	0	1
Smoking status									
Currently	2 (25%)	1 (13%)	1 (17%)	3 (38%)	1 (6·3%)	0 (0%)	0 (0%)	0 (0%)	8 (12%)
Previously	4 (50%)	1 (13%)	2 (33%)	0 (0%)	7 (44%)	0 (0%)	6 (75%)	1 (13%)	21 (32%)
Never	2 (25%)	6 (75%)	3 (50%)	5 (63%)	8 (50%)	4 (100%)	2 (25%)	7 (88%)	37 (56%)
Unknown	0	0	2	0	0	12	0	0	14
Comorbidities									
CVD	0 (0%)	0 (0%)	1 (13%)	1 (13%)	1 (6·3%)	5 (31%)	2 (25%)	0 (0%)	10 (13%)
Stroke	0 (0%)	0 (0%)	1 (14%)	0 (0%)	0 (0%)	1 (6·3%)	1 (13%)	0 (0%)	3 (3·8%)
Diabetes	6 (75%)	0 (0%)	1 (13%)	0 (0%)	5 (31%)	4 (25%)	2 (25%)	0 (0%)	18 (23%)
Type 1	0 (0%)	0 (NA%)	0 (0%)	0 (NA%)	0 (0%)	1 (25%)	0 (0%)	0 (0%)	1 (4·0%)
Type 2	6 (100%)	0 (NA%)	1 (100%)	0 (NA%)	4 (100%)	2 (50%)	2 (100%)	0 (0%)	15 (60%)
Asthma	2 (25%)	1 (13%)	1 (13%)	1 (13%)	0 (0%)	0 (0%)	1 (13%)	0 (0%)	6 (7·5%)
COPD	0 (0%)	0 (0%)	0 (0%)	0 (0%)	0 (0%)	0 (0%)	0 (0%)	0 (0%)	0 (0%)
Hypertension	3 (38%)	0 (0%)	4 (50%)	1 (13%)	5 (31%)	15 (94%)	2 (25%)	0 (0%)	30 (38%)
Unknown	0	0	0	1	0	0	0	0	3
Number of comorbidities									
0	1 (13%)	7 (88%)	3 (38%)	5 (63%)	7 (44%)	1 (6·3%)	1 (13%)	8 (100%)	33 (41%)
1	3 (38%)	1 (13%)	2 (25%)	3 (38%)	7 (44%)	7 (44%)	5 (63%)	0 (0%)	28 (35%)
2	2 (25%)	0 (0%)	3 (38%)	0 (0%)	1 (6·3%)	5 (31%)	2 (25%)	0 (0%)	13 (16%)
3	2 (25%)	0 (0%)	0 (0%)	0 (0%)	1 (6·3%)	3 (19%)	0 (0%)	0 (0%)	6 (7·5%)
Prior vaccine type									
AZD1222	8 (100%)	8 (100%)	8 (100%)	8 (100%)	15 (94%)	11 (69%)	7 (88%)	4 (50%)	69 (86%)
BNT162b2	0 (0%)	0 (0%)	0 (0%)	0 (0%)	1 (6·3%)	5 (31%)	1 (13%)	4 (50%)	11 (14%)
V3 vaccine type									
BNT162b2	5 (63%)	3 (38%)	4 (50%)	4 (50%)	7 (44%)	11 (69%)	6 (75%)	8 (100%)	45 (56%)
mRNA-1273	3 (38%)	5 (63%)	4 (50%)	4 (50%)	9 (56%)	5 (31%)	2 (25%)	0 (0%)	32 (40%)
Immunosuppressive therapy									
Anti-TNF	0 (0%)	4 (50%)	0 (0%)	2 (25%)	0 (0%)	0 (0%)	0 (0%)	0 (0%)	6 (7·5%)
Anti-TNF+ MTX	0 (0%)	0 (0%)	0 (0%)	6 (75%)	0 (0%)	0 (0%)	0 (0%)	0 (0%)	6 (6·5%)
Anti-CD20	0 (0%)	0 (0%)	8 (100%)	0 (0%)	0 (0%)	0 (0%)	8 (100%)	0 (0%)	16 (20%)
CNI	0 (0%)	0 (0%)	0 (0%)	0 (0%)	8 (50%)	7 (44%)	0 (0%)	0 (0%)	15 (19%)
CNI+MMF	0 (0%)	0 (0%)	0 (0%)	0 (0%)	8 (50%)	9 (56%)	0 (0%)	0 (0%)	17 (21%)
Vedolizumab	0 (0%)	4 (50%)	0 (0%)	0 (0%)	0 (0%)	0 (0%)	0 (0%)	0 (0%)	4 (5·0%)
Corticosteroid	0 (0%)	1 (13%)	4 (50%)	1 (13%)	5 (31%)	3 (19%)	0 (0%)	0 (0%)	14 (18%)
Number of immunosuppressive therapeutics									
0	8 (100%)	0 (0%)	0 (0%)	0 (0%)	0 (0%)	0 (0%)	0 (0%)	8 (100%)	16 (20%)
1	0 (0%)	7 (88%)	4 (50%)	2 (25%)	5 (31%)	6 (38%)	8 (100%)	0 (0%)	32 (40%)
2	0 (0%)	1 (13%)	4 (50%)	4 (50%)	8 (50%)	8 (50%)	0 (0%)	0 (0%)	25 (31%)
3	0 (0%)	0 (0%)	0 (0%)	2 (25%)	3 (19%)	2 (12%)	0 (0%)	0 (0%)	7 (8.8%)

[1]n (%); Median (Q1, Q3)

Table 6.2 TotalSeq-C CITE-Seq Markers

Marker	Clone	Marker	Clone
anti-human CD86	IT2.2	anti-human CD163	GHI/61
anti-human CD274 (B7-H1, PD-L1)	29E.2A3	anti-human CD83	HB15e
anti-human CD270 (HVEM, TR2)	122	anti-human CD124 (IL-4Rα)	G077F6
anti-human CD155 (PVR)	SKII.4	anti-human CD13	WM15
anti-human CD112 (Nectin-2)	TX31	anti-human CD2	TS1/8
anti-human CD47	CC2C6	anti-human CD226 (DNAM-1)	11A8
anti-human CD48	BJ40	anti-human CD29	TS2/16
anti-human CD40	5C3	anti-human CD303 (BDCA-2)	201A
anti-human CD154	24-31	anti-human CD49b	P1E6-C5
anti-human CD52	HI186	anti-human CD81 (TAPA-1)	5A6
anti-human CD3	UCHT1	anti-human IgD	IA6-2
anti-human CD8	SK1	anti-human CD18	TS1/18
anti-human CD56	5.1H11	anti-human CD28	CD28.2
anti-human CD19	HIB19	anti-human CD38	HIT2
anti-human CD33	P67.6	anti-human CD127 (IL-7Rα)	A019D5
anti-human CD11c	S-HCL-3	anti-human CD45	HI30
anti-human HLA-A,B,C	W6/32	anti-human CD22	S-HCL-1
anti-human CD45RA	HI100	anti-human CD71	CY1G4
anti-human CD123	6H6	anti-human CD26	BA5b
anti-human CD7	CD7-6B7	anti-human CD36	5-271
anti-human CD105	43A3	anti-human CD158 (KIR2DL1/S1/S3/S5)	HP-MA4
anti-human/mouse CD49f	GoH3	anti-human CD49a	TS2/7
anti-human CD194 (CCR4)	L291H4	anti-human CD49d	9F10
anti-human CD4	RPA-T4	anti-human CD73 (Ecto-5'-nucleotidase)	AD2
anti-mouse/human CD44	IM7	anti-human TCR Vα7.2	3C10
anti-human CD14	M5E2	anti-human TCR Vδ2	B6
anti-human CD16	3G8	anti-human LOX-1	15C4
anti-human CD25	BC96	anti-human CD158b (KIR2DL2/L3, NKAT2)	DX27
anti-human CD45RO	UCHL1	anti-human CD158e1 (KIR3DL1, NKB1)	DX9
anti-human CD279	EH12.2H7	anti-human CD319 (CRACC)	162.1
anti-human TIGIT (VSTM3)	A15153G	anti-human CD99	3B2/TA8
Mouse IgG1, κ isotype Ctrl	MOPC-21	anti-human CLEC12A	50C1
Mouse IgG2a, κ isotype Ctrl	MOPC-173	anti-human CD352 (NTB-A)	NT-7
Mouse IgG2b, κ isotype Ctrl	MPC-11	anti-human CD94	DX22
Rat IgG2b, κ Isotype Ctrl	RTK4530	anti-human Ig light chain κ	MHK-49
anti-human CD20	2H7	anti-human CD85j (ILT2)	GHI/75
anti-human CD335 (NKp46)	9E2	anti-human CD23	EBVCS-5
anti-human CD31	WM59	anti-human Ig light chain λ	MHL-38
anti-human CD146	P1H12	anti-human CD328 (Siglec-7)	6-434
anti-human IgM	MHM-88	anti-human GPR56	CG4
anti-human CD5	UCHT2	anti-human HLA-E	3D12
anti-human CD183 (CXCR3)	G025H7	anti-human CD82	ASL-24
anti-human CD195 (CCR5)	J418F1	anti-human CD101 (BB27)	BB27
anti-human CD32	FUN-2	anti-human CD88 (C5aR)	S5/1
anti-human CD196 (CCR6)	G034E3	anti-human CD224	KF29
anti-human CD185 (CXCR5)	J252D4	anti-human CD244 (2B4)	C1.7
anti-human CD103 (Integrin αE)	Ber-ACT8	anti-human CD169 (Sialoadhesin, Siglec-1)	7-239
anti-human CD69	FN50	anti-human/mouse integrin β7	FIB504
anti-human CD62L	DREG-56	anti-human CD268 (BAFF-R)	11C1
anti-human CD161	HP-3G10	anti-human CD42b	HIP1
anti-human CD152 (CTLA-4)	BNI3	anti-human CD54	HA58
anti-human CD223 (LAG-3)	11C3C65	anti-human CD62P (P-Selectin)	AK4
anti-human KLRG1 (MAFA)	SA231A2	anti-human CD119 (IFN-γ R α chain)	GIR-208
anti-human CD27	O323	anti-human TCR α/β	IP26
anti-human CD107a (LAMP-1)	H4A3	Rat IgG1, κ isotype Ctrl	RTK2071
anti-human CD95 (Fas)	DX2	Rat IgG2a, κ Isotype Ctrl	RTK2758
anti-human CD134 (OX40)	Ber-ACT35 (ACT35)	Armenian Hamster IgG Isotype Ctrl	HTK888
anti-human HLA-DR	L243	anti-human CD122 (IL-2Rβ)	TU27
anti-human CD1c	L161	anti-human CD267 (TACI)	1A1
anti-human CD11b	ICRF44	anti-human FcεRIα	AER-37 (CRA-1)
anti-human CD64	10.1	anti-human CD41	HIP8
anti-human CD141 (Thrombomodulin)	M80	anti-human CD137 (4-1BB)	4B4-1
anti-human CD1d	51.1		
anti-human CD314 (NKG2D)	1D11		
anti-human CD35	E11		
anti-human CD57 Recombinant	QA17A04		
anti-human CD272 (BTLA)	MIH26		
anti-human/mouse/rat CD278 (ICOS)	C398.4A		
anti-human CD58 (LFA-3)	TS2/9		
anti-human CD39	A1		
anti-human CX3CR1	K0124E1		
anti-human CD24	ML5		
anti-human CD21	Bu32		
anti-human CD11a	TS2/4		
anti-human CD79b (Igβ)	CB3-1		

Table 6.3 Expanded B cell clones

Ag = SARS-CoV-2 Spike specific, CD45 = background. LT = Liver transplant, Cirr = Cirrhosis, RT = Renal transplant, RA = rheumatoid arthritis

Clone ID	Donor ID	Clinical group	Source	IGH V gene	IGH C gene	Cell type	Number of cells	Mean CDR3 SHM
11314	60	LT	CD45	IGHV3-48*02	IGHA1	Memory B cells	1	0.14
11314	60	LT	CD45	IGHV3-48*02	IGHA2	Plasma cells	1	0.14
11812	118	LT	CD45	IGHV3-33*01	IGHM	Naive B cells	2	0.1
12545	60	LT	CD45	IGHV3-7*01	IGHA1	Memory B cells	1	0.12
12545	60	LT	CD45	IGHV3-7*01	IGHA2	Memory B cells	1	0.08
13756	54	LT	CD45	IGHV4-34*01	IGHM	Naive B cells	5	0.11
13756	54	LT	CD45	IGHV4-34*01	IGHM	Memory B cells	8	0.11
15113	71	Cirr	CD45	IGHV3-7*01,IGHV3-7*03	IGHM	Naive B cells	1	0.06
15113	71	Cirr	CD45	IGHV3-7*01,IGHV3-7*03	IGHM	Memory B cells	5	0.05
1745	56	Cirr	Ag	IGHV3-33*01	IGHM	Memory B cells	1	0.09
1745	56	Cirr	CD45	IGHV3-33*01	IGHM	Naive B cells	3	0.08
1745	56	Cirr	CD45	IGHV3-33*01	IGHM	Memory B cells	10	0.08
1745	56	Cirr	CD45	IGHV3-33*01,IGHV3-33*04	IGHM	Naive B cells	1	0.07
1746	56	Cirr	CD45	IGHV3-33*06	IGHM	Naive B cells	1	0.07
1746	56	Cirr	CD45	IGHV3-33*06	IGHM	Memory B cells	9	0.07
1748	56	Cirr	CD45	IGHV3-33*01	IGHM	Memory B cells	3	0.07
19138	118	LT	CD45	IGHV3-23*01,IGHV3-23D*01	IGHM	Memory B cells	1	0.17
19138	118	LT	CD45	IGHV3-23*01,IGHV3-23D*01	IGHM	Plasma cells	1	0.13
19929	9	RA	Ag	IGHV3-33*08	IGHG1	Memory B cells	2	0.07
20907	54	LT	CD45	IGHV3-23*04	IGHM	Naive B cells	1	0.1
20907	54	LT	CD45	IGHV3-23*04	IGHM	Memory B cells	1	0.05
2245	58	Cirr	CD45	IGHV3-15*01,IGHV3-15*02	IGHM	Memory B cells	6	0.06
2588	60	LT	Ag	IGHV2-5*02,IGHV2-5*09	IGHG2	Memory B cells	1	0.14
2588	60	LT	CD45	IGHV2-5*02,IGHV2-5*09	IGHG2	Memory B cells	1	0.16
2589	60	LT	CD45	IGHV2-5*02,IGHV2-5*09	IGHG2	Memory B cells	3	0.13
3526	68	LT	CD45	IGHV3-11*01	IGHM	Memory B cells	3	0.06
3667	68	LT	Ag	IGHV3-11*01	IGHM	Memory B cells	3	0.06
3667	68	LT	CD45	IGHV3-11*01	IGHM	Naive B cells	64	0.06
3667	68	LT	CD45	IGHV3-11*01	IGHM	Memory B cells	103	0.06
3828	76	RT	CD45	IGHV3-49*04	IGHM	Memory B cells	2	0.02
6769	72	LT	CD45	IGHV3-23*01,IGHV3-23D*01	IGHA2	Memory B cells	3	0.07
6945	118	LT	CD45	IGHV3-23*01,IGHV3-23*04,IGHV3-23D*01	IGHM	Memory B cells	1	0.09
6945	118	LT	CD45	IGHV3-23*01,IGHV3-23D*01	IGHM	Memory B cells	3	0.09
9208	68	LT	Ag	IGHV3-33*01,IGHV3-33*03	IGHM	Memory B cells	1	0.11
9208	68	LT	CD45	IGHV3-33*01,IGHV3-33*03	IGHG1	Memory B cells	1	0.11
9208	68	LT	CD45	IGHV3-33*01,IGHV3-33*03	IGHM	Naive B cells	15	0.1
9208	68	LT	CD45	IGHV3-33*01,IGHV3-33*03	IGHM	Memory B cells	11	0.1
9440	732	RA	Ag	IGHV4-34*01	IGHG3	Memory B cells	1	0.01
9440	732	RA	CD45	IGHV4-34*01	IGHG3	Naive B cells	1	0.01
9440	732	RA	CD45	IGHV4-34*01	IGHG3	ABCs	2	0.01
9440	732	RA	CD45	IGHV4-34*01	IGHG3	Memory B cells	26	0.02
9558	71	Cirr	CD45	IGHV3-74*01	IGHM	Memory B cells	2	0
9558	71	Cirr	CD45	IGHV3-74*01,IGHV3-74*03	IGHM	Memory B cells	2	0.01
9619	9	RA	Ag	IGHV1-69*01,IGHV1-69D*01	IGHG1	Memory B cells	2	0.01

7 Conclusions and future directions

In this thesis I demonstrated that factors associated with the COVID-19 vaccine regimen and the vaccine recipient have a considerable impact on vaccine-induced T and B cell mediated immune responses. In summary, I : 1) revealed the extreme variability of COVID-19 vaccine responses across and within various secondary immunodeficiencies (**Fig. 7.1)**, 2) demonstrated the dominant impact of dosing interval on the vaccine-induced antigen-specific T cell response to ChAdOx1 nCoV-19 and BNT162b2 COVID-19 vaccines (**Fig. 7.2)**, 3) comprehensively phenotyped the pre- and post-vaccination circulating immune system in individuals with secondary immunodeficiencies to identify immune predictors of vaccine responsiveness (**Fig. 7.3)**, 4) discovered pathways of impairment in the functionality and differentiation of vaccine-induced antigen-specific B and T cells in individuals with secondary immunodeficiencies (**Fig. 7.4)**. This work provides new insight into the immune effectiveness of important vaccine platforms in clinically vulnerable people, with broad relevance to vaccine design and the biology of secondary immunodeficiencies.

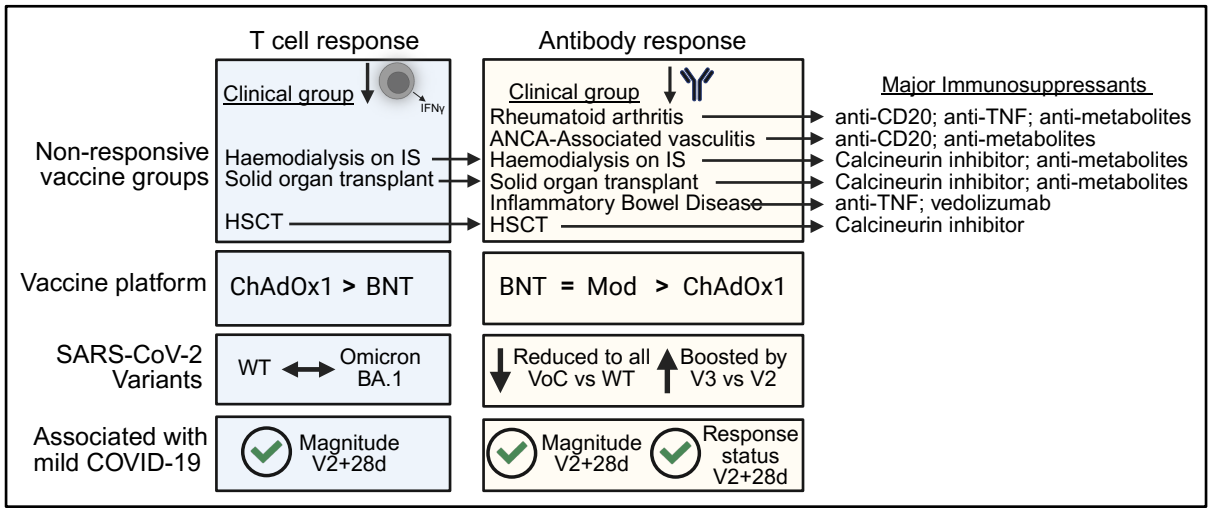

Fig. 7.1 Summary of key findings in chapter 3
IS = immunosuppressive therapy, BNT = BNT162b2, ChAdOx1 = ChAdOx1 nCoV-19, Mod = mRNA-1273 (Moderna), WT = wild-type, VoC = variant of concern, V = vaccine

7.1 Individuals with certain immunosuppressive conditions have impaired antibody and T cell responses to COVID-19 vaccines

In this thesis, I present work from two large cohort studies of COVID-19 vaccine

immunogenicity across various SIs. It was clear from these studies that the term 'immunocompromised' encapsulates a highly heterogeneous group with differing intensity and phenotypes of immune impairment and complex interactions between diseases and immunosuppressive therapies. These studies however identified certain groups particularly at risk of vaccine non-responsiveness, including individuals on aCD20 therapy and transplant recipients.

Understanding which groups were particularly at risk of vaccine immune non-responsiveness is important in multiple ways. First, this information could be used to prioritise groups for alternative therapies; indeed, data from the OCTAVE and OCTAVE DUO studies were used to inform UK government guidelines on social shielding and COVID-19 vaccination in immunocompromised individuals early in the COVID-19 pandemic (*379*). However, vulnerability to infection in immunocompromised populations is an ongoing concern and individuals with some SIs continue to remain shielded from society. Ongoing work to assess vaccine-induced immunogenicity and protection against infection after repeated booster COVID-19 vaccines (now up to 10 doses (*200*)) will help determine which groups can be successfully vaccinated after many doses of mRNA or ChAdOx1 vaccines. Findings from these studies also have relevance to preparedness against possible future pandemics, where these adaptable vaccine technologies would likely be implemented to provide protection (*506*).

Second, by comparing the varying impact of SIs on different vaccine platforms we gain insight into their mechanisms of immunogenicity. For example, cirrhosis disease severity significantly reduced vaccine immunogenicity to one dose of mRNA but not ChAdOx1 COVID-19 vaccine. This was similarly observed in HSCT recipients compared to healthy individuals (*295*). mRNA and ChAdOx1 vaccines variably require $CD4^+$ T cell help to optimally induce cytotoxic T cell responses and antibody production (*507-509*) and therefore may be differentially impacted by such disease states. Further work is required to delineate these mechanisms in mice, but studies of vaccine immunogenicity in immunocompromised individuals provide initial evidence

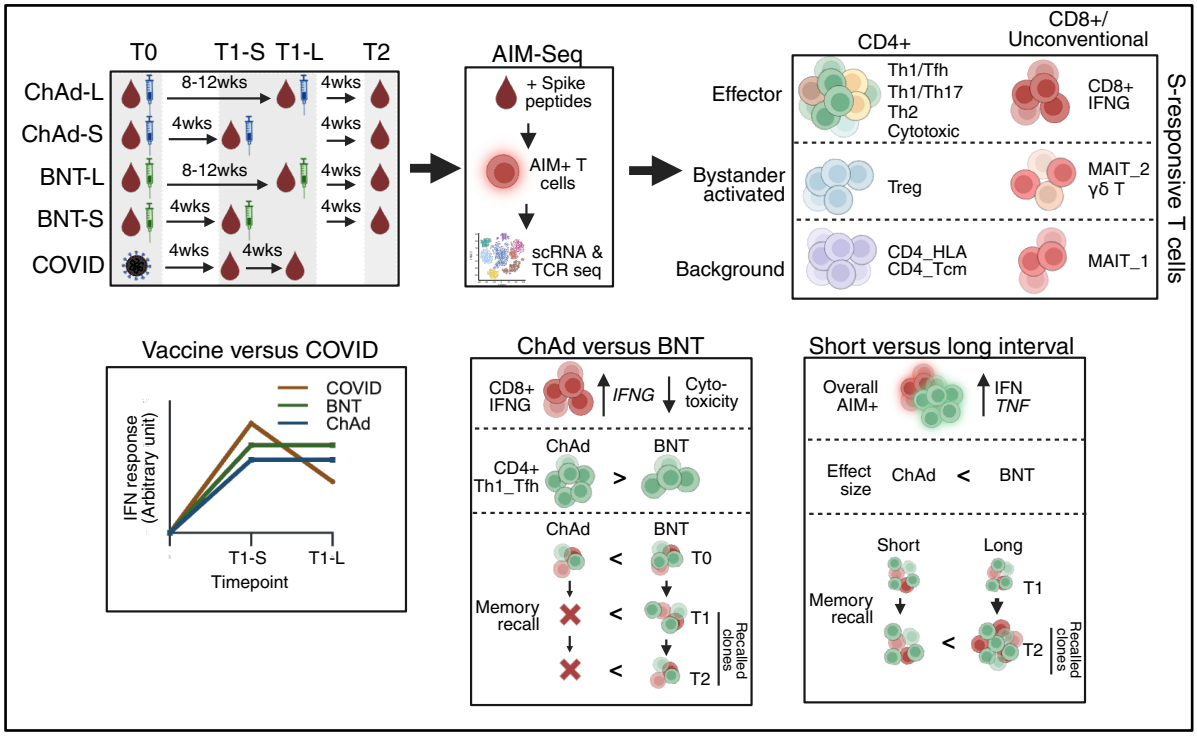

Fig. 7.2 Summary of key findings in chapter 4
Study overview and key findings from comparisons.
ChAd = ChAdOx1 nCoV-19, BNT = BNT162b2, COVID = SARS-CoV-2 infection, S = short, L = long, AIM = activation induced marker, MAIT = mucosal associated invariant T cell, IFN = Interferon

for the importance of these different pathways in humans. Such information can also be used as rationale to target specific vaccine platforms for use in certain immunosuppressive groups. An ongoing study to investigate the SARS-CoV-2 spike-responsive T and B cells induced by mRNA compared with ChAdOx1 vaccines in HSCT recipients and healthy individuals will provide further insight into the conserved/impaired immunogenicity pathways of COVID-19 vaccines in these patients.

7.2 Activation induced markers with single-cell RNA sequencing to study antigen-specific T cell responses to vaccination

Key to improving understanding of vaccine immunogenicity is the ability to effectively measure relevant, functional responses. This is especially challenging with T cells, due to their high functional heterogeneity (*502*), the complex combinations of possible HLA-epitope combinations (*313*) and technical limitations in accurately capturing T cell functionality (*310, 353*). In this thesis, I present data generated by the integration of an AIM flow cytometry assay with single-cell RNA and TCR sequencing (AIM-seq) – a recently developed approach which

is increasingly being employed in vaccine studies (*25, 342, 510*). Using this approach in healthy and immunocompromised individuals in two separate studies, I demonstrate its ability to resolve heterogenous SARS-CoV-2 spike-responsive $CD4^+$ and $CD8^+$ T cell subsets. This work highlighted the important role of bystander activation in assays of T cell functionality, particularly $CD4^+$ T_{reg} populations and unconventional T cell subsets – consistent with the ability of these T cell subsets to respond to cytokine independently of TCR stimulation (*247, 285, 311, 314, 326*). Whether the bystander-activated T cells measured in these assays in blood have any functional role in the T cell response to vaccine remains to be understood. In chapter 4, the $CD4^+$ T_{reg} population was the sole population that expressed *IL7* – important for T cell survival and activation (*511*) and a promotor of mRNA vaccine immunogenicity (*512*). SARS-CoV-2 spike-responsive AIM^+ $CD4^+$ T_{reg}s were also identified in multiple tissue types after COVID-19 vaccination where they are more likely to exert their regulatory function (*342*). MAIT cells have been shown to enhance ChAdOx1-induced $CD8^+$ T cell responses (*351*), highlighting a possible role for these cells in enhancing antigen-specific T cell responses. Alteration of markers used in the AIM assay may exclude these populations (*314*), but before excluding these cells from future studies further functional work is required to understand their relevance in the vaccine-induced response.

In healthy individuals, I used the AIM-seq assay to demonstrate that a short dosing interval between mRNA or ChAdOx1 nCoV-19 vaccination prime and boosting doses induced post-boost T cells with a phenotype that was more inflammatory and less associated with a memory recall response. This is consistent with observations from IFNγ ELISpot data in larger cohort studies (*71, 284*), but provides new insight into the antigen-specific cell subsets responsible for this phenotype. Given the growing use of mRNA vaccines for infectious disease and cancer - which differ in their requirement for memory or cytotoxic/inflammatory (*16, 513*) T cell responses, respectively, these findings have broad relevance for the optimisation of the vaccine regimen to tailor the T cell phenotype for the given vaccine target.

In the OCTAVE DUO study, I used AIM-seq to reveal pathways of reduced differentiation and activation of CD4⁺ and CD8⁺ T cells in solid organ transplant recipients on high intensity immunosuppression compared to other immunocompromised groups. I also identified an activated CD8⁺ T cell population with a unique exhaustion phenotype in this group. *In vitro* and

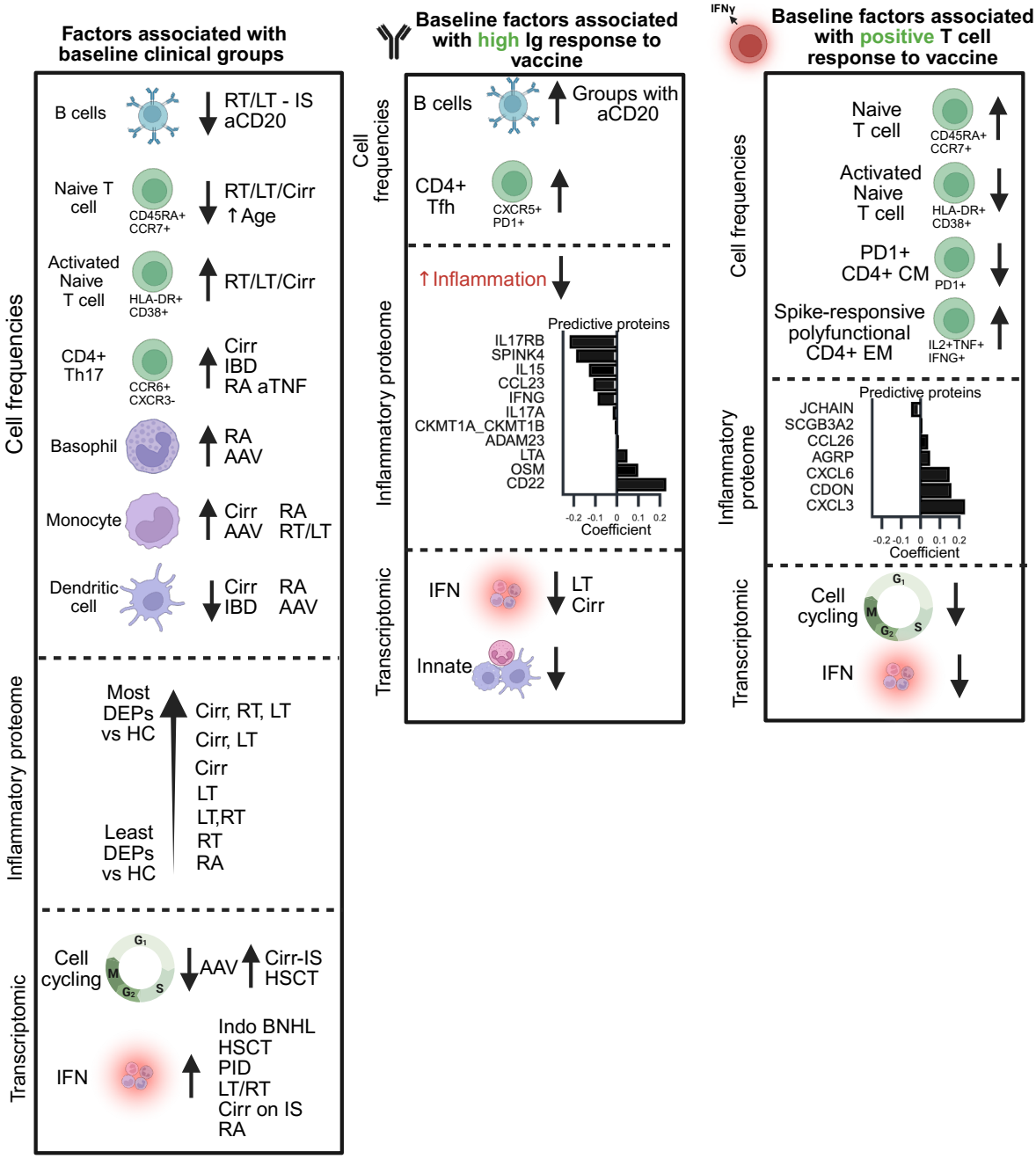

Fig. 7.3 Summary of key findings in chapter 5
Notable baseline features associated with specific disease groups compared to healthy individuals or other disease groups (left panel), or associated with antibody titres (middle panel) or IFNγ T cell responses (right panel) to SARS-CoV-2 at the 21 days post third vaccine timepoint. DEPs = differentially expressed proteins

mice studies previously demonstrated that solid organ transplant related immunosuppressive

agents can reduce T cell differentiation and cytokine production and lead to an altered $CD8^+$ T cell exhaustion/effector phenotype in models of graft versus host disease (*132, 514, 515*). However, little is known about the mechanisms of these drugs in specifically altering *de novo* responses to vaccines. Further investigation into the contribution of the unique $CD8^+$ population identified here to the vaccine-induced response in patient samples and models of transplant associated immunosuppression in mice will give insight into its importance. Identification of possible methods to reverse this phenotype may also offer means by which to improve vaccine-responsiveness in this at-risk population.

7.3 Immune predictors of mRNA vaccine responsiveness in immunocompromised individuals

Baseline immunophenotyping of immunosuppressive individuals was highly informative of disease specific and disease-spanning immune features. Identification of broad transcriptional groupings at baseline that were associated with vaccine responsiveness supports the concept that despite large clinical heterogeneity immune phenotype may converge into relatively few broad, functionally relevant, signatures (*393*). Nevertheless, I also identified several transcriptomic measures associated with vaccine-responsiveness that were distinct to several groups. Delineating these different pathways has relevance to future optimisation of vaccination strategies. It is not possible to overcome a lack of B cells, for instance in individuals with aCD20 therapies, by modifying vaccine strategies. However, it may be possible to overcome the reduced class-switching observed in solid organ transplantation through employing methods to augment T cell help for B cells at the time of vaccination. “Molecular adjuvants”, such as IL-12p70 (*516*), IL-7 (*512*), encoded using gene delivery vehicles (such as mRNA-LNPs) and administered alongside vaccine may specifically enhance elements of the vaccine immunogenicity pathway to overcome such impairments. Research into the design and use of molecular adjuvants for use in specific immunosuppressive conditions is

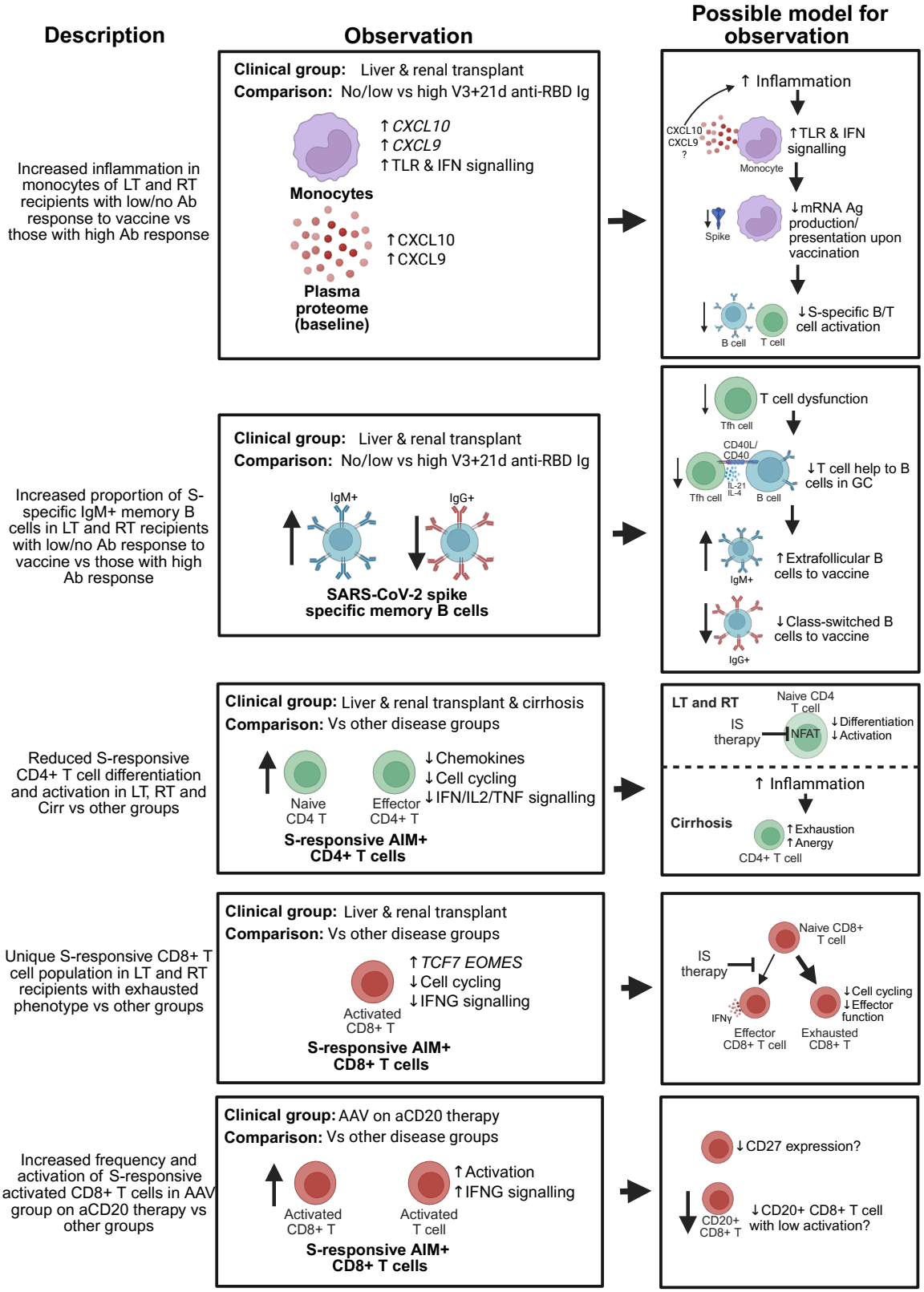

Fig. 7.4 Summary of key findings in chapter 6
Key observations made in chapter 6 and possible biological models to explain their observation. AIM = activation induced marker, S-responsive = SARS-CoV-2 spike responsive, Ag = antigen, NFAT = nuclear factor of activated T cells, LT = liver transplant, RT = renal transplant, Cirr = cirrhosis, AAV = ANCA-associated vasculitis

largely unexplored but may be a promising avenue for future research.

Immunosuppressive agents clearly impacted the germinal centre in differing ways. Considering the enhancing effect of aCD20 therapy on T cell responses to vaccine, elucidating the pathway that leads to this phenomenon – and harnessing this knowledge to improve the T cell immunogenicity of vaccines, has relevance for the design of vaccines which induce high magnitudes of cytotoxic T cells, for use for instance in cancer (*513*). The impact of calcineurin inhibitors and anti-proliferative therapies on the human lymph node has previously been explored in observational studies (*279*), however, mechanistic studies to investigate the pathways by which this impairs vaccine responsiveness are required. In addition, the study of other immunosuppressive therapies, such as anti-TNF, on *de novo* vaccine responses in the lymph node is essential and will be a primary focus of my future work.

Finally, a key finding was that a limited collection of inflammatory proteins measurable in blood at baseline could accurately predict antibody and T cell non-responsiveness after vaccination in immunocompromised groups. Given the success in using circulating protein concentrations as prognostic biomarkers of disease (*517-519*), it is feasible that assays to predict vaccine-responsiveness may be developed to avoid unnecessary vaccine usage and prioritise individuals for alternative therapy. To develop this work further, I will repeat the proteomics assays performed here on an independent cohort of immunocompromised individuals to validate the predictive markers. If predictive biomarkers that span both cohorts can be identified, a small number of proteins will be taken forward to develop cost-effective quantification methods in blood.

In conclusion, this thesis provides new insight into the impact of secondary immune deficiencies and the vaccine regimen on COVID-19 vaccine immunogenicity. In doing so, it highlights potential pathways for the optimisation of vaccine strategies for at-risk populations, identifies immune features that are essential for vaccine immunogenicity, and demonstrates the clinical importance of vaccine immunogenicity for protection against severe disease in immunocompromised groups.

8 References

1. W. Msemburi *et al.*, The WHO estimates of excess mortality associated with the COVID-19 pandemic. *Nature* **613**, 130-137 (2023).
2. M. Nicola *et al.*, The socio-economic implications of the coronavirus pandemic (COVID-19): A review. *Int J Surg* **78**, 185-193 (2020).
3. H. E. Davis, L. McCorkell, J. M. Vogel, E. J. Topol, Long COVID: major findings, mechanisms and recommendations. *Nature Reviews Microbiology* **21**, 133-146 (2023).
4. R. A. Evans *et al.*, Impact of COVID-19 on immunocompromised populations during the Omicron era: insights from the observational population-based INFORM study. *The Lancet Regional Health – Europe* **35**, (2023).
5. A. K. Clift *et al.*, Living risk prediction algorithm (QCOVID) for risk of hospital admission and mortality from coronavirus 19 in adults: national derivation and validation cohort study. *Bmj* **371**, m3731 (2020).
6. I. L. Ward *et al.*, Risk of covid-19 related deaths for SARS-CoV-2 omicron (B.1.1.529) compared with delta (B.1.617.2): retrospective cohort study. *Bmj* **378**, e070695 (2022).
7. J. Valabhji *et al.*, Prevalence of multiple long-term conditions (multimorbidity) in England: a whole population study of over 60 million people. *Journal of the Royal Society of Medicine* **117**, 104-117 (2024).
8. F. Krammer, The role of vaccines in the COVID-19 pandemic: what have we learned? *Seminars in Immunopathology* **45**, 451-468 (2024).
9. J. Cui, F. Li, Z.-L. Shi, Origin and evolution of pathogenic coronaviruses. *Nature Reviews Microbiology* **17**, 181-192 (2019).
10. R. Yadav *et al.*, Role of Structural and Non-Structural Proteins and Therapeutic Targets of SARS-CoV-2 for COVID-19. *Cells* **10**, (2021).
11. M. Cascella, M. Rajnik, A. Aleem, S. Dulebohn, R. Di Napoli, Features, Evaluation, and Treatment of Coronavirus (COVID-19). *StatPearls*, (2023).
12. D. G. Augusto *et al.*, A common allele of HLA is associated with asymptomatic SARS-CoV-2 infection. *Nature* **620**, 128-136 (2023).
13. E. K. Stokes *et al.*, Coronavirus Disease 2019 Case Surveillance - United States, January 22-May 30, 2020. *MMWR Morb Mortal Wkly Rep* **69**, 759-765 (2020).
14. J. Li *et al.*, Epidemiology of COVID-19: A systematic review and meta-analysis of clinical characteristics, risk factors, and outcomes. *Journal of Medical Virology* **93**, 1449-1458 (2021).
15. S. Riedel, Edward Jenner and the history of smallpox and vaccination. *Proc (Bayl Univ Med Cent)* **18**, 21-25 (2005).
16. A. J. Pollard, E. M. Bijker, A guide to vaccinology: from basic principles to new developments. *Nature Reviews Immunology* **21**, 83-100 (2021).
17. B. Pulendran, P. S. Arunachalam, D. T. O'Hagan, Emerging concepts in the science of vaccine adjuvants. *Nature Reviews Drug Discovery* **20**, 454-475 (2021).
18. F. Alnaimat *et al.*, Vaccination in the Era of Immunosuppression. *Vaccines (Basel)* **11**, (2023).
19. I. McDonald, S. M. Murray, C. J. Reynolds, D. M. Altmann, R. J. Boyton, Comparative systematic review and meta-analysis of reactogenicity, immunogenicity and efficacy of vaccines against SARS-CoV-2. *npj Vaccines* **6**, 74 (2021).
20. N. Pardi, M. J. Hogan, F. W. Porter, D. Weissman, mRNA vaccines — a new era in vaccinology. *Nature Reviews Drug Discovery* **17**, 261-279 (2018).
21. E. M. Mucker *et al.*, Comparison of protection against mpox following mRNA or modified vaccinia Ankara vaccination in nonhuman primates. *Cell* **187**, 5540-5553.e5510 (2024).
22. P. M. Folegatti *et al.*, Vaccines based on the replication-deficient simian adenoviral

vector ChAdOx1: Standardized template with key considerations for a risk/benefit assessment. *Vaccine* **40**, 5248-5262 (2022).
23. E. Kon *et al.*, A single-dose F1-based mRNA-LNP vaccine provides protection against the lethal plague bacterium. *Science Advances* **9**, eadg1036 (2023).
24. X. Wang *et al.*, Strong immune responses and protection of PcrV and OprF-I mRNA vaccine candidates against Pseudomonas aeruginosa. *npj Vaccines* **8**, 76 (2023).
25. Z. Sethna *et al.*, RNA neoantigen vaccines prime long-lived CD8+ T cells in pancreatic cancer. *Nature*, (2025).
26. M. V. R. Chengalvala *et al.*, Adenovirus vectors for gene expression. *Current Opinion in Biotechnology* **2**, 718-722 (1991).
27. A. Syyam *et al.*, Adenovirus Vector System: Construction, History and Therapeutic Applications. *BioTechniques* **73**, 297-305 (2022).
28. J. Alonso-Padilla *et al.*, Development of Novel Adenoviral Vectors to Overcome Challenges Observed With HAdV-5-based Constructs. *Mol Ther* **24**, 6-16 (2016).
29. S. A. Mendonça, R. Lorincz, P. Boucher, D. T. Curiel, Adenoviral vector vaccine platforms in the SARS-CoV-2 pandemic. *npj Vaccines* **6**, 97 (2021).
30. N. Tatsis, H. C. Ertl, Adenoviruses as vaccine vectors. *Mol Ther* **10**, 616-629 (2004).
31. M. Sumida Shawn *et al.*, Neutralizing Antibodies and CD8+ T Lymphocytes both Contribute to Immunity to Adenovirus Serotype 5 Vaccine Vectors. *Journal of Virology* **78**, 2666-2673 (2004).
32. F. Farina Steven *et al.*, Replication-Defective Vector Based on a Chimpanzee Adenovirus. *Journal of Virology* **75**, 11603-11613 (2001).
33. G. A. O'Hara *et al.*, Clinical Assessment of a Recombinant Simian Adenovirus ChAd63: A Potent New Vaccine Vector. *The Journal of Infectious Diseases* **205**, 772-781 (2012).
34. J. E. Ledgerwood *et al.*, Chimpanzee Adenovirus Vector Ebola Vaccine. *New England Journal of Medicine* **376**, 928-938 (2017).
35. M. D. J. Dicks *et al.*, A Novel Chimpanzee Adenovirus Vector with Low Human Seroprevalence: Improved Systems for Vector Derivation and Comparative Immunogenicity. *PLOS ONE* **7**, e40385 (2012).
36. G. Asthagiri Arunkumar *et al.*, Vaccination with viral vectors expressing NP, M1 and chimeric hemagglutinin induces broad protection against influenza virus challenge in mice. *Vaccine* **37**, 5567-5577 (2019).
37. R. D. Antrobus *et al.*, Clinical Assessment of a Novel Recombinant Simian Adenovirus ChAdOx1 as a Vectored Vaccine Expressing Conserved Influenza A Antigens. *Molecular Therapy* **22**, 668-674 (2014).
38. P. M. Folegatti *et al.*, Safety and immunogenicity of a candidate Middle East respiratory syndrome coronavirus viral-vectored vaccine: a dose-escalation, open-label, non-randomised, uncontrolled, phase 1 trial. *The Lancet Infectious Diseases* **20**, 816-826 (2020).
39. N. K. Alharbi *et al.*, ChAdOx1 and MVA based vaccine candidates against MERS-CoV elicit neutralising antibodies and cellular immune responses in mice. *Vaccine* **35**, 3780-3788 (2017).
40. J. A. Wolff *et al.*, Direct Gene Transfer into Mouse Muscle in Vivo. *Science* **247**, 1465-1468 (1990).
41. N. Chaudhary, D. Weissman, K. A. Whitehead, mRNA vaccines for infectious diseases: principles, delivery and clinical translation. *Nature Reviews Drug Discovery* **20**, 817-838 (2021).
42. D. Weissman, mRNA transcript therapy. *Expert Review of Vaccines* **14**, 265-281 (2015).
43. M.-G. Alameh *et al.*, Lipid nanoparticles enhance the efficacy of mRNA and protein subunit vaccines by inducing robust T follicular helper cell and humoral responses.

Immunity **54**, 2877-2892.e2877 (2021).
44. N. Pardi *et al.*, Expression kinetics of nucleoside-modified mRNA delivered in lipid nanoparticles to mice by various routes. *Journal of Controlled Release* **217**, 345-351 (2015).
45. F. Heil *et al.*, Species-Specific Recognition of Single-Stranded RNA via Toll-like Receptor 7 and 8. *Science* **303**, 1526-1529 (2004).
46. M. Schlee *et al.*, Recognition of 5′ Triphosphate by RIG-I Helicase Requires Short Blunt Double-Stranded RNA as Contained in Panhandle of Negative-Strand Virus. *Immunity* **31**, 25-34 (2009).
47. A. Pichlmair *et al.*, Activation of MDA5 Requires Higher-Order RNA Structures Generated during Virus Infection. *Journal of Virology* **83**, 10761-10769 (2009).
48. A. De Beuckelaer *et al.*, Type I Interferons Interfere with the Capacity of mRNA Lipoplex Vaccines to Elicit Cytolytic T Cell Responses. *Mol Ther* **24**, 2012-2020 (2016).
49. Z. Wang *et al.*, Reducing cell intrinsic immunity to mRNA vaccine alters adaptive immune responses in mice. *Molecular Therapy Nucleic Acids* **34**, (2023).
50. K. Karikó, M. Buckstein, H. Ni, D. Weissman, Suppression of RNA Recognition by Toll-like Receptors: The Impact of Nucleoside Modification and the Evolutionary Origin of RNA. *Immunity* **23**, 165-175 (2005).
51. K. Karikó, H. Muramatsu, J. Ludwig, D. Weissman, Generating the optimal mRNA for therapy: HPLC purification eliminates immune activation and improves translation of nucleoside-modified, protein-encoding mRNA. *Nucleic Acids Research* **39**, e142-e142 (2011).
52. O. Andries *et al.*, N1-methylpseudouridine-incorporated mRNA outperforms pseudouridine-incorporated mRNA by providing enhanced protein expression and reduced immunogenicity in mammalian cell lines and mice. *Journal of Controlled Release* **217**, 337-344 (2015).
53. N. Kaur *et al.*, Genetic comparison among various coronavirus strains for the identification of potential vaccine targets of SARS-CoV2. *Infect Genet Evol* **89**, 104490-104490 (2021).
54. N. Le Bert *et al.*, SARS-CoV-2-specific T cell immunity in cases of COVID-19 and SARS, and uninfected controls. *Nature* **584**, 457-462 (2020).
55. J. Pallesen *et al.*, Immunogenicity and structures of a rationally designed prefusion MERS-CoV spike antigen. *Proceedings of the National Academy of Sciences* **114**, E7348-E7357 (2017).
56. D. Wrapp *et al.*, Cryo-EM structure of the 2019-nCoV spike in the prefusion conformation. *Science* **367**, 1260-1263 (2020).
57. E. E. Walsh *et al.*, Safety and Immunogenicity of Two RNA-Based Covid-19 Vaccine Candidates. *New England Journal of Medicine* **383**, 2439-2450 (2020).
58. P. M. Folegatti *et al.*, Safety and immunogenicity of the ChAdOx1 nCoV-19 vaccine against SARS-CoV-2: a preliminary report of a phase 1/2, single-blind, randomised controlled trial. *The Lancet* **396**, 467-478 (2020).
59. N. van Doremalen *et al.*, ChAdOx1 nCoV-19 vaccine prevents SARS-CoV-2 pneumonia in rhesus macaques. *Nature* **586**, 578-582 (2020).
60. M. N. Ramasamy *et al.*, Safety and immunogenicity of ChAdOx1 nCoV-19 vaccine administered in a prime-boost regimen in young and old adults (COV002): a single-blind, randomised, controlled, phase 2/3 trial. *The Lancet* **396**, 1979-1993 (2020).
61. K. S. Corbett *et al.*, SARS-CoV-2 mRNA vaccine design enabled by prototype pathogen preparedness. *Nature* **586**, 567-571 (2020).
62. A. B. Vogel *et al.*, BNT162b vaccines protect rhesus macaques from SARS-CoV-2. *Nature* **592**, 283-289 (2021).
63. Z. Zhang *et al.*, Humoral and cellular immune memory to four COVID-19 vaccines.

Cell **185**, 2434-2451.e2417 (2022).
64. X. Liu *et al.*, Safety and immunogenicity of heterologous versus homologous prime-boost schedules with an adenoviral vectored and mRNA COVID-19 vaccine (Com-COV): a single-blind, randomised, non-inferiority trial. *The Lancet* **398**, 856-869 (2021).
65. A. S. V. Stuart *et al.*, Immunogenicity, safety, and reactogenicity of heterologous COVID-19 primary vaccination incorporating mRNA, viral-vector, and protein-adjuvant vaccines in the UK (Com-COV2): a single-blind, randomised, phase 2, non-inferiority trial. *Lancet* **399**, 36-49 (2022).
66. R. H. Shaw *et al.*, Effect of priming interval on reactogenicity, peak immunological response, and waning after homologous and heterologous COVID-19 vaccine schedules: exploratory analyses of Com-COV, a randomised control trial. *Lancet Respir Med* **10**, 1049-1060 (2022).
67. X. Liu *et al.*, Safety and immunogenicity of heterologous versus homologous prime-boost schedules with an adenoviral vectored and mRNA COVID-19 vaccine (Com-COV): a single-blind, randomised, non-inferiority trial. *Lancet* **398**, 856-869 (2021).
68. A. Y. Collier *et al.*, Differential Kinetics of Immune Responses Elicited by Covid-19 Vaccines. *N Engl J Med* **385**, 2010-2012 (2021).
69. H. Parry *et al.*, Differential immunogenicity of BNT162b2 or ChAdOx1 vaccines after extended-interval homologous dual vaccination in older people. *Immun Ageing* **18**, 34 (2021).
70. L. Henze *et al.*, Primary ChAdOx1 vaccination does not reactivate pre-existing, cross-reactive immunity. *Frontiers in Immunology* **14**, (2023).
71. R. P. Payne *et al.*, Immunogenicity of standard and extended dosing intervals of BNT162b2 mRNA vaccine. *Cell* **184**, 5699-5714.e5611 (2021).
72. A. Flaxman *et al.*, Reactogenicity and immunogenicity after a late second dose or a third dose of ChAdOx1 nCoV-19 in the UK: a substudy of two randomised controlled trials (COV001 and COV002). *The Lancet* **398**, 981-990 (2021).
73. M. Voysey *et al.*, Single-dose administration and the influence of the timing of the booster dose on immunogenicity and efficacy of ChAdOx1 nCoV-19 (AZD1222) vaccine: a pooled analysis of four randomised trials. *The Lancet* **397**, 881-891 (2021).
74. R. H. Shaw *et al.*, Effect of priming interval on reactogenicity, peak immunological response, and waning after homologous and heterologous COVID-19 vaccine schedules: exploratory analyses of Com-COV, a randomised control trial. *The Lancet Respiratory Medicine* **10**, 1049-1060 (2022).
75. V. Hall *et al.*, Protection against SARS-CoV-2 after Covid-19 Vaccination and Previous Infection. *New England Journal of Medicine* **386**, 1207-1220 (2022).
76. V. G. Hall *et al.*, Delayed-interval BNT162b2 mRNA COVID-19 vaccination enhances humoral immunity and induces robust T cell responses. *Nat Immunol* **23**, 380-385 (2022).
77. K. W. Ng *et al.*, Preexisting and de novo humoral immunity to SARS-CoV-2 in humans. *Science* **370**, 1339-1343 (2020).
78. A. Grifoni *et al.*, Targets of T Cell Responses to SARS-CoV-2 Coronavirus in Humans with COVID-19 Disease and Unexposed Individuals. *Cell* **181**, 1489-1501.e1415 (2020).
79. S. M. Murray *et al.*, The impact of pre-existing cross-reactive immunity on SARS-CoV-2 infection and vaccine responses. *Nature Reviews Immunology* **23**, 304-316 (2023).
80. L. Swadling *et al.*, Pre-existing polymerase-specific T cells expand in abortive seronegative SARS-CoV-2. *Nature* **601**, 110-117 (2022).
81. L. Loyal *et al.*, Cross-reactive CD4+ T cells enhance SARS-CoV-2 immune

responses upon infection and vaccination. *Science* **374**, eabh1823 (2021).
82. C.-Y. Lin *et al.*, Pre-existing humoral immunity to human common cold coronaviruses negatively impacts the protective SARS-CoV-2 antibody response. *Cell Host & Microbe* **30**, 83-96.e84 (2022).
83. E. M. Anderson *et al.*, Seasonal human coronavirus antibodies are boosted upon SARS-CoV-2 infection but not associated with protection. *Cell* **184**, 1858-1864.e1810 (2021).
84. A. L. McNaughton *et al.*, Fatal COVID-19 outcomes are associated with an antibody response targeting epitopes shared with endemic coronaviruses. *JCI Insight* **7**, (2022).
85. A. M. Carabelli *et al.*, SARS-CoV-2 variant biology: immune escape, transmission and fitness. *Nature Reviews Microbiology* **21**, 162-177 (2023).
86. P. V. Markov *et al.*, The evolution of SARS-CoV-2. *Nature Reviews Microbiology* **21**, 361-379 (2023).
87. E. C. f. D. P. a. Control. (2025).
88. W. F. Garcia-Beltran *et al.*, mRNA-based COVID-19 vaccine boosters induce neutralizing immunity against SARS-CoV-2 Omicron variant. *Cell* **185**, 457-466.e454 (2022).
89. D. Planas *et al.*, Reduced sensitivity of SARS-CoV-2 variant Delta to antibody neutralization. *Nature* **596**, 276-280 (2021).
90. M. Andre *et al.*, From Alpha to Omicron: How Different Variants of Concern of the SARS-Coronavirus-2 Impacted the World. *Biology (Basel)* **12**, (2023).
91. Y. Chen *et al.*, Immune recall improves antibody durability and breadth to SARS-CoV-2 variants. *Science Immunology* **7**, eabp8328 (2022).
92. W. Dejnirattisai *et al.*, SARS-CoV-2 Omicron-B.1.1.529 leads to widespread escape from neutralizing antibody responses. *Cell* **185**, 467-484.e415 (2022).
93. C. Hyams *et al.*, Severity of Omicron (B.1.1.529) and Delta (B.1.617.2) SARS-CoV-2 infection among hospitalised adults: a prospective cohort study in Bristol, United Kingdom. *The Lancet Regional Health – Europe* **25**, (2023).
94. A. R. Branche *et al.*, Comparison of bivalent and monovalent SARS-CoV-2 variant vaccines: the phase 2 randomized open-label COVAIL trial. *Nature Medicine* **29**, 2334-2346 (2023).
95. N. G. Marchevsky *et al.*, An exploratory analysis of the response to ChAdOx1 nCoV-19 (AZD1222) vaccine in males and females. *eBioMedicine* **81**, 104128 (2022).
96. G. Li *et al.*, Safety and immunogenicity of the ChAdOx1 nCoV-19 (AZD1222) vaccine in children aged 6–17 years: a preliminary report of COV006, a phase 2 single-blind, randomised, controlled trial. *The Lancet* **399**, 2212-2225 (2022).
97. J. Tran *et al.*, Patterns and temporal trends of comorbidity among adult patients with incident cardiovascular disease in the UK between 2000 and 2014: A population-based cohort study. *PLoS Med* **15**, e1002513 (2018).
98. E. J. Anderson *et al.*, Safety and Immunogenicity of SARS-CoV-2 mRNA-1273 Vaccine in Older Adults. *New England Journal of Medicine* **383**, 2427-2438 (2020).
99. H. Parry *et al.*, Differential immunogenicity of BNT162b2 or ChAdOx1 vaccines after extended-interval homologous dual vaccination in older people. *Immunity & Ageing* **18**, 34 (2021).
100. K. Abu Jabal *et al.*, Impact of age, ethnicity, sex and prior infection status on immunogenicity following a single dose of the BNT162b2 mRNA COVID-19 vaccine: real-world evidence from healthcare workers, Israel, December 2020 to January 2021. *Eurosurveillance* **26**, 2100096 (2021).
101. L. Müller *et al.*, Age-dependent Immune Response to the Biontech/Pfizer BNT162b2 Coronavirus Disease 2019 Vaccination. *Clinical Infectious Diseases* **73**, 2065-2072 (2021).

102. H. M. El Sahly *et al.*, Humoral Immunogenicity of the mRNA-1273 Vaccine in the Phase 3 Coronavirus Efficacy (COVE) Trial. *The Journal of Infectious Diseases* **226**, 1731-1742 (2022).
103. M. J. Divo, C. H. Martinez, D. M. Mannino, Ageing and the epidemiology of multimorbidity. *Eur Respir J* **44**, 1055-1068 (2014).
104. D. Frasca, B. B. Blomberg, B cell function and influenza vaccine responses in healthy aging and disease. *Current Opinion in Immunology* **29**, 112-118 (2014).
105. H. Chi, M. Pepper, P. G. Thomas, Principles and therapeutic applications of adaptive immunity. *Cell* **187**, 2052-2078 (2024).
106. P. K. Gregersen, L. M. Olsson, Recent advances in the genetics of autoimmune disease. *Annu Rev Immunol* **27**, 363-391 (2009).
107. Q. Li, P. Lan, Activation of immune signals during organ transplantation. *Signal Transduction and Targeted Therapy* **8**, 110 (2023).
108. A. Di Matteo, J. M. Bathon, P. Emery, Rheumatoid arthritis. *The Lancet* **402**, 2019-2033 (2023).
109. A. R. Kitching *et al.*, ANCA-associated vasculitis. *Nature Reviews Disease Primers* **6**, 71 (2020).
110. G. Mieli-Vergani *et al.*, Autoimmune hepatitis. *Nature Reviews Disease Primers* **4**, 18017 (2018).
111. T. Alexander, R. Greco, Hematopoietic stem cell transplantation and cellular therapies for autoimmune diseases: overview and future considerations from the Autoimmune Diseases Working Party (ADWP) of the European Society for Blood and Marrow Transplantation (EBMT). *Bone Marrow Transplantation* **57**, 1055-1062 (2022).
112. M. R. Lucey, K. N. Furuya, D. P. Foley, Liver Transplantation. *New England Journal of Medicine* **389**, 1888-1900 (2023).
113. C. Thongprayoon *et al.*, Recent Advances and Clinical Outcomes of Kidney Transplantation. *J Clin Med* **9**, (2020).
114. M. Meneghini, O. Bestard, J. M. Grinyo, Immunosuppressive drugs modes of action. *Best Practice & Research Clinical Gastroenterology* **54-55**, 101757 (2021).
115. Q. Guan, A Comprehensive Review and Update on the Pathogenesis of Inflammatory Bowel Disease. *Journal of Immunology Research* **2019**, 7247238 (2019).
116. A. Albillos *et al.*, Cirrhosis-associated immune dysfunction. *Nature Reviews Gastroenterology & Hepatology* **19**, 112-134 (2022).
117. M. V. Dhodapkar, K. M. Dhodapkar, Immune Modulation in Hematologic Malignancies. *Semin Oncol* **42**, 617-625 (2015).
118. M. A. A. Boyd, D. van Bockel, C. M. L. Munier, A. D. Kelleher, Navigating the complexity of chronic HIV-1 associated immune dysregulation. *Current Opinion in Immunology* **76**, 102186 (2022).
119. R. Berry, G. M. Watson, S. Jonjic, M. A. Degli-Esposti, J. Rossjohn, Modulation of innate and adaptive immunity by cytomegaloviruses. *Nat Rev Immunol* **20**, 113-127 (2020).
120. M. Patel *et al.*, HCMV-Encoded NK Modulators: Lessons From in vitro and in vivo Genetic Variation. *Front Immunol* **9**, 2214 (2018).
121. B. D. Griffin *et al.*, EBV BILF1 evolved to downregulate cell surface display of a wide range of HLA class I molecules through their cytoplasmic tail. *J Immunol* **190**, 1672-1684 (2013).
122. D. Li *et al.*, Down-Regulation of MHC Class II Expression through Inhibition of CIITA Transcription by Lytic Transactivator Zta during Epstein-Barr Virus Reactivation1. *The Journal of Immunology* **182**, 1799-1809 (2009).
123. L. K. Dropulic, H. M. Lederman, Overview of Infections in the Immunocompromised

Host. *Microbiol Spectr* **4**, (2016).
124. S. Ilham *et al.*, Cancer incidence in immunocompromised patients: a single-center cohort study. *BMC Cancer* **23**, 33 (2023).
125. G. Russell, R. Graveley, J. Seid, A.-K. Al-Humidan, H. Skjodt, Mechanisms of action of cyclosporine and effects on connective tissues. *Seminars in Arthritis and Rheumatism* **21**, 16-22 (1992).
126. S. Otsuka *et al.*, Calcineurin inhibitors suppress acute graft-versus-host disease via NFAT-independent inhibition of T cell receptor signaling. *The Journal of Clinical Investigation* **131**, (2021).
127. H. Chi, Regulation and function of mTOR signalling in T cell fate decisions. *Nature Reviews Immunology* **12**, 325-338 (2012).
128. L. J. Appleman, A. Berezovskaya, I. Grass, V. A. Boussiotis, CD28 costimulation mediates T cell expansion via IL-2-independent and IL-2-dependent regulation of cell cycle progression. *J Immunol* **164**, 144-151 (2000).
129. J. D. Powell, G. M. Delgoffe, The Mammalian Target of Rapamycin: Linking T Cell Differentiation, Function, and Metabolism. *Immunity* **33**, 301-311 (2010).
130. O. Traitanon *et al.*, Differential Effects of Tacrolimus versus Sirolimus on the Proliferation, Activation and Differentiation of Human B Cells. *PLOS ONE* **10**, e0129658 (2015).
131. E. F. Wallin, D. L. Hill, M. A. Linterman, K. J. Wood, The Calcineurin Inhibitor Tacrolimus Specifically Suppresses Human T Follicular Helper Cells. *Front Immunol* **9**, 1184 (2018).
132. K. Tsuda *et al.*, Calcineurin inhibitors suppress cytokine production from memory T cells and differentiation of naïve T cells into cytokine-producing mature T cells. *PLoS One* **7**, e31465 (2012).
133. G. Whitehouse *et al.*, IL-2 therapy restores regulatory T-cell dysfunction induced by calcineurin inhibitors. *Proceedings of the National Academy of Sciences* **114**, 7083-7088 (2017).
134. D. Presser *et al.*, Differential kinetics of effector and regulatory T cells in patients on calcineurin inhibitor based drug regimens. *Kidney International* **76**, 557-566 (2009).
135. K. Araki *et al.*, Pathogenic virus-specific T cells cause disease during treatment with the calcineurin inhibitor FK506: implications for transplantation. *Journal of Experimental Medicine* **207**, 2355-2367 (2010).
136. J. R. Azzi, M. H. Sayegh, S. G. Mallat, Calcineurin Inhibitors: 40 Years Later, Can't Live Without …. *The Journal of Immunology* **191**, 5785-5791 (2013).
137. Z. Zou, T. Tao, H. Li, X. Zhu, mTOR signaling pathway and mTOR inhibitors in cancer: progress and challenges. *Cell & Bioscience* **10**, 31 (2020).
138. N. A. Pilch, L. J. Bowman, D. J. Taber, Immunosuppression trends in solid organ transplantation: The future of individualization, monitoring, and management. *Pharmacotherapy* **41**, 119-131 (2021).
139. J. R. Azzi, M. H. Sayegh, S. G. Mallat, Calcineurin Inhibitors: 40 Years Later, Can't Live Without …. *The Journal of Immunology* **191**, 5785 (2013).
140. J. Listing, K. Gerhold, A. Zink, The risk of infections associated with rheumatoid arthritis, with its comorbidity and treatment. *Rheumatology* **52**, 53-61 (2012).
141. S. Ramamoorthy, J. A. Cidlowski, Corticosteroids: Mechanisms of Action in Health and Disease. *Rheum Dis Clin North Am* **42**, 15-31, vii (2016).
142. L. Quéméneur *et al.*, Differential control of cell cycle, proliferation, and survival of primary T lymphocytes by purine and pyrimidine nucleotides. *J Immunol* **170**, 4986-4995 (2003).
143. J. C. A. Broen, J. M. van Laar, Mycophenolate mofetil, azathioprine and tacrolimus: mechanisms in rheumatology. *Nature Reviews Rheumatology* **16**, 167-178 (2020).
144. A. Krawczyk, B. Kravčenia, T. Maślanka, Mycophenolate mofetil: an update on its

mechanism of action and effect on lymphoid tissue. *Front Immunol* **15**, 1463429 (2024).
145. B. N. Cronstein, T. M. Aune, Methotrexate and its mechanisms of action in inflammatory arthritis. *Nature Reviews Rheumatology* **16**, 145-154 (2020).
146. C. F. Spurlock Iii *et al.*, Increased sensitivity to apoptosis induced by methotrexate is mediated by JNK. *Arthritis & Rheumatism* **63**, 2606-2616 (2011).
147. M. A. Sheiko *et al.*, Outcomes in Pediatric Autoimmune Hepatitis and Significance of Azathioprine Metabolites. *J Pediatr Gastroenterol Nutr* **65**, 80-85 (2017).
148. M. Ladrière, [Current indications of azathioprine in nephrology]. *Nephrol Ther* **9**, 8-12 (2013).
149. A. V. Anstey, S. Wakelin, N. J. Reynolds, Guidelines for prescribing azathioprine in dermatology. *Br J Dermatol* **151**, 1123-1132 (2004).
150. O. H. Nielsen, J. T. Bjerrum, H. Herfarth, G. Rogler, Recent advances using immunomodulators for inflammatory bowel disease. *J Clin Pharmacol* **53**, 575-588 (2013).
151. A. D. Goralczyk *et al.*, Calcineurin inhibitor sparing with mycophenolate mofetil in liver transplantion: a systematic review of randomized controlled trials. *Am J Transplant* **12**, 2601-2607 (2012).
152. S. S. Mustafa, Steroid-induced secondary immune deficiency. *Annals of Allergy, Asthma & Immunology* **130**, 713-717 (2023).
153. M. Bianchi, C. Meng, L. B. Ivashkiv, Inhibition of IL-2-induced Jak-STAT signaling by glucocorticoids. *Proc Natl Acad Sci U S A* **97**, 9573-9578 (2000).
154. M. D. Elftman, C. C. Norbury, R. H. Bonneau, M. E. Truckenmiller, Corticosterone impairs dendritic cell maturation and function. *Immunology* **122**, 279-290 (2007).
155. A. E. Coutinho, K. E. Chapman, The anti-inflammatory and immunosuppressive effects of glucocorticoids, recent developments and mechanistic insights. *Mol Cell Endocrinol* **335**, 2-13 (2011).
156. H. Akiho *et al.*, Promising biological therapies for ulcerative colitis: A review of the literature. *World J Gastrointest Pathophysiol* **6**, 219-227 (2015).
157. K. R. VanDerMeid *et al.*, Cellular Cytotoxicity of Next-Generation CD20 Monoclonal Antibodies. *Cancer Immunol Res* **6**, 1150-1160 (2018).
158. S. Lara, J. Heilig, A. Virtanen, S. Kleinau, Exploring complement-dependent cytotoxicity by rituximab isotypes in 2D and 3D-cultured B-cell lymphoma. *BMC Cancer* **22**, 678 (2022).
159. M. Croft, The role of TNF superfamily members in T-cell function and diseases. *Nature Reviews Immunology* **9**, 271-285 (2009).
160. G. van Loo, M. J. M. Bertrand, Death by TNF: a road to inflammation. *Nature Reviews Immunology* **23**, 289-303 (2023).
161. R. Kado, G. Sanders, W. J. McCune, Suppression of normal immune responses after treatment with rituximab. *Current Opinion in Rheumatology* **28**, (2016).
162. T. A. Davis, D. K. Czerwinski, R. Levy, Therapy of B-cell lymphoma with anti-CD20 antibodies can result in the loss of CD20 antigen expression. *Clin Cancer Res* **5**, 611-615 (1999).
163. R. Kumar, S. Kumar, S. S. Prakash, Compensated liver cirrhosis: Natural course and disease-modifying strategies. *World J Methodol* **13**, 179-193 (2023).
164. H. Tilg *et al.*, Serum levels of cytokines in chronic liver diseases. *Gastroenterology* **103**, 264-274 (1992).
165. M. Buck *et al.*, Novel inflammatory biomarkers of portal pressure in compensated cirrhosis patients. *Hepatology* **59**, (2014).
166. R. Wiest, A. Albillos, M. Trauner, J. S. Bajaj, R. Jalan, Targeting the gut-liver axis in liver disease. *Journal of Hepatology* **67**, 1084-1103 (2017).
167. K. A. Tazi *et al.*, Upregulation of TNF-alpha production signaling pathways in

monocytes from patients with advanced cirrhosis: Possible role of Akt and IRAK-M. *Journal of Hepatology* **45**, 280-289 (2006).
168. L. Muñoz *et al.*, Mesenteric Th1 polarization and monocyte TNF-alpha production: first steps to systemic inflammation in rats with cirrhosis. *Hepatology* **42**, 411-419 (2005).
169. D. L. Shawcross, N. A. Davies, R. Williams, R. Jalan, Systemic inflammatory response exacerbates the neuropsychological effects of induced hyperammonemia in cirrhosis. *Journal of Hepatology* **40**, 247-254 (2004).
170. I. A. Rajkovic, R. Williams, Abnormalities of Neutrophil Phagocytosis, Intracellular Killing and Metabolic Activity in Alcoholic Cirrhosis and Hepatitis. *Hepatology* **6**, (1986).
171. M. Lario *et al.*, Defective thymopoiesis and poor peripheral homeostatic replenishment of T-helper cells cause T-cell lymphopenia in cirrhosis. *Journal of Hepatology* **59**, 723-730 (2013).
172. H. Doi *et al.*, Dysfunctional B-cell activation in cirrhosis resulting from hepatitis C infection associated with disappearance of CD27-Positive B-cell population. *Hepatology* **55**, (2012).
173. F. Gomez, P. Ruiz, A. D. Schreiber, Impaired Function of Macrophage Fcγ Receptors and Bacterial Infection in Alcoholic Cirrhosis. *New England Journal of Medicine* **331**, 1122-1128 (1994).
174. T. Xing, L. Li, H. Cao, J. Huang, Altered immune function of monocytes in different stages of patients with acute on chronic liver failure. *Clinical and Experimental Immunology* **147**, 184-188 (2006).
175. A. B. Hauser *et al.*, Characteristics and causes of immune dysfunction related to uremia and dialysis. *Perit Dial Int* **28 Suppl 3**, S183-187 (2008).
176. M. R. Sharif *et al.*, Immune disorders in hemodialysis patients. *Iranian journal of kidney diseases* **9**, 84-96 (2015).
177. C. T. Kassakian, S. Ajmal, R. Y. Gohh, P. E. Morrissey, G. P. Bayliss, Immunosuppression in the failing and failed transplant kidney: optimizing outcomes. *Nephrology Dialysis Transplantation* **31**, 1261-1269 (2015).
178. I. Aggeletopoulou, P. Davoulou, C. Konstantakis, K. Thomopoulos, C. Triantos, Response to hepatitis B vaccination in patients with liver cirrhosis. *Rev Med Virol* **27**, (2017).
179. D. A. Roni *et al.*, Safety and efficacy of hepatitis B vaccination in cirrhosis of liver. *Adv Virol* **2013**, 196704 (2013).
180. S. Subesinghe, K. Bechman, A. I. Rutherford, D. Goldblatt, J. B. Galloway, A Systematic Review and Metaanalysis of Antirheumatic Drugs and Vaccine Immunogenicity in Rheumatoid Arthritis. *J Rheumatol* **45**, 733-744 (2018).
181. Y. Hagihara *et al.*, Infliximab and/or immunomodulators inhibit immune responses to trivalent influenza vaccination in adults with inflammatory bowel disease. *Journal of Crohn's and Colitis* **8**, 223-233 (2014).
182. E. A. Blumberg *et al.*, The Immunogenicity of Influenza Virus Vaccine in Solid Organ Transplant Recipients. *Clinical Infectious Diseases* **22**, 295-302 (1996).
183. A. L. Ryan *et al.*, Immunogenicity of the inactivated influenza vaccine in children who have undergone allogeneic haematopoietic stem cell transplant. *Bone Marrow Transplantation* **55**, 773-779 (2020).
184. S. van Assen *et al.*, Humoral responses after influenza vaccination are severely reduced in patients with rheumatoid arthritis treated with rituximab. *Arthritis Rheum* **62**, 75-81 (2010).
185. J. H. Koh *et al.*, Safety, and humoral and cell-mediated immune responses to herpes zoster vaccine in patients with rheumatoid arthritis. *Journal of Rheumatology* **45**, 465-469 (2018).

186. H.-J. Cheong *et al.*, Humoral and cellular immune responses to influenza vaccine in patients with advanced cirrhosis. *Vaccine* **24**, 2417-2422 (2006).
187. L. Simeng *et al.*, Covid-19 vaccine-induced antibodies are attenuated and decay rapidly in infliximab treated patients. *Nature Portfolio*, (2021).
188. R. Redjoul, A. Le Bouter, F. Beckerich, S. Fourati, S. Maury, Antibody response after second BNT162b2 dose in allogeneic HSCT recipients. *The Lancet* **398**, 298-299 (2021).
189. S. K. Mahil *et al.*, The effect of methotrexate and targeted immunosuppression on humoral and cellular immune responses to the COVID-19 vaccine BNT162b2: a cohort study. *The Lancet Rheumatology*, (2021).
190. K. Maneikis *et al.*, Immunogenicity of the BNT162b2 COVID-19 mRNA vaccine and early clinical outcomes in patients with haematological malignancies in Lithuania: a national prospective cohort study. *The Lancet Haematology* **8**, e583-e592 (2021).
191. J. L. Alexander *et al.*, COVID-19 vaccine-induced antibody responses in immunosuppressed patients with inflammatory bowel disease (VIP): a multicentre, prospective, case-control study. *Lancet Gastroenterol Hepatol* **7**, 342-352 (2022).
192. N. A. Kennedy *et al.*, Infliximab is associated with attenuated immunogenicity to BNT162b2 and ChAdOx1 nCoV-19 SARS-CoV-2 vaccines in patients with IBD. *Gut* **70**, 1884-1893 (2021).
193. P. J. Thuluvath, P. Robarts, M. Chauhan, Analysis of antibody responses after COVID-19 vaccination in liver transplant recipients and those with chronic liver diseases. *J Hepatol* **75**, 1434-1439 (2021).
194. S. M. Murray *et al.*, Impaired humoral and cellular response to primary COVID-19 vaccination in patients less than 2 years after allogeneic bone marrow transplant. *British Journal of Haematology* **n/a**, (2022).
195. E. J. Carr *et al.*, Neutralising antibodies after COVID-19 vaccination in UK haemodialysis patients. *Lancet* **398**, 1038-1041 (2021).
196. M. Prendecki *et al.*, Immunological responses to SARS-CoV-2 vaccines in kidney transplant recipients. *Lancet* **398**, 1482-1484 (2021).
197. M. Jiménez *et al.*, Cellular and humoral immunogenicity of the mRNA-1273 SARS-CoV-2 vaccine in patients with hematologic malignancies. *Blood Adv* **6**, 774-784 (2022).
198. B. Dhakal *et al.*, Response to SARS-CoV-2 vaccination in patients after hematopoietic cell transplantation and CAR T-cell therapy. *Blood* **138**, 1278-1281 (2021).
199. P. Bergman *et al.*, Safety and efficacy of the mRNA BNT162b2 vaccine against SARS-CoV-2 in five groups of immunocompromised patients and healthy controls in a prospective open-label clinical trial. *EBioMedicine* **74**, 103705 (2021).
200. L. Mumford *et al.*, Impact of SARS-CoV-2 spike antibody positivity on infection and hospitalisation rates in immunosuppressed populations during the omicron period: the MELODY study. *The Lancet* **405**, 314-328 (2025).
201. D. T.-H. Chen *et al.*, Uptake, effectiveness and safety of COVID-19 vaccines in individuals at clinical risk due to immunosuppressive drug therapy or transplantation procedures: a population-based cohort study in England. *BMC Medicine* **22**, 237 (2024).
202. F. A. Pearce *et al.*, Antibody prevalence after three or more COVID-19 vaccine doses in individuals who are immunosuppressed in the UK: a cross-sectional study from MELODY. *The Lancet Rheumatology* **5**, e461-e473 (2023).
203. K. R. Kukurba, S. B. Montgomery, RNA Sequencing and Analysis. *Cold Spring Harb Protoc* **2015**, 951-969 (2015).
204. Helder I. Nakaya *et al.*, Systems Analysis of Immunity to Influenza Vaccination across Multiple Years and in Diverse Populations Reveals Shared Molecular

Signatures. *Immunity* **43**, 1186-1198 (2015).
205. D. Kazmin *et al.*, Systems analysis of protective immune responses to RTS,S malaria vaccination in humans. *Proceedings of the National Academy of Sciences* **114**, 2425-2430 (2017).
206. H.-C. S. P. Team *et al.*, Multicohort analysis reveals baseline transcriptional predictors of influenza vaccination responses. *Science Immunology* **2**, eaal4656 (2017).
207. J. S. Tsang *et al.*, Improving Vaccine-Induced Immunity: Can Baseline Predict Outcome? *Trends Immunol* **41**, 457-465 (2020).
208. P. S. Arunachalam *et al.*, Systems vaccinology of the BNT162b2 mRNA vaccine in humans. *Nature* **596**, 410-416 (2021).
209. F. Tang *et al.*, mRNA-Seq whole-transcriptome analysis of a single cell. *Nature Methods* **6**, 377-382 (2009).
210. D. Jovic *et al.*, Single-cell RNA sequencing technologies and applications: A brief overview. *Clin Transl Med* **12**, e694 (2022).
211. R. Sparks *et al.*, Influenza vaccination reveals sex dimorphic imprints of prior mild COVID-19. *Nature* **614**, 752-761 (2023).
212. M. P. Mulè *et al.*, Integrating population and single-cell variations in vaccine responses identifies a naturally adjuvanted human immune setpoint. *Immunity* **57**, 1160-1176.e1167 (2024).
213. M. Wilhelm *et al.*, Mass-spectrometry-based draft of the human proteome. *Nature* **509**, 582-587 (2014).
214. P. Steffen *et al.*, Protein species as diagnostic markers. *J Proteomics* **134**, 5-18 (2016).
215. S. A. Williams *et al.*, Plasma protein patterns as comprehensive indicators of health. *Nature Medicine* **25**, 1851-1857 (2019).
216. D. A. Gadd *et al.*, Blood protein assessment of leading incident diseases and mortality in the UK Biobank. *Nature Aging* **4**, 939-948 (2024).
217. G. H. Eldjarn *et al.*, Large-scale plasma proteomics comparisons through genetics and disease associations. *Nature* **622**, 348-358 (2023).
218. B. B. Sun *et al.*, Plasma proteomic associations with genetics and health in the UK Biobank. *Nature* **622**, 329-338 (2023).
219. M. Cui, C. Cheng, L. Zhang, High-throughput proteomics: a methodological mini-review. *Laboratory Investigation* **102**, 1170-1181 (2022).
220. L. Wik *et al.*, Proximity Extension Assay in Combination with Next-Generation Sequencing for High-throughput Proteome-wide Analysis. *Mol Cell Proteomics* **20**, 100168 (2021).
221. D. J. Schneider *et al.*, in *RNA Therapeutics,* P. H. Giangrande, V. de Franciscis, J. J. Rossi, Eds. (Academic Press, 2022), pp. 171-260.
222. F. J. Ryan *et al.*, A systems immunology study comparing innate and adaptive immune responses in adults to COVID-19 mRNA and adenovirus vectored vaccines. *Cell Rep Med* **4**, 100971 (2023).
223. C. Bergamaschi *et al.*, Systemic IL-15, IFN-γ, and IP-10/CXCL10 signature associated with effective immune response to SARS-CoV-2 in BNT162b2 mRNA vaccine recipients. *Cell Rep* **36**, 109504 (2021).
224. K. M. McKinnon, Flow Cytometry: An Overview. *Curr Protoc Immunol* **120**, 5.1.1-5.1.11 (2018).
225. L. A. Herzenberg *et al.*, The History and Future of the Fluorescence Activated Cell Sorter and Flow Cytometry: A View from Stanford. *Clinical Chemistry* **48**, 1819-1827 (2002).
226. J. P. Robinson, Flow Cytometry: Past and Future. *BioTechniques* **72**, 159-169 (2022).

227. A. J. Konecny, P. L. Mage, A. J. Tyznik, M. Prlic, F. Mair, OMIP-102: 50-color phenotyping of the human immune system with in-depth assessment of T cells and dendritic cells. *Cytometry Part A* **105**, 430-436 (2024).
228. S. A. Apostolidis *et al.*, Cellular and humoral immune responses following SARS-CoV-2 mRNA vaccination in patients with multiple sclerosis on anti-CD20 therapy. *Nature Medicine* **27**, 1990-2001 (2021).
229. N. G. Nuñez *et al.*, High-dimensional analysis of 16 SARS-CoV-2 vaccine combinations reveals lymphocyte signatures correlating with immunogenicity. *Nature Immunology* **24**, 941-954 (2023).
230. N. Faulkner *et al.*, Reduced antibody cross-reactivity following infection with B.1.1.7 than with parental SARS-CoV-2 strains. *eLife* **10**, e69317 (2021).
231. A. Ogbe *et al.*, T cell assays differentiate clinical and subclinical SARS-CoV-2 infections from cross-reactive antiviral responses. *Nat Commun* **12**, 2055 (2021).
232. L. Wik *et al.*, Proximity Extension Assay in Combination with Next-Generation Sequencing for High-throughput Proteome-wide Analysis. *Molecular & Cellular Proteomics* **20**, 100168 (2021).
233. S. Chen, Y. Zhou, Y. Chen, J. Gu, fastp: an ultra-fast all-in-one FASTQ preprocessor. *Bioinformatics* **34**, i884-i890 (2018).
234. R. Patro, G. Duggal, M. I. Love, R. A. Irizarry, C. Kingsford, Salmon provides fast and bias-aware quantification of transcript expression. *Nature Methods* **14**, 417-419 (2017).
235. Y. Zhang, G. Parmigiani, W. E. Johnson, ComBat-seq: batch effect adjustment for RNA-seq count data. *NAR Genomics and Bioinformatics* **2**, (2020).
236. M. I. Love, W. Huber, S. Anders, Moderated estimation of fold change and dispersion for RNA-seq data with DESeq2. *Genome Biology* **15**, 550 (2014).
237. S. Hänzelmann, R. Castelo, J. Guinney, GSVA: gene set variation analysis for microarray and RNA-Seq data. *BMC Bioinformatics* **14**, 7 (2013).
238. S. Li *et al.*, Molecular signatures of antibody responses derived from a systems biology study of five human vaccines. *Nature Immunology* **15**, 195-204 (2014).
239. G. Korotkevich *et al.*, Fast gene set enrichment analysis. *bioRxiv*, 060012 (2021).
240. T. Wu *et al.*, clusterProfiler 4.0: A universal enrichment tool for interpreting omics data. *The Innovation* **2**, (2021).
241. Z. Gu, R. Eils, M. Schlesner, Complex heatmaps reveal patterns and correlations in multidimensional genomic data. *Bioinformatics* **32**, 2847-2849 (2016).
242. Y. Hao *et al.*, Integrated analysis of multimodal single-cell data. *Cell* **184**, 3573-3587.e3529 (2021).
243. P. Germain, A. Lun, C. Garcia Meixide, W. Macnair, M. Robinson, Doublet identification in single-cell sequencing data using scDblFinder [version 2; peer review: 2 approved]. *F1000Research* **10**, (2022).
244. C. S. McGinnis *et al.*, MULTI-seq: sample multiplexing for single-cell RNA sequencing using lipid-tagged indices. *Nature Methods* **16**, 619-626 (2019).
245. M. D. Robinson, D. J. McCarthy, G. K. Smyth, edgeR: a Bioconductor package for differential expression analysis of digital gene expression data. *Bioinformatics* **26**, 139-140 (2010).
246. R. A. Watson *et al.*, Immune checkpoint blockade sensitivity and progression-free survival associates with baseline CD8+ T cell clone size and cytotoxicity. *Science Immunology* **6**, eabj8825 (2021).
247. L. C. Garner *et al.*, Single-cell analysis of human MAIT cell transcriptional, functional and clonal diversity. *Nature Immunology* **24**, 1565-1578 (2023).
248. Z. Gu, L. Gu, R. Eils, M. Schlesner, B. Brors, circlize implements and enhances circular visualization in R. *Bioinformatics* **30**, 2811-2812 (2014).
249. E. J. Haas *et al.*, Impact and effectiveness of mRNA BNT162b2 vaccine against

SARS-CoV-2 infections and COVID-19 cases, hospitalisations, and deaths following a nationwide vaccination campaign in Israel: an observational study using national surveillance data. *Lancet* **397**, 1819-1829 (2021).
250. E. Pritchard *et al.*, Impact of vaccination on new SARS-CoV-2 infections in the United Kingdom. *Nat Med* **27**, 1370-1378 (2021).
251. T. Nyberg *et al.*, Comparative analysis of the risks of hospitalisation and death associated with SARS-CoV-2 omicron (B.1.1.529) and delta (B.1.617.2) variants in England: a cohort study. *Lancet* **399**, 1303-1312 (2022).
252. T. Marjot *et al.*, Outcomes following SARS-CoV-2 infection in patients with chronic liver disease: An international registry study. *J Hepatol* **74**, 567-577 (2021).
253. L. Turtle *et al.*, Outcome of COVID-19 in hospitalised immunocompromised patients: An analysis of the WHO ISARIC CCP-UK prospective cohort study. *PLOS Medicine* **20**, e1004086 (2023).
254. H. J. Whitaker *et al.*, Pfizer-BioNTech and Oxford AstraZeneca COVID-19 vaccine effectiveness and immune response amongst individuals in clinical risk groups. *Journal of Infection* **84**, 675-683 (2022).
255. S. A. Madhi *et al.*, Durability of ChAdOx1 nCoV-19 (AZD1222) vaccine and hybrid humoral immunity against variants including omicron BA.1 and BA.4 6 months after vaccination (COV005): a post-hoc analysis of a randomised, phase 1b–2a trial. *The Lancet Infectious Diseases* **23**, 295-306 (2023).
256. M. Wu *et al.*, Three-dose vaccination elicits neutralising antibodies against omicron. *The Lancet* **399**, 715-717 (2022).
257. C. J. Reynolds *et al.*, Immune boosting by B.1.1.529 (Omicron) depends on previous SARS-CoV-2 exposure. *Science* **377**, eabq1841 (2022).
258. E. Barnes *et al.*, SARS-CoV-2-specific immune responses and clinical outcomes after COVID-19 vaccination in patients with immune-suppressive disease. *Nature Medicine* **29**, 1760-1774 (2023).
259. S. M. Murray *et al.*, Immune responses and clinical outcomes after COVID-19 vaccination in patients with liver disease and liver transplant recipients. *Journal of Hepatology* **80**, 109-123 (2024).
260. B. F. J. Goudsmit *et al.*, Validation of the Model for End-stage Liver Disease sodium (MELD-Na) score in the Eurotransplant region. *Am J Transplant* **21**, 229-240 (2021).
261. *Clerical Changes for Implementation of Adding Serum Sodium to the MELD Score.* (2015).
262. "World Health Organization. Living guidance for clinical management of COVID-19: living guidance, 23 November 2021," (World Health Organization, 2021).
263. S. Elbe, G. Buckland-Merrett, Data, disease and diplomacy: GISAID's innovative contribution to global health. *Glob Chall* **1**, 33-46 (2017).
264. D. T. Skelly *et al.*, Two doses of SARS-CoV-2 vaccination induce robust immune responses to emerging SARS-CoV-2 variants of concern. *Nature Communications* **12**, 5061 (2021).
265. U. Cillo *et al.*, Immunosuppressive regimens for adult liver transplant recipients in real-life practice: consensus recommendations from an Italian Working Group. *Hepatology International* **14**, 930-943 (2020).
266. C. Millson *et al.*, Adult liver transplantation: UK clinical guideline - part 2: surgery and post-operation. *Frontline Gastroenterology* **11**, 385 (2020).
267. D. S. Khoury *et al.*, Neutralizing antibody levels are highly predictive of immune protection from symptomatic SARS-CoV-2 infection. *Nature Medicine* **27**, 1205-1211 (2021).
268. M. J. Scurr *et al.*, Magnitude of venous or capillary blood-derived SARS-CoV-2-specific T cell response determines COVID-19 immunity. *Nat Commun* **13**, 5422 (2022).

269. P. B. Gilbert *et al.*, Immune correlates analysis of the mRNA-1273 COVID-19 vaccine efficacy clinical trial. *Science* **375**, 43-50 (2022).
270. V. Fumagalli *et al.*, Antibody-independent protection against heterologous SARS-CoV-2 challenge conferred by prior infection or vaccination. *Nature Immunology* **25**, 633-643 (2024).
271. K. Maneikis *et al.*, Immunogenicity of the BNT162b2 COVID-19 mRNA vaccine and early clinical outcomes in patients with haematological malignancies in Lithuania: a national prospective cohort study. *Lancet Haematol* **8**, e583-e592 (2021).
272. V. Furer *et al.*, Immunogenicity induced by two and three doses of the BNT162b2 mRNA vaccine in patients with autoimmune inflammatory rheumatic diseases and immunocompetent controls: a longitudinal multicentre study. *Ann Rheum Dis* **81**, 1594-1602 (2022).
273. A. M. Spanjaart *et al.*, Poor outcome of patients with COVID-19 after CAR T-cell therapy for B-cell malignancies: results of a multicenter study on behalf of the European Society for Blood and Marrow Transplantation (EBMT) Infectious Diseases Working Party and the European Hematology Association (EHA) Lymphoma Group. *Leukemia* **35**, 3585-3588 (2021).
274. P. Ljungman *et al.*, COVID-19 and stem cell transplantation; results from an EBMT and GETH multicenter prospective survey. *Leukemia* **35**, 2885-2894 (2021).
275. S. H. Lim *et al.*, Antibody responses after SARS-CoV-2 vaccination in patients with lymphoma. *Lancet Haematol* **8**, e542-e544 (2021).
276. M. Kantauskaite *et al.*, Intensity of mycophenolate mofetil treatment is associated with an impaired immune response to SARS-CoV-2 vaccination in kidney transplant recipients. *American Journal of Transplantation* **22**, 634-639 (2022).
277. A. Abhishek *et al.*, Effect of a 2-week interruption in methotrexate treatment versus continued treatment on COVID-19 booster vaccine immunity in adults with inflammatory conditions (VROOM study): a randomised, open label, superiority trial. *The Lancet Respiratory Medicine* **10**, 840-850 (2022).
278. M. Kantauskaite *et al.*, Immune response to third SARS-CoV-2 vaccination in seronegative kidney transplant recipients: Possible improvement by mycophenolate mofetil reduction. *Clinical Transplantation* **36**, e14790 (2022).
279. K. Lederer *et al.*, Germinal center responses to SARS-CoV-2 mRNA vaccines in healthy and immunocompromised individuals. *Cell* **185**, 1008-1024.e1015 (2022).
280. L. Quéméneur *et al.*, Mycophenolic Acid Inhibits IL-2-Dependent T Cell Proliferation, But Not IL-2-Dependent Survival and Sensitization to Apoptosis1. *The Journal of Immunology* **169**, 2747-2755 (2002).
281. S. Eickenberg *et al.*, Mycophenolic acid counteracts B cell proliferation and plasmablast formation in patients with systemic lupus erythematosus. *Arthritis Research & Therapy* **14**, R110 (2012).
282. J. J. H. Smeets, H. van Malenstein, S. van der Merwe, F. Nevens, J. Verbeek, SARS-CoV-2 anti-spike IgG antibodies are present in all liver transplant recipients after fifth vaccine dose. *Journal of Hepatology* **80**, e284-e286 (2024).
283. D. Cromer *et al.*, Neutralising antibody titres as predictors of protection against SARS-CoV-2 variants and the impact of boosting: a meta-analysis. *The Lancet Microbe* **3**, e52-e61 (2022).
284. S. C. Moore *et al.*, Evolution of long-term vaccine-induced and hybrid immunity in healthcare workers after different COVID-19 vaccine regimens. *Med* **4**, 191-215.e199 (2023).
285. D. Paprckova, E. Salyova, J. Michalik, O. Stepanek, Bystander activation in memory and antigen-inexperienced memory-like CD8 T cells. *Current Opinion in Immunology* **82**, 102299 (2023).
286. R. Nesamari *et al.*, Post-pandemic memory T cell response to SARS-CoV-2 is

durable, broadly targeted, and cross-reactive to the hypermutated BA.2.86 variant. *Cell Host Microbe* **32**, 162-169.e163 (2024).
287. L. Guo *et al.*, Durability and cross-reactive immune memory to SARS-CoV-2 in individuals 2 years after recovery from COVID-19: a longitudinal cohort study. *The Lancet Microbe* **5**, e24-e33 (2024).
288. E. C. Wall *et al.*, AZD1222-induced neutralising antibody activity against SARS-CoV-2 Delta VOC. *The Lancet* **398**, 207-209 (2021).
289. H. Ward *et al.*, Population antibody responses following COVID-19 vaccination in 212,102 individuals. *Nature Communications* **13**, 907 (2022).
290. M. J. van Gils *et al.*, Antibody responses against SARS-CoV-2 variants induced by four different SARS-CoV-2 vaccines in health care workers in the Netherlands: A prospective cohort study. *PLOS Medicine* **19**, e1003991 (2022).
291. A. S. V. Stuart *et al.*, Immunogenicity, safety, and reactogenicity of heterologous COVID-19 primary vaccination incorporating mRNA, viral-vector, and protein-adjuvant vaccines in the UK (Com-COV2): a single-blind, randomised, phase 2, non-inferiority trial. *Lancet* **399**, 36-49 (2022).
292. P. Martin *et al.*, Comparison of immunogenicity and clinical effectiveness between BNT162b2 and ChAdOx1 SARS-CoV-2 vaccines in people with end-stage kidney disease receiving haemodialysis: A prospective, observational cohort study. *Lancet Reg Health Eur* **21**, 100478 (2022).
293. K. J. Hassett *et al.*, mRNA vaccine trafficking and resulting protein expression after intramuscular administration. *Molecular Therapy Nucleic Acids* **35**, (2024).
294. S. Marquez-Martinez, N. Salisch, J. Serroyen, R. Zahn, S. Khan, Peak transgene expression after intramuscular immunization of mice with adenovirus 26-based vector vaccines correlates with transgene-specific adaptive immune responses. *PLOS ONE* **19**, e0299215 (2024).
295. H. Colton *et al.*, Greater preservation of SARS-CoV-2 neutralising antibody responses following the ChAdOx1-S (AZD1222) vaccine compared with mRNA vaccines in haematopoietic cell transplant recipients. *British Journal of Haematology* **205**, 2206-2218 (2024).
296. M. Stone *et al.*, Evaluation of Commercially Available High-Throughput SARS-CoV-2 Serologic Assays for Serosurveillance and Related Applications. *Emerg Infect Dis* **28**, 672-683 (2022).
297. A. A. Manu *et al.*, Development and utility of a SARS-CoV-2 pseudovirus assay for compound screening and antibody neutralization assays. *Heliyon* **10**, (2024).
298. S. Feng *et al.*, Correlates of protection against symptomatic and asymptomatic SARS-CoV-2 infection. *Nat Med* **27**, 2032-2040 (2021).
299. P. B. Gilbert *et al.*, Immune correlates analysis of the mRNA-1273 COVID-19 vaccine efficacy clinical trial. *Science* **375**, 43-50 (2022).
300. S. Ahmed *et al.*, Postvaccination antibody titres predict protection against COVID-19 in patients with autoimmune diseases: survival analysis in a prospective cohort. *Annals of the Rheumatic Diseases* **81**, 868-874 (2022).
301. A. J. Mentzer *et al.*, Human leukocyte antigen alleles associate with COVID-19 vaccine immunogenicity and risk of breakthrough infection. *Nature Medicine* **29**, 147-157 (2023).
302. E. Phillips *et al.*, Comparison of two T-cell assays to evaluate T-cell responses to SARS-CoV-2 following vaccination in naïve and convalescent healthcare workers. *Clinical and Experimental Immunology* **209**, 90-98 (2022).
303. Q. Ma *et al.*, Global Percentage of Asymptomatic SARS-CoV-2 Infections Among the Tested Population and Individuals With Confirmed COVID-19 Diagnosis: A Systematic Review and Meta-analysis. *JAMA Network Open* **4**, e2137257-e2137257 (2021).

304. R. Baden Lindsey *et al.*, Efficacy and Safety of the mRNA-1273 SARS-CoV-2 Vaccine. *New England Journal of Medicine* **384**, 403-416 (2021).
305. F. P. Polack *et al.*, Safety and Efficacy of the BNT162b2 mRNA Covid-19 Vaccine. *New England Journal of Medicine* **383**, 2603-2615 (2020).
306. R. Kundu *et al.*, Cross-reactive memory T cells associate with protection against SARS-CoV-2 infection in COVID-19 contacts. *Nature Communications* **13**, 80 (2022).
307. C. Dong, Cytokine Regulation and Function in T Cells. *Annual Review of Immunology* **39**, 51-76 (2021).
308. A. Binayke *et al.*, A quest for universal anti-SARS-CoV-2 T cell assay: systematic review, meta-analysis, and experimental validation. *npj Vaccines* **9**, 3 (2024).
309. A. Ogbe *et al.*, T cell assays differentiate clinical and subclinical SARS-CoV-2 infections from cross-reactive antiviral responses. *Nature Communications* **12**, 2055 (2021).
310. J. C. Law, T. H. Watts, Considerations for Choosing T Cell Assays during a Pandemic. *The Journal of Immunology* **211**, 169-174 (2023).
311. H. Lee, S. Jeong, E.-C. Shin, Significance of bystander T cell activation in microbial infection. *Nature Immunology* **23**, 13-22 (2022).
312. T. M. Williams, Human leukocyte antigen gene polymorphism and the histocompatibility laboratory. *J Mol Diagn* **3**, 98-104 (2001).
313. E. Arrieta-Bolaños, D. I. Hernández-Zaragoza, R. Barquera, An HLA map of the world: A comparison of HLA frequencies in 200 worldwide populations reveals diverse patterns for class I and class II. *Frontiers in Genetics* **14**, (2023).
314. M. Z. M. Zheng *et al.*, Deconvoluting TCR-dependent & -independent activation is vital for reliable Ag-specific CD4+ T cell characterization by AIM assay. *bioRxiv*, 2024.2012.2010.627643 (2024).
315. A. Lemieux *et al.*, Enhanced detection of antigen-specific T cells by a multiplexed AIM assay. *Cell Rep Methods* **4**, 100690 (2024).
316. G. Bowyer *et al.*, Activation-induced Markers Detect Vaccine-Specific CD4$^+$ T Cell Responses Not Measured by Assays Conventionally Used in Clinical Trials. *Vaccines (Basel)* **6**, (2018).
317. S. Reiss *et al.*, Comparative analysis of activation induced marker (AIM) assays for sensitive identification of antigen-specific CD4 T cells. *PLoS One* **12**, e0186998 (2017).
318. A. Tarke *et al.*, SARS-CoV-2 vaccination induces immunological T cell memory able to cross-recognize variants from Alpha to Omicron. *Cell* **185**, 847-859.e811 (2022).
319. S. L. Gray-Gaillard *et al.*, SARS-CoV-2 inflammation durably imprints memory CD4 T cells. *Sci Immunol* **9**, eadj8526 (2024).
320. Y. Gao *et al.*, Immunodeficiency syndromes differentially impact the functional profile of SARS-CoV-2-specific T cells elicited by mRNA vaccination. *Immunity* **55**, 1732-1746.e1735 (2022).
321. J. Mateus *et al.*, Low-dose mRNA-1273 COVID-19 vaccine generates durable memory enhanced by cross-reactive T cells. *Science* **374**, eabj9853 (2021).
322. L. Garcia-Alonso *et al.*, Single-cell roadmap of human gonadal development. *Nature* **607**, 540-547 (2022).
323. S. A. Schattgen *et al.*, Integrating T cell receptor sequences and transcriptional profiles by clonotype neighbor graph analysis (CoNGA). *Nat Biotechnol* **40**, 54-63 (2022).
324. G. E. Hoffman, E. E. Schadt, variancePartition: interpreting drivers of variation in complex gene expression studies. *BMC Bioinformatics* **17**, 483 (2016).
325. N. M. Provine, P. Klenerman, MAIT Cells in Health and Disease. *Annu Rev Immunol* **38**, 203-228 (2020).
326. Y. Hu *et al.*, γδ T cells: origin and fate, subsets, diseases and immunotherapy. *Signal*

Transduction and Targeted Therapy **8**, 434 (2023).
327. B. Zhang *et al.*, Multimodal single-cell datasets characterize antigen-specific CD8+ T cells across SARS-CoV-2 vaccination and infection. *Nature Immunology* **24**, 1725-1734 (2023).
328. R. V. Luckheeram, R. Zhou, A. D. Verma, B. Xia, $CD4^+$T cells: differentiation and functions. *Clin Dev Immunol* **2012**, 925135 (2012).
329. C.-H. Koh, S. Lee, M. Kwak, B.-S. Kim, Y. Chung, CD8 T-cell subsets: heterogeneity, functions, and therapeutic potential. *Experimental & Molecular Medicine* **55**, 2287-2299 (2023).
330. A. Chaudhry *et al.*, Interleukin-10 signaling in regulatory T cells is required for suppression of Th17 cell-mediated inflammation. *Immunity* **34**, 566-578 (2011).
331. A. O'Garra, P. L. Vieira, P. Vieira, A. E. Goldfeld, IL-10-producing and naturally occurring CD4+ Tregs: limiting collateral damage. *J Clin Invest* **114**, 1372-1378 (2004).
332. M. Efremova, M. Vento-Tormo, S. A. Teichmann, R. Vento-Tormo, CellPhoneDB: inferring cell–cell communication from combined expression of multi-subunit ligand–receptor complexes. *Nature Protocols* **15**, 1484-1506 (2020).
333. K. A. Lagattuta *et al.*, The T cell receptor sequence influences the likelihood of T cell memory formation. *Cell Reports* **44**, (2025).
334. D. Zemmour *et al.*, Single-cell gene expression reveals a landscape of regulatory T cell phenotypes shaped by the TCR. *Nature Immunology* **19**, 291-301 (2018).
335. N. J. Tubo *et al.*, Single Naive CD4+ T Cells from a Diverse Repertoire Produce Different Effector Cell Types during Infection. *Cell* **153**, 785-796 (2013).
336. T. Guo *et al.*, A Subset of Human Autoreactive CD1c-Restricted T Cells Preferentially Expresses TRBV4-1(+) TCRs. *J Immunol* **200**, 500-511 (2018).
337. P. Dash *et al.*, Quantifiable predictive features define epitope-specific T cell receptor repertoires. *Nature* **547**, 89-93 (2017).
338. Y. Elhanati, Z. Sethna, C. G. Callan, Jr., T. Mora, A. M. Walczak, Predicting the spectrum of TCR repertoire sharing with a data-driven model of recombination. *Immunol Rev* **284**, 167-179 (2018).
339. T. Mora, A. M. Walczak, Quantifying lymphocyte receptor diversity. *bioRxiv*, 046870 (2016).
340. J. Liu *et al.*, The peripheral differentiation of human natural killer T cells. *Immunol Cell Biol* **97**, 586-596 (2019).
341. I. Van Rhijn *et al.*, TCR Bias and Affinity Define Two Compartments of the CD1b–Glycolipid-Specific T Cell Repertoire. *The Journal of Immunology* **192**, 4054-4060 (2014).
342. J. Davis-Porada *et al.*, Maintenance and functional regulation of immune memory to COVID-19 vaccines in tissues. *Immunity* **57**, 2895-2913.e2898 (2024).
343. S. I. Koizumi, H. Ishikawa, Transcriptional Regulation of Differentiation and Functions of Effector T Regulatory Cells. *Cells* **8**, (2019).
344. J. I. Rodriguez-Barbosa *et al.*, HVEM, a cosignaling molecular switch, and its interactions with BTLA, CD160 and LIGHT. *Cellular & Molecular Immunology* **16**, 679-682 (2019).
345. E. N. McNamee, D. Korns Johnson, D. Homann, E. T. Clambey, Hypoxia and hypoxia-inducible factors as regulators of T cell development, differentiation, and function. *Immunologic Research* **55**, 58-70 (2013).
346. L. Gattinoni, D. E. Speiser, M. Lichterfeld, C. Bonini, T memory stem cells in health and disease. *Nature Medicine* **23**, 18-27 (2017).
347. S. Crotty, Do Memory CD4 T Cells Keep Their Cell-Type Programming: Plasticity versus Fate Commitment? Complexities of Interpretation due to the Heterogeneity of Memory CD4 T Cells, Including T Follicular Helper Cells. *Cold Spring Harb Perspect*

Biol **10**, (2018).
348. G. T. Nepom, MHC class II tetramers. *J Immunol* **188**, 2477-2482 (2012).
349. J. E. Ussher *et al.*, CD161++CD8+ T cells, including the MAIT cell subset, are specifically activated by IL-12+IL-18 in a TCR-independent manner. *European Journal of Immunology* **44**, 195-203 (2014).
350. N. M. Provine *et al.*, Unique and Common Features of Innate-Like Human Vδ2(+) γδT Cells and Mucosal-Associated Invariant T Cells. *Front Immunol* **9**, 756 (2018).
351. N. M. Provine *et al.*, MAIT cell activation augments adenovirus vector vaccine immunogenicity. *Science* **371**, 521-526 (2021).
352. B. E. Freeman, E. Hammarlund, H.-P. Raué, M. K. Slifka, Regulation of innate CD8+ T-cell activation mediated by cytokines. *Proceedings of the National Academy of Sciences* **109**, 9971-9976 (2012).
353. W. Mandala, V. Harawa, A. Munyenyembe, M. Soko, H. Longwe, Optimization of stimulation and staining conditions for intracellular cytokine staining (ICS) for determination of cytokine-producing T cells and monocytes. *Curr Res Immunol* **2**, 184-193 (2021).
354. K. J. Ewer *et al.*, T cell and antibody responses induced by a single dose of ChAdOx1 nCoV-19 (AZD1222) vaccine in a phase 1/2 clinical trial. *Nat Med* **27**, 270-278 (2021).
355. A. N. Hegazy *et al.*, Plasticity and lineage commitment of individual TH1 cells are determined by stable T-bet expression quantities. *Science Advances* **10**, eadk2693 (2024).
356. A. Angyal *et al.*, T-cell and antibody responses to first BNT162b2 vaccine dose in previously infected and SARS-CoV-2-naive UK health-care workers: a multicentre prospective cohort study. *The Lancet Microbe* **3**, e21-e31 (2022).
357. C. Saggau *et al.*, The pre-exposure SARS-CoV-2-specific T cell repertoire determines the quality of the immune response to vaccination. *Immunity* **55**, 1924-1939.e1925 (2022).
358. C. Li *et al.*, Mechanisms of innate and adaptive immunity to the Pfizer-BioNTech BNT162b2 vaccine. *Nat Immunol* **23**, 543-555 (2022).
359. J. E. Teigler, M. J. Iampietro, D. H. Barouch, Vaccination with adenovirus serotypes 35, 26, and 48 elicits higher levels of innate cytokine responses than adenovirus serotype 5 in rhesus monkeys. *J Virol* **86**, 9590-9598 (2012).
360. M. De Giovanni *et al.*, Spatiotemporal regulation of type I interferon expression determines the antiviral polarization of CD4+ T cells. *Nature Immunology* **21**, 321-330 (2020).
361. N. S. Joshi *et al.*, Inflammation Directs Memory Precursor and Short-Lived Effector CD8+ T Cell Fates via the Graded Expression of T-bet Transcription Factor. *Immunity* **27**, 281-295 (2007).
362. F. Cappuccini, S. Stribbling, E. Pollock, A. V. Hill, I. Redchenko, Immunogenicity and efficacy of the novel cancer vaccine based on simian adenovirus and MVA vectors alone and in combination with PD-1 mAb in a mouse model of prostate cancer. *Cancer Immunol Immunother* **65**, 701-713 (2016).
363. F. Cappuccini *et al.*, Safety and immunogenicity of novel 5T4 viral vectored vaccination regimens in early stage prostate cancer: a phase I clinical trial. *Journal for ImmunoTherapy of Cancer* **8**, e000928 (2020).
364. B. Essink *et al.*, The safety and immunogenicity of two Zika virus mRNA vaccine candidates in healthy flavivirus baseline seropositive and seronegative adults: the results of two randomised, placebo-controlled, dose-ranging, phase 1 clinical trials. *The Lancet Infectious Diseases* **23**, 621-633 (2023).
365. H. Fu *et al.*, The response to influenza vaccination is associated with DNA methylation-driven regulation of T cell innate antiviral pathways. *Clinical Epigenetics*

16, 114 (2024).
366. S. Falahi, A. Kenarkoohi, Host factors and vaccine efficacy: Implications for COVID-19 vaccines. *J Med Virol* **94**, 1330-1335 (2022).
367. S. Fourati *et al.*, Pan-vaccine analysis reveals innate immune endotypes predictive of antibody responses to vaccination. *Nature Immunology* **23**, 1777-1787 (2022).
368. T. Hagan *et al.*, Transcriptional atlas of the human immune response to 13 vaccines reveals a common predictor of vaccine-induced antibody responses. *Nature Immunology* **23**, 1788-1798 (2022).
369. John S. Tsang *et al.*, Global Analyses of Human Immune Variation Reveal Baseline Predictors of Postvaccination Responses. *Cell* **157**, 499-513 (2014).
370. M. Cortese *et al.*, System vaccinology analysis of predictors and mechanisms of antibody response durability to multiple vaccines in humans. *Nature Immunology* **26**, 116-130 (2025).
371. S. Fourati *et al.*, Pre-vaccination inflammation and B-cell signalling predict age-related hyporesponse to hepatitis B vaccination. *Nature Communications* **7**, 10369 (2016).
372. T. D. Querec *et al.*, Systems biology approach predicts immunogenicity of the yellow fever vaccine in humans. *Nature Immunology* **10**, 116-125 (2009).
373. D. E. Zak *et al.*, Merck Ad5/HIV induces broad innate immune activation that predicts CD8+ T-cell responses but is attenuated by preexisting Ad5 immunity. *Proceedings of the National Academy of Sciences* **109**, E3503-E3512 (2012).
374. P. Drennan *et al.*, Immunogenicity of MVA-BN Vaccine Deployed as Mpox Prophylaxis: A Prospective Cohort Study and Analysis of Transcriptomic Predictors of Response. *SSRN*, (2024).
375. J. García-Arriaza *et al.*, A Candidate HIV/AIDS Vaccine (MVA-B) Lacking Vaccinia Virus Gene C6L Enhances Memory HIV-1-Specific T-Cell Responses. *PLOS ONE* **6**, e24244 (2011).
376. Y. Liu *et al.*, Clinical characteristics, risk factors and antiviral treatments of influenza in immunosuppressed inpatients in Beijing during the 2015-2020 influenza seasons. *Virol J* **19**, 11 (2022).
377. M. Lemaitre *et al.*, Association Between Use of Thiopurines or Tumor Necrosis Factor Antagonists Alone or in Combination and Risk of Lymphoma in Patients With Inflammatory Bowel Disease. *JAMA* **318**, 1679-1686 (2017).
378. Z. Huo *et al.*, Cancer Risks in Solid Organ Transplant Recipients: Results from a Comprehensive Analysis of 72 Cohort Studies. *OncoImmunology* **9**, 1848068 (2020).
379. C. S. Goodyear *et al.*, Immunogenicity of third dose COVID-19 vaccine strategies in patients who are immunocompromised with suboptimal immunity following two doses (OCTAVE-DUO): an open-label, multicentre, randomised, controlled, phase 3 trial. *The Lancet Rheumatology* **6**, e339-e351 (2024).
380. L. Mol, P. B. Ottevanger, M. Koopman, C. J. A. Punt, The prognostic value of WHO performance status in relation to quality of life in advanced colorectal cancer patients. *European Journal of Cancer* **66**, 138-143 (2016).
381. J. H. Friedman, T. Hastie, R. Tibshirani, Regularization Paths for Generalized Linear Models via Coordinate Descent. *Journal of Statistical Software* **33**, 1 - 22 (2010).
382. U. Groemping, Relative Importance for Linear Regression in R: The Package relaimpo. *Journal of Statistical Software* **17**, 1 - 27 (2006).
383. K. D. Deane *et al.*, Genetic and environmental risk factors for rheumatoid arthritis. *Best Pract Res Clin Rheumatol* **31**, 3-18 (2017).
384. J. E. Locke *et al.*, Quantifying Sex-Based Disparities in Liver Allocation. *JAMA Surgery* **155**, e201129-e201129 (2020).
385. G. Katz-Greenberg, S. Shah, Sex and Gender Differences in Kidney Transplantation. *Semin Nephrol* **42**, 219-229 (2022).

386. K. C. Thandra *et al.*, Epidemiology of Non-Hodgkin's Lymphoma. *Med Sci (Basel)* **9**, (2021).
387. S. Tahtinen *et al.*, IL-1 and IL-1ra are key regulators of the inflammatory response to RNA vaccines. *Nature Immunology* **23**, 532-542 (2022).
388. N. A. Bezman *et al.*, Molecular definition of the identity and activation of natural killer cells. *Nature Immunology* **13**, 1000-1009 (2012).
389. P. Bohacova *et al.*, Multidimensional profiling of human T cells reveals high CD38 expression, marking recent thymic emigrants and age-related naive T cell remodeling. *Immunity* **57**, 2362-2379.e2310 (2024).
390. G. Strauss *et al.*, CD95 co-stimulation blocks activation of naive T cells by inhibiting T cell receptor signaling. *J Exp Med* **206**, 1379-1393 (2009).
391. S. Simon, N. Labarriere, PD-1 expression on tumor-specific T cells: Friend or foe for immunotherapy? *Oncoimmunology* **7**, e1364828 (2017).
392. J. R. Groom, A. D. Luster, CXCR3 in T cell function. *Exp Cell Res* **317**, 620-631 (2011).
393. R. Sparks *et al.*, A unified metric of human immune health. *Nature Medicine* **30**, 2461-2472 (2024).
394. G. Wang, H. L. Bonkovsky, A. de Lemos, F. J. Burczynski, Recent insights into the biological functions of liver fatty acid binding protein 1. *J Lipid Res* **56**, 2238-2247 (2015).
395. E. Noiri *et al.*, Urinary fatty acid-binding protein 1: an early predictive biomarker of kidney injury. *Am J Physiol Renal Physiol* **296**, F669-679 (2009).
396. L. Rump, D. L. Mattey, O. Kehoe, J. Middleton, An initial investigation into endothelial CC chemokine expression in the human rheumatoid synovium. *Cytokine* **97**, 133-140 (2017).
397. S. Cambier, M. Gouwy, P. Proost, The chemokines CXCL8 and CXCL12: molecular and functional properties, role in disease and efforts towards pharmacological intervention. *Cellular & Molecular Immunology* **20**, 217-251 (2023).
398. T. Iwamoto *et al.*, Monocyte chemoattractant protein-4 (MCP-4)/CCL13 is highly expressed in cartilage from patients with rheumatoid arthritis. *Rheumatology* **45**, 421-424 (2005).
399. J. Chen *et al.*, CCL7 promotes macrophage polarization and synovitis to exacerbate rheumatoid arthritis. *iScience*, 112177 (2025).
400. Y. Bian *et al.*, Immunomodulatory roles of metalloproteinases in rheumatoid arthritis. *Front Pharmacol* **14**, 1285455 (2023).
401. D. I. Jang *et al.*, The Role of Tumor Necrosis Factor Alpha (TNF-α) in Autoimmune Disease and Current TNF-α Inhibitors in Therapeutics. *Int J Mol Sci* **22**, (2021).
402. A. K. Mehta, D. T. Gracias, M. Croft, TNF activity and T cells. *Cytokine* **101**, 14-18 (2018).
403. M. Schulz, H. Dotzlaw, G. Neeck, Ankylosing Spondylitis and Rheumatoid Arthritis: Serum Levels of TNF-α and Its Soluble Receptors during the Course of Therapy with Etanercept and Infliximab. *BioMed Research International* **2014**, 675108 (2014).
404. A.-M. Tsimberidou, T. Waddelow, H. M. Kantarjian, M. Albitar, F. J. Giles, Pilot study of recombinant human soluble tumor necrosis factor (TNF) receptor (p75) fusion protein (TNFR:Fc; Enbrel) in patients with refractory multiple myeloma: increase in plasma TNFα levels during treatment. *Leukemia Research* **27**, 375-380 (2003).
405. M. L. Nowlan *et al.*, Systemic cytokine levels and the effects of etanercept in TNF receptor-associated periodic syndrome (TRAPS) involving a C33Y mutation in TNFRSF1A. *Rheumatology* **45**, 31-37 (2005).
406. N. Morozova, M. Z. Avramovič, G. Markelj, N. Toplak, T. Avčin, Dynamics of serum levels of TNF-α in a longitudinal follow-up study in 98 patients with juvenile idiopathic arthritis treated with anti-TNF-α biological drugs. *Clinical Rheumatology* **43**, 2287-

2293 (2024).
407. A. Kassambara *et al.*, RNA-sequencing data-driven dissection of human plasma cell differentiation reveals new potential transcription regulators. *Leukemia* **35**, 1451-1462 (2021).
408. S. Palmer, L. Albergante, C. C. Blackburn, T. J. Newman, Thymic involution and rising disease incidence with age. *Proceedings of the National Academy of Sciences* **115**, 1883-1888 (2018).
409. Z. L. Piedra-Quintero, Z. Wilson, P. Nava, M. Guerau-de-Arellano, CD38: An Immunomodulatory Molecule in Inflammation and Autoimmunity. *Frontiers in Immunology* **11**, (2020).
410. S. De Biasi *et al.*, Marked T cell activation, senescence, exhaustion and skewing towards TH17 in patients with COVID-19 pneumonia. *Nature Communications* **11**, 3434 (2020).
411. B. Bauvois *et al.*, Upregulation of CD38 Gene Expression in Leukemic B Cells by Interferon Types I and II. *Journal of Interferon & Cytokine Research* **19**, 1059-1066 (1999).
412. B.-N. Kang *et al.*, Transcriptional regulation of CD38 expression by tumor necrosis factor-α in human airway smooth muscle cells: role of NF-κB and sensitivity to glucocorticoidsTranscriptional regulation of CD38 expression by tumor necrosis factor-α in human airway smooth muscle cells: role of NF-κB and sensitivity to glucocorticoids. *The FASEB Journal* **20**, 1000-1002 (2006).
413. J. Yunis, K. R. Short, D. Yu, Severe respiratory viral infections: T-cell functions diverging from immunity to inflammation. *Trends in Microbiology* **31**, 644-656 (2023).
414. H. Arasanz *et al.*, PD1 signal transduction pathways in T cells. *Oncotarget* **8**, (2017).
415. W. Li, L. Liang, Q. Liao, Y. Li, Y. Zhou, CD38: An important regulator of T cell function. *Biomedicine & Pharmacotherapy* **153**, 113395 (2022).
416. R. Zonozi *et al.*, T cell responses to SARS-CoV-2 infection and vaccination are elevated in B cell deficiency and reduce risk of severe COVID-19. *Science Translational Medicine* **15**, eadh4529.
417. H. Rincon-Arevalo *et al.*, Impaired humoral immunity to SARS-CoV-2 BNT162b2 vaccine in kidney transplant recipients and dialysis patients. *Science Immunology* **6**, eabj1031 (2021).
418. N. S. Abed, J. H. Chace, A. L. Fleming, J. S. Cowdery, Interferon-gamma regulation of B lymphocyte differentiation: activation of B cells is a prerequisite for IFN-gamma-mediated inhibition of B cell differentiation. *Cell Immunol* **153**, 356-366 (1994).
419. N. Obeng-Adjei *et al.*, Malaria-induced interferon-γ drives the expansion of Tbethi atypical memory B cells. *PLOS Pathogens* **13**, e1006576 (2017).
420. N. Gill, G. Paltser, A. A. Ashkar, Interleukin-15 expression affects homeostasis and function of B cells through NK cell-derived interferon-γ. *Cellular Immunology* **258**, 59-64 (2009).
421. W. Chen *et al.*, The kinetics of IgG subclasses and contributions to neutralizing activity against SARS-CoV-2 wild-type strain and variants in healthy adults immunized with inactivated vaccine. *Immunology* **167**, 221-232 (2022).
422. P. Irrgang *et al.*, Class switch toward noninflammatory, spike-specific IgG4 antibodies after repeated SARS-CoV-2 mRNA vaccination. *Science Immunology* **8**, eade2798 (2023).
423. K. Matsushita *et al.*, Soluble CD22 as a tumor marker for hairy cell leukemia. *Blood* **112**, 2272-2277 (2008).
424. E. A. Clark, N. V. Giltiay, CD22: A Regulator of Innate and Adaptive B Cell Responses and Autoimmunity. *Front Immunol* **9**, 2235 (2018).
425. V. Upadhyay, Y. X. Fu, Lymphotoxin signalling in immune homeostasis and the control of microorganisms. *Nat Rev Immunol* **13**, 270-279 (2013).

426. O. V. Britanova *et al.*, Age-related decrease in TCR repertoire diversity measured with deep and normalized sequence profiling. *J Immunol* **192**, 2689-2698 (2014).
427. E. Liaskou *et al.*, High-throughput T-cell receptor sequencing across chronic liver diseases reveals distinct disease-associated repertoires. *Hepatology* **63**, 1608-1619 (2016).
428. S. Heidt *et al.*, Calcineurin inhibitors affect B cell antibody responses indirectly by interfering with T cell help. *Clin Exp Immunol* **159**, 199-207 (2010).
429. S. Pineda *et al.*, Characterizing pre-transplant and post-transplant kidney rejection risk by B cell immune repertoire sequencing. *Nature Communications* **10**, 1906 (2019).
430. R. J. M. Bashford-Rogers *et al.*, Analysis of the B cell receptor repertoire in six immune-mediated diseases. *Nature* **574**, 122-126 (2019).
431. M. P. Mulè, A. J. Martins, J. S. Tsang, Normalizing and denoising protein expression data from droplet-based single cell profiling. *Nature Communications* **13**, 2099 (2022).
432. C. Domínguez Conde *et al.*, Cross-tissue immune cell analysis reveals tissue-specific features in humans. *Science* **376**, eabl5197.
433. J. Ye, N. Ma, T. L. Madden, J. M. Ostell, IgBLAST: an immunoglobulin variable domain sequence analysis tool. *Nucleic Acids Research* **41**, W34-W40 (2013).
434. N. Nouri, S. H. Kleinstein, Somatic hypermutation analysis for improved identification of B cell clonal families from next-generation sequencing data. *PLOS Computational Biology* **16**, e1007977 (2020).
435. N. Nouri, S. H. Kleinstein, A spectral clustering-based method for identifying clones from high-throughput B cell repertoire sequencing data. *Bioinformatics* **34**, i341-i349 (2018).
436. G. Yaari *et al.*, Models of Somatic Hypermutation Targeting and Substitution Based on Synonymous Mutations from High-Throughput Immunoglobulin Sequencing Data. *Frontiers in Immunology* **4**, (2013).
437. E. Dann, N. C. Henderson, S. A. Teichmann, M. D. Morgan, J. C. Marioni, Differential abundance testing on single-cell data using k-nearest neighbor graphs. *Nature Biotechnology* **40**, 245-253 (2022).
438. E. Rosati *et al.*, A novel unconventional T cell population enriched in Crohn's disease. *Gut* **71**, 2194 (2022).
439. P. Giuffrida, G. R. Corazza, A. Di Sabatino, Old and New Lymphocyte Players in Inflammatory Bowel Disease. *Digestive Diseases and Sciences* **63**, 277-288 (2018).
440. A. Liberzon *et al.*, The Molecular Signatures Database (MSigDB) hallmark gene set collection. *Cell Syst* **1**, 417-425 (2015).
441. A. Wesa, A. Galy, Increased production of pro-inflammatory cytokines and enhanced T cell responses after activation of human dendritic cells with IL-1 and CD40 ligand. *BMC Immunology* **3**, 14 (2002).
442. N. Sanarico *et al.*, Human monocyte-derived dendritic cells differentiated in the presence of IL-2 produce proinflammatory cytokines and prime Th1 immune response. *Journal of Leukocyte Biology* **80**, 555-562 (2006).
443. H. Gary-Gouy, P. Lebon, A. H. Dalloul, Type I Interferon Production by Plasmacytoid Dendritic Cells and Monocytes Is Triggered by Viruses, but the Level of Production Is Controlled by Distinct Cytokines. *Journal of Interferon & Cytokine Research* **22**, 653-659 (2002).
444. J. Yang, L. Zhang, C. Yu, X.-F. Yang, H. Wang, Monocyte and macrophage differentiation: circulation inflammatory monocyte as biomarker for inflammatory diseases. *Biomarker Research* **2**, 1 (2014).
445. S.-M. Ong *et al.*, The pro-inflammatory phenotype of the human non-classical monocyte subset is attributed to senescence. *Cell Death & Disease* **9**, 266 (2018).

446. T. S. Kapellos *et al.*, Human Monocyte Subsets and Phenotypes in Major Chronic Inflammatory Diseases. *Front Immunol* **10**, 2035 (2019).
447. T. Condamine *et al.*, Tmem176B and Tmem176A are associated with the immature state of dendritic cells. *Journal of Leukocyte Biology* **88**, 507-515 (2010).
448. A. L. Shaffer *et al.*, Blimp-1 Orchestrates Plasma Cell Differentiation by Extinguishing the Mature B Cell Gene Expression Program. *Immunity* **17**, 51-62 (2002).
449. A. Caraux *et al.*, Circulating human B and plasma cells. Age-associated changes in counts and detailed characterization of circulating normal CD138- and CD138+ plasma cells. *Haematologica* **95**, 1016-1020 (2010).
450. K. A. Wietschel *et al.*, Non-cross-reactive epitopes dominate the humoral immune response to COVID-19 vaccination – kinetics of plasma antibodies, plasmablasts and memory B cells. *Frontiers in Immunology* **15**, (2024).
451. D. D. Jones *et al.*, mTOR has distinct functions in generating versus sustaining humoral immunity. *J Clin Invest* **126**, 4250-4261 (2016).
452. T. N. Iwata, J. A. Ramírez-Komo, H. Park, B. M. Iritani, Control of B lymphocyte development and functions by the mTOR signaling pathways. *Cytokine Growth Factor Rev* **35**, 47-62 (2017).
453. D. P. Calado *et al.*, The cell-cycle regulator c-Myc is essential for the formation and maintenance of germinal centers. *Nature Immunology* **13**, 1092-1100 (2012).
454. F. Salerno *et al.*, An integrated proteome and transcriptome of B cell maturation defines poised activation states of transitional and mature B cells. *Nature Communications* **14**, 5116 (2023).
455. K. Takahashi *et al.*, CCL3 and CCL4 are biomarkers for B cell receptor pathway activation and prognostic serum markers in diffuse large B cell lymphoma. *Br J Haematol* **171**, 726-735 (2015).
456. H. Y. Wong, A. Prasad, S. U. Gan, J. J. E. Chua, H. Schwarz, Identification of CD137-Expressing B Cells in Multiple Sclerosis Which Secrete IL-6 Upon Engagement by CD137 Ligand. *Front Immunol* **11**, 571964 (2020).
457. H. Ghadially *et al.*, Differential Regulation of CCL22 Gene Expression in Murine Dendritic Cells and B Cells1. *The Journal of Immunology* **174**, 5620-5629 (2005).
458. M. Kremlitzka *et al.*, Complement receptor type 1 (CR1, CD35) is a potent inhibitor of B-cell functions in rheumatoid arthritis patients. *Int Immunol* **25**, 25-33 (2013).
459. J. Stavnezer, J. E. Guikema, C. E. Schrader, Mechanism and regulation of class switch recombination. *Annu Rev Immunol* **26**, 261-292 (2008).
460. J. M. Di Noia, M. S. Neuberger, Molecular mechanisms of antibody somatic hypermutation. *Annu Rev Biochem* **76**, 1-22 (2007).
461. E. Blanco *et al.*, Age-associated distribution of normal B-cell and plasma cell subsets in peripheral blood. *Journal of Allergy and Clinical Immunology* **141**, 2208-2219.e2216 (2018).
462. F. Horns, C. L. Dekker, S. R. Quake, Memory B Cell Activation, Broad Anti-influenza Antibodies, and Bystander Activation Revealed by Single-Cell Transcriptomics. *Cell Reports* **30**, 905-913.e906 (2020).
463. R. Hong *et al.*, Distinct roles of BCNP1 in B-cell development and activation. *International Immunology* **32**, 17-26 (2020).
464. F. Castellino *et al.*, Chemokines enhance immunity by guiding naive CD8+ T cells to sites of CD4+ T cell–dendritic cell interaction. *Nature* **440**, 890-895 (2006).
465. F. Macdonald, J. van Loosdregt, D. M. W. Zaiss, T cell derived HB-EGF prevents Th17 cell differentiation in an autocrine way. *bioRxiv*, 2021.2002.2009.430418 (2021).
466. R. E. Owen *et al.*, Loss of T cell responses following long-term cryopreservation. *J Immunol Methods* **326**, 93-115 (2007).
467. H. Gudmundsdottir, A. D. Wells, L. A. Turka, Dynamics and requirements of T cell

clonal expansion in vivo at the single-cell level: effector function is linked to proliferative capacity. *J Immunol* **162**, 5212-5223 (1999).
468. C. Poloni *et al.*, T-cell activation–induced marker assays in health and disease. *Immunology & Cell Biology* **101**, 491-503 (2023).
469. K. Ohtani *et al.*, Cell growth-regulated expression of mammalian MCM5 and MCM6 genes mediated by the transcription factor E2F. *Oncogene* **18**, 2299-2309 (1999).
470. F. Calmon-Hamaty, B. Combe, M. Hahne, J. Morel, Lymphotoxin α revisited: general features and implications in rheumatoid arthritis. *Arthritis Res Ther* **13**, 232 (2011).
471. T. Kim, S. C. Bae, C. Kang, Synergistic activation of NF-κB by TNFAIP3 (A20) reduction and UBE2L3 (UBCH7) augment that synergistically elevate lupus risk. *Arthritis Res Ther* **22**, 93 (2020).
472. M. Park *et al.*, NF-κB-responsive miR-155 induces functional impairment of vascular smooth muscle cells by downregulating soluble guanylyl cyclase. *Experimental & Molecular Medicine* **51**, 1-12 (2019).
473. A. F. Christiaansen *et al.*, CD11a and CD49d enhance the detection of antigen-specific T cells following human vaccination. *Vaccine* **35**, 4255-4261 (2017).
474. T. O. Bose *et al.*, CD11a regulates effector CD8 T cell differentiation and central memory development in response to infection with Listeria monocytogenes. *Infect Immun* **81**, 1140-1151 (2013).
475. M. A. Paley *et al.*, Progenitor and Terminal Subsets of CD8+ T Cells Cooperate to Contain Chronic Viral Infection. *Science* **338**, 1220-1225 (2012).
476. J. Zhang, T. Lyu, Y. Cao, H. Feng, Role of TCF-1 in differentiation, exhaustion, and memory of CD8+ T cells: A review. *The FASEB Journal* **35**, e21549 (2021).
477. D. Mittal *et al.*, CD96 Is an Immune Checkpoint That Regulates CD8(+) T-cell Antitumor Function. *Cancer Immunol Res* **7**, 559-571 (2019).
478. Z. Z. Yang *et al.*, TIGIT Expression Is Associated with T-cell Suppression and Exhaustion and Predicts Clinical Outcome and Anti-PD-1 Response in Follicular Lymphoma. *Clin Cancer Res* **26**, 5217-5231 (2020).
479. C. V. Jakubzick, G. J. Randolph, P. M. Henson, Monocyte differentiation and antigen-presenting functions. *Nature Reviews Immunology* **17**, 349-362 (2017).
480. K. L. Hilligan, F. Ronchese, Antigen presentation by dendritic cells and their instruction of CD4+ T helper cell responses. *Cellular & Molecular Immunology* **17**, 587-599 (2020).
481. J. Austermann, J. Roth, K. Barczyk-Kahlert, The Good and the Bad: Monocytes' and Macrophages' Diverse Functions in Inflammation. *Cells* **11**, (2022).
482. R. J. Schutte, A. Parisi-Amon, W. M. Reichert, Cytokine profiling using monocytes/macrophages cultured on common biomaterials with a range of surface chemistries. *J Biomed Mater Res A* **88**, 128-139 (2009).
483. C. De Haro, R. Méndez, J. Santoyo, The eIF-2α kinases and the control of protein synthesis. *The FASEB Journal* **10**, 1378-1387 (1996).
484. S.-L. Liang, D. Quirk, A. Zhou, RNase L: Its biological roles and regulation. *IUBMB Life* **58**, 508-514 (2006).
485. T. Schmidt *et al.*, Cellular immunity predominates over humoral immunity after homologous and heterologous mRNA and vector-based COVID-19 vaccine regimens in solid organ transplant recipients. *American Journal of Transplantation* **21**, 3990-4002 (2021).
486. A. Favà *et al.*, A comprehensive assessment of long-term SARS-CoV-2–specific adaptive immune memory in convalescent COVID-19 Solid Organ Transplant recipients. *Kidney International* **101**, 1027-1038 (2022).
487. A. Aranburu *et al.*, Human B-cell memory is shaped by age- and tissue-specific T-independent and GC-dependent events. *European Journal of Immunology* **47**, 327-344 (2017).

488. M. Seifert *et al.*, Functional capacities of human IgM memory B cells in early inflammatory responses and secondary germinal center reactions. *Proc Natl Acad Sci U S A* **112**, E546-555 (2015).
489. B. Budeus, A. Kibler, R. Küppers, Human IgM–expressing memory B cells. *Frontiers in Immunology* **14**, (2023).
490. A. J. McAdam *et al.*, ICOS is critical for CD40-mediated antibody class switching. *Nature* **409**, 102-105 (2001).
491. K. Warnatz *et al.*, Human ICOS deficiency abrogates the germinal center reaction and provides a monogenic model for common variable immunodeficiency. *Blood* **107**, 3045-3052 (2006).
492. J. L. Karnell *et al.*, Mycophenolic acid differentially impacts B cell function depending on the stage of differentiation. *J Immunol* **187**, 3603-3612 (2011).
493. S. Tritschler *et al.*, Concepts and limitations for learning developmental trajectories from single cell genomics. *Development* **146**, dev170506 (2019).
494. W. Saelens, R. Cannoodt, H. Todorov, Y. Saeys, A comparison of single-cell trajectory inference methods. *Nature Biotechnology* **37**, 547-554 (2019).
495. J. Cao *et al.*, The single-cell transcriptional landscape of mammalian organogenesis. *Nature* **566**, 496-502 (2019).
496. R. Kraaijeveld *et al.*, Inhibition of T Helper Cell Differentiation by Tacrolimus or Sirolimus Results in Reduced B-Cell Activation: Effects on T Follicular Helper Cells. *Transplantation Proceedings* **51**, 3463-3473 (2019).
497. R. Alfonso-Dunn *et al.*, Strong T-cell activation in response to COVID-19 vaccination in multiple sclerosis patients receiving B-cell depleting therapies. *Front Immunol* **13**, 926318 (2022).
498. C. Ulutekin *et al.*, B cell depletion attenuates CD27 signaling of T helper cells in multiple sclerosis. *Cell Reports Medicine* **5**, (2024).
499. Y. S. Kap, N. van Driel, J. D. Laman, P. P. Tak, B. A. 't Hart, CD20+ B Cell Depletion Alters T Cell Homing. *The Journal of Immunology* **192**, 4242-4253 (2014).
500. K. Shinoda *et al.*, Differential effects of anti-CD20 therapy on CD4 and CD8 T cells and implication of CD20-expressing CD8 T cells in MS disease activity. *Proc Natl Acad Sci U S A* **120**, e2207291120 (2023).
501. Z. Chen *et al.*, TCF-1-Centered Transcriptional Network Drives an Effector versus Exhausted CD8 T Cell-Fate Decision. *Immunity* **51**, 840-855.e845 (2019).
502. L. Sun, Y. Su, A. Jiao, X. Wang, B. Zhang, T cells in health and disease. *Signal Transduction and Targeted Therapy* **8**, 235 (2023).
503. P. L. Smith, K. Piadel, A. G. Dalgleish, Directing T-Cell Immune Responses for Cancer Vaccination and Immunotherapy. *Vaccines (Basel)* **9**, (2021).
504. C. Ferreira *et al.*, Type 1 Treg cells promote the generation of CD8+ tissue-resident memory T cells. *Nature Immunology* **21**, 766-776 (2020).
505. F. Song, G. M. A. Chan, Y. Wei, Flexible experimental designs for valid single-cell RNA-sequencing experiments allowing batch effects correction. *Nature Communications* **11**, 3274 (2020).
506. J. Jeon, E. Kim, Exploring Future Pandemic Preparedness Through the Development of Preventive Vaccine Platforms and the Key Roles of International Organizations in a Global Health Crisis. *Vaccines (Basel)* **13**, (2025).
507. L. Yong, C. Hutchings, E. Barnes, P. Klenerman, N. M. Provine, Distinct Requirements for CD4+ T Cell Help for Immune Responses Induced by mRNA and Adenovirus-Vector SARS-CoV-2 Vaccines. *European Journal of Immunology* **55**, e202451142 (2025).
508. W. S. Foster *et al.*, Tfh cells and the germinal center are required for memory B cell formation & humoral immunity after ChAdOx1 nCoV-19 vaccination. *Cell Reports Medicine* **3**, (2022).

509. J. S. Chen *et al.*, High-affinity, neutralizing antibodies to SARS-CoV-2 can be made without T follicular helper cells. *Science Immunology* **7**, eabl5652 (2022).
510. R. da Silva Antunes *et al.*, Evolution of SARS-CoV-2 T cell responses as a function of multiple COVID-19 boosters. *bioRxiv*, (2025).
511. L. Belarif *et al.*, IL-7 receptor blockade blunts antigen-specific memory T cell responses and chronic inflammation in primates. *Nature Communications* **9**, 4483 (2018).
512. L. Wang *et al.*, IL-7 promotes mRNA vaccine-induced long-term immunity. *Journal of Nanobiotechnology* **22**, 716 (2024).
513. T. Fan *et al.*, Therapeutic cancer vaccines: advancements, challenges and prospects. *Signal Transduction and Targeted Therapy* **8**, 450 (2023).
514. Y. Wang *et al.*, Calcineurin inhibition rescues alloantigen-specific central memory T cell subsets that promote chronic GVHD. *The Journal of Clinical Investigation* **134**, (2024).
515. H. Senjo *et al.*, Calcineurin inhibitor inhibits tolerance induction by suppressing terminal exhaustion of donor T cells after allo-HCT. *Blood* **142**, 477-492 (2023).
516. B. Brook *et al.*, Adjuvantation of a SARS-CoV-2 mRNA vaccine with controlled tissue-specific expression of an mRNA encoding IL-12p70. *Science Translational Medicine* **16**, eadm8451.
517. M. A. Y. Al-Nesf *et al.*, Prognostic tools and candidate drugs based on plasma proteomics of patients with severe COVID-19 complications. *Nature Communications* **13**, 946 (2022).
518. O. Repetto, R. Vettori, A. Steffan, R. Cannizzaro, V. De Re, Circulating Proteins as Diagnostic Markers in Gastric Cancer. *Int J Mol Sci* **24**, (2023).
519. Y. Zhou *et al.*, Tumor biomarkers for diagnosis, prognosis and targeted therapy. *Signal Transduction and Targeted Therapy* **9**, 132 (2024).